THE
PHYSICAL REVIEW

A journal of experimental and theoretical physics established by E. L. Nichols in 1893

SECOND SERIES, VOL. 79, NO. 1 JULY 1, 1950

John Torrence Tate

THE Physical Review must now give its pages to John Torrence Tate who for nigh on a quarter of a century gave them to the physicists of the United States and of the world. On Saturday morning, May 27, 1950, while enjoying the garden at his home, he was stricken by a cerebral hemorrhage. Death came a few hours later at the hospital of the University of Minnesota. Dr. Tate had been on leave from active duties since December, 1949, when he suffered a light stroke. He had been able, however, to attend the recent meetings of the American Physical Society, the American Philosophical Society, and the National Academy of Sciences, of all of which he was a member.

Dr. Tate was born in Lennox, Iowa, on July 28, 1889. In 1910, he received the degree of Bachelor of Science at the University of Nebraska, and two years later he earned the Master of Arts. He then attended the University of Berlin and won the degree of Doctor of Philosophy in 1914. Two years were spent on the staff at the University of Nebraska, and in 1916 he came as an instructor to the University of Minnesota. At the close of each of his first three years on the staff, the University raised his rank, first to assistant professor, then to associate professor, and in 1919 to full professor. The University of Nebraska granted him the honorary degree of Doctor of Science in 1938, and in 1946 he was honored by a similar degree from the Case Institute of Technology.

In 1937 he was appointed Dean of the College of Science, Literature, and the Arts at the University of Minnesota. This position he resigned in 1943 and accepted appointment as research professor of physics.

During World War I, Dr. Tate served as first lieutenant in the Signal Corps and Air Service. In World War II, he served as Chief of Division 6 of the National Defense Research Committee. This division was responsible for research in and development of undersea warfare. He was also a member of Division 3, NDRC, and the Scientific Council of the Commander-in-Chief, U. S. Navy. At the time of his death he was Chairman of the Committee on Undersea Warfare of the National Research Council. From 1946 to 1949 he served as Chairman of the Board of Governors of the Argonne National Laboratory, one of the regional laboratories of the Atomic Energy Commission. Thereafter he continued as a member of the Council of Representatives of Participating Institutions of that laboratory.

For his service during World War II, our government awarded him the Presidential Medal of Merit, with citation, and the British bestowed upon him the King's Medal for service in the cause of freedom.

In 1926 Dr. Tate was selected by the American Physical Society to be its Managing Editor. As such, he was editor of *The Physical Review;* and his enormous service in this post is his monumental contribution to the science of the world. During this period the size of the *Physical Review* more than doubled with a greater than corre-

sponding increase in the burden carried by the Managing Editor. Dr. Tate tenaciously subscribed to the principle that a research is not completed until the results are published, and succeeded in winning effective support for that point of view. He also contended that progress and eventual security and welfare for all were best obtained by a free exchange of ideas, although he recognized that the exigencies of the times did not always permit the ideal. Under his guidance and editorship the American Physical Society founded two new journals: the *Reviews of Modern Physics* in 1929, and in 1931 the journal *Physics*, which is now the *Journal of Applied Physics*.

Dr. Tate was one of the founders of the American Institute of Physics, and throughout its existence has been its Adviser on Publications. During the period 1936–1939 he was Chairman of the Governing Board of the Institute. The American Physical Society chose him for its President in 1939.

His research at the University of Minnesota dealt with the phenomena arising in the collision of electrons with atoms and molecules. Many of the publications from the physics laboratory at Minnesota are by students of his. Seldom did he permit his name to be listed as co-author.

Providence did not grant him the three score and ten years in which men normally complete the tasks apportioned to them in accordance with their talents. But in the years allotted to him, Dr. Tate has in his quiet way contributed in full measure to his science, to his country, to his University, and to the community at large. Science has lost one of its statesmen, the University a revered teacher, research leader, and counselor, and all of us a friend.

Dr. Tate was married in 1917 to Lois Fossler who died in 1939; a son, John Torrence Tate, Jr., was born to them. In 1945 Dr. Tate was married to Madeline M. Mitchell, at that time Publications Manager of the American Institute of Physics, who survives him as does his son. We extend our warmest sympathies to them.

Delayed Neutrons from U^{238} and Th^{232} Fission*

K. H. SUN, R. A. CHARPIE, F. A. PECJAK, AND B. JENNINGS
Westinghouse Research Laboratories, East Pittsburgh, Pennsylvania
AND
J. F. NECHAJ AND A. J. ALLEN
University of Pittsburgh, Pittsburgh, Pennsylvania
(Received March 22, 1950)

The half-lives of the delayed neutron emitters from U^{238} and Th^{232} fission were found to be 0.4, 1.7, 5.8, 22.6, and 55.2, and 0.41, 1.4, 4.4, 20, and 56 sec., respectively, by using fast neutrons from 15-Mev cyclotron deuterons on a thick carbon target. These, when compared with those from the slow neutron fission of Pu^{239} and U^{235}, indicate that delayed neutron emitters from fission of Pu^{239}, U^{235}, U^{238}, and Th^{232} are identical. The delayed neutron yield after saturation bombardment was about 8 per 100 fissions. A preliminary survey indicated that the 22 and 56 sec. half-lives were also present when LiF or B_4C instead of carbon was used as the cyclotron target for producing faster neutrons.

SINCE the earlier work of Roberts *et al.*[1] many investigations have been carried out on the delayed neutrons from fission. At least five periods have been established[2–6] for the delayed neutrons from slow neutron fission of both U^{235} and Pu^{239} which were found to be the same for both fissionable nuclei. Two of the longest periods were attributed[7] to Br^{87} and I^{137}. Recently, Greveling *et al.*[8] found that four of the five known periods were also present in the fast neutron fission of Th^{232}. The present study of the delayed neutrons from fission was extended to include the fission of U^{238} as well as Th^{232} with fast neutrons varying in maximum energy from 14 to 29 Mev. The results indicated that there are at least five periods of delayed neutron emitters associated with fast neutron fission of U^{238} and Th^{232} and that these periods are identical, within the experimental error, with those found in the slow neutron fission of U^{235} and Pu^{239}. The yield of delayed neutrons per fission was found to be higher than that for the U^{235} and Pu^{239}.

The fast neutron source used was a thick target of C, LiF or B_4C bombarded with a 2 μa 15-Mev external deuteron beam from the University of Pittsburgh cyclotron. The Be-target was found to be undesirable because it yields large amounts of delayed photoneutrons due to the intense γ-rays which were always present immediately after cyclotron bombardment. The uranium or thorium sample was placed behind the neutron producing target and behind this target was placed a paraffin-surrounded $B^{10}F_3$ proportional counter (Fig. 1). The pulses from the counter were amplified by a linear amplifier and fed to a scaler capable of scaling down from 2^3 or 2^{12} to 1. The output pulses were registered on a paper tape traveling at a constant speed by an automatic pen recorder. A relay was placed in the circuit so that the pulse recording would start the moment the cyclotron bombardment was stopped. High scaling factors were used in the initial stage of counting, and as the rate of emission of delayed neutrons decreased, it was possible to shift to the lower scales without introducing extra pulses. The information recorded on the tape was then translated into the rate of decay of the delayed neutron emitters as a function of time. The data were then plotted and analyzed as described later.

About 5 pounds of uranium metal or 10 pounds of thorium oxide were used in the half-life measurements, and 168.1 g of metallic uranium or 41.36 g of thorium were used in the absolute yield determinations. The fission rate due to the fast neutron flux at the location where the uranium or thorium sample was placed was determined with a fission ionization chamber which contains a standard thin layer of uranium (7.8×10^{-4} g) or thorium (5.0×10^{-4} g). This made it possible to measure the rate of fission per unit weight of uranium or thorium under the same conditions as the delayed neutron measurement, which in turn yields direct information on the total number of fissions in the uranium or thorium sample for the delayed neutron study. The measurement of the absolute yield of delayed neutrons was made possible by assuming spherical symmetry of the neutron distribution, and by calibrating the $B^{10}F_3$ counter with a standard Ra–Be neutron source placed at the location of the uranium or thorium sample. The Ra–Be standard used was calibrated with the help of Dr. D. J. Hughes at the Argonne National Laboratory, and was found to emit 1.0×10^4 neutrons/sec. A previous study indicated that the counter used was almost energy independent for neutrons from Sb^{124}–Be (neutron energy 0.03 Mev), Na^{24}–D (0.22 Mev), Na^{24}–Be (0.83 Mev) to Ra–Be. Since the uranium samples used were natural isotopic mixtures, containing 0.7 percent U^{235}, they were wrapped in cadmium sheets to eliminate the slow neutron fission of U^{235}. An independent study of

* Assisted by the joint program of AEC and ONR.
[1] Roberts, Meyer, and Wang, Phys. Rev. **55**, 510 (1939); Roberts, Meyer, Hafstad, and Wang, Phys. Rev. **55**, 664 (1939).
[2] Snell, Nedzel, Ibser, Levinger, Wilkinson, and Sampson, Phys. Rev. **72**, 541 (1947).
[3] F. de Hoffmann and B. T. Feld, Phys. Rev. **72**, 567 (1947).
[4] W. C. Redman and D. Saxon, Phys. Rev. **72**, 570 (1947).
[5] Hughes, Dobbs, Cahn, and Hall, Phys. Rev. **73**, 111 (1948).
[6] De Hoffmann, Feld, and Stein, Phys. Rev. **74**, 1330 (1948).
[7] Snell, Levinger, Meiners, Sampson, and Wilkinson, Phys. Rev. **72**, 545 (1947).
[8] Greveling, Hood, and Pool, Phys. Rev. **76**, 946 (1949).

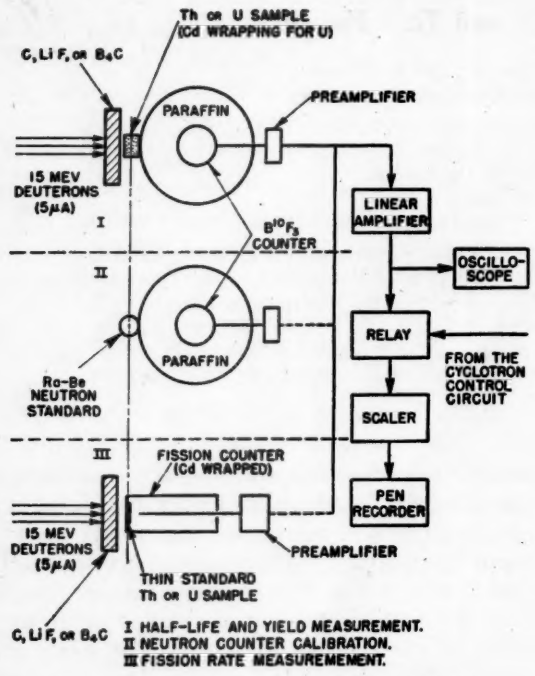

FIG. 1. Fast neutron fission of U^{238} and Th^{232}.

the neutron flux from a 15-Mev deuteron bombardment on a similar target revealed that the slow neutron flux near the target was only about one percent of that of the fast neutrons. It was therefore assumed that the delayed neutrons resulting from slow neutron fission of the U^{235} inside the Cd-enclosed natural uranium samples were negligible.

The information from the recording mentioned above was converted into the logarithm of the counting rate and plotted against time. The conventional *peeling off* technique was then applied to resolve the various half-lives (Fig. 2). A bombardment of 300 sec., which approached the saturation bombardment of all periods, made it possible to evaluate the three long half-lives, namely those of 56, 22, and 5 sec. The relative yields were obtained by reading the intercepts made by the straight lines of these periods on the axis at *zero time* (the end of the bombardment). In measuring the absolute yield, the decay rate at *zero time* was obtained by a short extrapolation in the semilog plot and was equal to the rate of production of the delayed neutron emitter for a saturation bombardment. Knowing the rate of fission, the yield was obtained. The two short periods (0.4 and 1.6 sec. half-lives) were obtained from data taken after a relatively short bombardment (0.8 to 2 sec.). The counting rate at 10 sec. after the end of the short bombardment was considered due to the neutron emitters with the three long half-lives. Their relative contribution at this instant (10 sec.) was calculated from their relative yield and their disintegration constants. Three corresponding straight lines were drawn and subtracted from the experimental data for the short bombardment. This provided the evaluation of the two short periods (Fig. 3). The process was repeated once again to allow for correction of the contribution made by the neutron emitter with a 1.6-sec. half-life. The relative yield of the short periods with respect to that of the 5-sec. half-life was obtained from the bombardment time, their disintegration constants and their intercepts on the semilog plot at zero time.[9]

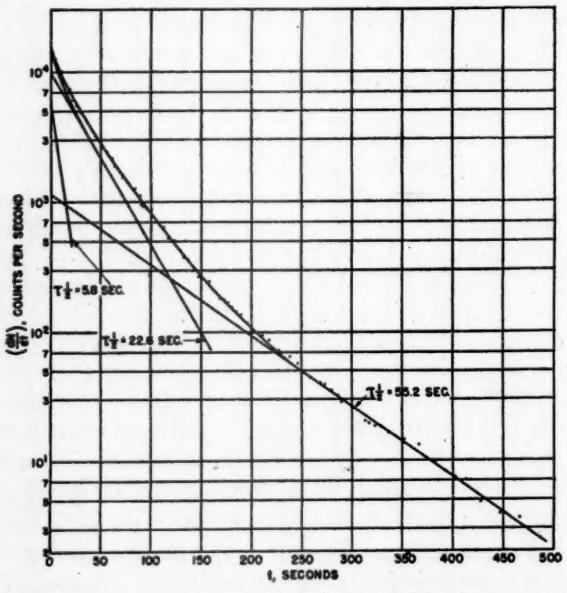

FIG. 2. Delayed neutrons from fission of U^{238} by fast neutrons from 15-Mev deuterons on carbon. Bombardment time=300 sec. (Run 45).

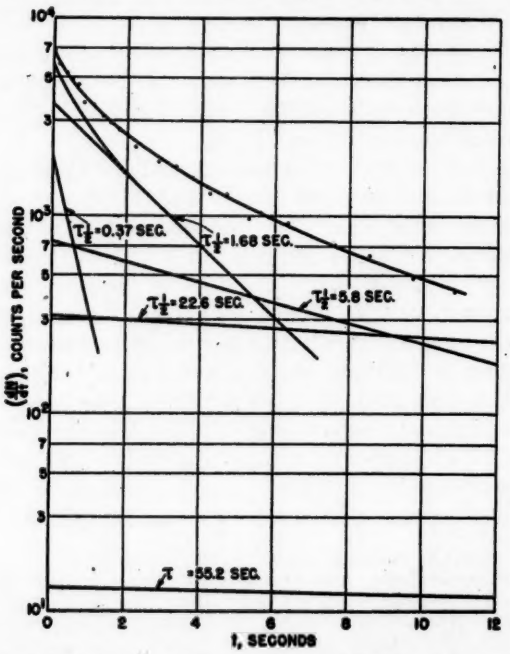

FIG. 3. Delayed neutrons from fission of U^{238} by fast neutrons from 15-Mev deuterons on carbon. Bombardment time=1.8 sec. (Run 26).

[9] $P=D/[1-\exp(-\lambda t_b)]$, where P=rate of production, D=rate of decay at end of bombardment, t_b=bombardment time, λ=disintegration constant.

TABLE I. Delayed neutrons from fission.

Nucleus	Neutron source	Neutron energy	Half-lives in seconds (relative yields in parentheses)												Reference
			Uncertain		0.4		1.6		5		22		56		
U^{235}	Chain reactor	Thermal	0.05	(0.12)	0.43	(0.40)	1.52	(1.13)	4.51	(1.00)	22.0	(0.78)	55.6	(0.12)	(5)
U^{235}	Chain reactor	Thermal	0.006		0.36	(0.26)	1.8	(0.94)	5.47	(1.00)	22.5	(0.99)	55.4	(0.18)	(6)
U^{235}	7.5-Mev deuterons on Be and slowed down	Slow			0.4	(0.36)	1.8	(0.45)	4.4	(1.00)	23.0	(0.91)	56.0	(0.13)	(2)
U^{235}	Chain reactor	Thermal					1.13	(1.21)	4.43	(1.00)	22.47	(0.74)	55.0	(0.11)	(4)
Pu^{239}	Chain reactor	Thermal					1.1	(0.81)	5.2	(1.00)	22.6	(0.78)	55.2	(0.11)	(3)
Pu^{239}	Chain reactor	Thermal					1.05	(1.10)	4.5	(1.00)	22.4	(0.92)	55.0	(0.09)	(4)
U^{238}	15-Mev deuterons on C	14-Mev (max.)			0.40	(0.64)	1.7	(2.0)	5.8	(1.00)	22.6	(1.5)	55.2	(0.18)	This paper
U^{238}	15-Mev deuterons on LiF	29-Mev (max.)									22.0	(6.0)	54.0	(1.00)	This paper
Th^{232}	10-Mev deuterons on Li	24-Mev (max.)	0.13	(0.88)			1.51	(0.92)	4.5	(1.00)	22.0	(0.5)	55.6	(0.14)	(8)
Th^{232}	15-Mev deuterons on C	14-Mev (max.)			0.41	(0.17)	1.4	(0.63)	4.4	(1.00)	20	(1.05)	56	(0.45)	This paper
Th^{232}	15-Mev deuterons on LiF	29-Mev (max.)							4.5	(1.00)	23	(0.6)	57	(0.3)	This paper
Th^{232}	15-Mev deuterons on B_4C	28-Mev (max.)							4.5	(1.00)	21	(0.85)	58	(0.43)	This paper

Several runs were made and an average taken. These results are summarized in Table I, in which the delayed neutron emitters of various half-lives and yields from fission of U^{235}, Pu^{239}, and Th^{232} by various investigators were also included for comparison. Using 15-Mev deuterons on a thick carbon target as the neutron source, the result of the analysis may be expressed as follows:

Delayed neutrons from U^{238}:

$$(dN/dt)_t = C_U(0.64e^{-1.7t} + 2.0e^{-0.40t} + 1.0e^{-0.12t} + 1.5e^{-0.031t} + 0.18e^{-0.013t}). \quad (1)$$

Delayed neutrons from Th^{232}:

$$(dN/dt)_t = C_{Th}(0.17e^{-1.7t} + 0.63e^{-0.50t} + 1.0e^{-0.16t} + 1.1e^{-0.035t} + 0.45e^{-0.012t}), \quad (2)$$

where $(dN/dt)_t$ is the rate of delayed neutron emission at t sec. after the fast neutron bombardment, and C is a constant. Half-lives shorter than 0.4 sec., or possibly 0.1 sec., are not included. The data for those, using neutrons from 15-Mev deuterons on B_4C and LiF, were incomplete. However, they indicated that the half-lives of the delayed neutron emitters from the fast neutron fission of U^{238} and Th^{232} are the same regardless of the neutron energy up to about 29 Mev.

The absolute yield of the delayed neutrons was estimated to be 8 ± 3 per 100 fissions after saturation bombardment using 15-Mev deuterons on C, B_4C, or LiF as a neutron source. Assuming three instantaneous neutrons per fission, the delayed neutrons are about 2.7 percent of the instantaneous neutrons emitted, which is greater than that of the slow neutron fission of U^{235} (0.76 percent)[5] by 4 times and Pu^{239} ($\frac{1}{2}$ that of U^{235})[3,4] by 8 times. It should be noted that in addition to the excess energy available, caused by that from the impinging fast neutrons, the compound nuclei formed before fission in the present study are of odd mass number while for the slow neutron fission of U^{235} and Pu^{239} they are of even mass number. These might account for the high yield of the delayed neutrons.

Angular Distributions of Ground-State Protons from $B^{10}+D^*$

W. C. REDMAN†
Sloane Physics Laboratory, Yale University, New Haven, Connecticut‡
(Received March 13, 1950)

The angular distributions of the ground-state protons resulting from the deuteron bombardment of B^{10} has been investigated at six energies in the 1- to 4-Mev interval. The reaction protons were recorded photographically at all angles from 5° to 165° and their distribution was determined by microscopic examination of the photographic emulsion. The resulting intensity variation with angle can be expressed within experimental error as a second-order Legendre polynomial series for all energies except the highest, for which a fourth-order series is required. *S*-wave deuterons predominate in producing this reaction, but *p*-wave effects occur even for the lowest energy distribution studied. *D*-wave contributions are noticed for deuteron energies above 3 Mev. The behavior of the coefficients in the series representation shows that several broad overlapping resonance levels, of both even and odd parity, in the compound nucleus probably enter into this reaction.

I. INTRODUCTION

INCREASING attention has been given recently to angular distribution studies as a fruitful approach to the field of nuclear spectroscopy. Recent work on *d*, *p* reactions by Heydenburg, Inglis, and co-workers[1] has indicated that an investigation of other similar reactions may furnish useful information.

The high energy release, $Q=9.14$ Mev, in the $B^{10}(d, p)B^{11}$ reaction makes it convenient for such a study. Because of the high excitation energy of the $B^{10}+D$ system, about 25 Mev for zero energy bombarding deuterons, no abrupt changes in the distribution with varying energy are to be expected, a favorable factor in view of the appreciable energy spread of the Yale cyclotron beam. In spite of this limitation, a knowledge of the trend in the angular distribution with increasing bombardment energy and information about the nature of this particular reaction should result. Photographic detection provides good discrimination against the prolific neutron yield from competing reactions, and through all-angle recording the presence or absence of appreciable fine structure in these distributions can be determined.

II. APPARATUS AND PRELIMINARY TESTS

A schematic plan of the combination bombardment chamber and angular distribution camera used is shown in Fig. 1. Similar chambers described by Wilkins[2] and Rubin[3] have influenced the design. This chamber is mounted past the magnetic deflector of the cyclotron with the photographic plates in a plane parallel to the direction of the stray magnetic field (<100 oersteds) in this region. The deuteron beam is stopped down to reduce its area, and is finally collimated into a $\frac{3}{16}$-in. diameter stream which strikes a solid target. The target support is attached to a Stupakoff metal-glass seal which passes through the base-plate of the chamber. Thus the target is insulated from the chamber which in turn is insulated from the cyclotron by Lucite bushings surrounding the bolts. The target mounting is a C-shaped, sandwich-type holder, permitting the observation of reaction particles emitted from both faces of the target. Beyond the target in the beam path is located a small window. This contains a fluorescent screen used for obtaining proper alignment of the chamber. Aluminum absorbers are interposed in the beam path to vary the bombarding energy. A fraction of the reaction particles pass through aluminum absorber foils mounted over an extended slit in the inner cylinder and enter the photographic emulsion at small angles with respect to the plane of the plates. Three 1×3-in. Ilford 100μ-type *C*-2 plates record these emitted particles at all angles from 0° to ~170° in the emulsion plane. The plates fit tightly in a holder which is positioned slightly below and parallel to the axis of the beam. In construction, all components were located relative to the fixed base-plate.

Solid targets of B_2O_3 from $\frac{1}{2}$ to 1 cm air equivalent were prepared by evaporating boracic acid, H_3BO_3, from a tungsten filament onto 5-cm air equivalent gold foil. Because of the long range of the end-group protons from $B^{10}(d, p)B^{11}$, these protons are easily separated from the oxygen and other boron charged particle groups by aluminum absorbers interposed between the target and photographic plates. Photographic plates are comparatively insensitive to the emitted neutrons due to the dependence on the neutron-proton scattering cross section for the production of recoil proton tracks. At the higher energies of bombardment the deuteron beam which passes through the target backing is absorbed in a gold foil mounted on the inner cylinder.

Ilford emulsions showed less tendency to crack or peel from their glass backing than did other similar

* Part of a dissertation presented to the Faculty of the Graduate School of Yale University in candidacy for the degree of Doctor of Philosophy.

† Now at Argonne National Laboratory, Chicago, Illinois.

‡ Assisted by the joint program of the ONR and AEC.

[1] N. P. Heydenburg and D. R. Inglis, Phys. Rev. **73**, 230 (1948); Heydenburg, Inglis, Whitehead, and Hafner, Phys. Rev. **75**, 1147 (1949); Krone, Hanna, and Inglis, Phys. Rev. **75**, 335(A) (1949); I. Resnick and S. S. Hanna, Phys. Rev. **76**, 168(A) (1949).

[2] T. R. Wilkins, Phys. Rev. **60**, 365 (1941).

[3] S. Rubin, Phys. Rev. **72**, 1176 (1947).

plates tested for performance during lengthy use in the evacuated chamber. For uniform development throughout such thick emulsions, the normal procedure is to soak the plates in developer at a low temperature before processing. However, to enhance the development of the initial part of the proton tracks for which the grain density is least and to supress the recoil proton tracks under the emulsion surface, this presoaking was eliminated in the plate processing procedure.

In order to check the range-energy relation for these emulsions, to test the techniques used to process the plates and observe the track distribution, and to determine the purity of the B_2O_3 targets used, the stopping power was determined for proton groups of three energies. The results were in essential agreement with published values[4] and there was no indication of extraneous tracks.

III. EXPERIMENTAL PROCEDURE

The aluminum foils necessary to reduce the incident deuteron energy to the desired value were inserted in the beam path. In addition to the gold foil to absorb the deuterons transmitted by the target backing, aluminum absorber thicknesses sufficient to cut off all emitted charged particles except the end-group protons were mounted on the inner cylinder. Because of the large variation of range with angle, increasing absorption was introduced with decreasing angle so that only the single group of protons would be recorded in the emulsion. Since data are lost at small angles with respect to the target and in the vicinity of the discontinuities in absorption, two sets of plates were exposed for each bombarding energy with the target at 70° and 110° with respect to the incident beam direction and the discontinuities at different angles. A normalization of the two exposures could be effected with data from angular regions common to the two sets of plates.

TABLE I. Summary of the six bombardment runs.

Mean deuteron energy (Mev)	Target thickness (cm air equiv.)	Beam axis -emulsion plane separation (cm)	Total tracks counted	Number of angles of observation
1.06	0.62	0.95	10620	17
1.50	0.81	1.41	11616	14
1.71	0.58	0.95	11137	17
2.36	0.92	0.95	12607	16
3.06	0.57	0.95	15953	19
3.68	0.94	0.95	9844	13

After development, the original position of the plates was duplicated and a very light grid of polar coordinates was scribed directly onto the emulsion surface. For each angle the end-group proton track density was determined microscopically over an average area 1 mm wide and 10 mm in length along the radial line. Each eyepiece of the binocular microscope contained a glass disk with rulings coincident with the objective image. On one disk was ruled a scale, useful for measuring proton track lengths, on the other a grid which divided the field of view into small squares, thereby simplifying the track density determination. A 43X achromatic objective in conjunction with 5X eyepieces provided the most convenient combination for the proton track lengths measured. Only those tracks satisfying certain requirements were counted. The track had to start at the surface of the emulsion, make no more than a 5° angle with the radial direction and be of the proper length. Tracks starting below the emulsion surface cannot be those of charged particles emitted by the target. The limiting angle acceptable for a track was decided from a maximum half-angle of 3.5° subtended

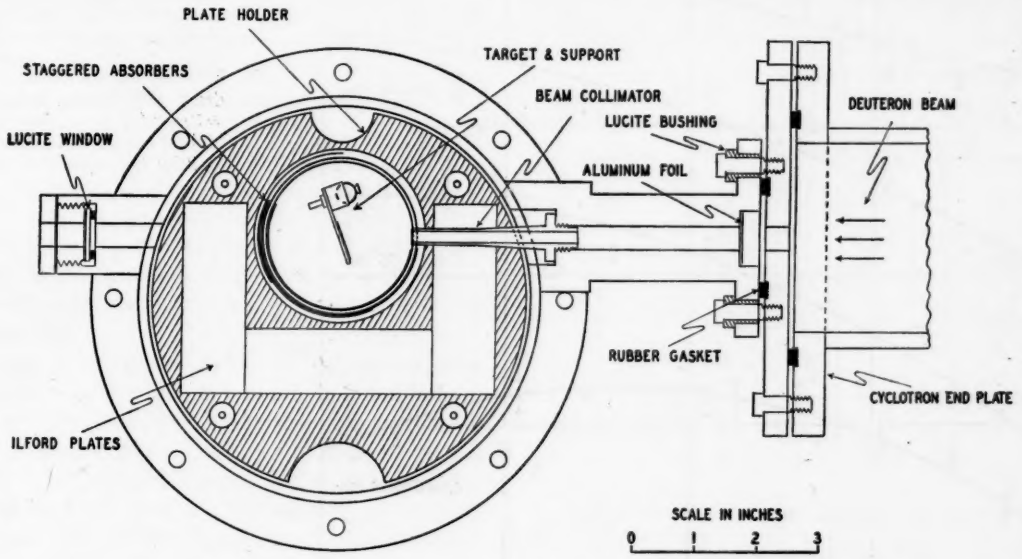

FIG. 1. Plan of the combination bombardment chamber and angular distribution camera.

[4] Lattes, Fowler, and Cuer, Proc. Phys. Soc. London 59, 883 (1947).

by the source at a point on the emulsion and an additional allowance of 1.5° for small-angle scattering of the proton by the gold and aluminum absorbers. The allowable length for the tracks was determined from a numbers-range plot of the first 150 tracks observed at a particular angle. It was then necessary only to count additional tracks satisfying the above criteria. The angular width of the area counted was always less than 2°.

IV. DATA AND ERRORS

Distribution measurements were made at six energies as given in Table I. Included in this table are the mean effective deuteron energy, the target thickness in cm air equivalent, the separation between beam axis and emulsion plane, the total number of end-group proton tracks counted, and the total number of angles for which the yield was determined. An average of 748 tracks for each of 16 angles, representing about 0.75 percent of the proton tracks recorded on the plates, constituted the distribution data determined at each energy. Normally, data were obtained at 15° intervals from 0° to 165° in the emulsion plane, and at such intermediate angles as were needed to define the distribution curve shape. Not included in Table I are two background runs made at full beam energy to test the track contribution

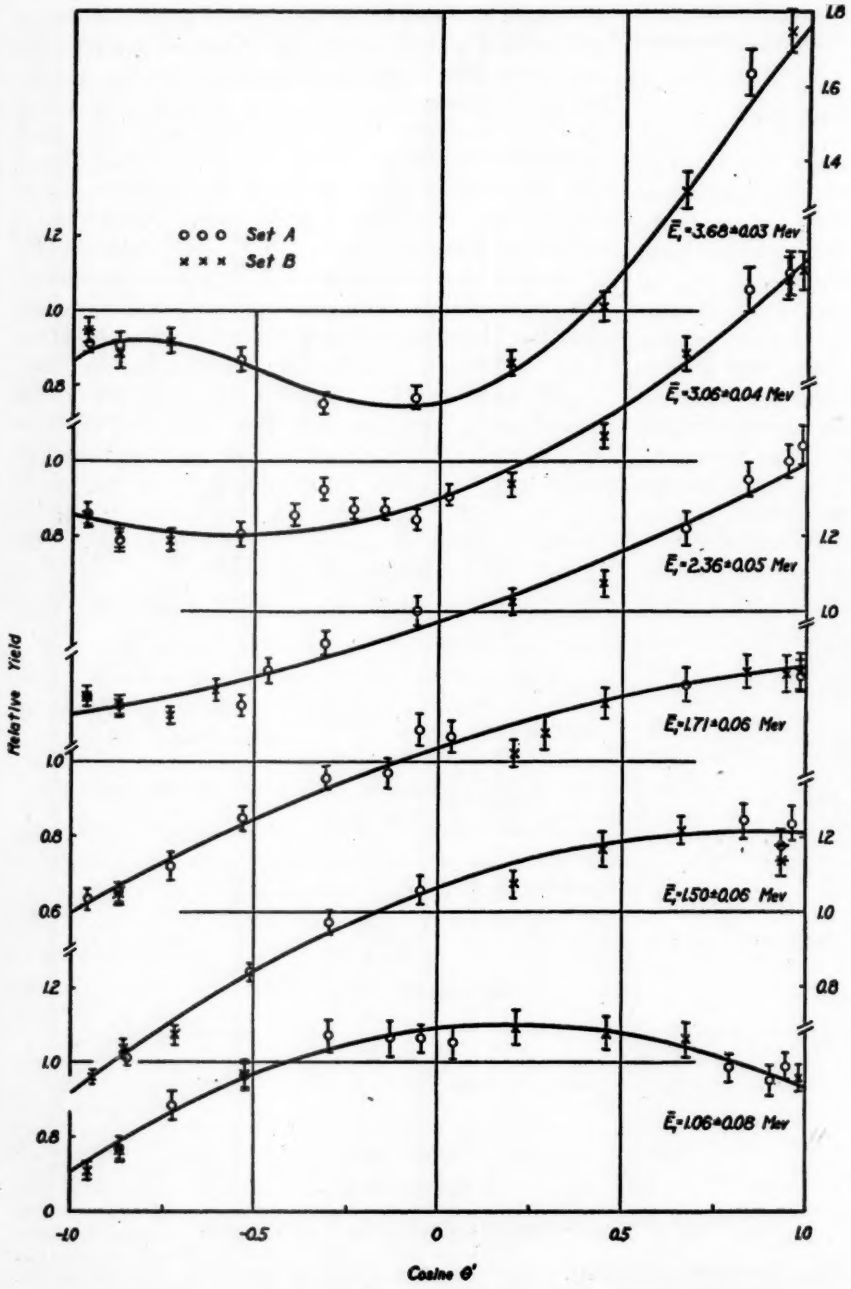

FIG. 2. Relative yield of the end-group protons from $B^{10}+D$ as a function of the cosine of the angle between the incident deuterons and emitted protons plotted in the center-of-mass system for various deuteron energies. The error limits indicated for the individual angular yields are those of statistical origin only. The coefficients listed in Table II were used to draw the curves, using $I(\mu)=\Sigma_i a_i P_i(\mu)$ up to $i=4$ for the highest energy distribution and $i=2$ for the other five.

TABLE II. Coefficients in the Legendre polynomial series representation of experimental angular distribution curves, normalized to a value of unity for a_0.

Mean deuteron energy (Mev)	Values of $a_i=\frac{1}{2}(2i+1)\int_{-1}^{+1} I(\mu)P_i(\mu)d\mu$ from experimental distribution curves							
	a_0	a_1	a_2	a_3	a_4	a_5	a_6	a_7
1.06	1.000	+0.111	−0.180	+0.007	−0.041	−0.010	−0.082	−0.023
1.50	1.000	+0.345	−0.134	+0.003	−0.046	−0.039	−0.091	−0.056
1.71	1.000	+0.325	−0.074	−0.017	−0.042	−0.029	−0.096	−0.054
2.36	1.000	+0.334	+0.057	+0.028	+0.033	−0.075	−0.150	−0.052
3.06	1.000	+0.341	+0.198	+0.041	−0.053	−0.089	−0.147	−0.061
3.68	1.000	+0.352	+0.414	+0.094	−0.101	−0.043	−0.193	−0.111

by the cyclotron, neutrons from the bombarded target and contaminants introduced in handling the target. No appreciable effect was observed.

The data obtained from the microscopic examination of the photographic plates must be related to $\sigma_{K,\theta}$, the cross section per unit solid angle for the emission of a particular type of particle K at an angle θ. Since the emulsion is at an angle with respect to the normal to the radial direction, the track density is proportional to r^{-3}, where r is the distance from the target center to a point on the emulsion. If N end-group proton tracks are counted in an area of width w extending from r_1 to r_2, the cross section is given by

$$\sigma_{K,\theta}=C(N/w)r_2^2r_1^2/(r_2^2-r_1^2). \quad (1)$$

The constant of proportionality, C, is dependent upon the number of target nuclei bombarded, the deuteron flux, the duration of bombardment, and the axis-plane separation. Actually the data are obtained at an angle ϕ in the plane of the emulsion. In terms of known quantities, θ is given by

$$\sin\theta=[\sin^2\phi+(h/d)^2]^{\frac{1}{2}}[1+(h/d)^2]^{-\frac{1}{2}}. \quad (2)$$

Here d is the distance in the emulsion plane from the point below the target center to the center of the area in which the tracks are observed, and h is the separation between the beam axis and the emulsion plane. For convenience in analyzing the resulting distributions, the data were expressed in the center-of-mass coordinate system, using the standard transformations for the angular coordinate and yield per unit solid angle.[5]

The largest error involved in these measurements is statistical, and it is the most difficult to reduce in the photographic method. For example, doubling the number of tracks counted would reduce the root-mean-square error, amounting to about ±4 percent here, by less than one-third.

The proton intensity deduced on the assumption that the angle of incidence for the protons is $\arcsin(h/r)$ would be in error by $100\gamma r/h$ percent if the emulsion surface is inclined at some angle γ with respect to the plane of the plate holder. Such a tilt in the emulsion plane can occur if the surface is not smooth or the glass backing is not uniform. An optical test of the emulsion smoothness showed that the variations were of the order of a wave-length of green light per cm, except at the edges which were avoided in these measurements. By counting tracks over a radial strip the effect of surface variations was to some extent further decreased. The plate thickness varied from plate to plate, but was essentially constant for a given plate. An upper limit of ±3 percent error introduced through this possible tilt of the emulsion surface seems reasonable, plus a ±1 percent error due to the change in h caused by the variation in plate thickness. For the run at 1.50 Mev, h was increased from 0.95 to 1.41 cm to reduce these errors.

The Coulomb scattering of the end-group protons by the gold target backing and aluminum absorbers will modify the actual intensity. This spreading of the proton flux initially headed for a part of the photographic plate is compensated for in part by the scattering of other protons into that region. As some large-angle scattering will always occur, this compensation will never be complete and will depend on the conditions of scatter-

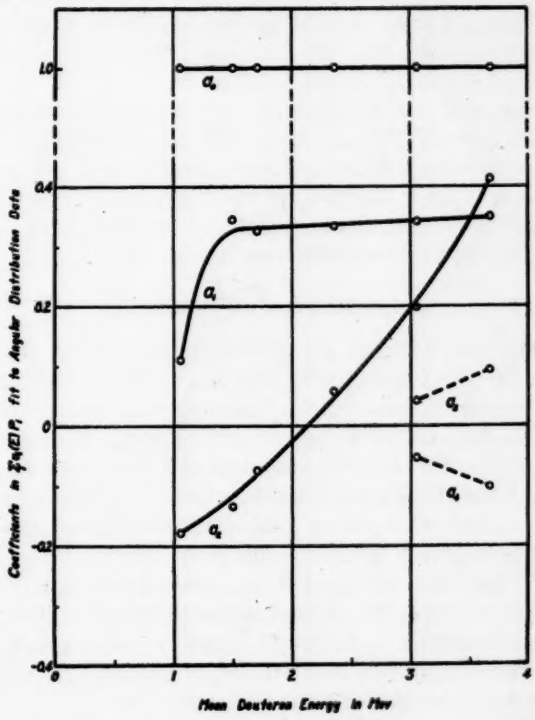

FIG. 3. Coefficients in the $\Sigma_i a_i(E)P_i(\mu)$ fit to the angular distribution data relative to a_0 plotted as a function of the deuteron mean energy.

[5] See L. I. Schiff, *Quantum Mechanics* (McGraw-Hill Book Company, Inc., New York, 1949), pp. 97–100.

ing, such as gold and aluminum path thickness and proton energy, prevailing at the adjacent angles. Each measured intensity will be reduced somewhat, but only the differential effect is of primary importance as an error source. Consideration of the effect of multiple small-angle scattering as treated by Breit, Thaxton, and Eisenbud,[6] and observation of the fraction of proton tracks of proper length which did not satisfy the ± 5 percent requirement place ± 2 percent as a reasonable estimate of the error introduced by not correcting each measured intensity for the effect of Coulomb scattering of the protons.

The selection of the extent of the proton group from the numbers-range curve and the measurement of the radial boundaries r_1 and r_2 of the area counted each introduces an error of the order of two percent. The effect of a possible displacement of the target source from its assumed position in the chamber and of the effective center due to non-uniformity of beam flux and/or target thickness is estimated as a possible ± 2 percent error for each. The scattering of protons out of the emulsion, the recoil proton contribution, the warp and creep of the emulsion and the assumption of a point source for the calculations each give rise to less than a ± 1 percent error.

The total expected error in each of the values of the relative intensity, compounded from the estimates of the effect of the individual sources of error discussed above, is ± 7 percent. In a number of these cases a pessimistic evaluation was made, while for others the error assigned was just a reasonable estimate. This ± 7 percent will about double the error limits shown in the graph of the data, as discussed below. There, only error of statistical origin is indicated.

The main uncertainty in the angular coordinate arises from the mechanics of scribing the coordinates on the emulsion surface, and the possibility of displacement, actual or effective, of the target center from the location assumed. Consequently, an uncertainty of $\pm\frac{1}{2}°$ is assigned to the angular coordinate.

V. DISCUSSION OF RESULTS

The observed intensity per unit solid angle as a function of the cosine of the angle is plotted in Fig. 2 for the center-of-mass system. Intensity values at the two angles common to the sets of data A and B are used to normalize the data at each energy. The error limits given for the six energies at which the distributions were observed are those resulting from the uncertainty in the measurement of the full beam energy.

In the wave mechanical representation of a nuclear reaction system the angular dependence of the emitted particles occurs in terms of Legendre polynomials. It is a well-known fact in the theory of Legendre functions that in the expansion of the intensity I as

$$I(\mu)=\Sigma_i a_i(E)P_i(\mu)$$

in a series of Legendre polynomials the energy-dependent coefficients a_i are given by

$$a_i=\tfrac{1}{2}(2i+1)\int_{-1}^{+1} I(\mu)P_i(\mu)d\mu. \tag{3}$$

Here μ is the cosine of the angle between the directions of the incident and emitted particles. A curve was drawn through the experimental points at each energy, and the values from this curve were used in a 20-part numerical integration to determine these coefficients. This method of fitting the distribution is noteworthy, for it is insensitive to the individual values or the detailed shape of the experimental curve. However, a certain amount of accidental personal judgment enters the operation of drawing the curve and the values of the a_i for higher values of the index i may therefore be inaccurate.

The values of a_i thus determined are given in Table II, normalized to a value of unity for a_0. As the values of a_3 and a_4 for all energies except the highest were less than the experimental error of ± 7 percent, a second-order series in $P(\mu)$ was used to represent these distributions. Two additional terms were used to fit the experimental intensity distribution at the highest energy. The values of the coefficients listed in Table II were used to draw the curves shown in Fig. 2, using $I(\mu)=\Sigma_i a_i P_i(\mu)$ up to $i=4$ for the highest energy distribution and $i=2$ for the other five. The agreement of these curves with the experimental data indicates that higher order Legendre polynomials are not needed. The magnitude of a_6 in each case is perhaps indicative of a consistent manner of terminating the curves drawn through the experimental points. For higher values of i, any slight irregularity in the curve drawn is magnified by the $\frac{1}{2}(2i+1)$ factor. The behavior of the coefficients in the analytical representation of the observed distributions is shown in Fig. 3. The values of a_3 and a_4 for $E=3.06$ Mev, although not used in the curve fitting because they are less than the experimental error, are included to show a possible trend.

The asymmetry of the observed distributions indicates that incident deuterons having both even and odd angular momentum values are effective in producing this reaction. The successful fit of the data with a second-order power series in angle for all but the highest energy implies that only s and p deuterons contribute appreciably to the reaction at low energies. Because the possible initial, compound and final quantum states for the $B^{10}(d, p)B^{11}$ reaction are so numerous, a unique explanation of the energy variation of the coefficients appears to be difficult.

At the lowest bombardment energy, the incident s-wave contribution predominates in the observed distribution. With increasing energy the incident p-wave contribution becomes sizeable, and for the highest energy d-wave effects in the distribution are

[6] Breit, Thaxton, and Eisenbud, Phys. Rev. **55**, 1018 (1939).

noticeable. It seems reasonable to assume that contributions by incident f-waves are negligible in the energy range covered, in view of the small effect observed for d-waves. The absence of abrupt changes in the distributions observed indicates that probably several broad overlapping resonances in the compound nucleus participate in this reaction, as anticipated because of the high degree of excitation of the $B^{10}+D$ system. Due to the observed asymmetry, these levels must differ in parity.

It is a sincere pleasure to acknowledge the guidance and encouragement provided by Professor R. F. Humphreys throughout this investigation. The many informative discussions with Professor G. Breit on the interpretation of angular distribution data are appreciated.

PHYSICAL REVIEW VOLUME 79, NUMBER 1 JULY 1, 1950

Low Energy Neutron Resonance Scattering and Absorption

S. P. Harris, C. O. Muehlhause, and G. E. Thomas
Argonne National Laboratory, Chicago, Illinois

(Received February 2, 1950)

Low energy neutron resonance absorption and scattering integrals have been measured, and resonance scattering fractions, Γ_n/Γ, have been determined for about thirty elements. Lightweight odd Z—even N and even Z—odd N isotopes are shown to have similar resonance phenomena. Correlations of level density and scattering fraction with atomic weight and nuclear type are presented.

I. INTRODUCTION

STRONG resonance absorption of slow neutrons has been observed for many elements since the discovery of neutron resonance phenomena by Fermi and others in 1936. The neutron spectrum of energies greater than thermal but less than 100 kev is usually referred to as the "epi-cadmium region," the "S-resonance region," or simply as the "resonance region." At these energies neutron scattering is almost entirely S-wave scattering. Though the existence of neutron resonance scattering was known experimentally and appreciated theoretically[1] as early as 1937, it was not until 1946 that Goldhaber[2,3] showed that in the case of $_{25}Mn^{55}$ neutrons at resonance ($\sim$300 ev) were scattered much more frequently than they were absorbed. Since that time, additional nuclei have been found which possess primarily scattering resonances. Some of these are: (a) $_{27}Co^{59}$ (115 ev)[4] 94 percent scattering; (b) $_{62}Sm^{152}$ (10 ev)[5] 66 percent scattering; (c) $_{74}W^{186}$ (18 ev)[6,7] 81 percent scattering.

The contribution to the total neutron cross section of scattering and absorption near resonance is given in the following simplified version of the Breit-Wigner formula[1]

$$\sigma_T(E)=\sigma_p+4\pi\lambda_0^2 g\frac{\Gamma_n^2}{\Gamma^2}\frac{1}{1+[(E-E_0)/(\Gamma/2)]^2}+4\pi\lambda_0^2 g\frac{\Gamma_n\Gamma_\gamma}{\Gamma^2}\frac{1}{1+[(E-E_0)/(\Gamma/2)]^2}$$

where: $\sigma_T(E)$—total neutron cross section at energy E; σ_P—potential scattering cross section; E_0—energy of resonance; λ_0—neutron wave-length (divided by 2π) at the resonance energy E_0; Γ_n—neutron resonance width at half-maximum; Γ_γ—γ-ray resonance width at half-maximum; Γ—total resonance width $(\Gamma_n+\Gamma_\gamma)$ at half-maximum g—$\frac{1}{2}[1\pm(1/2i+1)]$—statistical weight factor where "i" is the spin of the target (i.e., initial) nucleus. The second term in σ_T is the resonance scattering cross section, σ_{rs}, and the third term is the resonance absorption cross section, σ_{ra}.

The epi-cadmium neutron spectrum usually encountered (e.g., from a pile) is distributed in energy as $1/E$. An important measurable quantity, then, is the average epi-cadmium cross section for such a flux. In place of this, however, one usually considers a quantity proportional to the average epi-cadmium cross section, namely the resonance integral, Σ. This is defined as $\Sigma=\int\sigma_{res}dE/E$. Using the Breit-Wigner expressions for σ_{rs} and σ_{ra}, it can be readily shown that

$$\Sigma_s=(\pi/2)(4\pi\lambda_0^2 g\Gamma/E_0)\Gamma_n^2/\Gamma^2 \quad \text{res. scatt. integral,}$$
$$\Sigma_a=(\pi/2)(4\pi\lambda_0^2 g\Gamma/E_0)\Gamma_n\Gamma_\gamma/\Gamma^2 \quad \text{res. abs. integral,}$$
$$\Sigma_s+\Sigma_a=(\pi/2)(4\pi\lambda_0^2 g\Gamma/E_0)\Gamma_n/\Gamma \quad \text{total res. integral,}$$

---

[1] H. A. Bethe and G. Placzek, Phys. Rev. **51**, 450 (1937).
[2] M. Goldhaber and A. A. Yalow, Phys. Rev. **69**, 47(A) (1946).
[3] N. H. Barbre and M. Goldhaber, Phys. Rev. **71**, 141(A) (1947).
[4] Harris, Langsdorf, and Seidl, Phys. Rev. **72**, 866 (1947).
[5] M. Goldhaber and A. W. Sunyar, Phys. Rev. **76**, 189(A) (1949).
[6] M. Goldhaber and L. L. Lowry, Phys. Rev. **76**, 189(A) (1949).
[7] S. P. Harris and C. D. Muehlhause, Phys. Rev. **76**, 189(A) (1949).

TABLE I. Flux ratio for 7-cm separation in rabbit.

Nucleus	Thermal ratio $-g_{th}$	Resonance ratio Activation energy (ev)	g_r	Fast neutron ratio $-g_f$
Al	1.38			
Cu	1.38	0.6 to 1	1.57	
In		1.44	1.56	
Au		4.8	1.54	
Co		115	1.56	
Mn	1.38	345	1.56	
P				1.79
Average	1.38	1.56		1.79

from which

$$\Sigma_s/(\Sigma_s+\Sigma_a)=\Gamma_n/\Gamma \quad \text{and} \quad \Sigma_a/(\Sigma_s+\Sigma_a)=\Gamma_\gamma/\Gamma.$$

These ratios represent the probability of resonance scattering and of absorption, respectively. The resonance integrals are important in themselves, however, since they relate the various resonance parameters. For example, knowing Γ_n/Γ and E_0, it is possible to calculate $g\Gamma$ from either Σ_s or Σ_a.

It is the purpose of this paper to present measurements of Σ_s and Σ_a for a number of elements, and in addition to obtain average values of Γ_n/Γ. It will be demonstrated that, in general, resonance scattering is a prominent fraction of the total resonance integral.

II. DETERMINATION OF Σ_a

A. The Cadmium Ratio, Cd R

The neutron flux from the Argonne heavy water reactor is composed of two principal energy bands: thermal and epi-cadmium ($1/E$). The ratio of thermal absorption to epi-cadmium absorption for a given isotope in this flux can be determined by measuring the cadmium ratio. Since cadmium absorbs thermal neutrons exclusively, the ratio of absorption without cadmium to absorption with cadmium relates the thermal absorption cross section to the average epi-cadmium absorption cross section. Measurement of a cadmium ratio is usually accomplished by means of activation.

$$\text{Cd } R=\frac{\text{activation (no Cd)}}{\text{activation (with Cd)}}=1+\text{const. } \sigma_{tha}/\Sigma_a',$$

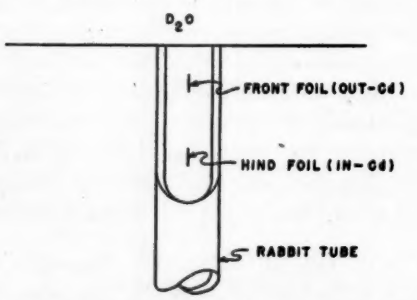

FIG. 1. Diagram of foil positions in rabbit flux.

TABLE II. Cadmium ratio for gold, indium, and boron in rabbit, port, and thimble fluxes.

Nucleus	Cadmium ratio (Cd-R) Rabbit	Thimble	Port (beam)
B	~70		
In	3.26	2.44	2.31
Au	2.91	2.25	

or

$$\Sigma_a'=K[\sigma_{tha}/(\text{Cd } R-1)]$$

K = constant (depending on flux only)

where σ_{tha} is the thermal activation cross section and Σ_a' is the resonance absorption integral plus any "$1/V$" absorption beyond the cadmium cut-off energy (~0.6 ev). With regard to this latter component of absorption, it should be noted that the thermal absorption cross section decreases with neutron energy as $1/E^{\frac{1}{2}}$. Since cadmium suddenly ceases to absorb neutrons at ~0.6 ev, some absorption or activation due to the thermal cross section is present even with a cadmium cover. This $1/V$ component of epi-cadmium absorption, $\Sigma_{1/v}$, is accounted for by writing

$$\Sigma_a'=\Sigma_a+\Sigma_{1/v}.$$

The proportionality constant, K, between thermal and resonance absorption is obtained by measuring the Cd R for a known resonance absorber such as gold, in which[8] $\Sigma_a=1296$b and[9] $\sigma_{tha}=93$b, where b indicates "barns" (1 barn$\equiv 10^{-24}$ cm^2). Then,

$$\Sigma_a'=(\text{Cd } R-1)_{\text{Au}}\frac{\Sigma_a'_{\text{Au}}}{\sigma_{tha\,\text{Au}}}\cdot\frac{\sigma_{tha}}{\text{Cd } R-1}\equiv K\frac{\sigma_{tha}}{\text{Cd } R-1}. \quad (1)$$

Therefore, by so comparing the Cd R of a substance with gold, and by knowing its thermal absorption cross section, Σ_a' can be evaluated. The advantage of this method is that only relative intensity measurements of the same activity are made. This can be done with high accuracy. Such a measurement of Σ_a' then depends on the more easily determined σ_{tha}. Measurements should be made with foils which are so thin that peak resonance absorption (i.e., at the maximum value of the resonance cross section) is a linear function of foil thickness.

It remains to be shown how the $1/V$-component of epi-cadmium absorption is determined. This is obtained from a measurement of the Cd R for a pure $1/V$-type absorber such as boron. In this case,

$$\Sigma_a'=\Sigma_{1/v}=K\frac{\sigma_{1/v}}{(\text{Cd } R-1)_{1/v}}\equiv k\sigma_{1/v}$$

where $\sigma_{1/v}$ is the thermal absorption cross section of the $1/V$ absorber. Therefore, the proper resonance ab-

[8] Best fit to Breit-Wigner formula using Columbia data by M. Goldhaber.

[9] Argonne mechanical velocity selector data by A. Wattenberg.

TABLE III. Resonance absorption integrals.

Isotope	Cd-R	$\frac{\Sigma_a'}{\sigma_{tha}}$	σ_{tha} (barns)	Σ_a' (barns)	$\Sigma_{1/v}$ (barns)	Σ_a (barns)	Source of σ_{tha}	10^{24} nuclei per cm^3 (isotopic)	Chemical form
$_{11}Na^{23}$	70.3	~0.4	0.52	~0.21	~0.21	~0	P	7.4×10^{-5}	NaF
$_{13}Al^{27}$	43.1	~0.65	0.22	~0.14	~0.09	~0.05	P	2.9×10^{-4}	Al
$_{15}P^{31}$	63.8	~0.44	0.23	~0.10	~0.09	~0.01	S	3.1×10^{-4}	P
$_{21}Sc^{45}$	69.0	~0.4	31.6	~12.6	~12.6	~0	P	2.6×10^{-5}	Sc_2O_3
$_{23}V^{51}$	70.6	~0.4	4.93	~2.0	~2.0	~0	P	2.1×10^{-5}	V_2O_5
$_{25}Mn^{55}$	35	~0.81	12.1	~9.8	~4.8	~5	P	6.5×10^{-5}	Mn
$_{27}Co^{59}$	23.8	1.20	34.3	41.2	13.7	27.5	P	6.1×10^{-5}	Co
$_{29}Cu^{63}$	30.8	0.92	3.62	3.35	1.45	1.90	P	1.4×10^{-4}	Cu
$_{29}Cu^{65}$	30.5	0.93						6.0×10^{-5}	Cu
$_{31}Ga^{69}$	5.79	5.72	1.40	8.01	0.56	7.45	S	3.1×10^{-5}	Ga_2O_3
$_{31}Ga^{71}$	7.96	3.94	3.36	13.2	1.3	11.9	S	2.0×10^{-5}	Ga_2O_3
$_{33}As^{75}$	4.36	8.15	3.87	31.5	1.6	29.9	P	6.0×10^{-5}	As
$_{35}Br^{79}$	3.25	12.2	10.9	133	4	129	S	1.0×10^{-5}	$PbBr_2$
$_{39}Y^{89}$	47.9	0.58	1.24	0.72	0.50	0.22	S	4.1×10^{-5}	Y_2O_3
$_{41}Nb^{93}$	9.59	3.19	1.31	4.19	0.52	3.67	P	2.5×10^{-5}	Nb_2O_5
$_{45}Rh^{103}$	7.94	3.95	149	589	60	529	S	2.6×10^{-5}	Rh
$_{47}Ag^{107}$	13.35	2.22	44.3	98.3	17.7	80.6	S	1.5×10^{-5}	Ag
$_{47}Ag^{109}$	3.20	12.5	97.0	1213	39	1174	S	Zero extrapolation	Ag
$_{49}In^{113}$	2.68	16.3	56.0	913	22	891	S	6.8×10^{-7}	In
$_{49}In^{115}$	3.26	12.1	196	2372	78	2294	S	1.5×10^{-6}	In
$_{51}Sb^{121}$	2.27	21.6	6.8	147	3	144	S	1.7×10^{-5}	Sb
$_{51}Sb^{123}$	~1.55	~50	2.5	~125	1	~124	S	1.3×10^{-5}	Sb
$_{53}I^{127}$	2.45	19.0	6.25	119	3	116	S	1.3×10^{-5}	PbI_2
$_{59}Pr^{141}$	30.9	0.92	10.1	9.3	4.0	5.3	S	1.8×10^{-5}	PrO_2
$_{62}Sm^{152}$	3.43	11.3	138	1559	55	1504	S	4.1×10^{-6}	Sm_2O_3
$_{63}Eu^{151}$	45.7	0.61	1380	842	552	290	S	8.3×10^{-6}	Eu_2O_3
$_{72}Hf^{180}$	14.9	1.97	10.0	19.7	4.0	15.7	S	8.0×10^{-6}	HfO_2
$_{72}Hf^{a11}$	~3.0	~14	~100	~1400	40	~1360	P	2.3×10^{-5}	HfO_2
$_{73}Ta^{181}$	25.1	25.1	20.6	517	10	507	S	2.7×10^{-5}	Ta
$_{74}W^{186}$	3.93	9.35	34.2	320	14	306	S	3.1×10^{-7}	W
$_{75}Re^{185}$	3.61	10.5	101	1061	40	1021	S	6.6×10^{-6}	Re
$_{75}Re^{187}$	8.50	3.65	75.3	275	30	245	S	1.1×10^{-5}	Re
$_{77}Ir^{191}$	9.37	3.27	1000	3270	400	2870	S	6.9×10^{-6}	Ir
$_{77}Ir^{193}$	3.89	9.48	128	1213	51	1162	S	1.1×10^{-5}	Ir
$_{79}Au^{197}$	2.91	14.35	93	1337	37	1296	Wattenberg	5.0×10^{-7}	Au
$_{81}Tl^{203}$	3.59	10.6	~12	127	~5	122	P	3.0×10^{-5}	Tl
$_{81}Tl^{205}$	7.12	4.48	~.17	.76	~.07	~.69	P	7.3×10^{-5}	Tl

Note.—Key to "source of σ_{tha}": P—pile (reference 10); S—Seren (reference 11).

sorption integral, Σ_a, is given by

$$\Sigma_a=\Sigma_a'-k\sigma_{tha}. \quad (2)$$

B. Energy and Space Distribution of the Flux

The so-called "rabbit flux" of the Argonne heavy water reactor was chosen as the most convenient neutron flux for making activation measurements. The rabbit consisted of a pneumatic tube which conducted a pair of samples to be bombarded into the pile at a position next to the heavy water tank, as illustrated in Fig. 1. One sample was covered with cadmium (in-Cd sample) while the other sample was not (out-Cd sample). Each sample pair was ejected after its proper time of bombardment. In-Cd and out-Cd samples were bombarded at the same time and were always separated 7 cm apart in the rabbit tube. This insured that (a) both samples received the same bombardment time at the same pile power, and (b) the neutron flux ratio (out-Cd to in-Cd) remained constant for all sample pairs.

Several experiments were performed to investigate the spacial distribution of the rabbit flux for various neutron energies.

(1) Pairs of thermal (i.e., $\sim 1/V$) absorber foils were activated 7 cm apart out of cadmium to determine the ratio of thermal neutron intensity for a 7-cm separation in the rabbit.

(2) Pairs of resonance absorber foils were activated 7 cm apart inside cadmium to determine this ratio for various energy resonance neutrons.

(3) Two phosphorus foils were activated 7 cm apart inside cadmium to determine this ratio for neutrons >1 Mev energy.

These results are given in Table I from which it can be seen that gr (flux ratio for resonance neutrons) is constant, i.e., is independent of energy. This is the only

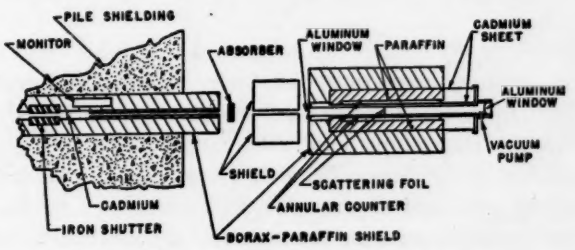

FIG. 2. Schematic diagram of scattering apparatus.

TABLE IV. Resonance scattering integrals.

Isotope	σ_{epi-Cd} (barns)	σ_P (barns)	σ_{tha} (barns)	Σ_a' (barns)	E_0 ev	Σ_s (barns)	Source of σ_P	10^{24} nuclei per cm³	Chemical form
$_6C^{12}$	4.60	4.60					*H*	4.5×10^{-3}	C
$_{11}Na^{23}$	7.6	4.4		27	~3000	~51	*H'*	1.4×10^{-4}	NaF
$_{13}Al^{27}$	1.80	1.46		2.9	>40 kev	~9	*H*	7.7×10^{-3}	Al
$_{21}Sc^{45}$	16.0		12.8	27	10^3–10^4	~60		8.7×10^{-5}	Sc_2O_3
$_{23}V^{51}$	16.2	5.0		94	~2700	~190	*H'*	5.0×10^{-4}	V
$_{24}Cr^{53}$	17.7		8.4	78	~4200	166		7.5×10^{-5}	$Cr_2{}^{53}O_3$
		Corrected							
$_{25}Mn^{55}$	35.4	3.8		265	345, 2400	425	*H*	7.4×10^{-5}	Mn
$_{27}Co^{59}$	42.5	7.3		296	115	435	*H*	9.9×10^{-5}	Co
$_{29}Cu^{nat}$	9.1	6.7		20	~10^3	~35	*H*	2.4×10^{-4}	Cu
$_{30}Zn^{67}$	36		7	244	480	410		7.3×10^{-5}	$Zn^{67}O$
$_{31}Ga^{nat}$	17.0	8.1		75	10^2–10^3	~126	*F*	2.2×10^{-4}	Ga
$_{33}As^{75}$	12.2	6.9		45	10^2–10^3	~76	*H*	8.0×10^{-5}	As
$_{35}Br^{nat}$	8.8	7.9		7.6	~10	~9.2	*H*	2.6×10^{-3}	CBr_4
$_{39}Y^{89}$	5.1		4.0	9.2	—			5.3×10^{-5}	Y_2O_3
$_{41}Nb^{93}$	7.7	7.2		4.2	—		*H*	6.4×10^{-4}	Nb
$_{45}Rh^{103}$	6.3		3.6	23	1.28	24		1.8×10^{-4}	Rh
$_{47}Ag^{107}$	7.4	6.8		5.0	~15	~6.2	*F*	4.9×10^{-5}	$Ag^{107}O$
$_{47}Ag^{109}$	12.4	7.7		39.5	5.2	46	*F*	4.7×10^{-5}	$Ag^{109}O$
$_{51}Sb^{nat}$	8.91	5.35		29.9	~10	~36.3	*H*	4.9×10^{-5}	Sb
$_{53}I^{127}$	10.0	5.15		40.7	20–30	~53	*H*	4.6×10^{-5}	PbI_2
$_{57}La^{139}$	10.1	9.1		8.4	—		*F*	3.7×10^{-5}	La_2O_3
$_{59}Pr^{141}$	15.0		8.0	59	~10(?)	~72		3.6×10^{-5}	PrO_2
$_{62}Sm^{nat}$	102		23	664	10	806		3.4×10^{-5}	Sm_2O_3
$_{63}Eu^{nat}$	34.1		30.1	34	~10	~41		3.3×10^{-5}	Eu_2O_3
$_{64}Gd^{nat}$	24		26					3.3×10^{-5}	Gd_2O_3
$_{72}Hf^{nat}$	53.8		26.0	234	7.7	279		2.8×10^{-5}	HfO_2
$_{73}Ta^{181}$	17.8	10.7		59.6	4.0	69	*H*	5.0×10^{-5}	Ta
$_{74}W^{186}$	149		23	1058	~15	~1330		2.6×10^{-5}	$W^{186}O_3$
$_{75}Re^{nat}$	22.2	15.2		58.8	2.3	64.6	*H*	3.2×10^{-5}	Re
$_{79}Au^{197}$	29.6	10.8		158	4.8, >345	~210	*H*	7.6×10^{-6}	Au
$_{81}Tl^{nat}$	14.7	11.7		25.2	260	39.8	*H*	3.0×10^{-4}	Tl

Note.—Key to "source of σ_P": *H*—reference 13; *H'*—unpublished; *F*—thick filter (see Section III-C).

quantity of actual importance in calculating the Cd *R* from the activity ratio of the two foils where:

front foil (nearest tank)≡out-Cd foil,
hind foil (farthest from tank)≡in-Cd foil.

The hind foil activity had therefore to be multiplied by the factor 1.56.

A second point of interest was to determine if the epi-cadmium neutron energy distribution of the rabbit flux was actually of the form $1/E$. This was accomplished by comparing the ratio of (Cd $R-1$) for two substances (1) and (2) measured in the rabbit flux and in the thimble flux (central vertical tube of the pile), which latter flux was known to vary as $1/E$. If both fluxes have the same epi-cadmium energy distribution, then:

$$[(\text{Cd } R-1)_1/(\text{Cd } R-1)_2]=[\sigma_{tha1}\Sigma_{a2}'/\sigma_{tha2}\Sigma_{a1}'].$$

This is to say that if two neutron fluxes differ only in the relative magnitudes of their thermal and epi-cadmium neutron intensities, the above quantity is a constant characteristic of the materials (1) and (2), and not of the fluxes. Table II gives data on gold and indium pertinent to the above point and, in addition, lists similar data for indium measured in a neutron beam from one of the reactor ports. The rabbit epi-cadmium flux is evidently distributed as $1/E$ since:

$$\left\{\frac{(\text{Cd } R-1)_{\text{In}}}{(\text{Cd } R-1)_{\text{Au}}}\right\}_{\text{Rabbit}}=1.18$$

and

$$\left\{\frac{(\text{Cd } R-1)_{\text{In}}}{(\text{Cd } R-1)_{\text{Au}}}\right\}_{\text{Thimble}}=1.15.$$

C. Calibration

Calculation of the constants "*K*" and "*k*" in formulas (1) and (2) is now possible from the data given in Table III.

First, from the light element data of Table III, $(\text{Cd } R)_{1/v}\simeq 70$. This is taken from the data on $_{11}Na^{22}$, $_{21}Sc^{45}$, and $_{23}V^{51}$. These isotopes have no known important neutron capture levels near zero energy which could cause any epi-cadmium neutron absorption other than $1/V$ absorption. Therefore:

$$k=K/(\text{Cd } R-1)_{1/v}=K/69.$$

Second, from the measured cadmium ratio of gold (2.91):

$$K=(\Sigma_a'_{\text{Au}}/\sigma_{tha\ \text{Au}})(\text{Cd } R-1)_{\text{Au}}$$
$$=[(1296+93k)/93]1.91.$$

These taken together yield $K=27.4$ and $k=0.4$. That is,

$$\Sigma_a'=27.4[\sigma_{tha}/(\text{Cd } R-1)] \quad \text{and} \quad \Sigma_{1/v}=0.4\sigma_{tha}.$$

$(\text{Cd } R)_{1/v}$ is of considerable significance when compared directly with another Cd R in the same neutron flux, since

$$(\text{Cd } R)_{1/v} > \text{Cd } R \rightarrow E_0 > 0.6 \text{ ev},$$
$$(\text{Cd } R)_{1/v} < \text{Cd } R \rightarrow E_0 < 0.6 \text{ ev}.$$

$(\text{Cd } R)_{1/v}$ therefore represents the critical case of nonresonance. If $\Sigma_a < 0$, the most prominent neutron absorption resonance has an energy <0.6 ev (cadmium cut-off energy). An example of this is ${}_{66}\text{Dy}^{164}$ where Cd $R \simeq 215$.

D. Preparation of Samples

Samples were usually of high purity. It was important that they be dry. This insured the absence of hydrogen in the samples, which if present would cause neutron moderation and consequent extra activation via thermal absorption of the in-Cd sample. Other impurities were less important since an activation technique permitted isolation of the period being studied. Unless in elemental foil form, all samples were fixed to a 1-cm² area and 1-mil thick puron (electrolytic iron) foil, which material becomes only slightly active under neutron bombardment. The powders (metals or oxides) were fixed by the application of one drop of thinned zapon (an organic adhesive), which substance when dry introduced a negligible amount of hydrogen into the sample and produced no measurable activity of its own. Such samples were usually <5.0 mg/cm². Strong resonance absorbers (Cd $R<5$) were either evaporated on the puron to thickness ~ 0.2 mg/cm² or zaponed to the puron to thicknesses ~ 1.0 mg/cm².

In preparing samples care was also taken to maintain equal thicknesses for the out-Cd and in-Cd samples. This was necessary to minimize (1) slight non-linear neutron resonance absorption, and (2) different radiation detection efficiencies.

E. Activation Measurements

Sample activities were either measured on a Geiger counter or in a no-window air ionization chamber. This latter instrument was especially useful in cases where (1) Cd $R>50$, since a greater intensity range was available with the ionization chamber than with the Geiger counter, and (2) the activity consisted largely of electrons too soft to penetrate a Geiger counter window.

When several activities had to be observed over a long period of time, activity standards such as uranium were employed. In short, when all the usual precautions were taken, these operations yielded results with a probable error of ~ 2 percent. Therefore, if the thermal absorption cross section was uncertain to only ~ 2 percent, the calculated resonance absorption integral, Σ_a, would be most limited by the five percent uncertainty in the gold standard. There were many cases, however, in which the thermal absorption cross section had an uncertainty of ~ 20 percent. This difficulty was at times avoided by the use of the pile neutron absorption cross section, σ_{pile}.[10] This is the neutron absorption cross section for a material placed in the center of the reactor (thimble). Such a pile cross section is made up principally of two parts, (a) the thermal absorption cross section, and (b) some fraction of the epi-cadmium absorption cross section (i.e., integral). In the Argonne heavy water reactor, σ_{pile} is given by $\sigma_{\text{pile}} = \sigma_{tha} + 0.054\Sigma_a$. When σ_{pile} had been measured with sufficiently thin samples, it could be combined with the value for Σ_a'/σ_{tha} (obtained from the Cd R measurement) to evaluate both Σ_a and σ_{tha}. When this was not the case, σ_{tha} was obtained from the neutron activation cross-section measurements of Seren[11] and others at Argonne. The source of σ_{tha} is indicated in column 8 of Table III.

Cd R of hafnium was determined by a different method[12] which will be described only briefly in this paper. The principal absorption in hafnium does not lead to an assigned activity.[12a] However, Cd R (Hf) was determined using the neutron beam from one of the pile ports and two anthracene scintillation γ-ray counters in coincidence. The capture γ-ray intensity from a thin Hf O_2 foil with and without cadmium in the beam was measured. This was then standardized with the Cd R for indium given in Table II.

F. Results of Σ_a

Table III lists values of Cd R, Σ_a'/σ_{tha}, σ_{tha}, Σ_a', $\Sigma_{1/v}$, Σ_a, sample thickness, and the source of σ_{tha}. Though the error in Σ_a'/σ_{tha} is less than five percent, other values are in general uncertain to 10 or 20 percent. Strong capture resonances are prominent in the region above zirconium but less than tin and in the region above lanthanum but less than lead.

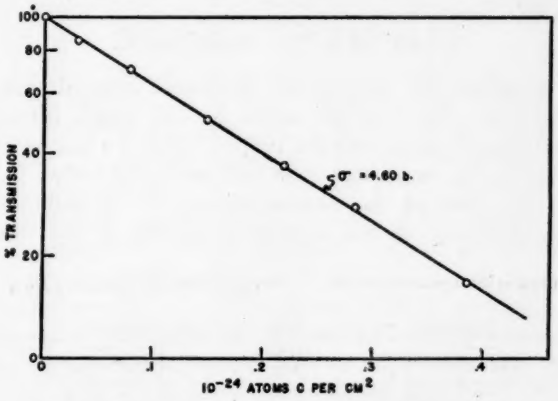

FIG. 3. Semilog plot of carbon transmission curve of carbon-detected epi-cadmium neutrons.

[10] Harris, Muehlhause, Rasmussen, Schroeder, and Thomas (to be published).
[11] Seren, Friendlander, and Turkel, Phys. Rev. 72, 888 (1947).
[12] C. O. Muehlhause, Phys. Rev. (to be published).
[12a] The unassigned 19-sec. Hf period may be an isomer of the stable isotope that results from the principal absorption in hafnium. There is evidence of this from the fact that Cd R (19-sec. Hf)$\simeq 3.1$ and Cd R (Hf)~ 3.0.

III. DETERMINATION OF Σ_s

A. Apparatus

The apparatus has been described in a previous paper.[4,13] Briefly, it consists of a 4π-annular proportional neutron counter filled with enriched BF_3 and surrounded by a paraffin reflector-moderator and shield. An evacuated hole through the center of the counter conducts a collimated beam of cadmium-filtered neutrons from the Argonne heavy water reactor. These neutrons give rise to a counting rate only when a scattering foil (termed the detector) is placed in the center of this tube transverse to the neutron beam. Provision is made for monitoring the neutron flux by simultaneously counting the pulses from a fission counter imbedded in the collimator. The chamber-circuit deadtime is 15 μsec. The equipment is illustrated schematically in Fig. 2.

B. Flux Conditions

Though the epi-cadmium neutron beam from the reactor is distributed in energy as $1/E$, the counting rate using a flat detector foil (i.e., one in which the scattering cross section is constant) falls off more rapidly with neutron energy than $1/E$. This results from the fact that though the paraffin reflector markedly increases the sensitivity of the boron counter at high energies, the efficiency still decreases with increasing neutron energy. Experimentally, the counter sensitivity has been shown to decrease as log$E$ (logarithm of neutron energy)[14] falling off by a factor of $\sim$8.0 between 0.5 ev (cadmium cut-off energy for the beam) and 1.5 Mev (mean fission energy). One can express the the counter sensitivity at energy E, $S(E)$, relative to the counter sensitivity at cadmium cut-off energy, $S(\mathrm{Cd})$, by:

$$[S(E)/S(\mathrm{Cd}) \simeq 1-0.0587 \log 2E.$$

This means that a scattering resonance integral measured with this counter would be too small. Simple analysis will show that the proper value of a scattering integral, Σ_s, is greater than the measured value, Σ_s', by the ratio of the counter sensitivity at cadmium cut-off energy to the counter sensitivity at the resonance energy, E_0. That is

$$\Sigma_s=[S(\mathrm{Cd})/S(E_0)]\Sigma_s'. \quad (3)$$

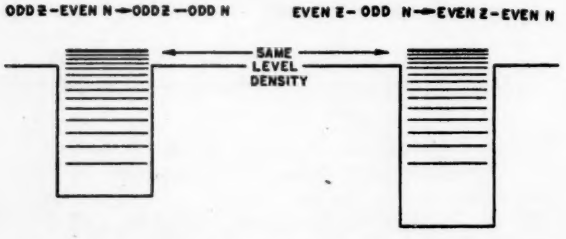

FIG. 4. Compound nuclei resulting from a neutron plus an odd Z—even N and an even Z—odd N nucleus.

C. Theory of Measurement

When a thin detector foil (i.e., scattering foil) is placed in the center of the annular chamber, the counting rate due to neutrons scattered by the foil will be proportional to both its potential scattering cross section, σ_p, and to its effective resonance scattering integral, Σ_s'. The average scattering cross section of the foil, $\sigma_{\text{epi-Cd}}$, for epi-cadmium neutrons can be determined by comparing the neutron counting rate from the foil with that from a flat detector such as carbon: $\sigma_{\text{epi-Cd}}=\sigma_C(N/N_c)(n_c/n)$ where N and N_c are the counting rates of the foil and carbon, respectively, n and n_c are the atoms per cm^2 of the foil and carbon, respectively, and σ_C is the constant carbon scattering cross section.

If a given material possesses no resonance scattering (i.e., $\Sigma_s=0$), then the average epi-cadmium scattering cross section, $\sigma_{\text{epi-Cd}}$, is just equal to the potential scattering cross section, σ_p. It is reasonable to expect, and a simple analysis will show, that the effective resonance scattering integral, Σ_s', is proportional to the the difference between $\sigma_{\text{epi-Cd}}$ and σ_p. The sensitivity function determines the constant of proportionality to be about 8.4. That is

$$\Sigma_s'=8.4(\sigma_{\text{epi-Cd}}-\sigma_p). \quad (4)$$

Therefore, the measurement of $\sigma_{\text{epi-Cd}}$ and σ_p will yield the effective resonance scattering integral, Σ_s', which can be corrected to the proper scattering resonance integral, Σ_s, when the resonance energy, E_0 is known.

Three principal sources or methods for determining the potential or off-resonance scattering cross section, σ_p, are available. (1) Neutrons near the resonance energy, E_0, are removed from the neutron beam with a thick filter of the material being studied. This filter is placed in the neutron beam outside the counter shield. A comparison of counting rates with carbon is again made which will now yield σ_p. (2) Numerous values of σ_p are available from the work of Hibdon and Muehlhause.[13] Those relevant to this paper have been used. (3) Lacking both of the above sources of σ_p, the thermal scattering cross section can be used in place of σ_p.

In the above discussion, carbon is assumed to be a flat detector (i.e., σ_C is independent of the energy). This is admittedly not quite true over the entire energy range. At energies up to about 5000 ev, our measurements indicate $\sigma_C=4.72b$. However, the neutron spectrum extends to energies at which σ_C is as low as $2.0b$. For practical purposes the average epi-cadmium cross section of carbon serves very well. This is determined by measuring the total cross section of carbon using a carbon detector. Figure 3 is a semilog plot of the epi-cadmium neutron transmission of carbon using a carbon detector. The transmission curve is a straight line

[13] C. T. Hibdon and C. O. Muehlhause, Phys. Rev. **76**, 100 (1949).
[14] R. W. Gurney (private communication).

TABLE V. Resonance scattering fraction: Γ_n/Γ.

Isotope	E_0 ev	Σ_a	Σ_s	Σ_Γ	Γ_n/Γ	Comments
$_{13}Al^{27}$	>40 kev	0.05	~9	~9	>0.99	
$_{25}Mn^{55}$	345, 2400	~5	425	430	~0.99	$J_1=3$
$_{27}Co^{59}$	115	27.5	435	463	0.94	
$_{29}Cu^{all}$	10^3–10^4	1.90	~35	~37	0.95	
$_{31}Ga^{all}$	10^2–10^3	7.45	~126	~133	~0.95	
$_{33}As^{75}$	10^2–10^3	29.9	~76	~106	~0.72	
$_{45}Rh^{103}$	1.28	529	24	553	0.043	
$_{47}Ag^{107}$	~15	80.6	~6.2	~86.8	~0.071	
$_{47}Ag^{109}$	5.1	1174	46	1220	0.038	
$_{51}Sb^{all}$	~10	136	~36.3	~172	~0.21	
$_{53}I^{127}$	20–30	116	~53	~169	~0.31	
$_{59}Pr^{141}$	~10(?)	5.3	72	~77	~0.94	
$_{62}Sm^{152}$	10	1504	2975	4479	0.66	
$_{72}Hf^{all}$	<10	1360	279	1639	0.17	$\Gamma_n \sim \Gamma_\gamma$ at 7.7 ev
$_{73}Ta^{181}$	4.0	507	69	576	0.12	
$_{74}W^{186}$	~15	306	~1340	~1646	~0.81	
$_{75}Re^{all}$	2.3	531	64.6	596	0.11	
$_{79}Au^{197}$	4.8, >345	1296	~210	1506	0.14	$\Gamma_n/\Gamma>0.9$ for $E_0>345$ ev
$_{81}Tl^{all}$	260	36.5	39.8	76.3	.52	Probably Tl^{203}

whose slope yields the proper epi-cadmium total cross section. Since carbon is very nearly a pure scatterer (i.e., no absorption), this value of 4.60*b* can be used for σ_C.

D. Preparation of Samples

Whenever possible, the elemental foil form was used for detectors. Otherwise dry powders (metals, oxides, fluorides) were fixed to 0.5-mil aluminum foils. The fixing was accomplished as described in Section II-D. Again it was important to insure a minimum presence of hydrogen. In this case, the presence of hydrogen caused an extra counting rate due to its high scattering cross section (~20*b*). The backing was accounted for by measuring the counting rate from a 0.5-mil aluminum foil with the same amount of zapon attached.

E. Counting Technique

Counting rate measurements were always made with and without the detector foil in place. In the case of powders fixed to aluminum, the background was considered to be that from an aluminum foil having the same number of zapon drops as were used to fix the powders. The scattering due to oxygen or fluorine was subtracted according to their known[13] potential scattering cross sections

$$\sigma_p(\text{oxygen})=4.12b, \quad \sigma_p(\text{fluorine})=3.62b.$$

All counting rates were monitored by the fission counter and corrected for deadtime losses. These measurements had a probable error of about two percent.

F. Results on Σ_s

Table IV lists the data on $\sigma_{\text{epi-Cd}}$, σ_p or the thermal scattering cross section σ_{ths}, Σ_s', and, when possible, Σ_s. In addition, the source of σ_p is indicated. These results have a probable error of 10 to 20 percent. This large uncertainty arises from two sources. First, the sensitivity function, $S(E)$, which determines both the correction factor in Eq. (3) and the scale factor in Eq. (4) is known only to about 10 percent. Second, in many cases σ_p is known only to about 10 percent since it is not always measurable by any of the procedures employed (Section III-C and reference 13). For example, the general depression in the scattering cross section of $_{25}Mn^{55}$ ($E_0=345$ and ~2400 ev)[15] below 50 ev is due to the destructive interference of resonance and potential scattering. This is operative even in the thermal region, as is evidenced by the fact that manganese exhibits a negative scattering phase at thermal energies.[16] An asymtotic cross section (i.e., using thick filters (Section III-C) or a thermal scattering cross section ($\sigma_{ths}=2.6$b) is, therefore, different from the proper value of σ_p.

In the case of hafnium, the large resonance scattering observed is due principally[16a] to a resonance level at 7.7 ev.[17]

Σ_s' for gold is too large to be accounted for by the 4.8-ev resonance level.[18] It is probably due to a prominent scattering resonance >345 ev, since strong resonance overlapping between gold and manganese has been reported.[13]

The large resonance scattering in $_{11}Na^{23}$ indicates a low energy scattering resonance. Details of this resonance at ~3000 ev have been reported.[19]

Observation of Table IV reveals 10 elements or isotopes out of 31 in which $\Sigma_s>100$b. Sizable resonance scattering at low energies appears to be associated with

[15] High speed Argonne resonance time-of-flight velocity selector data by W. Selove.
[16] E. Fermi and L. Marshall, Phys. Rev. **71**, 666 (1947).
[16a] A boron transmission curve of hafnium scattered neutrons indicated a resonance energy of ~7.5 ev. See reference 13 for details of method.
[17] Havens, Wu, Rainwater, and Meaker, Phys. Rev. **71**, 165 (1947), Zr curve.
[18] Reference 17, Au curve.
[19] Hibdon, Muehlhause, Selove, and Woolf, Phys. Rev. **77**, 730 (1950).

odd Z-even N and even Z-odd N lightweight isotopes.[20] In the medium heavy region, certain even Z-even N isotopes have very large scattering resonance integrals (e.g., $_{62}Sm^{152}$, $_{72}Hf^{even}$, $_{74}W^{186}$). The heavy elements may also exhibit sizable resonance scattering for resonance levels ~100 ev (e.g., $_{79}Au^{197}$, $_{81}Tl^{odd}$).

In the light element region (less than 50 neutrons), many unreported even Z-even N isotopes were examined and found to have no observable resonance scattering. From this we may conclude that the nearest level to zero energy is greater than 10 kev. On the other hand, in two cases[21,22] of Oak Ridge separated even Z-odd N isotopes[23,24] ($_{24}Cr^{53}$ at ~4200 ev, $_{30}Zn^{67}$ at 480 ev) strong resonance scattering was found which accounted for all of the observed resonance scattering of the normal element. Evidently the odd Z-even N and even Z-odd N isotopes have comparable level densities in their respective compound nuclei near the neutron binding energy. This situation is depicted in Fig. 4. An odd Z-even N isotope forms an odd Z-odd N compound nucleus with a shallow well whose first excited state is not far off ground. An even Z-odd N isotope forms an even Z-even N isotope with a deep well whose first excited state is far above the ground level. It is not unreasonable to expect such nuclei to have about the same level spacing near binding (i.e., near zero energy for the incoming neutron). Such a picture is in agreement with observations on neutron induced radioactivity (e.g., Mattauch's rules[25]).

It remains to be shown why the even Z-even N isotopes have a greater level separation near binding in the compound nucleus. In the medium heavy region, the even Z-even N isotopes display level spacings of the order of 10 to 100 times greater than their odd Z or odd N neighbors. Therefore, if this level spacing factor is maintained in the lightweight region, no resonance levels <10 kev would be expected for even Z-even N isotopes.

One further observation not complete in Table IV should be made. No significant resonance scattering or absorption exists for $_{40}Zr^{90}$ (50 neutrons), $_{50}Sn$ (50 protons), $_{57}La^{139}$ (82 neutrons), or $_{83}Bi^{209}$ (126 neutrons). These elements are at magic number positions.[26,27] It is furthermore true that neutron resonance levels are more widely separated in the region following a magic number. The closed shells perhaps account for (a) the appearance of strong capture resonances (i.e., high level density) soon after the element zirconium, (b) the disappearance of dense levels near tin (50 protons), (c) the reappearance of dense levels in the rare earth region after lanthanum (82 neutrons), and (d) the second disappearance of dense levels near lead (82 protons) and bismuth (126 neutrons).

IV. THE SCATTERING FRACTION, Γ_n/Γ

Table V re-lists the measured values of Σ_s and Σ_a for cases in which the scattering fraction Γ_n/Γ is calculated. For most of the isotopes studied $\Gamma_n/\Gamma>0.1$. The light odd Z-even N and even Z-odd N are such that $\Gamma_n/\Gamma\sim0.9$. The scattering fraction decreases with increasing atomic weight principally because resonance levels appear which are nearer zero neutron energy. It appears that resonance scattering and absorption are comparable for resonance energies of about 10 to 50 ev. Below 10 ev, capture is the principal resonance component. Above 50 ev, scattering is the principal resonance component. Many of the features indicated in Section III are also revealed in Table V.

[20] S. P. Harris, and A. S. Langsdorf, Phys. Rev. **74**, 1216(A) (1948).
[21] Preliminary results on the odd isotope of germanium (73) indicate that the prominent (see reference 22) resonance at ~95 ev is primarily a scattering resonance and due to $_{32}Ge^{73}$.
[22] Wu, Rainwater, and Havens, Phys. Rev. **71**, 174 (1947).
[23] W. W. Havens and L. J. Rainwater, Phys. Rev. **75**, 1296(A) (1949).
[24] Goldsmith, Ibser, and Feld, Rev. Mod. Phys. **19**, 259 (1947).
[25] J. Mattauch, *Kernphysikalische Tabellen* (Verlag. Julius Springer, Berlin, 1942).
[26] M. G. Mayer, Phys. Rev. **74**, 235 (1948).
[27] M. G. Mayer, Phys. Rev. **75**, 1969 (1949).

The Disintegration of As^{72}*

J. Y. Mei, Allan C. G. Mitchell, and C. M. Huddleston
Indiana University, Bloomington, Indiana
(Received March 23, 1950)

The spectra of the various radioactive arsenics produced by high energy alpha-particle bombardment of gallium have been studied using a magnetic lens spectrograph. These isotopes consist of As^{72} (26 h), As^{74} (19.5 d), As^{73} (90 d) and As^{71} (60 h). The main investigation concerns As^{72}. This element is found to emit five positron groups of end-point energies 3.339 (19.3 percent), 2.498 (64.6 percent), 1.844 (12.1 percent), 0.669 (5.0 percent) and 0.271 (2.0 percent) Mev. A strong gamma-ray of energy 0.835 Mev together with many weak gamma-rays with energies up to 3 Mev have been found. The levels of the product nucleus Ge^{72} agree well with those found from a study of Ga^{72}. The highest energy positron group has a forbidden shape. The spectrum of As^{74} consists of one gamma-ray of energy 0.593 Mev, two negatron groups of energies 1.45 and 0.82 Mev together with a positron group of energy about 0.96 Mev. As^{73} disintegrates by K-electron capture and the emission of an internal conversion line corresponding to a gamma-ray of 0.052 Mev. An internal conversion line corresponding to a gamma-ray at 0.162 Mev is ascribed to As^{71}.

I. INTRODUCTION

THE study of the spectrum of As^{72} was undertaken in order to obtain more evidence about the various energy levels of Ge^{72}, since As^{72} is a positron emitter which leads to Ge^{72}. The states of Ge^{72} have been investigated by Mitchell, Zaffarano, and Kern[1] and by Haynes[2] through an investigation of the beta- and gamma-rays of Ga^{72}. The spectrum of Ga^{72} turned out to be extremely complicated, consisting of seven beta-ray groups and some eight or nine gamma-rays, most of them weak. The two sets of independent investigators are in reasonable agreement on the level scheme determined from their data. About the only point of divergence is the question as to where to place an internally converted gamma-ray of 0.700 Mev energy. This line was originally discovered by Bowe, Goldhaber, Hill, Meyerhoff, and Sala[3] with the help of coincidence counting techniques. They showed that coincidences between disintegration electrons and the internal conversion electrons from the gamma-ray in question are delayed. They therefore assumed that the state giving rise to the internally converted gamma-ray was a metastable one of about 30 μsec. half-life and followed a weak beta-ray transition. Mitchell, Zaffarano, and Kern placed this transition rather high in the disintegration scheme and thought that they had found a gamma-ray in the photo-electron spectrum corresponding to the internally converted gamma-ray in question.

In order to obtain corroborative evidence on the levels of Ge^{72}, the investigation of As^{72} was undertaken. In the process of producing As^{72}, the radioactive nuclei As^{71}, As^{73}, and As^{74} were also produced and information concerning the spectra of these elements was also obtained.

As^{72} was produced in the cyclotron by bombarding gallium with 23-Mev alpha-particles. Since gallium has two stable isotopes, Ga^{69} and Ga^{71}, it is clear that As^{72} (26 hours) and As^{74} (17.5 days) will both be produced as a result of an (α,n) reaction. It was found also that As^{71} and As^{73} were formed by an $(\alpha,2n)$ reaction.

II. PREPARATION OF THE SOURCES

In order to prepare the sources, Ga_2O_3 was pressed into grooves in the target plate of the cyclotron and bombarded with 23-Mev alpha-particles for a total irradiation of 80 to 125 microampere hours. The target material was placed in a distilling flask with 1 gram of hydrazine sulfate and 75 ml concentrated HCl, together with a small amount of arsenic carrier, and the $AsCl_3$ distilled over. The arsenic was finally precipitated with H_2S.

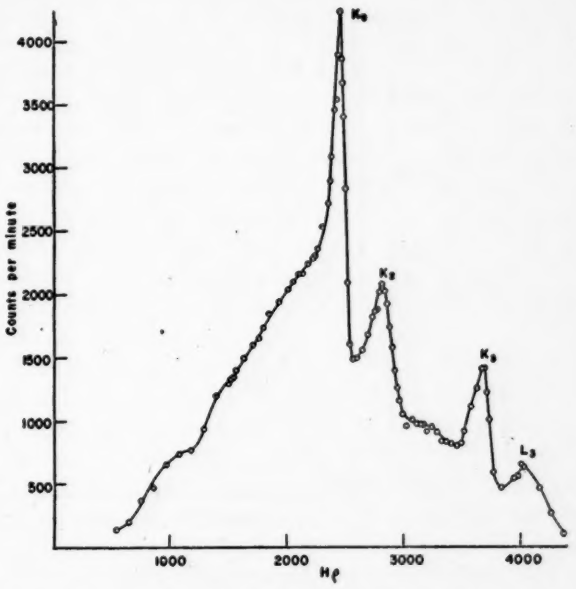

FIG. 1. Gamma-rays from As^{72} and As^{74}; distribution of photo-electrons (U radiator).

* This research was assisted by the joint program of the ONR and AEC.

[1] Mitchell, Zaffarano, and Kern, Phys. Rev. **73**, 1424 (1948).
[2] S. K. Haynes, Phys. Rev. **74**, 423 (1948).
[3] Bowe, Goldhaber, Hill, Meyerhoff, and Sala, Phys. Rev. **73**, 1219A (1948).

TABLE I. Energy levels of Ge^{72} (Mev).

Levels obtained from Ga^{72} (MZK)	(H)	Levels obtained from As^{72} Allowed Positron energy	Levels	Forbidden Positron energy	Levels
0	0	3.386	0.0	3.339	0.0
0.835	0.84	2.486	0.900	2.498	0.841
1.47	1.47	1.849	1.537	1.844	1.495
2.16	—	—	—	—	—
2.52	2.52	0.669	2.717	0.669	2.67
3.02	3.05	0.255	3.131	0.271	3.07
3.34	3.35		—	—	—

III. THE SPECTRUM OF As^{72}

A preliminary investigation of As^{72} by Mitchell, Jurney, and Ramsey,[4] using absorption and coincidence counting methods, indicated that the beta-ray end point was 2.78 Mev, that there was a gamma-ray of about 2.4 Mev, as determined by the coincidence absorption of Compton electrons, and that the spectrum was complex.

In the present investigation, the gamma-ray spectrum was determined by measuring the distribution of photo-electrons ejected from a uranium or lead radiator, in a magnetic lens spectrograph. The uranium radiator had a surface density of 90 mg/cm². Various lead radiators were used having surface densities from 15 to 77 mg/cm². The result of a typical experiment, using a uranium radiator, is shown in Fig. 1. Only that portion of the curve below about 1 Mev is shown. Beyond 1 Mev the gamma-ray intensity is quite weak and it is practically impossible to find lines with any certainty. The highest energy gamma-ray appears to be around 3 Mev. In Fig. 1 the following lines are to be seen: K_1, the K photo-line for annihilation radiation; K_2, the K photo-line for a gamma-ray of energy 0.593 Mev, coming from As^{74}; K_3, L_3, the K and L lines for a gamma-ray of energy 0.835 Mev from As^{72}. By observing the decay of the spectrum it was shown that all of the radiation of energy greater than 1 Mev comes from As^{72}.

The line at 0.835 Mev is the strongest line in the As^{72} spectrum and is also the strongest line in the spectrum of Ga^{72}. There is some evidence for a line at 1.05 Mev, obtained with a lead radiator, which was also observed in the spectrum of Ga^{72}. A careful search was made for a line at 0.637 Mev, observed as a strong line in Ga^{72}, but this was not observed in any intensity. It is apparent, from studying the data, that the many weak lines of high energy, seen in Ga^{72}, are making a contribution to the high energy part of the spectrum of As^{72}. However, the relative intensity of these lines, compared to the line at 0.835 Mev, appears to be considerably less than in Ga^{72}.

The beta-ray spectrum of the arsenic produced from the irradiation of gallium was next investigated. It was found that if the full energy of the beam of 23-Mev alpha-particles was used to produce the source, certain internal conversion lines owing to As^{71} and As^{73} appear. If, however, the energy of the beam was limited to 12 to 13 Mev by placing thin aluminum sheets in front of the target, the extraneous lines disappeared. Figure 2 shows the spectrum of the beta-rays from arsenic under conditions in which the lines from As^{71} and As^{73} do not appear. The spectrum consists of radiations from As^{72} and As^{74}. One feature to be noted in the spectrum is the

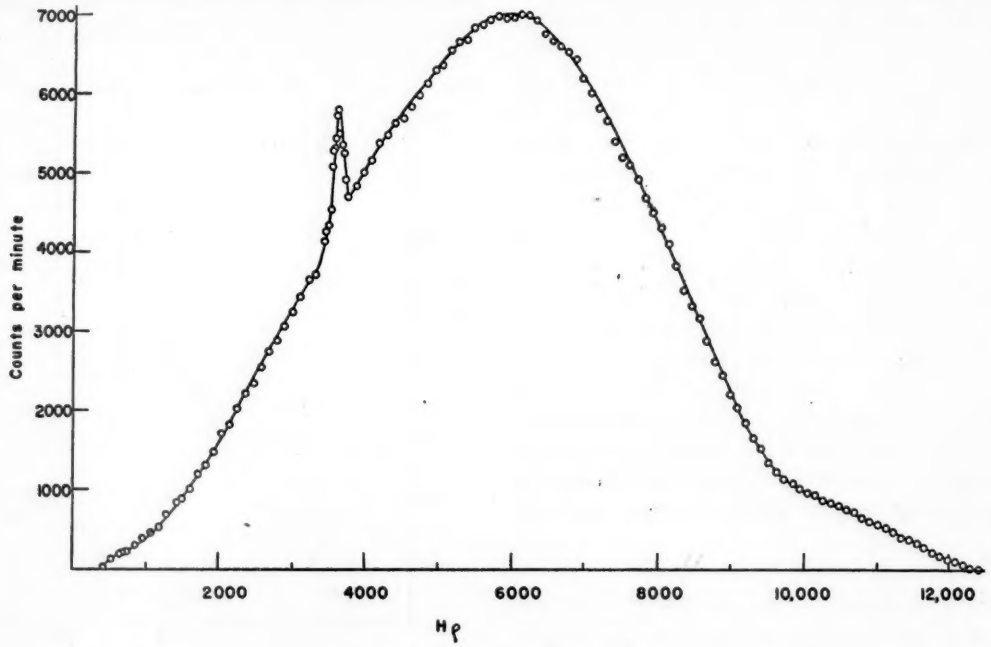

FIG. 2. Beta-ray spectrum of As^{72}.

[4] Mitchell, Jurney, and Ramsey, Phys. Rev. **71**, 825 (1947).

internal conversion line at 3631 gauss-cm—corresponding to a gamma-ray energy of 0.700±0.003 Mev.

In order to analyze this spectrum, the As^{72} (26 hours) was allowed to decay completely and measurements were made on the remaining As^{74} (17.5 days). The original data were then corrected for the presence of As^{74}. Since the end-point energy of As^{74} is approximately 1.45 Mev, no corrections were necessary at energies higher than this.

After the corrections mentioned were made to the data, the beta-ray distribution was analyzed by the usual method of Fermi-plots. In the first analysis it was assumed that all of the spectra involved have an allowed shape. Under this assumption it was found that the spectrum could be resolved into five groups having the end point energies shown in column 3 of Table I. Table I also shows the energy levels of Ge^{72}, obtained from a study of Ga^{72} by Mitchell, Zaffarano, and Kern (MZK) and Haynes (H). It will be seen at once that, while the difference in energies of the two highest energy beta-ray groups is of the right order of magnitude to account for the gamma-ray at 0.835 Mev, the fit is not good enough and as a result the levels of Ge^{72}, determined in this manner, are raised above the levels as determined from Ga^{72}.

An inspection of the Fermi plot of the high energy group revealed that it has a slight curvature, concave toward the energy axis. Such a behavior suggests that the transition is forbidden. The most obvious shape factors to try for this type of behavior are (a) first forbidden $\Delta j=\pm 2$, change of parity and (b) second forbidden $\Delta j=\pm 3$, no change of parity. Both possibilities were tried with the result that the second forbidden shape did not fit the data whereas the shape corresponding to first forbidden, $\Delta j=\pm 2$, change of parity gave a very good fit. The analysis of the complete spectrum was then carried out under the assumption that the high energy group has the forbidden shape given under assumption (a) above. The results are shown in the last two columns of Table I. It will be seen that the difference in energy of the two most energetic groups, 0.841 Mev, is in good agreement with the energy of the gamma-ray, 0.835 Mev, and furthermore that the levels of Ge^{72}, determined in this manner, show quite good agreement with those determined from Ga^{72}. The relative abundances and comparative half-lives of the group are given in Table II.

As has already been mentioned, the shape of the spectrum of the highest energy group implies that it belongs to the first forbidden class with $\Delta j=\pm 2$ and a change of parity. Shull and Feenberg[5] have collected information on some eleven disintegrations of this class. They point out that the quantity $(W_0^2-1)ft$ is approximately 10^{10} for all of these nuclei. For the highest energy group of As^{72} the quantity $(W_0^2-1)ft=1.1\times 10^{10}$, which agrees with the classification of Shull and Feenberg.

[5] F. B. Shull and E. Feenberg, Phys. Rev. **75**, 1768 (1949).

TABLE II. Positron groups of As^{72}.

End-point energy Mev	Relative abundance (percent)	Ft. (sec.)
3.339	19.3	2.0×10^8
2.498	61.6	1.8×10^7
1.844	12.1	5.4×10^6
0.669	5.0	0.97×10^6
0.271	2.0	5×10^4

An attempt can be made to correlate these findings with predictions based on the nuclear shell model. The ground state of the product nucleus $_{32}Ge^{72}$ should have zero spin and even parity. The parent nucleus $_{33}As^{72}$ is a nucleus of the odd-odd type and it is therefore somewhat difficult to predict its configuration. According to Mayer[6] the odd proton should be in a $p_{3/2}$ state. This is in agreement with the fact that the spin of $_{33}As^{75}$ is 3/2. The next higher proton state would be $f_{5/2}$. The thirty-ninth neutron is expected to go into a $p_{1/2}$ state and the next higher state would be $g_{9/2}$. The shell model would predict a state $(p_{3/2}p_{1/2})$ for As^{72}. Now in order to account for the fact that the shape of the high energy spectrum is first forbidden, $\Delta j=\pm 2$ with a change of parity, it is necessary that the ground state of As^{72} have odd parity with a spin of 2. This could be accounted for by the configuration $(f_{5/2}g_{9/2})$. The configuration $(p_{1/2}p_{3/2})$ would not be in agreement with the data since this state would have even parity and the transition would display a shape which would not fit the data.

The energy levels of Ge^{72} as determined from the analysis of the beta-ray spectrum of As^{72} are in quite good agreement with those determined from the spectrum of Ga^{72}. The experiments on As^{72} definitely show that the first excited state of Ge^{72} lies at 0.835 Mev above the ground state. This, of course, could only be inferred in the study of the spectrum of Ga^{72}. It remains to explain why the line at 0.835 Mev is so much more intense than all the other lines in the spectrum of As^{72}, while this is not the case in Ga^{72}. An inspection of Table II shows that 62 percent of all the beta-ray transitions lead to the 0.835-Mev level and only 18 percent to higher levels. In Ga^{72}, on the other hand,[1] 75 percent of the beta-ray transitions lead to levels 3 Mev and more above the ground state. This easily accounts for the lack of intensity of the other lines of the spectrum.

The question of the short-lived metastable state connected with the internally converted line corresponding to a gamma-ray at 0.700 Mev still poses an enigma. The ratio of the number of internal conversion electrons to the total number of positrons from As^{72} is 0.012 while the ratio to the total number of beta-rays in Ga^{72} is 0.005. There is no evidence from the analysis of the positrons of As^{72} or the negatrons of Ga^{72} that there is a level at 0.700 Mev above the ground state. If the

[6] M. G. Mayer, Phys. Rev. **78**, 16 (1950).

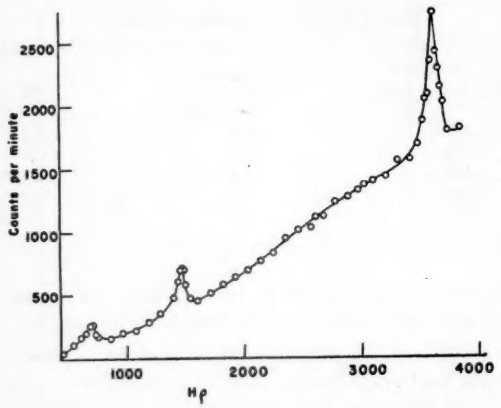

FIG. 3. Internal conversion lines in As^{72}, As^{73}, and As^{71}.

level is placed higher in the level scheme, as was proposed in Ga^{72}, it is necessary to assume that its enhanced population in the decay of As^{72} is occasioned by K-electron capture.

IV. REMARKS ON THE SPECTRA OF As^{74}, As^{73}, As^{71}

It has already been noted that the species As^{74}, As^{73}, and As^{71} were produced in the experiments in which 23-Mev alpha-particles bombarded gallium. While the investigation of these elements was not the main purpose of this research, and since the method of production was not designed to give the maximum yield of these species, still the results obtained appear to be worth mentioning.

As^{74}

The spectrum of As^{74} (17.5 days) has been studied by several investigators. Sagane, Kojima, Miyamoto, and Ikawa[7] investigated the particle spectrum with the help of a cloud chamber. They found that both negatrons and positrons were emitted. They gave the negatron end point as 1.3 Mev and the positron end point as 0.9 Mev. Deutsch and Roberts,[8] using a magnetic lens spectrograph, have shown that there is a gamma-ray emitted having an energy of 0.582 Mev.

In the present experiments, the gamma-ray (see Fig. 1) was measured together with the gamma-rays of As^{72}. The energy of the gamma-ray was found to be 0.593 $\pm$0.003 Mev. The particle spectrum was measured using a source in which both As^{71} and As^{73} were produced, activation by 10 to 12-Mev alpha-particles, and from which the As^{72} has been allowed to die out. The resulting spectrum was relatively weak but it was possible to make a Fermi plot of the data. The result of the analysis shows two negatron groups of end-point energies 1.45 Mev (47 percent) and 0.82 Mev (53 percent), and one positron group of energy 0.96 Mev. The ratio of electrons to positrons is approximately 2. The mismatch of about 7 percent between the difference in energy of the two electron groups and the gamma-ray energy is caused by the low intensity and complexity of the spectrum

As^{73} and As^{71}

The spectrum of As^{73} has been investigated by Elliott and Deutsch,[9] using a magnetic lens spectrometer. This isotope decays by K-electron capture, with a half-life of 90 to 100 days, and emits internal conversion electrons from a gamma-ray of energy 0.052 Mev. In the present experiments, when 23-Mev alpha-particles bombard gallium, an internal conversion line corresponding to a gamma-ray of 0.052 Mev has been found. This is seen on Fig. 3. The half-life of this line has been measured and found to be approximately 90 days. These experiments confirm the findings of Elliott and Deutsch.

The beta-ray spectrum of arsenic, obtained when 23-Mev alpha-particles are used, also shows a line at 0.162 Mev (see Fig. 3). The decay of this line was followed and was found to show a half-life of about 60 hours. This line is evidently associated with the disintegration of As^{71}. Hopkins and Cunningham[10] have ascribed a period of 52 min. to As^{71} and also, according to Seaborg and Perlman,[11] one of 60 hours. The 52-min. activity occurs in the chain

$$Se^{71} \xrightarrow[44\text{ min.}]{\beta^+} As^{71} \xrightarrow[52\text{ min.}]{\beta^+} Ge^{71} \xrightarrow[40\text{ hr.}]{} Ga^{71}.$$

Since it does not seem possible to associate the line at 0.162 Mev with a 52-min. activity or any of its disintegration products, it is natural to associate it with the 60 hr. As^{71}, or possibly with some of its disintegration products if any. Further work will be necessary to work out the final assignment.

The authors wish to express their thanks to Dr. Milo B. Sampson and the cyclotron crew for making the bombardments. They are also indebted to Miss Elma Lanterman for performing the chemical separations.

[7] Sagane, Kojima, Miyamoto, and Ikawa, Proc. Phys. Math. Soc. Japan **21**, 728 (1939).
[8] M. Deutsch and A. Roberts, Phys. Rev. **60**, 362 (1941).
[9] L. G. Elliott and M. Deutsch, Phys. Rev. **63**, 457 (1943).
[10] H. H. Hopkins, Jr. and B. B. Cunningham, Phys. Rev. **73**, 1406 (1948).
[11] G. T. Seaborg and I. Perlman, Rev. Mod. Phys. **20**, 585 (1948).

The Detection of Positron-Conjoint Nuclear Gamma-Radiation*

HERBERT E. KUBITSCHEK†
University of Illinois, Urbana, Illinois
(Received February 20, 1950)

An absorption technique is described for the rapid detection and measurement of nuclear gamma-radiation from positron emitters. Applicability of the method was shown in the verification of the energy and intensity of the gamma-ray from Cu^{64}. The method was further used to find a new gamma-ray of 0.81 ± 0.01 Mev from Ti^{45}; the number of positrons per gamma is $(19\pm2):1$. The positron maximum energy of 1.00 ± 0.02 Mev was also observed, and K-electron capture demonstrated.

1. INTRODUCTION

THE search for nuclear gamma-radiation from positron emitters can be carried out readily with the techniques commonly used for beta-emitters only when the gamma-radiation is present to at least the same order of magnitude as is the positron component, unless the energy is rather large. If this is not the case, conventional absorption methods fail because of the extensive production of annihilation radiation in the region of the detector.

Gamma-ray spectroscopy can be used in the exploration for low intensity radiation, and is especially effective when radioactive lifetimes are long enough to permit the minute investigation required with these high resolution instruments. But positron emitters usually may be expected to have short lifetimes in view of the alternative mode of decay by electron capture, which is always possible energetically. Thus the investigation of such sources requires a large number of activations to ascertain their spectra completely. For these reasons, we may anticipate hitherto undetected gamma-radiation to be associated with a number of such sources. A prominent example indicating these difficulties is the discovery of gamma-radiation from Cu^{64} by Bradt *et al.*,[1] using the method of coincidence absorption, about a decade after sufficiently intense sources for that purpose were available.

Professor M. Goldhaber proposed an absorption technique which greatly increases the probability of observing low intensity radiation. The basis of the method consists in the discrimination against the detection of annihilation radiation, as will be described more fully.

2. ABSORPTION APPARATUS

The source was suspended in a vacuum chamber on an aluminum backing 0.76 mg/cm² thick, and was held in a vertical position by fine wires. Since the source was thin most of the positrons escaped to the walls of the chamber before annihilation. However, the counter was shielded from the radiation from these walls, as shown in Fig. 1, and detected mainly the radiation from the source itself. The customary technique of absorption in lead could now be carried out to search for gamma-radiation and to measure energies.

In order to reduce the annihilation radiation arising from positrons emitted in the direction of the counter, and diametrically opposite to it, it was necessary to apply a magnetic field across the chamber. The thin source was placed normal to this field, so that if the field were flat no positron could re-enter the source once it had left it, as would have been the case were it parallel to the field. Actually, with single pole pieces the capture of positrons in the source increased with field strength because the field was not flat, and trochoidal trajectories were set up for many of the lower energy positrons which allowed them to strike the source. This field was improved by using the double auxiliary pole pieces shown in the figure, which, in the vicinity of the source, bent the flux lines away from the normal to the source, thereby reducing the number of capture trajectories. Still, one must expect an optimum field strength, again stemming from the fact that flux lines are not normal to the source: for very large fields many trajectories will have too small a curvature to miss the source. For Cu^{64} positrons the optimum currents were 2.5 amperes in both the field coils and the auxiliary pole coils, and gave a field strength at the center of the source of about

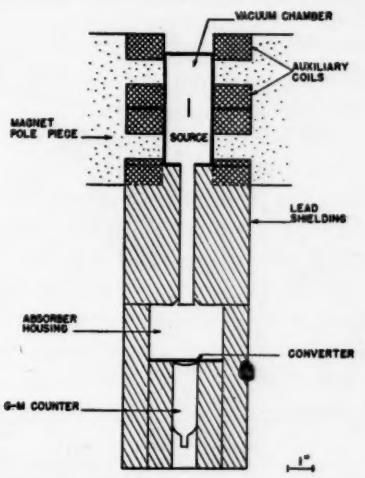

FIG. 1. Diagram of experimental arrangement.

* This work was supported by the ONR.
† Now at the Institute of Radiobiology and Biophysics, University of Chicago, Chicago, Illinois.
[1] Bradt, Gugelot, Huber, Medicus, Preiswerk, and Scherrer, Helv. Phys. Acta 19, 219 (1946).

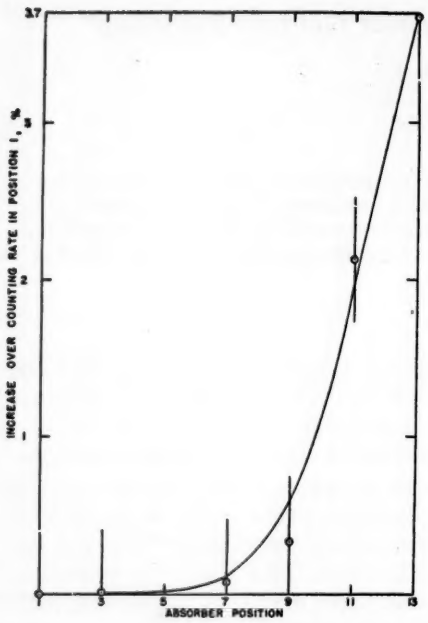

FIG. 2. Calibration of counting rates with absorber position.

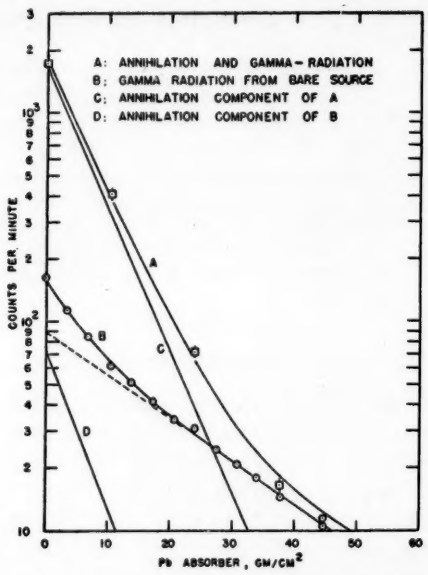
A: ANNIHILATION AND GAMMA-RADIATION
B: GAMMA RADIATION FROM BARE SOURCE
C: ANNIHILATION COMPONENT OF A
D: ANNIHILATION COMPONENT OF B
COUNTS PER MINUTE
Pb ABSORBER, GM/CM²

FIG. 4. Absorption curves for Cu^{64} radiation.

1200 gauss, compared to 1570 gauss between the poles. With this arrangement the counting rate with the field was about 30 percent lower than in its absence.

The nuclear gamma-radiation was detected by a halogen-filled end window G-M counter through the secondary radiation produced in a lead radiator of 0.935 g/cm². The energy was measured by successively intercepting the radiation with eighth-inch lead absorbers, the half-value thickness being characteristic of the energy. However, accuracy required a correction for forward Compton scattered gamma-rays which could record. This was accomplished by measuring the counting rate for a single absorber as a function of position. Assigning "excellent" geometry to that position farthest from the counter, that is, a negligible increase in counting rate due to singly scattered gamma-rays, the curve of Fig. 2 was obtained. Here we see that the correction is indeed negligible for the first five positions, but reaches a value of 3.7 percent for the absorber in position No. 13 adjacent to the converter. Since this position effect involves small corrections only, to good approximation the combined effect for a number of absorbers is their sum. When all the absorbers were simultaneously used, the reduction to be applied to the counting rate was 10.6 percent. All such corrected absorption curves for monochromatic gamma-rays were exponential to the maximum absorber thickness of 44.5 g/cm² of lead.

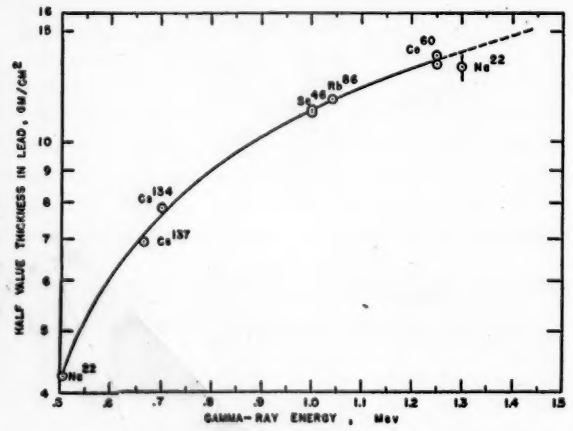

FIG. 3. Calibration of standard geometry for measurement of gamma-ray energies.

The half-value thickness as a function of energy was determined empirically for this geometry by using a number of radioactive sources for which the energies are known from spectroscopic measurements. The energies were taken from Seaborg and Perlman[2] except for Co^{60} which were taken from Lind, Brown, and DuMond.[3] The average energy is taken in those cases where two gamma-rays of equal intensity are present (Sc^{46}, Co^{60}, Cs^{134}). The calibration is shown in Fig. 3.

3. GAMMA-RADIATION FROM Cu^{64}

The apparatus was tested by examining the well-known nuclear gamma-radiation from Cu^{64}. Disks of copper 0.1 mil thick and 2.1 cm in diameter, were activated in the pile of the Oak Ridge National Laboratory. The results of measurements on one of these are shown in Fig. 4. Curve *B* indicates the counting rate observed with the bare source; the dotted line is the asymptote to this curve and indicates the nuclear gamma-intensity. Curve *D* is the annihilation component of *B*, the difference between the observed curve *B* and its asymptote. Curve *A* is the activity measured with the source covered with an eighth of an

[2] G. T. Seaborg and I. Perlman, Rev. Mod. Phys. **20**, 585 (1948).
[3] Lind, Brown, and DuMond, Phys. Rev. **76**, 1838 (1949).

inch of aluminum; the increased intensity here is due to the fact that the positrons are now all captured in the aluminum, and give rise to annihilation radiation. Curve *C* results from the subtraction of the nuclear gamma-component from *A*. Comparison with *D* shows the reduction of the annihilation component to be 96 percent.

The weighted average over several such measurements gave a half-value thickness for the hard component of *B* of 14.5±0.5 g/cm², which corresponds to an energy of 1.38±0.06 Mev, in agreement with the work of Deutsch[4] (1.35 Mev), and of Kurie and Ter-Pogossian[5] (1.34±0.01 Mev). The soft component of *B* has the half-value thickness 4.2 g/cm², appropriate to annihilation radiation.

If the counter efficiency is known as a function of energy the number of annihilation gamma-rays per nuclear gamma-ray can be calculated directly from the values of the intensities at zero absorber. The relative efficiency at different energies for the counter used in these measurements was taken from the work of Bradt *et al.*,[6] who calibrated counters of various cathode materials with wall thicknesses always greater than the ranges of the secondary electrons.

Using the efficiencies listed for counters with brass walls as good approximation to those for the iron-walled counter here, the efficiency for 1.35-Mev gamma-rays is a factor of 2.9 greater than for annihilation radiation. This includes a minor correction for the contribution from the lead converter, the area of which was found to be 12 percent of the effective counter wall area. Including small corrections for positioning, for absorption of gamma-radiation by the converter, and for absorption of annihilation radiation by the aluminum around the source, the emission ratio for annihilation radiation to nuclear gamma-rays is 62±10.

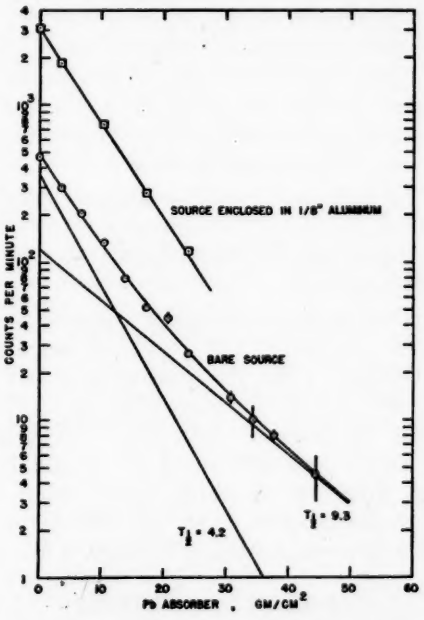

FIG. 5. Absorption of radiation from Ti^{45}.

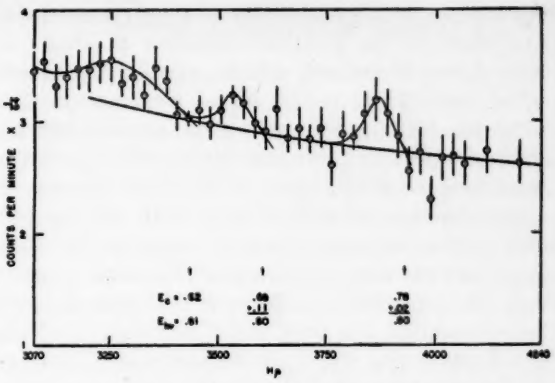

FIG. 6. Compton and photo-electrons from Ti^{45}.

Since two quanta are emitted on positron annihilation the ratio of emission of positrons to nuclear gamma-rays is 31±5, which again is in reasonable agreement with the work of Deutsch (40±5). By far the largest contribution to the error here is the fact that a small change in slope near the end of the absorption curve implies a large change in the extrapolated zero absorber intensity of the nuclear gamma-component. The error does not include the minor contribution of annihilation of positrons in motion, nor does it include any errors in the measurement of efficiencies by Bradt *et al.*

4. GAMMA-RADIATION FROM Ti^{45}

The production of Ti^{45} was first accomplished in 1941 by Allen, Pool, Kurbatov, and Quill.[7] They observed an activity due to positrons, with a maximum energy of 1.2 Mev according to a cloud-chamber histogram, and with a half-life for the radioisotope of 3.08±0.06 hours. They also observed the presence of a few electrons and gamma-rays, but assumed these probably to be due to the annihilation radiation.

In the experiments described below, Ti^{45} was usually produced according to the reaction $Sc^{45}(p, n)Ti^{45}$. Bombardments were made with 10-Mev molecular hydrogen ions from the University of Illinois cyclotron. A spectroscopic analysis of the Sc_2O_3 used as the target showed no Ti greater than 10 ppm, nor other impurities greater than 1 ppm. A deuteron bombardment was tried, but discarded since the competitive reaction $Sc^{45}(d, p)Sc^{46}$ appeared too prominently.

The chemical separation used was a carrier modification of the quantitative separation of titanium from aluminum as detailed in Treadwell and Hall.[8] The radioactive mixture of 0.3 to 0.4 g was washed into 100

[4] M. Deutsch, Phys. Rev. **72**, 729 (1947).
[5] N. D. Kurie and M. Ter-Pogossian, Phys. Rev. **74**, 677 (1948).
[6] Bradt, Gugelot, Huber, Medicus, Preiswerk, and Scherrer, Helv. Phys. Acta **19**, 77 (1946).
[7] Allen, Pool, Kurbatov, and Quill, Phys. Rev. **60**, 425 (1941).
[8] F. P. Treadwell and W. T. Hall, *Analytical Chemistry* (John Wiley and Sons, Inc., New York, 1935), Vol. II.

cc of water, to which was added 50 cc of concentrated H_2SO_4. Most of the material dissolved in about 15 minutes. 1.6 g of tartaric acid in solution and about 2 mg of inert Ti in acid solution were added. The titanium was then precipitated by the dropwise addition of 1.5 cc of 4 percent cupferron, filtered, and ignited to constant weight of titanium oxide. Thin deposits of the oxide were formed on aluminum after wetting with a dilute solution of Duco cement in acetone. The total preparation time was about two and one-half hours.

With this procedure the decay of Ti^{45} was observed to be exponential for over eight half-lives, and the weighted value for the half-lifetime was 3.09 ± 0.03 hours, in agreement with Allen *et al.*

The gamma-ray absorption curve for Ti^{45} is shown in Fig. 5. The resulting half-value thicknesses are 9.3 ± 0.2 and 4.2 ± 0.2 g/cm^2. The corresponding gamma-ray energies[9] are 0.82 ± 0.03 Mev and 0.51 ± 0.02 Mev.

From the data of Fig. 5 the ratio of the number of positrons to gamma-rays can be determined, as in the case of Cu^{64}. The counter efficiency for 0.8 Mev is 1.5 times as great as at 0.51 Mev, from which the positron frequency is 19 ± 2 per gamma-ray.

5. SPECTROSCOPIC VERIFICATION

It was felt that any remaining doubt about the merits of this absorption technique for positron emitters, or the existence of the gamma-ray line found with it, might be dispelled by confirming the existence of the line by gamma-ray spectroscopy. For this purpose, a variable field, current regulated, 180° spectrometer using end window G-M counter detection was employed. Trajectories in focus has a radius of 7 cm, and the instrument was usually operated with a resolution of 3 percent. A foil of uranium one mil thick was used to convert the gamma-radiation.

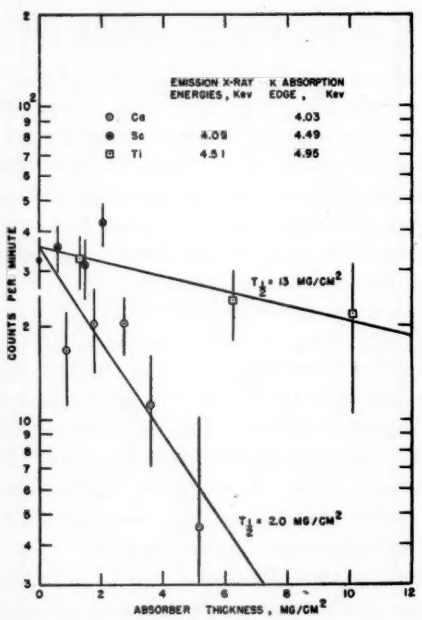

FIG. 7. Critical absorption of x-rays.

The spectrometer was calibrated against the K and L photo-conversion lines of the gamma-rays from Co^{60} and the annihilation radiation from Ti^{45}. The average root mean square deviation from linearity between measured magnetic field and electron momentum was 0.5 percent. The conversion electron momenta were measured directly from the extrapolated values to the upper end point of the photo-electron distributions. Verification of the calibration was provided here by measuring the beta-end point of Cs^{134}. The value of 0.64 ± 0.01 Mev is in good agreement with the values of

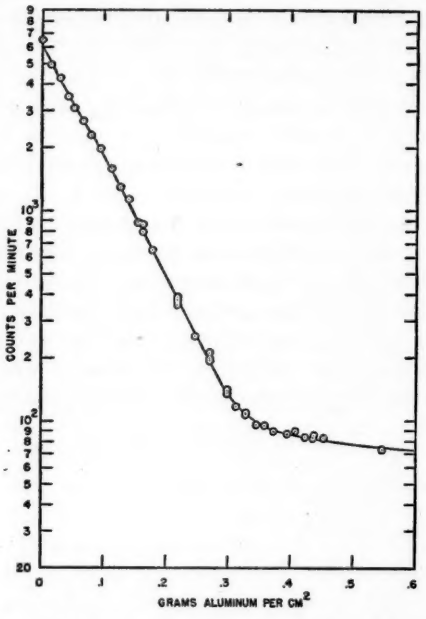

FIG. 8. Absorption of Ti^{45} positrons in aluminum.

Siegbahn and Deutsch[10] (0.645 ± 0.02), and Elliot and Bell[11] (0.658 ± 0.15).

The decay-corrected conversion electron spectrum obtained for Ti^{45} is shown in Fig. 6. Although the statistical errors are large, due mainly to a large background counting rate, three peaks are evident on the annihilation background. Assuming that these peaks correspond to the Compton and the K and L photo-conversion lines, the following values result for the gamma-ray energy: 0.81, 0.80, and 0.80 Mev, respectively, with an average value of 0.80 ± 0.01 Mev.

6. *K*-ELECTRON CAPTURE

The existence of a gamma-ray line of intermediate energy indicated that orbital electron capture might be

[9] The lower energy corresponds to annihilation radiation, and does not appear to have the nuclear component indicated in a preliminary report by Kubitschek, Longacre, and Goldhaber, Phys. Rev. **77**, 742 (1950).

[10] K. Siegbahn and M. Deutsch, Phys. Rev. **71**, 483 (1947).

[11] L. G. Elliot and R. E. Bell, Phys. Rev. **72**, 979 (1947).

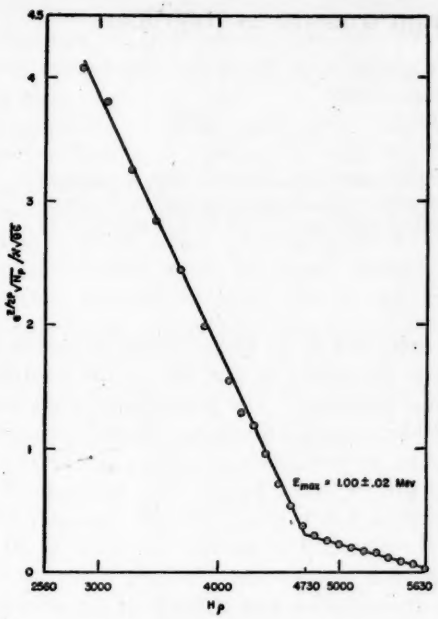

FIG. 9. Kurie plot for Ti^{45}.

observable for Ti^{45}. This proved to be the case, using the method of critical absorptions.

The positron background was excluded by placing the source in the absorption geometry previously described, and the G-M counter was placed as close as possible to the exit aperture. A preliminary absorption in aluminum indicated a very soft component of about 3 mg/cm² half-value thickness, which was present at zero absorber thickness to about 30 percent above a hard background intensity. To prove that these were x-rays a set of critical absorbers was made from the oxides of Ca, Sc, and Ti, by brushing the powders onto an aluminum backing of 0.76 mg/cm² and cementing them in place with a thin layer of Duco cement. A calibration by absorption of the x-rays from a tungsten target tube set for a maximum energy of 21 kev showed the absence of any peculiarities for these absorbers.

The critical absorption, after subtraction of the large background, is shown in Fig. 7. The data show that the x-rays were strongly absorbed only in Ca, and not in either Sc or Ti, so that the emission x-ray energy must lie between the K absorption edges of Ca and Sc. This condition is satisfied by the K x-rays from Sc.

7. POSITRON MAXIMUM ENERGY

An early estimate for the maximum energy of the positrons had been made during the course of these experiments, indicating about 0.98 Mev from their range in aluminum, Fig. 8. Since this result is in discord with that of Allen *et al.*, another determination was made with the spectrometer. The Kurie plot obtained with the spectrometer is shown in Fig. 9, and gives the positron maximum energy of 1.00±0.02 Mev at the knee of the curve. The contribution beyond this break is due to the poor shielding against annihilation radiation, which occurred because of the large value for the resolution: positrons could annihilate near the counter housing and thereby record. Hence, the positron spectrum was not accurately obtainable. The discrepancy with the cloud-chamber data of Allen *et al.* may be accounted for by the poor statistics of their method, in addition to the apparent extension toward higher energies due to scattering in their cloud chamber.

8. DISCUSSION

The absorption method with shielding of the detector from annihilation radiation has a sensitivity comparable to that of a high transmission spectrometer. In addition, it has the advantage of covering the spectrum within a small number of measurements, thus allowing rapid qualitative investigation for the presence of gamma-radiation.

High sensitivity depends upon obtaining both high source activity and negligible self-absorption for positrons; with intensities available at present, gamma-radiation with a frequency less than one percent of that of the positron component can be detected. When the lifetime of the source is greater than one hour identification may be made with a single activation.

The author expresses appreciation to Professor M. Goldhaber for suggesting the problem and its mode of solution, and to Professor A. Longacre for setting up the original apparatus and for his interest throughout the experiment. Thanks are also due the cyclotron crew of the University of Illinois for activation of the sources, Professor C. W. Sherwin for the use of the gamma-ray spectrometer, and Dr. S. Siegel, of the Illinois Institute of Technology, for spectrographic analyses. The author gratefully acknowledges the support of an AEC Predoctoral Fellowship.

Total Neutron Cross Section of Vanadium from 10 to 1000 Kev

J. MORRIS BLAIR AND J. R. WALLACE
Argonne National Laboratory, Chicago, Illinois
(Received March 16, 1950)

The total cross section of vanadium for neutrons of 10 to 1000 kev has been measured with an energy resolution of ±6 kev. For low energy neutrons the values of the cross sections fluctuate rapidly, leveling off to an average of about 3 barns above 500 kev. By using a filtering technique a cross section of 0.0±0.5 barn was measured at 105 kev.

I. INTRODUCTION

THE detailed measurements of total neutron cross sections made previously have been, in the case of elements heavier than aluminum, for elements having two or more isotopes.[1–4] For measurements made with neutrons having rather poorly defined energies, which are intended to verify theories predicting the general trends of cross sections with neutron energy and atomic weight, the differences between the cross sections of the several isotopes of an element may not be significant. However, to study the detailed variations in the neutron cross section which show up so well, for example, in the case of aluminum,[5] for neutrons whose spread in energy is 10 kev, one should be free from the complication of having several isotopes of comparable abundances. Vanadium consists only of atoms of mass 51, with the exception of ¼ percent of the recently discovered isotope of mass 50.[6] Since it is anticipated that the resonances in the neutron cross sections of heavier elements are more closely spaced, there is a practical limit of the mass of an element whose cross section will reveal such sharp variations, due to the spread in the energy of neutrons produced at the target of an electrostatic accelerator. As illustrated below, the resonances in the vanadium cross section seem to be resolved in the lower part of the neutron energy range covered in these measurements, but not at the higher energies.

II. PROCEDURE

The total neutron cross section of vanadium was measured for neutrons having energies between 10 kev and 1000 kev. The method used was similar to that described by Barschall and collaborators.[2,5] The neutrons were produced with the recently completed Argonne National Laboratory electrostatic accelerator by bombarding thin lithium targets with protons. The targets used had 5- to 10-kev stopping power for the protons as measured by the rise in the neutron yield just above threshold.[4] The preliminary work was done with a 10-kev target while more detailed measurements were made, at energies where the cross section varies rapidly, with a 5-kev target. The neutrons were detected with a 3-inch long, one inch diameter BF_3 proportional counter. The counter was filled to 30 cm Hg pressure with gas enriched in the mass 10 isotope. Around the counter was a layer of paraffin one-half inch thick and outside of the paraffin was a layer of boron carbide one-quarter inch thick. The whole unit was covered with cadmium. The neutron production was monitored by measuring the proton charge accumulated by the accelerator target during a run with a simple current integrator circuit. This quantity was used to normalize the runs taken with and without the scattering sample in place at each energy investigated.

The scattering sample used throughout this experiment was a cylinder of vanadium metal 1.750 inches in diameter and 1.000 inch long. It was borrowed from the Metallurgy Division of the Argonne Laboratory, and it was stated that its only known impurity was ¼ percent of carbon. The percentage transmission of this sample varied from 50 to 70 percent over most of the energy range investigated except at the sharp peaks and dips in the cross section.

For the measurements using neutrons of 120 kev and above, the neutron counter and scattering sample were placed 12 and 6 inches, respectively, directly in front of the lithium target producing the neutrons. The sample was supported in a reproducible manner in a triangle of steel wires. To obtain measurements of the portion of the counts recorded which were caused by neutrons not traveling directly from the target to the counter, a cone of paraffin and boron carbide could be placed between the target and the counter. The background count thus obtained was found to vary gradually from 3 to 10 percent over this energy range.

Since the neutron energy in the forward direction becomes confused by a group of slower neutrons[7] below 120 kev the measurements at the lower energies were made with the counter and scatterer at an angle of 120° from the line of the proton beam. In this position

[1] Barschall, Bockelman, and Seagondollar, Phys. Rev. **73**, 659 (1948).
[2] Adair, Barschall, Bockelman, and Sala, Phys. Rev. **75**, 1124 (1949).
[3] Bockelman, Peterson, Adair, and Barschall, Phys. Rev. **76**, 277 (1949).
[4] Barschall, Bockelman, Peterson, and Adair, Phys. Rev. **76**, 1146 (1949).
[5] L. W. Seagondollar and H. H. Barschall, Phys. Rev. **72**, 439 (1947).
[6] D. C. Hess and M. G. Inghram, Phys. Rev. **76**, 1717 (1949); W. T. Leland, Phys. Rev. **76**, 1722 (1949).
[7] R. F. Taschek and A. Hemmendinger, Phys. Rev. **74**, 373 (1948).

it was convenient to place the counter 25 inches and the scattering sample 12.5 inches from the target spot. A correspondingly longer paraffin cone was used in this position also.

The energy of the protons striking the lithium target was measured with an electrostatic analyzer (25° deflection) which was used on the mass 2 beam. The spread in proton energy of this accelerator has not been carefully studied, but has been estimated from the sharpness of the threshold of the Li (p, n) reactions as being 3 or 4 kev. For the work in the forward direction the spread in the energy of the neutrons due to the angle subtended at the target by the counter was one to two kev. In this position the total estimated spread in the neutron energies was 10 to 12 kev for the thinner target and 15 to 18 kev for the thicker target. When working at 120° to the line of the proton beam the total energy spread was estimated as 4 kev at 10 kev and 15 kev at 120 kev (the variation in energy with angle changes rapidly in this region).

III. RESULTS

The observed transmission data were corrected for the scattering of neutrons into the counter by the sample on the assumption that the neutron scattering was isotropic in the laboratory coordinate system. In the 0° position this effect was 2.1 percent of the scattered neutrons, while at 120°, due to the greater spacings, the correction was reduced to 0.5 percent of the scattered neutrons. The corrected transmissions were converted to cross sections on the basis of an exponential decrease in the neutron flux on passing through the sample (no correction for multiple scattering). The resulting cross section was finally corrected for the effect of the $\frac{1}{4}$ percent of carbon in the sample using the published carbon scattering cross section.[8] The results are plotted in Fig. 1. A sufficient number of neutrons was counted for each point to make the probable error due to random fluctuations approximately 2 percent. The points represented by crosses were taken with the 10-kev target; the circle points were taken with the 5-kev target.

The five points (at 50, 60, 105, 225, and 270 kev) lying below the main set of data represent cross sections obtained using a filter technique. Since the spread in neutron energies was probably somewhat greater than the width of several of the narrow dips in the cross section curve, the spread in the energy of the neutrons hitting the sample could be reduced (when operating near the energy of one of these dips) by filtering them through an additional thickness of vanadium before they struck the sample. With sufficient vanadium between the target and sample only those neutrons would strike the sample for which the cross section was the lowest. The low points at 225 and 270 kev were taken with a filter 5 inches long composed of vanadium powder contained in a thin copper cone. The other points were taken at 120°, so there was room for a cone of vanadium powder 10.5 inches long. The shorter cone gave a thickness of vanadium, in grams per square centimeter, of three times that of the sample, while the larger cone was equivalent to six times the thickness of the original sample. When the cones were in place the transmission of the sample was obtained in the usual way. Since the

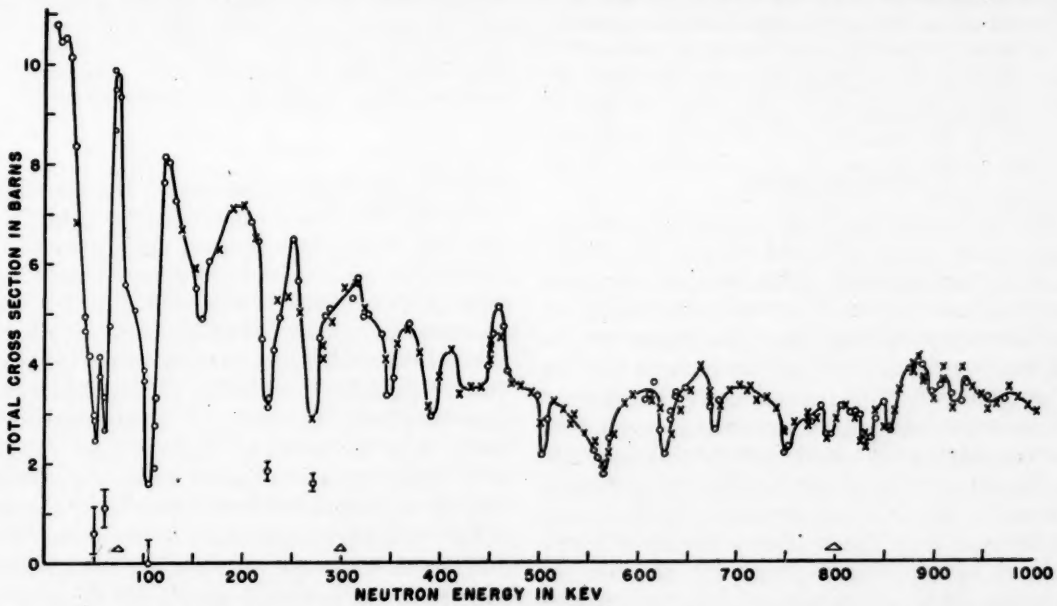

FIG. 1. Total neutron cross section for vanadium. The cross points (×) were taken with a 10-kev thick target, the circle points (o) with a 5-kev thick target. The probable error of each point is ±2 percent. The approximate energy spread of the neutrons is given by the small triangles.

[8] Goldsmith, Ibser, and Feld, Rev. Mod. Phys. 19, 259 (1947).

vanadium cones did not completely remove all of the neutrons except those with the lowest cross section, the positions of those points do not necessarily represent the lowest value of the cross section for that neutron energy. However, it is interesting to note that the observed cross section at 105 kev was zero with a probable error of one-half barn. The narrow peak between the low points at 50 and 60 kev was checked to make sure that there was not a broad minimum in the curve instead of two minima close together.

For neutron energies greater than 640 kev one might expect the measured cross sections to be influenced by the presence of the low energy group of neutrons which has recently been studied by the photographic plate technique.[9,10] However, the cross sections were recalculated between 640 and 1000 kev on the basis that the low energy neutrons provide 8 percent of the flux at 1000 kev and decrease linearly in intensity towards their threshold.[10] (The greater sensitivity of the neutron detector for the lower energy group of neutrons was taken into account.) The results of this correction were hardly noticeable, the cross section at most points being changed by less than the 2 percent probable error mentioned above.

The authors would like to express their appreciation for the work of Rolland Perry, formerly of the Argonne National Laboratory, now at Utah State College of Engineering and Agriculture, in designing and constructing the Argonne electrostatic generator with which these measurements were taken. The neutron detector used was constructed by Warren Stubbins, now at the University of Cincinnati. We would also like to thank A. S. Langsdorf, Jr. and Albert Wattenberg for advice concerning various phases of the experiment.

[9] Johnson, Laubenstein, and Richards, Phys. Rev. **77**, 413 (1950).
[10] B. Hammermesh and V. Hummel, Phys. Rev. **78**, 73 (1950).

PHYSICAL REVIEW VOLUME 79, NUMBER 1 JULY 1, 1950

Consistency of Nuclear Radii of Even-Even Nuclei from Alpha-Decay Theory*

I. PERLMAN AND T. J. YPSILANTIS
Radiation Laboratory and Department of Chemistry, University of California, Berkeley, California
(Received March 16, 1950)

It is shown possible to obtain a consistent function for nuclear radii if the quantitative treatment of the alpha-decay process is applied to even-even isotopes of the heavy elements. The nuclear radii so calculated for even-even isotopes of emanation, radium, thorium, uranium, plutonium, and curium, conform to the expression $r=1.48\cdot10^{-13}\cdot A^{\frac{1}{3}}$ cm which defines the *normal nuclear radii*. The agreement is within 1 percent for the majority of the cases and there is reason to question the experimental data used in the calculations for at least part of those which do not show such close agreement. In cases of fine structure in alpha-decay of even-even nuclei, the radii calculated from the separate alpha-groups are compatible. The polonium isotopes and Em^{212} form a special group showing departures from normal nuclear radii explainable by consideration of shells in nuclear structure.

I. INTRODUCTION

RECENTLY there has been renewed interest in alpha-decay systematics and alpha-decay theory stimulated by the discovery within the past few years of many new alpha-emitters. In a recent communication[1] from this laboratory regularities in alpha-decay energies and half-lives were dealt with at some length and the correlation observed which is pertinent to the present paper is that only the even-even nuclei give evidence of quantitative agreement with present alpha-decay theory. The observation of significance was that on a *decay energy vs. half-life* plot *even* isotopes of an *even* element define a line which is close to the curve which is calculated by selecting a reasonable function for nuclear radius. This type of plot will be presented and discussed in the last part of this paper. The nuclear radius is the single parameter in the equation which cannot be determined experimentally with the desired precision. While the even-even nuclei showed this consistency, the nuclei with odd nucleons almost invariably departed from these curves in the direction which corresponds to prohibition of alpha-decay, that is, the half-lives were too long for the particular decay energies. The reasons for prohibition of alpha-decay in such cases have been discussed[1] and the phenomenon is mentioned here in order to dismiss these categories of nuclear type in attempting to obtain a consistent function for nuclear radius from alpha-decay theory.

The present communication treats the even-even nuclides to determine their nuclear radii assuming the validity of the one-body theory for alpha-decay. The significance of the nuclear radius in alpha-decay is in determining the height and breadth of the potential barrier for a given nuclear charge. In the one-body theory, the alpha-particle being emitted is considered

* This paper is based on work performed under the auspices of the U. S. AEC.
[1] Perlman, Ghiorso, and Seaborg, Phys. Rev. **77**, 26 (1950).

to be acted upon by the potential field of the product nucleus. Accordingly, the nuclear charge, barrier height, and radius employed are those of the product after alpha-emission. From the considerations of this problem to be presented here, we shall see that in most cases the simplifying assumptions inherent in the one-body theory probably do not produce inconsistencies in the calculated nuclear radii although the absolute values obtained may vary somewhat with different treatments. This follows if most parent-daughter pairs have about the same nuclear radius, which indeed does seem to be the case for a wide group which we shall define as *normal nuclei*. The meaning of the calculated nuclear radius becomes less definite where there is a large change in nuclear radius between parent and daughter, since in such a case the contribution of the parent nucleus is tacitly ignored and any effect it may have is attributed to the daughter. More basically, it should be realized that nuclear radii calculated from alpha-decay theory will depend upon the nuclear model employed and may be expected to differ from those obtained from other phenomena related to a different model or for which the calculated radii are not sensitive to the model selected. The objective of the present paper is to test the consistency of nuclear radii as calculated from alpha-decay data of even-even nuclei; it is probable that different treatments will be equivalent in this regard even though the absolute values of the radii may differ somewhat. In the present study the expression used was selected because of its relative simplicity and relates the decay constant, decay energy, atomic number, and nuclear radius as follows (see Bethe[2]):

$$\log_{10}\lambda = 21.843 + \tfrac{1}{2}\log_{10}E - \log_{10}r + 0.217\frac{4}{A-4} - 1.104\frac{(Z-2)}{\{E[1+(4/A-4)]\}^{\frac{1}{2}}}\alpha_0 + 1.104\frac{(Z-2)}{\{E[1+(4/A-4)]\}^{\frac{1}{2}}}\sin\alpha_0\cos\alpha_0,$$

with

$$\cos\alpha_0 = 0.5893[Er/(Z-2)]^{\frac{1}{2}}.$$

The numerical coefficients were calculated to give λ in units of sec.$^{-1}$ with E (Mev) the alpha-decay energy, r (cm$\times 10^{13}$) the radius of the product nucleus, while Z and A are the charge and mass number, respectively, of the emitting nucleus. The principal approximation in this expression involves taking the coefficient, K, in the formula $\lambda = Ke^{-2G}$ simply as v/r, where v is the relative velocity of the alpha-particle. Biswas[3] has tested alpha-decay data using a similar expression and Preston[4] has developed a more rigorous expression for alpha-decay which he and Biswas and Patro[5] have used in calculating nuclear radii. The values obtained from Preston's expression appear to be a few percent larger than those from the approximate solution which we employ. Of more significance, these authors and others make no distinction between different nuclear types so that a nuclear radius so calculated is an "effective nuclear radius" which appears abnormally small when alpha-decay is forbidden for *any* reason.

TABLE I. Calculated nuclear radii of even-even nuclides.

Nuclide	α-energy (Mev)	Abundance of alpha-group	Half life	Nuclear radius[a] r	Deviation of r from normal (percent)
Cm^{242}	6.18		150 days	9.14	−0.4
Cm^{240}	6.37		30 days	9.02	−1.4
Pu^{238}	5.59		92 yr.	9.06	−0.7
Pu^{236}	5.85		2.7 yr.	9.10	0.0
U^{238}	4.25		4.51×10^{9} yr.	9.41	+3.2
U^{234}	4.84		2.35×10^{5} yr.	9.22	+1.7
U^{232}	5.40		70 yr.	9.14	+1.1
U^{230}	5.96		20.8 days	9.15	+1.5
Th^{232}	4.05		1.39×10^{10} yr.	9.41	+4.0
Th^{230}	4.76	0.80	1.0×10^{5} yr.	9.09	+0.9
	4.69	0.20	4.0×10^{5} yr.	9.04	+0.4
Th^{228}	5.52	0.72	2.64 yr.	8.97	−0.2
	5.43	0.28	6.79 yr.	9.03	+0.5
Th^{226}	6.41		30.9 min.	9.09	+1.4
Ra^{226}	4.88	0.96	1700 yr.	8.98	+0.2
	4.70	0.04	4.0×10^{4} yr.	8.92	−0.4
Ra^{224}	5.78		3.64 days	8.97	+0.4
Ra^{222}	6.63		38 sec.	8.98	+0.9
Em^{222}	5.59		3.83 days	8.95	+0.4
Em^{220}	6.39		54.5 sec.	8.94	+0.7
Em^{218}	7.25		0.019 sec.	9.03	+2.0

[a] The nuclear radius is that of the α-decay daughter calculated using the measured half-life and α-energy and is expressed in units of 10^{-13} cm.

In the present paper, calculations of nuclear radius were made for 25 even-even nuclides, and of these three have more than one recognized alpha-group for each of which separate computations were made. With a few exceptions, which may be due to inaccuracies in the available data, the nuclear radii from emanation (element 86) to curium (element 96) show remarkably good agreement with the simple expression $r = 1.48A^{\frac{1}{3}} \times 10^{-13}$ cm. For convenience we shall call the nuclear radius determined from this relationship the *normal nuclear radius*. The polonium isotopes show unmistakably lower values for their nuclear radii, as will be discussed.

The selection of 1.48 as the coefficient for the nuclear radius expression was not arrived at by a statistical analysis weighting all of the available data equally as will be apparent by examining Table I in which it will be seen that the deviations to be discussed below are distributed heavily on one side. It will be seen that the principal uncertainties in the calculation of nuclear radii insofar as experimental data are concerned are inaccuracies in alpha-energies. As a result, greater weight was given to the relatively few determinations made by alpha-ray spectroscopy, especially since for many of the other nuclei there is reason to suspect inaccuracies, and for some it is known that the probable error is in the right direction.

[2] H. A. Bethe, Rev. Mod. Phys. **9**, 69, 161 (1937).
[3] S. Biswas, Ind. J. Phys. **23**, 51 (1949).
[4] M. A. Preston, Phys. Rev. **71**, 865 (1947).
[5] S. Biswas and A. P. Patro, Ind. J. Phys. **22**, 539 (1948).

TABLE II. Nuclear radii in cases of α-decay fine structure.

Nuclide Z^A	Decay energies and references	Abundance of group	Partial alpha-half-life	Calculated radius for $(Z-2)^{A-4}$	Deviation of r from "normal" (percent)
Th^{230}(Io)	4.74[a]		8.0×10^4 yr.	9.23	+2.4
	GpO 4.76[b]	0.80	1.0×10^5 yr.	9.09	+0.9
	GpI 4.69[b]	0.20	4.0×10^5 yr.	9.04	+0.4
Th^{228}(RdTh)	5.48[c]		1.90 yr.	9.21	+2.5
	GpO 5.52[d]	0.72	2.64 yr.	8.97	−0.2
	GpI 5.43[d]	0.28	6.79 yr.	9.03	+0.5
Ra^{226}(Ra)	4.88		1622 yr.	9.01	+0.6
	GpO 4.88[e]	0.96	1700 yr.	8.98	+0.2
	GpI 4.70[e]	0.04[f]	4.0×10^4 yr.	8.92	−0.4
	GpI 4.70	0.10[e]	1.6×10^4 yr.	9.08	+1.3
	GpI 4.70	0.018[g]	9.0×10^4 yr.	8.78	−2.0

[a] See reference 11.
[b] See reference 12.
[c] See references 8 and 9.
[d] Rosenblum, Valadares, and Perey, Comptes Rendus **228**, 385 (1949).
[e] See reference 13.
[f] A. Ghiorso (private communication).
[g] See reference 14.

Table I shows the even-even nuclides from emanation to curium with the alpha-energies and half-lives used in calculating the nuclear radii. The last two columns list the calculated nuclear radii and the deviations of these radii from the *normal* values (given from the expression $r=1.48A^{\frac{1}{3}}\times10^{-13}$ cm). In examining the results, one should first of all consider the possible errors in the two experimentally determined parameters, the decay constant, and the decay energy. The calculated value for the nuclear radius is fairly insensitive to a variation in decay constant; for example, a 10 percent error in the half-life determination would only change the radius by about $\frac{1}{4}$ percent. However, an error of only 0.02 Mev in decay-energy will change the radius by 1 percent, and it may be remarked that the energies of most of the nuclides shown in Table I are possibly in error by this amount and some by more.

It should be pointed out that the details of nuclear binding for this broad region are not sufficiently well known to give an *a priori* reason why all nuclear radii in this region should not deviate from the normal by more than some arbitrary degree such as 1 percent. Nevertheless, because of the agreement in so many cases, it is worth while examining the experimental data for those few cases which deviate by significantly more than 1 percent.

The first such example from Table I is that of U^{238} whose radius calculated from its measured energy and decay constant is 3 percent too high. In making this calculation, the alpha-particle energy selected was 4.18 Mev (decay energy 4.25 Mev) measured by Clark, Spencer-Palmer, and Woodward[6] using an ionization chamber coupled to a pulse height discriminator. To eliminate the 3 percent discrepancy in radius, it would be necessary to increase the particle energy only to 4.23 Mev. It is undoubtedly worth re-examining the alpha-energy for U^{238}, particularly since older values are higher than the one we have chosen; see for example, 4.21 Mev by Schintlmeister and Lintner[7] and 4.23 Mev by Sizoo and Wytzes.[8]

The calculated radius for Th^{232} is 4 percent high, and here even more than was the case with U^{238}, there may be reason to question the measured alpha-energy before ascribing a real difference from the normal nuclear radius. In arriving at the nuclear radius, the alpha-particle energy selected[9] was 3.98 Mev while values as high[10] as 4.20 Mev have been reported. The value which would be required to eliminate the discrepancy in radius is 4.06 Mev. While the two cases cited represent the greatest differences between calculated and normal nuclear radii, there are others which will probably be changed by redetermination of alpha-energies.

The few examples of alpha-particle fine structure in even-even nuclides are of special interest since the correlations[1] showed that each of the alpha-groups appeared with its partial half-life in conformity with its decay energy. The quantitative agreement may be tested by the calculation of the nuclear radius since that calculated for one group should agree with that calculated from the other and both should agree with the *normal* relationship for an even-even nucleus. It is found that within experimental uncertainty these conditions do apply to even-even nuclei. Another way of stating this effect is to say that each alpha-group decays in an allowed manner as though it came from a separate even-even nucleus. In contrast, it has been shown[1] that wherever fine structure appears in nuclei with an odd nucleon, the ground state transition is highly forbidden and shorter range groups become progressively less prohibited.

Table II shows data on three cases of well-defined

[6] Clark, Spencer-Palmer, and Woodward, British Atomic Energy Project Report BR 522 (October, 1944).

[7] J. Schintlmeister and K. Lintner, Sitzber. Akad. Wiss. Wien, Abt. IIa, **148**, 279 (1939).
[8] G. J. Sizoo and S. A. Wytzes, Physica **4**, 791 (1937).
[9] Clark, Spencer-Palmer, and Woodward, British Atomic Energy Project Report BR 584 (March, 1945).
[10] J. Schintlmeister, Sitzber. Akad. Wiss. Wien, Abt. IIa, **146**, 371 (1937).

alpha-particle fine structure in even-even nuclei. For ionium the first value for the energy which is listed[11] is that of measurements which did not separately measure the different groups and resulted in something approaching a weighted mean. The next set of data[12] comes from a more recent determination in which the fine structure was determined. The differences in calculated nuclear radii illustrate the extreme sensitivity to alpha-energy, and show that in this case, the calculated nuclear radius is in better agreement with the normal value, using the refined measurements in which fine structure was separated. In the case of radiothorium, the same situation is found as that discussed for ionium.

The third example shown in Table II is that of radium, in which the uncertainty in experimental data was not in the energy of the short-range group but in its abundance. The energy of the ground state transition is known accurately as 4.877 Mev and the nuclear radius calculated from this is in good agreement with the normal. There is agreement among different investigators that the short-range group has a lower energy by 180 to 190 kev than the ground state transition. However, one published measurement of the abundance of this group gives about 10 percent,[13,*] while another gives 1.8 percent[14] resulting respectively in a positive and negative deviation from normal nuclear radius as shown in Table II. Recently, in this laboratory,[15] the abundance of this group has been redetermined as 4.3 percent which can be seen to give good agreement between calculated nuclear radius and the normal value.

The above examples were selected for discussion because of their classical importance and because some gave calculated radii with the greatest differences from the normal. One could discuss in turn all of the other nuclides shown in Table I in order to examine differences in calculated radii from the normal in terms of uncertainty in experimental data. For such a discussion to be profitable, more precise energy values should be available, since many of the values are not known to better than 20 to 30 kev and this uncertainty virtually encompasses the spread of deviations. It may also be noted that certain even-even nuclides such as Pu^{232}, Pu^{234}, and U^{228} were not included in these calculations. This was done principally because of the uncertainty in alpha-decay half-life for these electron capture unstable nuclides.

The even-even polonium isotopes are treated separately in Table III because it appears clear that these

TABLE III. Calculated nuclear radii for polonium isotopes.

Nuclide	α-energy	Half-life	Nuclear radius r	Deviation of r from normal (percent)
Po^{218}	6.11	3.05 min.	8.80	−0.6
Po^{216}	6.89	0.158 sec.	8.73	−1.1
Po^{214}	7.83	1.5×10^{-4} sec.	8.67	−1.5
Po^{212}	8.95	3.0×10^{-7} sec.	8.45	−3.6
Po^{210}	5.40	138 days	8.04	−8.0
Po^{208}	5.24	3.0 yr.	7.90	−9.3
Em^{212}	6.29	23 min.	8.36	−4.7

belong to a family in which some members have deviations of radii from the *normal* which are real. It is seen that from Po^{218} to Po^{208} there is a progressive shinkage in the nuclear radius, which shows its greatest increments between Po^{214} and Po^{212} and between Po^{212} and Po^{210}.

It has been suggested that in cases in which there may be a discontinuity in the value of the nuclear radius between parent and daughter, the meaning of the radius as calculated by the one-body theory is indefinite. The calculated deviation from the normal may be that of the parent, daughter, or of some hybrid depending upon the contribution of each form to the effective potential barrier. Perhaps some qualitative deductions on the contribution of parent and daughter can be made from an examination of Table III, bearing in mind the discontinuity in nuclear binding which occurs at neutron number 126 and proton number 82. The nucleus which contains both of these numbers is Pb^{208}. It would seem that the effect of 82 protons (in the daughter nucleus) on nuclear stability begins to disappear if there is a large neutron excess, since the calculated radii for Po^{218} and Po^{216} show scarcely significant departures from the normal. Either this is so or the daughter nuclear radius is non-operative in determining the potential barrier. For Po^{212} the observed negative departure could be explained by the effect of the daughter nucleus, Pb^{208}, on the potential barrier. The further shrinkage shown for Po^{210} must bring in the contribution of the parent, which in this case has 126 neutrons. We might then picture the effective potential barrier as some hybrid dependent upon both the parent and daughter nuclei. The similar large departure from the normal for Po^{208} simply means that a discontinuity in nuclear binding at a closed shell occurs only above the closed shell, and that the binding energies of nucleons in the vicinity below are as great or greater as that which completes the shell.

There is one other known even-even nuclide, Em^{212}, in which the neutron number 126 appears and should affect the nuclear radius. The facts of its low energy and measurable half-life alone attest to the correctness of this view as has already been discussed.[1,15] The present calculation shows a negative departure of nuclear radius of 4.7 percent.

[11] H. Geiger, Zeits. f. Physik **8X**, 45 (1922).
[12] Rosenblum, Valadares, and Vial, Comptes Rendus **227**, 1088 (1948).
[13] S. Rosenblum, Nucleonics 4, No. 3, 38 (1949).
* *Note added in proof:* Rosenblum, Guillot, and Bastin-Scoffier, Comptes Rendus **229**, 191 (1949) have obtained more accurate data on the alpha-particle groups of Ra^{226}. In particular, they list the abundance of the group at about 4.61 Mev (particle energy) as 6.9 percent which brings about better agreement between measured half-life and that calculated.
[14] W. Y. Chang, Phys. Rev. **70**, 632 (1946).
[15] Ghiorso, Meinke, and Seaborg, Phys. Rev. **76**, 1414 (1949).

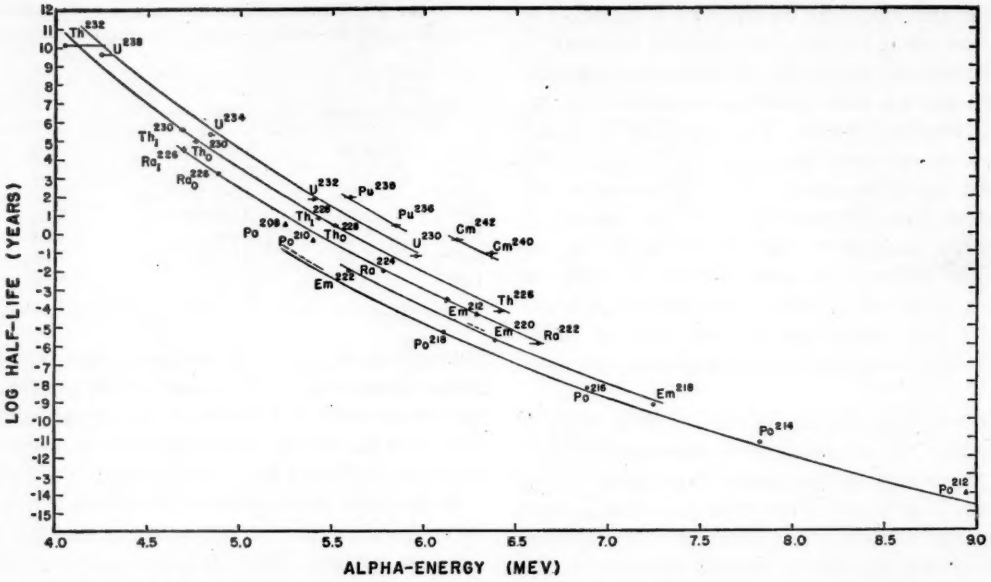

FIG. 1. Calculated curves and experimental points for the half-life *vs.* decay-energy relationship. ○ Alpha-emitters which may have normal nuclear radii. △ Alpha-emitters with abnormally small nuclear radii.

One of the graphical methods for comparing the variables which describe the alpha-decay process consists of a plot of half-life, or decay constant, against the decay energy in which the variable Z is eliminated as an arbitrary variable by joining points of constant Z.[1,3] This results in a family of curves which for the even-even nuclides are sufficiently regular[1] that it may be deduced that the position of a point is either insensitive to nuclear radius or that nuclear radii vary in a regular fashion, as has already been assumed. It is possible to justify a comparison of such empirical curves with theoretical curves defined by assuming values for the nuclear radius. In defining the *normal* nuclear radii as a simple function of the mass number and realizing that for normal nuclei the decay energy varies regularly with mass number for each element,[1] it is seen that single curves of the type shown in Fig. 1 will result.

Figure 1 shows experimental points in comparison with theoretical curves which were constructed in the following manner. For each measured even-even nuclide or alpha-group, the half-life was calculated by using its measured energy and assigning it a *normal* nuclear radius. These points define the curves of Fig. 1; the excellent agreement of most of the experimental data indicates the validity of the assumptions and of the theory. The agreement in the case of fine structure is worthy of special note. As already mentioned, a point below the curve, such as is the case for U^{238}, may mean that the measured energy is in error or that its nuclear radius is greater than normal. Its half-life could hardly be sufficiently in error to bring about the observed disagreement. A point above the curve may mean an experimental error in the opposite direction, an abnormally low nuclear radius, or, as is the case for odd nuclei, the alpha-decay may be forbidden for reasons peculiar to such nuclei.

Special mention should be made of the polonium curve since this illustrates the difficulties in presenting data on this type of plot for nuclei in which the nuclear radii are obviously not normal. The portion of the curve between the positions of Po^{218} and Po^{212} is normal and the half-lives taken from the curve may be thought of as those which each isotope would have if its decay-energy were as measured, but its nuclear radius were normal. This would mean in the case of Po^{212}(ThC′) that its short half-life is 0.3 microsecond would actually be less than 0.1 microsec. if it were *normal*. Returning to the polonium curve of Fig. 1 in the energy region below Po^{218}, this portion of the curve now applies to isotopes of higher mass numbers (at present not known) and those of low mass number such as Po^{210}, and is therefore not a single curve. By estimating the alpha-energy of Po^{220} as 5.3 Mev, it is possible to calculate its half-life and extend the normal curve shown as the solid line in Fig. 1. However, because of the great difference in mass number, the normal curve for Po^{208} and Po^{210} would lie somewhat higher and is indicated as a segment of broken line. This segment represents the hypothetical half-life *versus* decay-energy curve for polonium isotopes in this mass-number range if they could have both normal nuclear radii and the measured energies. Its only significance is that it should be the baseline for comparing half-lives in ascertaining the effect of nuclear radius on prohibition of alpha-decay. It will be noted that the one other even-even nuclide in this category Em^{212}, should be treated similarly.

We wish to thank Dr. Kenneth Street for valuable discussions and suggestions concerning this paper.

On the Magnetic Moments of Tl^{203}, Tl^{205}, Sn^{115}, Sn^{117}, Sn^{119}, Cd^{111}, Cd^{113}, and Pb^{207}*,†

W. G. Proctor
Department of Physics, Stanford University, Stanford, California
(Received February 17, 1950)

A radiofrequency spectrometer for observing nuclear induction signals is described. The use of crossed radiofrequency coils allows, in a simple fashion, the determination of the signs of the magnetic moments. The spectrometer has been used to determine the magnetic moments and magnetic moment ratios given in Table II. These values are based on a proton moment, without diamagnetic correction, of (2.7935±0.0003) nuclear magnetons.

I. INTRODUCTION

THE phenomenon termed "nuclear magnetic resonance absorption"[1] or "nuclear induction"[2] by the two originating groups at Harvard and Stanford, respectively, has certain characteristic advantages for the observation of nuclear moments. One of them, its high accuracy, is of particular interest for the results obtained on the lightest nuclei,[3–8] since they can be readily interpreted in terms of nuclear forces. Another advantage lies in the fact that it can be applied to practically any element, and it is this feature which has been partially used in the work presented here, on the magnetic moments of Tl^{203}, Tl^{205}, Sn^{115}, Sn^{117}, Sn^{119}, Cd^{111}, Cd^{113}, and Pb^{207}.

In the design of apparatus used to measure a variety of nuclei two principal aspects must be kept in mind. The first is that, due to sample limitations such as low natural abundances, limitations in solubility, or unfavorable relaxation times, signals may occur with amplitude less than the noise contained in a convenient audio band-width within which nuclear induction signals are usually amplified. Through a radiofrequency amplification stage, preceding the rectifier and subsequent audio amplifier, it is possible to reduce the noise, due to shot effect, to a point at which the Johnson noise of the receiving circuit represents substantially the only limitation. A further reduction of the noise can then be obtained only by extending the observation over a longer time so that the noise fluctuations are largely canceled out; a practical method for achieving this aim is the use of a narrow band width. A second aspect is due to the circumstance that the magnetic moments and spins may only be approximately known or not known at all, so that the frequency of resonance cannot be anticipated. This calls for an automatic apparatus which can be made to examine a given range of radiofrequencies while making a record of any resonance that may occur. An instrument combining these two features was first devised and used successfully by Pound, and we have, in some respects, followed his design.[9]

Through mutual exchange of experience and parallel improvements, the originally rather different techniques employed at Harvard and Stanford have now developed to a point at which they are similar in many respects. We should like, however, to emphasize one of the main differences: While in the Harvard technique one observes the voltage induced by the precession of the nuclear moments in the same coil which provides the driving r-f field, a separate "receiver coil," wound at right angles both to the driving "transmitter coil" and to the d.c. magnetic field, is used in the Stanford technique for the observation of nuclear induction. It is primarily a matter of habit and experience which of the two arrangements one considers to be the simpler and easier to operate. The crossed coil arrangement has, however, the undeniable advantage that it gives directly the sign of the magnetic moment. This arises from the circumstance that the crossed coils intrinsically imply a sense of rotation around the d.c. field, a feature which the single coil arrangement does not possess. The fact that the sign of a nuclear moment is one of the relevant pieces of information to be obtained seemed to us to be a sufficient justification for our preference of crossed coils. The comparison of signs is one of the simple and regular routines which have been carried out in the performance of the measurements presented here.

Throughout this work we have used liquid samples with the advantage that narrow lines can usually be expected and that the addition of paramagnetic catalysts for the rapid establishment of thermal equilibrium is relatively simple. The chemical composition of the solute and that of the catalyst have been chosen in every case to obtain solutions of appropriate concentration.

To measure the gyromagnetic ratio of a nucleus, its resonance frequency is compared in the same field

* This paper is based on a thesis to be submitted to the Department of Physics and the Committee on Graduate Study of Stanford University in partial fulfillment of the requirements for the degree of Doctor of Philosophy.

† Assisted by the joint program of the AEC and ONR.

[1] Purcell, Torrey, and Pound, Phys. Rev. **69**, 37 (1946).
[2] Bloch, Hansen, and Packard, Phys. Rev. **69**, 127 (1946).
[3] H. L. Anderson and A. Novick, Phys. Rev. **71**, 372 (1947).
[4] Bloch, Graves, Packard, and Spence, Phys. Rev. **71**, 373, 551 (1947).
[5] Bloch, Levinthal, and Packard, Phys. Rev. **72**, 1125 (1947).
[6] Bloch, Nicodemus, and Staub, Phys. Rev. **74**, 1025 (1948).
[7] H. L. Anderson and A. Novick, Phys. Rev. **73**, 919 (1948).
[8] H. L. Anderson, Phys. Rev. **76**, 1460 (1949).

[9] R. V. Pound, Phys. Rev. **72**, 527, 1273 (1947); **73**, 523, 1112 (1948). The essential feature of Pound's apparatus, the use of a self-excited oscillating receiver of special design, is not incorporated in our spectrometer.

with that of another nucleus, the gyromagnetic ratio of which is known. The two frequencies would be in proportion to their gyromagnetic ratios, if it were not for the diamagnetic field corrections, due to atomic electrons, which are only known with limited accuracy. A summary of results, presented in Table II, has not included any diamagnetic correction in the computation for magnetic moments; instead, the magnitude of this correction has been given separately, in order to keep the experimental and the theoretical values distinct.

The uncertainty of the diamagnetic field corrections, however, does not enter into the calculation for the ratio of the gyromagnetic ratios of isotopes, since the same percentage corrections apply here for each. The elements whose nuclei have been chosen for measurement (except Pb^{207}) have been those which have isotopes of the same spin, so that the relatively small effect on the magnetic moment by adding two neutrons to a nucleus may be measured with good accuracy. Tin is the only element which has three stable isotopes of substantial abundance, Sn^{115}, Sn^{117}, and Sn^{119} each having a spin $\frac{1}{2}$ and differing in turn by two neutrons. For this reason, this sequence was considered particularly interesting; together with the cadmium isotopes Cd^{111} and Cd^{113} one obtains a sequence of five nuclei differing in turn by two nucleons.

II. APPARATUS AND METHOD

A. Outline of Spectrometer Design

The operation of the spectrometer is best understood with the aid of the block diagram, given in Fig. 1. The rectifier supplies current for the magnet; this current is regulated by hard tubes in the regulator. The d.c. magnetic field produced is modulated at a rate of 92.5 c.p.s. by the driver unit, which supplies current at this frequency to coils mounted on the nuclear induction head, located between the pole faces of the magnet. The head, described in greater detail below, contains a transmitter coil which is part of the plate impedance of a radiofrequency oscillator. The head also contains a tuned receiver coil, perpendicular to the transmitter coil and to the magnetic field, in which the nuclear signals are induced. The induced

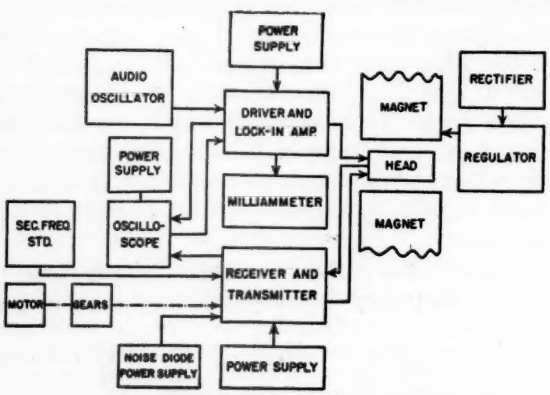

FIG. 1. Block diagram of the spectrometer.

voltages are first amplified by a radiofrequency amplifier; after rectification by a diode, the nuclear induction signals are further amplified at audiofrequencies by an amplifier, built in the oscilloscope, and presented as vertical deflections on the screen. The horizontal deflection of the oscilloscope trace is provided by a voltage derived from the driver and therefore of the same frequency as the modulating field. If, for a given radiofrequency, the range of the modulated magnetic field includes the resonance value, there will thus be traced upon the screen two resonances during each cycle of the field modulation. Except for the introduction of the

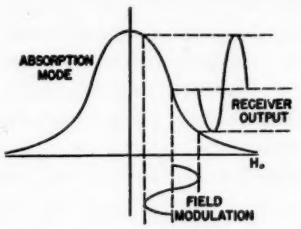

FIG. 2. Absorption mode for slow passage, illustrating receiver output for a sinusoidal field modulation.

radiofrequency amplification stage preceding the rectifying diode, the method described so far is largely the same as that explained in detail in the original paper of Bloch, Hansen, and Packard.[10]

The nuclear induction signals, in order to be observable on the oscilloscope screen, must be larger than the noise also presented there. If, for reasons such as those given in the introduction, this is not the case, they can nevertheless be made visible by taking a photograph of the oscilloscope screen, making a long exposure so that the random noise fluctuations are smoothed out.[11] Another alternative is based upon reduction of the band width; it is this method, first outlined by Pound[9] and by Bloembergen, Purcell, and Pound,[12] which we have followed and which is described below.

The radiofrequency flux intensities from the nuclei in the receiver coil can be resolved into two characteristic phase components, one in phase with the impressed radiofrequency field and one 90° behind it; the latter corresponds to dispersion and is called the *u*-mode, while the former is the *v*-mode and corresponds to absorption.[13] Either mode can be observed by homodyning the nuclear induction voltage with a radiofrequency voltage which is large compared to the maximum amplitude of the former and of the same phase as the desired mode.[12] Described as a function of the radiofrequency deviation from resonance $\Delta\omega$, the amplitude of each mode has its characteristic shape and magnitude. The work described in this paper has been done using the *v*-mode signal under slow passage conditions described by Bloch who derived the formula

$$v = M_0 \frac{\gamma H_1 T_2}{1+(\Delta\omega T_2)^2+\gamma^2 H_1^2 T_1 T_2}, \qquad (1)$$

[10] Bloch, Hansen, and Packard, Phys. Rev. **70**, 474 (1946).
[11] F. Bloch and D. H. Garber, Phys. Rev. **76**, 585 (1949).
[12] Bloembergen, Purcell, and Pound, Phys. Rev. **73**, 679 (1948).
[13] F. Bloch, Phys. Rev. **70**, 460 (1946).

where M_0 is the equilibrium polarization per unit volume of the sample, H_1 the half-amplitude of the exciting radiofrequency field, T_1 and T_2 the longitudinal and transverse relaxation times, respectively, and γ the gyromagnetic ratio of the nucleus in question.

In Fig. 2 we have plotted the v-mode as it would appear upon slow, monotonic variation of the d.c. field H_0 in the neighborhood of resonance. If, instead, the field is modulated sinusoidally over a relatively small region as indicated, one will obtain from the audio output of the receiver a signal which contains principally the first harmonic of the modulating frequency. It appears with the largest amplitude and opposite phase if the center of the modulation is located near one or the other of the two points of inflection of the v-mode, and its first harmonic content is here comparable to the maximum of this mode, if the sweep amplitude is chosen to be of the order of the line width. The observation of the first harmonic alone gives under these conditions practically the full magnitude of the available signal, while sweep amplitudes which are either small or large compared to the line width result in an appreciable loss of signal magnitude.

The output of the receiver is analyzed, as indicated in Fig. 1, by a "lock-in amplifier"[14] for the presence of voltages of the sweep frequency, resulting in a direct current whose magnitude is proportional to the amplitude and whose sign depends on the phase of the input voltage. This current is smoothed by an RC-filter, and it is registered on a chart by a recording, d.c. milliammeter. If the frequency response of the recording milliammeter is sufficiently high, one has an output band width of the spectrometer given by $1/\pi RC$, where RC is the product of the resistance R and capacitance C determining the final output time constant. With a noise voltage proportional to the square root of the pass-band width, one thus obtains upon the milliammeter record a signal-to-noise ratio equal to (signal-to-noise ratio present at the receiver output) $(\pi RC \times$ receiver-band width in c.p.s.$)^{\frac{1}{2}}$ (α), where α is a number less than unity which has been introduced to account for the loss of signal described above. By utilizing this method within practical limits, a large improvement in the signal-to-noise ratio can be realized.

If the transmitter and receiver are tuned together while the frequency is varied slowly and the magnetic field remains fixed, the recording milliammeter will record the presence of a resonance. In this way the apparatus may be used to search for nuclear resonances. It is only necessary that the rate at which the radiofrequency is changed is such that the time which it takes to vary the frequency through a line width is long compared to RC. With a sweep amplitude comparable to the line width one records, in this way, essentially the derivative of the resonance line as a function of the frequency.

It was pointed out in the introduction that the use of crossed transmitter and receiver coils enables the spectrometer to distinguish the sign of nuclear moments. This is due to the fact that the phase relation between the nuclear signal induced in the receiver coil and the radiofrequency voltage across the transmitter coil is inverted for nuclear moments with opposite sign. Superimposed in a linear detector upon the homodyning "local oscillator" voltage derived from the driving radiofrequency field, the radiofrequency nuclear induction signal manifests this phase relation through the sign of the audiofrequency signal, which, according to Fig. 2, will determine the sign of the recorded trace. Hence, if two nuclei are observed, leaving all radiofrequency and sweep-frequency conditions unchanged and achieving their respective resonances through a

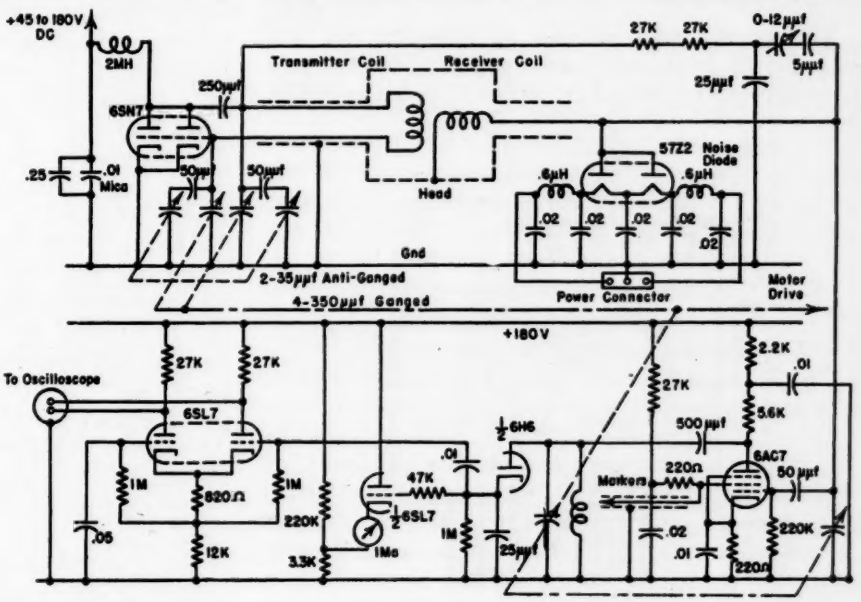

FIG. 3. Circuit diagram of the transmitter and the receiver.

[14] R. Dicke, Rev. Sci. Inst. 17, 268 (1946).

mere change of the d.c. field, the relative sign of their recorded signals will tell directly whether the signs of their magnetic moments are the same or opposite.

With the sign of the moment manifested in the manner described and the gyromagnetic ratio given by the value of the resonance frequency, there remains one more important piece of information, furnished by the magnitude of the signal. Indeed, the voltage induced in the receiver coil by the nuclei is, among other factors, strongly dependent upon their spin. Its value could be ascertained from the magnitude of the recorded signal by calibrating the total gain of the radiofrequency, audio, and d.c. circuits. A simpler procedure is, however, to compare the signal magnitudes from the nucleus of type a under observation and from a nucleus of type b with known spin by merely changing the value of the field H_0, leaving all other conditions of observation unchanged, as in the determination of the relative signs mentioned. Indeed, if H_1 is made small, so that $\gamma^2 H_1^2 T_1 T_2 \ll 1$, and if the signals are modulated with a small amplitude of magnetic field, it follows from Eq. (1) and the Curie expression for M_0 that

$$r=[n_a I_a(I_a+1)\gamma_a{}^3 T_{2a}{}^2]/[n_b I_b(I_b+1)\gamma_b{}^3 T_{2b}{}^2], \quad (2)$$

is the ratio of the maximum derivative of the signal from n_a nuclei of spin I_a to that of n_b nuclei of spin I_b, contained in the sample where $\gamma_{a,b}$ and $T_{2a,b}$ are their respective gyromagnetic ratios and transverse relaxation times. With I_b being known and the other quantities readily measureable, I_a can thus be determined from (2). Throughout this work we have made use of this relationship to check spin values, although in the instances observed so far this has merely served as a verification of results known previously from hyperfine structure measurements.

B. Detailed Description of Principal Components

The magnet used with the spectrometer has pole faces $7\frac{13}{16}$ in. in diameter and a gap of $1\frac{3}{4}$ in. The pole faces have been shimmed to obtain a more homogeneous field in the central region, but this procedure has not been carried out to the highest perfection. For a typical cylindrical sample contained in a test tube, 1.3 cm in diameter and 2.5 cm in length, the variation of the magnetic field over the region occupied by the sample was about 3×10^{-3} percent.

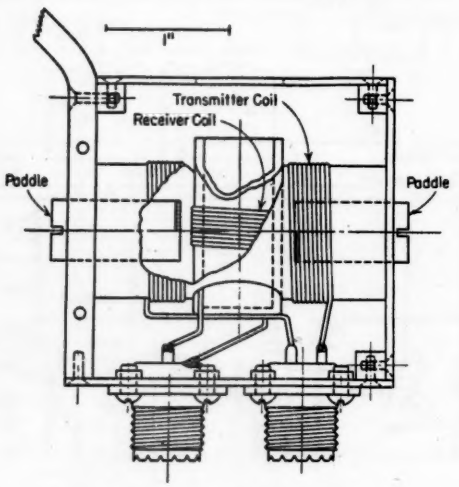

FIG. 4. Side view of the head, with cut.

There are two water-cooled windings, one around each pole piece. Each winding consists of about 17,000 turns of B and S No. 18 copper wire, so that the magnetization arises from a large number of turns rather than from a large current. This feature makes it possible to regulate the current by hard tubes, specifically eight $304TL$'s in parallel. In the unsaturated region the magnetic field changes by 10 gauss/ma; a current of 2 amp. produces slightly less than 12 kgauss. The voltage for 2 amp. is about 3000 v, which is supplied, after transformer step-up, by full-wave rectification from the 220-v, 3-phase lines. To obtain current regulation the magnet current is passed through a variable resistor of high wattage. The difference of the voltage across this resistor and that of a 28.5-v battery is amplified in a d.c. amplifier of two stages with a total gain of 1600. The output is applied to the grids of the hard tubes, thus providing a feedback capable of reducing line voltage variations of five percent to current variations of 0.0005 percent approximately, depending on the magnitude of the variable resistor. The warming up of the magnet windings causes current drifts which, however, subside about one hour after turning on.

The essential radiofrequency components of a nuclear induction apparatus are the transmitter, providing the driving radiofrequency field, the "head" in which the sample is located, and the receiver circuit. They are diagrammatically shown in Fig. 3. The transmitting circuit is a Colpitts oscillator, with a capacitance feedback ratio almost exactly equal to two. A series of commercial B-batteries serves as a source of constant plate voltage variable between 45 and 180 v. The half-amplitude H_1 of the driving radiofrequency field increases with increasing voltage and can be varied between 0.13 and 0.82 gauss. The same set of batteries also supplies 180 v for the plate voltage in the receiver circuit. The inductance of the transmitter coil in the head is resonated by variable condensers ganged with the tuning condensers of the receiver. This allows a continuous frequency variation between 4.35 and 9.00 Mc and thereby in the range of d.c. field between 12,000 and 1020 gauss the observation of nuclei with gyromagnetic ratios ranging between 2.28×10^3 and 5.52×10^4 gauss^{-1} sec.$^{-1}$. As standards of comparison in this range we have used the nuclei H^1, Na^{23}, and H^2, for which the spins as well as the signs and, with high accuracy, the magnetic moments are known.

The construction of the head is shown in its side view, Fig. 4, with one shielding plate removed. It is of the type first used by Bloch and Garber[11] with the advantage over previously described forms[15] that the

[15] M. Packard, Rev. Sci. Inst. 19, 435 (1948).

sample can be simply inserted through an opening without interruption of the operation of the apparatus. This is achieved by splitting the transmitter coil into two halves of approximate Helmholtz proportions, leaving the center free for the hollow receiver coil form, shown in the cut with an inner diameter sufficient to accommodate 15-mm test tubes. Receiver and transmitter coils are held rigidly on Lucite forms and are shielded by a silver-plated brass shell. Two Lucite "paddles,"[10] carrying semicircular copper disks at their inner ends, are used to control by their rotation the inductive coupling of the receiver coil to the transmitter coil. The head has a depth of $1\frac{1}{4}$ in.; its other dimensions are indicated by the scale given in Fig. 4. The coils which are used to modulate the field H_0 are cemented to the outside of the shielding plates, and they are likewise of Helmholtz proportions.

The receiver coil is resonated in order to enhance the induced voltage by the resonance rise factor Q. This enhanced voltage appears across a tuning condenser in the receiver, from which point it is amplified as a radiofrequency voltage, detected, and amplified again as an audio signal, the audio band width of the detector time constant and amplifier band pass being 5 kc. The radiofrequency amplifier, detector, and audio amplifier are conventional, although there are some unusual features which merit a short discussion.

There are two controls used to adjust the magnitude and phase of the radiofrequency "leakage" voltage applied to the grid of the radiofrequency amplifier for the purpose of serving as a homodyning voltage for the nuclear induction signals. The amplitude and phase of this leakage voltage is important for detector sensitivity and for determining which mode of the resonance is to be observed. The purpose of the 35-$\mu\mu$f antiganged condensers shown in Fig. 3 across two of the principal tuning condensers is to change the ratio of the capacitances of these two tuning condensers without changing their total capacitance. By this change the center point of the radiofrequency voltage across the transmitter coil can be varied without changing the frequency. Since the receiver coil is grounded at one end, its effective capacitive coupling to the transmitter coil is sensitively dependent upon the center voltage of the latter. The above-mentioned change of the 35-$\mu\mu$f condensers provides thus a variable, capacitively induced voltage in the receiver circuit. This voltage has the same phase as that across the transmitter coil and therefore controls the v-mode leakage. The RC network indicated in the upper right of Fig. 3 provides principally a potential across the capacitance which lags in phase 90° behind the potential across the transmitter coil and thus contributes to the homodyning phase component of the u-mode. A small voltage of this phase is coupled to the radiofrequency amplifier grid by means of the 0- to 12-$\mu\mu$f variable capacitance shown. By means of these two controls it is possible to observe either the pure v-mode or the pure u-mode or any mixture of them.

TABLE I. Data from the measurements on Sn^{115}.

Nucleus	Time of resonance in minutes	Resonance frequency in kilocycles
Sn^{115}	9	6236.2
	60	6236.7
	106	6236.7
	328	6236.3
	378	6236.0
Na^{23}	27	5044.9
	75	5044.7
	161	5044.6
	343	5044.5
	396	5044.5

To obtain, for example, the pure v-mode, the paddles are first adjusted to eliminate the principal part of the in-phase voltage, which is induced in the receiver coil. Proper setting of the 0- to 12-$\mu\mu$f condenser provides cancellation of the remaining u-mode leakage and the antiganged 35-$\mu\mu$f condensers, serving as a fine control for the in-phase leakage, are adjusted to provide, after amplification, a homodyning voltage of approximately 0.2 v r.m.s., sufficient for linear detection. Conversely, by using the u-mode control to obtain a sufficient voltage of the other phase component and canceling the remaining in-phase leakage by means of the v-mode control, one can observe the pure u-mode.

The noise diode, shown connected directly to the receiver coil, serves the purpose of calibrating the observed noise against the known shot noise in the diode. It is inoperative when its filaments are cold, and is turned on by applying heater power through the indicated connector. For low levels of oscillation, a noise figure of four is obtained; this means that the noise power per unit band width in the spectrometer output is four times as great as that which one would expect, were there no noise other than the amplified Johnson noise from the resonated receiver coil.

The harmonics of a 25-kc multivibrator from a commercial secondary frequency standard are coupled to the screen grid of the radiofrequency amplifier. Tube currents proportional to the product of the control grid and screen grid potentials give rise to audio beats between the radiofrequency leakage from the transmitter and these harmonics. When the beat frequency is near the sweep frequency, the beats are detected by the lock-in amplifier, and a characteristic mark is made on the tape of the recording milliammeter.

The meter shown carries a current proportional to the average cathode potential of the detecting diode; it serves to register the amplified amount of leakage, and its use is important during adjustment.

The ganged receiver and transmitter capacitors are turned by a clock motor. The rate is variable, and it is chosen according to the line width of the resonance being observed and the final band width of the spectrometer. As an example, a final band width frequently used is 0.069 c.p.s.; for nuclei with a gyromagnetic ratio of 10^4 gauss^{-1} sec.$^{-1}$, providing a line of one gauss

TABLE II. Magnetic moments and diamagnetic corrections.

Nucleus	Magnetic moment in nuclear magnetons	Diamagnetic correction in percent
Cd^{111}	-0.5923 ± 0.0001	0.47
Cd^{113}	-0.6196 ± 0.0001	0.47
Sn^{115}	-0.9134 ± 0.0002	0.50
Sn^{117}	-0.9951 ± 0.0002	0.50
Sn^{119}	-1.0411 ± 0.0002	0.50
Tl^{203}	1.5962 ± 0.0003	0.98
Tl^{205}	1.6118 ± 0.0003	0.98
Pb^{207}	0.5837 ± 0.0001	1.00

Ratios of magnetic moments

$\mu(Cd^{113})/\mu(Cd^{111}) = 1.0461\pm0.0001$
$\mu(Sn^{117})/\mu(Sn^{115}) = 1.0894\pm0.0001$
$\mu(Sn^{119})/\mu(Sn^{117}) = 1.0465\pm0.0001$
$\mu(Tl^{205})/\mu(Tl^{203}) = 1.0098\pm0.0002$

between points of maximum slope, a sufficiently slow rate is 2 kc/min. Searching the complete frequency range at this rate would require 39 hours.

In order to have constant leakage voltage over a wide frequency range it would be necessary that the capacities of the two tuning condensers of the transmitter remain equal to each other while the frequency changes. In practice, this cannot be achieved with sufficient accuracy since the leakage is very sensitive to any difference between these capacities. This imperfection is not serious, however, over a frequency interval of as much as 1 Mc, and the amplified leakage voltage in this interval remains less than 1 v r.m.s., causing no appreciable increase in the noise figure. The u-mode leakage is considerably less sensitive to frequency change and remains negligible if it is canceled at one frequency; hence, if the spectrometer is adjusted for v-mode observation, it will remain adjusted for this mode.

The lock-in amplifier has been described by Dicke.[14] We have used total output time constants of 1.2 and 4.7 sec., corresponding to final band widths of 0.28 c.p.s. and 0.069 c.p.s., and calculated reductions by factors of 130 and 270, respectively, of the noise voltage from the receiver output band pass of 5 kc.

C. Use of the Spectrometer

Before a nuclear resonance frequency can be measured with appreciable accuracy, the occurrence of the signal and its approximate frequency must first be established; consequently, the spectrometer is first used to search for the resonance of the nucleus in question.

Liquid samples are preferred because they usually lead to sharp lines, and because the nuclear relaxation times can be controlled by the addition of paramagnetic ions.[10,12] In these experiments the paramagnetic ion Mn^{++} has been used as catalyst and was brought into the solution by dissolving a suitable salt. Equation (1) may be used to show that v_{max}, the value of v for $\Delta\omega=0$, as a function of H_1 has a maximum $(v_{max})_{max} = (M_0/2)(T_2/T_1)^{\frac{1}{2}}$ for $H_1=1/\gamma(T_1T_2)^{\frac{1}{2}}$. To obtain signals of enhanced amplitude, it is helpful to shorten T_1 until it is comparable with T_2 which will normally be the case when the line broadening caused by the addition of paramagnetic ions is of the order of that due to field inhomogeneities. Mn^{++}, having a moment of 5.9 Bohr magnetons, provides a thermal relaxation time T_1 of about 3×10^{-5} sec. for protons in a 1.0 molar aqueous solution of $MnSO_4$. For other nuclei, and for other paramagnetic ions, the thermal relaxation time can be estimated[12] from the above value by taking the relaxation time to be inversely proportional to the product (concentration of paramagnetic atoms) (magnetic moment of paramagnetic atom)^2 (viscosity of sample) (gyromagnetic ratio of nucleus in question).[2] In view of the rather complicated features underlying the mechanism of relaxation, this relationship can claim only qualitative validity, but it is nevertheless useful as a guide for choosing a suitable concentration of paramagnetic salt.

To obtain suitable conditions for signal observation, the magnitudes of the sweep field and the radiofrequency field must be both chosen of the order of the expected line width, the amplified leakage voltage must be adjusted to about 0.5 v r.m.s. and the gain of the lock-in amplifier made large enough to make the expected signal visible on the tape. Guided by spectroscopic values, as we have been for all nuclei reported on here, a range of frequencies likely to contain the resonance is chosen. It is automatically explored as the clock motor provides a continuous frequency variation while a trace is drawn on the chart by the recording milliammeter. We have usually taken search runs of approximately 10-hr. duration, turning the apparatus on in the evening and examining the milliammeter record for a resonance the next morning.

Once the frequency of a nuclear resonance is known approximately, and it is desired to measure this resonance frequency as exactly as possible, the leakage phase is carefully adjusted for observation of the pure v-mode, and the secondary frequency standard is set to generate 25-kc markers. Since the frequency is known approximately, it is possible to set the transmitter to a frequency which is just below the first marker below resonance. Hence, after the motor has begun to turn the condensers, a marker is made, the resonance is drawn, and a second marker is made, whereupon the sought-for resonance frequency can be determined by interpolation between the two markers. To calibrate the gyromagnetic ratio against that of a known nucleus, it is necessary to observe similarly the resonance frequency of the latter by turning the condensers to an appropriate position, without changing the magnetic field.

Since the two resonances are not observed at the same time, one has to anticipate the possibility of drifts in the magnetic field between their observation. We therefore have followed the procedure of alternately repeating, at least three times, the pattern of the two

resonances in the fashion described. The time at which each resonance occurs is automatically recorded by the recording milliammeter, since the chart moves at a uniform speed. The resonance frequencies of the two nuclei may be plotted as a function of time, and by interpolation their values can be obtained as they would appear if measured at the same time and hence at the same value of the magnetic field. Typical data, from the measurements on Sn^{115} and Na^{23}, are given in Table I.

III. MEASUREMENTS

We shall give here a detailed description of a series of measurements which have been made, using the methods and apparatus described in the preceding section. Short reports of the results have already been published.[16–18]

A. Measurements on Tl^{203} and Tl^{205}

At the time when the measurements to be described were made, the magnetic moment of Tl^{205} was well known from nuclear induction;[19] the best value for Tl^{203}, however, depended on the spectroscopically determined ratio of the magnetic moments of these two isotopes.[20] It seemed worth while to determine the ratio of these two moments with higher accuracy while the measurement of the magnetic moment of Tl^{205} served merely as a check upon the previously published result.

The sample consisted of an aqueous solution of 2.6 molar $Tl(C_2H_3O_2)$ with 0.03 molar $MnSO_4$. Eight experiments were made in which the resonances of Tl^{203}, Tl^{205}, and H^1 from the same sample were in turn observed four times. The first four of these experiments were performed at 1500 gauss and the last four at 1900 gauss.[21] The final frequency ratios were determined to be

$$\nu(Tl^{203})/\nu(H^1)=0.5714\pm0.0001 \quad (3)$$

$$\nu(Tl^{205})/\nu(H^1)=0.5770\pm0.0001 \quad (4)$$

$$\nu(Tl^{205})/\nu(Tl^{203})=1.0098\pm0.0002. \quad (5)$$

The value (4) agrees well with Poss' value,[19] as do the ratios (3) and (5) with those subsequently published by Poss.[22] The ratio (5) is in good agreement with the spectroscopic value

$$\mu(Tl^{205})/\mu(Tl^{203})=1.00966\pm0.0004,$$

given by Schüler and Korsching.[20]

With the magnetic moment of the proton taken to be[23] $(2.7935\pm0.0003)\mu_N$ and with the spin of both isotopes having a value $\frac{1}{2}$, one obtains directly from the frequency ratios,

$$\mu(Tl^{203})=(1.5962\pm0.0003)\mu_N, \quad (6)$$

$$\mu(Tl^{205})=(1.6118\pm0.0003)\mu_N. \quad (7)$$

The magnitude of the diamagnetic correction to be applied is given in column 3 of Table II, where all of the experimental results are summarized. The corrections indicated are to be applied in such a direction as to increase the magnitudes of the magnetic moments listed in the second column. The diamagnetic correction will be discussed in the final paragraph of this section.

The signs of both thallium nuclear magnetic moments were verified to be positive by the procedure outlined in Section II. The resonances of Tl^{203}, Tl^{205}, and H^1 were observed in a small frequency range, sufficient for their respective line widths, by changing the magnetic field accordingly. Since very little change in frequency takes place, there is no possibility that a leakage phase reversal of 180° could have taken place; hence the relative signs of their magnetic moments were determined upon inspection of the signals on the tape.

By the procedure outlined in Section II, a comparison of the maximum of the recorded resonances of H^1 and Tl^{205} led to a spin $\frac{1}{2}$ for Tl^{205}. Since the proton signal would otherwise have been about 60 times greater, it was attenuated in the audio system so as to make it comparable to that of Tl^{205}. The ratio of the signal amplitudes of the two thallium isotopes was in good agreement with the ratio of the abundances,[24] so that the spin of Tl^{203} was also indicated to be $\frac{1}{2}$. These results are in agreement with spectroscopic measurements.[25]

B. Measurements on Sn^{115}, Sn^{117}, and Sn^{119}

Spectroscopically the nuclei Sn^{115}, Sn^{117}, and Sn^{119} have been known[26,27] to have a spin of $\frac{1}{2}$, and their magnetic moments were determined to be $-0.86\mu_N$,[27] $-0.9\mu_N$,[28] and $-0.9\mu_N$,[28] respectively. Since the isotopes Sn^{117} and Sn^{119} have, respectively, natural abundances of 7.51 percent and 8.45 percent,[29] a short calculation reveals that a signal-to-noise ratio of about 10 should be available from a 5 molar solution of a tin salt in water and that their respective abundances should be sufficiently different to distinguish between the two resonances. Accordingly, an aqueous 5.3 molar solution of $SnCl_2$ with 1.0 molar $MnCl_2$ was used, and their resonances were found about 300 kc apart in the neighborhood of 7.0 Mc, with a magnetic field of 4500 gauss.

The resonances of Sn^{117}, Sn^{119}, and Na^{23} were then observed in turn until about three of each had been

[16] W. G. Proctor, Phys. Rev. **75**, 522 (1949).
[17] W. G. Proctor, Phys. Rev. **76**, 684 (1949).
[18] W. G. Proctor and F. C. Yu, Phys. Rev. **76**, 1728 (1949).
[19] H. L. Poss, Phys. Rev. **72**, 637 (1947).
[20] H. Schüler and H. Korsching, Zeits. f. Physik **105**, 168 (1937).
[21] The magnet used for the last four experiments was a battery-operated magnet with pole faces 10 in. in diameter, spaced $1\frac{15}{16}$ in. apart. All other measurements reported in this paper have been carried out with the magnet described in Section II.
[22] H. L. Poss, Phys. Rev. **75**, 600 (1949).
[23] H. Taub and P. Kusch, Phys. Rev. **75**, 1481 (1949).
[24] A. O. Nier, Phys. Rev. **54**, 275 (1938).
[25] H. Schüler and J. E. Keyston, Zeits. f. Physik **70**, 1 (1931); H. Schüler and T. Schmidt, Zeits. f. Physik **104**, 468 (1937).
[26] H. Schüler and H. Westmeyer, Naturwiss. **21**, 660 (1933).
[27] M. Gurevitch, Phys. Rev. **75**, 767 (1949).
[28] S. Tolansky, Proc. Roy. Soc. **144**, 574 (1934).
[29] Hintenberger, Mattauch, Seelmann-Eggebert, Zeits. f. Naturforschung **3a**, 413 (1948).

recorded; these observations were repeated once again. The resonance of sodium was obtained by exchanging the sample above with one composed of an aqueous solution of 0.69 molar NaCl with 1.0 molar $MnCl_2$. By the graphical method of interpolation mentioned in Section II to correct for field drifts, we find as the result of both experiments the following frequency ratios:

$$\nu(Sn^{117})/\nu(Na^{23}) = 1.3468 \pm 0.0001, \quad (8)$$

$$\nu(Sn^{119})/\nu(Na^{23}) = 1.4090 \pm 0.0001, \quad (9)$$

$$\nu(Sn^{119})/\nu(Sn^{117}) = 1.0465 \pm 0.0001. \quad (10)$$

Since the abundance of the isotope Sn^{115} is only 0.33 percent,[29] its resonance was not observed with the first sample. It was found, however, about 700 kc below that of Sn^{117} at the same magnetic field, using a sample prepared by dissolving $SnCl_2 \cdot 2H_2O$ in 2.0 molar $MnSO_4$ at the temperature of boiling water. This supersaturated solution of tin would not crystallize at room temperature for several hours; with the search extending over many hours, it was necessary to heat it at intervals. The concentration of tin in this sample proved to be about 2.5 times that of the first sample, and $MnSO_4$ was present to a molar concentration of 0.7. The frequency of resonance of Sn^{115} was compared to that of Na^{23} using a sample containing 0.2 molar NaCl with 0.2 molar $MnSO_4$. The signal-to-noise ratio of the recorded resonance was about two; the resonances of Sn^{115} and Na^{23} were recorded five times each, with the results shown in Table I. From these data we compute that

$$\nu(Sn^{115})/\nu(Na^{23}) = 1.2362 \pm 0.0001. \quad (11)$$

By dividing (8) by (11), one obtains

$$\nu(Sn^{117})/\nu(Sn^{115}) = 1.0894 \pm 0.0001. \quad (12)$$

With the magnetic moment of Na^{23} taken to be[30] $(2.2166 \pm 0.0004)\mu_N$, one obtains

$$\mu(Sn^{115}) = (-0.9134 \pm 0.0002)\mu_N, \quad (13)$$

$$\mu(Sn^{117}) = (-0.9951 \pm 0.0002)\mu_N, \quad (14)$$

$$\mu(Sn^{119}) = (-1.0411 \pm 0.0002)\mu_N. \quad (15)$$

These values differ from those reported earlier[31] because the diamagnetic correction has not been included in making these calculations and a slightly different value of the magnetic moment of Na^{23} has been taken. The ratios of these magnetic moments are given accurately by the expressions (10) and (12).

The isotopes Sn^{117} and Sn^{119}, with a known abundance ratio[29] 0.89, were identified by the ratio of the amplitudes of their signals. This same ratio, derived from the amplitude ratio of the two signals, was found to be 0.95 ± 0.06, while the opposite assignment would have given 1.05 ± 0.07, showing beyond reasonable doubt that the former assignment is the correct one.

Inspection of the recorded signals showed that the tin nuclei had the same sign of magnetic moment. A comparison of signals for the sign between Sn^{119} and Na^{23} showed these nuclei to have magnetic moments of the opposite sign, thus verifying that all three tin isotopes have negative magnetic moments.[32]

The spin of the tin nuclei were verified to be $\frac{1}{2}$ from a comparison of their signal amplitudes with each other and with that from Na^{23}.

C. Measurements on Pb^{207}

Of all the naturally occurring isotopes of lead, only one, the isotope 207, with an abundance of 21.1 percent, has an odd number of neutrons. Since hyperfine structure measurements have indicated a spin[33] of $\frac{1}{2}$ and a magnetic moment of 0.6 nuclear magnetons,[34] one has sufficient data to calculate that a reasonably concentrated solution of some lead salt would provide a detectable signal. Accordingly, a sample containing an aqueous solution of 1.0 molar $Pb(C_2H_3O_2)_2$ with 0.8 molar $Mn(C_2H_3O_2)_2$ was prepared, and a signal was observed in the neighborhood of 5.8 Mc with a magnetic field of 6600 gauss.

The lead resonance was compared in frequency with that from Na^{23}, which was obtained by exchanging the the sample above with one composed of an aqueous solution of 0.69 molar NaCl and 1.0 molar $MnCl_2$. After four alternate measurements, the following frequency ratio was found:

$$\nu(Pb^{207})/\nu(Na^{23}) = 0.7901 \pm 0.0001, \quad (16)$$

which leads to

$$\mu(Pb^{207}) = (0.5837 \pm 0.0001)\mu_N. \quad (17)$$

The positive sign was verified by comparing the signal trace from the lead resonance to that obtained from the sodium resonance, when they both were made at the same frequency and no possibility of a change of leakage phase could have occurred.

Several measurements were made to determine the relative signal amplitudes of the sodium and lead resonances with the result that the spin of Pb^{207} was verified to be $\frac{1}{2}$.

D. Measurements on Cd^{111} and Cd^{113}

Various spectroscopic measurements on the hyperfine structure of cadmium were carried out before the publication of the review article by Bethe and Bacher,[34] who conclude that the isotopes Cd^{111} and Cd^{113} each have a spin $\frac{1}{2}$ and the same magnetic moment of -0.65

[30] The magnitude was computed using $\nu(Na^{23})/\nu(H^1) = 0.26450 \pm 0.0003$ given by F. Bitter, Phys. Rev. 75, 1326 (1949) and the value of the magnetic moment of the proton given by Taub and Kusch, reference 23.

[31] See references 17 and 18. Furthermore, it will be noted that the uncertainty in the frequency ratios given in (8)–(10), and (16) is smaller than given in the early report, reference 17. The improvement arises from correcting an error made in the previous calculations.

[32] The positive sign of Na^{23} has been taken from J. B. M. Kellogg and S. Millman, Rev. Mod. Phys. 18, 323 (1946).

[33] H. Kopfermann, Zeits. f. Physik 75, 363 (1932).

[34] H. A. Bethe and R. F. Bacher, Rev. Mod. Phys. 8, 82 (1936).

nuclear magnetons. Cadmium has eight naturally occurring isotopes but only Cd^{111} and Cd^{113} have an odd mass number, and these occur with an abundance of 13.0 and 12.3 percent, respectively.[35] The resonances were found at a field of 6600 gauss, with radiofrequencies in the neighborhood of 6.0 Mc, using a saturated sample of $CdCl_2$ in 0.3 molar $MnSO_4$. The frequency ratios were found to be

$$\nu(Cd^{111})/\nu(Na^{23}) = 0.8016 \pm 0.0001, \quad (18)$$

$$\nu(Cd^{113})/\nu(Na^{23}) = 0.8386 \pm 0.0001, \quad (19)$$

$$\nu(Cd^{113})/\nu(Cd^{111}) = 1.0461 \pm 0.0001. \quad (20)$$

Because of the equality of the spins, the last ratio again gives the ratio of the magnetic moments of the cadmium isotopes. The Na^{23} was obtained from an aqueous solution of 0.1 molar NaCl with 0.2 molar $MnSO_4$. These frequency ratios lead to the values

$$\mu(Cd^{111}) = -(0.5923 \pm 0.0001)\mu_N, \quad (21)$$

$$\mu(Cd^{113}) = -(0.6196 \pm 0.0001)\mu_N. \quad (22)$$

The signs were determined by comparing, under identical radiofrequency conditions, the cadmium resonances and that of I^{127}, the magnetic moment of which is positive.[36] The cadmium isotopes were identified by their different signal magnitudes, using samples[37] enriched to about 80 percent in Cd^{111} and Cd^{113}. Through comparison of the recorded signal magnitudes from cadmium and sodium, a spin of $\frac{1}{2}$ for both cadmium isotopes has been verified.

The sequence of isotopes, Cd^{111}, Cd^{113}, Sn^{115}, Sn^{117}, Sn^{119} was of interest to us since each of these nuclei differs from the preceding one by the addition of two nucleons. Without change in spin and sign, the magnitude of the moment shows a steady increase, in the ratio 1.000:1.046:1.542:1.680:1.758. While the significance of this fact is not yet capable of direct interpretation in terms of nuclear structures, it is likely to be connected with the circumstance that a "proton shell"[38] comes to a conclusion with tin. It also seems plausible that the relatively much larger increase, from Cd^{113} to Sn^{115}, caused by the addition of two protons is due to their charge, while the addition of two neutrons in the other cases, as in Tl^{203} and Tl^{205}, causes only an increase of a few percent. In this connection it may be worth noticing that the ratio of the magnetic moments of Cd^{113} to Cd^{111} is very nearly equal to that of Sn^{119} to Sn^{117}.

E. Discussion of Accuracy

The present spectrometer measures resonance frequencies with accuracies of about one part in 10^4. This corresponds to about 500 c.p.s. for the radio frequencies used, or a distance on the recording tape of 1 mm, since a rate is used such that a frequency interval of 25 kc is equivalent to 60 mm. This limitation is dictated by the signal-to-noise ratios available in the present experiments, uncertainty of leakage phase, and by small, random magnetic field changes. There is little reason to suspect that the magnetic moment ratios of isotopes determined above have any other limitations in accuracy than those just mentioned. Systematic sources of error, such as non-uniform spacing of frequency markers and lag of information recorded on the tape, have been examined and found to be negligible. Since the head only accommodates one sample, samples containing different nuclei have always been accurately located in the same position in the magnetic field.

The situation is different from that met with in the comparison of isotopes when nuclei of different elements are compared, and particularly when one attempts to give the final results in terms of the nuclear magneton μ_N. As far as the latter is concerned, the accuracy depends ultimately on that with which the proton moment is known, and which, at present,[22] is given to be $(2.7935 \pm 0.0003)\mu_N$. Another source of error arises from the diamagnetic correction, which takes account of the shielding due to extranuclear electrons and has to be applied when comparing moments of different elements. The diamagnetic corrections listed in column 3 of Table II have been linearly interpolated from values for specific atoms given by Lamb[39] using Hartree fields. Calculations[40] were made on six of the atoms reported by Lamb, using hydrogen-like wave functions and empirical shielding constants proposed by Slater.[41] In each case, the Hartree field value and the calculated value agreed to within two percent. This agreement suggests that a smaller error in the magnitude of the diamagnetic correction will be made by using interpolated Hartree values instead of Lamb's formula.

The uncertainties and corrections given in Table II have been arrived at from those mentioned, and it would have seemed that their enumeration was essentially complete. We have recently observed,[42] however, that the resonance lines of N^{14} show a marked dependence on the chemical compound containing nitrogen. For example, in an aqueous solution of NH_4NO_3 there appear two resonances, evidently from the NH_4^+ and NO_3^- ions, separated in frequency by as much as 0.03 percent. Similar, although not quite so pronounced, effects have been found for F^{19} by W. C. Dickinson,[43] and it is possible that they occur for many other nuclei, including those the moments of which have been under

[35] A. O. Nier, Phys. Rev. **50**, 1041 (1936).
[36] T. Schmidt, Zeits. f. Physik **112**, 199 (1939).
[37] These samples were kindly lent to us by Dr. B. J. Moyer of the Radiation Laboratory of the University of California.
[38] E. Feenberg and K. C. Hammack, Phys. Rev. **75**, 1877 (1949); L. W. Nordheim, Phys. Rev. **75**, 1894 (1949); M. Mayer, Phys. Rev. **75**, 1969 (1949).
[39] W. E. Lamb, Jr., Phys. Rev. **60**, 817 (1941).
[40] These calculations were made by Dr. F. C. Yu, Department of Physics, Stanford University.
[41] J. C. Slater, Phys. Rev. **36**, 57 (1930).
[42] W. G. Proctor and F. C. Yu, Phys. Rev. **77**, 717 (1950).
[43] We are grateful to Professor F. Bitter for sending us a preliminary report of these findings.

investigations in this paper. While these effects are evidently due to extranuclear electrons and possibly of an origin related to that of the hitherto considered diamagnetic effects, they are not sufficiently understood at the present moment to evaluate properly the corresponding corrections in the moment values. Further investigations, now in progress, are necessary before this is possible, and we have to limit ourselves at this stage to the concluding remark that the present estimate of accuracies is under serious doubt.

The author is deeply grateful to Professor Felix Bloch for generous and helpful advice throughout the course of this work. He would also like to express his gratitude to Dr. F. C. Yu who worked with him during the period of the measurements upon the isotopes Cd^{111}, Cd^{113}, and Sn^{115}.

PHYSICAL REVIEW VOLUME 79, NUMBER 1 JULY 1, 1950

Negative Energy Neutron Resonance in Cl^{35}

C. T. HIBDON AND C. O. MUEHLHAUSE
Argonne National Laboratory, Chicago, Illinois

(Received March 28, 1950)

The neutron scattering cross section of chlorine has been measured at various energies in the range from 0 to 3000 ev. These data have been fitted to a one-level Breit-Wigner scattering formula. A single real level (i.e., one of negative energy with respect to binding) in Cl^{36} at -75 ev is sufficient to account for the observed slow neutron properties of chlorine.

I. INTRODUCTION

NO positive energy neutron resonance below 3000 ev is known for chlorine. However, there is abundant evidence for the existence of a negative energy neutron resonance (i.e., a real level) in Cl^{35}. A level just below neutron binding in Cl^{36} is consistent with the following facts: (a) the scattering cross section of chlorine markedly decreases with increasing neutron energy up to at least 3000 ev, (b) the thermal and coherent scattering cross sections σ_s and σ_{coh} of chlorine are unequal[1] and the thermal scattering phase of chlorine is positive, (c) the thermal scattering cross section, σ_s, of chlorine is much larger than $4\pi R^2$, where R is the nuclear radius, (d) the thermal capture cross section, σ_{tha}, of Cl^{35} (75 percent abundant[2] -42.0b) is large, (e) the deep potential well of the odd Z-odd N, Cl^{36} nucleus ($\sim$9.8 Mev) implies an unusually high level density near neutron binding,[3] and (f) Cl^{37} (25 percent abundant) is a closed shell nucleus;[4] therefore, it is expected to have a large level separation.[5] This in turn makes the existence of a neutron level near binding in Cl^{37} improbable.

[1] E. O. Wollan and C. G. Shull, Phys. Rev. **73**, 830 (1948).
[2] Harris, Muehlhause, Rasmussen, Schroeder, and Thomas, Phys. Rev. (to be published).
[3] The depth of the well can be calculated from mass values. Evidence of a deep well is indicated by the facts that the n,p reaction on Cl^{35} is exoergic, and that the average number γ-rays per neutron capture from Cl^{35} is high. C. O. Muehlhause, Phys. Rev. (to be published).
[4] M. G. Mayer, Phys. Rev. **75**, 1969 (1949).
[5] Harris, Muehlhause, and Thomas, Phys. Rev. **79**, 11 (1950).

II. THEORY

The Breit-Wigner[6] one-level scattering cross section, $\sigma_s(E)$, as a function of energy is given by:

$$\sigma_s(E)=\sigma_p+\pi p g\lambda_0\Gamma_n\frac{\lambda_0\Gamma_n+4R(E-E_0)}{(E-E_0)^2+\Gamma^2/4}.$$

where σ_p is the potential scattering cross section; p is the fractional abundance of the isotope having the resonance, R is the nuclear radius, and $g=\frac{1}{2}[1\pm 1/(2i+1)]$, where i=spin of initial nucleus. The other symbols have their usual meanings. For a negative energy level in which Γ is small compared to the resonance energy, the scattering cross section can be written as

$$\sigma_s(E)=\sigma_p+\pi p g\lambda_0\Gamma_n[\lambda_0\Gamma_n+4R(E+E_0)]/(E+E_0)^2.$$

E_0 in this expression is positive, and

$$\lambda_0=[(2.60\times 10^6)/4\pi E_0]^{\frac{1}{2}}.$$

This work will be concerned with fitting measured values of the scattering cross section, $\sigma_s(E)$, at different neutron energies to the Breit-Wigner expression in order to obtain the parameters of the resonance.

First, the quantity $\lambda_0\Gamma_n$ can be evaluated in terms of E_0. This relation is given in terms of the thermal $[\sigma_s(0)=14.2\text{ b}]$ and the coherent $[\sigma_{coh}(0)=11.5\text{ b}]$ scattering cross sections.[1]

$$(\sigma_s-\sigma_{coh})/4\pi=pg(1-pg)(\lambda_0\Gamma_n/2E_0)^2.$$

For Cl^{35}, $p=3/4$ and $g=5/8$ or $3/8$ (spin of $Cl^{35}=3/2$).

[6] H. A. Bethe, Rev. Mod. Phys. **9**, 69 (1937).

This results in two choices of $\lambda_0\Gamma_n/2E_0$:

$$\lambda_0\Gamma_n/2E_0=\begin{cases}0.921 \text{ for } g=5/8,\\ 1.020 \text{ for } g=3/8.\end{cases}$$

Either "g" value will satisfactorily fit the data given in Section III. A more reasonable value of the nuclear radius, however, is obtained for $g=5/8$. In this paper it will be assumed, then, that $g=5/8$. However, the case for $g=3/8$ has equal validity.

The final equation to be fitted takes the form:

$$\sigma_s(E)=\sigma_p+[10.85RE_0/(E+E_0)]+[4.99E_0^2/(E+E_0)^2]. \quad (1)$$

This equation contains three unknown parameters: σ_p, E_0, and R.

Since the measurements consist in determining the total cross section, $\sigma_T(E)$, of chlorine at various neutron energies, E, it is necessary to subtract the absorption cross section, $\sigma_a(E)$, from $\sigma_T(E)$. Chlorine is an almost pure $1/v$-type absorber, i.e., $\sigma_a(E)\alpha 1/E^{\frac{1}{2}}$. Therefore, the absorption cross section at any energy, E, is given in terms of the thermal absorption cross section via the relation

$$\sigma_a(E)=31.5/(40E)^{\frac{1}{2}}.$$

$\sigma_s(E)$ is then calculated from the equation

$$\sigma_s(E)=\sigma_T(E)-31.5/(40E)^{\frac{1}{2}}.$$

As a further point of interest the radiation width, Γ_γ, can be calculated after the resonance energy, E_0, has been determined from the fit. This is obtained from the following Breit-Wigner expression for the thermal absorption cross section, σ_{tha}:

$$\sigma_{tha}=4\pi pg(\lambda_0\Gamma_n/2E_0)\cdot(\lambda_{th}\Gamma_\gamma/2E_0), \quad (2)$$

where λ_{th} is the neutron wave-length at thermal energy (0.025 ev), and $\sigma_{tha}=31.5$ b.

III. MEASUREMENT OF $\sigma_T(E)$

Neutron energies were selected by using the property of neutron resonance scattering in certain elements. The substances chosen were Co^{59} (120 ev),[7] Mn^{55} (345 ev),[8] and V^{51} (~2700 ev).[9] Thin foils of these materials were used to scatter neutrons from a cadmium-filtered neutron beam emanating from the Argonne heavy water reactor. The resonance-scattered neutrons were detected in a BF_3 proportional neutron counter[10] (see Fig. 1, of reference 10). Transmission curves of CCl_4 were measured for the three resonance scattering detectors. Proper total cross sections were obtained from the asymptotic slopes of semilog transmission plots.[10] One-fourth of the potential scattering cross section of carbon (4.72 b)[5] plus $\sigma_a(Cl)$ was subtracted from $\sigma_T(C_4Cl)$ to obtain $\sigma_s(Cl)$.

Table I. Neutron scattering cross sections.

Set	Detector	Energy ev	$\sigma_s(E)$ exp. (barns)	$\sigma_s(E)$ from fit (barns)
A		0	14.2	14.2
B	$_{27}Co^{59}$	120	5.12	5.14
C	$_{25}Mn^{55}$	345	3.02	2.95
D	$_{23}V^{51}$	~2700	1.60	1.59

Values for the net scattering cross section of chlorine are given in column 2 of Table I. Any three of the four sets of data yield the unknown resonance parameters. All combinations involving set A (Table I) were used and average values were calculated.

IV. RESULTS AND DISCUSSION

Table I lists the four sets of data and the calculated values of σ_s determined by the best fit. The manganese measurement is somewhat perturbed by an additional scattering resonance in manganese at ~2400 ev.[8] Equation (1) becomes:

$$\sigma_s(E)=1.43+[580/(E+75)]+[28100/(E+75)^2].$$

This, taken together with Eq. (2), yields the following values for the resonance parameters: $\sigma_p=1.43$ b; $E_0=75$ ev (proper sign); $R=0.72$ $b^{\frac{1}{2}}$ (units of 10^{-12} cm); $\Gamma_n=2.63$ ev; $\Gamma_\gamma=0.30$ ev; and $\Gamma=\Gamma_n+\Gamma_\gamma=2.93$ ev.

It can be seen that a reasonable fit is obtained since E_0 has the proper sign and $\Gamma\ll E_0$.

The case of Cl^{35} may be similar to that of N^{14}. It has been suggested[11] that N^{15} possesses a negative energy neutron level sufficiently close to binding to explain the behavior of the N^{14} neutron scattering cross section at energies below ~100 kev. There is evidence from the capture γ-ray spectrum[12] of $N^{14}+n\rightarrow N^{15}$ that one or two real levels just below binding (10.8 Mev) in N^{15} may exist.

[7] Harris, Langsdorf, and Seidl, Phys. Rev. **72**, 866 (1947).
[8] Neutron resonance region time-of-flight velocity selector data by W. Selove.
[9] M. Hammermesh and C. O. Muehlhause, Phys. Rev. **77**, 175 (1950).
[10] C. T. Hibdon and C. O. Muehlhause, Phys. Rev. **76**, 100 (1949).
[11] E. Melkonian, Phys. Rev. **76**, 1750 (1949).
[12] Kinsey, Bartholomew, and W. H. Walker, Phys. Rev. **77**, 723 (1950).

Lambda-Temperatures of Solutions of He^3 in He^4 below 1°K*

J. G. DAUNT AND C. V. HEER
The Mendenhall Laboratory, The Ohio State University, Columbus, Ohio
(Received March 2, 1950)

Measurements have been made of the transition (lambda) temperatures at which solutions of He^3 in He^4 first show superfluidity by observation of the thermal isolation of a vessel which contained the solutions and which was cooled to low temperature by a paramagnetic salt. The incidence of superfluidity was accompanied by a high heat influx to the solution produced by a convection of film flow to the high temperature together with return flow in the vapor phase. The solution with the highest concentration, namely 89 percent He^3, had a lambda-temperature of 0.38°K; solutions with smaller He^3 content (concentrations down to 42 percent He^3 were investigated) showed higher lambda-temperatures ranging up to 1.15°K. It was concluded that pure He^3 could not be superfluid above 0.25°K and most probably is not superfluid down to 0°K. From the results conclusions have been drawn regarding the free energy of pure He^4 in the liquid II state on the basis of the two-fluid model.

1. INTRODUCTION

IN 1947 it was shown by Daunt, Probst, Johnston, Aldrich, and Nier[1] that in dilute solutions of He^3 in He^4, the He^3 did not partake in superfluid flow. This was confirmed by another method, also using dilute solutions, by Lane, Fairbank, Aldrich, and Nier.[2] It had been suggested by Pollard and Davidson[3] and by Franck[4] that the criterion for the superfluid flow of the helium isotopes was whether they obeyed the Bose-Einstein statistics, in which the low temperature degeneration phenomenon was responsible, according to the theory of F. London,[5] for the occurrence of the superfluid properties of liquid He^4. Although the early experiments[1,2,2a] on dilute mixtures of He^3 in He^4 lent considerable support to this view of the importance of the statistics, a contrary opinion was subsequently put forward by Landau and Pomeranchuk[6] who suggested that in very dilute solutions any solute would not partake in superfluid flow. Subsequent and more decisive evidence has been gained from the measurements of Osborne, Weinstock, and Abraham[7] on the flow properties of pure liquid He^3 which showed no sign of superfluidity at any temperature between 1.05°K and its boiling point[8] (3.2°K), thus favoring the basic theory of F. London. It was considered to be of interest to extend to lower temperatures the experimental tests for the superfluidity of He^3 and details of these observations down to a temperature of 0.25°K are given in this paper. A second point of interest to which the experiments reported herewith are pertinent concerns the thermodynamics of solutions of He^3 in He^4. From measurements of the vapor pressures of such solutions, it has recently been concluded by Taconis, Beenakker, Nier, and Aldrich[9] that for dilute solutions in the helium II phase the He^3 dissolves in the "normal" constituent of the liquid only, resulting in high concentrations of He^3 in the vapor phase of low temperatures.[9a] Some conclusions that can be drawn from this peculiar law for the solubility of He^3 in liquid helium II have been made by Stout,[10] de Boer,[11] and by de Boer and Gorter,[12,12a] who have calculated the variation of the lambda-temperature, T_λ, with He^3 concentration, even up to 100 percent concentration. Since these theoretical calculations differed markedly from one another in the high concentration range, because of basically different assumptions regarding the free energy of liquid helium, it was of interest to investigate the variation of T_λ in He^3+He^4 mixtures. Some results on this up to 28 percent He^3 concentration have been published by

* Assisted by a contract between the ONR and The Ohio State University Research Foundation.

[1] Daunt, Probst, Johnston, Aldrich, and Nier, Phys. Rev. **72**, 502 (1947). See also, Daunt, Probst, and Johnston, J. Chem. Phys. **15**, 759 (1947).

[2] Lane, Fairbank, Aldrich, and Nier, Phys. Rev. **73**, 256 (1948).

[2a] See also Daunt, Probst, and Johnston, Phys. Rev. **73**, 638 (1948).

[3] E. C. Pollard and W. L. Davidson, *Applied Nuclear Physics* (John Wiley and Sons, Inc., New York, 1942), p. 183.

[4] J. Franck, Phys. Rev. **70**, 561 (1946).

[5] F. London, Nature **141**, 643 (1938) and Phys. Rev. **54**, 947 (1938).

[6] L. Landau and I. Pomeranchuk, Comptes Rendus Acad. Sci. U.S.S.R. **59**, 669 (1948).

[7] Osborne, Weinstock, and Abraham, Phys. Rev. **75**, 988 (1949).

[8] See Sydoriak, Grilly, and Hammel, Phys. Rev. **75**, 303 (1949).

[9] Taconis, Beenakker, Nier, and Aldrich, Physica **15**, 733 (1949) and Phys. Rev. **75**, 1966 (1949).

[9a] The marked differences between the values of the distribution coefficient (C_V/C_L) obtained by Taconis, Beenakker, Nier, and Aldrich and those obtained previously by Fairbank, Lane, Aldrich, and Nier [Phys. Rev. **73**, 729 (1948)] and by Daunt, Probst, and Smith [Phys. Rev. **74**, 495 (1948)], are undoubtedly partly due to the improved stirring of the liquid adopted by Taconis *et al.*, thereby avoiding concentration gradients in the liquid with the lower concentration of He^3 on the surface. It would, however, also be expected that the concentration gradients would be less marked at higher average concentrations of the liquid owing to the automatic stirring produced by differences in vapor pressure for different concentrations. Indeed calculations indicate that such an effect may contribute in large measure to the variations in the results of the three different experiments quoted above, their results indicating that without exception increasingly large values of C_V/C_L were observed for increasing average concentrations. Such an explanation seems more straightforward than that based on the special assumptions put forward by F. London and O. K. Rice (Phys. Rev. **73**, 1188 (1948)).

[10] J. W. Stout, Phys. Rev. **76**, 864 (1949) and **74**, 605 (1948).

[11] J. de Boer, Phys. Rev. **76**, 852 (1949).

[12] J. de Boer and C. J. Gorter (to be published in Physica); Phys. Rev. **77**, 569 (1950).

[12a] We are grateful to Professor J. de Boer for kindly sending us the manuscript of this paper before publication.

Abraham, Weinstock, and Osborne,[13] whereas our investigations reported here extend to 89 percent He^3 concentration, which involved measurements down to 0.2°K.

The general method for finding the λ-temperatures adopted by us depended on the anomalously high heat influx into vessels partially filled with liquid helium below the λ-point, first observed for pure liquid He^4 by Rollin[14] and by Rollin and Simon.[15] This anomalously high heat influx is due to the motion of the helium film formed from helium II up the walls of the tube connecting the helium vessel to its surroundings, such motion being toward the warmer end where it is partially or completely evaporated, as has been investigated in detail by Daunt and Mendelssohn.[16] This upward flow of matter in the film is compensated by a downward flow in the vapor phase, bringing down to the helium vessel the large heat of condensation of the vapor. The λ-point can be detected, therefore, as the temperature at which this large heat influx first occurs, due to the two phase convection process. In the experiments described below we investigated the heat influx into vessels partially filled with solutions of He^3 in He^4 below 1°K in order to determine their λ-points.[16a] In adopting this technique it was assumed that even in the high concentration ranges a mobile helium film would be formed from the liquid phase II, an assumption which appears to be valid in view of the observation of the superfluidity of the He^4 component in concentrations up to 28 percent He^3 by Abraham, Weinstock, and Osborne.[13] One advantage of our technique was that concentration of the solution remained essentially constant (see section on "Results") during the course of any one experiment.

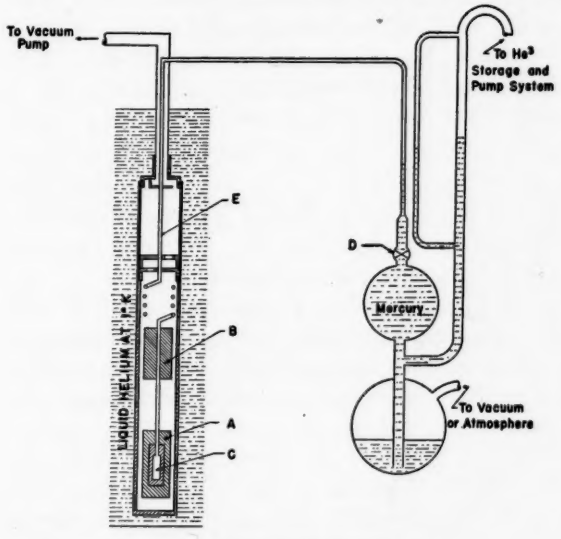

FIG. 1. Experimental apparatus.

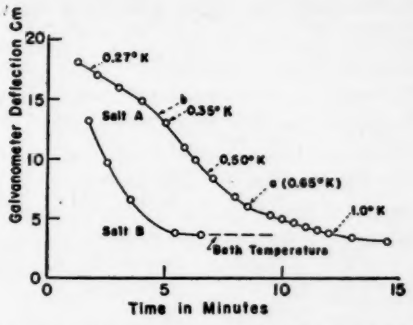

FIG. 2. Observed warm-up curves for the 79 percent He^3 solution.

2. THE EXPERIMENTAL METHOD

A volume of 3.2 cm^3 of gas at N.T.P. of a He^3+He^4 mixture of concentration 89 percent He^3 was kindly supplied by the Isotopes Division of the AEC. In order to cool the liquid formed from this mixture to very low temperatures the gas was pumped by a Toepler pump, "*D*" (see diagram given in Fig. 1) via a fine bore stainless steel capillary, "*E*" (inside diameter 0.24 mm) into a copper reservoir "*C*" inside the cryostat. This reservoir, which was of 6-mm^3 volume, was pressed inside a cylindrical pill, "*A*," made up of 5 grams of chromium potassium alum powder compressed under 200-atmospheres pressure, a technique which was found to give good thermal contact between the reservoir and the salt. This arrangement of reservoir and salt was mounted in a vacuum jacket on which was wound the mutual inductance for measurement of the susceptibility of the salt.[16b] It was cooled to helium temperatures by immersing it in a Dewar filled with liquid helium from a small Simon-type expansion liquefier[17] and temperatures below 1°K were attained by equipment identical with that previously described.[18–19]

In order to reduce the heat influx to the reservoir "*C*" at low temperatures, a second salt cylinder, "*B*," of mass 5 grams, also of pressed chromium potassium alum powder, was mounted higher up the stainless steel

[13] Abraham, Weinstock, and Osborne, Phys. Rev. **76**, 864 (1949).
[14] B. V. Rollin, Proc. VII Int. Congress of Refrigeration **1**, 187 (1936). See also Kurti, Rollin, and Simon, Physica **3**, 266 (1936).
[15] R. V. Rollin and F. Simon, Physica **6**, 219 (1939).
[16] J. G. Daunt and K. Mendelssohn, Nature **141**, 911 (1938) and Proc. Roy. Soc. **A170**, 423, 439 (1939).
[16a] Another possibility of making thermal observations of λ-points would be by measuring the heat conductivity of the solutions themselves and noting the temperature at which such heat conductivity first begins to get anomalously large, such as one could observe in pure liquid He^4. Such a procedure, however, was thought to be less readily interpretable than the method outlined above using the two phase convection process since (a) over a long column of the solution, such as would be necessary from technical considerations, quite appreciable concentration gradients might be set up owing to internal convection of the superfluid and normal constituents within the liquid itself, thus possibly falsifying the measurements, and (b) the heat influx to the lower temperature end might be so large that accuracy of temperature measurement of the temperatures below 1°K would be impaired.
[16b] See Daunt and Heer (Phys. Rev. **76**, 1324 (1949)) for further details of such arrangements.
[17] Daunt, Heer, and Silvidi, Phys. Rev. **75**, 1113 (1949).
[18] J. G. Daunt and C. V. Heer, Phys. Rev. **76**, 715 (1949).
[19] J. G. Daunt and C. V. Heer, Phys. Rev. **76**, 1324 (1949).

TABLE I. λ-temperatures, T_λ, of solutions of He^3 in He^4 for various concentrations, X, of He^3. Column 5 gives the fractional value of the λ-temperature of the solutions compared with the λ-temperature, (2.18°K), of pure He^4.

Date	Run	X (percent)	T_λ °K	T_λ °K/2.18
Aug. 30	#1	89±2	0.37±0.03	0.17±0.015
	#2	89±2	0.38±0.03	0.175±0.015
Oct. 20	#1	81±2	0.54±0.03	0.25±0.015
	#2	81±2	0.57±0.03	0.26±0.015
	#3	81±2	0.58±0.03	0.27±0.015
Oct. 27	#1	78±2	0.65±0.03	0.30±0.015
	#2	78±2	0.64±0.03	0.30±0.015
Nov. 1	#1	71±2	0.69±0.03	0.32±0.015
	#2	71±2	0.71±0.03	0.32±0.015
	#3	71±2	0.68±0.03	0.31±0.015
Nov. 3	#1	61±2	0.81±0.03	0.37±0.015
	#2	61±2	0.83±0.03	0.38±0.015
	#3	42±2	1.15±0.05	0.52±0.025

capillary (see Fig. 1), so as to serve as a heat barrier to the flow of heat along the capillary from the helium bath maintained at about 1.1°K to the reservoir. This barrier salt, "*B*," was also cooled magnetically simultaneously with the lower pill, "*A*," it being situated in the fringing field of the magnet which served to magnetize the latter. Magnetic measurements of the temperatures of the barrier salt, "*B*," could be made alternately with those of the lower salt, "*A*" surrounding the reservoir, by means of a second mutual inductance.

In order to test the apparatus, and in particular to make sure of the efficacy of the thermal contact between the reservoir and the salt "*A*," an experiment was carried out using pure He^4 in the reservoir space. Sufficient He^4 was liquefied to fill the reservoir about half-full at 1.2°K. The salts were then cooled, salt "*A*" to 0.15° curie and salt "*B*" to 0.3° curie and the warm-up time observed. This was very fast (2 minutes) corresponding to an average heat influx of 600 ergs/sec. This high heat influx[19a] was due, as described earlier, to the motion of the helium film up the walls of the capillary tube to the warmer end where it was evaporated. This upward flow of matter was compensated by a downward flow in the vapor phase, bringing down to the lower temperature the large heat of condensation of the vapor. From this experiment it was concluded that the thermal contact and time for establishment of thermal equilibrium between the reservoir, "*C*," and the salt "*A*" were satisfactory for measurements down to 0.2° curie.

An identical experiment using pure He^4 in the reservoir space was carried out at the end of the long series of runs on He^3+He^4 mixtures, in order to check for possible changes in the apparatus with time, which yielded a result identical with the first after a period of over four months.

The experiments on solutions of He^3 in He^4 were carried out in the following manner. First, the salt "*B*" and the salt "*A*" together with its reservoir, "*C*," almost filled with solution were demagnetized simultaneously to low temperatures and then the rise of temperature of both salts with time observed magnetically. The temperature on the T^* or "Curie scale" was calculated in the usual manner,[20-21] by assuming Curie's law for the paramagnetic susceptibility of the chromium potassium alum in the temperature range involved. The calculation of the temperature of the helium bath, necessary for calibrating the apparent Curie constant for our arrangement, was made from vapor pressure measurements, using the tables given by Van Dijk and Shoenberg.[22]

Diagrams giving typical warm-up curves for both the salts "*A*" and "*B*" are given in Figs. 2 and 3, which give the results of one measurement on the 79 percent He^3 solution. Figure 3 is an enlarged diagram of the results shown in Fig. 2 near the λ-point at 0.65°K. The curves show the galvanometer deflections plotted against the time, where the galvanometer deflections are proportional to $1/T^*$. For the temperature range used the specific heat of the salt is proportional to $1/T^2$ and hence the slopes of the curves plotted in Figs. 2 and 3 are directly proportional to the heat influx.

From Fig. 2 it will be seen that the salt "*B*" which acted as a heat barrier warmed up to the temperature of the bath relatively quickly. This was due mainly to the fact that it absorbed the heat of condensation of the

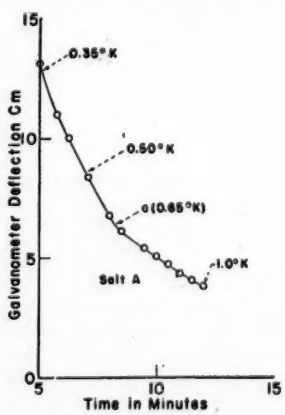

FIG. 3. Enlarged picture of the warm-up curve for 79 percent He^3 solution near the λ-point (marked "*a*" on the curve).

[19a] Much smaller average heat influxes have been observed in a somewhat similar arrangement employed by Hudson, Hunt, and Kurti [Proc. Phys. Soc. London 62, 392 (1949)] for other purposes. In comparing this work, however, it must be remembered that the pressure head establishing the vapor flow is given by the helium vapor pressure at the temperature of the bath, which for the temperature of 0.9°K reported in Hudson, Hunt, and Kurti's work was smaller by more than a factor of 10 than in our experiments. Our calculations of the considerable effect that the bath temperature has on the net heat influx to the salts in our arrangement were checked by making several demagnetizations with pure He^4 in the reservoir starting from different bath temperatures between 1.05°K and 1.3°K.

[20] N. Kurti and F. Simon, Proc. Roy. Soc. **A149**, 152 (1935) and W. J. de Haas and E. C. Wiersma, Physica **2**, 335 (1935).
[21] N. Kurti and F. Simon, Phil. Mag. **26**, 849 (1938).
[22] H. Van Dijk and D. Shoenberg, Nature **164**, 151 (1949).

gas in the capillary which flowed down immediately after demagnetization.[22a]

The salt "*A*" initially warmed up slowly, so long as salt "*B*" was well below 1°K, due to the small pressure difference in the capillary between them. When salt "*B*" reached the bath temperature, however, salt "*A*" commenced to warm up rapidly, at the well-marked point "*b*" in the curve (see Fig. 2). This rapid warming up of "*B*" was due, as described previously, to the two phase convective process of heat influx operative below the λ-point of the solution, and continued until the λ-point was reached (point "*a*" of Figs. 2 and 3). Above the λ-point (point "*a*") the heat influx to salt "*A*" became much smaller, owing to the breakdown of the two phase convection. These λ-points, observed by the change in slope of the $(1/T)$ *versus* time curves, were always clearly observable, as is shown in Fig. 3, where the heat influx to salt "*A*" changed from 140 ergs/sec. above point "*a*" to 50 ergs/sec. below point "*a*."

Curves similar to that of Fig. 2 were observed for the other concentrations of He^3, the lower concentrations being obtained by adding measured volumes of pure He^4.

3. RESULTS

The observed values of the λ-temperature, as interpreted by the technique reviewed in the previous section, for various concentrations of He^3 are given in Table I and are shown graphically by the circled points of Figs. 4 and 5. The four points marked □ in Figs. 4 and 5 are the results obtained by a different method in the liquid helium temperature range of Abraham, Weinstock, and Osborne.[13]

The possible errors in assessing the concentration of He^3 in the solutions are due to (a) possible inaccuracy in measurement of the concentration in the unrefrigerated gas, and, (b) possible differences in the concentration in the solution and in the unrefrigerated gas. Under (a), the initial concentration of the gas mixture was measured before dispatch by the AEC with an optical spectrograph and stated to be 88.7 percent He^3 with He^4 as diluent. In diminishing the concentration, measured volumes of pure He^4 were added, the accuracy of estimation of any one concentration value thus produced being ±1.0 percent, this error being due to possible inaccuracy of assessment of the original volume. As a final check, the concentration of the most diluted mixture was measured mass-spectroscopically giving a result in agreement with our calculation. Under item (b), two possible causes of discrepancies between the solution concentration and the unrefrigerated gas concentration need to be considered. First the solution concentration may be diminished owing to the relatively large concentration in the vapor.[9] This effect was negligible, however, owing to the small vapor volume available and to the small vapor pressures below 1°K. Secondly the heat influx to the solution in the reservoir would cause internal convection of the superfluid and normal constituents within the liquid and thus tend, since the He^3 does not partake in superfluid flow,[1] to produce a vertical concentration gradient in the solution. At such high average concentrations and with such small liquid depths (6 mm) as used here, however, the vapor pressure gradients which would accompany such concentration gradients would provide adequate stirring (see reference 9a). It was concluded that the effective solution concentration would not differ from the unrefrigerated concentration by more than 2 percent.

The possible errors in assessment of the λ-temperature on the absolute scale could arise from, (a) differences between the Curie scale for a spherical specimen,[21] T_s^*, and the absolute scale, T°K, (b) effects due the shape of salt "*A*" on the evaluation of T_s^*, and (c) difficulties in interpretation of the exact transition point from the measured warm-up curves (see Figs. 2 and 3). Under (a), it is estimated that in the temperature range involved, 0.35 degrees and upward, $T°K - T_s^*$ for chromium potassium alum is less than 0.01 degrees.[23]

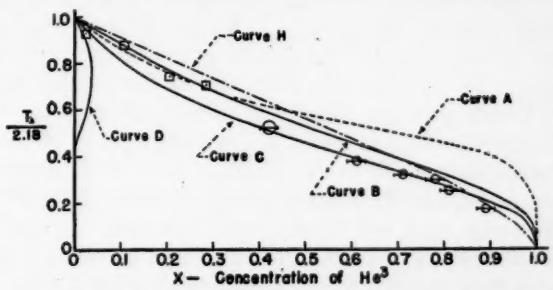

FIG. 4. Plot of the λ-temperatures, T_λ, of the solutions (as a fraction of the λ-temperature, 2.18°K, of pure liquid He^4) against He^3 concentration. The points marked ○ are the results reported herewith. The points marked □ are the results obtained by Abraham, Weinstock, and Osborne, reference 13. Curve *A* is the theoretical result of Stout, reference 10. Curve *B* is the theoretical result of de Boer and Gorter, reference 12. Curves *C* and *D* are for first-order transitions calculated by de Boer, reference 11 (see text).

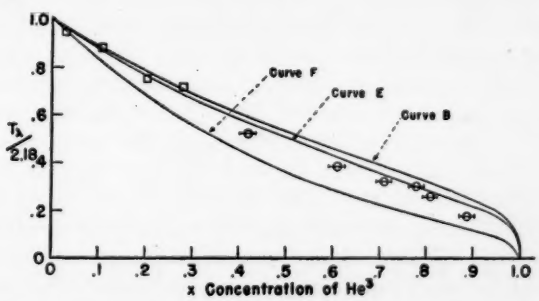

FIG. 5. Plot of the λ-temperatures, T_λ, of the solutions (as a fraction of the λ-temperature, 2.18°, of pure liquid He^4) against He^3 concentration, X. Points marked ○ are the results reported herewith. Points marked □ are the results of Abraham, Weinstock, and Osborne, reference 13. Curve *B* is the theoretical result of de Boer and Gorter, reference 12. Curves *E* and *F* are theoretical results reported herewith (see text).

[22a] This was checked (a) by the fact that the observed vapor pressure of the solution fell with time along a curve identical with that for the susceptibility of salt "*B*" and (b) by demagnetizing from various initial temperatures.

[23] J. H. Van Vleck, J. Chem. Phys. **5**, 320 (1937); M. H. Hebb and E. M. Purcell, J. Chem. Phys. **5**, 388 (1937).

Under (b), it should be stated that the temperatures quoted in this paper are uncorrected for the shape factor of the salt "*A*". Its interior contained the irregularly shaped reservoir which rendered corrections difficult to assess. It was estimated, however, from the geometry of our arrangement that the temperatures quoted here are not *smaller* than T_s* by more than 0.03 degree. Finally under (c), we estimated T_λ from the tangents drawn to the curves at either side of the λ-point. This results in a possible error estimated to be ±0.02 degrees. The λ-point at the 42 percent concentration was, owing to the fast warm-up encountered at the high temperature involved, in more doubt that the λ-points observed below 1°K. The results of these considerations in temperature and concentration assessment are collected in Table I.

4. DISCUSSION

(A) The Superfluidity

The lowest λ-temperature observed in these experiments was 0.38°K for the 89 percent He^3 solution. If pure He^3 were to show superfluidity, its λ-temperature would therefore be below 0.38°K, and from extrapolation of the experimental results it would certainly be below 0.25°K. Moreover from the agreement between the results and the thermodynamical theory,[12] (to be discussed), which is based on the assumption of non-superfluidity of He^3 at all temperatures, it is concluded that liquid He^3 is a non-superfluid liquid. This is in agreement with the theory of F. London,[5] in which superfluidity of the liquid phase would occur only for the isotope obeying the Bose-Einstein statistics.[23a] It is of interest to note, however, that many of the detailed properties of the condensed state of pure He^3 were predicted exactly by de Boer and Lunbeck,[24] independently of consideration of the statistics involved.

(B) Statistical and Thermodynamic Considerations

Two basic properties of pure liquid He^3 and of solutions of He^3 and He^4, based on experimental evidence, have enabled statistical thermodynamic formulations to be evolved for the variation of the λ-temperature with change in concentration of He^3. These properties are (1) the non-superfluidity of pure liquid He^3, as discussed previously, and (2) the unusual solubility law for He^3 in liquid helium II. Under item (2), it was found by Taconis and co-workers[9] that the results of their measurements of the vapor pressures of such solutions could be explained by assuming that He^3 does not dissolve in the superfluid part of liquid helium II. Assuming these two properties, the variation of the λ-temperature with He^3 concentration has been calculated by Stout,[10] de Boer,[11] and by de Boer and Gorter.[12] The results of these calculations are given in Fig. 4, where curve *A* is due to Stout and curve *B* to de Boer and Gorter. Both curves *A* and *B* represent the λ-temperatures for transitions of second order. Curves *C* and *D* give the phase diagram for transitions of first order as calculated by de Boer[11] and by de Boer and Gorter.[12] A first-order transition would result in the solution splitting into two separate phases, helium I and helium II, such that the helium II phase contains only a small fraction of the He^3 atoms. (In Fig. 4, curve *C* is for the helium I phase and curve *D* for the helium II phase.)

The large differences between curves *A* and *B*, both of which refer to transitions of second order, are due to differences in arbitrary assumptions made regarding the free energy of liquid helium II, (pure He^4). It would appear that the choice made by de Boer and Gorter (curve *B*) for this free energy is in closer agreement with experiment.[24a]

The points obtained by Abraham, Weinstock, and Osborne,[13] as shown in Fig. 4, together with our results for the higher concentration range, form a moderately continuous curve. The slight discrepancies may be due partly to the difference in the methods of observation of the λ-temperatures and partly to the difficulties that arise at higher temperatures in assessing the concentration of He^3 in the solution, due to the high concentrations in the vapor phase.[9] Unfortunately, it is not possible from these results to decide whether the transition is of first or second order, although the observed λ-temperatures lie close to those calculated for a first-order transition (curve *C*). This uncertainty is due to the fact that small differences in the assumptions made regarding the free-energy of helium II make large differences in the computed T_λ *versus* concentration curves. It can only be concluded that, if the transition is of first order, the free energy expression adopted by de Boer and Gorter,[12] yielding curve *C*, is satisfactory.

On the other hand, if the transition is of second order, as seems to be indicated by recent vapor pressure measurements of Weinstock, Osborne, and Abraham,[25] Fig. 5 shows some of the T_λ *versus* concentration curves that can be computed. In Fig. 5 curve *B* is due to de Boer and Gorter;[12] curves *E* and *F* have been computed using similar methods, adopting the assumption that the "normal" density ρ_n of helium II is proportional to T^7, rather than T^6 as assumed by de Boer and Gorter. This seventh-power variation of ρ_n seems probable at the lower temperatures from the recent measurements of Andronikashvilli.[26] Curve *E* is for a linear variation with temperature of the free energy, *G* at $\rho_n = \rho$ (total)

[23a] As a further check it would be of interest to investigate the properties of He^6 in liquid He^4, perhaps by a method analogous to that used first by Daunt *et al.* (see reference 1) for dilute solutions of He^3 in He^4.

[24] J. de Boer and R. J. Lunbeck, Physica **14**, 510 (1948).

[24a] For further detail regarding this phenomenological approximation for the free-energy of helium I, see C. J. Gorter, Physica **15**, 523 (1949).

[25] Weinstock, Osborne, and Abraham, Phys. Rev. **77**, 400 (1950).

[26] Andronikashvilli, J. Exp. Theor. Phys. U.S.S.R. **18**, 429 (1948).

whereas curve F is for quadratic variation[26a] (see de Boer, reference 11). It will be seen from Fig. 5 that the experimental points lie somewhere in between the various theoretical curves, all of which differ only slightly in the phenomenological basis for their computation.

It is concluded, therefore, (a) that the experimental results do not provide evidence for establishing whether the λ-transition of the solutions is of first or second order; (b) from the general agreement of the results with the theories of de Boer and Gorter, that the basic assumptions of non-superfluidity of pure liquid He^3 and of the Taconis solubility law receive welcome confirmation, and (c) that the general type of free-energy function for liquid helium II (pure He^4) which forms the basis of the computations shown in Fig. 5 is satisfactory for both types of transition, even down to the lowest λ-temperature measured (0.38°K).

As is well known the "condensation" temperature, T_λ, of a perfect Bose-Einstein gas is proportional to the number density of particles to the two-thirds power. The observed decrease in the λ-temperature of liquid He^4+He^3 solutions with decreasing He^4 concentration, as reported herewith, might be ascribed therefore to this decrease in the number density of Bose-Einstein particles. Although the conditions obtaining in a perfect gas cannot adequately represent those of liquid helium, it was considered to be of interest to calculate the expected variation of T_λ for a perfect He^3+He^4 gas mixture with concentration, x, of He^3, assuming the liquid mixture densities. The liquid mixture densities were calculated by assuming the law for perfect solutions using the known values of the molar volumes of pure liquid He^4 (27.6 cc) and pure liquid He^3 (37.5 cc) at the lowest temperatures. The result of this calculation is given by curve H of Fig. 4, T_λ at $x=0$ being normalized to 2.18°K. In view of the range of experimental error in measurement of T_λ (especially, as noted, that for the point at $x=42$ percent) it would appear that curve H represents the results as adequately as curves B and E which are the closest fit to the experimental results on the basis of the theory of de Boer and Gorter.[12] It is hoped to present later the detailed relationship between these various methods of calculation of T_λ.

Note added in proof.—O. G. Engel and O. K. Rice [Phys. Rev. **78**, 55 (1950)] have recently also proposed a thermodynamic model to allow calculation of T_λ as a function of x for high concentrations of He^3. In it, as in the models discussed above, the observed results can only be calculated after making *ad hoc* assumptions regarding the free energy of pure liquid He^4 in the normal state. A detailed discussion must, however, be postponed for a subsequent communication.

[26a] The quadratic temperature function is indicated by extrapolation of the entropy *versus* temperature curve below T_λ (see Daunt and Mendelssohn, Proc. Roy. Soc. **A185**, 237 (1946)) and is the same as that obtained for the roton spectrum postulated by Landau (J. Phys. U.S.S.R. **11**, 91 (1947)).

PHYSICAL REVIEW VOLUME 79, NUMBER 1 JULY 1, 1950

On the Azimuthal Asymmetry of Cosmic-Ray Intensity above the Atmosphere at the Geomagnetic Equator*

J. A. Van Allen and A. V. Gangnes
Applied Physics Laboratory, Johns Hopkins University, Silver Spring, Maryland
(Received January 16, 1950)

By means of Geiger-Mueller tube telescopes in an Aerobee sounding rocket fired to high altitude at the geomagnetic equator, information on the azimuthal asymmetry of the cosmic-ray intensity above the atmosphere has been obtained. These results, in conjunction with previously reported vertical intensities and specific ionizations at $\lambda=0°$ and $\lambda=41°$N, are consistent with the hypothesis that most of the primaries are positively charged protons with differential number spectrum of the form $dN=KE^{-1.9}dE$ in the energy region 5 to 23 Bev.

1. INTRODUCTION

A PREVIOUS paper[1] reports cosmic-ray intensities above the atmosphere at the geomagnetic equator as obtained by means of Aerobee sounding rocket A10 fired from the USS Norton Sound on March 17, 1949. From the same set of data, information on the azimuthal asymmetry[2] has been derived by a detailed analysis of the variation of the counting rate of telescopes *AOB*, *XOY* (axes at 45° to the rocket axis) as the rocket rotated about its longitudinal axis. This information is presented herein.

2. EXPERIMENTAL RESULTS

It is essential in measurements of this type to know the angular motion of a system of axes fixed in the rocket, and hence of the telescope axes, during the flight of the rocket above the appreciable atmosphere. Two devices were used in the A10 flight for this purpose. The first was a system of sixteen photoelectric cells, whose apertures were systematically arranged to cover

* Supported by the Navy Bureau of Ordnance under Contract NOrd 7386.
[1] J. A. Van Allen and A. V. Gangnes, Phys. Rev. **78**, 50 (1950).
[2] A preliminary and partially incorrect report was given at the Echo Lake Conference (June, 1949). A corrected manuscript was subsequently submitted for inclusion in the report of the conference.

various angles of view. By means of this system, a more-or-less continuous record of the angle between the longitudinal axis of the rocket and the "solar vector" (sun's rays) was obtained. The second device was a total-field magnetometer[3] equipped with auxiliary coils through which known calibrating currents were passed periodically. Analysis of the magnetometer data provided a record of the angle between the longitudinal axis of the rocket and the local terrestrial magnetic field vector.

In general, two widely different angular positions of the rocket axis (on the two intersections of two cones) simultaneously satisfy the photo-cell and the magnetometer data at any one instant. An unambiguous choice is made possible by following the progression of positions from launching.

The results of this analysis are shown in Fig. 1, in which are plotted the zenith angle and azimuth of the longitudinal axis of the rocket. Accuracy of the plot is estimated at $\pm 3°$ in zenith angle and $\pm 5°$ in azimuth over most of the range shown.

Throughout the flight era considered, the period of roll of the rocket about its longitudinal axis was accurately constant at 3.53 seconds, as determined by both photoelectric cells and magnetometer.

Fiducial marks were placed on the long strip of telemetering record at the successive times at which a particular photo-cell was centered on the solar vector. The intervals between such marks were divided into 18 equal segments, corresponding to 20° intervals of roll angle. Each telescope coincidence (unassociated with a guard count) *AOB*, *XOY* was then recorded in the appropriate interval of roll angle so as to build up the histogram shown in Fig. 2. (Counts *XOY* were shifted 180°, then added to counts *AOB* to yield the composite histogram.) An equation of the form $y=a_0+R\cos(\phi+\delta)$ was then fitted to the histogram by least squares technique. The result is shown as a smooth curve in Fig. 2. The values of the parameters, with their statistical probable errors are as follows: $a_0=18.7\pm0.7$, $R=3.6\pm1.0$, $\delta=87°\pm15°$. The maximum of the fitted curve occurs at a geomagnetic azimuth of $268°\pm15°$ (i.e., approximately west). The ratio $2R/a_0=0.39\pm0.11$. For a telescope of effective azimuthal acceptance angle 2α, the observed asymmetry must be increased by a factor $\alpha/\sin\alpha$. The corrected value $2R/a_0$ is

$$0.41\pm0.11.$$

In order to confirm the significance of the parameters in the above fitted curve, histograms were prepared for *AOB* and *XOY* separately and also for a shorter interval of flight time during which the rocket axis was more nearly vertical. The sense and phase of the asymmetry agreed in all cases with those of the total histogram and the magnitudes of the parameters likewise agreed within their statistical significance. The multiple particle events were found to exhibit *no* significant correlation with azimuth of the telescopes.

Unfortunately, not enough data were obtained during transit through the Pfotzer maximum to either confirm or contradict the asymmetry measurements of Johnson and Barry.[4]

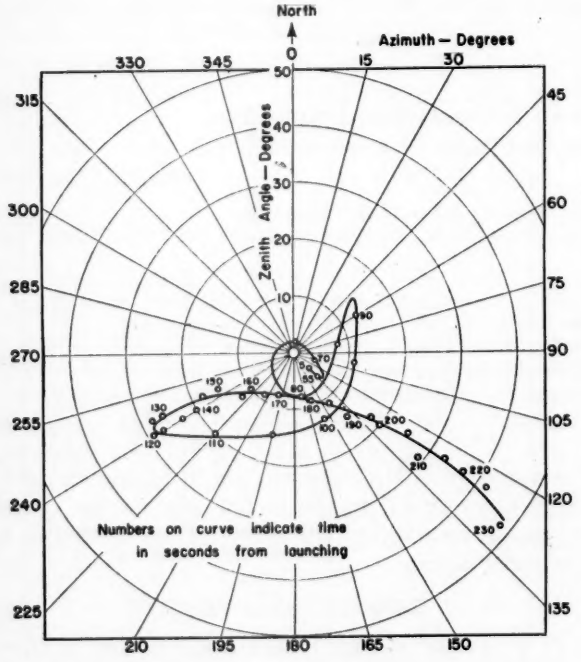

FIG. 1. Trace of forward end of rocket axis on a unit hemisphere, whose axis is vertical.

3. INTERPRETATION

The above value $2R/a_0$ cannot be simply interpreted as a conventional east-west asymmetry because of the fact that the rocket axis was not vertical. In order to arrive at an understanding of the result, we have proceeded as follows:

(a) The data of Fig. 1 were plotted on a graduated sphere.

(b) Corresponding to points on this plot, circles were drawn on the sphere to represent the trace of the axes of the *AOB*, *XOY* telescopes as the rocket rotated about its longitudinal axis.

(c) The sphere was then marked at various zenith and azimuth coordinates with the geomagnetic cut-off energies[5,6] (for protons).

(d) Finally, from the composite of telescope axis traces, the average cut-off energies corresponding to the azimuths of maximum and minimum counting rate were estimated to be 11 Bev and 23 Bev, respectively.

Thus the apparent directional intensity of particles of energy greater than 11 Bev is found to be 0.048 ± 0.003/sec./cm²/steradian; and that of particles of energy greater than 23 Bev, to be 0.031 ± 0.003/sec./cm²/steradian.

[3] The magnetometer was supplied by the Naval Ordnance Laboratory of White Oak, Maryland. We are particularly indebted to Mr. W. A. Bowen of NOL and Dr. S. F. Singer of this Laboratory for this phase of the work.

[4] T. H. Johnson and J. G. Barry, Phys. Rev. **55**, 503 (1939); **56**, 219 (1939).

[5] M. S. Vallarta, Phys. Rev. **74**, 1837 (1948).

[6] R. A. Alpher (private communication).

In the previous paper[1] it was found that a zenith angle dependence of intensity, averaged over all azimuths, of

$$0.028(1+0.6\sin\theta) \qquad (1)$$

is consistent with the intensity measurements by the various telescopes in this flight at $\lambda=0°$. On the other hand the geomagnetic theory predicts, for a reasonable power law spectrum of protons, a slight fall-off of intensity with increase of zenith angle.

Thus, it appears that Eq. (1) provides evidence for the increasing importance of atmospheric albedo at increasing zenith angles. This effect is no doubt present to an even greater extent in balloon measuremnts of the total intensity within the atmosphere.

If one temporarily ignores this evidence and the untenable result that the intensity of 0.031 for particles

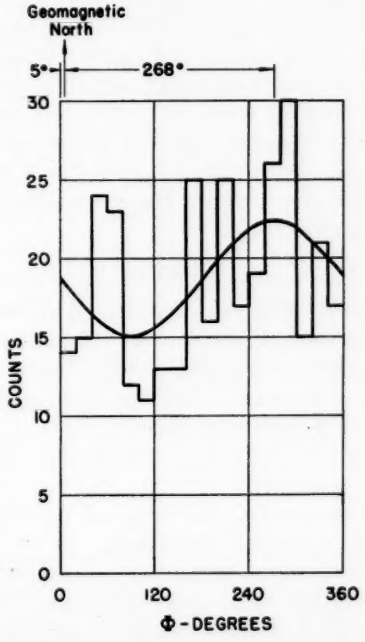

FIG. 2. Composite histogram of counts (unassociated with guard counts) from telescopes *AOB* and *XOY* in 20° segments of azimuth from an arbitrary zero, taken over 137.21 seconds of flight time during the interval 61.17 to 201.92 seconds after lauching. The smooth curve is a least squares fit to the histogram of the form $y=a_0+R\cos(\phi+\delta)$.

of energy greater than 23 Bev is higher than the (vertical) intensity of 0.028 for particles of energy greater than 14 Bev, and sets

$$(0.048/0.031)=(23/11)^{\gamma-1},$$

then $\gamma=1.6$. This is the exponent of a supposed power law differential spectrum of primaries—a value similar to, but less than, the value 1.9 deduced in the previous paper from comparison of vertical intensities at $\lambda=0°$ and $\lambda=41°$N.

In view of the conclusions of reference 1 and the foregoing discussion, it is likely that both the "11-Bev" and "23-Bev" intensities contain a significant contribution of secondaries. An equal subtraction of reasonable magnitude from each of these figures increases the calculated value of γ, and tends to bring it into agreement with the value deduced from the latitude effect.

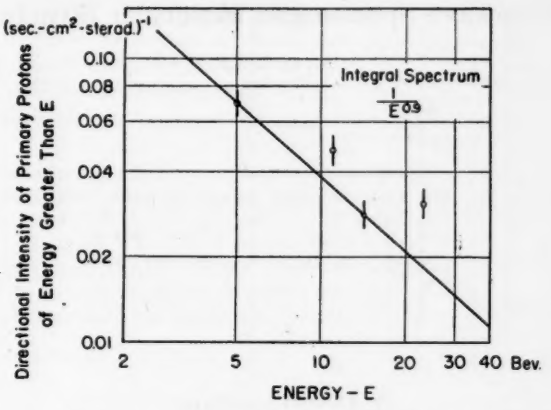

FIG. 3. A provisional integral spectrum, in absolute units, of the directional intensity of primary protons of energy greater than E as a function of E.

4. CONCLUSIONS

Thus, it appears that the measured asymmetry above the atmosphere at the geomagnetic equator can be regarded as consistent with the already widely held belief that most of the cosmic-ray primaries are ordinary positively charged protons. In this connection there may be mentioned a previous experiment[7] at $\lambda=41°$N and a subsequent one[8] at $\lambda=0°$, which have shown by direct measurement that the high energy charged particles above the atmosphere are predominantly *singly charged.*

A provisional *integral* number spectrum is plotted in Fig. 3, giving absolute intensities of primary protons of energy greater than E as a function of E. The curve of the form of $E^{-0.9}$ has been passed through the two "latitude" points; the deviation of the "asymmetry" points is evident.

This expedition was made possible by the continuing support of the U. S. Navy Bureau of Ordnance and by the cooperation of many other branches of the Naval organization: in particular, the Naval Unit of the White Sands Proving Ground, the USS Norton Sound, the USS Agerholm, and the USS Richard B. Anderson.

We are indebted to Professor M. S. Vallarta and to Dr. S. F. Singer for discussion of the results. Mr. L. W. Fraser of this Laboratory and Mr. R. F. Ohlemacher of the New Mexico College of Agriculture and Mechanic Arts have contributed essentially in accomplishing this experiment.

[7] S. F. Singer, Phys. Rev. **76**, 701 (1949).
[8] S. F. Singer, Echo Lake Conference (June, 1949).

Microwave Spectra and Molecular Structures of Methyl Cyanide and Methyl Isocyanide*

MYER KESSLER,† HAROLD RING,‡ RALPH TRAMBARULO, AND WALTER GORDY
Department of Physics, Duke University, Durham, North Carolina

(Received March 30, 1950)

Certain of the pure rotational lines of methyl cyanide and methyl isocyanide have been measured and the following molecular properties have been obtained. The moments of inertia, I_B, $\times 10^{-4}$ g cm^2, are: for $C^{12}H_3C^{12}N^{14}$, 91.20_{34}; for $C^{12}H_3C^{13}N^{14}$, 91.24_{86}; for $C^{12}D_3C^{12}N^{14}$, 106.76_{66}; for $C^{12}D_3C^{13}N^{14}$, 106.89_{48}; for $C^{12}H_3N^{14}C^{13}$, 83.45_{50}; for $C^{12}H_3N^{14}C^{13}$, 86.52_{77}; for $C^{12}D_3N^{14}C^{13}$, 97.75_{79}; and for $C^{12}D_3N^{14}C^{13}$, 101.33_{91}. The molecular dimensions are: for CH_3CN, $d_{CH}=1.092$A, $d_{CC}=1.460$A, $d_{CN}=1.158$A, and $\angle HCH=109°8'$; for CH_3NC, $d_{CH}=1.094$A, $d_{CN}=1.427$A, $d_{NC}=1.167$A, and $\angle HCH=109°46'$. The nuclear coupling for N^{14} is -4.35 Mc/sec. in CH_3CN and is $<|0.5|$ in CH_3NC.

I. INTRODUCTION

METHYL cyanide and methyl isocyanide have been previously investigated by means of infra-red[1] and Raman spectra[1] as well as by electron diffraction.[2–4] The infra-red and Raman spectral studies have shown that both methyl cyanide and methyl isocyanide have symmetric-top configurations. Electron diffraction work has provided values, accurate to about two percent, for the distances between the heavier atoms. The present work allows a more accurate evaluation of these distances, and in addition provides the first determination of the CH distances and of the HCH bond angles. An evaluation of the nuclear quadrupole coupling of N^{14} is also made. Preliminary results[5] for the most abundant isotopes were reported earlier.

II. EXPERIMENTAL PROCEDURE

The lines were detected by a method previously described[6] and were measured with a frequency standard[7] monitored by station WWV. Most of the measurements were made at dry ice temperatures and at pressures of about 5×10^{-3} mm of Hg.

The samples of methyl cyanide and of methyl isocyanide were synthesized essentially by the methods of Guillemard.[8,9] Methyl isocyanide was prepared by heating 0.4 g (2.8 mmole) of methyl iodide with 0.8 g (6.0 mmole) of silver cyanide at 80°C for four hours in a sealed tube. The resulting product was diluted with several milliliters of water and made strongly basic with potassium hydroxide. The methyl isocyanide was removed by distillation and purified in a vacuum system by successive evaporations and condensations. Methyl cyanide was obtained by heating methyl isocyanide in a sealed tube for four hours at 260°C and purified by fractionation in a vacuum system. Silver cyanide with the C^{13} content enriched to 14 percent and deuterated methyl iodide were used in the syntheses of the appropriate isotopic species.

III. RESULTS

Table I lists the frequencies measured for the different molecules. In methyl cyanide the N^{14} nuclear quadrupole coupling splits the rotational lines into a number of frequencies. A comparison of the calculated and observed hyperfine structure for the $J=1\rightarrow2$ transition of $C^{12}H_3C^{12}N^{14}$ is given in Table II. For methyl isocyanide N^{14} quadrupole splitting was too small to be resolved. Nevertheless, the lines of different K are separated by centrifugal distortions.

Rotational lines of molecules in excited bending vibrational states were also measured. For methyl cyanide the lines of the vibrational state consist of a widely spaced triplet. For the isocyanide the central line of this triplet is split into a doublet with components separated by 2.48 Mc/sec. The structure of the lines for the excited vibrational states has been satisfactorily accounted for by Nielsen.[10] Details of the theory, which is applicable to other symmetric rotators in excited bending vibrational states, may be found in Nielsen's recent paper.[10]

Table III lists the B values, the moments of inertia, centrifugal stretching constants and nuclear couplings. Table IV lists the interatomic distances and bond angles. For each molecule there are four structural parameters. Thus, the four different isotopic species are just sufficient for a complete determination of the structures. The accuracy of these determinations is limited by the zero-point energy effects to about one percent. The equations used in calculating the struc-

* This work was supported by Contract W19-122-ac-35 with the Geophysical Research Directorate of the Air Force Cambridge Research Laboratories and by a grant from the Research Corporation. It was submitted by Myer Kessler in partial fulfillment for the requirements of the Ph.D. degree.

† Frederick Gardner Cottrell Fellow. Present address: Department of Physics, Brandeis University, Waltham, Massachusetts.

‡ Frederick Gardner Cottrell Fellow. Present address: E. I. du Pont de Nemours Company, Wilmington, Delaware.

[1] G. Herzberg, *Infrared and Raman Spectra of Polyatomic Molecules* (D. Van Nostrand Company, Inc. New York, 1945), p. 332.

[2] Pauling, Springall, and Palmer, J. Am. Chem. Soc. **61**, 927 (1939).

[3] L. O. Brockway, J. Am. Chem. Soc. **58**, 2516 (1936).

[4] W. Gordy and L. Pauling, J. Am. Chem. Soc. **64**, 2952 (1942).

[5] Ring, Edwards, Kessler, and Gordy, Phys. Rev. **72**, 1262 (1947).

[6] W. Gordy and M. Kessler, Phys. Rev. **72**, 644 (1947).

[7] R. R. Unterberger and W. V. Smith, Rev. Sci. Inst. **19**, 580 (1948).

[8] H. Guillemard, Ann. Chim. Phys. **14**, 311 (1908).

[9] H. Guillemard, Chem. Zentr. **I**, 948 (1907).

[10] H. Nielsen, Phys. Rev. **77**, 130 (1950).

TABLE I. Observed frequencies for methyl cyanide and methyl isocyanide.

Species	Transition			Frequency[a] (Mc/sec.)
$C^{12}H_3N^{14}C^{12}$	$J=1\rightarrow2$,	$K=0\rightarrow0$		40,211.16
	$J=1\rightarrow2$,	$K=1\rightarrow1$		40,210.27
				40,313.37
	$J=1\rightarrow2$,	For excited vib. state $\omega_8(e)$		40,364.07
				40,366.55
				40,424.49
$C^{12}H_3N^{14}C^{13}$	$J=1\rightarrow2$,	$K=0\rightarrow0$		38,783.21
	$J=1\rightarrow2$,	$K=1\rightarrow1$		38,782.21
$C^{12}D_3N^{14}C^{12}$	$J=1\rightarrow2$,	$K=0\rightarrow0$		34,327.82
	$J=1\rightarrow2$,	$K=1\rightarrow1$		34,327.23
	$J=2\rightarrow3$,	$K=0\rightarrow0$		51,490.90
	$J=2\rightarrow3$,	$K=1\rightarrow1$		51,490.05
	$J=2\rightarrow3$,	$K=2\rightarrow2$		51,487.51
$C^{12}D_3N^{14}C^{13}$	$J=2\rightarrow3$,	$K=0\rightarrow0$		49,671.19
	$J=2\rightarrow3$,	$K=1\rightarrow1$		49,670.43
	$J=2\rightarrow3$,	$K=2\rightarrow2$		49,668.07
$C^{13}H_3C^{12}N^{14}$	$J=1\rightarrow2$,	$K=1\rightarrow1$,	$F=1\rightarrow2$	36,793.64
	$J=1\rightarrow2$,	$K=0\rightarrow0$, $K=1\rightarrow1$,	$F=0\rightarrow1$ $F=2\rightarrow2$	36,794.26
	$J=1\rightarrow2$,	$K=1\rightarrow1$,	$F=2\rightarrow3$	36,794.88
	$J=1\rightarrow2$,	$K=0\rightarrow0$,	$F=2\rightarrow3$ $F=1\rightarrow2$	36,795.38
	$J=1\rightarrow2$,	$K=1\rightarrow1$,	$F=0\rightarrow1$	36,796.27
	$J=1\rightarrow2$,	$K=0\rightarrow0$,	$F=1\rightarrow1$	36,797.52
				36,942.15
	$J=1\rightarrow2$,	For $\omega_8(e)$ excited vib. state with hyperfine structure unresolved		36,903.40
				36,870.94

tures are:

$$I_B=\tfrac{3}{2}M_H(d_{CH}\sin\alpha)^2+1/M\{d_{C'N}{}^2M_N(M-M_N)+d_{CC'}{}^2(M_N+M_{C'})(M_C+3M_H)+3(d_{CH}\cos\alpha)^2M_H(M-3M_H)+2d_{C'N}d_{CC'}M_N(M_C+3M_H)+6d_{C'N}d_{CH}\cos\alpha M_NM_H+6d_{CC'}d_{CH}\cos\alpha M_H(M_N+M_{C'})\}$$

for CH_3CN, and

$$I_B=\tfrac{3}{2}M_H(d_{CH}\sin\alpha)^2+1/M\{d_{NC'}{}^2M_{C'}(M-M_{C'})+d_{CN}{}^2(M_{C'}+M_N)(M_C+3M_H)+3(d_{CH}\cos\alpha)^2M_H(M-3M_H)+2d_{NC'}d_{CN}M_{C'}(M_C+3M_H)+6d_{NC'}d_{CH}\cos\alpha M_{C'}M_H+6d_{CN}d_{CH}\cos\alpha M_H(M_{C'}+M_N)\}$$

for CH_3NC, where I_B is the moment of inertia about an axis perpendicular to the figure axis, M is the mass of the molecule, α is the angle between the C−H bond and the figure axis. (C′ designates the carbon atom adjacent to the nitrogen in CH_3CN and the terminal carbon atom in CH_3NC.) All the remaining symbols have the usual significance. For the isotopic species the appropriate masses were substituted in the above expressions, and the distances and angles found from the resulting simultaneous equations.

TABLE I. (*Continued.*)

Species	Transition			Frequency[a] (Mc/sec.)
$C^{12}H_3C^{13}N^{14}$	$J=1\rightarrow2$,	$K=0\rightarrow0$,	$F=2\rightarrow3$ $F=1\rightarrow2$	36,777.18
$C^{12}D_3C^{12}N^{14}$	$J=2\rightarrow3$,	$K=0\rightarrow0$,	$F=3\rightarrow4$ $F=2\rightarrow3$ $F=1\rightarrow2$	47,147.60
	$J=2\rightarrow3$,	$K=1\rightarrow1$,	$F=3\rightarrow4$ $F=1\rightarrow2$	47,147.00
	$J=2\rightarrow3$,	$K=1\rightarrow1$,	$F=2\rightarrow3$	47,146.68
	$J=2\rightarrow3$,	$K=0\rightarrow0$, $K=1\rightarrow1$, $K=2\rightarrow2$,	$F=3\rightarrow3$ $F=3\rightarrow3$ $F=1\rightarrow2$	47,146.00
	$J=2\rightarrow3$,	$K=2\rightarrow2$,	$F=3\rightarrow4$ $F=3\rightarrow3$ $F=3\rightarrow2$	45,145.20
	$J=2\rightarrow3$,	$K=2\rightarrow2$,	$F=2\rightarrow3$ $F=2\rightarrow2$	47,143.85
$C^{12}D_3C^{13}N^{14}$	$J=2\rightarrow3$,	$K=0\rightarrow0$,	$F=3\rightarrow4$ $F=2\rightarrow3$ $F=1\rightarrow2$	47,091.05
	$J=2\rightarrow3$,	$K=1\rightarrow1$,	$F=3\rightarrow4$ $F=1\rightarrow2$	47,090.41
	$J=2\rightarrow3$,	$K=0\rightarrow0$, $K=1\rightarrow1$, $K=2\rightarrow2$,	$F=3\rightarrow3$ $F=3\rightarrow3$ $F=1\rightarrow2$	47,089.43
	$J=2\rightarrow3$,	$K=2\rightarrow2$,	$F=3\rightarrow4$ $F=3\rightarrow3$ $F=3\rightarrow2$	47,088.69
	$J=2\rightarrow3$,	$K=2\rightarrow2$,	$F=2\rightarrow3$ $F=2\rightarrow2$	47,087.39

[a] Frequency is for ground vibration state unless otherwise specified.

IV. DISCUSSION OF THE STRUCTURES

It is of interest that the CH lengths and bond angles to the C are, within the limits of error, equivalent to those in methane. This is true also for the CH_3 group of methyl alcohol,[11] and approximately true for the methyl halides.[12] Such uniformity in the configuration of the CH_3 group in organic compounds has been generally assumed, but before the development of microwave spectroscopy this assumption could not be widely tested. Electron diffraction, the principal method then used for determining the structures of organic molecules, did not, in general, locate the hydrogen atom.

The CC bond found for $H_3C-C\equiv N$ is 0.03A shorter than the previously reported electron diffraction value, and is 0.08A shorter than the CC bond in ethane and similar hydrocarbons. The effective single-bond radius of C joined by a triple bond is smaller by about 0.03A than the usual single-bond C radius. The additional shortening can be accounted for by a contribution of about 10 percent to the ground state of the molecule

[11] Edwards, Gilliam, and Gordy (unpublished results).
[12] Gordy, Simmons, and Smith, Phys. Rev. 74, 243 (1948).

TABLE II. Comparison of calculated and observed hyperfine structure for the $J=1\rightarrow2$ transition of $C^{13}H_3C^{12}N^{14}$.

K	$F\rightarrow F'$	Frequency in Mc/sec. Calc.[a]	Obs.	Relative intensity Calc.	Obs.
0	1→1	36,797.51	36,797.52	18	20
0	2→1	36,796.20	36,796.27	1	15
1	0→1	36,796.25		18	
0	2→3	36,795.42		100	
0	1→2	36,795.33	36,795.38	54	160
1	2→1	36,795.27		1	
1	2→3	36,794.88	36,794.88	75	70
1	1→1	36,794.62	—	13	—
0	0→1	36,794.24	36,794.26	24	25
1	2→2	36,794.19		13	
0	2→2	36,794.02	—	18	—
1	1→2	36,793.55	36,793.64	40	30

[a] Calculated with $eQ(\partial^2V/\partial z^2)=-4.35$ Mc/sec. and $D_{JK}=0.18$ Mc/sec.

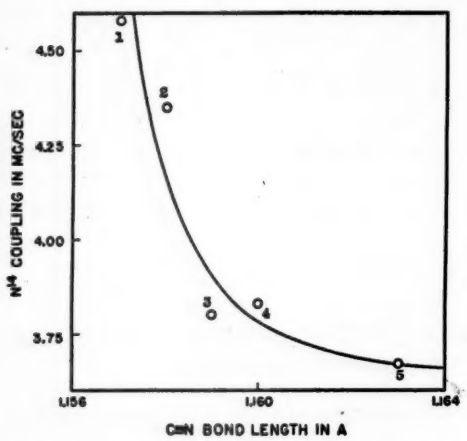

FIG. 1. Relation of the C≡N bond length to the N^{14} nuclear quadrupole coupling in XC≡N compounds. (1) Represents HCN, (2) CH_3CN, (3) ICN, (4) BrCN, (5) ClCN.

by hyperconjugated structures of the type:

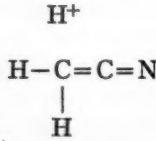

This amount of hyperconjugation would have a negligible effect on the CN and CH lengths, but should decrease the nuclear coupling of the N^{14} a measurable amount. The magnitude of coupling found for N^{14} is 0.23 Mc/sec. less than that in hydrogen cyanide. Figure 1 shows the variation of the N^{14} coupling with the CN length for all the cyanides so far studied with microwave spectroscopy.

TABLE III. Molecular constants.

Molecule	B_0 Mc/sec.	I_B $\times10^{-40}$ g cm²	D_{JK} Mc/sec.	$eQ(\partial^2V)/(\partial z^2)$ for N^{14} Mc/sec.
$C^{12}H_3C^{12}N^{14}$	9198.83	91.20_{34}	0.17_8	-4.35 ± 0.20[a]
$C^{12}H_3C^{13}N^{14}$	9194.28	91.24_{86}	—	−4.35
$C^{12}D_3C^{12}N^{14}$	7857.93	106.76_{66}	0.11_3	−4.35
$C^{12}D_3C^{13}N^{14}$	7848.51	106.89_{48}	0.11_0	−4.35
$C^{12}H_3N^{14}C^{12}$	10,052.90	83.45_{50}	0.22_8	$<\lvert0.5\rvert$
$C^{12}H_3N^{14}C^{13}$	9695.91	85.52_{77}	—	$<\lvert0.5\rvert$
$C^{12}D_3N^{14}C^{12}$	8582.06	97.75_{79}	0.14_1	$<\lvert0.5\rvert$
$C^{12}D_3N^{14}C^{13}$	8278.79	101.33_{91}	0.13_0	$<\lvert0.5\rvert$

[a] This value is smaller than the preliminary one given in reference 5.

TABLE IV. Molecular structures.

CH_3CN	d_{CH} 1.092A	d_{CC} 1.460A	d_{CN} 1.158A	∠HCH 109°8′
CH_3NC	d_{CH} 1.094A	d_{CN} 1.427A	d_{NC} 1.167A	∠HCH 109°46′

The early electron diffraction value for the CN length in CH_3NC, 1.48A, found by Brockway[3] was revised downward by the remeasurements of Gordy and Pauling.[4] The present microwave work revises this distance further downward to 1.427A. This is some 0.05A shorter than the usual CN single bond. If we assume, as for C, a shortening of the nitrogen single bond radius of 0.03A by the adjacent multiple bond, there is still a shortening of 0.02A to be accounted for. Hyperconjugated structures of type III are probably not very important because of the unstable charge distribution.[4]

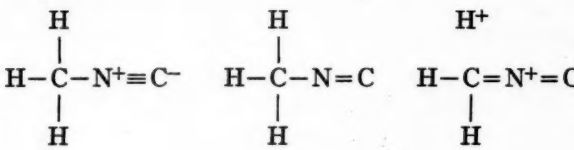

I II III

It seems more likely that the shortening of the CN bond is due to a decrease in the nitrogen radius because of the positive formal charge on N in the most important structure type I. The NC length is slightly longer than the CN length in HCN or CH_3CN. This might be explained by postulating contribution from structure II. However, very significant contributions from II are precluded by the linear configuration of CNC and by the absence of detectable N^{14} hyperfine structure for this molecule. In structures I and III the valence orbitals of N are symmetrically filled and, if distortion effects are neglected, $(\partial^2V)/(\partial z^2)$ would be zero.

The Scattering of Protons by Protons near 30 Mev, Photographic Method*

WOLFGANG K. H. PANOFSKY AND FRANKLIN L. FILLMORE
Radiation Laboratory, Department of Physics, University of California, Berkeley, California

(Received February 20, 1950)

The scattering of 29.4-Mev protons by hydrogen gas at one atmosphere pressure has been studied with the beam of the Berkeley linear accelerator. The beam, collimated to a diameter of $\frac{1}{16}$ in., passes through the gas and constitutes a line source of scattered protons. The scattering angle of the scattered protons is measured directly in the emulsion of 50μ Ilford C-2 emulsions. Measurements of the range of the scattered protons was made on a fraction of the tracks. From range-energy relations established in the magnetic field of the 184-in. cyclotron for the emulsions used, the primary energy of the protons before scattering was found to be 29.4 $\pm$0.1 Mev. Protons were observed in the angular range $10° \leqslant \theta_{lab} \leqslant 80°$; two independent sets of scattering data in the angular region greater or less than 45° are thus obtained; a valuable internal check on observational errors or background or impurity effects is thus possible. No statistically significant difference in the two regions was observed. 10,934 tracks have been tabulated; this results in the statistical error approximately matching systematic errors such as those due to tolerance of plate geometry, observational error, etc. Cross sections obtained are absolute; the beam is measured by absorption in a Faraday cup and charge integration on a low leakage condenser. The most significant result of these experiments is the apparent absence of expected repulsive P wave and of D wave effects.

I. INTRODUCTION

THE scattering of protons by protons has been studied by many observers[1–15] covering an energy range up to 14.5 Mev,[9] and recently at 240 Mev[14] and 340 Mev.[15] Unfortunately, the accuracy of the experiments in the region above 7 Mev and below this work has not been sufficient to permit significantly different conclusions to be drawn as compared to the conclusions obtained from the more precise low energy experiments. With possible small deviations all low energy experiments can be interpreted[16] in terms of scattering in the lowest state of angular momentum only. As has been shown by Schwinger,[17] Blatt,[18] and others[19] this permits the determination of only two parameters of an assumed potential of interaction between the particles. The essential conclusion drawn from these experiments is the fact that these parameters calculated from the $p-p$ S wave interaction are essentially the same as the parameters calculated for the $n-p$ S wave interaction in the singlet state.

This investigation was undertaken in order to extend $p-p$ scattering data into the region where the contribution from scattering in higher states of angular momentum should certainly become significant. The protons used in this experiment were produced by the Berkeley linear accelerator. This accelerator provides a beam up to an energy of 32 Mev, the beam being of small diameter and small angular divergence and thus

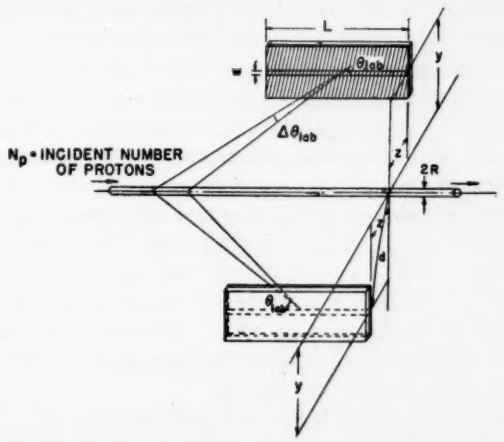

FIG. 1. Relative geometry of a photographic plate "pair" to the beam. Geometrical parameters shown are: L=length of swath scanned; W=swath width; Z=off-set of emulsion surface from beam center line; y=distance of swath from plane through beam normal to emulsion surface; $d=(Z^2+y^2)^{\frac{1}{2}}$=distance of beam center line to swath; R=beam radius; θ_{lab}=laboratory scattering angle.

* This work was done under the auspices of the AEC.

[1] W. H. Wells, Phys. Rev. **47**, 591 (1935).

[2] M. G. White, Phys. Rev. **49**, 309 (1936).

[3] Tube, Heydenburg, and Hafstad, Phys. Rev. **50**, 806 (1936); 600–900 kev.

[4] Hafstad, Heydenburg, and Tuve, Phys. Rev. **53**, 239 (1938).

[5] Heydenburg, Hafstad, and Tuve, Phys. Rev. **56**, 1078 (1939); 867, 680, 776 kev.

[6] Herb, Kerst, Parkinson, and Plain, Phys. Rev. **55**, 998 (1939); 860, 1200, 1390, 2105, 2392 kev.

[7] R. R. Wilson, Phys. Rev. **71**, 384 (1947); 10 Mev.

[8] R. R. Wilson and E. C. Creutz, Phys. Rev. **71**, 339 (1947); 10 Mev.

[9] Wilson, Lofgren, Richardson, Wright, and Shankland, Phys. Rev. **71**, 560 (1947); 14.5 Mev.

[10] Dearnley, Oxley, and Perry, Phys. Rev. **73**, 1290 (1948); 7 Mev. J. Rouvina (private communication).

[11] Blair, Freier, Lampi, Sleator, and Williams, Phys. Rev. **74**, 553 (1948); 2.42, 3.04, 3.27, 3.53 Mev.

[12] Ragan, Kanne, and Taschek, Phys. Rev. **60**, 628 (1941); 176 and 200 kev.

[13] Bondelid, Bohlman, and Mather, Phys. Rev. **76**, 865 (1949); 5.11 Mev.

[14] C. L. Oxley, Phys. Rev. **76**, 461 (1949), 240 Mev.

[15] O. Chamberlain and C. Wiegand, Phys. Rev. **79**, 81 (1950).

[16] For a review of the present state of the interpretation of $p-p$ scattering experiments see: H. A. Bethe, Phys. Rev. **76**, 38 (1949); also J. D. Jackson, M.I.T. Tech. Report No. 29 (July 15, 1949); also Jackson and Blatt, Rev. Mod. Phys. **22**, 77 (1950).

[17] J. Schwinger, Phys. Rev. **72**, 742(A) (1947); lecture notes on nuclear physics, Harvard (1947). (As quoted by Blatt and Jackson, reference 18.)

[18] J. M. Blatt, Phys. Rev. **74**, 92 (1948) and J. M. Blatt and J. D. Jackson, Phys. Rev. **76**, 18 (1949).

[19] J. Smorodinski, J. Phys. U.S.S.R. **8**, 219 (1944); **11**, 195 (1947).

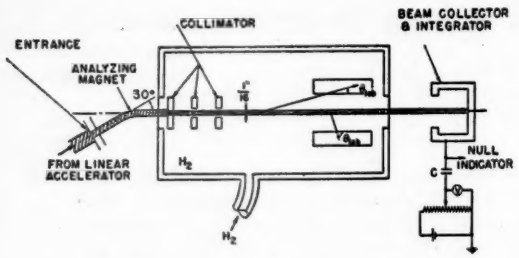

FIG. 2. Schematic layout of collimating system, scattering chamber, and integrator.

well suited to scattering experiments. The authors are greatly indebted to the members of the linear accelerator crew for their efficient operation of the machine during the bombardments.

It was felt that the importance of the problem of $p-p$ scattering in the 30-Mev range justified that the experiments be performed by two entirely independent methods. Cork, Johnston, and Richman[20] have undertaken the study by means of a proportional counter method; their methods and results are given in an adjoining paper. This paper describes the results obtained by means of an apparatus using photographic plates as detectors. The results reported here are not final; it was felt, however, since most of the theoretical implication of this work does not rest on the features requiring the highest attainable accuracy, that publication at this stage of the work was advisable.

II. DESCRIPTION OF APPARATUS

A. Ideal Geometry

The first use of photographic plate techniques in the study of $p-p$ scattering was made at the University of Rochester[10] at 7 Mev. In the Rochester experiment an annular exit slit was employed which resulted in a one to one correspondence between track position and scattering angle. This reduced analysis of the plates to a simple counting operation. The problems associated with slit scattering and penetration to be expected at 30 Mev led us to adopt the more laborious method, namely of actually measuring the scattering angle of all tracks directly in the emulsion. The method is made practical in this energy region by the small multiple Coulomb scattering in the emulsion. Range measurements were also made whenever the track length permitted us to do so. This permitted an internal check as to the primary energy.

The proton beam from the linear accelerator is first monochromatized and collimated to $\frac{1}{16}$ in. diameter by means of equipment described below. The beam then passes into the scattering chamber in which plates are disposed symmetrically about the beam in the manner shown in Figs. 1 and 2. The solid angle subtended by a swath of width W and length L parallel to the beam is then directly defined by the distance d from the swath to the centerline of the beam and the offset Z of the plane of the emulsion and the beam. It is easily shown by elementary calculation that, if the finite beam size is ignored, the number of tracks N_t for a given number of incident protons N_p is given by

$$\frac{N_t}{N_p}=N_v\left(\frac{d\sigma}{d\omega}\right)_{cm}\frac{WLZ}{d^2}\frac{\Delta\omega_{cm}}{2\pi}, \tag{1}$$

where N_v is the number of scattering centers per unit volume and $(d\sigma/d\omega)_{cm}$ is the differential cross section in the center-of-mass coordinates. $\Delta\omega_{cm}$ represents the increment of solid angle in the center-of-mass frame corresponding to the range $\Delta\theta_{\text{lab}}$ in the laboratory angle θ_{lab} within which the N_t tracks have been recorded. This equation can be written in the equivalent form

$$\frac{N_t}{N_p}=N_v\left(\frac{d\sigma}{d\omega}\right)_{cm}\frac{WLZ}{d^2}\Delta\,(\cos 2\theta_{\text{lab}}), \tag{2}$$

which forms the basis for all cross-section computations. It is to be noted that in this simple geometry the number of tracks corresponding to a given interval in solid angle is simply proportional to the differential cross section without any further angular dependence.

B. Non-Ideal Geometry—Design of Plate Holder

The scattering geometry depends linearly on the offset Z of the emulsion face toward the beam center. In the apparatus as described here $Z\cong 0.070$ in. and therefore if data were based on the tracks as measured in a single plate, an excessive dependence of the calculated absolute cross section on beam position would result. To obviate this difficulty the plates were arranged in a symmetrical array about the beam center. Figure 1 shows one pair of plates only. It is easy to show that if the measurement of cross section is based on the *sum* of the tracks measured in paired plates (see Fig. 1),

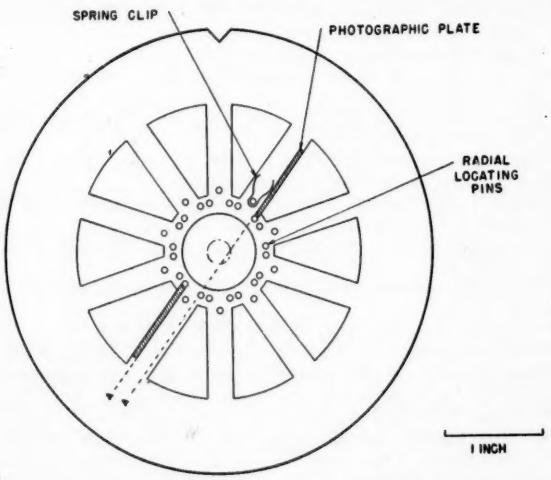

FIG. 3. Diagram of base plate of cartridge showing the means of radial and azimuthal localization of the plates. The distance $A-A$ corresponds to the interface distance D of Eq. (4).

[20] Cork, Johnston, and Richman, Phys. Rev. **79**, 71 (1950).

then the fractional error ϵ_Z due to an error δ_Z in beam centering parallel to Z is given by

$$\epsilon_Z = 3(\delta_Z)^2/(y^2+Z^2), \quad (3)$$

while the fractional error ϵ_D due to an error δ_D in the face to face distance D between the emulsion faces is given by

$$\epsilon_D = \delta_D/D \quad (4)$$

and the error ϵ_y due to an error δ_y in y, where $2y$ is the edge-to-edge distance between paired plates, is given by

$$\epsilon_y = 2\delta_y/y. \quad (5)$$

The ratio between the number of tracks recorded in the two members of a pair of plates depends linearly on the off-center displacement of the beam. If N_1 and N_2 are the tracks recorded in the two members of a pair, it is easy to show that

$$(N_1-N_2)/(N_1+N_2) = \delta_Z/Z \quad (6)$$

and hence

$$\epsilon_Z = [(N_1-N_2)/(N_1+N_2)]^2 \cdot [3Z^2/(y^2+Z^2)]. \quad (7)$$

The error in absolute cross section due to lack of beam centering can thus be evaluated directly by an internal check on the symmetry of the track counts. Experimentally it has been possible to keep the error ϵ_Z well below 0.1 percent corresponding to a centering error δ_Z of less than 0.01 in. A similar calculation can be made on the effect of beam centering in the y direction. It is to be noted that this, and other possible geometrical errors, have no bearing upon the relative cross section but only on the absolute measurements.

The errors ϵ_D and ϵ_y are independent of beam position and are only dependent on the accurate *relative* location of the plates. To achieve this required accuracy, a precision plate holder-cartridge was machined out of Lucite and Duraluminum. Figure 3 shows the base diagram of the cartridge end plates. The faces $A-A$ are held to a tolerance of ± 0.0005 in. by means of go/no-go gauges which were applied before and after every run. The cartridge was designed to hold up to 20 plates for simultaneous exposure. This design was adopted during the initial stages of testing of the Berkeley linear accelerator when it appeared that the proton beam current might be very small. Since the current is now more than adequate for this experiment only six of the plate positions are occupied. It also seemed inadvisable to place plates with their emulsions facing one another, since calculation shows that the probability of a proton scattering out of one emulsion face and entering the opposite emulsion cannot be considered negligible.

In addition to the precision gauging of the distance $A-A$ (Fig. 3), precise determination of the face to face distance requires also knowledge of the photographic plate glass thickness and flatness and also knowledge of the emulsion thickness. The plates were measured after processing to ± 0.0004 in. using surface plate and dial gauge equipment. A correction was applied for emulsion shrinkage using a shrinkage factor of 2.0. Since the emulsion thickness used is only $50\mu = 0.002$ in., the uncertainty in shrinkage factor produces negligible error.

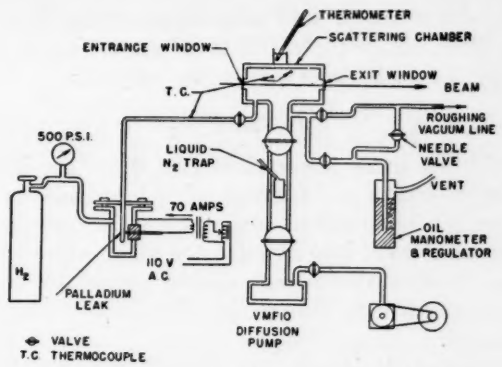

FIG. 4. Schematic diagram of gas handling system. Oil manometer and regulator regulates H_2 pressure and meters it against atmospheric pressure.

The plates are held onto the cartridge precision faces by means of light springs which assure positive contact with the surfaces $A-A$. The cartridge is always kept either in vacuum or in a desiccator to avoid possible warping due to moisture absorption.

The cartridge is centered in the barrel of the gas handling system by means of six steel balls, two of which are spring-loaded, thus providing a correct kinematic support. The collimator (see Fig. 2) is aligned with the barrel to within ± 0.004 in. As a result of this, it is assumed that if the beam is centered at one point of the scattering volume, it is centered at all points. The final centering of the beam is made by adjusting the analyzing magnet current and checking with a fluorescent screen. The final criterion as to centering does of course rest on the actual track count as outlined above.

Equation (2), on which the cross-section calculations are based, is strictly true only if the incoming beam constitutes an ideal line source. Errors caused by the finite diameter of the beam have been investigated in detail. The result is as follows. If the radius of the beam is R, then the ideal formula Eq. (2) is multiplied by a correction factor of

$$1+\tfrac{1}{4}(R/d)^2[\cos\theta_{cm}(\cos\theta_{cm}-1)-\tfrac{1}{2}] \quad (8)$$

where the integration over the beam has been carried out under the assumption that the differential cross section is constant over the range of integration. Since R is of the order of $\frac{1}{32}$ in. and $d>0.500$ in. this correction never exceeds 0.15 percent for all angles and is therefore negligible.

The finiteness of the scattering length of the beam does not introduce a correction but simply introduces limits on the range of angles which can be considered as originating in the gas. This restricts the smallest

angle which can be read unambiguously to 3° on the inner edge of the plate and to 8° on the outer edge. In practice angles were read in the interval:

$$10° \leq \theta_{lab} \leq 80°. \quad (9)$$

A further small geometrical error worth considering is the obliquity of incidence of the protons on the photographic emulsion. An elementary calculation, which also takes into account the finite width of the beam, shows that this error cannot exceed 0.1° and is usually much less. This source of error has thus been neglected.

A further deviation from "ideal" geometry which has been considered is the probability that a proton will enter the emulsion, then scatter back out again and re-enter the emulsion at a "hill" in the emulsion. This effect can be estimated with knowledge of the waviness of the emulsion. A microscopic measurement was made of the flatness of unprocessed emulsion surfaces and it was found that the "waviness" amounts to less than 1μ in height per 150,000 sq. μ of emulsion surface. By combining this information with calculation of the emulsion scattering, this effect appears negligible.

C. Vacuum and Gas Handling System

The hydrogen scattering chamber is separated from the linear accelerator vacuum by means of an entrance window, $\frac{1}{4}$-in. diameter, made of 0.001-in. aluminum.

The chosen operating pressure of H_2 was one atmosphere; for 30-Mev protons the broadening of the beam due to multiple scattering in the chamber is only 0.011 in. Multiple Coulomb scattering of sufficient magnitude to enter the plates is thus excluded. The nuclear cross sections are sufficiently small such that plural nuclear events are excluded also.

Figure 4 shows a schematic diagram of the gas system. In a $p-p$ scattering experiment with a gas target one of the main problems is that of gas purity; at this energy however, this problem is of course less significant than at lower energy since the Coulomb cross section falls off faster with energy than the nuclear scattering yields. The principal source of impurities proved to be water vapor or other contaminants evolved from the photographic plates themselves. Since the scattering angles cover the range of $10° \leq \theta_{lab} \leq 80°$ it was possible to check the presence of impurities by an asymmetry of tracks about a laboratory angle of 45°. These tests indicate that it was necessary to dehydrate the plates for at least four hours in high vacuum before data could be taken. Figure 5 shows a typical dehydration curve of the plates, showing that after a pump-out time of four hours the partial pressure of impurities would not rise to more than 0.05 percent of the total pressure in a 30-min. bombardment.

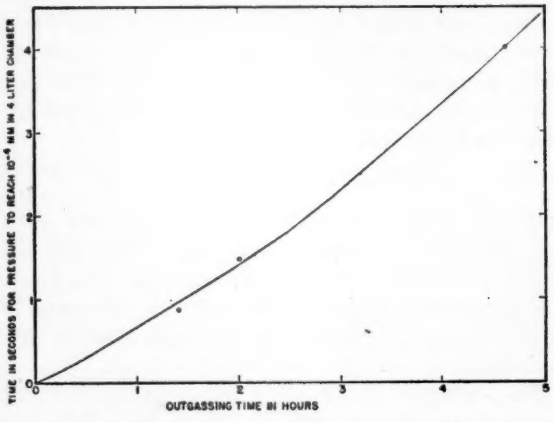

FIG. 5. Outgassing curve of 50μ Ilford C-2 plates during typical run. The accumulated impurity contribution during a run is estimated from this type of data.

Considerable trouble was encountered from peeling of the emulsion from the glass surface when this outgassing procedure was used. After many unsuccessful experiments to reduce peeling by taping the emulsion edges, covering the plates with collodium, etc., an emulsion (Ilford C-2; 50μ thickness, Emulsion No. Z2199) was found which withstood the outgassing treatment without peeling difficulties. All attempts to use Eastman-Kodak NTB emulsions proved unsuccessful.

After pump-out the scattering chamber was isolated from the pump and liquid nitrogen trap (to preserve thermal equilibrium) and hydrogen was admitted through a palladium leak. This leak (Fig. 6), designed by Mr. L. Johnston and Mr. E. A. Day, consists of a palladium tube of $\frac{1}{4}$-in. diameter and 0.006-in. wall thickness, internally supported by ceramic rings. It was heated to a temperature slightly below red heat by passing a current of approximately 70 amp. directly through the tube, corresponding to a dissipation of approximately 250 watts. The external pressure was maintained at a pressure of 500 p.s.i. of H_2. At this pressure differential the chamber (volume $\sim$4 liters) could be filled in 20 min. to a pressure of one atmosphere. The leak was outgassed by heating in vacuum before every run and tested for imperviousness to gases other than hydrogen by an external helium atmosphere.

The pressure was maintained at a constant pressure differential against atmospheric pressure by means of an oil-filled manometer which simultaneously served as a pressure regulator. During the run the palladium leak was operated continuously thus changing the H_2 gas once every 20 min. Most of the gas was removed by a vacuum pump throttled by a needle valve; a slight excess bubbled out through a manometer-regulator. The density of the oil in the manometer ("Litton" diffusion pump oil) was determined by weighing. The pressure excess used was of the order of 10 in. of oil, i.e., only two percent of the total pressure. The atmospheric pressure was read to 0.1 mm on a precision mercurial barometer. Difference in altitude between locations of the barometer and scattering chamber introduced a correction of 0.6 mm of Hg.

The gas temperature was read by means of an accurate thermometer in contact (maintained by a water cup) with the heavy brass barrel containing the gas and plate cartridge. The only question then is whether the beam barrel is in temperature equilibrium with the gas. This point was investigated by introducing thermocouples into the hydrogen gas and onto other points. Couples were located: (1) near the center of the vessel in the scattering region; (2) at the outer edge of the hydrogen volume; (3) along the copper tubing leading hydrogen into the chamber. The three couples showed differentials corresponding to less than 1°C. One of the couples was surrounded by a radiation shield consisting of a polished aluminum cylinder; presence or absence of this shield did not affect the temperature readings. Problems regarding temperature equilibrium appear to be insignificant here, as contrasted to earlier work on this subject; the reason is presumably the high pressure of hydrogen used.

D. Beam Collimation

In any high energy experiment of this kind the principal concern is the reduction of background. "Background" tracks observed were principally attributed to the following causes: (1) slit scattering on collimator apertures; (2) particles starting from chamber walls and from plate holders; (3) protons generated by $n-p$ collisions in the chamber gas; and (4) neutron knock-ons and neutron-induced nuclear processes in the emulsion. Let us now discuss the various measures taken to reduce the sources of background.

Figure 7 shows the relative disposition of collimator and the photographic plates. Two considerations affect the choice of collimator material: one is the neutron production in the collimator parts, and the other is the fraction of incident protons which will scatter out of the slit after having penetrated the material. The first point makes carbon a logical choice: the total yield for neutron production in carbon is only approximately 10^{-3} at 30 Mev and the energetic upper limit on the possible neutron energy is 10 Mev. This means that a

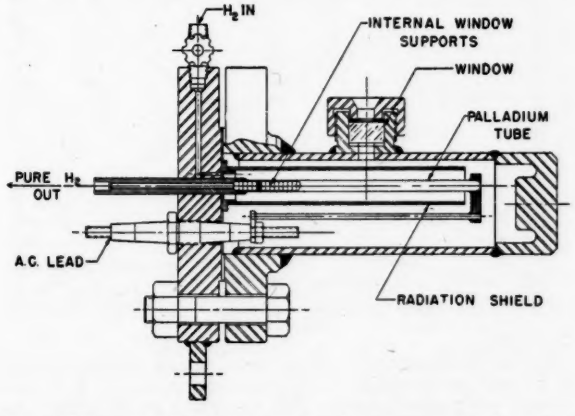

FIG. 6. Diagram of 500 p.s.i. external pressure palladium leak. Note that the palladium tube is directly heated.

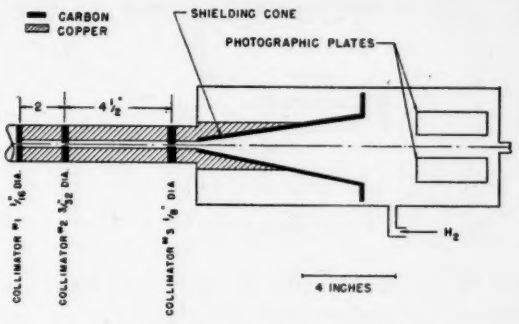

FIG. 7. Diagram of collimating system.

neutron formed on carbon does not have sufficient energy to produce a nuclear reaction when impinging on graphite. Accordingly, the collimating disks were made of graphite and in addition the faces of the plate holder which could "see" the photographic plates were lined with graphite. As to the second point, namely the problem of the proton scattering out of the slit after initial penetration, calculations† show that if the edges of a carbon slit of full range thickness is hit by a beam of 30-Mev protons, an amount will scatter out of the slit corresponding to the number of protons incident over a strip of width 0.001 in. For lead the corresponding number is 0.007 in. A low atomic number collimating disk is thus of advantage here. From this point of view either Be or C are favored; however, the small neutron binding energy in Be makes the choice of carbon the most reasonable. It is essentially impossible to design a collimator such that no secondary protons can reach the photographic plates; the present design (Fig. 7) simply minimizes the slit scattered protons, consistent with a given length of collimator. The number of slit-scattered protons can of course be further reduced by lengthening of the collimator, however at the expense of decreased mechanical tolerances. There are still a large number of slit scattered tracks on the plates (for statistics see Section III-B) but these cannot fall on the plates at an angle exceeding 8° and are therefore not included in the tabulation range.

In order to attenuate the neutron flux through the scattering regions and the region of the plates, the collimating disks were surrounded by copper pieces. Copper has a mean free path of approximately 4 in. for inelastic events for fast neutrons and hence appreciable flux reduction is possible. Also an additional 2-mm aperture was introduced ahead of the analyzing magnet (see Fig. 2) which reduced the number of protons incident on the collimator and hence reduced the neutron flux.

One of the effects of neutrons in the hydrogen chamber is to produce $n-p$ collisions resulting in erroneous proton tracks. In order to reduce the hydrogen volume "seen" by the plates a cone turned of graphite was intro-

† This calculation was made by E. A. Martinelli, to whom the authors are indebted.

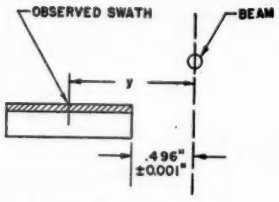

FIG. 8. Measurement of y.

duced to cut off the hydrogen region not traversed by hydrogen scattered protons (see Fig. 7).

It should be pointed out that the efficacy of the background reduction measures does not have to be evaluated by calculation but is experimentally determined both by background runs and by the symmetry of tabulated tracks about a laboratory angle of 45°. (See Sections III and V.)

E. Integrator

The beam, after passage through the scattering chamber is integrated by collection in a Faraday cup. The integrator was constructed by Mr. Lee Aamodt. The charge is collected on a low leakage condenser. Details of construction of the instrument, the method of calibration and the test for secondary emission are described in the adjoining report by Cork, Johnston, and Richman.[20]

III. TECHNIQUE OF GATHERING DATA

A. Microscope Technique

The plates are scanned under a high power microscope to count the number of scattered proton tracks. A 97x oil immersion objective is used with 7.5x eyepieces. The data required are the angle θ_{lab} and the distance d of the entering point of the track from the beam center. We recorded θ_{lab} and the coordinates x_0, y_0 of the point where the track enters the emulsion. x_0 was recorded to enable one to relocate individual tracks when checking the counting which another person has done; this will be discussed later. The actual recording is done by photographing the readings of three rotary counters which are connected to the microscope drives by flexible shafts. A Recordak Jr., Model J.C. microfilm recorder‡ was rented for this purpose, and the three counters placed on the stage of the microfilm recorder. One eyepiece has a specially built worm drive attachment so that it can be rotated for measuring the angle of the scattered proton tracks. It has a reticle with a hair line ruled on it for this purpose as well as a scale representing a length of 100μ (actually 102.0 $\pm$0.5μ) so that ranges of tracks can be measured accurately. The other eyepiece has two accurately parallel hair lines which correspond to a separation of 127.0 $\pm$0.5μ. Tracks which enter the emulsion between these lines are counted, so that a swath 127μ wide the length of the plate is read at one setting of the microscope carriage y coordinate.

The plate holder on the microscope carriage was designed and constructed by W. W. Brower to permit very accurate alignment of the plates in the microscope and accurate re-inserting of a plate if it has to be removed from the microscope at any time. Plates were re-inserted accurately in the plate holder to closer than 0.001 in. after a 6-month interval. The plate is clamped securely by a spring which presses it against two indexing ledges, one at each end of the plate, which correspond in position to the indexing surfaces in the scattering chamber plate holder. These indexing ledges were observed to be accurately parallel to the axis of the lead screw on the microscope carriage x coordinate drive to within 1/1000 of a radian. The hair line in the goniometer eyepiece can be set parallel to these indexing ledges to within 3/1000 of a radian. The accuracy of its alignment is checked every few hundred tracks to insure that the mechanism has not slipped. Thus any systematic error in measuring θ_{lab} is less than 0.2°.

The rotary counter which records θ_{lab} can be read to 0.1°. Back-lash in the mechanism is less than 0.3°. The vernier scale on the x and y coordinate lead screws of the microscope carriage are graduated in thousandths of an inch and were checked against a Bausch and Lomb standard showing that they were accurate to closer than one part in a thousand. The separation of inside plate edges of paired plates in the scattering chamber plate holder was measured to be 0.992$\pm$0.002 in. The y distance from the axis of the geometry to the center of a swath is obtained by adding half of 0.992 in. to the distance from the edge of the plate to the center of the swath as read from the y coordinate of the microscope. Thus the distance y to the center of a swath is measured to within about $\pm$0.001 in. (See Fig. 8.)

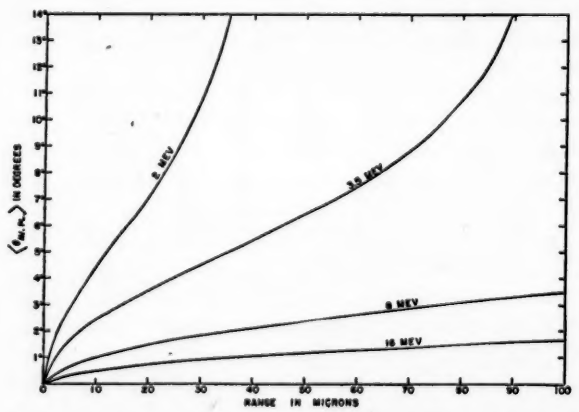

FIG. 9. Plane projected root mean square scattering angle plotted as a function of the distance along a proton track. Various primary energies are shown. This scattering angle is the r.m.s. of the plane projection of the angle of the tangent to the track with the initial direction.

‡ Can be rented from: Recordak Corporation, 561 Clay Street, San Francisco, California.

B. Criteria for Reading Tracks

When one looks at a plate it becomes quite evident that many of the tracks seen are obviously not scattered protons at 30 Mev, but are what we call a non-confusable background. Such tracks are caused by scatterinf from the collimating slits, neutrons producing knock-on protons in the gas and plate holder material, protons scattered backwards from the 1-mil aluminum exit foil, or scattered protons which strike the walls of the chamber and are there scattered through a large angle either elastically or inelastically. The majority of such tracks are non-confusable since they are observed to have quite low energies. This non-confusable background, including slit scattering which enters at $\theta_{lab}<8°$, is very roughly double in number to the number of good tracks on the plate.

In addition to this obviously non-confusable background, one sees tracks which can easily be mistaken for good scattered proton tracks but which upon more careful consideration can be shown to be spurious. Such tracks are due to the small fraction of the background protons mentioned in the preceeding paragraph which happen to enter the emulsion at an energy very nearly correct for their scattering angle θ. These tracks are about eight percent of the good tracks, and their detection is a matter which requires a fair amount of skill and judgement on the part of the observer. Since it was desired to have several observers counting tracks it was necessary to undertake a training program which would insure that all observers were competant to detect these barely non-confusable tracks and eliminate them. To this end several criteria were established for the judging of each track, and each observer was carefully instructed in their application. Spot checks on the counting of each observer have been made and an estimate of the reliability will be given later. In order to establish the basis for the criteria and also to consider the angular accuracies of this method it is first necessary

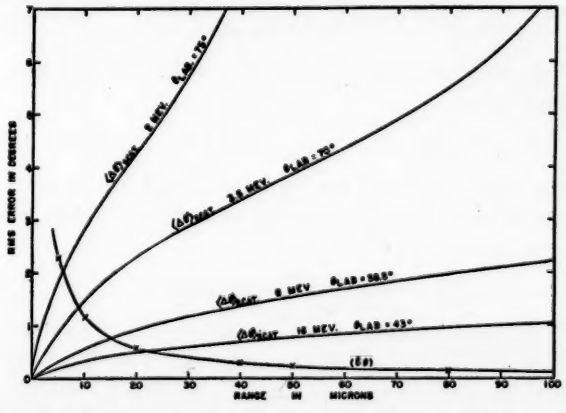

FIG. 10. Root-mean-square error $\langle\Delta\theta\rangle_{scat}$ in measuring θ_{lab} due to scattering, obtained by comparing the direction from the point of entry to a point along the track with the initial direction, plotted as a function of range. Also shown is the error $\langle\delta\theta\rangle$ in measuring θ_{lab} due to finite grain size, plotted as a function of the length of track used in making the measurement.

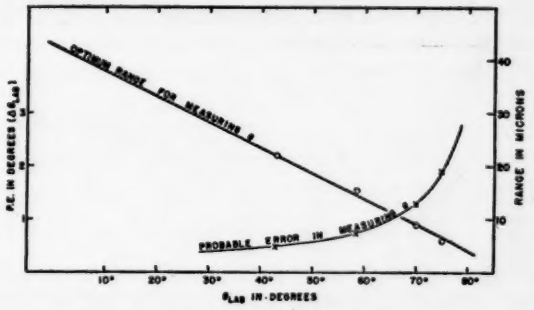

FIG. 11. Plot of optimum range for angle measurement as obtained equalizing scattering and grain size errors. The resulting over-all probable error $\Delta\theta_{lab}$ is also shown.

to investigate the multiple scattering of protons in the emulsion.

The mean square of the plane projection of the scattering angle of a particle of unit charge, momentum p and mass m, traveling a distance x in an absorber of atomic number Z and numerical density N is[21,22]

$$\langle\theta_{Av.pl.}\rangle^2=(4\pi e^4Z^2Nx/p^2v^2)\ln(\theta_{max}/\theta_{min}) \quad (10)$$

where $\theta_{min}=mcZ^{\frac{1}{2}}/p181=\lambda Z^{\frac{1}{2}}/137^2r_0$ is given by screening and $\theta_{max}=\lambda/(0.57r_0Z^{\frac{1}{3}})$ is given by the finite size of the nucleus. Thus Eq. (10) can be written (non-relativistically)

$$\langle\theta_{Av.pl.}\rangle^2=[2\pi r_0^2/(E/mc^2)^2]xNZ^2\ln(181Z^{\frac{1}{3}}) \quad (11)$$

where $r_0=2.82\times10^{-13}$ cm, m is the electron mass, and E is the energy and is assumed constant along the path. The composition of the Ilford C-2 emulsions used is given in an article by J. H. Webb.[23] The result of summing Eq. (11) over the components of the emulsion is found to be

$$\langle\theta_{Av.pl.}\rangle^2=19.7x/E^2 \quad (12)$$

where x is in cm and E is in Mev. The square root of Eq. (12) can be interpreted as the slope of a trajectory after having undergone the r.m.s. scattering. Since E will vary along the path, we must find $\langle\theta_{Av.pl.}\rangle$ as a function of x by a numerical integration along the path (Fig. 9). We can then find the mean displacement y as a function of x by a numerical integration. The measurement of the scattering angle θ_{lab} is done by measuring the secant over a certain optimum length x of track. The r.m.s. error is this measurement due to scattering will thus be

$$\langle\Delta\theta\rangle_{scat}=\arctan(y/x). \quad (13)$$

A plot of $\langle\Delta\theta\rangle_{scat}$ *vs.* x for various energies is shown in Fig. 10.

The determination of the optimum length of track for measuring θ_{lab} will now be discussed. There will be an error in θ_{lab} due to inaccuracy in setting the goniometer eyepiece hair line. This is due to finite width of the

[21] B. Rossi and K. Greisen, Rev. Mod. Phys. 13, 240 (1941).
[22] H. A. Bethe, Phys. Rev. 70, 821 (1946).
[23] J. H. Webb, Phys. Rev. 74, 511 (1948).

TABLE I. Typical data.

Plate	Length scanned	Total tracks	Good tracks	Spurious tracks: Tracks obviously not confusable	Grain density wrong	Dives too steeply	Angle inconsistent with range
P190	0.222 in.	83	35	45	2	1	0
P191	0.355 in.	131	39	90	1	1	0
P192	0.450 in.	149	67	77	1	3	1
P193	0.291 in.	179	35	139	2	3	0
P194	0.292 in.	170	44	121	2	3	0
P195	0.300 in.	132	44	85	0	3	0

hair line and grain diameter. The value we adopt for for this error is

$$\langle\delta\theta\rangle = d/2x \tag{14}$$

where d is the grain diameter which is about 0.3μ according to Webb[23] while we obtained a slightly higher value, namely about 0.46μ, using formulas he gives. We will use the value 0.4μ for d. Values of $\langle\delta\theta\rangle$ are plotted in Fig. 10 along with those of $\langle\Delta\theta\rangle_{\text{scat}}$. In order to minimize the error in angular measurement we must adjust x so as to equalize these two errors. A plot of optimum x *vs.* θ_{lab} is given in Fig. 11. The probable error of the angular measurement $\Delta\theta_{\text{lab}}$ is now given by $0.6745\sqrt{2}$ times the value of $\langle\Delta\theta\rangle_{\text{scat}}$ read at the crossing points on the curves in Fig. 10. A plot of $\Delta\theta_{\text{lab}}$ *vs.* θ_{lab} is shown in Fig. 11. We have neglected scattering in the H_2 after proton scattering but this has a negligible effect on the results. An experimental range-angle plot of 130 tracks to be discussed presently shows good agreement with the above values of $\Delta\theta_{\text{lab}}$.

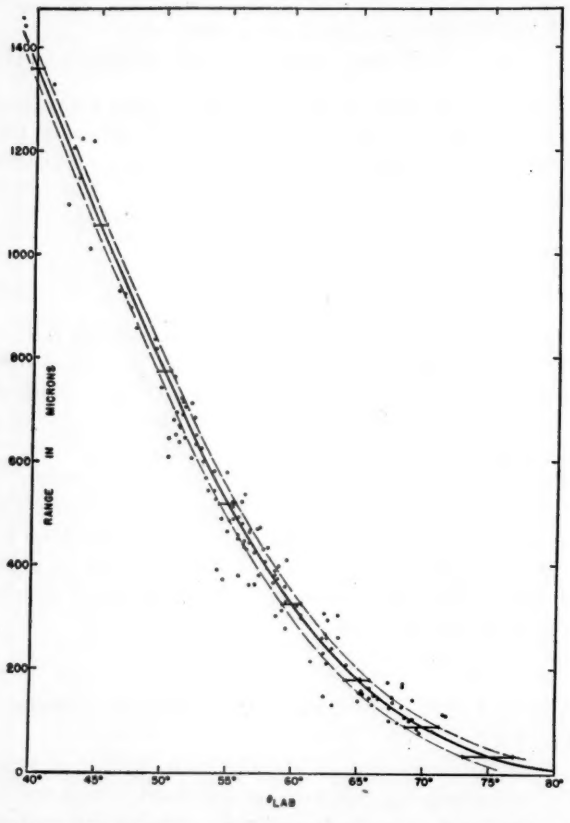

FIG. 12. Plot of the ranges and laboratory scattering angles of 130 protons. The solid line is the best fit for a curve based on a range energy relation of the form $R=\alpha E^{1.72}$ and on the conservation laws. The dashed curves represent the deviation from this curve caused by the probable error in angle measurement as obtained from Fig. 11.

It is evident from Fig. 11 that the probable error in measuring θ_{lab} becomes excessive as θ_{lab} approaches 80°. A more accurate measurement can be made by obtaining θ_{lab} from the experimental range-energy relation of protons in the emulsion used, shown in Fig. 12. The plot contains 130 tracks, and the solid curve represents the best fit based on a range energy relation of the form $R=\alpha E^{1.72}$ which is the range-energy equation given by Bradner *et al.*[24] Since $E\cong E_0\cos^2\theta_{\text{lab}}$, the probable error in θ_{lab} is found to be

$$\Delta\theta_{\text{lab}} = 16.7^\circ\,(\Delta R/R)\cot\theta_{\text{lab}} \tag{15}$$

where ΔR is the probable error in the range measurement. $\Delta R/R$ ranges from about three percent at 65° to about 15 percent at 80°. This gives $\Delta\theta_{\text{lab}}=0.23°$ at 65° and $\Delta\theta_{\text{lab}}=0.44°$ at 80°. While the probable error in angle could be improved by using the range method down to $\theta_{\text{lab}}=60°$ or even lower, the authors decided upon placing the limit at 65° where the error in direct angular measurement is not excessive, because the range measurement is quite time-consuming for the longer tracks.

Since the plates are inclined at a small angle to the beam and the thickness of the emulsion is known, one can calculate the range in which a given proton will dive clear through the emulsion. Let us call this dive distance ξ. The angle β at which a proton enters the emulsion is easily obtained for various θ_{lab} from the geometrical dimensions cited earlier. To β we must add the effect due to scattering in the emulsion, the maximum value for which was taken to be $3\langle\Delta\theta\rangle_{\text{scat}}$. If E is constant along the track, it can be shown that the mean displacement is given by[21,22]

$$\langle y\rangle^2 = \tfrac{1}{3}x^2\langle\theta_{\text{Av.pl.}}\rangle^2, \tag{16}$$

where x is measured along the track, and hence approximately

$$\langle\Delta\theta\rangle_{\text{scat}}\cong[\langle y\rangle^2/x^2]^{\frac{1}{2}}=[\langle\theta_{\text{Av.pl.}}\rangle^2/3]^{\frac{1}{2}}=2.56(x)^{\frac{1}{2}}/E. \tag{17}$$

The unprocessed 50μ emulsion will shrink about 16 percent when dried by evacuation, so we have the following equation to solve for ξ:

$$[\beta+7.68(\xi)^{\frac{1}{2}}/E]\xi=4.2\times10^{-3}\text{ cm}. \tag{18}$$

β was taken at its maximum value over the beam for a given θ_{lab} thus giving the shortest possible ξ. The resulting values of ξ at different positions on the plate are plotted *vs.* θ_{lab} in Fig. 13, which also shows 247 experimental points taken at the center of the plate. On the basis of these points, the minimum value for ξ

[24] Bradner, Smith, Barkas, and Bishop, Phys. Rev. **77**, 462 (1950).

was lowered 15 percent from the theoretical curve and this was used as a criterion in determining which tracks were good. It is thus presumed that if a track dives through the emulsion too steeply it did not come directly from the beam and thus is spurious.

We may now summarize our criteria for determining good tracks. (1) Each track must have $\theta_{lab} \geq 10°$ and $\theta_{lab} \leq 80°$ as determined by a range of 8μ. ($R \geq 8\mu$.) (2) The energy of the track as estimated by its grain density must not be inconsistent with its angle. This is done by visually comparing the grain density of the track in question to the grain density of good tracks at close to the same θ_{lab}. This requires careful judgement on the part of the observer, but since only about three percent of the tracks counted were at all questionable from this point of view the probable error of the results will not be greatly affected by this. (3) For θ_{lab} between 65° and 80° where the grain density criterion is difficult to apply, a better criterion is available; namely, a comparison of range *vs.* angle. If the angle of a track as measured with the goniometer eyepiece disagreed with the angle as determined by the range measurement by more than four times the probable error as computed by the scattering formula above, the track was discarded. (4) Each track had to satisfy the dive distance criterion as discussed in the previous paragraph.

Table I gives a typical sample of the total number of tracks scanned, the number of those accepted as good and the number rejected with the reason for rejection.

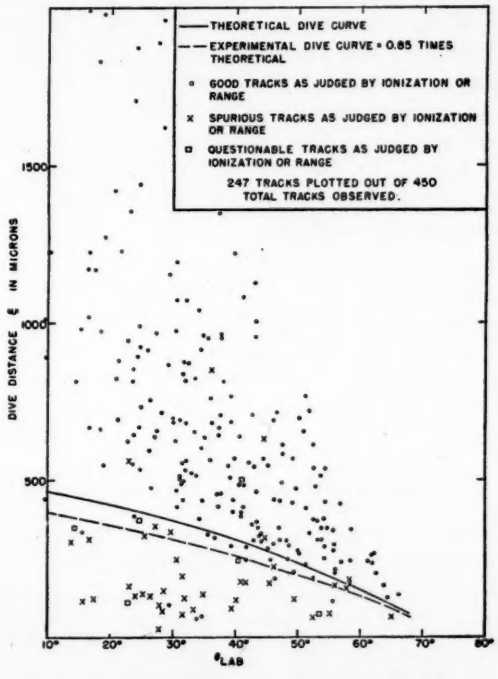

FIG. 13. The range ξ of 247 tracks before "diving" through the emulsion, plotted as a function of laboratory scattering angle. The solid line is the theoretical "limit" of dive distance based on a scattering of three times standard deviation. The dashed line is the experimental "limit curve" used as a criterion for accepting tracks.

It might be remarked here that although this procedure appears to be a somewhat elaborate analysis of the plates, it simply uses fully the information contained in nuclear tracks; namely, track position, ionization, and direction. The rejection of tracks entering at an incorrect angle is equally justifiable as is the selection of a particle trajectory by two counters in coincidence.

C. Background Runs

Since the elimination of all "confusable" background tracks is not possible it is necessary to make some measurements to see how much background is present. The causes of background have already been discussed so we will only describe here the methods of measuring background. Two types of background runs have been made; one, wherein the chamber is kept evacuated during the run, while in the other hydrogen was admitted as in the scattering runs but a graphite tube $\frac{3}{4}$ in. in diameter was inserted axially in the scattering chamber so as to surround the beam and thus prevent scattered protons from reaching the plates. All other geometrical factors were the same as in the scattering runs. These background runs were made immediately after the scattering runs.

Comparison of the counting of tracks on the background runs with that for the scattering runs showed that the high vacuum runs gave about 0.7 percent confusable tracks and the run with the graphite tube gave about 2.1 percent confusable tracks. No angular dependence was observed in the vacuum run. The back-

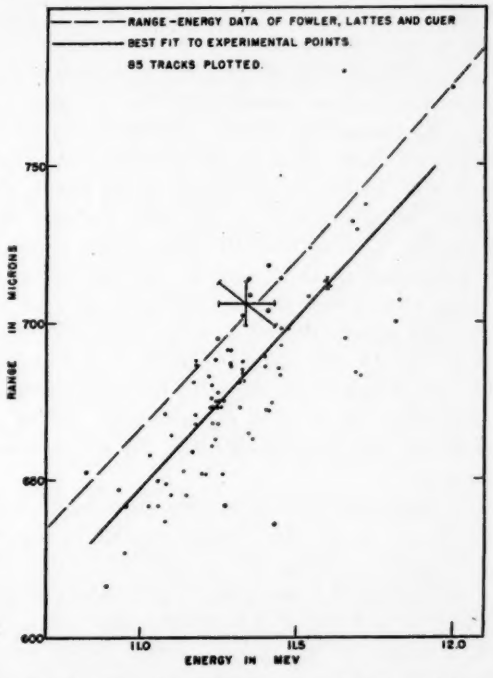

FIG. 14. Ranges and energies of 85 tracks exposed to protons in the 184-in. cyclotron. Emulsions used were the same and received the same treatment as in the $p-p$ scattering runs. Solid line is best fit; dashed line is from the data of Fowler, Lattes, and Cüer.

TABLE II. Run 37.

Original observer	No. of tracks counted	No. of tracks re-counted by F.L.F.	No. of tracks missed	No. of tracks incorrectly counted	No. of tracks which could not be relocated	No. of tracks recorded twice	Net correction per observer (percent)
S.G.A.	894	200	3	4	1	1	+1.5
F.L.F.	5320	610	7	6	1	3	+0.8
W.K.H.P.	1736	253	14	4	3	1	−2.4

ground in the graphite tube run was concentrated toward scattering angle $\theta_{lab}>50°$. It is believed that the background is due to inelastic events in the carbon and does not represent an applicable correction. The vacuum background has been applied as a correction to the absolute cross section.

IV. PRIMARY ENERGY

The primary energy can be obtained by comparing the measured range of the scattered protons as a function of angle in the emulsion with the experimentally known range-energy relation. In the work of Bradner *et al.*[24] it was found that the relativistically extrapolated range-energy relation given by Fowler, Lattes, and Cüer[25] was essentially correct, but that small variations occur when one compares different emulsion batches. They also found a small effect caused by varying the amount of dehydration of the emulsion just prior to exposure. Because of these variations, the accuracy claimed for the range-energy relation $E=0.251\ R^{0.581}$ given by Bradner *et al.*[24] was ±2 percent. In order to cut down on the error in the energy measurement, the authors have calibrated the emulsion used in this experiment at an energy near that at which comparison with the energy of the scattered protons is to be made. The method used is the same as that described by Bradner *et al.* Plates were exposed in the 184-in. cyclotron after being pumped in the high vacuum of the cyclotron for 6 hr. so that the plates were thoroughly dehydrated just as they were in the scattering runs. The range and energy was measured for 85 tracks and the resulting points plotted on a range-energy diagram, shown in Fig. 14. The data of Fowler *et al.*[25] are shown by the dotted line while the solid line representing the best empirical fit to the experimental points gives ranges which are 2.5 percent below the ranges given by Fowler *et al.*[25]

The probable error in the energy measurement of the proton by radius and field measurements in the cyclotron is found to average 0.8 percent while that of the range measurement is one percent plus 0.95 percent for straggling or a total of 1.4 percent per point. These errors, assumed to be random normal errors, are then combined in the usual manner to give the probable error of the experimental curve, which is thus found to be 0.17 percent. This error is a spread normal to the curves of Fig. 14 and corresponds to 0.24 percent in range.

The experimental range-energy plot for hydrogen scattered protons in this experiment is shown in Fig. 12, where the solid line is the best fit of the form $E=0.251\ R^{0.581}$ (determined empirically by counting the number of points lying above and below the curve), and the dashed curves represent the theoretical probable error $\Delta\theta_{lab}$ calculated earlier. By counting the number of tracks in the four sections of the graph, we conclude that the theoretical values for $\Delta\theta_{lab}$ are sufficiently accurate for our needs. The observed range for $\theta_{lab}=45°$ is 1058μ. When the 2.5 percent experimental correction obtained above is applied to the Fowler *et al.*[25] range-energy data, this corresponds to an energy of 14.59 Mev at the plates. The energy lost in the hydrogen after scattering at 45° is 24 kev, so the energy after scattering at 45° is 14.61 Mev. The relativistically correct formula for the kinetic energy of a scattered proton whose primary energy is E_0 in the lab system is given by

$$E=\frac{E_0\cos^2\theta_{lab}}{1+(E_0/2Mc^2)\sin^2\theta_{lab}}. \tag{19}$$

This gives the energy before scattering to be 29.4 Mev.

The probable error of the observed range is seen from Fig. 12 to be ±5.4μ or 0.51 percent which when combined with the probable error of the range energy relation gives a total probable error of 0.56 percent for the range; using the exponent in the Bradner *et al.*, range-energy relation this corresponds to a probable error in the primary energy of 0.33 percent or ±0.1 Mev. Note that this represents the probable error of defining the central value of the energy and not necessarily the energy spread. By analysis of the geometry of the analyzing magnet it can be shown that the beam is monochromatic to ±0.18 Mev.

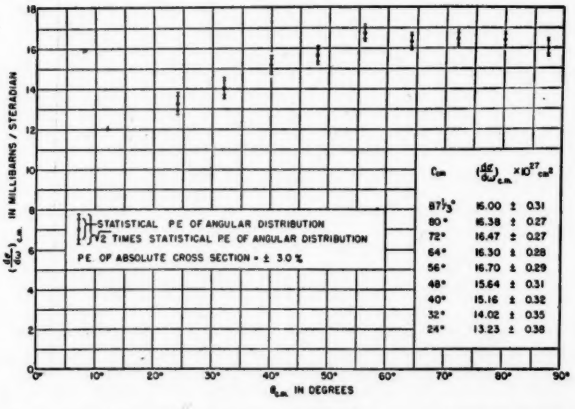
IN MILLIBARNS / STERADIAN
STATISTICAL PE OF ANGULAR DISTRIBUTION
√2 TIMES STATISTICAL PE OF ANGULAR DISTRIBUTION
PE OF ABSOLUTE CROSS SECTION = ± 3.0 %
IN DEGREES

FIG. 15. Observed differential cross section (center-of-mass system) as a function of center-of-mass scattering angle. Probable errors of the relative cross section are shown plotted with the points; these are based either on purely statistical errors or a conservative estimate of systematic deviations. The probable error of the absolute scale is ±3.0 percent.

[25] Lattes, Fowler, and Cüer, Proc. Phys. Soc. London **59**, 883 (1947).

V. ESTIMATE OF ACCURACY

A. Errors Affecting the Relative Cross Section

In discussing the errors in this experiment it is necessory to distinguish those errors which affect the accuracy of the absolute cross section only from those affecting the angular distribution. Let us discuss the latter first.

1. Statistics

10,934 tracks have been tabulated. The number of subdivisions in angle is of course arbitrary and has to be chosen in accordance with the rate of angular variation of the observed cross section. If the data are tabulated in 4° intervals in the laboratory system (Fig. 15), then the maximum rate of variation per point is about two probable errors and therefore probably significant. At this angular interval the statistical probable errors vary from ±2.3 percent (at 43° laboratory angle) to ±3.3 percent (at 12° laboratory angle).

2. Reliability of Observers

About two-thirds of the tabulated tracks have been read by one of us (F.L.F.) and the remainder by the other author (W.K.H.P.) and Mrs. Sue Gray Al-Salam, to whom the authors are greatly indebted. To check the reliability of observers F.L.F. has re-read samples of plates read by other observers. The re-reading cannot be done in a manner which is completely independent of the first reading because it is impossible to reset the swath position to closer than about $\pm 5\mu$. This means that tracks which are near the edge of a swath might correctly be counted inside by one observer and outside by another. The method used was to scan along a swath until a good track is found and then to look at the other observers' data and see if they had counted this track. In tabulating tracks missed, allowance is made for tracks which start near the edge of a swath. It is felt that the number of tracks missed by both observers is less than one-half percent so that to a good approximation we may tabulate the difference between the first observer's count and both observer's count as being the number missed by the first observer. The results of the principal run are given in Table II. No systematic difference in angular distribution was discovered in the tracks missed.

3. Accuracy of Angular Measurement

It was shown in Section III that in the interval $10° \leq \theta_{lab} \leq 65°$, where the angle is determined by direct measurement, the probable error in θ_{lab} varies from $\Delta\theta_{lab} = \pm 0.3°$ at $\theta_{lab} = 10°$ to $\Delta\theta_{lab} = \pm 1.0°$ at $\theta_{lab} = 65°$. In the interval $65° \leq \theta_{lab} \leq 80°$, where θ_{lab} is determined from range measurement, $\Delta\theta_{lab} = \pm 0.23°$ at $\theta_{lab} = 65°$ and $\Delta\theta_{lab} = \pm 0.44°$ at $\theta_{lab} = 80°$. Owing to the slow variation of cross section with angle, the angular uncertainties do not contribute appreciably to the error in the relative cross section.

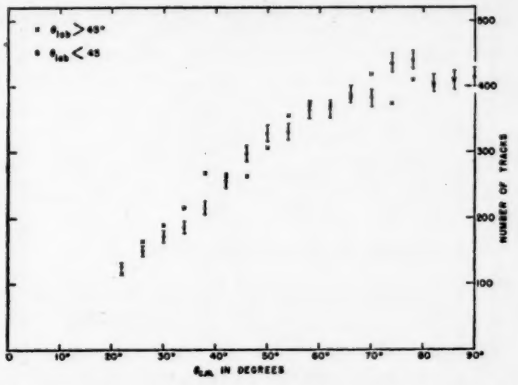

FIG. 16. Track counts plotted separately for laboratory scattering angle >45° and <45°. Equality between the count at a given angle and its complement serves as a criterion of like particle scattering.

4. Geometrical Errors

None of the geometrical errors discussed contribute to the uncertainty in relative cross section.

5. Impurities and Background

The total number of "confusable" tracks observed in the background runs was 0.7 percent with no significant angular correlation. Thus background effects to not appreciably contribute to the probable error of the relative cross section.

The impurity content can be estimated from the rate of rise of pressure with the chamber isolated and the rate of pure gas exchange. The results gives 4×10^{-5} for the maximum impurity content. Even at $\theta_{lab} = 10°$ the Coulomb contribution to the scattering yield due to the impurity (taken as $Z=8$) is thus only 7×10^{-4} of the observed proton yield.

All background effects, impurity scattering and systematic observational errors, are detectable by the fact that they presumably do not possess the symmetry about a laboratory angle of 45° characteristic of like particle scattering. Figure 16 shows the data plotted separately in the angular intervals $\theta_{lab} \gtrless 45°$. There is no statistically significant disagreement between the data in the two angular intervals. Nevertheless, the statistical error of any internal check of this kind is twice as large as the statistical error of the combined data. One can therefore conclude from the absence of any systematic dissymmetry that the effect of impurity scattering and background is not larger than the statistical error of the combined data; by the preceding arguments it is probably much smaller than this.

It appears as the result of this discussion that a conservative estimate for the probable error of the differential cross section is $\sqrt{2}$ times the statistical error of the combined data.

B. Errors Affecting the Absolute Cross Section

As was discussed in Section II-B the error is greatly reduced if the absolute cross section is obtained by

TABLE III. Data from individual plates. (The notation is that of Section II-B.)

Pair No.	Pair	Number of tracks	$\Sigma L/y^2$	Number of tracks weighted by scanned area and swath distance	$\frac{\delta Z}{Z}=\frac{N_1-N_2}{N_1+N_2}$	ϵ_Z percent
A	1	1127	10.94	103.0	0.1237	0.021
	2	1412	10.69	132.1		
B	1	1006	16.00	91.5	0.1766	0.044
	2	1449	11.08	130.8		
C	1	1299	11.24	115.5	0.0538	0.004
	2	1072	10.34	103.7		
					Mean error	0.023 percent

adding the tracks counted on symmetrically located pairs of plates. The basic formula for the absolute cross section is then

$$\left(\frac{d\sigma}{d\omega}\right)_{cm}=\frac{\Sigma N_t}{WN_pN_v\Delta(\cos\theta_{cm})}\times\frac{1}{\Sigma(LZ/y^2+Z^2)_1+\Sigma(LZ/y^2+Z^2)_2}, \quad (20)$$

where ΣN_t represent the sum of all tracks counted in the increment $\Delta(\cos\theta_{cm})$ in plates 1 and 2. The summations in the denominator give the solid angle factor weight for each swath, this being necessary since L and y are different for each swath. We will now discuss the errors contributed by each factor in Eq. (20); these errors will be denoted by ϵ with appropriate subscripts.

1. Statistics

Owing to the fact that the observed differential cross section is essentially flat near $\theta_{lab}=45°$, the tracks in the angular range $40°\leq\theta_{lab}\leq50°$ have been combined to give the absolute cross-section data. There are 1350 tracks in this angular range on which the computation is based, corresponding to a statistical probable error of $\epsilon_s=1.84$ percent.

2. Pressure Measurements

The pressure measurement is certainly accurate to 0.3 mm of Hg which corresponds to an accuracy of 0.2 mm of Hg in the reading of the mercury barometer and 2 mm in the reading of the oil manometer. This gives $\epsilon_p=0.04$ percent.

3. Temperature Measurement

The principal question as to accuracy of temprature measurement rests on the problem of temperature equilibrium discussed in Section II-C. It was concluded that equilibrium was established to within 1°C, corresponding to $\epsilon_T=0.3$ percent.

4. Errors in Beam Integration

(*a*) *Standard condenser.*—A polystyrene insulated condenser of nominal capacity 0.01 μf was sealed in a glass tube and calibrated against a General Radio Company standard condenser (certified accurate to 0.1 percent) by means of a ballistic galvanometer method. The calibration was made both before the runs and six months later; during this time a shift of 0.75 percent occurred. Owing to the slide-back system used no correction for lead and collecting cup capacity is necessary. We consider this equivalent to a 0.4 percent probable error.

(*b*) *Condenser voltage.*—The condenser voltage was measured by a standard cell-potentiometer method, accurate to 0.1 percent.

(*c*) *Condenser time constant.*—The condenser time constant was in all cases greater than 500 hr.; this corresponds to a possible error of 0.2 percent.

(*d*) *Secondary particles from collector.*—The tests made to check on secondary particles are described in the adjoining paper by Cork, Johnston, and Richman. It is concluded there that the effect of secondaries is less than 1.0 percent provided a proper high retarding voltage is used. We shall use a 1.0 percent probable error for this effect. Combining the integration errors we obtain: $\epsilon_I=1.1$ percent.

5. Plate Separation

The error in plate spacing is defined by the machining tolerance of ±0.0005 in. of the plate holder, 0.001 in. can thus be considered a limit of error and 0.0005 in. a probable error. The plate thickness measurement has a probable error of ±0.0004 in. These errors combine quadratically to give $\epsilon_D=1.11$ percent.

6. Swath Separation in the y Direction

The error in plate edge-to-edge separation was measured to a probable error of ±0.002 in. A swath is about 0.006 in. wide, so the value of y in the cross-section formula has a maximum uncertainty due to swath width of ±0.003 in. Taking half of this for the probable error we find $\delta_y=\pm0.0018$ in., whence $\epsilon_y=0.36$ percent.

7. Beam Centering Errors

As has been discussed in Section II-B the errors due to beam centering as affecting the cross section derived from adding counts in pairs of plates can be calculated from the difference in the counts in pairs of plates. In Table III 7843 counts from the individual plates as obtained in Run 37 have been listed. This source of error is thus seen to be negligible.

8. Swath Width

The swath width of $W=127\mu$ has a probable error of $\pm0.5\mu$ or 0.40 percent.

9. Other Geometrical Errors

Other geometrical errors which have been considered and found negligible are: (a) errors caused by lack of centering in the y direction; (b) errors caused by "scattering out" of tracks; (c) errors in knowing length of swath L.

10. Observational Errors

The observational error is much more serious in the case of the absolute cross section than it is in the case of the relative cross sections. The tabulation in Section IV-A shows that different observers diverge by a r.m.s. amount of 1.7 percent. This has been taken as the observational probable error in absolute cross section. The absolute cross section has a correction of -0.1 percent applied to take care of the tracks missed and duplicated. (See Section V-A-2.)

11. Uncertainty in Background

A correction of -0.7 percent has been applied as a background correction. The probable error of this correction is taken as ± 0.5 percent.

12. Combination of Errors

If the errors enumerated above are combined quadradically we obtain: $\epsilon_{\text{absolute cross section}} = \pm 3.0$ percent.

VI. RESULTS

A. Summary of Runs

Table IV summarizes the four runs upon which these results are based. We list all of the data taken for each run except for the detailed breakdown of the number of tracks counted in each angular interval.

B. Absolute Cross Section

The absolute cross section for a set of paired plates is calculated from Eq. (20) with N_p expressed in terms of the condenser voltage and capacitance, and N_v expressed in terms of pressure and temperature. The number of tracks observed in the two plates between $\theta_{cm}=80°$ to $100°$ is weighted by the solid angle factor as previously explained. The results thus obtained for the three sets of plates are then weighted according to their statistics and averaged giving the final result. For this calculation we have used the results of Run 37 only since the total charge collected in the earlier Run 28 was not known to better than about two percent. We thus obtain 15.94 ± 0.48 millibarn/sterad. for the absolute value of the cross section at $\theta_{cm}=90°$ at an energy of 29.4 ± 0.1 Mev.

C. Angular Dependence

The angular dependence of the cross section is found by dividing the number of tracks counted in each angular interval on all the plates by the sine of twice the laboratory angle at the center of each interval respectively. This gives relative values for the cross section which are then normalized to the absolute value over the interval $40° \leq \theta_{\text{lab}} \leq 50°$. The probable errors to be attached to each value thus obtained depend only on statistics as previously explained. The results are shown in Fig. 15.

VII. DISCUSSION OF RESULTS

A detailed analysis of these data has been undertaken at this laboratory by Christian and Noyes[26] and is being presented in an adjoining paper. It might be well here to discuss some of the conclusions.

In all prior $p-p$ scattering work only S-wave contributions were obtainable but in the interpretation of the low energy work[27] it has been frequently attempted to interpret small repulsive P-interactions from the data. The principal result of the present work is the approximate absence of any apparent higher angular momentum contribution, be it caused by a real absence of such terms or a fortuitous masking effect. The fact that this work disagrees even qualitatively from the

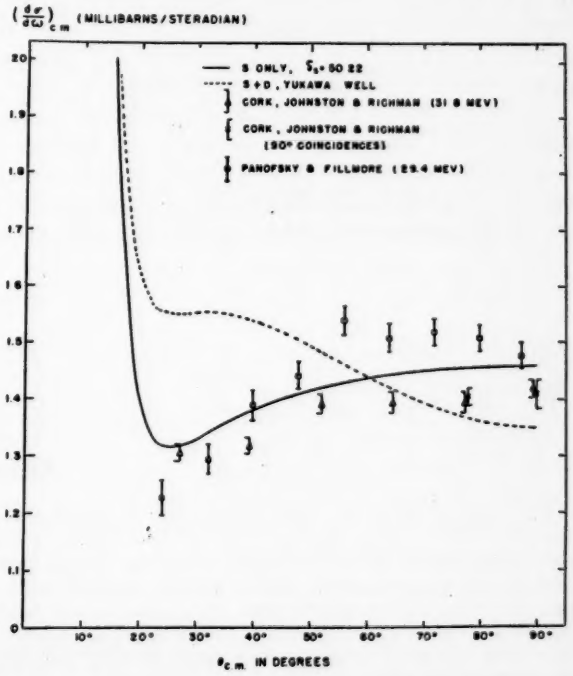

FIG. 17. Differential cross sections of Panofsky and Fillmore and of Cork, Johnston, and Richman (see reference 20) plotted together reduced to a common primary energy of 32.0 Mev by an assumed $1/E$ dependence of cross section. The two sets of data are *not* normalized but the absolute cross-section values are independent. Two theoretical curves (kindly supplied by Mr. P. Noyes) are shown: (a) pure S scattering using $\delta_s = 50.22°$; (b) total singlet scattering ($S+D$ scattering) using a Yukawa well and the same S phase shift. (Note suppressed zero of ordinate scale.)

[26] R. Christian and P. Noyes, Phys. Rev. **79**, 85 (1950).
[27] See, e.g., L. I. Foldy, Phys. Rev. **72**, 125, 731 (1947); also reference 10.

TABLE IV. Summary of runs.

Run No.	Date	Type of run	Time for pressure to reach 10^{-4} mm (sec.)	Temp. (°C)	Pressure (mm of Hg)	Charge collected (coulombs)	N_s	N_p	Total No. tracks counted
28	2–7 –49	Scattering	5.2	18	747.6	1.6×10^{-8}	4.95×10^{19}	1×10^{11}	3091
37	3–11–49	Scattering	3.9	24.3	757.0	1.401×10^{-8}	4.912×10^{19}	0.8745×10^{11}	7843
33	2–26–49	Background	1.2	—	10^{-4}	1.5×10^{-8}	—	0.94×10^{11}	12 confusable
38	3–12–49	Background	3.0	21.5	761.0	1.59×10^{-8}	4.98×10^{19}	0.99×10^{11}	37 confusable

expected results is the reason that this work is being presented now in its admittedly unfinished form.

At this energy also D-wave contributions should be appreciable and in particular an angular distribution including the singlet D-interaction can be computed from the low energy data, since the range and depth of the potential are known to good precision. The apparent absence of this contribution also means that there is either a very fundamental difficulty with the analysis of the data by a static potential or that a masking effect occurs. Christian and Noyes have investigated this point and have shown that it is formally possible at least to produce such a masking by a strong tensor interaction. Also such a strong tensor term accounts, at least qualitatively, for the large absolute differential cross section observed at a primary proton energy of 340 Mev[15] and 240 Mev.[14]

Figure 17 shows the data as obtained here plotted together with those of Cork, Richman, and Johnston.[20] Note that the primary proton energy of the two experiments differs by 2.4 Mev so that the absolute cross section measurements can be considered to be in agreement with an approximate $1/E$ variation of differential cross section and the assigned probable errors of the two experiments. It is also felt that the differences in shape between the two curves cannot be considered significant.

Figure 17 shows also the curve computed on the basis of singlet S and D interactions alone; it is thus seen clearly that neither of the experimental data are compatible with a central force static potential.

VIII. ACKNOWLEDGMENTS

The authors have benefited by the active cooperation of many members of this laboratory. In particular, thanks are due Mr. Al Kaehler for mechanical design, Mr. Lee Aamodt for construction of the integrator, Mrs. Sue Al-Salam and Miss Amy Bates for aid in reading and tabulating tracks. We have enjoyed the cooperation and advice of Messrs. Cork, Richman and Johnston in discussing our mutual difficulties, but it is believed that the results can be considered fully independent. The bombardments were carried out by the linear accelerator crew under the direction of Mr. Saul Lissauer.

Announcement

From time to time, the Institute has received inquiries from subscribers for information as to where and how they may have their copies bound. After investigation the Institute has found that this may be best accomplished by selecting a capable bindery that will work to our specifications and produce a well-bound volume at as low a price as possible. The necessary arrangements have been completed with the Book Shop Bindery, 308 West Randolph Street, Chicago 6, Illinois.

The volumes will be bound in the best grade of washable buckram with facsimile gold stamping on the spine and the subscriber's name in gold on the front cover. A distinctive color for each of the Journals has been selected as listed below. Advertising matter and covers are removed before binding. The price of $3.00 per volume applies to any of these journals regardless of size. Issues, comprising complete volumes, should be sent by prepaid express or parcel post to the Book Shop Bindery. Bound volumes will be shipped approximately 30 days after receipt. Return transportation will be prepaid when remittance accompanies order.

No deviation in color or specification can be allowed in view of the favorable price.

Physical Review	Green
Reviews of Modern Physics	Orange
Journal of the Optical Society	Brown
Journal of the Acoustical Society	Orange
American Journal of Physics	Black
Review of Scientific Instruments	Grey
Journal of Chemical Physics	Blue
Journal of Applied Physics	Red
Physics Today	Purple

Proton-Proton Scattering at 31.8 Mev, Proportional Counter Method*

BRUCE CORK, LAWRENCE JOHNSTON,** AND CHAIM RICHMAN
Radiation Laboratory, University of California, Berkeley, California

(Received February 20, 1950)

Differential cross-section measurements for proton-proton scattering have been made with protons of 31.8-Mev incident energy, scattered from hydrogen at one atmosphere pressure. Seven increments of angles from 15° to 51° in the laboratory system of coordinates have been measured simultaneously using proportional counters. In order that measurements could be made with very small currents, axially symmetrical defining slits and counters were made to include large solid angles. A 90° coincidence method was also used at large angles to give an independent geometry and to detect the possibility of slit and contamination scattering. The ratio of the differential cross section at 30° to that at 90°, center of mass system, is observed to be compatible with pure S-wave scattering of approximately 50° phase shift.

INTRODUCTION

THE scattering of protons on protons has been carried out by many investigators at successively higher energies,[1–13] and the analysis[14–19] of these experiments has provided us with a phenomenological picture of the nuclear interaction between two protons. The experiments which have been carried out so far which use protons of incident energy up to 14.5 Mev can all be explained on the basis of pure S-wave scattering. If there are effects in this energy region due to the scattering of the P-wave they appear to be small. It was very desirable therefore that experiments be made at higher energies to see if one could observe the scattering of the higher angular momentum waves. With the completion of the Berkeley linear accelerator such an experiment became possible.

The Berkeley linear accelerator[20] gives an external beam of well-collimated 32-Mev protons. This makes it practically an ideal machine with which to do scattering experiments. Two independent experiments were undertaken. One experiment, performed by Panofsky and Fillmore, uses nuclear emulsions as detectors of the scattered protons. The second experiment which is described below uses proportional counters to detect the scattered protons, and a completely different geometry. The apparatus was designed and constructed before the linear accelerator was completed. Since the magnitude of the anticipated beam was not known it was desirable to construct the apparatus so that as many of the scattered protons would be detected as possible.

Each proportional counter was thus constructed to intercept as large a solid angle as conveniently possible, and the scattering into seven angular intervals was measured simultaneously. To determine the internal consistency of the data, two different scattering geometries were used simultaneously, namely "singles" and "90° coincidence." By singles is meant that a count is registered every time a single proton goes into a particular counter. The scattering geometry for the singles is defined by the two coaxial cylinders and the zonal apertures of the individual counters as shown in Fig. 2.

When identical particles collide elastically their trajectories are at 90° to each other (including relativistic effects for 32-Mev incident protons the angle is 89.6°) in the laboratory system. Thus, a proton-proton collision can also be measured as a 90° coincidence by arranging the counters in the proper manner. The 90° coincidence[7] method is included for large angles to investigate the possibility of errors caused by slit scattering and contamination scattering, to reduce the effective background counts, and to give a geometry independent of the geometry of the singles counting method. The coincidence method depends only on the entrance apertures to the coincidence counters for the definition of the geometry.

DESIGN OF SCATTERING APPARATUS

The complete scattering apparatus is shown in Fig. 1. With one atmosphere of hydrogen in the scattering chamber a current of 10^{-13} ampere is sufficient to give a good counting rate of scattered protons. The accelerator was found capable of accelerating more than 10^5 times this amount of current. The protons were made

* This work was performed under the auspices of the AEC.
** Now at the University of Minnesota, Minneapolis, Minnesota.

[1] H. W. Wells, Phys. Rev. **47**, 591 (1935).
[2] M. G. White, Phys. Rev. **49**, 309 (1936).
[3] Tuve, Heydenburg, and Hafstad, Phys. Rev. **50**, 806 (1936).
[4] Hafstad, Heydenburg, and Tuve, Phys. Rev. **53**, 239 (1938).
[5] Heydenburg, Hafstad, and Tuve, Phys. Rev. **56**, 1078 (1939).
[6] Herb, Kerst, Parkinson, and Plain, Phys. Rev. **55**, 998 (1939).
[7] R. R. Wilson, Phys. Rev. **71**, 384 (1947).
[8] R. R. Wilson and E. C. Creutz, Phys. Rev. **71**, 339 (1947).
[9] Wilson, Lofgren, Richardson, Wright, and Shankland, Phys. Rev. **71**, 560 (1947).
[10] Dearnly, Oxley, and Perry, Phys. Rev. **73**, 1290 (1948). J. Rouvina (private communication).
[11] Blair, Freier, Lampi, Sleator and Williams, Phys. Rev. **74**, 553 (1948).
[12] Ragan, Kanne, and Taschek, Phys. Rev. **60**, 628 (1941).
[13] Bondelid, Bohlman, and Mather, Phys. Rev. **76**, 865 (1949).
[14] Yost, Wheeler, and Breit, Phys. Rev. **49**, 174 (1936).
[15] Breit, Condon, and Present, Phys. Rev. **50**, 825 (1936).
[16] Breit, Thaxton, and Eisenbud, Phys. Rev. **55**, 1018 (1939).
[17] Hoisington, Share, and Breit, Phys. Rev. **56**, 884 (1939).
[18] H. A. Thaxton and L. Hoisington, Phys. Rev. **56**, 1194 (1939)
[19] H. A. Bethe, Phys. Rev. **76**, 38 (1949).
[20] Bradner, Crawford, Gordon, and Woodyard, Phys. Rev. **73**, 534A (1948).

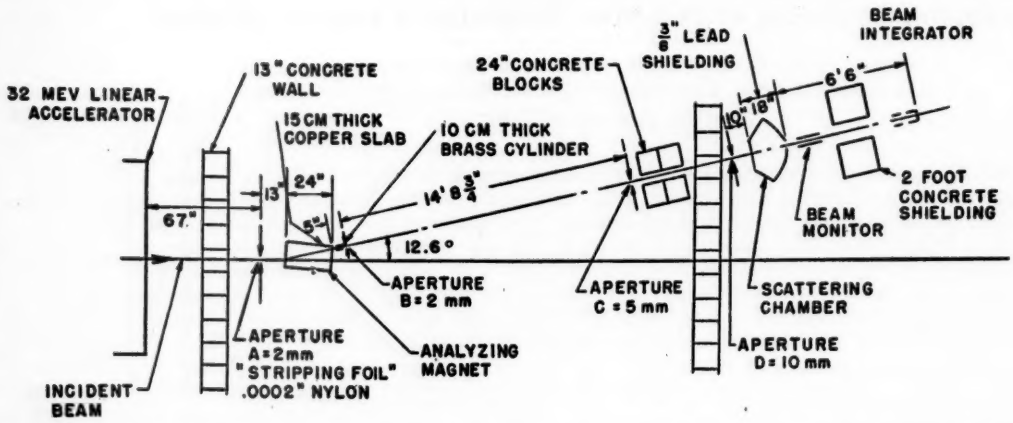

FIG. 1. General arrangement of apparatus.

monoenergetic by means of an analyzing magnet, and advantage was taken of the large available current to further collimate the beam to ± 0.05 degree by means of a slit system and tube approximately 5 meters long.

The scattering chamber is shown in Fig. 2. The proton beam is incident from the left and scattered from the region defined by two coaxial cylinders. In order that a favorable solid angle for detection of the scattered protons will result, the proportional counters have been made to detect simultaneously all protons scattered into various zones of a sphere. The two angle-defining cylinders limit the source of the scattered protons, and these plus the zonal apertures define the singles scattering geometry.

Since it is desirable to evacuate the scattering chamber and the proportional counter independently, considerable care was necessary in the mechanical design of the supporting structure. The main body of the chamber is constructed of a welded cone of cold-rolled steel $\frac{3}{8}$ in. thick and nickel plated. Supporting struts (see Fig. 2) were likewise made of welded cold-rolled steel in the form of cones coaxial with the main body cone. These were spaced at the dividing zones of the increments of angle by radial struts which are welded to the main center hub.

The angle-defining plate, which is a section of a sphere, was carefully machined on a lathe, starting with a 600-pound slab of cold-rolled steel. The critical dimensions of the apparatus are thus determined by the dimensions of this plate and can be easily measured.

All of the windows for the counters were made by inserting a single 0.025 in. aluminum spinning over the angle-defining plate. Ring-type rubber gaskets sealed the scattering chamber and the counter chamber to the aluminum spinning. The counter chamber was made of a heavy aluminum spinning with conical aluminum partitions between the counters. Aluminum absorbers (see Table II) were placed in the small-angle counters to degrade the energy of the protons and increase their specific ionization. These absorbers also kept slit-scattered protons of low energy from penetrating into the counters.

Each counter is a torus of approximately a rectangular cross section, and the collecting electrode consists of a 0.002-in. diameter tungsten wire supported by 12 radial silk threads.

The 45° counter is split azimuthally into two 180° sectors, top and bottom, so that 90° coincidence between the top and bottom halves results. Likewise, the 39° and 51° counters are arranged so that the top-half of the 51° counter will give a 90° coincidence with the bottom half of the 39° counter, and vice versa.

Two 0.0002 in. Nylon foils rotated so that the "grain" in each is lined up at 90° to the other, form the diaphragm separating the hydrogen system from the linear accelerator. Hydrogen is admitted through a palladium leak to the collimator (Fig. 2) and allowed to diffuse through the scattering region. Most of the incident protons continue on through the chamber and are collected in the charge integrator, which will be described later. For convenience in sending beam-monitoring information back to the accelerator control desk, an ionization chamber has been included as indicated.

A mechanical shutter shown in Fig. 2, consisting of a cylinder, coaxial with the defining cylinders, is operated through a Wilson seal. Background runs are made with this shutter moved to the forward position, so that the aperture between the defining cylinders is closed.

DETECTION OF SCATTERED PROTONS

The signals from the proportional counters were transmitted through Kovar seals with Kovar guard rings to the grid of a 4-tube amplifier and cathode follower. The gas multiplication was approximately 100, but was changed during the process of determining the plateau for detecting all the scattered protons, which will be discussed in more detail later. The maximum gain of the 4-tube amplifier was 3000; the band-width was 0.9 megacycle. The output from each cathode follower operated a 5-tube channel consisting of a variable discriminator, gate tube, and scale of 4, with mechanical register. Signals from the 51°, 45°, and 39° discriminators were also sent to 3 coincidence units and to one unit that measured the number of accidental coincidences.

The resolving time of the singles scaling circuit is limited by the discriminator circuit. This resolving time was measured using a double-pulse signal generator, and it was observed that two signals closer than 5 microseconds will be counted as a single count. The resultant correction to our data was always less than 2 percent.

The mechanical registers used with the scale of 4 units are known to be reliable for 15 impulses per second, but of course they will not register two impulses during the same 300 microsecond interval. The counting rate was sufficiently small that, on the average, the mechanical register operated only once in eight pulses of the linear accelerator, making negligibly small the chance of getting two (scaled×4) impulses during a linear accelerator pulse.

MEASUREMENT OF ENERGY

The diameters of the collimators (Fig. 1) are as follows: *A*, 2.0 mm; *B*, 2.0 mm; *C*, 5.0 mm; *D*, 10 mm; *E*, 12 mm. Collimators *A*, *B*, and *C* used in conjunction with the magnet allow the proton energy to be selected to ±0.5 Mev. The integral of the magnetic field along the trajectory of the protons has been measured to ±½ percent by a group working with Mr. Duane Sewell. This plus the angular deflection of the beam is sufficient[21] to define the energy of the beam. The energy was also measured using proportional counters coincident in depth, plus aluminum absorbers to obtain first an integral curve and then a differential absorption curve. Each of these methods gives an energy of 31.8±0.3 Mev for the incident beam, corrected for energy loss in the nylon foil and hydrogen.

Since some ionized hydrogen molecules are accelerated to 16 Mev by the accelerator, it is necessary to insert a thin foil ahead of the magnet to "strip" the molecule, thus changing its charge to mass ratio so that it will not have the same $H\rho$ as a 32-Mev proton. A 0.0002 in. nylon foil mounted at collimator *A* was used to accomplish this stripping.

MEASUREMENT OF INCIDENT PROTON FLUX

The beam-integrating equipment is shown physically in Fig. 3 and electrically in Fig. 4. Protons enter the

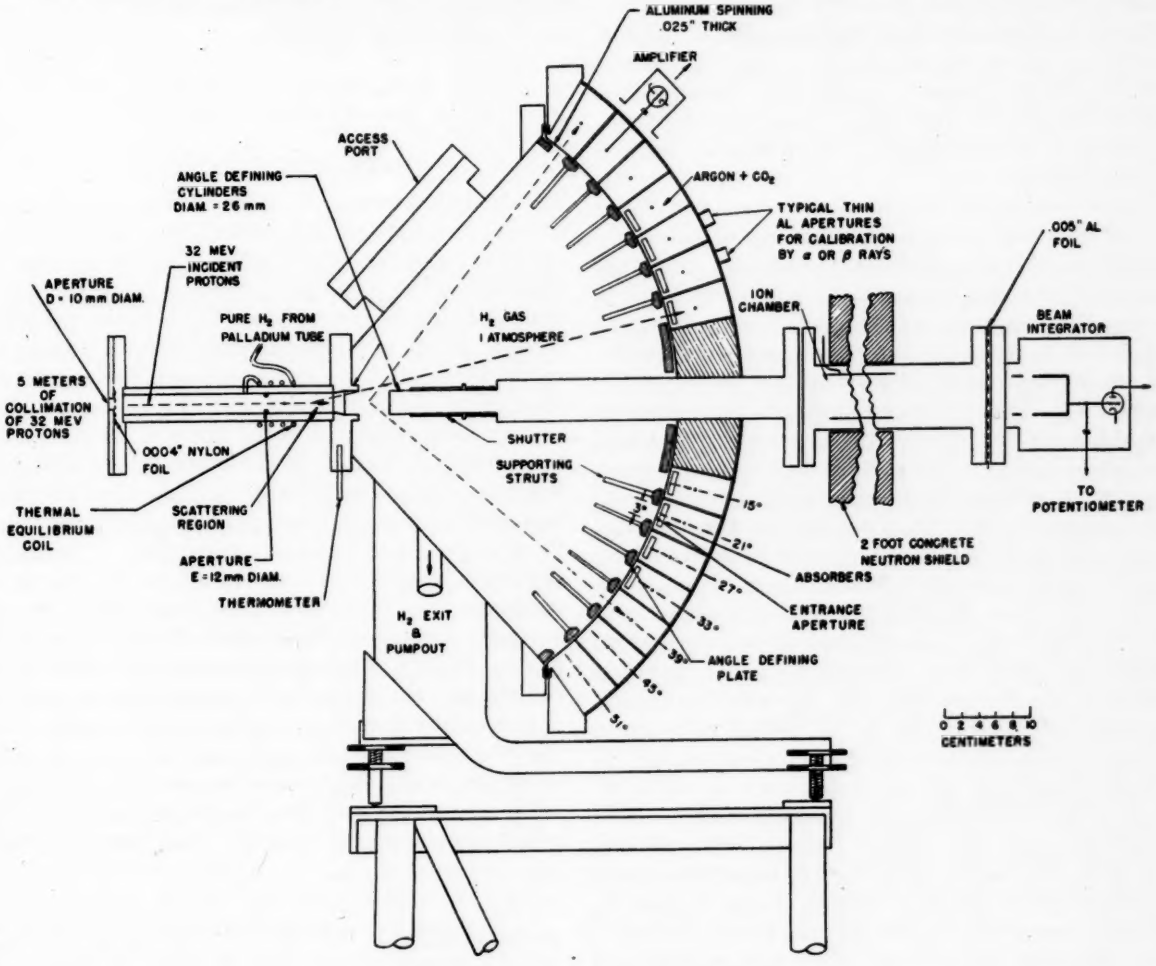

FIG. 2. Proton-proton scattering chamber.

[21] R. R. Wilson and E. C. Creutz, Rev. Sci. Inst. **17**, 385 (1946)

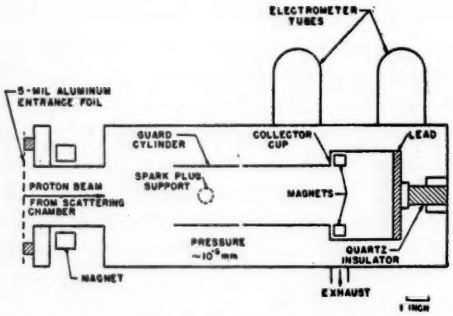

FIG. 3. Mechanical layout of charge integrator.

high vacuum region of the collector through a 5-mil aluminum foil and pass through a guard cylinder into the collector cup, where they are stopped in lead. The guard cylinder is maintained at -200 volts in order to trap secondary electrons, which are produced by the beam at the aluminum entrance foil and in the cup. As an added precaution against secondaries, small permanent magnets were mounted at the foil and in the cup to produce a field of about 50 gauss at the proton path.

The size of the beam and its orientation in the cup were determined by exposing an x-ray film to the beam, indicating that the beam was quite well defined with a diameter of about 2 centimeters. Clearances were considered adequate to the walls of both the cup and the guard cylinder.

The integrator circuit (Fig. 4) functions as follows: Protons collected in the cup charge the condenser $C_1=0.001071$ microfarad, causing a voltage V to appear across it. The charge is calculated as V times C_1. V is measured by manually adjusting the standard potentiometer P_1 to make the cup remain at ground potential, whereupon V is read as the voltage on the potentiometer dial. The electrometer tube and galvanometer comprise a vacuum tube voltmeter which is used as a null instrument to indicate when the cup is at ground potential. It will be seen that the potentiometer needs to be adjusted accurately only at the beginning and end of a run; it was kept in rough adjustment during a run, however, to monitor the collected charge.

To avoid errors due to stray lead capacitance and possible sensitivity to air pressure it was decided to measure the integrating capacitor C_1 in its operating position in the vacuum chamber. The effective capacitance for beam integration is the mutual capacitance between the cup and the potentiometer lead marked A, and is independent of the capacitance of either to ground; this was measured by comparison with a standard variable air condenser both at 1000 cycles and at very low frequency (actually d.c. impulses about 5 seconds long) by suitable bridges. These checked to within 0.2 percent, which was taken as the limit of short-time soakage in the condenser. Long-time soakage and leakage were also shown to be less than 0.1 percent for half-hour runs. The calibration of the variable condenser was also checked against a standard mica condenser at 1000 cycles. C_1 is a polystyrene insulated unit, made by the Fast Company. A series of $p-p$ scattering runs was made as a function of the potential on the guard cylinder, and another set as a function of gas pressure in the integrator, from which it was concluded that errors due to secondary electrons and gas multiplication would be negligible. The grid current of the electrometer tube was measured after each series of runs for which a correction of approximately one percent was necessary. We have assigned a probable error of $\pm\frac{1}{2}$ percent to the beam measurements. This integrator was developed by Mr. Lee Aamodt, to whom we are indebted.

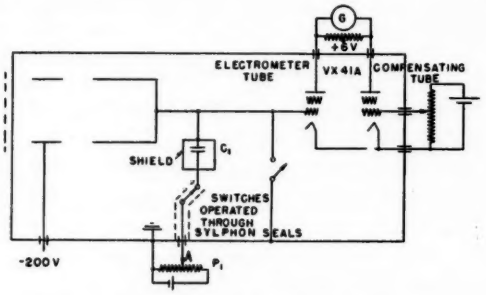

FIG. 4. Electrical circuit of charge integrator, slide-back type of potentiometer.

HYDROGEN GAS SUPPLY

Pure hydrogen gas for the scattering chamber was obtained by passing tank hydrogen through a heated palladium thimble. This device is similar to the one described in the preceding paper and hence will not be discussed. Before entering the chamber, the gas passes through a coil of copper tubing wrapped around the collimator tube, to insure thermal equilibrium with the walls of the chamber. The temperature is measured by a thermometer embedded in the flange of the collimating tube during a run. All joints in the tube carrying gas from the palladium tube to the chamber are made without rubber gaskets, using either metal flared fittings or threaded joints waxed with Cenco "Sealstix." Hydrogen enters the chamber in the middle of the collimator and from there flows continually out into the main volume of the chamber. It will be seen that most of the scattering takes place in the interior of the collimating tube where the hydrogen is most pure; this is particularly true of scattering at small angles, where the effects of Coulomb scattering from contaminating gases are most likely to be encountered. The excess hydrogen escapes from the chamber via an oil-lock tube which regulates the pressure and prevents back-

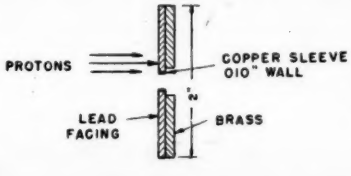

FIG. 5. Circular apertures, arranged with lead facing to reduce the neutron background.

TABLE I. Scattering data. Geometrical scattering length = 5.38 cm. Normalized for collected charge = 317.1×10^{-12} coulombs. Mean energy = 31.8±0.3 Mev. 89.7° *T* and *B* refers to top half and bottom halves of a given counter. All counts ×4.

Run	Date	Counter potential volts	Singles mean angles, center of mass 89.7°*T*	89.7°*B*	77.6°*B*	64.7°	52.5°	39.8°	27.3°	Coincidence angles (center of mass) Av. back-grnd. %	$Q\times10^{-12}$ coulombs	90°−90°	102°−78°
1	7-15-49	3200*	590	623	582	1072	—	728	492	21	316	136	—
2		3200*	623	585	594	1061	929	706	494	28	316	132	138
3		3100*	625	625	600	1077	—	720	480	11	316	140	134
4		3100*	590	612	617	1085	—	690	494	13	316	138	139
5		3000	585	597	561	1125	—	641	459	10	316	127	128
6		3000	623	599	596	1088	—	668	447	5	316	134	137
7		3000	618	612	610	1084	—	677	474	5	316	138	136
8		2800	612	604	516	1016	—	616	416	2	316	128	124
9		Av. values	607	611	598	1074	(929)	711	490		1.264	136.5	137
10	7-22-49	3100*	655	630	602	1068	977	705	497	54	318	157	141
11		3000*	613	623	585	1039	948	713	485	25	318	140	141
12		3000*	614	647	601	1110	971	715	506	34	318	136	135
13		Av. values	628	633	596	1072	965	711	496		954	144	139
14	8-29-49	2700*	574	594	584		925	707	470	24	317	139	141
15		2700*	627	631	586		940	729	502	19	317	153	138
16		2700*	599	622	599		938	743	515	33	317	153	142
17		Av. values	600	616	590		934	726	496		951	148	140
18	9-1-49	2900*	607	607	598	1055	—	674	486	25	211	141	139
19		2800*	611	623	610	1091	—	742	514	25	211	153	142
20		2800*	657	625	608	1145		706	506	20	211	144	138
21		2800*	596	595	603	1059	—	710	485	26	211	126	135
22		2800*	582	606	589	1106	—	727	470	21	211	131	147
23		Av.	611	611	602	1091	—	712	492		1055	139	140
24	9-8-49	2800*	603	626	603	1151	963	745	512	35	211	139	139
25		2800*	595	605	606	1114	947	690	512	35	211	129	138
26		Av.	599	615	605	1132	955	717	512		422	134	139
27		Wtd. mean	610.1	616.9	597.5	1085	943	715	494.9			140.7	138.9
28		RMS Dev.	±.77	±.59	±.38	±1.1	±.78	±.36	±.70			±1.6	±.35
29		*G* factor	0.3108		0.3128	0.3444	0.3955	0.4937	0.7054			2.685	2.710
30		Abs. $(d\sigma/d\Omega)$c.m.	14.30		14.05	14.05	14.02	13.27	13.13			14.21	14.15
31		Prob. error (differential)	±1.1%		±1.1%	±1.4%	±1.2%	±1.1	±1.2			±1.8%	±1.1%

diffusion of air into the system. The hydrogen flow normally used was sufficient to change the gas completely in 90 minutes; this swept out contaminating gases evolved from the chamber walls with sufficient speed. Tests for determining gas contamination will be described in a later section.

BACKGROUND EVALUATION

Reduction of background counts was the greatest single difficulty encountered in doing this experiment, and it is felt that anyone starting to work with protons of this energy or above would do well to use coincidence counter telescopes, and fast circuits. By carefully shielding against x-rays and neutrons we were able to obtain data with a background of about 20 percent. Of this background, about $\frac{1}{4}$ is x-rays and $\frac{3}{4}$ neutrons.

The x-rays are generated by stray electrons accelerated to a few hundred kilovolts between the drift tubes of the linear accelerator. These were effectively reduced by covering the scattering chamber with $\frac{3}{8}$ in. of lead. The neutrons are produced wherever the beam strikes matter, with only slight dependence on the nuclear species. Rough experiments indicated that lead and bismuth gave approximately $\frac{1}{2}$ the background effect observed in carbon, copper or aluminum. Hence lead was used to stop the protons wherever practicable. A typical collimator disc is shown in Fig. 5. Most of the protons to be rejected by the disk strike the lead facing, while the hole itself is lined with a thin collar of copper to reduce scattering from the collimator edge.

The neutron flux at the counters is greatly reduced also by arranging the collimating system so that all protons to be rejected are stopped at some distance from the counters, and several feet of concrete are interposed between the counters and the last collimating disc. Note that the main proton beam does not strike any solids after collimator *C*, until it is stopped in lead at the integrator. The integrator is placed 6 feet behind the counters, in order to allow extra concrete shielding between them.

Background caused by cosmic rays and other accelerators in the vicinity was reduced to a very small

TABLE II. Absorbers installed in counter windows.

(Laboratory system) θ_{max}	θ_{min}	Total aluminum absorber mg/cm²	Residual range of 31-Mev incident proton mg/cm² Al
16.31°	11.00°	867	183
23.05°	16.76°	709	116
29.71°	22.51°	530	230
36.36°	28.49°	351	229
43.24°	34.39°	179	221
49.67°	40.00°	179	81
56.38°	46.00°	179	—

fraction of the total background by gating on the counters only during a pulse of the linear accelerator.

Since the background was large, it had to be evaluated accurately; and unfortunately the background varied with time by as much as 25 percent. Thus a single background run would not give a good correction. It was necessary to break up the running time into a series of short scattering runs alternated with background runs, so that the fluctuations in background would average out over the series. The only assumption necessary here is that background fluctuations are random with regard to whether the run is for measuring scattering or background, and we feel that this condition has been fulfilled. Background variations were caused by the operating conditions of the accelerator, and hence one might suspect that the accelerator crew would have been more careful in their operation during a scattering run than during a background run. Accordingly, precautions were taken to insure that the crew would not find out during a series, which runs were for background. The general background level in the room was continuously monitored by an auxiliary proportional counter of geometry similar to the proton counters and located adjacent to the scattering chamber. The readings on this counter were used to approximately normalize each background run to the general background level during the preceding scattering run. By these devices we were able to reduce to about $\frac{1}{2}$ percent the effect of background variation on our results, as judged from the internal consistency of the series of five runs listed in Table I.

A further item of importance is to show that the true background is being measured, i.e., that closing the shutter to cut off the scattered protons from the counters does not appreciably change the background counts.

The two principal avenues by which this could occur are here discussed: 1. Hydrogen-scattered protons which normally are counted, or which strike opaque zones of the steel defining plate, will instead strike the shutter and make a nuclear reaction which can produce a count. This will be a small effect, since such a nuclear reaction will have a yield of about 10^{-5}, and the resulting particles will be counted with low efficiency by the counters. 2. Any neutrons which enter the chamber co-linearly with the incident proton beam could produce $n-p$ scattering in the H_2 gas, which would be recorded as $p-p$ scattering since the shutter would cut out the scattered protons during background runs. In all counters, except the 77.6° one (all angles are expressed in the center of mass system), protons would not have sufficient energy to penetrate the absorbers placed in the counter windows unless they were scattered from neutrons of at least 22 Mev energy. The corresponding minimum neutron energy at the 77.6° counter is 18 Mev. We have shown in another experiment that the yield of high energy neutrons by 32-Mev proton bombardment on copper or lead is less than 10^{-6} using the carbon $(n, 2n)$ reaction as the detector. This reaction has a neutron threshold of 20 Mev. The most likely place for these neutrons to be produced is at collimator C, and, allowing that 100 times as much beam is stopped at this collimator as is transmitted, and that the neutrons generated spread out with a full angle at $\frac{1}{2}$ intensity of 10°, the neutron intensity inside the defining cylinders is less than 10^{-6} of the incident proton beam. Since $n-p$ and $p-p$ scattering cross sections are comparable in magnitude, $n-p$ scattered protons will be less than 10^{-6} of the $p-p$ scattered ones. The above is consequently a negligible source of error.

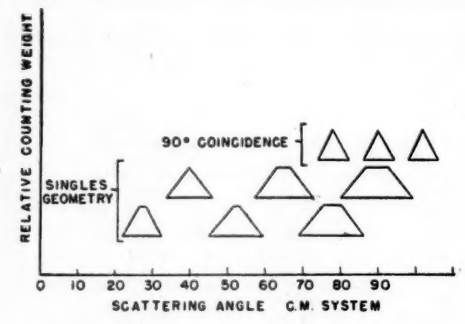

FIG. 6. Weighing factors of various counters.

EVALUATION OF PROTONS SCATTERED FROM SLITS, GAS CONTAMINATION, ETC.

Reference to Fig. 2 will show that it is impossible for a primary proton to scatter from the Nylon foil or any of the metal apertures and get into a counter, without scattering once more in the process from another body. The probability of such an event is rather complicated to calculate, so we relied on experiments in which we looked for residual scattering counts when the chamber was highly evacuated. No effect was observable above background. Thus this source of error would be less than 1 percent at all angles.

A possible event not covered by the above experiment would be that protons, scattered from hydrogen gas near the entrance foil at small angles, would strike the defining cylinders and thence bounce into a counter.

To test this, it was necessary to have hydrogen atoms in the coilimating tube to illuminate the edges of the defining cylinders with scattered protons, but it was also necessary to have no hydrogen in the scattering region from which "honest" scattered protons could reach the counters. This was arranged by placing an extra nylon foil 5 mils thick in the collimating tube at the plane of collimator E (Fig. 2). This foil is calculated to produce Rutherford scattering equivalent to filling the collimating tube with 100 atmospheres of H_2 gas. Residual scattering was now looked for with the chamber evacuated, but none was observed. One atmosphere of H_2 gas normally present in the collimator will produce less than a 0.1 percent error in the 27.3° counter, due to this event.

To determine the tolerance on gas impurities for this

experiment, the scattering of 32 Mev protons in air was measured with the same apparatus. From this we concluded that our hydrogen should contain less than 0.01 percent of nitrogen or oxygen in order to reduce the resultant scattering to 0.1 percent of the $p-p$ scattering. To determine the rate of evolution of contaminating gases from the chamber walls, the chamber was evacuated before each run, and the rate of increase of pressure measured on the chamber with the (cold) palladium tube connected. This rate never exceeded 10^{-5} atmospheres per hour, which, combined with the hydrogen flushing period of $1\frac{1}{2}$ hours, gives a maximum impurity content of 0.001 percent for the gas in the main chamber. Thus the feature of introducing the pure hydrogen gas into the scattering region of the chamber is not absolutely necessary, but it does provide a gross experimental check on the contamination of the main chamber, as follows:

At the end of a series of runs, a run was made in which the supply of pure hydrogen was cut off, so that any contamination in the main chamber would diffuse into the scattering region. The measured cross section was the same, to within its probable error of 2 percent, as in the runs in which the gas was flowing. The palladium tube was tested for perforation before and after each series of runs. In view of the measured low rate of evolution of contaminating gases, and the continuous renewal of hydrogen in the scattering region, we consider the scattering due to gas contamination to be negligible.

It is possible for hydrogen-scattered protons to strike the radial and conical supporting struts in the chamber and thence scatter into the counters. The corrections for these scattered protons have been estimated on the basis of Williams' equation,[22] and were less than 0.1 percent at all angles.

DETERMINATION OF GEOMETRICAL FACTORS

The basic differential equation defining scattering yields (ratio of scattered to incident protons) is

$$dY=(d\sigma/d\Omega)_{c.m.}N dt d\Omega$$

where dY is the yield of protons scattered into the solid angle $d\Omega$ from a path length dt of incident beam. N is the number of scattering nuclei per unit volume.

Reference to Fig. 2 shows that scattering occurs over such an extended region in this apparatus that the solid angle subtended by a given counter will vary considerably over the scattering region, and hence many of the usual simplifying assumptions made in other scattering experiments are not justified here. The above quantity was integrated over the solid angle $d\Omega_{c.m.}$ and along the scattering length dt. The geometry was evaluated in terms of a factor G, defined as,

$$1/G=\int d\Omega dt.$$

Then,

$$(d\sigma/d\Omega)_{c.m.}=GY/N$$

The assumption is made that $(d\sigma/d\Omega)_{c.m.}$ is a linear function of the scattering angle θ within the range of θ accepted by a given counter, for lack of previous knowledge of the real shape of the curve. The errors introduced by this assumption are calculated to be less than $\frac{1}{2}$ percent, if one accepts the theoretical curve for $\delta_s=49°21.6'$ in Fig. 7, as the true one. Table II indicates the angular interval covered by each of the counters, ranging from 10.6° for the 27.3° counter (all angles are in center of mass system) to 19.4° for the 89.7° counter. The entire angular interval does not have the same weight of course, since relatively fewer protons of extreme angles can get in. The weighting functions for protons of various angles getting into a given counter are roughly symmetrical trapezoids as shown in Fig. 6.

For purposes of plotting the data, the effective angle of each counter is taken as half-way between the two extreme angles which the counter "sees."

The G factors were evaluated by two independent methods: first by graphical integration from an accurate full-scale drawing, and then by an analytic method. We wish to acknowledge the material assistance of Mr. F. Fillmore in developing the latter approach. The two methods agreed at all angles to better than $\frac{1}{2}$ percent. A number of small corrections to the above are necessary, due to simplifying assumptions made in the calculations. The value of these will be given for a typical counter, the 64.7° one:

1. -1.5 percent, due to scattered protons penetrating the corners of the defining cylinders (copper). It is assumed that the protons are not scattered in the copper, since roughly as many will scatter into a given counter as get scattered out. All protons are assumed to reach the counters if the thickness of copper they must penetrate leaves them enough energy to penetrate the aluminum absorber at the counter window. This energy threshold of the counters greatly reduces the effect of penetration of the copper.

2. $+0.16$ percent, caused by "tunnel effect" of the parallel sides of the apertures of the counter windows.

3. A correction for finite width of the incident beam was necessary for the small angle counters, amounting to -0.35 percent at 27.3°. The original calculations assumed the beam to be a line source.

4. It was discovered that certain dimensions of the chamber were warped when it was assembled, since it was necessary to draw the peripheral ring of bolts tight to make the major vacuum seals. Hence it was necessary to measure all the essential dimensions while it was assembled. This was done by means of various gauges inserted through the access port. The radius of the

[22] E. J. Williams, Proc. Roy. Soc. **169**, 531 (1939).

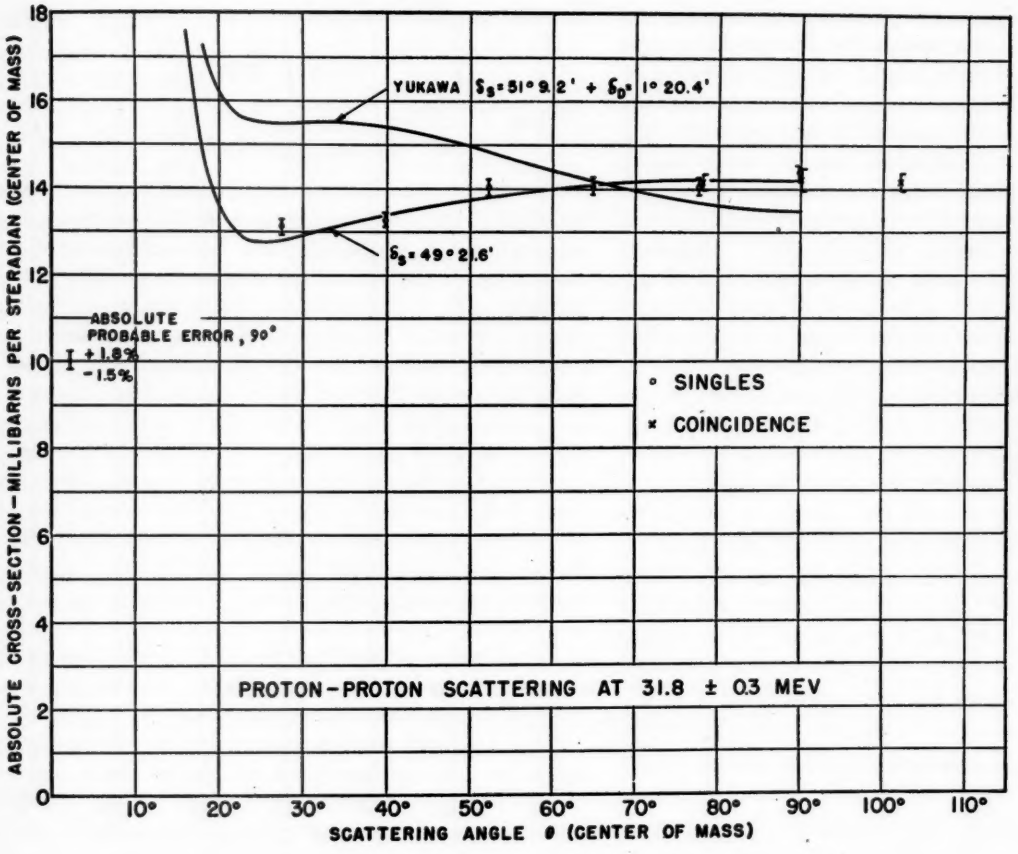
ABSOLUTE CROSS-SECTION - MILLIBARNS PER STERADIAN (CENTER OF MASS)
YUKAWA $\delta_S = 51° 9.2' + \delta_D = 1° 20.4'$
$\delta_S = 49° 21.6'$
ABSOLUTE PROBABLE ERROR, 90°
+1.8%
-1.5%
° SINGLES
× COINCIDENCE
PROTON-PROTON SCATTERING AT 31.8 ± 0.3 MEV
SCATTERING ANGLE θ (CENTER OF MASS)

FIG. 7. Absolute differential cross-section for proton-proton scattering at 31.8±0.3 Mev. The theoretical curves are indicated by the solid lines.

counter windows from the center of the chamber was measured at six points for each counter, and the width of each counter aperture was measured at 18 points. The angular position of each counter aperture relative to the center of the chamber was measured by calipers and calculated by trigonometry. The aperture between the defining cylinders was measured, as well as their diameters and their position relative to the center of the chamber. Corrections were derived from these data for each counter, amounting to +2.4 percent for the 64.7° counter. It is believed that the result of these measurements is good to ±0.2 percent.

The corrected G factors are listed in Table I.

PROCEDURE

The alignment of collimators and the scattering chamber was accomplished as follows:

The position of the beam at the exit of the linear accelerator is determined by observing fluorescence caused by the incident protons. A limiting aperture A is then inserted, and the position of the deflected beam is observed in the region of the exit to the analyzing magnet chamber. A second limiting aperture B is inserted at this point and the position of the beam is observed in the region of the scattering chamber. Aperture C is then installed, and the axis of the deflected beam is determined by apertures B and C. Cross-hairs are installed in apertures B, C, and D, the angle-defining cylinders and the main supporting hub. Aperture D, the angle-defining cylinder, and the hub are first adjusted until coaxial. The entire scattering chamber is supported on three adjustable screws for vertical deflection. The front and back can be moved independently in a horizontal direction by means of adjusting screws and sliding planes.

With the aid of the cross-hairs and a transit-type cathetometer, the apparatus was aligned with the axis of the beam to better than ±0.010 in. The general alignment is checked by illuminating a photographic plate with the proton beam in the region of the charge integrator.

The foils were then installed in aperture D, and the chamber was filled with hydrogen (see above). The correct amplification for each counter must be determined so that all of the protons are counted but as few background counts as possible result. Since the background was due to photoelectrons and to knock-on collisions of neutrons with the walls and gas of the counters, a nearly continuous spectrum of background pulse heights was present. Increasing the gas multiplication of the counter increases the background at a very rapid rate. The technique used for setting the gas multiplication was as follows: (1) The counter apparatus was allowed to come to equilibrium by operating for an hour. (2) A pulsed signal generator was connected to the discriminator input of all 12 channels,

and the discriminators were adjusted to operate at the same predetermined pulse height. (3) The gain was measured and adjusted so that all amplifiers had nearly the same gain. (4) A high voltage from a single source was applied to the tungsten wires of each of the proportional counters. A phosphorous source of beta-rays was then placed in turn at each of the 0.001 in. dural windows in the counter (see Fig. 2). The potentiometers supplying the potentials for each wire were then adjusted to give approximately the same counting rate in each counter.

This procedure greatly facilitated the adjustment of the many counters. To make a scattering run, the above procedure was followed; the chamber was filled with hydrogen to one atmosphere; a measurement was made of the beam energy; the accelerator was adjusted to give a maximum beam through the analyzer into the charge integrator and its magnitude was then adjusted to give a satisfactory counting rate into the counters.

Before a run the shutter was opened, and the gas multiplication adjusted to the maximum value without overload. Next, the incident proton beam was intercepted by a "flip gate"; the counters were turned off; the charge collector cup was grounded; and the initial readings of the mechanical registers recorded.

To start a run, the charge collector cup was ungrounded; the counters were turned on; the "flip gate" was opened; and the run continued until a predetermined charge was collected on the cup. The time of the run, the pressure and temperature of the scattering hydrogen, and a total of 15 independent register readings were recorded (4 small angles, 3 large angle split counters, 3 coincidences, 1 accidental coincidence, and the background monitor).

The background run is then made by closing the shutter and repeating the above procedure. After the same amount of charge is collected, the counter readings were recorded. The background monitor counter readings were compared with the proton run, and a correction was made to the singles background for each counter by a factor equal to the ratio of the two background counts. Table I lists the difference between the proton run and the corrected background run, corrected to 0°C and 760 mm Hg, and for counter resolving time. (Less than 2 percent correction.) These average data weighted according to total collected charge are then multiplied by the geometrical factor G, listed below, which includes the geometrical functions required for conversion to the differential scattering cross section in the center of mass system. These conversion factors are listed in row 29 and the values of the cross sections are listed in row 30 of Table I.

To determine the plateau for counting all of the scattered protons, runs are made in turn by reducing the gas multiplication of each counter until counts are missed. The knee of the plateau is thus determined and scattering data (marked *) are then taken for values of gas multiplication well up on the plateau of the counters.

The data from which the plateau is determined, and the percent background are tabulated in Table I. The pressure of the argon-carbon dioxide counting gas mixture was reduced for row 10 and succeeding runs. Thus the plateau occurred at a lower counter potential.

RESULTS

Table I lists the number of proton counts, corrected for x-ray and neutron background, and resolving time of the counters, and normalized for a collected charge of 317×10^{-12} coulombs. The column Q gives the actual collected charge for each run and is used as the weighting factor in computing averages.

The plateau for the proportional counters was determined by the method described under *Procedure* above. Rows 1 to 8 give typical data for determining a plateau. The counter supply potential is listed for convenience. The actual wire potential was derived from a potentiometer connected to this supply and was approximately 60 percent of the recorded values.

The slope of the plateau was determined for the sum of all the counters by comparing the proton counts as a function of the counter potential. It was observed that statistically the plateau happened to decrease 1.6 percent for a 100 volt increase in wire potential. All data used in computing averages were well up on the plateau, and a reasonable probable error of +1 percent −0 percent is assumed because of uncertainty in the slope of the plateau.

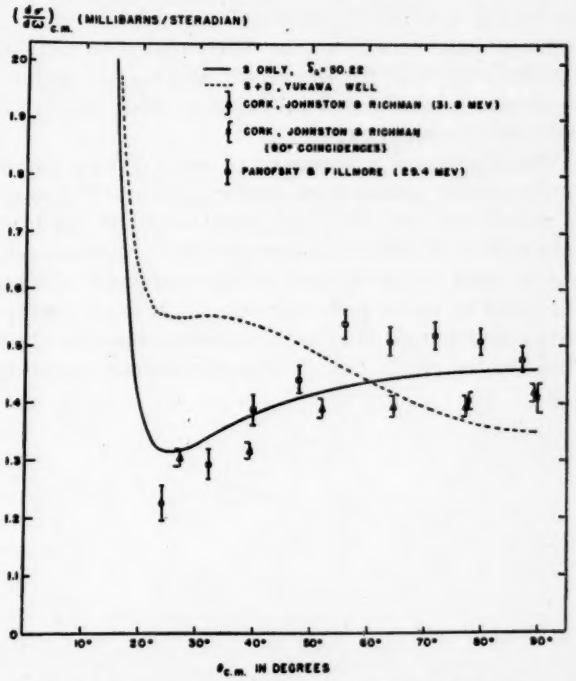

FIG. 8. Absolute differential cross-section for proton-proton scattering. The data are normalized to 32.0 Mev assuming a $1/E$ dependence of cross-section. The theoretical curves were calculated by Christian and Noyes, as follows: (a) Pure S scattering using $\delta_s=50.22°$. (b) Total singlet scattering ($S+D$) using a Yukawa well and the same S phase shift.

The large angle counters are split into top and bottom sections. The 89.7°T and 89.7°B counters are observed to agree within statistics. After careful investigation, the particular amplifier used with the 77.6°T counter was observed to give double counts for very large input signals. The differential cross section is thus calculated using the value of counts in the 77.6°B counter.

The average background counts are listed in column 12. It is observed that the background is a rapidly changing function of the counter potential.

The mean values of proton counts weighted according to collected incident proton charge are tabulated in row 27. Row 28 is a tabulation of the percent r.m.s. deviation of the mean result. This is computed by dividing the root-mean-square deviation of the result of each series by the square root of the number of series of runs. The geometrical conversion factors are listed in row 29, and the absolute values of the differential cross section in the center of mass system are listed in row 30, expressed in millibarns (10^{-27} cm^2) per steradian. These are plotted in Fig. 7.

The assigned probable errors for 90° in the center of mass system are as follows: (a) collected charge $\pm\frac{1}{2}$ percent, (b) mean energy ± 1 percent, (c) measurement of temperature and pressure $\pm\frac{1}{3}$ percent, (d) slope of plateau (maximum) $+1$ percent, -0, (e) (percent r.m.s. deviation of counts) $\pm\frac{1}{2}$ percent, and (f) calculated geometry $\pm\frac{3}{4}$ percent.

The root sum square value of these probable errors is $+1.8$ percent, -1.5 percent, indicated by the vertical bar in Fig. 7, beside the ordinate axis.

The probable errors for the differential cross sections are the root sum square values of (d), (e), and (f) above and are indicated in Table I. Note that (e) is different at each angle.

The experiment was planned to provide two separate checks on the symmetry of scattering about 90° (center of mass), one from the single count data and one from coincidence. Singles data from the 102° counter could not be used, however, because the aluminum window could not be made quite thin enough to admit protons of maximum angle (and hence minimum energy) which the counter could "see." The coincidence geometry admits only protons of energy high enough to get into both the 78° and the 102° counters, and hence a check is provided. The close agreement between the 77.6° singles data and the 78°–102° coincidence data indicates that the measured cross section at 102° is probably not smaller than that at 78° by more than 1 percent. The coincidence data are also given in Table I.

The results indicated by Fig. 7 are different from the results expected, if one assumes the usual static potential theory. The theoretical curve for an S-wave phase shift of $\delta_s = 49°21.6'$ is included. Also, the theoretical curve, if one assumes a Yukawa potential well adjusted to fit the low energy data and having $\delta_s = 51°9.2'$ plus a $\delta_D = 1°20.4'$, is plotted in Fig. 7. A comparison with the data using the photographic emulsion detectors is given by Fig. 8.

The analysis of these data, given in a paper by Christian and Noyes in this issue of *The Physical Review* shows that the shape of the differential cross section curve is compatible with pure S-wave scattering.

Christian and Noyes show that, if one compares the proton-proton scattering at 32 Mev with the neutron-proton scattering data obtained with 40 Mev incident neutrons, one must conclude that the hypothesis of the charge independence of nuclear forces is not valid. Furthermore the absence of a repulsive force in the P state coupled with the fact that in the case of the $n-p$ interaction the repulsive forces are weak makes it difficult to understand the saturation of nuclear forces.

ACKNOWLEDGMENTS

We are greatly indebted to Mr. Edward Day for the mechanical design of the scattering chamber, to Mr. John Harvie's shop for the accurate construction of the mechanical apparatus, and to the linear accelerator crew for careful operation of the machine.The authors have profited from many stimulating discussions with Professor Robert Serber, Dr. Geoffery Chew, Mr. Richard Christian, and Mr. Pierre Noyes. It is a pleasure to thank Professor L. W. Alvarez for much helpful guidance and for suggesting the problem. We wish to thank Professor E. O. Lawrence for continued encouragement and interest in the work.

Proton-Proton Scattering at 340 Mev*

OWEN CHAMBERLAIN AND CLYDE WIEGAND
Department of Physics, Radiation Laboratory University of California, Berkeley, California
(Received February 20, 1950)

Measurements of the proton-proton differential scattering cross section using 340-Mev protons show a cross section approximately constant between 41° and 90° in the center of mass system. Two methods of counting the scattered protons have been used. The first method uses a counter telescope to count the scattered protons. The second method utilizes coincidences between counters which record the two protons involved in a single scattering process. The first method gives slightly higher cross sections; the average value of the differential cross section is $(5.5\pm1.0)\times10^{-27}$ cm² steradian^{-1} in the center of mass system. Although the scattering appears isotropic it is larger than can be accounted for with pure S-scattering. There is a strong suggestion, but no positive proof, that n-p and p-p forces are different.

The p-p scattering at high energy is even qualitatively different from n-p scattering at comparable energy. In the p-p scattering the presence of other than S-wave scattering is evidenced in the magnitude of the cross section but not in the angular dependence in the range 41° to 90° center of mass system.

INTRODUCTION

IN spite of the incompleteness of the results it seems proper to report at this time on the proton-proton differential scattering cross section measurements made with the 340-Mev external proton beam from the 184-inch Berkeley cyclotron. The importance of the work stems from the short de Broglie wave-length of the protons in the beam. As is well known, only with short wave-lengths (high energies) can the details of the nucleon-nucleon forces be seen.

While meson theories are at present inadequate to give quantitative predictions, they do predict the range of the nuclear forces to be approximately $\hbar/mc$ (the Compton wave-length of the meson divided by 2π) where m is the mass of the meson. This range is in qualitative agreement with the observed range of nuclear forces if the π-meson is accepted as the particle giving rise to the forces and is then 1.4×10^{-13} cm.

If we cannot look to meson theories for a more detailed description of nuclear forces, then we must fall back on the concept of a potential giving rise to the nuclear forces: moreover since no reliable relativistic theory exists we may ask under what circumstances the available non-relativistic scattering theory is applicable. A restriction, presumably not any too stringent, is that the kinetic energy of the nucleons involved be less than their rest energy. For comparison with the range of nuclear forces given above we may state this restriction in terms of the de Broglie wave-length; the de Broglie wave-length of the proton divided by 2π should be greater than 0.12×10^{-13} cm.

The energy of the protons used in this experiment is of course determined by the cyclotron which is available to us. It so happens that this energy is such that the wave-length divided by 2π (in the center of mass system of two protons) is 0.50×10^{-13} cm, and thus falls within the limiting values mentioned above. It is still not possible to show that relativistic corrections are small.

One very interesting result of the present experiment is that the p-p scattering is even qualitatively very different from the n-p scattering. Because the Pauli principle excludes triplet states of even orbital angular momentum and singlet states of odd angular momentum from the p-p scattering it is not possible to conclude directly that the n-p and p-p interactions are different. However, we will review some arguments which make it seem fairly plausible that these interactions are indeed different.

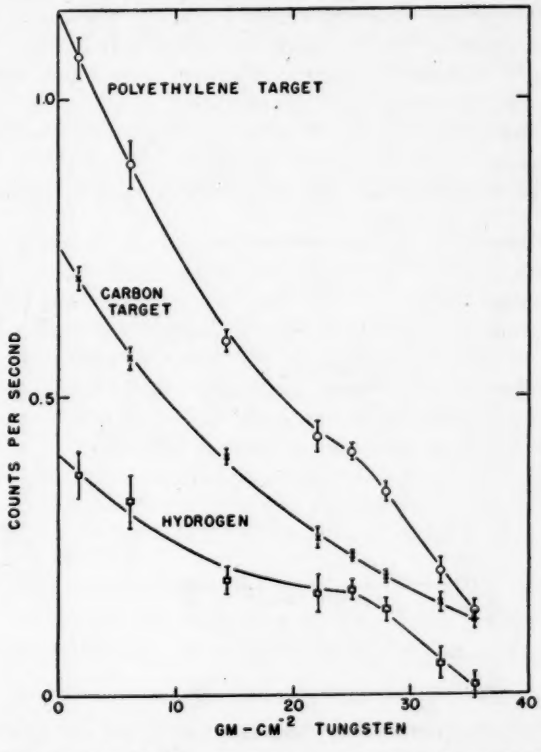

FIG. 1. Coincidence counting rate at average beam level *vs.* thickness of absorber placed before last counter of counter telescope. (Method I.) The counting rate for carbon has been scaled (multiplied by 0.70) to be equivalent to the carbon in the polyethylene target. The hydrogen curve is obtained from the other two curves by subtraction.

* Through the Radiation Laboratory this work has been supported by the AEC.

EXPERIMENTAL ARRANGEMENT

The beam is deflected within the cyclotron tank by a pulsed electric deflector, passes away from the main magnetic field in an iron channel, is deflected about 20 degrees by an auxiliary magnetic field (often called the steering magnet) and then travels 20 feet to the scattering apparatus which is outside of the ten-foot thick concrete shield. A collimator can be placed in the beam path before the steering magnet, and a four-foot long collimating hole may be arranged where the beam passes through the concrete shield. The paths of the protons in the beam at the shielding are parallel to within 0.002 radian, so good collimation can be employed at the shielding, giving beams down to 1.3 cm diameter.

The beam passes through a 0.010 in. thick aluminum window into the atmosphere, traverses a thin-walled air-filled ionization chamber, passes through the target and is stopped in a thick concrete wall ten feet from the apparatus. The target is of polyethylene or graphite (surface density 0.1 to 3.0 g/cm^2). The ionization chamber is used to determine the beam intensity as will be described below.

PROTON COUNTING—METHOD I

The scattered protons have been counted in each of two ways, both employing three proportional counters in coincidence. Method I uses a counter telescope of three counters (3.8 cm diameter, 10-cm active length) with a variable tungsten absorber before the last counter.[1] Counting rates are measured as a function of the amount of tungsten absorber to identify the proton component of the scattered radiation by its range.

The counting rate with equivalent carbon target must be subtracted from the counting rate with polyethylene target to obtain the effect due to hydrogen alone. The thickness of a carbon target is adjusted to the same stopping power as the polyethylene target used in conjunction with it. The carbon targets thus have 1.4 times the surface density of the carbon surface density in the polyethylene targets. The counting rates with carbon target are multiplied by $1/1.4=0.7$ to obtain the counting rates due to carbon in the polyethylene target. Figure 1 shows typical absorption curves for both target materials and the difference attributable to hydrogen.

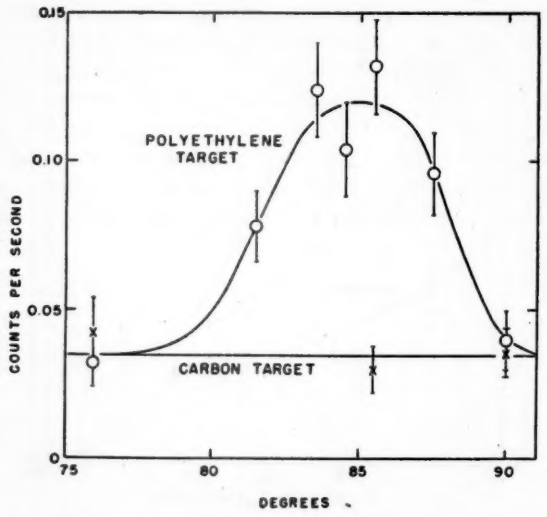

FIG. 2. Coincidence counting rate at average beam level *vs.* the angle between small counter telescope and large counter as seen from the scattering target. (Method II.)

The sensitivity of the proportional counters is adjusted approximately by insertion within the counter gas of a small polonium source, highly collimated. Precise adjustment of the sensitivity is accomplished by the study of the plateau curve (coincidence counting rate *vs.* voltage) which is measured at the time of the experiment using the protons scattered from either carbon or polyethylene.

In all cases the counting rates are very low. The proton beam from the cyclotron comes in pulses less than one microsecond long, 60 pulses per second. Since the pulse time is shorter than the resolving time of the proportional counters, each counter must on the average count much less than once each beam pulse. In typical operation the single counters count from 1 to 10 counts per second and the coincidence rate is about 0.5 per second. The cyclotron beam intensity has been varied over a large factor and it has been demonstrated that the operating intensity is so low that the coincidence rate is a linear function of intensity, as it should be.

The absorber curves (hydrogen counting rate *vs.* absorber thickness) have all shown the expected behavior near the end of the range of the scattered proton (25 to 35 g/cm^{-2} tungsten, Fig. 1). At most angles the cutoff at the end of the range is not sharp, since the finite range of scattering angles accepted by the counters allows a significant spread in energy and range in the scattered protons. Likewise the thickness of the target is reflected in a gradual rather than sharp cutoff in the absorption curves. For absorber thickness less than the range of the scattered protons (0 to 25 g cm^{-2} tungsten, Fig. 1) the absorption curves show a smooth slope attributable to multiple Rutherford scattering and to nuclear collisions in the tungsten absorber. That the multiple scattering is by far more important is seen from the fact that the effective cross section of tungsten as read from the slope of the absorption curves is several times the geometrical cross section of the tungsten nucleus. Near zero absorber the absorption curves have large statistical errors due to the large amount of scattering by carbon. (The counting rate due to carbon may be regarded as a background to which the counting rate of hydrogen is added.) Down to as little absorber as 2 g/cm^2 of tungsten there is no indication that any of the counting rate is due to other than the high energy proton-proton scattering. At zero absorber the hydrogen

[1] Hadley, Kelly, Leith, Segrè, Wiegand, and York, Phys. Rev. **75**, 351 (1949), Fig. 2.

TABLE I. Results and probable errors.

Method	ϕ (center of mass system)	$\sigma(\phi)$ (center of mass system) in units of 10^{-27} cm^2 sterad^{-1}
I	60°	6.0±0.5
I	64°	5.6±0.7
I	85°	6.5±0.7
I	90°	5.8±0.6
II	41°	5.5±0.7
II	43°	5.3±1.0
II	49°	5.1±1.0
II	62°	5.0±0.5
II	90°	4.8±0.4

counting rate has seemed slightly higher than at 2 g/cm^2 tungsten though the counting statistics do not allow proof.

PROTON COUNTING—METHOD II

Method II has also been used, in which both the scattered and scattering protons are observed.

Two counters of the type described above form a counter telescope to detect one proton; the other proton involved in the scattering process is detected by a third larger counter (7.6 cm diameter, 30 cm long). As viewed from the scattering target the small counter telescope and the large counter are slightly less than 90° apart; the deviation from 90° is a relativistic effect. No absorbers are involved in Method II.

Although it has been necessary to count exceedingly slowly with this method, the background from carbon of the polyethylene is very much reduced. Figure 2 shows typical data for the triple coincidence counting rate as a function of the angle between the two counter arms. It is of considerable importance that the counting rate due to hydrogen is zero when the angle between the counters is 90°, for it indicates that the protons counted include a negligible number of very low energy. All of the pairs of protons observed from hydrogen are at less than 90 degrees in the laboratory coordinate system and hence must be caused by incoming protons with relativistic energies. The calculated angle between protons from hydrogen is 85.5 degrees for the case shown in the figure.

The coincidence counting rate has been measured as a function of the height of the counters, and the height adjusted to maximum counting rate. This guarantees that the plane of the counters contains the beam. Plateau curves—coincidence counting rates *versus* the voltage on all counters—have been run in all cases and are quite satisfactory. It is essential that the large counter be large enough and close enough to count every proton whose counterpart traverses the small counters. To obtain assurance of this condition we have measured the counting rate as a function of the distance of the large counter from the target, and have found that the counting rate due to hydrogen remains constant over a wide range of this distance.

The background counting rate caused by carbon is due principally to accidental coincidences. This is known from the fact that the counting rate due to carbon varies as the square of the beam intensity.

MEASUREMENT OF BEAM INTENSITY

In all cases the beam is monitored with a thin-walled ionization chamber. The ionization chamber has parallel plate electrodes and contains air at atmospheric pressure. The plates of the chamber are circular with useful diameter five inches. The essential elements are two 0.003 in. aluminum foils, spaced one inch apart; one is the sensitive electrode and is connected by a 50-foot cable to a vacuum tube voltmeter, the other is the high voltage electrode and is maintained at −600 volts. On each side of these essential elements are 0.001 in. aluminum shielding foils at ground potential. The proton beam passes through the chamber normal to the foils.

The vacuum-tube voltmeter acts as a beam integrator, for the charge collected in the ionization chamber serves to charge the cable and input capacity of the voltmeter circuit. Fairly exhaustive tests have shown that the voltmeter is correctly calibrated throughout its range 0–1 volt, that its input impedance is adequately high, that its zero drift is negligible, that the total input circuit capacitance including cable behaves like a perfect condenser without dielectric absorption of charge, that only one percent of the charge collected is due to long-life (>100 sec.) radioactivity, and that the electric field is more than adequate to collect all the ions formed in the air of the chamber at the beam intensities used.

The method of calibrating the ionization chamber is by direct comparison with a Faraday cup apparatus made by V. Z. Peterson of the Radiation Laboratory. The proton beam passed through the thin-walled ionization chamber and then impinged on the Faraday cup. The Faraday cup is inside an evacuated enclosure; the beam enters this enclosure through a thin window. In this case of a very penetrating beam the cup consists of a piece of brass six inches thick and six inches in diameter. The Faraday cup apparatus has been carefully calibrated and its performance studied as a function of the electric field around the cup to make certain secondary electron emission was not a source of error.

RESULTS

The differential scattering cross section in the laboratory coordinate system is defined by the equation:

$$C=nN_T\Omega\sigma(\Phi),$$

where C is the number of counts in a counter subtending the solid angle Ω at angle Φ from the beam direction (laboratory coordinate system); N_T is the number of hydrogen atoms per square centimeter of target, measured in the direction of the beam; n is the number of incident protons in the beam; and $\sigma(\Phi)$ is the differ-

tial scattering cross section, laboratory system. The differential scattering cross section in the center of mass (zero momentum) coordinate system is then

$$\sigma(\phi)=\frac{[1+(E/2Mc^2)\sin^2\Phi]^2}{1+(E/2Mc^2)}\left(\frac{1}{4\cos\Phi}\right)\sigma(\Phi),$$

where ϕ is the angle between the direction of the scattered particle and the beam direction in the center of mass coordinate system, corresponding to Φ in the laboratory system; and E is the energy of the incident protons in the laboratory coordinate system, and M is the proton mass.

The results, with their relative probable errors, are shown in Table I.† To obtain the absolute error an estimated 10 percent error due to uncertainty in determination of the beam intensity should be superimposed on the errors given in the table. $\sigma(\phi)$ is the differential scattering cross section (center of mass system) at angle ϕ (center of mass system).

The correct $\sigma(\phi)$ is guaranteed to be the same as $\sigma(\pi-\phi)$. Method I has shown this property in the case of 60° and 120°, and the results are lumped together in the $\sigma(\phi=60°)$ in the table. Method II utilizes both outgoing particles, so the symmetry of $\sigma(\phi)$ around 90° is guaranteed beforehand.

INTERPRETATION

The most striking characteristic of the results is that they are consistent with isotropic scattering and yet the differential cross section is about twice the theoretical maximum for S-scattering alone. (The theoretical maximum for $\sigma(\phi)$ is $\lambda^2/4\pi^2=2.5\times10^{-27}$ cm^2 sterad^{-1}.) This is evidence that the cross section is inconsistent with any of the usually considered short range central force potentials, which at $\phi=90°$ predict zero P-wave and destructive interference between S- and D-waves.

A similar phenomenon has occurred in the case of the 30-Mev p-p scattering experiments of Panofsky and Fillmore[2] and Cork, Johnston, and Richman.[3] At that energy the cross section appears (if analyzed into the partial waves of a central force interaction) as S-scattering, showing interference with Coulomb scattering; there is no P-wave or D-wave in evidence. The absence of P-wave could be explained (as in the neutron-proton scattering mentioned below) with the use of a potential which gives no scattering in odd angular momentum states. However, any likely central force potential which gives the proper scattering in the S-state and has the effective range required by experiments below 10 Mev, should at 30 Mev show D-scattering in amount not consistent with the experimental results.

This is to be contrasted with the results of n-p scattering experiments[4] at 40, 90, and 270 Mev. These experiments are in at least qualitative accord with a central force interaction which is about half ordinary, half exchange force. They show, in the center of mass system, a large cross section for scattering in both the forward and backward directions. A detailed calculation of the n-p scattering has been given by Christian and Hart.[5] They find that the radial dependence of the potential is not well determined by the experiments to date, but the Yukawa well shape gives a reasonably good fit to the experiment. The use of a potential giving little scattering in P-states is necessary to obtain a total cross section as small as that obtained experimentally.

The p-p scattering at 340 Mev presents somewhat the opposite difficulty, for the differential scattering cross section is larger than can readily be explained by S- and D-scattering alone, especially at 90°. Christian and Noyes,[6] working with Professor Serber in the theoretical group of the Radiation Laboratory, have shown that the p-p scattering can likewise be explained by a potential interaction but with a very different potential. The outstanding characteristic of this potential is that it is a pure tensor interaction in the triplet state. The tensor interaction gives rise to scattered waves not present with central interaction. In particular there appear three P-waves in place of the one P-wave for central force, because with the tensor force the orbital angular momentum is not conserved—only the total angular mementum is conserved.

The 30-Mev p-p scattering cross section can also be explained with the tensor interaction and a radial dependence which is quite normal—such as the Yukawa potential. To give the observed scattering at 340 Mev, the potential must be given a strong singularity at the origin—such as $1/r^2$. In all cases the singlet potential has been adjusted to fit the data below 10 Mev, and the triplet potential adjusted to the 30-Mev data.

It is interesting to note that the singularity at the origin necessary to explain the 340-Mev p-p scattering has practically no effect on the calculations at 30 Mev. This implies that to some extent it may be possible to adjust a different part of the radial dependence function for the explanations of scattering at different energies. If so, it may be impossible to challenge the potential concept on the basis of scattering experiments alone.

PROPOSED CHANGES OF METHOD

After the bulk of the present data were taken, a new method of obtaining the external charged-particle beams from the cyclotron was developed by Leith.[7] A

† *Note added in proof:* The cross sections in the abstract and Table I should be reduced by the factor 1.11. Recent observations of the effect of scattering in the walls of the counters have necessitated this change. The conclusions are not altered.

[2] W. K. H. Panofsky and F. L. Fillmore, Phys. Rev. **79**, 57 (1950).

[3] Cork, Johnston and Richman, Phys. Rev. **79**, 71 (1950).

[4] See E. Segrè, International Conference on Nuclear Physics, Basil, *High Energy Neutron-proton and Proton-proton Scattering*, Helv. Phys. Acta (to be published), a review article.

[5] R. S. Christian and E. W. Hart, Phys. Rev. **77**, 441 (1950).

[6] R. S. Christian and H. P. Noyes, Phys. Rev. **79**, 85 (1950).

[7] C. E. Leith, Phys. Rev. **78**, 89 (1950).

thin thorium foil can be placed in the internal beam of the cyclotron. The multiple Rutherford scattering in this foil is sufficient to give a r.m.s. deflection of 1.5° and causes some of the internal beam to enter the magnetic channel which can lead this part of the beam away from the cyclotron magnetic field in the usual way. In this process there is no pulsed electrostatic deflector used. This "scattered beam" comes in 60 pulses per second as does the electrostatically deflected beam, but has the advantage of being spread (each pulse) over a period of about 25 microseconds (whereas the electrostatistically deflected pulses last less than 1 μsec. each).

As long as the beam pulses were of less than 1 μsec. duration there seemed little hope of developing a coincidence counting system with resolving time much shorter than the beam pulse time. With the advent of the scattered beam comes the expectation that many resolving times may be contained in the beam pulse time, and far more effective coincidence techniques used.

Now under construction are very fast amplifiers and coincidence circuits for use with stilbene scintillation counters. It is hoped that fast circuits will lessen the background due to particles penetrating the cyclotron shielding and due to the strong diffraction scattering in the forward direction by carbon in the polyethylene targets. If so, the measurements can be extended to a wider range of angles and improved in accuracy.

Also under consideration is a liquid hydrogen target to reduce the scattering by heavier nuclei in the target.

DISCUSSION

Christian and Noyes have shown remarkable agreement between the observed p-p scattering and that calculated using a strongly singular tensor interaction of protons in the triplet state. The great difference between the n-p potential of Christian and Hart and the p-p potential of Christian and Noyes suggests strongly that the interactions are different; unfortunately there is no rigorous proof of this difference.

The present experiments extend only to angles where the S- and D-scattering are expected (by comparison with the n-p scattering experiment) to be small compared to the observed cross section. The S- and D-scattering should become more important as the range of angles is extended toward the beam direction.

ACKNOWLEDGMENTS

The first steps in this work were taken at the suggestion of Professor E. Segrè. Professor Segrè has continued to give us help and encouragement. The operating crew of the cyclotron, directed by James Vale, has been most helpful and patient through many tedious hours of delicate adjustment.

PHYSICAL REVIEW VOLUME 79, NUMBER 1 JULY 1, 1950

The Proton-Proton Interaction*

R. S. CHRISTIAN AND H. P. NOYES
Radiation Laboratory, University of California, Berkeley, California
(Received February 20, 1950)

This paper presents a phenomenological analysis of the proton-proton scattering observed at 32 and 340 Mev in terms of static nuclear potentials. Comparison of these results with the neutron-proton scattering at 40, 90, and 280 Mev analyzed previously indicates that nuclear forces are not charge independent. In particular, there is definite evidence in the $n-p$ scattering data that but little scattering occurs in the odd parity states, whereas the high $p-p$ cross section apparently must be due to scattering in the (odd parity) triplet states. (This holds true even if velocity dependent spin orbit forces, i.e., $\boldsymbol{\sigma}\cdot\mathbf{L}$, are included.)

It is possible that the radial dependences found necessary for $p-p$ scattering would be acceptable for the $n-p$ scattering even though the exchange behavior is different. A definite statement regarding this must await detailed calculations, however.

Finally, we must take notice of the fact that no large repulsive forces have shown up in either the $n-p$ or the $p-p$ system of sufficient magnitude to account for nuclear saturation if saturation is to be predicted from two body forces. In both cases they would have been very easily detected, independent of the potential model assumed.

INTRODUCTION

IN this paper we shall attempt to fit the proton-proton scattering data at 32[1,2] and 340 Mev[3] by the use of static nuclear potentials. This description is phenomenological and as such may be considered a sequel to the report concerned with determining the $n-p$ interaction from the scattering [4-7] at 40, 90, and 280 Mev.

* The work described in this paper was performed under the auspices of AEC.

[1] W. K. H. Panofsky and F. Fillmore, Phys. Rev. **79**, 57 (1950).
[2] Cork, Johnston, and Richman Phys. Rev. **79**, 71 (1950).
[3] O. Chamberlain and C. Wiegand, Phys. Rev. **79**, 81 (1950).
[4] Hadley, Kelly, Leith, Segrè, and York, Phys. Rev. **75**, 351 (1949).
[5] Brueckner, Hartsough, Hayward, and Powell, Phys. Rev., **75**, 555 (1949).
[6] R. S. Christian and E. W. Hart, Phys. Rev. **77**, 441 (1950).
[7] See E. Segrè, International Conference on Nuclear Physics, Basil, *High Energy Neutron-proton and Proton-proton Scattering*,

The success that was obtained in the $n-p$ system would seem to be sufficient grounds for expecting that $p-p$ scattering would likewise be interpretable by means of static potentials. In fact we might be tempted to predict the $p-p$ nuclear potential from our knowledge of the $n-p$ potential as determined by the high energy scattering. This prediction could be made either on the hypothesis that the nuclear potential is charge independent (i.e., depends only upon whether the two particles are in a singlet or triplet spin state), or in terms of an attempt to explain the saturation of nuclear forces.

If we were to follow the first assumption (the so-called charge symmetry hypothesis) there would be no free parameters entering the $p-p$ theory, since the results of the $n-p$ experiments are quite definite. For both singlet and triplet states these experiments show that there are no (or very small) odd parity forces. Therefore on the basis of charge symmetry one might expect that the $n-p$ and $p-p$ scattering would be quite simila-. This is in obvious disagreement with the experimental results as is seen in Fig. 1.

In order to better understand the prediction of the charge symmetric theory we must consider in more detail the fundamental differences between $n-p$ and $p-p$ scattering. Firstly, for 32-Mev protons the Coulomb repulsion is dominant in the scattering at angles less than 20°. Between 20° and 40° or 50° the angular variation is governed by the nuclear-Coulomb interference terms. The remaining region around 90° is virtually the same as for simple nuclear scattering. Secondly, the $p-p$ system, being composed of identical particles

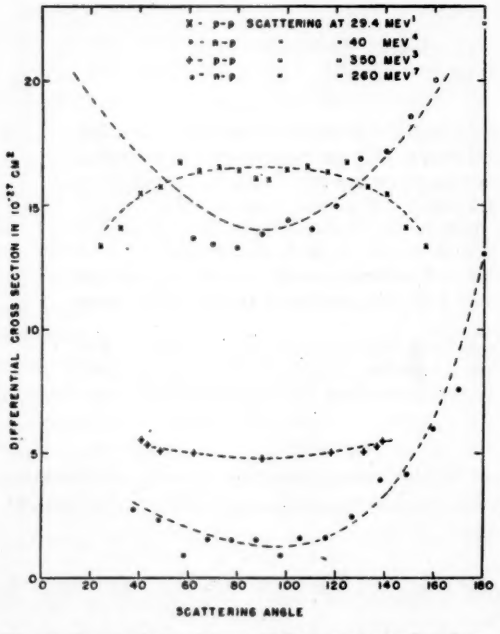

FIG. 1. Comparison of $n-p$ and $p-p$ scattering data.

obeying the exclusion principle, has fewer states than the $n-p$ system. Specifically only even parity singlet states and odd parity triplet states can be present. Thus scattering occurs only in ^1S, ^3P, ^1D, ^3F, $\cdots$ states, and the charge symmetric theory predicts the virtual absence of triplet scattering. The $n-p$ system, on the contrary, has scattering from both singlet and triplet even parity states so that a direct comparison must be justified. In order to learn what part of the complete $n-p$ scattering is singlet scattering we must recall that in order to lead to the low total $n-p$ cross section the singlet range must be greater than 2×10^{-13} cm. This gives an angular distribution for the singlet cross section that has an even higher ratio of $\sigma(180°)/\sigma(90°)$ than the complete scattering from both states, making a direct comparison of the relative angular variation of the complete $n-p$ and $p-p$ cross sections possible in the region from 50° to 90°. Thus the 32-Mev $p-p$ results show that the charge symmetry hypothesis is untenable.

Alternatively we could attempt to predict the $p-p$ scattering by directing our attention to the phenomenon of the saturation of nuclear forces. The $n-p$ experiments rule out the possibility of $n-p$ repulsive forces of anything like the magnitude required to explain saturation. The low energy experiments show that the singlet $p-p$ forces are attractive. Thus the only remaining way for the $p-p$ forces to lead to saturation would be the existence of strong repulsive forces in the triplet state. Since the triplet scattering amplitude is antisymmetric, the scattering from a central triplet potential is zero at 90°. Hence such repulsive forces would lead to an angular cross section rising even more rapidly on either side of 90° than that predicted by the charge symmetric theory and are conclusively excluded by the data.

Thus both the hypothesis of the charge independence of nuclear forces and the possibility of strong repulsive forces in the triplet $p-p$ state such as seem to be required for the saturation of nuclear forces are already disallowed by the $p-p$ scattering at 32 Mev. The 340-Mev scattering is even more strikingly anomalous (see Fig. 1). The experiments indicate a nearly spherically symmetric distribution over the range from 41° to 90° having an absolute magnitude that is twice the maximum possible for S wave scattering alone. Since the $n-p$ scattering at 280 Mev was in good agreement with a non-relativistic potential model it is difficult to accept this as a relativistic effect. Again both charge symmetry and repulsive triplet forces would lead to scattering strongly peaked at 0° and 180° and an order of magnitude lower in value at 90° than the observed $p-p$ cross section, and are conclusively disproved. This scattering is superficially similar to classical hard sphere scattering. However, since the wave-length of 340 Mev protons is only three or four times shorter than the range of the attractive region that must surround

Helv. Phys. Acta (in press, a review article). Also E. Segrè, private communication.

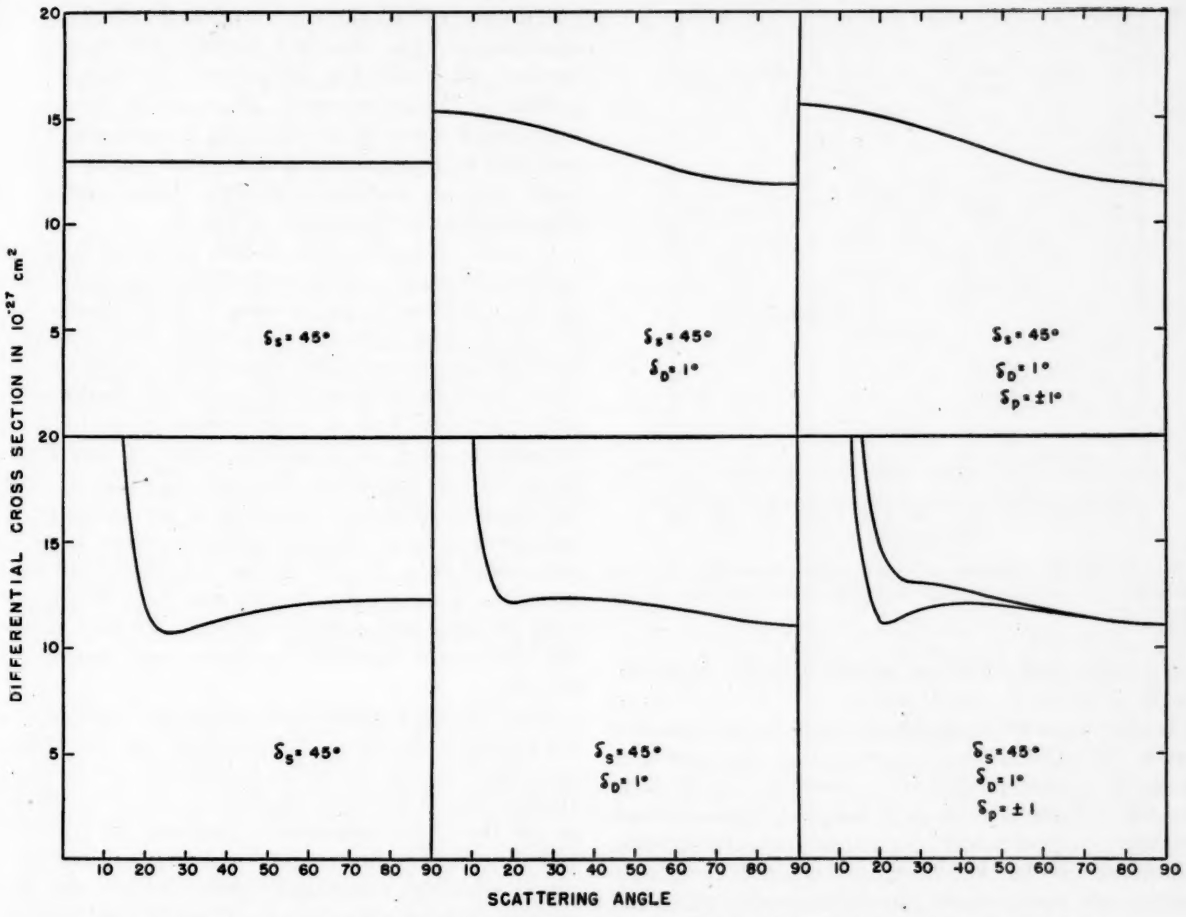
DIFFERENTIAL CROSS SECTION IN 10^{-27} cm^2
$\delta_s = 45°$
$\delta_s = 45°$ $\delta_D = 1°$
$\delta_s = 45°$ $\delta_D = 1°$ $\delta_p = \pm 1°$
$\delta_s = 45°$
$\delta_s = 45°$ $\delta_D = 1°$
$\delta_s = 45°$ $\delta_D = 1°$ $\delta_p = \pm 1$
SCATTERING ANGLE

FIG. 2. Effects of S, D, and P waves on 32-Mev scattering. The upper set of curves give the nuclear scattering. The lower set include the effects of Coulomb forces.

and include such a sphere in order to explain the low energy results, the sphere cannot be made large enough to give classical hard sphere scattering at this energy. This point is discussed in more detail below.

In spite of the surprising divergence of the observed $p-p$ scattering from that which had been expected previous to the experiments, it has proved possible to reconcile all the existing data with the scattering predicted from a static nuclear potential. This model consists of a shallow singlet potential and a highly singular triplet tensor potential. The main body of this paper is concerned with justifying this model.

In view of the apparently fundamental differences between the expected and the observed $p-p$ scattering, and the various complicating factors in the analysis of the data, we have devoted the first part of this report to a more or less qualitative discussion of $p-p$ scattering. In this section we will give typical results for various potential models but will not discuss which radial dependence is to be preferred. Rather we wish to emphasize the salient features in the analysis in order to furnish a basis for understanding the calculations which follow in Part II.

PART 1. QUALITATIVE DISCUSSION

It has been shown by many authors that the experiments below 14 Mev are compatible with S wave scattering alone[8] and that these experiments have determined only the scattering length and effective range.[9] This indicates that no one of the radial forms usually assumed is to be preferred. It need hardly be emphasized that the low energy experiments give little information concerning the interactions in states of higher angular momentum (especially the P state) other than putting upper limits on the magnitudes of the interactions in these states.

The $n-p$ experiments at 40 Mev[4-6] have shown that there is scattering in the D state and little scattering in the P state, and that the magnitudes of these interactions could be determined. It was therefore expected that since the range of forces for the $p-p$ system is

[8] Yost, Wheeler, and Breit, Phys. Rev. **49**, 174 (1936). Breit, Condon, and Present, Phys. Rev. **50**, 825 (1936). Breit, Thaxton, and Eisenbud, Phys. Rev. **55**, 1018 (1939). Hoisington, Share, and Breit, Phys. Rev. **56**, 884 (1939). H. M. Thaxton and L. E. Hoisington, Phys. Rev. **56**, 1194 (1939).

[9] J. Schwinger, Phys. Rev. **72**, 742A (1947). J. M. Blatt and J. D. Jackson, Phys. Rev. **76**, 18 (1949), Rev. Mod. Phys. **22**, 77 (1950). H. A. Bethe, Phys. Rev. **76**, 38 (1949).

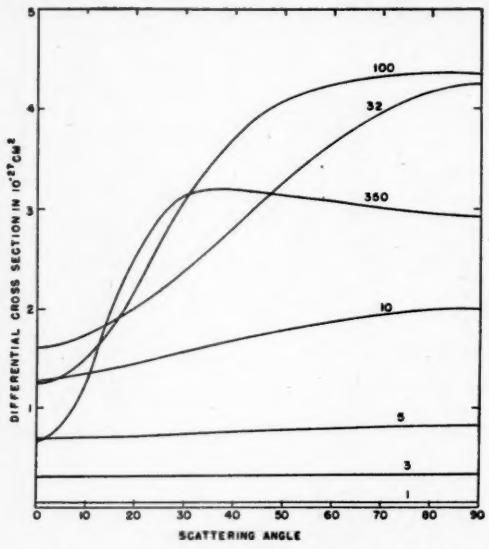

FIG. 3. Tensor scattering from a singular potential at various energies. The energies in Mev are given parametrically on the curves.

comparable, the scattering would likewise occur primarily in the S, P, and D states.

It was observed immediately, as has been pointed out in the experimental papers,[1,2] that the data were in good agreement with that predicted by S wave scattering alone. This is in definite disagreement with the scattering predicted by the usual potential models. The reason is that the S state interaction completely specifies the entire singlet interaction, and in particular the effective range is so long that the D wave predicted at this energy is incompatible with the experimental results. (It would of course be possible to choose a potential that would give only S scattering at 32 Mev, but the effective range of such a potential would then be much too short to fit the low energy region.)

If we consider in detail the predictions of the usual models we find that even for the most cut-off potential (the square well) the D phase shift is already too large (0.77°), and as is to be expected the more long-tailed Yukawa potential has an even larger D phase shift (1.4°). The adverse effect of such D phase shifts on the angular distribution can be readily seen by reference to the second panel of Fig. 2. The origin of this effect is destructive interference between S- and D-wave scattering in the region around 90°. This interference term is proportional to $\sin\delta_S \sin\delta_D \cos(\delta_S-\delta_D)P_2$. ($P_2(\cos\theta)=\frac{3}{2}\cos^2\theta-\frac{1}{2}$.) The usual models predict positive values for δ_S and δ_D, so that this term has a minimum at 90° as is observed in the $n-p$ scattering but not in the $p-p$ case. (Figure 2 also demonstrates that the Coulomb scattering has little effect in the region from 50° to 90° and hence cannot alter this conclusion.)

The central triplet scattering amplitude being antisymmetric leads to a cross section that is zero at 90°, and since there is no interference with the singlet state it can only add to the rise away from 90°. Therefore scattering in this state will increase the discrepancy between the predictions made from the central force model and the experiments. Alternatively we can see this directly from the fact that the P scattering is proportional to $\sin^2\delta_P \cos^2\theta$, showing that the $\cos^2\theta$ term must have a positive coefficient. These effects are illustrated in the third panel of Fig. 2.

In order to explain the 32-Mev data, we require a model that would predict essentially spherically symmetric scattering in the absence of the Coulomb field. We have already seen that central force scattering predicted by monatonically decreasing potential models of the usual radial form is in qualitative disagreement with experiment. Conceivably a more complicated radial dependence, such as a repulsive lip on a square well, could lead to negligible D phase shifts at 32 Mev. Attempts to build such models have been unsuccessful because they have effective ranges too short to fit the low energy data. In view of the straightforward interpretation of the $n-p$ scattering and the inherent difficulty of using such a model to fit the 350-Mev data, it did not appear profitable to pursue such models any further.

The remaining alternative, within the framework of the potential picture, is the possibility that the D wave is masked by the scattering from tensor forces in the triplet state. A favorable result is predicted by the use of the Born approximation to compute the scattering (see Fig. 3). (The Born approximation is valid for the P waves since the centrifugal barrier reduces the effect of the nuclear potential to a small perturbation.) The scattering computed this way is peaked at 90°and hence can add to the singlet cross section, which dips at 90°, to give an almost flat nuclear cross section. When the coulomb effects are included the resulting angular distribution is quite similar to S wave scattering (see Fig. 4). Thus a proper choice of range and depth for the tensor potential can lead to agreement with the experiments. (An alternative way of understanding why the scattering can have a finite value at 90° even

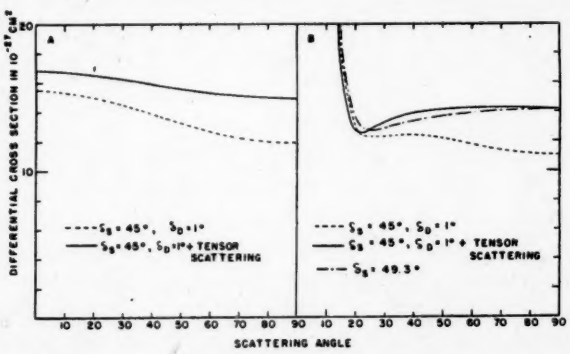
A
B
DIFFERENTIAL CROSS SECTION IN 10^{-27} CM^2
δ_S = 45°, δ_D = 1°
δ_S = 45°, δ_D = 1° + TENSOR SCATTERING
δ_S = 49.3°
SCATTERING ANGLE

FIG. 4. Effect of adding tensor scattering to the singlet scattering at 32 Mev. A. Nuclear scattering. B. Scattering including the effects of Coulomb forces. The tensor scattering is that from a potential of exponential radial dependence ($R=0.71\times10^{-13}$ cm, $V_t=\pm50$ Mev).

though it takes place in odd states is that the tensor force brings about a change in angular momentum, and tesseral harmonics other than the Legendre polynomials enter into the scattering amplitude. We can then see that the presence of $Y_1^1(\theta, \phi)=e^{i\phi}\sin\theta$ in addition to $Y_1^0(\theta, \phi)=\cos\theta$ leads to terms with a $\sin^2\theta$ symmetry which when added to the $\cos^2\theta$ symmetry terms in the singlet scattering could lead to a flat nuclear cross section.)

The 340-Mev data will first be analyzed independently of the 32-Mev data. The two models so derived will then be compared and reconciled. In order to further emphasize the anomalous nature of the high energy scattering, we note that if we assumed (arbitrarily) that there were no interactions in other than S states the predicted cross section would be spherically symmetric but ten or more times too small. (Recall that even the maximum possible S wave cross section is only one-half the measured value.) The Coulomb scattering falls to the value of the nuclear cross section between 6° and 7° so that Coulomb effects will be unimportant beyond about 12° and have been neglected in our analysis.

To analyze the situation in somewhat more detail we shall first consider the scattering that would result from the singlet state (since in this state the potential is completely specified by the assumption of a particular radial form). At 350 Mev the Born approximation is valid for central scattering and predicts the strong forward maximum illustrated in Fig. 5. Alternatively we may view the problem in terms of a partial wave decomposition. Only the even Legendre polynomials comprise the scattering amplitude. The even polynomials are all 1 at 0° and 180° and alternate in sign at 90° (e.g., $P_0(90°)=1$, $P_2(90°)=-0.5$, $P_4(90°)=0.375$, $\cdots$). Scattering by the usual monatonic potential models predicts that all phase shifts will have the same sign, so that there is constructive interference at 0° and 180° and destructive interference at 90°, giving a characteristic peaking of the angular distribution.

In order to obtain a flat cross section it would be necessary to require that the sine of the phase shifts of even parity alternate in sign with increasing l, resulting in a singlet cross section peaked at 90°. Then if this cross section were added to the central triplet cross section (which is always zero at 90°) a flat cross section would result. It does not appear possible, however, to find a singlet potential that will fit the scattering in the low energy region while at the same time predicting the required alternation in sign of the high energy phase shifts.

Before turning to tensor models we will first consider the so-called hard sphere scattering. To give this type of scattering phase shifts from high angular momentum states must be involved some of which must be greater than 180° in order to change the signs of the sines. One

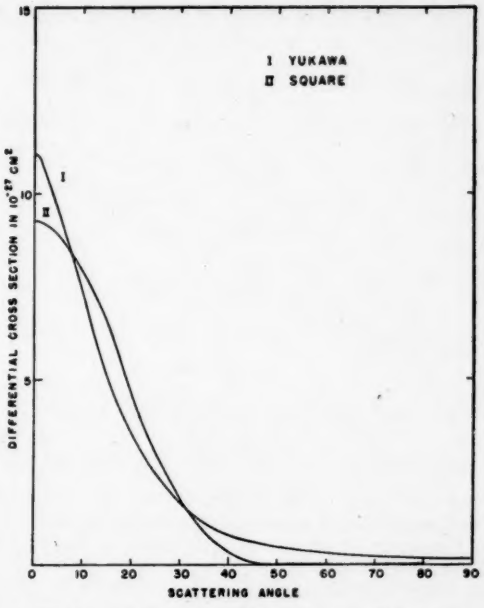

FIG. 5. Singlet scattering at 350 Mev as predicted for a potential having Yukawa radial dependence $R=1.1416\times10^{-13}$ cm and (II) for a square well potential $R=2.615\times10^{-13}$ cm.

can estimate by reference to Fig. 7 of Mott and Massey[10] that in order to give agreement with the experiments the phase shifts must be large for angular momentum states up to $l=20$. At this wave-length of 0.5×10^{-13} cm it might appear that a repulsive core in the central potential would give this result. An attempt was made using Morse potentials to find a model that would predict hard sphere scattering at 340 Mev. These potentials consisted of a repulsive core surrounded by an attractive region adjusted to give the correct scattering behavior at low energies. It is found that even in the limiting case where the repulsive core becomes infinitely high, the low energy experiments require the radius of the core to be so short (1.2×10^{-13} cm) that at 340 Mev only the lowest angular momentum states are involved in the scattering (for $l>6$, $\delta_l<0.1°$). It therefore appears that the effective range of the potential well will limit the radius of any potential to such an extent that hard sphere scattering cannot result. Alternatively we may note that even if we do not fit the low energy scattering, the absolute value of the cross section predicted by hard sphere scattering would be much too large. This can easily be seen by noting that the experimental value is $2\lambda^2$ per steradian while that predicted by hard sphere scattering must be of the order of $2(20\lambda)^2$ since the extent of the hard core must be approximately 20λ.

Again we must appeal to the tensor force in order to obtain agreement with the experimental data. In fact, if we recall that at 32 Mev we needed to add a triplet cross section that was peaked around 90° in order to

[10] N. F. Mott and H. S. W. Massey, *The Theory of Atomic Collisions*, (Oxford University Press, London, second edition) pp. 38–40.

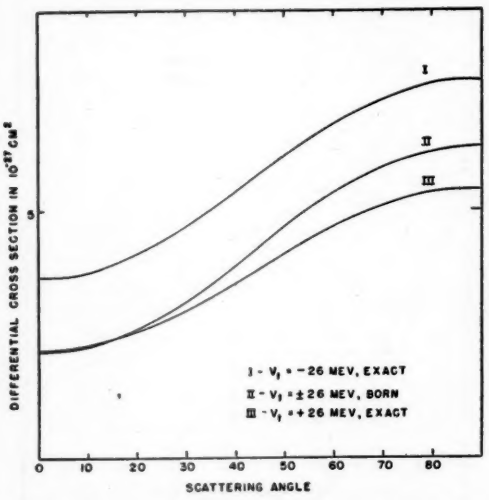

FIG. 6. Comparison of exact and Born calculations for tensor force scattering at 32 Mev from a potential of Yukawa radial dependence ($R=1.25\times10^{-13}$ cm).

mask the minimum in the singlet scattering we see that the situation at 350 Mev is very similar. We can again use the tensor force to obtain agreement, for in Born approximation scattering depends only on the combination kR where k is the wave number and R the range of the potential. That is, to produce the same scattering at a higher energy we need only contract the range by a factor that is the square root of the energy ratio, and adjust the depth to give the desired absolute magnitude to the scattering.

We therefore have indications of a tensor potential at both 32 and 350 Mev, and need only show that the requirements for the two cases are compatible. As the energy changes different regions of the potential will play the more dominant role. For example, at 32 Mev the potential region at distances of the order of 3 to 4×10^{-13} cm is most important while at 340 Mev the potential region at distances of the order of 1×10^{-13} cm has become important. By adjusting the range and depth of a tensor potential of any given radial form the predictions may be made to fit the 32 Mev experimental data. However, at 340 Mev the P wave protons are able to explore the potential into considerably shorter distances and it is necessary to have a strong interaction in this region in order to explain the very high 340-Mev cross section. The tensor scattering calculated for a singular potential in Born approximation as illustrated in Fig. 3 illustrates these remarks. From the foregoing curves we can also see that an appreciable fraction of the 32-Mev scattering must be explained in terms of tensor forces if we wish to obtain agreement with the high energy data. These curves further show that the tensor potential would probably have little effect below 10 Mev as the scattering amounts to less than one percent of the total scattering.

PART 2. CALCULATIONS

A. Methods

The singlet scattering from a potential of given radial form depending on two parameters is completely specified by the scattering length and effective range, which are determined by the scattering below 10 Mev. The general method of determining these parameters for a given radial dependence is discussed in detail by Blatt and Jackson.[9] The S scattering due to the nuclear potential alone at higher energies was calculated by direct numerical integration of the radial wave equation giving the S phase shift. The true S phase shift (in the presence of the Coulomb field) was then obtained by treating the Coulomb field as a perturbation according to the method of Chew and Goldberger.[11] The corrections amounted to approximately one degree or less. The D phase shift was calculated in Born approximation considering only the nuclear forces. (This method was checked by numerical integration in the case of the Yukawa potential, corrected for the Coulomb field as above. The results at 32 Mev: 1.33° for the Born approximation, 1.45° for the exact nuclear calculation, 1.40° with the Coulomb correction were assumed to be a satisfactory check.) Higher waves than the D were found to be negligible at 32 Mev.

As was shown in Part 1, it was not necessary to calculate any odd parity phase shifts due to central forces, but the tensor scattering was required. This was calculated with the exact values of the complex phase shifts, $\delta_l^{Jm_s}$, which enter into the tensor scattering. The result was in good agreement with that predicted by the Born approximation. There is a slight tendency for the Born approximation to predict somewhat larger angular variations than are found in the more exact calculations.

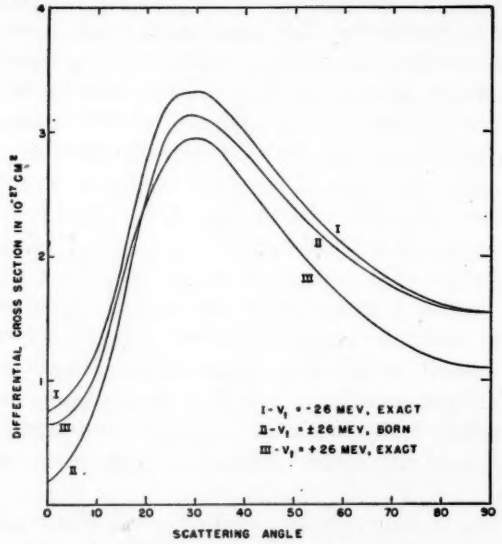

FIG. 7. Comparison of exact and Born calculations for tensor force scattering at 350 Mev from a potential of Yukawa radial dependence ($R=1.25\times10^{-13}$ cm).

[11] G. F. Chew and M. L. Goldberger, Phys. Rev. **75**, 1637 (1949).

TABLE I. Singlet phase shifts at 20 and 32 Mev for various radial forms adjusted to fit the low energy scattering.

Model	V_c	R	Phase shift 32 Mev S	32 Mev D	20 Mev S^*	20 Mev D
$V_c(r/R)=\begin{cases}V_c & r<R\\ 0 & r>R\end{cases}$	13.273 Mev	2.615×10^{-13} cm	41.99°	0.770°	48.5°	0.26°
$V_c(r/R)=V_c e^{-r/R}$	108.27 Mev	0.7088×10^{-13} cm	47.54°	1.20°		
$V_c(r/R)=\frac{V_c e^{-r/R}}{r/R}$	49.350 Mev	1.1417×10^{-13} cm	51.15°	1.40°	54.2°	0.7°

* Interpolated.

This can readily be understood in terms of the higher approximations of the Born approximation for then the scattering amplitude entering into each successive iteration (or each successive collision) is less well collimated than that entering the previous iteration, due to the scattering that occurs. A further small difference between the exact and the Born calculations occurs in the absolute magnitude, a tensor force taken with a positive sign (i.e., same sign as for the deuteron) always has less scattering in the exact calculation while the tensor force taken with a negative sign always has more scattering. A comparison between the exact predictions using the two signs and with the result of the Born approximation is afforded by reference to Figs. 6 and 7.

The phase shifts arising from the coupled states entering the exact calculations were carried out by iteration (in the manner described in reference 6) after they had been cast in the form of coupled integral equations. In the case of the uncoupled states any of the methods usually applicable to central scattering may be used. We found that the integral variational expression was sufficiently accurate when the proper component of the plane wave was used as a trial function.

From the relatively small differences shown in Figs. 6 and 7, we decided it was unnecessary to carry out the exact calculations for the nuclear part of the scattering. This is particularly so because we are able to offset any difference in absolute magnitude by choosing a slightly altered tensor depth (which will be determined only very roughly anyway from the present data). One difficulty with use of the Born approximation is that the interference term (see Appendix 1, for a derivation of this term) between the nuclear and Coulomb scattering identically vanishes, while the exact calculations at 32 Mev show that the P wave component of the nuclear scattering interferes appreciably with the Coulomb scattering. We had therefore to compute two uncoupled phase shifts, $\delta_1{}^{00}$ and $\delta_1{}^{1\pm}$, and also iterate the coupled ${}^3P_2+{}^3F_2$ state. The iteration process is rather tedious and as the magnitudes of the phase shifts were small compared with the uncoupled phase shifts, we used the *WKB* approximation to obtain these phase shifts. We shall consider this approximation in more detail below: If the two independent solutions of the coupled equations have the asymptotic form

$$a_{lL}\sim a_{lL}\sin(kx-l\pi/2+\delta_{lL}{}^J),$$

where $L=l$ or $2J-1$ depending upon which is the dominant state, then the nuclear phase shift may be easily shown to be given by

$$\exp(2i\delta_l{}^{Jm_s})=\frac{\exp[i(\delta_{ll}{}^J-\delta_{LL}{}^J)]-a_{lL}{}^J a_{Ll}{}^J\exp[i(\delta_{lL}{}^J-\delta_{Ll}{}^J)]+2i\left\{\frac{(2L+1)}{(2l+1)}\right\}^{\frac{1}{2}}\frac{\langle SLJm_s|SLOm_s\rangle}{\langle SlJm_s|SlOm_s\rangle}a_{lL}{}^J\sin(\delta_{ll}{}^J-\delta_{lL}{}^J)}{\exp[-i(\delta_{ll}{}^J+\delta_{lL}{}^J)]-a_{lL}{}^J a_{Ll}{}^J\exp[-i(\delta_{lL}{}^J+\delta_{Ll}{}^J)]}$$

where now $L=2J-1$ only, and we have set $a_{ll}{}^J=a_{LL}{}^J=1$. In the case of the ${}^3P_2+{}^3F_2$ state we have found that the Born approximation yields all quantities in this expression with the exception of $\delta_{11}{}^2$, with sufficient accuracy. This we have computed by using the "equivalent central potential" (see reference 6) in *WKB* approximation and then applying the Born approximation to this potential to obtain the phase shift. $\delta_{11}{}^2$ is then the sum of two terms one of which is identical with that predicted by the Born approximation applied directly to the coupled equations and the other is of the nature of a correction term, and has the value

$$\Delta_{11}{}^2=(36\cdot6/25\cdot10)1/kR\int_0^\infty[xV_t(x)]^2 g_1{}^2(kRx)dx,$$

where we have written the tensor potential,

$$S_{12}V_t(r/R)=[3(\sigma_1\cdot\mathbf{r})(\sigma_2\cdot\mathbf{r})/r^2-\sigma_1\cdot\sigma_2]V_t(x)$$

and

$$g_l(kx)=(\pi kx/2)^{\frac{1}{2}}J_{l+\frac{1}{2}}(kx).$$

This procedure applied to the exponential and Yukawa radial dependences yields the coefficients of the inter-

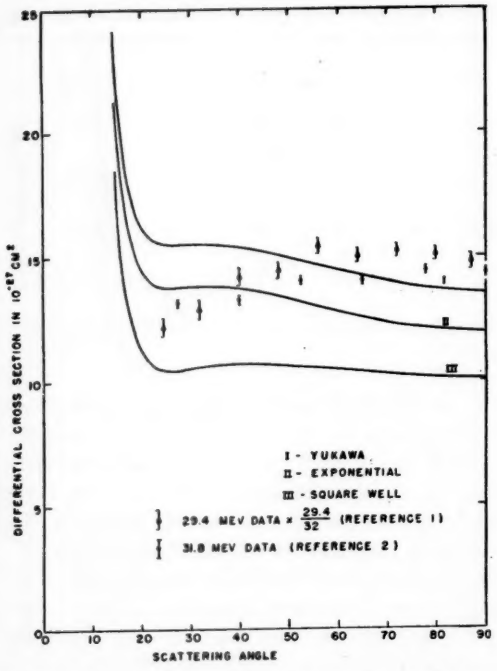
DIFFERENTIAL CROSS SECTION IN 10^{-27} CM^2
SCATTERING ANGLE
I - YUKAWA
II - EXPONENTIAL
III - SQUARE WELL
29.4 MEV DATA × 29.4/32 (REFERENCE 1)
31.8 MEV DATA (REFERENCE 2)

FIG. 8. Singlet scattering at 32 Mev from potentials with various radial forms adjusted to fit the low energy scattering. Data taken from reference 1 (29.4 Mev) and 2 (31.8 Mev).

ference terms within a few percent the coefficients determined from an exact calculation.

For the 340-Mev scattering the Coulomb scattering was neglected and the singlet scattering was computed in Born approximation.

B. Results

The singlet cross sections for the square, exponential, and Yukawa models are shown in Fig. 8. In each case the range and depth have been chosen to agree with Blatt and Jackson's low energy analysis. (The range and depth of the Yukawa potential and square well were determined independently by Chew and Goldberger before the results of Blatt and Jackson were available to us and agree within their assigned limits of error.) These parameters, together with the S and D phase shifts at 20 and 32 Mev, are collected in Table I. Clearly there are significant differences in the angular distributions predicted by the various models. However, the magnitude of the D phase shift is always large enough to yield a curve that has a characteristically different shape than the experimental results in the region from 50° to 90° and too low in absolute value at 90°. The principal reason for this is the presence of a P_2 coefficient in the nuclear scattering arising from the interference between the S and the D waves.

The addition of a central P wave does not change the cross section at 90° as can be seen in Fig. 9 where we have indicated the effect of adding positive and negative P phase shifts to the scattering predicted by the Yukawa model (which comes closest to fitting the 90° point). Clearly these curves do not agree with the experimental results, primarily because the nuclear cross section adds in the region from 50° to 90° (where the Coulomb interference can be neglected).

It is seen from Table I that the D phase shift increases as the potential becomes more long tailed. Since the D phase shift is too large even for the square potential we are forced to turn to more complicated radial forms, if we wish to account for the 32-Mev scattering by central interactions alone. Such a potential might be expected to be repulsive at long distances and attractive at short distances. Accordingly some attempts were made to annul the D wave by adding a repulsive lip to the square well. They met with little success, and having regard to the inherent difficulties implicit in such an approach when applied to attempt an explanation of the 340-Mev results, this approach was abandoned.

As discussed in Part 1, the effect of adding tensor force in the purely nuclear scattering is to produce a more nearly spherically symmetric angular distribution. The depth of the tensor potential and hence the amplitude of the scattering may be considered arbitrary, and must eventually be chosen to give agreement with the experimental data. In Fig. 10 we have shown the result of adding the tensor scattering to the singlet state scattering. Clearly, if the same radial dependence is assumed to hold for both singlet and triplet states, approximate agreement may be obtained for the exponential potential with depth $V_t = \pm 50$ Mev. If we drop the restriction that the singlet and triplet potentials have the same radial dependence, it is clear that we can obtain better agreement, especially with the

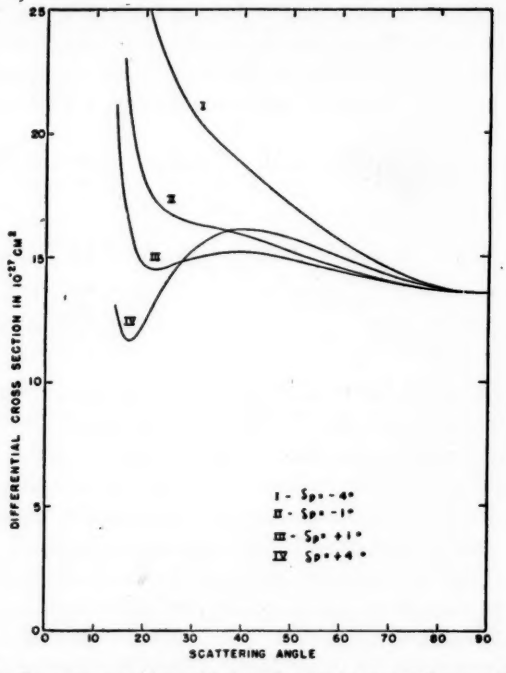

FIG. 9. P wave scattering added to the singlet scattering predicted by the Yukawa potential at 32 Mev.

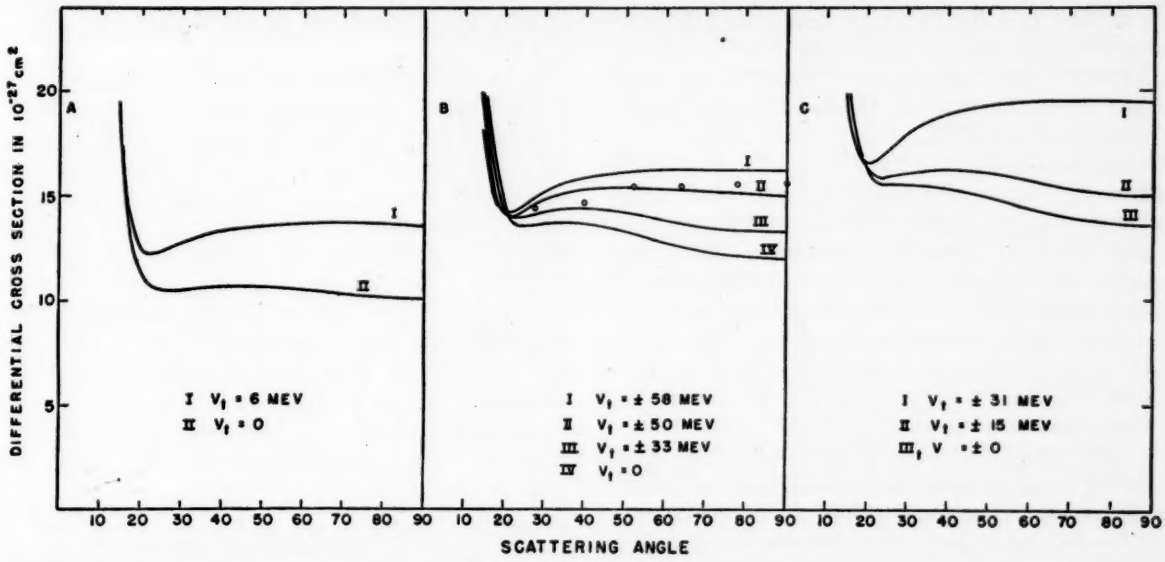
DIFFERENTIAL CROSS SECTION IN 10^{-27} cm^2
A
B
C
I V_t = 6 MEV
II V_t = 0
I V_t = ± 58 MEV
II V_t = ± 50 MEV
III V_t = ± 33 MEV
IV V_t = 0
I V_t = ± 31 MEV
II V_t = ± 15 MEV
III, V = ± 0
SCATTERING ANGLE

FIG. 10. Total scattering at 32 Mev by singlet and triplet tensor potentials of the same radial form. (The singlet potentials have range and depth adjusted to fit the low energy scattering.) A. Square. B. Exponential. C. Yukawa. Data taken from reference 2 (31.8 Mev).

photographic data, by using the combination of square well for the singlet potential and Yukawa for the triplet (see Fig. 11, curve I). (This combination utilizes a square well with the constants previously found for the singlet state and a tensor Yukawa well of range 1.25×10^{-13} cm and $V_t=\pm22$ Mev.)

This model gives an angular distribution essentially similar to S wave scattering at energies below 32 Mev. This is illustrated in Fig. 11 where the distribution due to this model at 32 and 20 Mev is compared to S wave scattering. Clearly a precise measurement would be needed even at 20 Mev in order to distinguish between this distribution and S wave scattering, although it could be distinguished from singlet scattering that included the D wave. Further, it has been found that the cross section at 90° for this model differs by at most three percent from that due to the partial S wave from a Yukawa potential below 32 Mev. Below 20 Mev the Yukawa singlet scattering at 90° (including the D wave) differs by at most $1\frac{1}{2}$ percent from the cross section predicted by this model.

As was remarked in Part 1 tensor scattering at 32 Mev is only able to explore the tail of the potential, and consequently there is little uniqueness to the radial form which can be established from the 32-Mev data. To illustrate this we may consider the Born approximation. In this approximation the triplet differential cross section (considering only the nuclear part) is proportional to

$$\sigma(\theta)\sim[C^2(\theta)+C^2(\pi-\theta)+C(\theta)C(\pi-\theta)],$$

where

$$C(\theta)=\frac{M}{\hbar^2K}\int_0^\infty V_t(r/R)g_2(Kr)rdr, \quad K=2k\sin\theta/2.$$

Plots proportional to $C(\theta)$ are shown in Fig. 12 as a function of $\alpha[2kR\sin(\theta/2)]$ where α has been adjusted such that each model predicts almost the same scattering at 32 Mev. (Recall that the Yukawa potential with $R=1.25\times10^{-13}$ cm gave a good fit to the data when combined with a shallow singlet potential.) From these

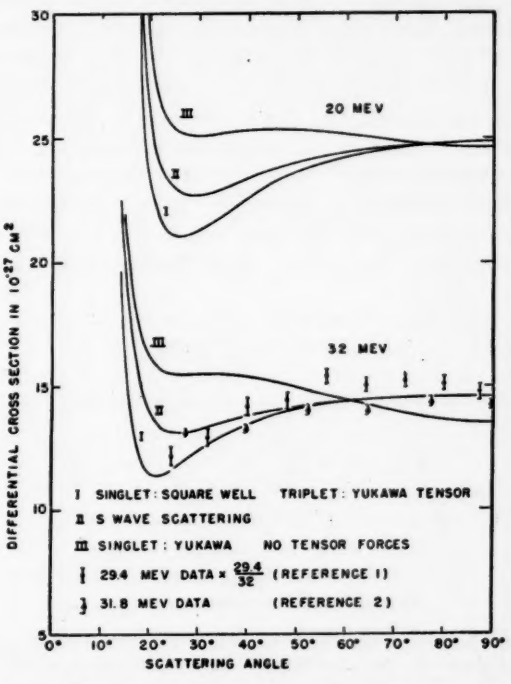
DIFFERENTIAL CROSS SECTION IN 10^{-27} cm^2
20 MEV
32 MEV
I SINGLET: SQUARE WELL TRIPLET: YUKAWA TENSOR
II S WAVE SCATTERING
III SINGLET: YUKAWA NO TENSOR FORCES
29.4 MEV DATA × 29.4/32 (REFERENCE 1)
31.8 MEV DATA (REFERENCE 2)
SCATTERING ANGLE

FIG. 11. Best fit at 32 Mev compared to S wave and singlet scattering at 32 and 20 Mev. I. Singlet square well $R=2.615\times10^{-13}$ cm and depth 13.273 Mev; triplet tensor Yukawa potential $R=1.25\times10^{-13}$ cm and $V_t=23$ Mev (or $S_{12}V_t\exp(-r/R)/(r/R)^2$ with $R=1.6\times10^{-13}$ cm and $V_t=18$ Mev). II. S wave scattering. III. Singlet scattering from Yukawa potential $R=1.1417\times10^{-13}$ cm and $V_c=49.350$ Mev; no tensor forces.

plots we find that the following ranges are practically equivalent with respect to the 32 Mev scattering: $R=3.8\times10^{-13}$ cm (square), $R=1.0\times10^{-13}$ cm (exponential), $R=1.25\times10^{-13}$ cm (Yukawa), $R=2.0\times10^{-13}$ cm^2 $(\exp(-r/R)/(r/R)^2)$.

In the plots of $C(\theta)$ we have chosen the scale of the abscissa such that $\alpha(2kR\sin\theta/2)=1$ for $\theta=90°$ with a k corresponding to 32 Mev. For other angles we move up and down the abscissa according to $\sin\theta/2$ (e.g., to obtain the value for $C(180°)$ at 32 Mev read the ordinate for an abscissa $2^{\frac{1}{2}}$). The 90° point at other energies can be readily located as it is given at an abscissa which is the square root of the ratio of that energy to 32 Mev. Thus to obtain the value of $C(90°)$ at 350 Mev read the ordinate at an abscissa of $(350/32)^{\frac{1}{2}}=3.30$.

As the energy increases a large difference in the scattering occurs between the various models. We shall first adjust the range and depth of the tensor potential to fit the data at 32 Mev, then examine the predictions of the various models at 340 Mev. From the predictions of the singlet cross section at 90° it seems reasonable to allow approximately one-third of the nuclear scattering at 32 Mev to be of tensor origin. This fixes the depths of the tensor potentials for a given range. The requirement that the tensor scattering at 32 Mev have sufficient angular variation to mask the singlet D wave sets limits on the range of the potentials.

The 340-Mev cross section is comparable with the fraction of the 32-Mev cross section attributed to tensor scattering. The square, exponential and Yukawa potentials all give too little scattering at 340 Mev (especially around 90°). Shorter ranges for these forms would give better agreement, but these ranges are incompatible with the 32-Mev data. Comparison between the radial forms indicates that a potential more singular than the Yukawa might give agreement. It was found that a tensor potential of the form $\exp(-r/R)/(r/R)^2$ with $R=1.6\times10^{-13}$ cm and $V_t=\pm18$ Mev gives a good fit to both the 32- and the 340-Mev data (see Figs. 11 and 13).

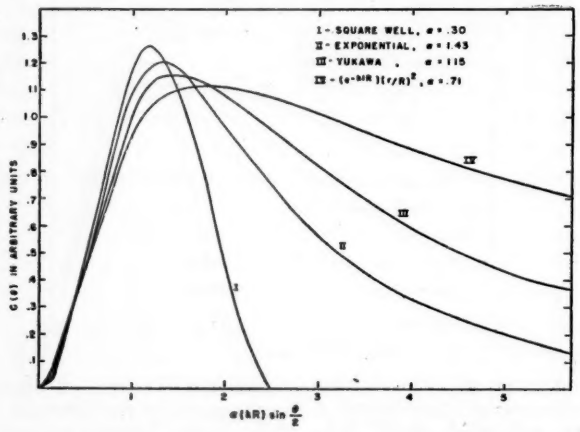

FIG. 12. Born tensor scattering amplitude for various potentials. The abscissa scale has been adjusted so that all potentials will give the same angular distribution at 32 Mev as the Yukawa potential with $R=1.25\times10^{-13}$ cm for a suitable choice of depth.

In order to indicate the essential features of the singular model, we again examine the curves in Fig. 12. Clearly a square well of range 4×10^{-13} cm gives scattering of the correct form to fit the 32 Mev data, while a square well of range 1×10^{-13} cm gives 340-Mev scattering approximating to that predicted by the singular model. By combining the shallow long range square well with a deep short range square well (which will not be explored by 32 Mev P wave protons) scattering approximating to that predicted by the singular model can be obtained. Thus a strong tensor interaction at distances less than 1×10^{-13} cm is indicated by the 340-Mev data, while the 32-Mev data gives evidence of interaction at greater distances (i.e., of a "tail" in the terminology of potential models.)

C. Summary of Results

We have shown that the 32-Mev data can be fitted by means of two combinations of central and tensor force. These both have the radial dependence singular for the tensor potential and shallow and cut off for the central potential. The best fit is with a singlet square well of range 2.6×10^{-13} cm and $V_t\exp(-r/R)/(r/R)$ radial dependence (with $R=1.25\times10^{-13}$ cm and $V_t=\pm23$ Mev) or with a more singular potential $V_t\exp(-r/R)/(r/R)^2$ with $R=1.6\times10^{-13}$ cm and $V_t=\pm18$ Mev. These combinations give better fits to the photographic data than to the counter data.

To fit the 340-Mev data we have shown that a very singular tensor force must be used, such as the $\exp(-r/R)/(r/R)^2$. The essential feature is that there must be a strong interaction in regions less than 0.5×10^{-13} cm.

The best fit of the combined data is therefore obtained by using the singular potential so adjusted that approximately one-third of the nuclear scattering at 32 Mev is accountable to tensor scattering.

It is clear that the present data are not sufficiently extensive to permit very precise specification of the radial forms; however, in the foregoing summary we have tried to emphasize the salient features of each model.

The effect of velocity dependent forces such as $\boldsymbol{\sigma}\cdot\mathbf{L}$ was not considered in this report because, as was mentioned in the introduction, they were not found necessary to fit the $n-p$ scattering.

CONCLUSIONS

We have shown that it is possible to fit all the present $p-p$ data by means of a shallow central potential for the singlet states and a singular tensor potential for the triplet states.

Quite apart from the potential models assumed however, even the most casual comparison of the $p-p$ data at 32 Mev with the $n-p$ data at 40 Mev and, especially

a comparison of the 340 Mev $p-p$ data with the 280 Mev $n-p$ data shows that nuclear scattering is charge dependent. This statement can be made more definite by an examination of the extent to which scattering in the odd parity triplet states can be tolerated in the $n-p$ system. Note from Fig. 3 that the tensor scattering adds about 4 mb/steradian to the $p-p$ cross section at energies between 32 and 340 Mev so that the same forces present in odd triplet $n-p$ states would increase the total $n-p$ cross section by nearly $\frac{1}{4}(4\pi)(4$ mb) or 12 mb. However the measured $n-p$ cross section at 90 Mev is 75 mb with less than 10 percent uncertainty while the lowest value predicted by a tensor model with only even parity states is 87 mb, so that an additional 12 mb is hard to tolerate. A similar situation exists at 40 and 280 Mev. Alternatively, a Yukawa tensor potential of range 1.35×10^{-13} cm must be 17.4 Mev deep to fit the 32 Mev data, while the maximum allowable depth of the $n-p$ tensor potential for the same states is 9 Mev (see Table III and Fig. 12, reference 6). We may further note that $\sigma\cdot\mathbf{L}$ forces have the same undesirable feature of increasing the $n-p$ total cross section.

It is possible that the radial dependences found necessary for $p-p$ scattering would be acceptable for $n-p$ scattering even though the exchange behavior is different. A definite statement regarding this must await detailed calculations, however.

Finally we must take notice of the fact that no large repulsive forces have shown up in either the $n-p$ or the $p-p$ system of sufficient magnitude to account for nuclear saturation if saturation is to be predicted from two body forces. In both cases they would have been very easily detected in the scattering independent of the potential model assumed.

ACKNOWLEDGMENTS

This analysis was originally started by G. F. Chew and M. L. Goldberger, to whom the analysis of the low energy data to obtain the singlet potential parameters and the original demonstration that the observed 32-Mev scattering is incompatible with central force models is due. We are indebted to J. M. Blatt and J. D. Jackson for receipt of their forthcoming paper on the analysis of the low energy proton-proton scattering prior to publication. We owe more than can be stated to the inspiration and guidance of Professor Robert Serber throughout this research.

APPENDIX I

The triplet cross section is given by

$$d\sigma/d\Omega=1/3k^2\sum_{m_s}(|R|^2+RN_0^*+N_0R^*+\sum_{\mu}N_\mu^*N_\mu), \quad (1A)$$

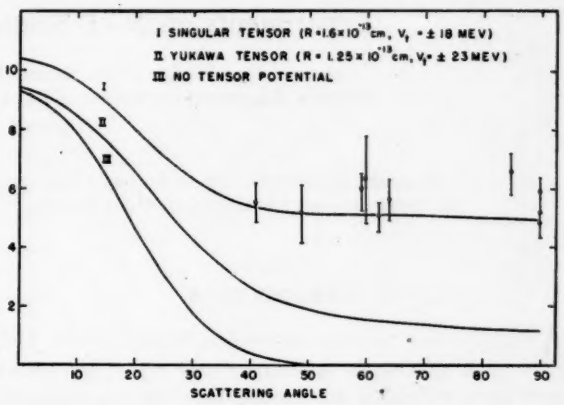

FIG. 13. Complete cross section at 350 Mev for various tensor models adjusted to fit the 32-Mev data. The legend shows the tensor model used. Data taken from reference 3.

where

$$R=\alpha/2i\left(\frac{\exp[-i\alpha\ln\sin^2(\theta/2)]}{\sin^2(\theta/2)}-\frac{\exp[-i\alpha\ln\cos^2(\theta/2)]}{\cos^2(\theta/2)}\right),$$

$$N_\mu=\sum_{J,l}[4\pi(2l+1)]^{\frac{1}{2}}\exp[2i(\sigma_l-\sigma_0)]\langle SlJm_s|Sl0m_s\rangle \times\langle SlJm_s-\mu|Sl\mu m_s-\mu\rangle[\exp(2i\delta_l^{Jm_s})-1]\bar{Y}_l^\mu(\theta,\phi),$$

$$\alpha=e^2/\hbar v,$$

$$\sigma_l-\sigma_0=\tan^{-1}(\alpha/l)+\tan^{-1}(\alpha/l-1)+\cdots+\tan^{-1}\alpha$$

$\bar{Y}_l^\mu(\theta,\phi)$ are the normalized tesseral harmonics and $\delta_l^{Jm_s}$ are the customary (complex) phase shifts that occur in tensor scattering (defined here in the presence of the Coulomb field).

In Eq. (1A) the term involving $|R|^2$ is just the usual triplet Coulomb scattering and the terms $\Sigma_\mu N_\mu^* N_\mu$ are the usual nuclear scattering. The remaining terms represent the interference between nuclear and Coulomb scattering.

In our calculations of the tensor scattering the Coulomb modification of the nuclear phase shift was neglected as the expected order of magnitude of this modification was very small compared to the P phase shifts. Further the nuclear-Coulomb interference terms were calculated only for the P wave part of the nuclear scattering. These terms can then be written

$$\frac{9P_1(\cos\theta)}{2k^2}\left[\frac{\sin\alpha_1}{S^2}-\frac{\sin\beta_1}{C^2}\right]\times(\tfrac{1}{3}\sin^2\delta_1^{00}+\tfrac{1}{3}\sin^2\delta_1^{1\pm}-\tfrac{1}{6}A_1^{2\pm}-\tfrac{1}{3}A_1^{20})$$
$$-\frac{9P_1(\cos\theta)}{2k^2}\left[\frac{\cos\alpha_1}{S^2}-\frac{\cos\beta_1}{C^2}\right]\times(\tfrac{1}{3}\sin\delta_1^{00}\cos\delta_1^{00}+\tfrac{1}{3}\sin\delta_1^{1\pm}\cos\delta_1^{1\pm}+\tfrac{1}{6}B_1^{2\pm}+\tfrac{1}{3}B_1^{20}), \quad (2A)$$

where

$$\alpha_1=\alpha\ln S^2+2(\sigma_1-\sigma_0)$$
$$\beta_1=\alpha\ln C^2+2(\sigma_1-\sigma_0)$$
$$S^2=\sin^2\theta/2$$
$$C^2=\cos^2\theta/2$$
$$A_l^{Jm_s}=Re[\exp(2i\delta_l^{Jm_s})-1]$$
$$B_l^{Jm_s}=Im[\exp(2i\delta_l^{Jm_s})]$$

Equation (2A) reduces to the expression given by Breit, Kittel, and Thaxton, Phys. Rev. **57**, 255 (1940), when the coupling between the $^3P_2$ and $^3F_2$ scattering is neglected.

Experiments on $N-P$ Scattering with 260-Mev Neutrons*

E. KELLY, C. LEITH, E. SEGRÈ, AND C. WIEGAND
Radiation Laboratory, Department of Physics, University of California, Berkeley, California
(Received March 29, 1950)

Neutrons produced by 350-Mev protons impinging on beryllium are scattered by hydrogen. The differential scattering cross section is measured as a function of the scattering angle.

I. INTRODUCTION

WHEN the circulating proton beam of the 184-inch cyclotron is intercepted by a beryllium target at a radius of 81 inches, high energy neutrons are produced in the forward direction with an energy distribution maximum at about 260 Mev. Using this neutron beam with a low energy cut-off at 200 Mev we have performed $n-p$ scattering experiments similar to those previously carried out with neutrons of 40- and 90-Mev mean energies.[1]

The methods and apparatus used will in general be described only where they differ from those of the previous work and the reader is referred to the earlier paper for the missing details and for notation.[2] The principle of the experiment is to measure the number of protons scattered from a hydrogenous target into a fixed solid angle $d\Omega = d\psi d\cos\Phi$ at angle Φ; this number is proportional to the differential cross section $\sigma(\Phi)$. From this we find the differential cross section $\sigma(\theta) = \sigma(\Phi)[d(\cos\Phi)/d(\cos\theta)]$ in the center-of-mass system. The direct measurement of $\sigma(\Phi)$ is not on an absolute scale, but we can normalize it and pass to an absolute scale by requiring that

$$\int \sigma(\Phi)d\Omega = \text{total scattering cross section} = \sigma_t.$$

In practice polyethylene was used for the hydrogenous target and the effect of the carbon was measured (using graphite) and then subtracted.

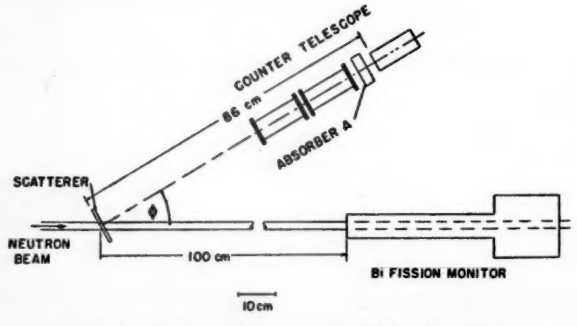

FIG. 1. General arrangement of apparatus.

The main results of the investigation are given in Tables I and II and Fig. 3. These results have been communicated in a preliminary form to Messrs. R. S. Christian and E. W. Hart, who have taken them into account in a theoretical paper endeavoring to interpret all $n-p$ scattering data through a suitable potential. We refer to their paper for the theoretical treatment of the data.[3]

II. APPARATUS

The arrangement of apparatus shown in Fig. 1 was used for all angles Φ. The diameter of the last counter has been increased to 5.1 cm and absorber A has been changed to the appropriate thickness of tungsten to give a primary neutron beam cut-off at an energy of 200 Mev; otherwise this apparatus is the same as apparatus A previously described in reference 1. The equipment was checked by all the performance tests described in Section II.E of reference 1. The approximate angular resolution of the telescope is 3°. The error in the value of $\sigma(\Phi)$ introduced by this lack of resolution is significant only for the value measured at $\Phi=0$; here we estimate that this effect would put the true cross section possibly 10 percent above the observed value (we have not made this correction to the data).

III. EFFECT OF ABSORBER A

The thickness of absorber A required to give a 200-Mev energy cut-off of the primary neutron beam (approximately 12 cm of Al or 4.5 cm of Pb at small angles) causes losses of the coincidence counting rate of the recoil protons and the variation of these losses with Φ is not small. These losses are due primarily to nuclear interaction, both elastic and inelastic, and to multiple small angle Rutherford scattering; estimates of the losses indicated tungsten to be a suitable material for absorber A and accordingly tungsten was used. It is not possible to calculate these losses accurately, due in part to lack of data and in part to the poorly defined geometry of the sensitive region of the counter behind absorber A.

To get an empirical measure of the loss due to absorber A the telescope was placed in the external deflected proton beam, the diameter of which was larger than that of the counters, and the attenuation of the telescope coincidence counting rate was measured for

* This work was performed under the auspices of the AEC.
[1] Hadley, Kelly, Leith, Segrè, Wiegand, and York, Phys. Rev. 75, 351 (1949).
[2] In formula (5) of reference 1, Θ should be replaced by Φ; in the sixth line, first column of page 361, $d(\cos\Omega)/d(\cos\theta)$ should be replaced by $d(\cos\Phi)/d(\cos\theta)$, and the formula of the second column of page 361 should read $V(r) = (g^2/r)e^{-Kr}(1/2)(1+P)$.
[3] R. S. Christian and E. W. Hart, Phys. Rev. 77, 441 (1950).

TABLE I. $\sigma(\Phi)$ in 10^{-27} cm² per steradian. All runs have been fitted to run 2, and normalized to the value of $\sigma_t = 0.035 \times 10^{-24}$ cm².

Run number Date Φ(deg.)	1 (3-10-49)	2 (3-23-49)	3 (3-31-49)	4 (4-7-49)	5 (4-14-49)	6 (4-21-49)	Weighted average	Transmission of absorber A
0			62±9				62.0±9.0	0.60
5			29±5			42.0±6.0	35.4±3.8	0.60
10	30±5	28.4±2.2	27±4			29.5±2.6	28.7±1.5	0.61
15		20.5±2.1	20±4				20.4±1.9	0.63
20		17.8±2.0				19.4±2.9	18.7±1.3	0.65
25		11.0±1.6					11.0±1.6	0.68
30		6.1±1.0				9.7±1.7	7.0±0.9	0.72
35		7.0±1.1		7.4±2.0	7.7±1.6	6.1±1.3	6.9±0.7	0.76
40		3.4±0.8					3.4±0.8	0.81
45	5.7±0.8	6.1±0.7		5.9±1.5	5.6±1.2	3.8±0.6	5.2±0.4	0.86
50				4.8±1.7			4.8±1.7	0.90
55				7.0±2.0	2.9±1.0		3.7±0.9	0.93
60					2.0±1.2		2.0±1.2	0.95
65				3.0±1.8	6.0±1.2		5.1±1.0	0.96
70				7.9±2.3	3.7±1.0		4.4±0.9	0.97

various thicknesses of tungsten placed in the position of absorber A. This was done as follows. In order to determine the number of incident protons an extra counter tube was placed in front of the telescope and electronically connected in triple coincidence with the first two counter tubes of the regular telescope. This electronic connection did not influence the operation of the regular telescope. In order to verify the voltage plateaus of the two systems of three counters the extra counter tube was de-sensitized by lowering its voltage so as to make it the controlling counter of the monitor coincidence circuit; the voltage on the regular telescope was then varied and in this way we could verify that the regular telescope was operating on a voltage plateau. Next, the sensitivity of the extra counter tube was increased until it was the same as that of the others and this was confirmed by the fact that, with no tungsten absorber, the regular telescope coincidence counting rate was 0.98 of the monitor coincidence counting rate. Finally the attenuation measurements were made.

The attenuation caused by the tungsten was found to be approximately linear with the thickness of the tungsten, ending in a sharp cut-off which gave the range of the proton beam. Data were taken at proton beam energies corresponding to ranges in tungsten of 109, 58, 38, and 24 g cm^{-2}. (The energy of the proton beam was varied by placing Al absorbers between the magnetic deflector and the focusing magnet of the cyclotron beam deflecting system.) On the basis of these data and the energy distribution of the neutron beam given in the next section, the attenuation due to absorber A was computed. Corrections for this have been applied to the differential cross sections given in Tables I and II and Fig. 3; the values of the transmission of absorber A are listed in Table I. We estimate these attenuation values to be good to about 10 percent.

IV. NEUTRON BEAM

The neutron beam was produced by intercepting the circulating beam of 350-Mev protons with a 5.08-cm thickness of beryllium. The beam was collimated in the forward direction by a hole in the 10-foot thick concrete walls of the cyclotron shield and emerged through an aperture whose diameter varied from 1 to 3 cm in the various runs; the neutron beam intensity at the scatterer was about 10^4 to 10^5 neutrons cm^{-2} sec.$^{-1}$. The equipment was accurately centered in the beam by the use of x-ray film preceded by a sheet of polyethylene for an intensifier.

An experimental determination of the energy distribution of the neutron beam was made by the method described in reference 1 of de-sensitizing the last counter of the telescope and varying the amount of tungsten placed in the position of absorber A. Allowing for the dependence of the $n-p$ scattering cross section on angle and energy and for the variation in loss due to different thickness of tungsten at the position of absorber A we obtain the results given in Fig. 2. For the 200 Mev cut-off used this gives a mean neutron energy of about 260 Mev.

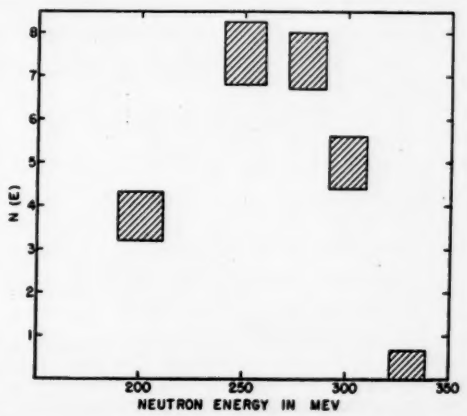

FIG. 2. Energy distribution of the primary neutrons in the beam in the forward direction obtained by 350 Mev protons incident on 5.08 cm thick beryllium. The width of the boxes represents the energy resolution of the detector and the height of the boxes represents the standard deviation due to counting statistics alone.

TABLE II. $\sigma(\theta)$ (center of gravity system) in 10^{-27} cm² per steradian; $\sigma(\theta)$ has been obtained by multiplying $\sigma(\Phi)$ of Table I by the appropriate values of d (cosΦ)/d (cosθ) for neutrons of 260-Mev energy.

Run number / Date / θ(deg.)	1 (3-10-49)	2 (3-23-49)	3 (3-31-49)	4 (4-7-49)	5 (4-14-49)	6 (4-21-49)	Weighted average
180			13.7±2.1				13.7 ±2.1
169.3			6.4±1.2			9.2±1.2	7.8 ±0.8
158.7	6.8±1.1	6.4±0.5	6.1±0.9			6.6±0.6	6.4 ±0.3
148.1		4.8±0.5	4.6±0.9				4.7 ±0.4
137.6		4.3±0.5				4.7±0.7	4.5 ±0.3
127.1		2.8±0.4					2.8 ±0.4
116.7		1.7±0.3				2.6±0.5	1.90±0.24
106.5		2.0±0.3		2.2±0.6	2.3±0.5	1.8±0.4	2.02±0.21
96.3		1.1±0.3					1.09±0.26
86.3	2.0±0.3	2.2±0.3		2.1±0.5	2.0±0.4	1.4±0.2	1.85±0.14
76.4				1.9±0.7			1.9 ±0.7
66.6				3.2±0.9	1.3±0.5		1.7 ±0.4
56.8					1.1±0.6		1.1 ±0.6
47.2				1.9±1.2	3.9±0.8		3.3 ±0.6
37.7				6.4±1.9	3.0±0.8		3.6 ±0.7

V. CONCLUSION

The normalized values of $\sigma(\Phi)$ for all the runs are given in Table I. The normalization is carried out as explained earlier by requiring that

$$\int \sigma(\Phi)d\Omega = \sigma_t = 0.035\times10^{-24}\ \text{cm}^2.$$

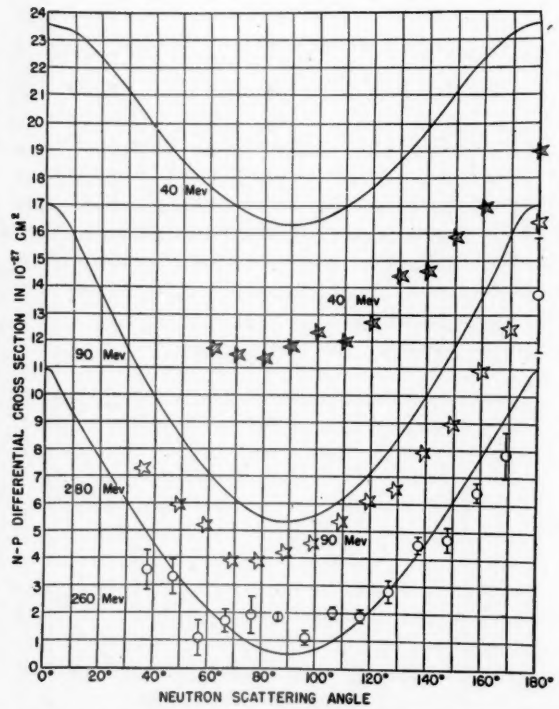

FIG. 3. Differential neutron proton cross section in the center-of-mass system in 10^{-27} cm² per steradian. The stars represent data published earlier but are included here for reference. The lowest curve represents the data taken with 260 Mev neutrons; the errors given are standard deviations due to counting statistics alone. The solid curves are the theoretical predictions for a Yukawa tensor force model and have been copied from Fig. 17 of reference 3. (The predicted cross section for 280 Mev $n-p$ scattering is 0.037×10^{-24} cm², the value quoted in reference 3 being incorrect.)

Since $\sigma(\Phi)$ is not known for the entire range of Φ we have arbitrarily extrapolated $\sigma(\Phi)$; using units of 10^{-27} cm² we have put $\sigma(\Phi)$ equal to 3.6 at 75°, 3.0 at 80°, 2.0 at 85° and 0 at 90°. The contribution of the extrapolated part of the curve to σ_t is 15 percent of the total. The value of σ_t has been measured in this laboratory,[4,5] using two types of detectors; the value of $\sigma_t = 0.035\times10^{-24}$ cm² has been taken as approximate average of these data. As was explained in Section III of reference 1 this value of σ_t is subject to considerable uncertainty (25 percent) because of the neutron energy distribution and the change of sensitivity with energy for the particular detectors used.

To find $\sigma(\theta)$, the center-of-mass differential cross section, the value of $\sigma(\Phi)$ must be multiplied by d cosΦ/d cosθ and the result paired with the value of θ corresponding to the Φ considered. This has been done using the appropriate values of d cosΦ/d cosθ for neutrons of 260 Mev energy and the results for all runs are given in Table II; the weighted averages of these data are shown in Fig. 3. For comparison we have included in Fig. 3 the previous measurements at 40 and 90 Mev which are shown as stars. The errors given in the tables are the standard deviations calculated from counting statistics only.

The weakest points of these experiments are the broadness of the primary neutron spectrum, the uncertainty in the total neutron cross section, and the fact that the form of the primary neutron spectrum is not well known. If a better neutron source (e.g., protons on deuterons) should be found, it would be worthwhile to repeat the whole experiment, possibly with considerable changes in technique, for example, with scintillation counters. In the meantime we have decided to publish the present results even though they are probably less reliable than those given in reference 1.

[4] R. Fox, C. Leith, K. McKenzie, and L. Wouters (to be published).
[5] J. DeJuren (to be published).

Proton Groups from the Deuteron Bombardment of Aluminum, Sodium, and Manganese*

W. D. WHITEHEAD†
University of Virginia, Charlottesville, Virginia

AND

N. P. HEYDENBURG
Department of Terrestrial Magnetism, Carnegie Institution of Washington, Washington, D. C.

(Received February 6, 1950)

Thin targets of sodium, aluminum, and manganese were bombarded with 3.0-Mev deuterons from the large electrostatic generator at the Department of Terrestrial Magnetism, and the protons were observed at 90 degrees to the beam with an argon filled proportional counter. The counter was biased to count protons at the end of their range and the ranges of the groups were measured in air and aluminum. Proton groups due to oxygen and carbon were found with all targets.

1. INTRODUCTION

MEASUREMENT of the energy of the proton groups emitted in the (d,p) reactions yields a method for determining the energy levels in the residual nucleus. A number of elements have been investigated with this type of reaction and extensive data are available on nuclear energy levels and energy level spacings.[1]

The proton groups from the $Na^{23}(d,p)Na^{24}$ were investigated by Lawrence[2] at a bombarding energy of 2.15 Mev and by Murrell and Smith[3] at a bombarding energy of 0.85 Mev. Lawrence found two groups of protons which gave Q-values of 4.92 and 1.72 Mev but the low energy groups were not investigated, Murrell and Smith found seven groups of protons, but two of these they attributed to $O^{16}(d,p)O^{17}$ and one to $H^2(d,p)H^3$, the remaining groups gave Q-values of 1.38, 3.50, 4.58 and 4.76 Mev respectively. The proton groups from the $Al^{27}(d,p)Al^{28}$ reaction were investigated by McMillan and Lawrence[4] at a bombarding energy of 2.2 Mev, by Schultz, Davidson, and Ott[5] at a bombarding energy of 3.2 Mev, rather thoroughly by Pollard, Sailor, and Wyly[6] with various bombarding energies and a maximum of 3.8 Mev, and by Allan and Clavier[7] at a bombarding energy of 0.9 Mev. McMillan and Lawrence found evidence of five distinct groups, while Schultz, Davidson, and Ott using a cloud chamber to detect the protons, found groups whose ranges were in rough agreement with those of McMillan and Lawrence but whose intensities differed. Allen and Clavier found three groups at the lower bombarding energy, while Pollard *et al.* found 14 groups of protons and 4 groups of alphas. The protons from $Mn^{55}(d,p)Mn^{56}$ were investigated by Martin[8] at a bombarding energy of 3.6 Mev; he resolved five groups of protons which he attributed to the $Mn^{55}(d,p)Mn^{56}$ reaction.

Two other reactions that have been investigated are the $O^{16}(d,p)O^{17}$ reaction,[9] and the $C^{12}(d,p)C^{13}$ reaction.[10] These two reactions are particularly important because the elements appear as contaminants on all targets unless special precautions are taken to remove them. Oxygen forms a thin oxide layer on the target, and since the cross section is large, the proton groups from this reaction are generally present. Thin layers of carbon are deposited on the targets from the diffusion pumps. The yield curves for these reactions have been determined[9,10] and by determining the yield-curve of a proton group which comes at the proper range for one of these contaminants the amount of the contaminant can be estimated.

The well-defined energy of the bombarding particles from the source, and the fact that the energy available was higher than with similar previous experiments, combined with a more detailed knowledge of the yield curves of carbon and oxygen, made it seem worth while to reinvestigate the proton groups from the (d,p) reactions of sodium, aluminum, and manganese.

2. EXPERIMENTAL APPARATUS

The pressurized electrostatic generator at the Department of Terrestrial Magnetism was used as the source of high energy deuterons. The voltage was measured with a generating voltmeter using the $Be(p,n)$ threshold (2.035 Mev), the $Li^7(p,n)$ threshold (1.87 Mev) and the fluorine (p,γ) 873-kev resonance as calibrating points. The current, which was generally of the order of one microampere, was measured with a current integrator designed by M. Sands.

* Part of thesis submitted in partial fulfillment of the requirements for the degree of Doctor of Philosophy at the University of Virginia.

† Part of this work done while an AEC Predoctoral Fellow. Now at Bartol Research Foundation, Swarthmore, Pennsylvania.

[1] E. C. Pollard, Nucleonics **2**, 4 (1948).

[2] E. O. Lawrence, Phys. Rev. **47**, 17 (1935).

[3] E. B. Murrell and C. L. Smith, Proc. Roy. Soc. **A173**, 410 (1939).

[4] E. M. McMillan and E. O. Lawrence, Phys. Rev. **47**, 343 (1935).

[5] Shultz, Davidson, and Ott, Phys. Rev. **58**, 1043 (1940).

[6] Pollard, Sailor, and Wyly, Phys. Rev. **75**, 727 (1949).

[7] H. R. Allan and C. A. Clavier, Nature **158**, 832 (1946).

[8] A. B. Martin, Phys. Rev. **72**, 378 (1947).

[9] N. P. Heydenburg and D. R. Inglis, Phys. Rev. **73**, 230 (1948).

[10] N. P. Heydenburg *et al.*, Phys. Rev. **75**, 1147 (1949).

In the early portion of the work the protons were detected with a 3-mm deep ionization chamber, but a proportional counter was found to be more satisfactory because of the shorter resolving time, and the gas amplification; and all of the data except the manganese number *vs.* range curve were taken with a proportional counter. These were the same counters that were used in this laboratory in the previous experiments with oxygen,[9] carbon,[10] and lithium.[11] The pulses from the counter were amplified by a preamplifier and a linear amplifier and counted with a scale of 64 counter and a mechanical register.

The counters were mounted at 90 degrees to the bombarding beam on a vernier screw so that the range in air could be changed accurately. Gross changes in the range were made using aluminum foils of 2.54 and 5.2 cm air equivalent, and the fine changes were made with the screw. The discriminator for the scaler was set to measure only those particles near the end of their ranges and the number of particles was corrected for the decrease in intensity with increasing range.

Thin targets were deposited on a backing foil and then mounted so that the beam struck them at an angle of 45 degrees, and the protons were observed at 90 degrees to the beam. The target chamber for aluminum and manganese was a brass tube with a side arm with an aluminum window mounted over the end. The targets were mounted and slipped in the end of the tube so that they were opposite the side arm. The sodium target chamber was similar but had a sodium boiler incorporated so that targets could be prepared in the vacuum system. The diameter of the beam was $\frac{1}{4}$ inch and the window on the front of the counter was 3×5 mm.

The sodium target was prepared by evaporating the pure metal from the boiler onto a $\frac{1}{32}$-in. silver foil mounted on a $\frac{1}{16}$-in. thick copper plate which held the silver in place and served as a heat conductor. Gold foil was tried as a target backing but sodium and gold form an amalgam which makes the target thick. The thickness of the sodium target was judged entirely by eye, and no measurements of thickness were made. The sodium was evaporated on until there was a visible even layer.

The aluminum and manganese targets were both prepared by evaporating the pure metal onto thin gold foils in an auxiliary vacuum system. Small pieces of aluminum and magnanese were melted onto tungsten filaments and then evaporated onto the foils. The thickness of the manganese target was measured by measuring the change in equivalent cm of air of the gold foil before and after the manganese was evaporated on. The change in range due to target thickness was less than 1 mm of air.

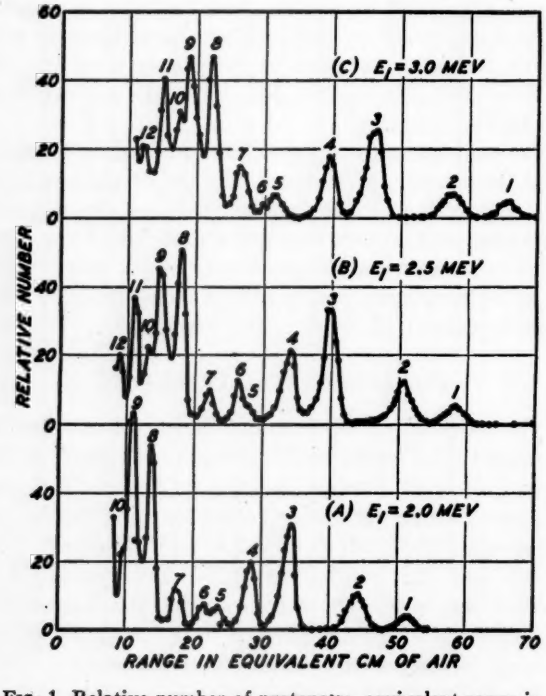

FIG. 1. Relative number of protons *vs.* equivalent range in air for protons from $Na^{23}(d,p)Na^{24}$; E_1 is bombarding energy.

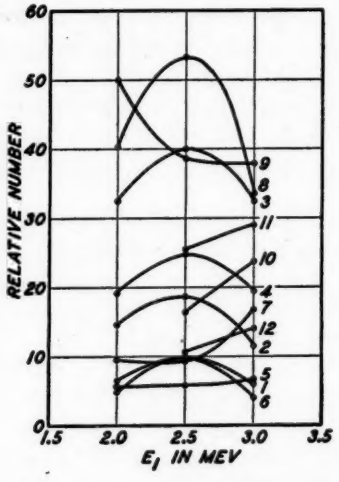

FIG. 2. Yield curve for proton groups taken from Fig. 1, *A*, *B*, *C*, normalized to group 3.

3. RESULTS

Nine groups of protons were found when the thin sodium target was bombarded with 2.0-Mev deuterons and 12 groups when the bombarding energy was 2.5 and 3.0 Mev. These groups are plotted in Fig. 1 in which the relative number of protons per integrator count is plotted *vs.* the equivalent range in air. The points on the higher intensity peaks represent several thousand protons. Two of the groups of protons (10, Fig. 1A) (7, 10, Fig. 1B, C) have the same ranges as the protons from the $O^{16}(d,p)O^{17}$ reaction, but they come in a region of high density of proton groups from the sodium and the intensities do not follow the observed yield curve for oxygen so the Q-values were computed as if the groups were from sodium. The range of group 5 does

[11] N. P. Heydenburg *et al.*, Phys. Rev. **74**, 405 (1948).

not vary with bombarding energy in the same fashion as does group 6 and must be from a different nucleus, and since it gives the correct Q-value for the $C^{12}(d,p)C^{13}$ reaction at all three bombarding energies we have attributed it to carbon, although the yield curve of this group does not follow that observed for carbon.

The number *vs.* range curves were all taken using the same sodium target, and after all the data were taken a yield curve was taken for group 3 to normalize the yields of the different groups at the different energies. The intensity of a group is approximately proportional to the product of the height of the group and the width at half-maximum. The intensities of the individual groups were determined in this way and Fig. 2 gives the excitation curve for the individual groups. The intensities of the complex groups were taken as the product of the group height and the width at half-maximum as determined from Bethe's straggling curves.[12]

The yield curve for group 5 (Fig. 2) does not follow the observed yield curve for carbon at higher energies the observed yields being

$$Y_{2.0}/Y_{2.5}=65/70, \quad Y_{2.0}/Y_{3.0}=65/30.$$

This discrepancy is probably due to the background of sodium protons. The yield curve for the long range oxygen group ($O_{L.R.}$) compares with group 7 as follows:

$$Y_{2.0}/Y_{2.5}=9.5/9.3, \quad O_{L.R.} \text{ observed } 9/16,$$
$$Y_{2.0}/Y_{3.0}=9.5/16.6, \quad O_{L.R.} \text{ observed } 9/32.$$

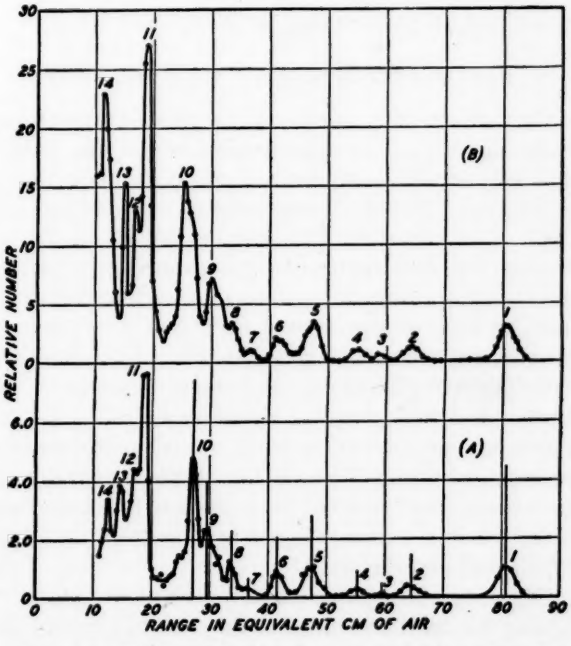

FIG. 3. Relative number of protons *vs.* equivalent range in air for protons from $Al^{27}(d,p)Al^{28}$. Curve *A* is thin target; Curve *B* is slightly thicker. Bombarding energy is 3.0 Mev.

[12] M. S. Livingston and H. A. Bethe, Rev. Mod. Phys. 9, 245 (1937).

TABLE I. Q-values for $Na^{23}(d,p)Na^{24}$.

Present experiment Bombarding energy 2.0	2.5	3.0	Murrel and Smith Bombarding energy 0.85	Lawrence Bombarding energy 2.15
4.81	4.82	4.69	4.76	4.92
4.25	4.28	4.16	4.38	
3.46	3.43	3.47	3.50	
2.92	2.95	2.94		
2.21	2.25	2.19		
1.29	1.34	1.36	1.38	1.72
0.93	0.95	1.01		
	0.74	0.83		
	0.47	0.53		
	0.14	0.11		

The yield curve for group 9 departs from the general shape of the long range groups, and all of the short range groups increase in intensity with bombarding energy. If group 10 were entirely due to oxygen the intensity would decrease as the energy was increased from 2.0 to 3.0 Mev, but the intensity increases by a factor of 1.5 so that the group must be due mostly to sodium. The total yield curve as measured by the radioactivity of the Na^{24} for the $Na^{23}(d,p)Na^{24}$ increases up to a bombarding energy of 5.5 Mev.[1] The Q-values for this reaction as computed from the number *vs.* range curves are given in Table I.

A thin target of aluminum was bombarded with 3-Mev deuterons and 14 groups of protons were observed (Fig. 3A). In general the number *vs.* range curve for this reaction is similar to that determined by Pollard *et al.* but there are discrepancies in the Q-values computed from these ranges. A slightly thicker target of aluminum was bombarded at 3.0 Mev, the thickness was not actually measured but the number of protons increased by a factor of four. The number *vs.* range curve for this target (Fig. 3B) was essentially the same as for the thin target, but the range of the peak of group ten had shifted one cm. Two of the fourteen groups of protons have the same ranges as the protons from $O^{16}(d,p)O^{17}$ (10, 11, Fig. 3) and one has the same range as the protons from $C^{12}(d,p)C^{13}$ (8, Fig. 3). The oxide layer is likely to be a constant independent of the thickness of target, but group 10 which comes at approximately the right range for the oxygen shifted about one cm in range when the target was made thicker, and must be partly due to oxygen and aluminum at slightly different ranges. The observed ratio of the intensities of the short range oxygen group to the long range group is 1.25 at 3.0 Mev and the ratio as determined from Fig. 3B is 26/31; the observed ratio for these groups (9, 10) at 2.2 Mev is 7 and the ratio is 12/20 when the bombarding energy is 2.2 Mev so that the groups must be due to aluminum. The vertical lines drawn through the peaks of the thin aluminum curve are proportional to the intensity and are equal to the product of the group height and the width of the group at half-maximum. This illustrates the role of straggling in determining the intensity, for although the group

TABLE II. Q-values for $Al^{27}(d,p)Al^{28}$.

Present experiment		Pollard *et al.*	Allan and Clavier
thin	½ thin		
5.71	5.72	5.45	5.49
4.71	4.71		
4.32	4.39	4.42	4.49
4.07	4.07	3.88	
3.49	3.49	3.29	3.34
3.04	3.06		
2.72	2.66	2.84	
2.39	2.40	2.48	
2.11	2.05	2.04	
1.59	1.80	1.55	
0.95	0.93	0.98	
0.70	0.70	0.73	
0.47	0.45	0.57	
−0.05	0.13	0.29	
		0.01	
		−0.31	

TABLE III. Q-values for $Mn^{55}(d,p)Mn^{56}$.

Present experiment	Martin
5.01	4.76
3.47	3.69
3.13	
2.85	2.99
0.48	2.28
0.13	1.15
−0.19	

TABLE IV. Range of protons scattered from silver foil.

Bombarding energy Mev	Scattered proton energy Mev	Range (NTP) cm	Range (Herb) cm	Range (Bethe) cm
1.1	1.066	2.46	2.48	2.54
1.2	1.163	2.83	2.85	2.92
1.5	1.45	4.12	4.10	4.15
1.6	1.55	4.58	4.57	4.63
1.8	1.745	5.63	5.53	5.63
2.0	1.94	6.72	6.62	6.74
2.25	2.18	8.11		8.25
2.5	2.42	9.59		9.75
3.1	3.005	14.10		14.15

heights of the long range groups are low, the intensities are high. The Q-values as computed from the number *vs.* range curves are given in Table II.

A thin manganese target was bombarded with 3.0 (Fig. 4) and 2.2-Mev deuterons and ten proton groups were observed at 3.0 Mev. Groups 6 and 7 have the same range as the oxygen groups and group 5 has the same range as the carbon group. In the observed yield curve the ratio of the intensities of the short range oxygen group to the long range oxygen group at 3.0 Mev is 1.25 and in this curve it is 1, while the ratio at 2.2 Mev is 7 and in this case it is 10. The discrepancies in these ratios are probably due to the background of protons from manganese, and the groups are probably mostly due to oxygen. Assuming that group 7 follows the yield curve for the short range oxygen group, group 5 increases by a factor of 2.5 as the bombarding energy is decreased from 3.0 to 2.2 Mev, while the observed yield for carbon increases by a factor of 3, and the group must be due to carbon. For the high intensity groups there were several hundred protons counted per point; while for the low intensity peaks there were of the order of 50 protons per point. There are 7 observed groups of protons which are attributed to manganese and the Q-values are listed in Table III.

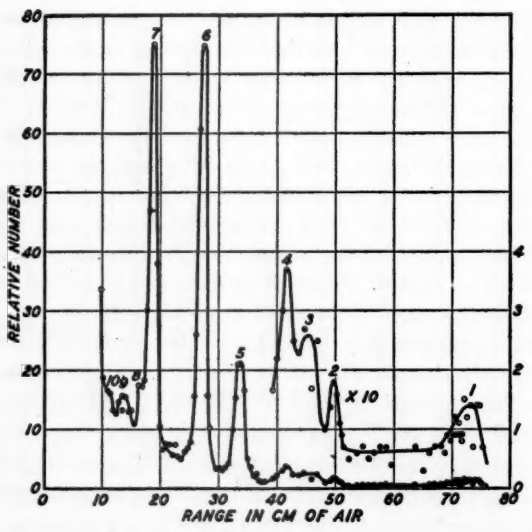

Fig. 4. Relative number of protons *vs.* equivalent range in air for protons from $Mn^{55}(d,p)Mn^{56}$; bombarding energy 3.0 Mev. The intensity is expanded by a factor of ten for the long range groups.

4. RANGE AND INTENSITY MEASUREMENTS

The range to the counter for each measurement was made up of the aluminum window on the target chamber, several centimeters of air, the aluminum absorbing foils, the aluminum counter window, and the argon in the counter. The stopping powers of the individual foils and windows were measured by measuring the change in range of protons of known energy scattered at 132.5 degrees from a silver leaf. The range to the center of the counter was then reduced to equivalent cm of air and plotted on the number *vs.* range curve. Since the actual range in air never exceeded 2.5 cm there was no correction made for temperature and pressure variation. The details of the conversion to equivalent cm of air from the aluminum foils have been discussed in a previous paper by Heydenburg, Inglis, Whitehead and Hafner.[10]

The range of a group of protons was computed by adding 0.2 cm to the range to the peak of a group. The counter was biased such that the maximum pulse height occurred when the counter straddled the Bragg peak; thus the range to the peaks in the number *vs.* range curve represents the mean range to the peak of the Bragg curve. The range of the group is this range plus

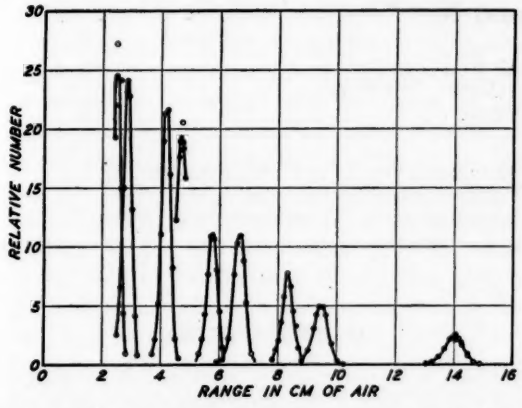

FIG. 5. Relative number of protons *vs.* range in air of protons scattered at 132.5 degrees from a silver leaf at bombarding energies of 1.1, 1.2, 1.5, 1.6, 1.8, 2.0, 2.25, 2.5, and 3.1 Mev.

0.2 cm as deduced from the Bragg curve for protons as given by Holloway and Moore.[13]

Figure 5 is the number *vs.* range curve for the protons scattered from a silver leaf at 132.5 degrees. In these curves corrections were made for temperature variations since most of the range is in air. The ranges deduced from the curve for the given energy are given in Table IV.

The intensity of the scattered protons should vary as

[13] M. G. Holloway, and B. L. Moore, Phys. Rev. **58**, 847 (1940).

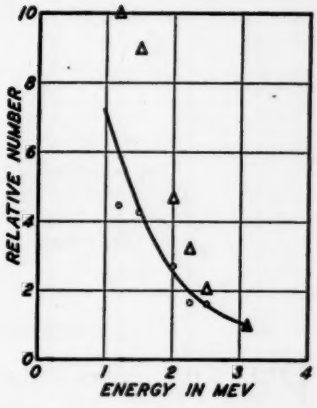

FIG. 6. Area under peaks of Fig. 5 *vs.* bombarding energy and peak heights of Fig. 5 *vs.* bombarding energy. Peak heights and areas are normalized for long range group. Solid line is $AE^{-2}\times 10$ with A an arbitrary constant.

AE^{-2} as the bombarding energy is increased, where A is an arbitrary constant. The ratio of the peak height to the 3.1-Mev peak and the ratio of the area under the peak to the area under the 3.1 new peak are plotted *vs.* energy in Fig. 6. A curve of the form AE^{-2} is normalized to this peak and from this can be seen that intensity is proportional to the area under the curve rather than to the peak height. This is to be expected since the counter measures number per unit length because of its finite depth, and the intensity of the product of the distance and this number.

One of us (W.D.W.) would like to thank, Dr. M. A. Tuve for making the facilities at the Department of Terrestrial Magnetism available for the work.

Radiations of Zr^{97} and Nb^{97}*

W. H. Burgus, J. D. Knight, and R. J. Prestwood
Los Alamos Scientific Laboratory, Los Alamos, New Mexico
(Received March 22, 1950)

The radiations of Zr^{97} and Nb^{97} have been examined by beta-ray spectrometry and coincidence counting. The 17.0-hr. Zr^{97} has been found to decay to a 60-sec. isomer of Nb^{97}, the latter undergoing isomeric transition to the 75-min. Nb^{97} ground state. The disintegration energies are: Zr^{97}, $E_\beta=1.91\pm0.02$ Mev; Nb^{97m}, $E_\gamma=0.747\pm0.005$ Mev; Nb^{97}, $E_\beta=1.267\pm0.02$ Mev; $E_\gamma=0.665\pm0.005$ Mev.

I. INTRODUCTION

PREVIOUS studies of the radiations of the 17.0-hr. Zr^{97}—75-min. Nb^{97} chain have been made by absorption methods.[1] On the basis of measurements on the mixture in transient equilibrium and on the niobium fraction separated from the mixture, the following beta- and gamma-ray energies have been reported: Zr^{97}: $E_\beta=2.2$ Mev, $E_\gamma\sim0.8$ Mev; Nb^{97}: $E_\beta=1.4$ Mev, $E_\gamma=0.78$ Mev.

The present report describes the results of an examination of the radiations and of the disintegration scheme of these nuclei by means of beta-ray spectrometry and coincidence counting techniques. The Zr^{97}—Nb^{97} samples used in this investigation were obtained by slow neutron irradiation of electromagnetically enriched Zr^{96} and by isolation from uranium fission products.[1a] Since in slow neutron uranium fission the 17.0-hr. Zr^{97} and the 65-day Zr^{95} are produced with nearly equal yields,[2] a certain amount of the Zr^{95} activity was always present in Zr^{97} sources of fission origin. However, by use of short neutron irradiations, with chemical separation and measurement within the 24 hr. following, it was possible to limit the Zr^{95} contribution to a few percent in the low energy range and to a negligible amount in the beta-energy region above 0.4 Mev.[3] To insure that the gamma-ray and conversion electron lines found belonged to the Zr^{97}—Nb^{97} chain, the sources were left in the spectrometer for a few days after measurement and the appropriate points were checked for a 17-hr. decay. The average of a number of decay measurements on Zr^{97} from $Zr^{96}(n,\gamma)$ has given $t_{\frac{1}{2}}=17.0\pm0.2$ hr.; for Nb^{97}, produced by $Mo^{98}(\gamma,p)$, $t_{\frac{1}{2}}=74\pm2$ min.

II. BETA-SPECTRA

The beta-ray spectrometer used in this investigation was of the single coil magnetic lens type, and has been described in an earlier paper from this laboratory.[4] Resolution could be varied from 2.4 to 6.4 percent by adjustment of a movable disk baffle. The detector was a G-M counter with 3.5-mg/cm² mica end window.

Beta-spectra were taken with two kinds of sources. The $Zr^{96}(n,\gamma)$ sources consisted of 13 to 14 mg of zirconium oxide spread over an area of 0.8 cm² and sandwiched between two layers of rubber hydrochloride film of 0.50-mg/cm² thickness each. The fission product Zr sources were 1.6 mg of zirconium oxide spread over 0.6 cm² and similarly mounted. Provision for electrical leakage was made by spraying the sources with a light coat of an Aquadag suspension. Since the beta-sources as described were thick enough to cause small distortions in the spectra, empirical energy calibrations were carried out using carrier-free P^{32} and Cs^{137}—Ba^{137m} sources evaporated down in inactive zirconium oxide and mounted in the same way as the active Zr—Nb sources.

The momentum distribution of the electrons from fission product Zr^{97} in transient equilibrium with the 75-min. Nb^{97} is shown in Fig. 1. Spectrometer resolution was 2.5 percent. The Fermi plot of this spectrum,

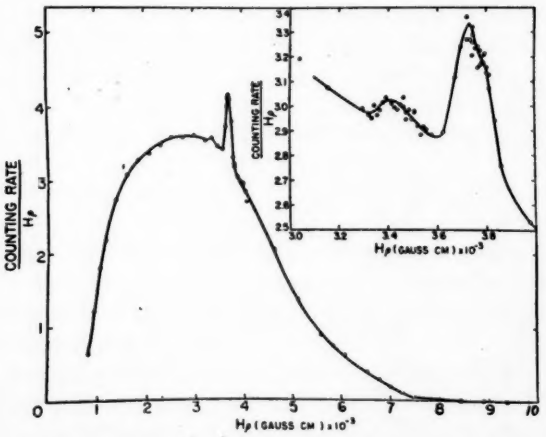

FIG. 1. The electron spectrum of Zr^{97} in transient equilibrium with Nb^{97}. Inset: Conversion peaks from Nb^{97m} and Nb^{97}.

* This document is based on work performed at Los Alamos Scientific Laboratory of the University of California under AEC Contract W-7405-Eng-36.

[1] S. Katcoff and B. Finkle, Plutonium Project Report CC-2310 (January, 1945), cited by G. T. Seaborg and I. Perlman, Rev. Mod. Phys. 20, 585 (1948).

[1a] The enriched Zr^{96} and Mo^{98} used in this investigation were supplied by Carbide and Carbon Chemicals Corporation, Y-12 Plant, Oak Ridge, Tennessee, on allocation from the Isotopes Division, U. S. AEC.

[2] Coryell, Sakakura, and Ross, Phys. Rev. 77, 755 (1950).

[3] The beta-spectrum of Zr^{95} is complex, with ~98 percent of the disintegrations having $E_{max}=0.394$ Mev and ~2 percent $E_{max}=1.0$ Mev (V. A. Nedzel and M. B. Sampson, Plutonium Project Report CC-2283 (October, 1944), cited by G. T. Seaborg and I. Perlman, reference 1).

[4] L. M. Langer, Phys. Rev. 77, 50 (1950).

shown in Fig. 2, exhibits straight-line components corresponding to beta-rays of energies 1.91±0.02 and 1.267±0.02 Mev, respectively. The results of two additional runs with somewhat heavier sources of fission and (n, γ) origin fell within the limits of error given above. The energy calibration was based on Ba^{137m} $E_{e^-}=0.626$ Mev.[5] The upward curvature in the series of points extending from about W=1.8 on backward on the Fermi plot is due presumably to source thickness distortions and to the presence of beta-rays from Zr^{95}.

In addition to the beta-spectrum, there is a line of conversion electrons at 0.726±0.005 Mev. From a measurement of the relative areas under the momentum distribution curve in Fig. 1, with the assumption that the conversion electron follows the 1.91-Mev beta-ray, there was obtained a conversion ratio $N_{e^-}/N_\beta=0.015$ ±0.002 for the transition. The 2.5 percent resolution of the spectrometer did not permit a separation of the K and L components of the conversion line. However,

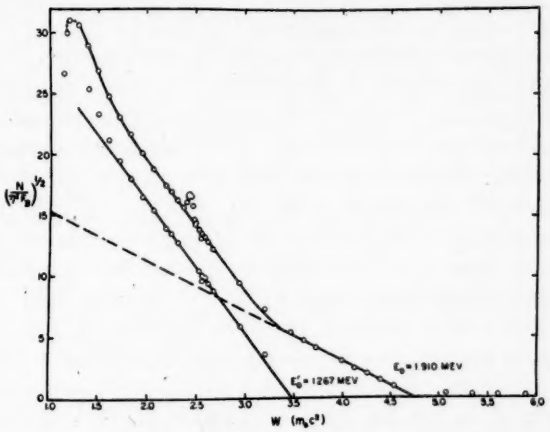

FIG. 2. Fermi plot of electron spectrum of Zr^{97} in transient equilibrium with Nb^{97}.

on the basis of a later run in which the conversion peak was carefully mapped (Fig. 1 inset) and its energy compared with the gamma-ray energy for this transition, it is estimated that at least 80 percent of the conversions occur in the K shell. There is also evidence for a weak conversion peak at 0.645±0.010 Mev, for which a rough estimate gives $N_{e^-}/N_\beta\sim0.0015$.

III. GAMMA-SPECTRA

Gamma-spectra were measured on $Zr^{97}-Nb^{97}$ from (n, γ) and fission product sources, using both gold and uranium radiators. The photo-electron spectrum for the uranium radiator and 2.5 percent spectrometer resolution is plotted in Fig. 3. It is seen that there are two prominent gamma-rays of about equal intensity, with $E_\gamma=0.749\pm0.005$ and 0.665±0.005 Mev, respectively, plus possibly two weaker ones at ~0.48 and ~0.56 Mev. A $Cs^{137}-Ba^{137m}$ source, with $E_\gamma=0.663$ Mev, was used as a gamma-standard.

[5] Townsend, Cleland, and Hughes, Phys. Rev. 74, 499 (1948).

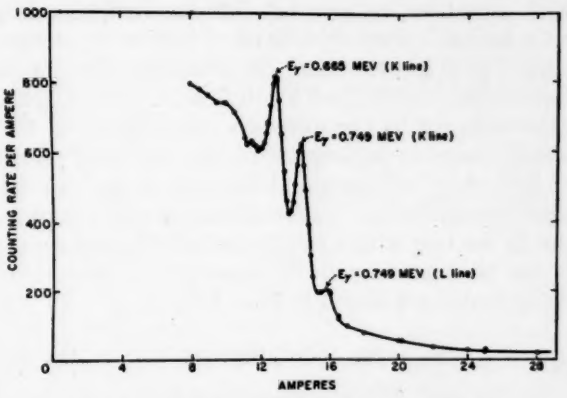

FIG. 3. Photo-electrons ejected from a 1-mil U radiator by gamma-rays from $Zr^{97}-Nb^{97}$.

IV. COINCIDENCE COUNTING

The harder of the two beta-rays has already been identified with the 17.0-hr. Zr^{97} on the basis of absorption studies.[1] While conventional separation and counting techniques have also shown that one of the gammas follows each beta, the small difference between the gamma-ray energies, together with the rapid growth of Nb^{97} into freshly purified Zr^{97} samples, has hitherto made it difficult to determine with any certainty the association of gamma- and beta-rays.

To clarify the decay relationships a series of beta-gamma-, gamma-gamma-, and beta-conversion electron measurements was made. In the first, a $Zr^{97}-Nb^{97}$ sample was mounted between two counter tubes face to face; one tube was shielded with sufficient aluminum to stop all betas, and beta-gamma-coincidences were measured as a function of absorber in front of the beta-counting tube. The results, plotted in Fig. 4, show a gradual decrease in $(\beta\text{-}\gamma)/\beta$ ratio with increasing absorber, extrapolating to zero at approximately 500 mg/cm² Al; this range corresponds to ~1.2 Mev, the Nb^{97} beta-energy. The sloping nature of the curve and the position of the $(\beta\text{-}\gamma)/\beta$ end point show that there is no gamma-ray in coincidence with the hard beta-ray. Measurements of beta-gamma-coincidences as a function of gamma-absorber gave a $(\beta\text{-}\gamma)/\gamma$ ratio which decreased slowly with increasing absorber thickness, indicating that the softer of the two gammas is the one which is in coincidence with the beta. No gamma-gamma-coincidences were found. Measurements of the beta-beta-coincidence rate gave a net $(\beta\text{-}e^-)/\beta$ ratio of $\leq6\times10^{-5}$. This ratio, as predicted from the effective geometry of the counting arrangement and the known internal conversion coefficient, should be $\geq4\times10^{-4}$ if the 0.726-Mev conversion electron were in coincidence with one of the beta-rays; in short, this conversion line and the harder of the two gammas are not in coincidence with either of the beta-transitions.

However, in view of the fact that the photo-electron spectrum showed the two gamma-rays to be of about equal intensity, and one was known to be associated

with each beta, it appeared that the Zr^{97} beta-decay must lead to a metastable state of Nb^{97} with a lifetime appreciably greater than the resolving time of the coincidence circuit ($\sim 0.5\times10^{-6}$ sec.). This suspicion was confirmed by the discovery of an isomer of Nb^{97}. Rapid chemical separation of the Zr from samples of $Zr^{97}-Nb^{97}$ mixtures and counting of the two fractions brought to light a gamma-emitter which grew into the Zr fraction with a 60 ± 8-sec. half-life and decayed in the Nb fraction with the same period. Growth and decay curves are shown in Figs. 5 and 6.

V. CONCLUSIONS

On the basis of the findings described in the preceding sections, the harder gamma-ray and its conversion electron are assigned to the 60-sec. isomeric transition of Nb^{97m}, and the softer gamma-ray to the 75-min. Nb^{97} decay. Also, since no evidence was found for beta-radiation harder than the 1.91-Mev component belonging to Zr^{97}, and the two gamma-rays occurred in about equal intensity in the $Zr^{97}-Nb^{97}$ equilibrium mixture, it is concluded that the 17.0-hr. Zr^{97} decays to the 75-min. Nb^{97} via the 60-sec. Nb^{97} isomer.*

Results of the energy measurements are summarized in Table I. The over-all results of this investigation are consistent with the disintegration scheme shown in Fig. 7. It is of interest to compare the *ft* values for Zr^{97} and Nb^{97} with those for Zr^{95} and Nb^{95}. The 17.0-hr. Zr^{97} decay, with *ft* $\sim1.4\times10^7$, is probably first forbidden; the 75-min. Nb^{97}, with *ft* $\sim2.6\times10^5$, should be allowed. The corresponding values for 65-day Zr^{95} (assuming all decay via the 0.394-Mev beta-ray) and 35-day Nb^{95} are 3.4×10^6 and 1×10^5, respectively. The Nb values compare well, suggesting that the same type of transition is involved in both cases. The *ft* for Zr^{95}, though also probably in the first forbidden category, is fourfold smaller than that of Zr^{97}; it appears that in this instance the two transitions are of different kinds.

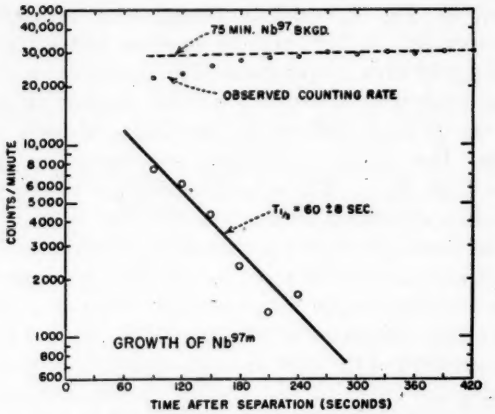

FIG. 5. Growth of Nb^{97m} into freshly separated Zr^{97}.

Some idea as to the order of the isomeric transition of Nb^{97m} may be obtained from the data in Table I. On the basis of half-life and energy for this transition, one finds, following the approximation treatment described by Segrè and Helmholz,[6] that the order of the transition lies between 4 and 5, being nearer the latter. Perhaps a better estimate may be made by a comparison of the observed conversion coefficient with the *K*-shell internal conversion coefficients recently calculated by M. E. Rose *et al.*[7] Coefficients for the most probable types of transition, obtained by interpolation from the tables of these authors, are given in Table II. The observed conversion coefficient for the 0.747-Mev transition is 0.015 ± 0.002, of which ≥80 percent is estimated to be *K* conversion. By reference to Table II, it appears that the transition is electric 2^5 or magnetic 2^4 or both,

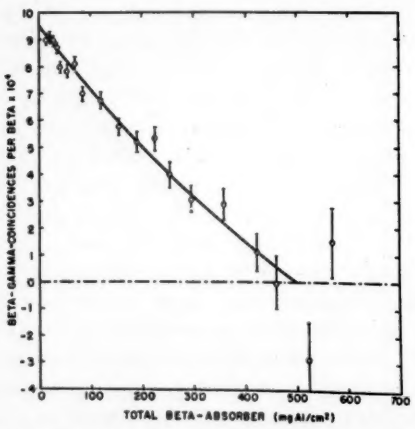

FIG. 4. Beta-gamma-coincidences as a function of beta-absorber thickness, $Zr^{97}-Nb^{97}$.

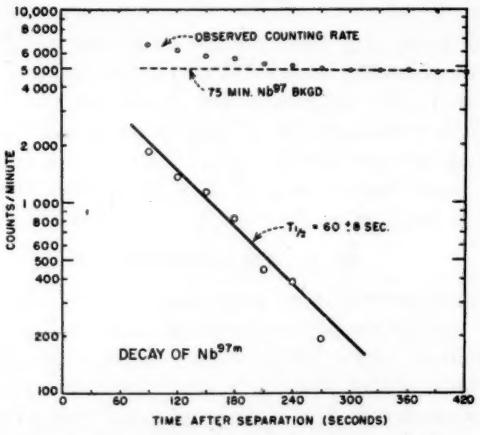

FIG. 6. Decay of Nb fraction separated from $Zr^{97}-Nb^{97}$ equilibrium mixture.

* *Note added in proof:* The 60-sec. Nb^{97m} has recently been produced by (γ,p) on enriched Mo^{98} with 20-Mev betatron gamma-rays. The activity level obtained was too low to permit an improvement in the half-life value given above.

[6] E. Segrè and A. C. Helmholz, Rev. Mod. Phys. **21**, 271 (1949).

[7] Rose, Goertzel, Spinrad, Harr, and Strong, Phys. Rev. **76**, 1883 (1949). We wish to thank Dr. Rose for providing us with a copy of these tables.

TABLE I. Summary of data.

	Beta-energy (Mev)	Conversion electron energy (Mev)	Gamma-energy (Mev)	Averaged value gamma-energy (Mev)	Estimated internal conversion (percent)
Zr^{97}	1.91 ±0.02				
Nb^{97m}		0.726	0.749	0.747±0.005	1.5±0.2
Nb^{97}	1.267±0.02	0.645	0.665	0.665±0.005	~0.15

TABLE II. K-shell internal conversion coefficients for $Z=41$, $E=0.747$ Mev.

Coefficient	Electric 2^4	Electric 2^5	Magnetic 2^3	Magnetic 2^4
N_e/N_γ	0.0071	0.0138	0.0082	0.0187

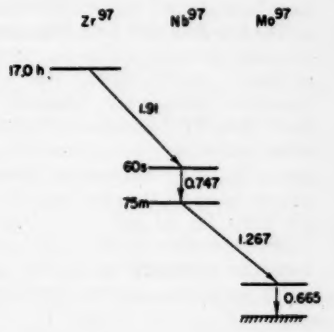

FIG. 7. Proposed disintegration scheme for $Zr^{97}-Nb^{97}$ chain.

and therefore that the order of the transition is probably 5.

We are greatly indebted to Robert E. Carter for his advice and assistance with the beta-ray spectrometer measurements. Our thanks are also due E. O. Swickard and Jane Heydorn of the Los Alamos Fast Reactor group for making the neutron irradiations and to Martin Warren of the betatron group for the gamma-ray irradiations.

APPENDIX I. PROCEDURE FOR ISOLATION OF FISSION PRODUCT Zr^{97}

Zr^{97} samples were isolated from fission product mixtures by the following procedure. The irradiated uranium metal was dissolved in a minimum quantity of hot 16 f. nitric acid. After solution, 10 mg of Zr^{+4} carrier was added, the solution boiled to expel any excess nitric acid, and a few drops of 5 f. hydroxylamine hydrochloride solution was added to insure reduction of neptunium. The solution was then made 6–10 f. in nitric acid, transferred to a Lusteroid centrifuge tube and made 2 f. in hydrofluoric acid. All further operations in which hydrofluoric acid was present were carried out in Lusteroid. Six successive lanthanum fluoride scavenging precipitations were then made by addition of 5-mg quantities of La^{+3} carrier to the solution. Each of the precipitates was centrifuged out and discarded.

From the solution remaining after the lanthanum fluoride scavenging, zirconium was then precipitated as barium fluozirconate by the addition of a fivefold excess of Ba^{++}. The precipitate was centrifuged out and the supernatant solution discarded. The barium fluozirconate precipitate was dissolved in several ml of water, several drops of 16 f. nitric acid, and a slight excess of saturated boric acid solution added to complex the fluoride. Barium fluozirconate was then reprecipitated by addition of an excess of hydrofluoric acid plus a small amount of Ba^{++}. It was centrifuged out as before and the supernatant liquid discarded. Resolution and reprecipitation of barium fluozirconate were twice repeated and the final precipitate was dissolved in a hydrochloric acid-boric acid mixture instead of the previously employed nitric acid-boric acid mixture.

The barium was removed by addition of a few drops of concentrated sulfuric acid and centrifugation of the resultant barium sulfate precipitate. The zirconium-containing solution was diluted to about 25 ml and a slight excess of six percent cupferron solution was added dropwise to precipitate the zirconium. The precipitate was filtered out on Whatman 42 filter paper and was ignited to zirconium dioxide. This zirconium dioxide served as the source material for some of the radioactivity measurements.

Low Energy Alpha-Particles from Fluorine Bombarded by Protons

C. Y. CHAO,* A. V. TOLLESTRUP, W. A. FOWLER, AND C. C. LAURITSEN
Kellogg Radiation Laboratory, California Institute of Technology, Pasadena, California
(Received March 6, 1950)

The low energy alpha-groups from the reaction $F^{19}(p, \alpha)O^{16*}$ have been studied at various resonances between proton energies of 340 kev and 1381 kev. Four groups have been identified. For the reaction energy of the α_π group, preceding the pair emission, we find $Q_\pi = 2.061 \pm 0.010$ Mev and for the three other groups preceding gamma-ray emission we find $Q_1 = 1.977 \pm 0.008$, $Q_2 = 1.204 \pm 0.008$ and $Q_3 = 1.002 \pm 0.008$ Mev. Each of the Q-values when added to the corresponding pair-energy or gamma-ray energy found by Rasmussen, Hornyak, Lauritsen, and Lauritsen gives a value for the total reaction energy of $F^{19}(p, \alpha)O^{16}$ which is the same for all the groups, namely 8.113 ± 0.030 Mev. The relative intensities of the α_1, α_2, and α_3 groups are found to vary from one resonance to another and the sum of their absolute yields per proton per 4π-steradians at 138° is found to be very close to the absolute yield of the gamma-rays per proton per 4π-steradians at 90° at all the resonances investigated, the gamma-ray yield being measured simultaneously with the alpha-particle yields. The absolute yield of the α_π-group agrees in order of magnitude with the pair yield determined in this laboratory and elsewhere. The small discrepancies can probably be attributed to angular distribution factors. The excitation functions of the α_1- and α_2-groups have been compared carefully with that of the gamma-rays over certain regions of the proton energy. Over each resonance, the excitation functions of the alpha-groups and the gamma-rays can be represented by the same curve by suitable normalizations. Our excitation curve of the α_π-group is found to run parallel with the excitation curve of the pairs found by Bennett *et al.*

I. INTRODUCTION

THE bombardment of fluorine by protons results in the production of high energy alpha-particles and several low energy groups. The high energy alpha-particles leave the residual nucleus, O^{16}, in the ground state and the low energy groups leave the O^{16} in one level which decays by the emission of a positive and negative electron-pair and several levels which decay by gamma-ray emission. The excitation function and absolute yield of the high energy alpha-particles, of the gamma-rays, and of the pairs were measured simultaneously by Streib, Fowler, and Lauritsen.[1] A review of the literature on the subject prior to 1941 will be found in their paper. The excitation function and yield of the gamma-radiation and of the pairs have also been measured by Kojima[2] and by Bonner and his collaborators.[3] The latter group used monoenergetic proton beams and thin targets and were able to ascertain the natural widths of the sharp resonance levels in the excitation curves with considerable precision.

The energy and intensity of the gamma-ray components have been measured by Walker and McDaniel[4] and recently by Rasmussen, Hornyak, Lauritsen, and Lauritsen,[5] who have also measured the energy and intensity of the pairs. The low energy alpha-particles have been studied by Freeman and Baxter[6] and by Burcham and Freeman.[7] The latter authors found that the observed low energy groups can be explained by assuming the existence of three gamma-ray emitting levels of O^{16} at 6.13, 6.94, and 7.15 Mev in addition to the pair emitting level at about 6.00 Mev. For convenience we shall call the alpha-group corresponding to the pair excitation the α_π-group, and those corresponding to the three gamma-ray levels the α_1-, α_2-, and α_3-groups in the order of decreasing alpha-energy.

We have recently measured the energy and intensity of the four low energy alpha-groups at most of the resonances between 340 kev and 1381 kev bombarding energy and have also determined the excitation functions for α_1, α_2, and α_π over two energy regions of particular interest. The Q-value we obtain for each group when added to the corresponding gamma-ray energy or pair energy found by Rasmussen, Hornyak, Lauritsen, and Lauritsen, gives a value for the total reaction energy of $F^{19}(p, \alpha)O^{16}$, which is constant over all the groups, namely 8.113 ± 0.030 Mev. The relative intensities of the α_1-, α_2-, and α_3-groups also agree very well with their relative gamma-ray intensities and the absolute yields of the alpha-groups agree with previous measurements of the absolute gamma-ray yields.[1] The absolute yield of the α_π-group agrees in order of magnitude with pair yields determined in this laboratory[1] and elsewhere.[3] The discrepancies can probably be attributed to angular distribution factors. The intensity ratios of α_1, α_2, and α_3 are found to vary in a complicated way from one resonance to another. For low bombarding energies and hence relatively low alpha-energies, the barrier effect apparently decreases the probability for the emission of α_2 and α_3 to the point where α_1 is by far the strongest component. Even at the higher energy resonances α_1 remains the strongest of the three, but in some cases α_2 and α_3 reach comparable intensities.

II. EXPERIMENTAL PROCEDURE

The protons were accelerated in an electrostatic generator and their energy was held constant within

* On leave from Institute of Physics, Academia Sinica, Nanking, China.

[1] Streib, Fowler, and Lauritsen, Phys. Rev. **59**, 253 (1941).
[2] S. Kojima, Proc. Imp. Acad. Toyko **19**, 282 (1943).
[3] Bennett, Bonner, Mandeville, and Watt, Phys. Rev. **70**, 882 (1946); T. W. Bonner and J. E. Evans, Phys. Rev. **73**, 666 (1948).
[4] R. L. Walker and B. D. McDaniel, Phys. Rev. **74**, 315 (1948).
[5] Rasmussen, Hornyak, Lauritsen, and Lauritsen, Phys. Rev. **77**, 617 (1950).
[6] J. M. Freeman and A. S. Baxter, Nature **162**, 696 (1948).
[7] W. E. Burcham and J. M. Freeman, Phys. Rev. **75**, 1756 (1949).

0.03 percent by an electrostatic analyzer which was calibrated by measurement on the strong gamma-ray resonance in the reaction $F^{19}(p, \alpha\gamma)$ at the proton energy of 873.5 kev.[8] The target consisted of a thin evaporated layer of ZnF_2 deposited on a copper surface. New targets were deposited on clean copper surfaces from time to time throughout the experiment. In general the targets had a stopping power of about 5 kev for 1-Mev protons. The alpha-particles emerging from the target in the angular interval 134.5° to 141.1° with respect to the incident beam were analyzed by a double focusing magnetic spectrograph[9] and detected with a scintillation counter.[10] The resolving power of the spectrograph in momentum was $R=P/\delta P=128$ and the solid angle of acceptance was 0.0061 steradian $\approx 1/2000$ of the whole sphere. The analyzer was calibrated by observations on protons scattered from copper surfaces into the spectrograph with known energy. The energy of the protons before scattering was determined by the electrostatic analyzer and the energy after scattering at the mean angle of 137.8° was calculated using the usual conservation laws of energy and momentum.

The gamma-ray intensity was measured by a Geiger-Müller counter set at a distance of 6.35 cm from the target in a direction perpendicular to the proton beam. At strong resonances, the counter was set at a distance of 12.7 cm in order to avoid too high a counting rate. The counter was surrounded by an aluminum cylinder of 0.1 inch wall thickness which was enclosed in a lead cylinder of 1 inch wall thickness. A window was cut in the front of the lead cylinder between counter and target and was covered with $\frac{1}{8}$ inch of lead during most of the experiments. In measuring the number of alpha-particles or the gamma-ray intensity, the proton beam was made to charge a condenser to a given voltage. The number of alpha-particles or of gamma-quanta then corresponds to a given number of microcoulombs of protons impinging on the target.

Two types of measurement were made for the low energy alpha-particles: (a) the momentum distribution of the alpha-particles near the exact resonances of the reaction and (b) the excitation functions for the different alpha-groups. For (a), the position of a resonance peak was first located by measuring the gamma-ray intensity or the pair intensity as a function of the proton energy. With the proton energy fixed at the setting corresponding to maximum yield,[10a] the number of alpha-particles which passed through the spectrograph was measured and plotted as a function of the fluxmeter reading, the latter being inversely proportional to the magnetic field of the spectrograph. The area under the profile of each group then gives a measure of the yield of the target for that group. For (b) the spectrograph field was always adjusted to give the maximum number of alpha-particles for the group investigated at any proton energy. This maximum number of alpha-particles was measured as a function of the proton energy and hence gives data from which the excitation curve for the particular group can be derived. The detailed methods of calculation are discussed below.

The maximum energy of the alpha-particles which could be deflected by the spectrograph was about

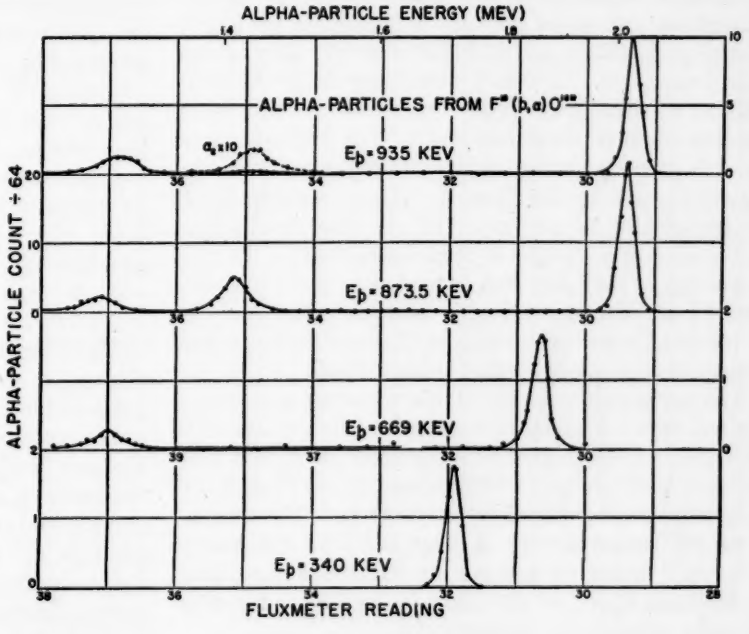

FIG. 1. Spectral distribution of low energy alpha-particles from fluorine bombarded by protons of energies 340, 669, 874, and 935 kev, at 138°.

[8] Herb, Snowdon, and Sala, Phys. Rev. 75, 246 (1949).
[9] Snyder, Fowler, Lauritsen, and Rubin, Phys. Rev. 74, 1564A (1948).
[10] Tollestrup, Lauritsen and Fowler, Phys. Rev. 76, 428 (1949).
[10a] This corresponds to the resonance energy plus one-half of the target thickness in energy units. This last value was always less than 5 kev.

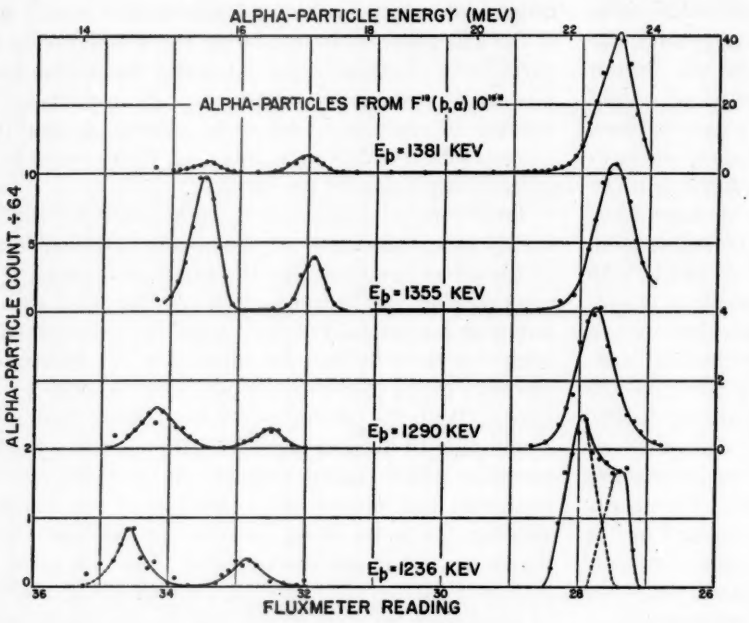

FIG. 2. Spectral distribution of low energy alpha-particles from fluorine bombarded by protons of of energies 1236, 1290, 1355, and 1381 kev at 138°.

2 Mev. When the energy of the alpha-particles exceeded this limit, aluminum foils, each of thickness about 0.2 mg/cm² were inserted before the spectrograph so as to reduce the energy of the alpha-particles to a value within the range of the spectrograph.

III. EXPERIMENTAL RESULTS ON *Q*-VALUES

The spectral distribution of the low energy alpha-particles was investigated at 9 proton energies corresponding to the more prominant resonances for the gamma-ray excitation between 340 kev and 1381 kev, and also at 843 kev and 1236 kev corresponding to two pair resonances. Figures 1 and 2 give the observed number of alpha-particles as functions of the fluxmeter reading for 8 of these resonances. The ordinate gives in each case the actual number of alpha-particles observed divided by 64 when the target received 26.85 microcoulombs of protons. The spectral distribution of the α_1- and α_r-groups in the neighborhood of the pair resonance at 843 kev was investigated for three different proton energies (Fig. 3) with the main purpose of resolving these two groups so that the intensity and energy of each group could be determined.

The excitation function of the α_1-group was investigated between the proton energies 870 kev and 970 kev, that of the α_2-group in the same range and also between 1240 kev and 1420 kev, and finally that of the α_r-group between 1050 kev and 1360 kev. These functions are shown in Fig. 4, together with the simultaneously measured gamma-ray excitation functions. In the same figure, we also show the excitation function for pairs measured by Bennett *et al.*[3]

As was mentioned above, in determining the spectral distribution of the alpha-particles at each resonance, the resonance peak was first located by taking the excitation curve of the gamma-rays. From the observed half-value width Γ' and the true half-value width Γ as given by Bonner and Evans,[3] we can calculate the target thickness ξ from the relation

$$\xi = (\Gamma'^2 - \Gamma^2)^{\frac{1}{2}}. \quad (1)$$

All quantities in (1) must be expressed in energy units. The proton beam was then adjusted to the peak intensity of the gamma-ray excitation and the alpha-particle spectrum determined. It is clear that the energy of the protons was at exact resonance at the middle layer of the target and that the energy of the alpha-particles produced in this layer represents the average energy of the group. This average energy is given by the peak of the symmetrical spectral distributions. The energy of these alpha-particles was reduced, however, by a certain amount in emerging from the target. This amount can be estimated from the target thickness ξ for the proton beam, the relative stopping power of the target for protons and alpha-particles of the appropriate energies, and the angles between the alpha-beam and proton beam and the normal to the target. In calculating the energy of each alpha-group we apply this correction[10b] throughout, which is about 3 percent in the most unfavorable case. For the sake of uniformity we take the resonance energies of Bonner and Evans and apply a correction factor such that the standard gamma-ray resonance is at 873.5 kev. From the measured alpha-particle and proton energies the energy released in the reaction, Q, can be computed by customary methods. Relativistic corrections to the alpha-particle and proton energy determinations have been made but they are less than 0.1 percent in relative magnitude.

[10b] The correction for the energy of the alpha-particles in emerging from the target is about 20 kev for the α_r- and α_1-groups, 26 kev for the α_2-group, and 28 kev for the α_3-group. The corrections in Q are about 25 percent greater.

For the evaluation of the Q-values, we use only those data which were obtained with fresh targets. The results are given in Table I, where Q_1, Q_2, Q_3, and Q_π are the Q's corresponding to the ejection of the α_1-, α_2-, α_3-, and α_π-groups, respectively. It is to be noted that most of the Q-values given in Table I were obtained at $E_p=874$ kev.

In our experiments, the α_π-group was completely resolved from the α_1-group only near 840 kev and it was analyzed by the magnetic spectrograph after passing through an Al foil of 0.2 mg/cm². The results for three bombarding energies, 842 kev and 851 kev both close to the pair resonance, and 874 kev the gamma-ray resonance, are shown in Fig. 3. The target used at 842 kev and 874 kev had an equivalent thickness of 5.2 kev and that used at 851 kev had an equivalent thickness of 2.7 kev. Note that at 874 kev the yield has been multiplied by a factor of 1/64. Note also the increase in energy of α_1 and α_π with increasing proton energy. The absolute energy of the α_π-group obtained using the Al foil is not as accurate as the energies of the other groups. However, the α_1-group energy was also measured after passage through the foil, as well as directly. From the data obtained using the foil we obtain $(Q_\pi-Q_1)$ with good accuracy. This value, when combined with the value of Q_1 determined directly, gives the value of Q_π.

The statistical probable errors of the Q-values given in Table I evaluated from the mean square deviation from the mean values vary from 0.1 percent in the case of Q_1 (± 2 kev) to 0.5 percent in the case of Q_3 (± 5 kev). We have attempted to estimate possible systematic errors in our experiments. We estimate these systematic errors to be 0.2 percent in the bombarding energy, 0.3 percent in the measured energy of the alpha-particles and 0.3° in the angle of observation. These various sources of error and the statistical error have been combined in the usual manner to give the results included in Table I. In general our Q-values are slightly higher than previously published results[7,11] although the recent values of Burcham and Freeman[7] agree with our values within their probable error (± 0.08 Mev). Our value for Q_1 also agrees with the value $Q_1=1.969$ Mev given recently by Strait *et al.*[12]

IV. DISCUSSION OF THE ENERGY MEASUREMENTS

By means of an electron spectrometer, Rasmussen, Hornyak, Lauritsen, and Lauritsen have recently made a careful study of the energies and intensities of the gamma-ray components and of the pairs of the reaction $F^{19}(p, \alpha)O^{16*}$. Each of our Q-values given in Table I when added to the corresponding pair-energy or gamma-ray energy will give the total Q of the reaction $F^{19}(p, \alpha)O^{16}$. Their experiment gives a unique answer for the energy of the pair and of the γ_1-component corresponding to the α_1-group. But their resolution was not high enough to resolve γ_2 and γ_3. They observed, however, in the intensity curve a shift of the common peak arising from these two components as the energy of the proton beam was changed from one resonance to another. This is because the relative intensities of the two components are not the same for all resonances. In other words, they have measured an average value of the gamma-ray energy weighted according to the relative intensities of the two gamma-rays. As will be discussed in more detail in a later section we have measured the alpha-particle intensities as well as the Q-values. We are thus able to calculate an appropriately averaged value for Q_2 and Q_3 which combined with the measured gamma-ray energy should give the total energy release in the reaction. Of course our intensity measurements on the alpha-particles were made at a specific angle of observation (138°) while the gamma-rays were observed in the forward direction. Thus our result may contain a small error if the angular distribution of the alpha-particles or gamma-rays is markedly anisotropic. The results are given in Table II. In determining the final mean value $Q_0=8.113\pm 0.030$ for the $F^{19}(p, \alpha)O^{16}$ reaction we give one-half weight to each of the two measurements based on the average results for the lower energy alpha-groups and the corresponding gamma-rays. The internal consistency of the results is excellent.

It is of some interest to compute the energy values of the excited states of O^{16} using the average value for Q_0

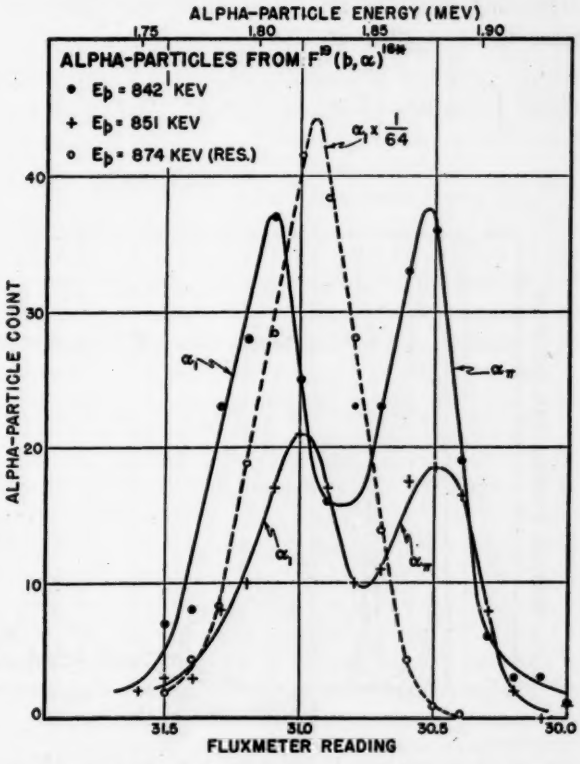

FIG. 3. Spectral distribution of α_1 and α_π groups in the neighborhood of the pair resonance at 843 kev. ($\theta=138°$.)

[11] Becker, Fowler, and Lauritsen, Phys. Rev. 62, 186 (1942).
[12] Strait, Van Patter, and Buechner, Phys. Rev. 78, 337A (1950).

calculated above and the measured values for Q_π, Q_1, Q_2, and Q_3. The results are given in the bottom line of Table I. The absolute probable errors are about 30 kev but the difference in any pair of values has an error of only 10 kev or less.

V. THE YIELD OF THE LOW ENERGY ALPHA-PARTICLES

Let $N_\alpha(I)$ be the number of alpha-particles observed at given fluxmeter[13] reading, I, of the spectrograph when q microcoulombs of protons are received by the target. Because of the loss of energy of the incident protons and of the emergent alpha-particles in the target material, the alpha-particles will be distributed over a finite interval in energy and momentum. Even with the thin targets used in these experiments this interval was larger than that accepted by the spectrograph. It was thus necessary to integrate the alpha-particle counts over all readings corresponding to one group to obtain the total yield for each group. Let $R=P/\delta P=|I/\delta I|$ be the momentum resolution of the spectrograph as determined by its entrance and exit slits and let Ω_c be the solid angle in the center-of-mass system within which alpha-particles can traverse the spectrograph from target to counter. Then the number of alpha-particles per proton per 4π-steradians per unit interval on the fluxmeter scale is

$$y(\alpha)=(4\pi R/q\Omega_c)(N_\alpha(I)/I)\times 1.602\times 10^{-13}. \quad (2)$$

Integrating over the total area under the peak corresponding to a given group we obtain

$$Y(\alpha)=\int y(\alpha)dI=(4\pi R/q\Omega_c)\int (N_\alpha(I)/I)dI \times 1.602\times 10^{-13}, \quad (3)$$

which is the yield in alphas per proton per 4π-steradians appropriate to the target thickness and angle of observation, 137.8°, used in the measurement of $N_\alpha(I)$. The integrals in (3) were evaluated graphically from plots of $N_\alpha(I)$ *vs.* I such as are shown in Figs. 1 and 2.

The quantity Ω_c can be calculated from the solid angle in the laboratory system, Ω, by the following formula

$$\Omega_c=\frac{(1+2\alpha\cos\theta_c+\alpha^2)^{\frac{3}{2}}}{1+\alpha\cos\theta_c}\Omega \approx(1+2\alpha\cos\theta_c)\Omega \quad \text{(for small values of } \alpha),$$

where

$$\alpha=\left[\frac{M_1M_2E_1}{(M_1+M_0)M_3Q+M_0M_3E_1}\right]^{\frac{1}{2}}$$

and where the angle of ejection in the center of mass system, θ_c, is related to that in the laboratory system, θ, by the equation

$$\cot\theta_c+\alpha\csc\theta_c=\cot\theta. \quad (5)$$

For small values of α useful forms of this last expression are

$$\cot\theta_c=\cot\theta-\alpha\csc\theta+\cdots,$$

and

$$\theta_c=\theta+\alpha\sin\theta-\alpha^2\sin^2\theta+\cdots.$$

In the expression for α, given above, M_0, M_1, M_2, and M_3 are the masses of the target nucleus, incident particle, ejected particle and residual nucleus while Q is the energy release, $(M_0+M_1-M_2-M_3)c^2$, in the reaction.

The quantity $4\pi R/\Omega$ was obtained by measuring the number of protons scattered by a copper target into the spectrograph and by calculating the number ex-

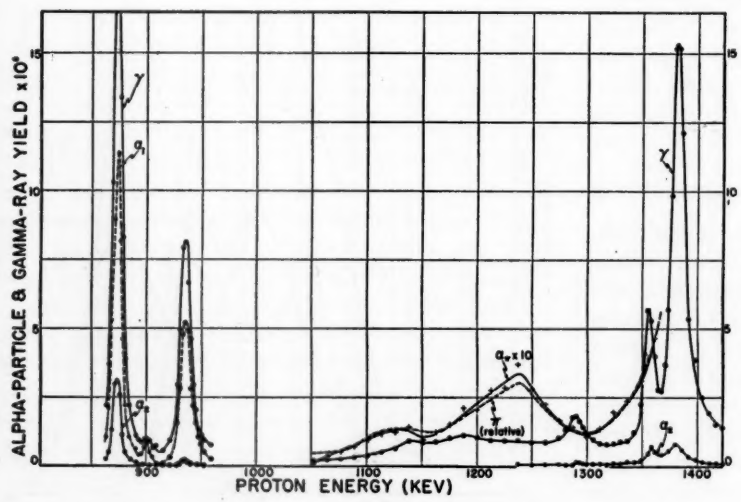

FIG. 4. Excitation functions of α_1-, α_2- and α_3-groups and of gamma-rays. ($\theta=138°$, target thickness=8 kev at 874 kev proton energy.)

[13] C. C. Lauritsen and T. Lauritsen, Rev. Sci. Inst. **19**, 916 (1948).
The fluxmeter reading is inversely proportional to the spectrograph field and thus inversely proportional to the momentum/charge of the particles traversing the spectrograph.

TABLE I. Q-values for $F^{19}(p, \alpha)O^{16*}$ (all in Mev).

E_p	Q_1	Q_2	Q_3	$Q_\pi - Q_1$	Q_π
0.340	1.982				
0.842				0.087	
0.851				0.080	
0.874	1.972				
0.874	1.974	1.212	1.010		
0.874	1.980	1.198	1.005		
1.353		1.203	0.990		
Mean	1.977±0.008	1.204±0.008	1.002±0.008	0.084±0.006	2.061±0.010
$h\nu$	6.136	6.909	7.111		6.052

$h\nu$ is calculated using $Q_0 = 8.113$ Mev.

TABLE II. Calculated energy for the $F^{19}(p, \alpha)O^{16}$ reaction (Mev).

Resonance	Alpha-group	Q_α†	$h\nu$	Q_0
1236	α_π	2.061±0.010	6.04±0.03	8.101±0.03
874, 935	α_1	1.977±0.008	6.14±0.04	8.117±0.04
874	α_2 and α_3	1.140±0.012	6.99±0.06	8.130±0.06
935	α_2 and α_3	1.024±0.012	7.09±0.06	8.114±0.06
		Weighted mean		8.113±0.030

† In the last two cases Q_α is averaged for α_2 and α_3 according to their relative intensities.

TABLE III. Relative yield of alpha-particles, gamma-rays, and pairs from $F^{19}(p, \alpha)O^{16*}$. Angles of observation: alphas, 138°; gammas, 90°; pairs, 13°. All yields are total yields at the resonance peaks and particularly in the case of α_π and π include some non-resonant background.

Level (kev)	$Y(\gamma)\cdot 10^5$	$Y(\alpha_1)\cdot 10^8$	$Y(\alpha_2)\cdot 10^8$	$Y(\alpha_3)\cdot 10^8$	$\Sigma Y(\alpha)\cdot 10^8$	$\Sigma Y(\alpha)/Y(\gamma)$
γ340	0.24	0.21	—	—	0.21+	0.88+
γ598	0.071	0.064	—	—	0.064+	0.90+
γ669	0.31	0.24	<0.02	0.06	0.30	0.97
γ874	18.4	10.80 (65%)	3.93 (24%)	1.78 (11%)	16.5	0.90
γ900	0.98	0.82	<0.04	—	0.82+	0.84+
γ935	8.5	5.73 (76.5%)	0.19 (2.5%)	1.58 (21%)	7.5	0.88
γ1290	1.74	1.28 (74.5%)	0.13 (7.5%)	0.31 (18%)	1.72	0.99
γ1355	6.6	3.42 (53.5%)	0.74 (11.5%)	2.25 (35%)	6.4	0.97
γ1381	15.1	11.58 (87%)	1.03 (8%)	0.71 (5%)	13.3	0.88
Level	$y(\pi)\cdot 10^{10}$	$Y(\alpha_\pi)\cdot 10^8$			$y(\alpha_\pi)\cdot 10^{10}$	$y(\alpha_\pi)/y(\pi)$
π843	1.1	0.12			2.5	~2
π1236	3.7	0.37			6.6	~2

pected per 4π-steradians using the Rutherford scattering law. The result was

$$(4\pi R)/\Omega = 2.63\times 10^5. \quad (6)$$

From the width of the slit at the detector, R is calculated to be 128 in agreement with observations on line shape. This yields $\Omega = 0.0061$ steradian which is in agreement with estimates of the solid angle based on the geometry of the spectrograph.

The measurements were in general restricted to counting the number of doubly ionized alpha-particles emerging from the target surface and entering the spectrograph. Small corrections were made to obtain the total number of particles, doubly ionized, singly ionized and neutral, in a manner similar to that previously described.[14]

As the low energy alpha-groups are followed by gamma-radiation and pair emission from the residual excited O^{16} nuclei, we have been interested in comparing the yields of the gamma-rays and pairs with the yields of the appropriate alpha-groups. Quantitative considerations aside, it is important to ascertain that the relative excitation curves for the alpha-groups and gamma-rays are identical functions of the proton energy. We have studied this question with greatest care for the α_1-group and the gamma-rays at the 874 and 935 kev resonances. The results are shown in Fig. 5 with the alpha-particle readings normalized at the peak values of the two resonances respectively. The detailed agreement in shape of the two excitation curves is satisfactory. Additional evidence for the correlation of the other alpha-groups with the appropriate gammas or pairs will be discussed below.

From the quantitative standpoint the absolute yield comparison is mainly of interest in that it serves as a check on computed efficiencies of Geiger counter detection of gamma-rays.[15] For the yield of gamma-rays per proton per 4π-steradians we have

$$Y(\gamma) = (4\pi/q\Omega_\gamma)(N_s/a\epsilon)\times 1.602\times 10^{-13}, \quad (7)$$

where N_s is the number of secondaries at a given angle of observation registered by the counter when q microcoulombs of protons impinge on the target, ϵ is the efficiency[15] of secondary production in the converter surrounding the counter, a is an absorption factor arising from material between target and counter, and $4\pi/\Omega_\gamma$ is the geometrical solid angle factor.

For the $F^{19}(p, \alpha\gamma)$ radiation ϵ varies from 0.042 to 0.045 depending on the relative intensities of the three components while $a = 0.90$ from the absorption of the radiation in $\frac{1}{8}$ inch of lead and $\frac{1}{10}$ inch of aluminum. The solid angle factor $4\pi/\Omega_\gamma$ equals 39.6 for a counter of diameter 1.8 cm and length 7.6 cm at a distance 6.35 cm from the target.[15]

For each of the gamma-ray resonances we have measured $Y(\gamma)$ at 90° and $Y(\alpha_1)$, $Y(\alpha_2)$ and $Y(\alpha_3)$ at 137.8° for the target employed at that resonance. $Y(\gamma)$ is the yield of all three components of the gamma-radiation. Fresh targets were employed at the different resonances but the same target was used throughout the measurements at any one resonance. As noted previously, after ascertaining the gamma-ray excitation curve the alpha-particle profile was obtained at the voltage giving the peak of the gamma-ray curve. The gamma-ray counter served as monitor throughout the profile measurements. The gamma-ray yields and the integrated profile yields for alphas are tabulated in Table III. The results for $Y(\gamma)$, $Y(\alpha_1)$, and $Y(\alpha_2)$ are shown graphically and in greater detail in Fig. 4. In

[14] Thomas, Rubin, Fowler, and Lauritsen, Phys. Rev. **75**, 1612 (1949).

[15] Fowler, Lauritsen, and Lauritsen, Rev. Mod. Phys. **20**, 236 (1949).

TABLE IV. Comparison of intensity ratios.

	$\left(\frac{\alpha_1}{\alpha_2}\right)$	$\left(\frac{\alpha_1}{\alpha_3}\right)$	$\left(\frac{\alpha_1}{\alpha_2+\alpha_3}\right)$	$\left(\frac{\alpha_1}{\alpha_2}\right)_{BF}$	$\left(\frac{\alpha_1}{\alpha_3}\right)_{BF}$	$\left(\frac{\gamma_1}{\gamma_2+\gamma_3}\right)_{RL}$
Angle	138°	138°	138°	83°	83°	13°
669	>12	4.0	>3		6.0	
874	2.7	6.1	1.9	3.0		2.5
935	30	3.6	3.2		3.7	3.3
1355	4.6	1.5	1.1			1.0
1381	11.2	16.3	6.7			4.7

this figure $Y(\alpha_1)$ and $Y(\alpha_2)$ are calculated from peak alpha-readings and from estimates of the shape of the group. At the resonances the shape was, of course, measured in detail and the yield normalized to that given by Eq. (3). For these excitation curves the thin ZnF_2 target had an equivalent thickness of 8 kev at 874 kev. In Table III we also tabulate $\sum_1^3 Y(\alpha)$ and its ratio to $Y(\gamma)$. In spite of the fact that the alpha-particle yields have been measured at 137.8° (~140° in the center of mass system) and the gamma-ray yields at 90° the ratio is very close to unity, having an average value of 0.92±0.03. Measurements on the angular distribution of the gamma-radiation have recently been made for the resonances below 900 kev by Devons and Hine.[16] They find isotropic distributions at all resonances except at 598 and 874 kev where the distributions follow $1+A\cos^2\theta$ with $A=0.2$ in the first case and $A=0.1$ in the second. Since our observations have been made at 90°, a correction factor $f=1+\frac{1}{2}A$ must be employed to give the total yield. We have $f=1.067$ at 598 kev and 1.033 at 874 kev; the correction is small. The angular distributions of the low energy alpha-particle groups have not been measured. Only for marked asymmetries will the total yields differ from our measured yields per 4π-steradians. The close agreement in our measurements between $\sum Y(\alpha)$ and $Y(\gamma)$ at all resonances as shown in Table III would seem to preclude the possibility of any *large* asymmetries in alpha- or gamma-distributions except for accidental effects. In any case the value 0.92±0.03 for $\sum Y(\alpha)/Y(\gamma)$ averaged over all resonances coupled with some assurance concerning the accuracy of alpha-particle counting definitely indicates that an error of at most 10 percent is involved in the calculation of counter efficiencies for gamma-rays up to 7 Mev made by Fowler, Lauritsen, and Lauritsen[15] in 1948. The efficiency curve given in this reference can thus be used with some confidence over the low energy region. It is hoped to make similar checks at higher energies in the near future.

We have also made a comparison of the excitation functions and yields of the α_π-group and the pairs. In Fig. 4 we show our measured excitation function for the α_π-group in comparison with the excitation curve for the pairs given by Bennett *et al.*[3] This latter curve has been normalized to give the best fit with our data and

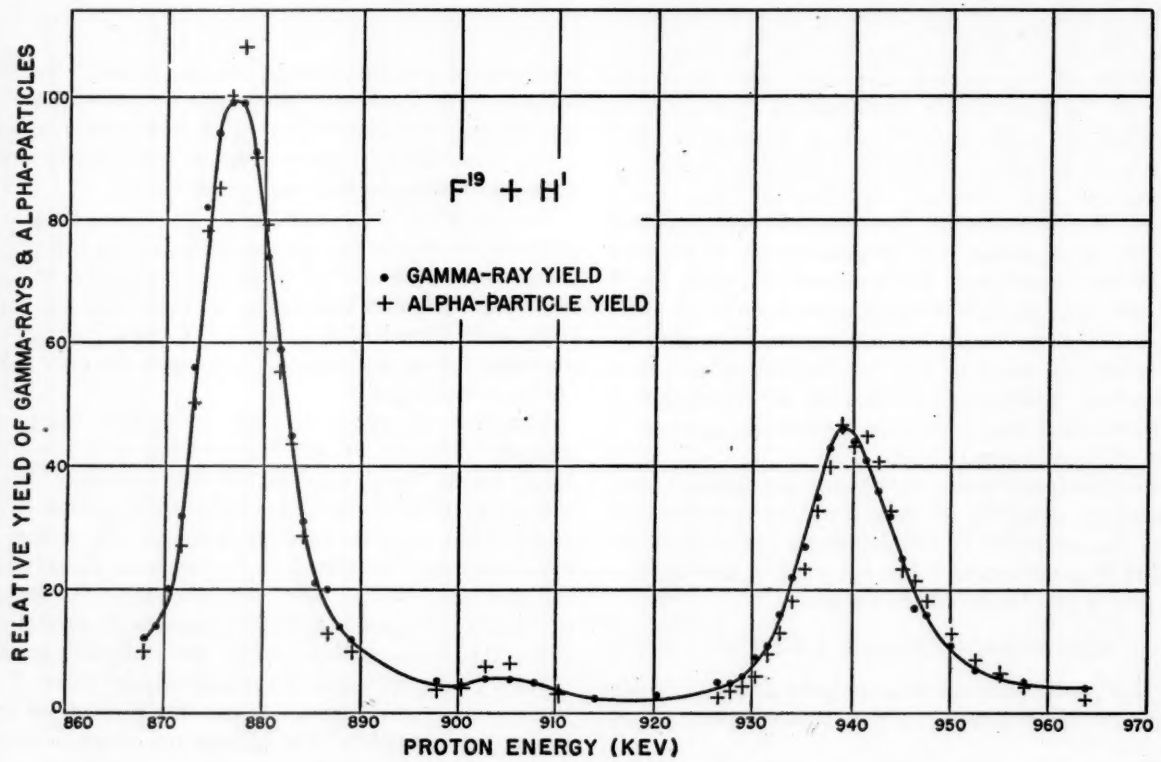

FIG. 5. Relative excitation curves for α_1-group and gamma-rays at the 874 and 935 kev resonances. ($\theta=138°$.)

[16] S. Devons and M. Hine, Proc. Roy. Soc. **199A**, 56 (1949).

TABLE V. Gamma-radiation from $F^{19}(p, \alpha\gamma)O^{16}$.

Resonance energy (kev)	Relative intensities of the three components 6.14 Mev	6.91 Mev	7.11 Mev	Thick CaF_2 target yield quanta/10^7 protons	Angular distribution A	Width Γ(kev)	Partial width $\omega\gamma$(ev)	Cross section $\sigma_R(10^{-27}$ cm^2)
222[a]				0.0002		<2[a]	0.03	>0.0002
340.4[b]	0.96	0.04		0.174*	0	1.7[a, b]	32	0.16
486	~0.8	~0.2		0.054*	0	<2[a]	11	>0.032
598				0.27*	0.2	37	55*	0.0071
669	0.75	<0.06	0.19**	0.48*	0	7.5	100	0.057
831				0.2		8.3	45	0.019
873.5[c]	0.65	0.24	0.11	3.7*	0.1	5.2	850*	0.54
900†	>0.95	<0.05		0.15		4.8	35	0.023
935.3†	0.76	0.025	0.21	2.0		8.0	470	0.18
1092				0.024		<1.2	6	>0.013
1137				0.1		4.1	25	0.015
1176				3.9		~130	1010	0.019
1290†	0.74	0.075	0.18	0.92		19.2	250	0.029
1355†	0.53	0.12	0.35	1.37		8.6†	360	0.089
1381†	0.87	0.08	0.05	8.2		15.0	2170	0.30

Resonance energies and widths: Bonner and Evans, Phys. Rev. **73**, 666 (1948). All resonance energies multiplied by 873.5/862. The energy at 873.5 kev was taken as a standard.
† Designates new determinations made in connection with investigations reported in this paper.
Yields: from measurements made in this laboratory.
* Designates total yields. Other yields are for 4π-steradians at 90°.
Angular distribution: Devons and Hine, Proc. Roy. Soc. **199A**, 56 (1949). $I(\theta)=1+A\cos^2\theta$.
Proportion of gamma-ray components: calculated from measurements on alpha-group intensities reported in this paper or from direct measurements of Walker and McDaniel, Phys. Rev. **74**, 315 (1948).
** Also 2 percent radiation near 13 Mev ($\omega\Gamma\gamma\sim 2$ ev, $\sigma_R\sim 10^{-27}$ cm^2), Devons and Hine, Nature **164**, 586 (1949).
[a] R. Tangen, Kgl. Norske. Vid. Sels. Skr., NR1 (1946).
[b] A. H. Morrish, Phys. Rev. **76**, 1651 (1949).
[c] Herb, Snowdon and Sala, Phys. Rev. **75**, 246 (1949).

it will be noted that the curves run almost parallel with each other over their full extent. In regard to absolute yields we have made a comparison with the pair yields at 13° with the incident beam reported by Rasmussen *et al.*[5] They report the yields, $y(\pi)$, for CaF_2 targets of one kev equivalent thickness, at 843 and 1236 kev. These values are given in the last two lines of the second column of Table III.[17] For a similar calculation for $Y(\alpha_\pi)$ we need to estimate the thickness of the target used in our pair measurement and this we have done by applying Eq. (1) to measurements with the same target on the gamma-ray breadth at 873.5 kev. Our measurements with very thin targets had confirmed the value $\Gamma=5.2$ kev given in reference 3 for the natural width of this resonance. Our results are given in the next to last column of Table III, and it will be noted that $y(\alpha_\pi)$ at 137.8° is approximately twice $y(\pi)$ at 13° both at 843 and 1236 kev. Since the pair emitting state presumably has angular momentum zero, it can be expected that the angular distribution for the pairs will be isotropic. Thus we have $y(\alpha_\pi, 141°)/\bar{y}(\alpha_\pi)\approx 2$. This would seem to indicate a marked asymmetry, something like a $\cos^2\theta$ distribution, for the angular distribution of the α_π-group.

In Table IV, columns two to four, we give also our intensity ratios of the α_1-, α_2-, and α_3-groups for certain resonances. Our ratios are compared on the one hand with the ratios given by Burcham and Freeman[7] (columns five and six) and on the other hand with the ratio $\gamma_1/(\gamma_2+\gamma_3)$ (column seven) given in references 5 as I_6/I_7.

Finally we give in Tables V, VI, and VII a tabulation of what we believe to be the best data on the gamma-radiation, pair radiation, and full energy alpha-particle emission from the bombardment of F^{19} with protons up to 1.4 Mev in energy. The values given have been selected from references 1, 3, 4, 8, and 15 as well as from the present work and from the work of Tangen[18] and of Morrish.[19] In the calculation of pair and full energy alpha-particle yields we have returned to the point of

TABLE VI. Electron-positron pair radiation from $F^{19}(p, \alpha\pi)O^{16}$.

Resonance energy (kev)	Thick CaF_2 target yield, pairs per 10^7 protons	Total width Γ(kev)	Partial width $\omega\gamma$(ev)	Cross section $\sigma_R(10^{-34}$ cm^2)
843†	0.048	30	12	0.0012
1115	0.089	60	22	0.0010
1236†	0.31	75	82	0.0025
1380	0.39	25	100	0.0085
1400*	0.85	$D\sim 1$ Mev	1600	0.0038*

Resonance energies: Bennett *et al.*, Phys. Rev. **70**, 882 (1946). All resonance energies multiplied by 873.5/862.
† designates new determinations made in connection with investigations reported in this paper.
Resonance yields and widths: taken from curves of Bennett *et al.*, normalized to yield at 1236 kev measured by Rasmussen *et al.*, Phys. Rev. **77**, 617 (1950). The yields and widths have been estimated assuming the resonance yield to be only that portion of the yield above a smooth curve drawn through the minima in the experimental excitation curve. As interference effects are almost certainly important the true widths of the level may be considerably greater than those tabulated.
Angular distribution of pairs: probably isotropic.
* Non-resonant yield: see remarks above. The cross section is that at 1.4 Mev and the partial width is calculated from the sum of this cross section and the corresponding cross section for the full energy alpha-particles assuming, D, the average separation between broad contributing levels to be ~1 Mev.

[17] Earlier results given in reference 1 were $y(\pi)=1.6\pm 0.6\times 10^{-10}$ pair/proton at 843 kev and $y(\pi)=3.6\pm 0.6\times 10^{-10}$ pair/proton at 1236 kev. These agree within their error limit with the results given in Table III.

[18] R. Tangen, Kgl. Norske. Vid. Sels. NR 1 (1946).
[19] A. H. Morrish, Phys. Rev. **76**, 1651 (1949).

TABLE VII. Full energy alpha-particles from $F^{19}(p, \alpha)O^{16}$.

Resonance energy (kev)	Thick CaF_2 target yield, alphas per 10^7 protons	Total width Γ(kev)	Partial width $\omega\gamma$(ev)	Cross section $\sigma_R(10^{-24}$ cm$^2)$
730	0.008	~30	1.6	~0.0002
850	0.006	~30	1.4	~0.0002
~1100	0.06	~60	15	~0.0006
1380	0.14	~25	36	~0.0031
1400*	0.5	D~1 Mev	1600	0.0013

Energies, yields, and widths: Streib *et al.*, Phys. Rev. **59**, 253 (1941).
* See remarks under Table VI concerning resonant and non-resonant yields and widths.
Angular distribution: not included but see Rubin, Phys. Rev. **72**, 1176 (1947).

view adopted in reference 1 where the yield below the minima in the thin target excitation curve was considered to be non-resonant. This non-resonant yield is believed to arise from the capture of *s*-wave protons by F^{19} in states of Ne^{20} having zero angular momentum and even parity from which alpha-particle transitions to the pair producing and ground states of O^{16} are highly probable giving large total widths and no marked resonance structure in the yield. From this point of view the non-resonant yield should follow the barrier penetration factor for *s*-wave protons multiplied by $\lambda^2 \sim 1/E$, and this is true experimentally to a fair approximation. The partial width for proton emission can be calculated at any point from the expression for the Breit-Wigner cross section averaged over many resonances,

$$\sigma = 2\pi^2\lambda^2(\omega\Gamma_p\Gamma_\alpha/D\Gamma) = 2\pi^2\lambda^2(\omega\gamma/D),$$

where D is the average separation of contributing levels in the region of interest. We arbitrarily assume $D \sim 1$ Mev and obtain a value for $\omega\Gamma_p \approx \omega\gamma = 1.6$ kev at 1.4 Mev from the sum of the α_0- and α_r-cross sections which is in reasonable agreement with the $\omega\Gamma_p$ for nearby gamma-ray resonances. On this picture the low yield of the long range alpha-particles and pairs relative to the gamma-radiation is not entirely unreasonable. Studies of the scattering of protons by F^{19} which are to be undertaken in this laboratory may yield some clarification of this point.

In conclusion the studies reported in this paper indicate the essential correctness of the general picture of the reactions following the disintegration of F^{19} by protons as worked out by numerous observers over the past decade. The yield and energy measurements on the short range alpha-particle groups correlate excellently with corresponding measurements on the pairs and gamma-rays which follow the emission of these groups. Among the numerous problems yet remaining are those having to do with the angular distributions of the reaction products and with the angular correlations between them as well as with those concerning the elastic scattering just discussed above.

In conclusion we wish to thank Dr. R. F. Christy for many illuminating discussions of this paper. This work was assisted by the joint program of the ONR and AEC.

On the Magnetic Shielding in He and H_2*

EGIL HYLLERAAS AND S. SKAVLEM
Institute for Theoretical Physics, University of Oslo, Oslo, Norway
(Received January 25, 1950)

The magnetic shielding constant for the He atom (i.e., the value of $(-\Delta H/H)$ at the nucleus), has been calculated to a high degree of accuracy by comparison of values obtained from a number of known first and higher approximations to the wave function. Its value is 5.9938×10^{-5}.

Next, the shielding constant for the H_2 molecule with respect to either of the nuclei has been found in the first approximation to be 2.6614×10^{-5}. The corresponding value derived from the Lamb formula is 3.1648×10^{-5}. The difference is due to the combined effect of both the center of mass and the center of the electronic charge lying outside either of the two nuclei. The numerical value 0.5034×10^{-5} of the difference fits well with the value 0.53×10^{-5} reported by N. F. Ramsay as derived from measurements of the spin-rotational interaction constant of the H_2 molecule.

However, there is also a second-order perturbation effect due to the perturbation of the ground state of the molecule by the magnetic field. By a special method its upper limit has been estimated to be 0.2864×10^{-5} and with a sign such as to weaken the magnetic field. Hence, the upper limit of the total shielding constant of H_2 should be 2.9478×10^{-5}.

I. INTRODUCTION

HIGH precision measurements of nuclear magnetic moments of light nuclei such as H and He^3 by the Rabi resonance method[1,2] have proved it necessary to take into account the faint shielding of the magnetic field in the nuclear region by the Larmor precession of the outer electronic shells. We are indebted to Dr. H. L. Anderson, for calling our attention to the importance of the problem.

As is well known,[3] the calculation of the magnetic shielding constant for an atom (with closed electronic shells) is easy in principle. If one knows the atomic wave function to some degree of accuracy, the rest of the work is to sum up the mean reciprocal values of the electronic distances from nuclei.

In the case of the He atom our interest was first concentrated on the rapidity of convergence of values obtained from the series of approximate wave functions used in our energy calculations.[4] To begin with, we were puzzled by the apparent lack of true convergence and a considerable spread among the values obtained from various kinds of wave functions. This indefiniteness, however, soon turned out to be caused by inaccurate determinations of the "flexibility" parameter, k, frequently used in energy calculations, which ensures that at the energy minimum the kinetic energy of the electrons is exactly half of the numerical value of the potential energy (virial theorem). It is not necessary that the rest of the variation parameters or expansion coefficients be very accurately chosen if only at the end the parameter k is carefully adjusted to the other given parameters so as to satisfy the virial theorem.

Following this principle, it turned out that for the He atom the shielding constant depends but very little on the accuracy of the wave function. The order of magnitude of improvement from the first to the sixth approximation is about 0.04 percent. This explains why by less accurate calculations the spread of the approximate values was more pronounced than was the real convergence of the true values. The small variations from the poor to the accurate approximation eigenfunctions make the repeated accurate calculations to some extent less important. On the other hand, we learn from this particular case of the He atom that for more complicated atomic configurations, as for instance the H_2 molecule, where accurate wave functions are not so easily obtained, we can rely rather safely even on the poorest first approximation.

II. GENERAL THEORY OF MAGNETIC SHIELDING

For a one-electron atom the diminution of a homogeneous magnetic field,

$$\mathbf{H}=\operatorname{curl}\mathbf{A},\quad \mathbf{A}=\tfrac{1}{2}\mathbf{H}\times\mathbf{r}, \tag{1}$$

at the center of the atom can be obtained from the Biot-Savart law

$$\Delta\mathbf{H}=-(e/c)(\mathbf{r}\times\mathbf{v})/r^3, \tag{2}$$

expressing $\mathbf{v}$ by the aid of the equation

$$m\mathbf{v}=\mathbf{p}+(e/c)\mathbf{A} \tag{3}$$

and averaging over a stationary state of the atom, usually the ground state.

If the angular momentum $\mathbf{r}\times\mathbf{p}$ is zero, there remains from (2)

$$\begin{aligned}-\Delta\mathbf{H}&=(e^2/mc^2)(\mathbf{r}\times\mathbf{A})/r^3\\&=(e^2/2mc^2)[\mathbf{r}\times(\mathbf{H}\times\mathbf{r})]/r^3.\end{aligned} \tag{4}$$

On averaging over a spherically symmetric state the result is

$$(-\Delta H/H)=\tfrac{1}{3}\alpha^2\langle a_H/r\rangle_{\text{Av}} \tag{5}$$

where a_H is the Bohr radius and α the fine structure constant.

* The investigation concerning H_2 is mainly due to Hylleraas.
[1] H. L. Anderson, Phys. Rev. **76**, 1460 (1949).
[2] E. M. Purcell, Phys. Rev. **76**, 1262 (1949).
[3] W. Lamb, Phys. Rev. **60**, 817 (1941).
[4] E. Hylleraas, Zeits. f. Physik **54**, 347 (1929).

TABLE I. Various approximations for the magnetic shielding in He.

φ	$-E/4Rh$	$(-\Delta H/H)/\frac{1}{3}\alpha^2$
$e^{-s/2}$	1.423828	3.375 $=4k$
$e^{-s/2}(1+c_2t^2)$ $c_2=0.01235$	1.438338	3.37112$=4k$
$e^{-s/2}\cosh c_2t/2)$ $c_2=0.295$	1.437831	3.37172$=4k$
$e^{-s/2}(1+c_1u)$ $c_1=0.0988,\quad k=0.92480$	1.445560	3.377830
$\exp(-s/2+c_1u/2)$ $c_1=0.137,\quad k=0.92898$	1.444809	3.37836

TABLE II. Improved approximations for the magnetic shielding in He.

φ	$-E/4Rh$	$(-\Delta H/H)/\frac{1}{3}\alpha^2$
$e^{-s/2}(1+c_1u+c_2t^2)$ $c_1=0.0803,\quad c_2=0.0099$ $k=0.908031$	1.451216	3.37606
$\exp(-s/2+c_1u/2)\cosh[c_2(1-c_1)t/2]$ $c_1=0.11375,\quad c_2=0.237$ $k=0.911817$	1.449767	3.37657

For many-electron atoms one should rather use the Hamiltonian

$$\mathcal{H}=V+\sum_i\left\{\frac{1}{2m}\mathbf{p}_i^2+\frac{e}{mc}(\mathbf{A}_i+\mathbf{a}_i)\cdot\mathbf{p}_i+\frac{e^2}{mc^2}\mathbf{A}_i\cdot\mathbf{a}_i\right\},$$
$$\mathbf{a}_i=(\boldsymbol{\mu}\times\mathbf{r}_i)/r_i^3, \tag{6}$$

where $\mathbf{a}_i$ is the vector potential of the nuclear magnetic moment. Writing

$$\mathbf{A}_i\cdot\mathbf{p}_i=\tfrac{1}{2}\mathbf{H}\cdot(\mathbf{r}_i\times\mathbf{p}_i), \tag{7}$$

and considering states with zero total angular momentum, the sum of terms in (7) is zero as well as the sum of the mean values of $(\mathbf{a}_i\cdot\mathbf{p}_i)$. Hence, from the last sum in the Hamiltonian (6), we obtain for spherically symmetric states in conformity with (5)

$$(-\Delta H/H)=\tfrac{1}{3}\alpha^2\sum_i\langle a_H/r_i\rangle_{\mathrm{Av}}. \tag{8}$$

A second-order perturbation energy arising from the term $\sum_i\mathbf{a}_i\cdot\mathbf{p}_i$ in (6) is quadratic in $\boldsymbol{\mu}$, and hence is insignificant in our problem.

III. APPLICATION TO THE He ATOM

Putting $\psi=\varphi(k\mathbf{r}_1, k\mathbf{r}_2)$, $s=r_1+r_2$, $t=r_2-r_1$, $u=r_{12}$, and taking $a_H/4$ for the unit of length, the result for various approximations of the He atom is given in Table I.

So far there is no indication of convergence, the dependence of the coordinate t tending to lower and that of u to raise the value of the magnetic shielding. Considering, however, both kinds of variations simultaneously, in the third-order approximation, we already get the rather definite results of Table II.

Finally, in the sixth approximation,

$$\varphi=e^{-s/2}(1+c_1u+c_2t^2+c_3s+c_4s^2+c_5u^2), \tag{9}$$

using the values of c_1 to c_5 found earlier by energy calculations,[4] and together with the corresponding best value of k, we get the figure 3.37628. As a final value we therefore choose

$$(-\Delta H/H)_{\mathrm{He}}=\tfrac{1}{3}\alpha^2(3.3764\pm0.0002). \tag{10}$$

IV. MAGNETIC SHIELDING IN THE HYDROGEN MOLECULE

For a molecular problem a more elaborate theory is needed. There is, for instance, the difference that the total angular momentum of the whole molecule including the nuclei is no longer a constant of the motion as soon as a magnetic field is applied, even though it may be quantized and can, for instance, be taken equal to zero in the absence of the field.

Denoting the electrons of H_2 by 1, 2, and the nuclei by a, b, and considering, for instance, the function

$$\psi=\psi(r_{1a}, r_{1b}, r_{2a}, r_{2b}, r_{12}, r_{ab}), \tag{11}$$

which is independent of the coordinates of the center of mass, and hence corresponds to zero total linear momentum, it is easily seen that it also represents states with zero total angular momentum.

If now we let the nuclear distance r_{ab} be "frozen" (i.e., disregard the nuclear oscillations), there still remains the freedom of rotation of the nuclear axis. Since the wave function (11) is independent of the angles of the axis with respect to a fixed coordinate system, we shall have to average over all possible orientations of the molecular axis. This being accepted, we can also disregard all effects of nuclear motion to the degree of accuracy m/M, and can transform the problem into an ordinary two-electron problem depending on an additional parameter $r_{ab}=2R$.

In contrast to many-electron atomic problems this procedure of disregarding the nuclear motion does not lead to a problem in which the total angular momentum of the electrons is a constant of the motion. To see the difference we need only compare the electronic wave function $\psi(r_1, r_2, r_{12})$ of the He ground state with the function (11) in which by given r_{ab} the center of mass is now considered to be at the middle point of the internuclear axis.

For this reason, as has been pointed out to us by Dr. Fermi and Dr. Anderson of the University of Chicago, there will be a second-order effect in the magnetic shielding due to the perturbation of the ground state of the molecule by the magnetic field. In this section, however, we shall disregard this second-order effect, since there is a much more important first-order effect to be evaluated. This effect, or perhaps rather the sum of the first and second-order effects, is closely connected with the measured spin-rotational

constant[5] as demonstrated by Ramsey.[6] To calculate the effect, we adopt the formal method suggested to us by Fermi and Anderson in which as in Eq. (6) the magnetic energy of the nuclei is included in the Hamiltonian of the system, since by a less rigorous method the term itself or at least its definiteness may easily be overlooked.

Denoting the magnetic moments of the nuclei by $\mathfrak{y}_a$ and $\mathfrak{y}_b$, writing for the corresponding vector potentials

$$\mathbf{a}_{1a}=(\mathfrak{y}_a\times\mathbf{r}_{1a})/r_{1a}^3,\quad \mathbf{a}_{1b}=(\mathfrak{y}_b\times\mathbf{r}_{1b})/r_{1b}^3,\text{ etc.},\quad (12)$$

the Lagrangian for the whole H_2 molecule including the nuclei has been found to be

$$L=T-V-\frac{e}{c}\{(\mathbf{v}_1+\mathbf{v}_a)\cdot\mathbf{A}_{1a}+(\mathbf{v}_2+\mathbf{v}_b)\cdot\mathbf{A}_{2b}+\mathbf{v}_{1a}\cdot\mathbf{a}_{1a}+\mathbf{v}_{1b}\cdot\mathbf{a}_{1b}+\mathbf{v}_{2a}\cdot\mathbf{a}_{2a}+\mathbf{v}_{2b}\cdot\mathbf{a}_{2b}\}\quad (13)$$

from which we obtain the Hamiltonian

$$\begin{aligned}\mathfrak{H}=&\frac{1}{2m}(\mathbf{p}_1^2+\mathbf{p}_2^2)+\frac{1}{2M}(\mathbf{p}_a^2+\mathbf{p}_b^2)+V\\&+\frac{e}{mc}\{(\mathbf{A}_{1a}+\mathbf{a}_{1a}+\mathbf{a}_{1b})\cdot\mathbf{p}_1+(\mathbf{A}_{2b}+\mathbf{a}_{2a}+\mathbf{a}_{2b})\cdot\mathbf{p}_2\}\\&+\frac{e}{Mc}\{(\mathbf{A}_{1a}-\mathbf{a}_{1a}-\mathbf{a}_{2a})\cdot\mathbf{p}_a+(\mathbf{A}_{2b}-\mathbf{a}_{1b}-\mathbf{a}_{2b})\cdot\mathbf{p}_b\}\\&+\frac{e^2}{mc^2}\{\mathbf{A}_{1a}\cdot(\mathbf{a}_{1a}+\mathbf{a}_{1b})+\mathbf{A}_{2b}\cdot(\mathbf{a}_{2a}+\mathbf{a}_{2b})\}\\&-\frac{e^2}{Mc^2}\{\mathbf{A}_{1a}\cdot(\mathbf{a}_{1a}+\mathbf{a}_{2a})+\mathbf{A}_{2b}\cdot(\mathbf{a}_{1b}+\mathbf{a}_{2b})\}\end{aligned}\quad (14)$$

in which quadratic terms in the vector potentials are omitted.[7]

Due to the appearance of purely relative vector potentials, the total linear momentum commutes with $\mathfrak{H}$ and is a constant of the motion. The total angular momentum, however, ceases to be a constant of the motion when the magnetic field is different from zero, and the wave function (11) is perturbed into a more general function of relative coordinates.

Disregarding nuclear motion (except for the free orientation of nuclear axis), i.e., disregarding terms of the order of magnitude m/M, the Hamiltonian (14) simplifies to

$$\begin{aligned}\mathfrak{H}=&\mathfrak{H}_0+\frac{e}{mc}\{(\mathbf{A}_{1a}+\mathbf{a}_{1a}+\mathbf{a}_{1b})\cdot\mathbf{p}_1+(\mathbf{A}_{2b}+\mathbf{a}_{1b}+\mathbf{a}_{2b})\cdot\mathbf{p}_2\}\\&+\frac{e^2}{mc^2}\{\mathbf{A}_{1a}\cdot(\mathbf{a}_{1a}+\mathbf{a}_{1b})+\mathbf{A}_{2b}\cdot(\mathbf{a}_{2a}+\mathbf{a}_{2b})\}\\=&\mathfrak{H}_0+\mathfrak{H}_1+\mathfrak{H}_2,\end{aligned}\quad (15)$$

where $\mathfrak{H}_0$ is the Hamiltonian for zero magnetic field.

The mean value for the ground state of the molecule of the first perturbing term $\mathfrak{H}_1$ which contains $\mathbf{p}_1$ and $\mathbf{p}_2$ in the first power is zero. From the last term, considering that $\mathbf{r}_{1b}=\mathbf{r}_{1a}-2\mathbf{R}$ and $\mathbf{r}_{2a}=\mathbf{r}_{2b}+2\mathbf{R}$, $\mathbf{A}_{1a}=\frac{1}{2}\mathbf{H}\times\mathbf{r}_{1a}$, $\mathbf{A}_{2b}=\frac{1}{2}\mathbf{H}\times\mathbf{r}_{2b}$, where $2\mathbf{R}=\mathbf{r}_{ba}$, we obtain the first-order perturbation energy with respect to the magnetic moment $\mathfrak{y}_a$ of the nucleus a

$$\Delta E=\frac{e^2}{3mc^2}(\mathbf{H}\cdot\mathfrak{y}_a)\left\langle\frac{1}{r_{1a}}+\frac{\mathbf{r}_{2a}^2-2\mathbf{R}\cdot\mathbf{r}_{2a}}{r_{2a}^3}\right\rangle_{Av}\quad (16)$$

corresponding to a mean diminution of the magnetic field at $\mathbf{r}_a$ of amount

$$(-\Delta H/H)_{H_2}=\tfrac{1}{3}\alpha^2 a_H\cdot 2\left\langle\frac{1}{r_a}-\frac{Rz_a}{r_a^3}\right\rangle_{Av},\quad (17)$$

r_a denoting either of the electronic distances from the nucleus a, since the wave function is symmetric in the two electrons.

V. NUMERICAL VALUES OF THE MAGNETIC SHIELDING IN HYDROGEN

Let the unit of length be $a_H/2k$ and consider a wave function

$$\psi_0=(\tfrac{1}{2})^{\frac{1}{2}}\{\psi+\bar{\psi}\},\quad (18)$$

ψ being a normalized function and $\bar{\psi}$ being obtained from ψ by an interchange of the electronic coordinates. Then the normalization integral will be $N=1+\bar{N}$ where $\bar{N}$ is the product integral. If we take the normalization factor for ψ into the volume element $d\tau$ we may write in the first approximation

$$\psi=\exp[-\tfrac{1}{2}(r_{1a}+r_{2b})],\quad \bar{\psi}=\exp[-\tfrac{1}{2}(r_{1b}+r_{2a})].\quad (19)$$

Squaring (18) and considering (17) we are lead to the integral

$$I=\int\{\exp(-r_a)+2\bar{N}e^{-R\xi}+\exp(-r_b)\}\left(\frac{1}{r_a}-\frac{Rz_a}{r_a^3}\right)d\tau,$$

$$d\tau=\tfrac{1}{4}r_a^2\sin\vartheta_a dr_a d\vartheta_a=\tfrac{1}{4}R^3(\xi^2-\eta^2)d\xi d\eta,$$

$$\bar{N}=e^{-R}S(R),\quad S(R)=1+R+\tfrac{1}{3}R^2,\quad (20)$$

where ξ, η are elliptic coordinates. Equation (17) is then

[5] Kellog, Rabi, Ramsey, and Zacharias, Phys. Rev. **57**, 691 (1940).

[6] N. F. Ramsay, Phys. Rev. **78**, 699 (1950).

[7] Since the Lorentz term of the applied field in L might as well have been written $(\mathbf{v}_1+\mathbf{v}_b)\cdot\mathbf{A}_{1b}+(\mathbf{v}_2+\mathbf{v}_a)\cdot\mathbf{A}_{2a}$, there is an indefiniteness in the Lagrangian corresponding to the function $\mathbf{v}_{12}\cdot\mathbf{A}_{ba}-\mathbf{v}_{ba}\cdot\mathbf{A}_{1a}$ times an aribtrary constant. As the calculation has been made such a term contributes neither to the first nor to the second-order perturbation energy. There are also two other linearly independent expressions which could be added to the Lagrangian without altering the equations of motion. The corresponding additional terms in the Hamiltonian do not, however, contribute to the resulting energy, as can easily be seen from the symmetry of the terms.

replaced by

$$-\Delta H/H=\tfrac{1}{3}\alpha^2\cdot 2kI/N. \tag{21}$$

It is found that

$$I=\left(\frac{1}{2}+\frac{1}{2R}\right)(1-e^{-2R})+e^{-2R}(1+R)S(R)$$
$$-\frac{1}{4R}[1-e^{-2R}(1+R+\tfrac{1}{2}R^2)^2]$$
$$-6\left\{\frac{1}{2R}[e^{-2R}S^2(R)(C+\ln 2R)\right.$$
$$\left.-S(R)S(-R)Ei(-2R)]-e^{-2R}S(R)(1+\tfrac{1}{2}R)\right\}. \tag{22}$$

On the other hand, the energy minimum is obtained from

$$E=-(L-L'-N/R)^2/NM, \tag{23}$$

where

$$M=2+2e^{-2R}S(R)(1+R-\tfrac{1}{3}R^2), \tag{23a}$$

$$L=\left(2+\frac{2}{R}\right)(1-e^{-2R})+4e^{-2R}S(R)(1+R), \tag{23b}$$

$$L'=\frac{1}{R}[1-e^{-2R}(1+R)]-e^{-2R}(\tfrac{3}{8}+\tfrac{3}{4}R+\tfrac{1}{6}R^2)$$
$$+\frac{1}{5}\left\{\frac{6}{R}[e^{-2R}S^2(R)(C+\ln R)\right.$$
$$-2S(R)S(-R)Ei(-2R)$$
$$+e^{2R}S^2(-R)Ei(-4R)]$$
$$\left.-\left[-\frac{25}{8}+\frac{23}{4}R+3R^2+\frac{1}{3}R^3\right]e^{-2R}\right\}. \tag{23c}$$

The energy minimum is found to be

$$E=-2.278387 \quad \text{for} \quad R=1.65, \quad k=1.166176. \tag{24}$$

corresponding to the dissociation energy

$$E_D=3.769 \text{ ev} \quad \text{and} \quad R_0=R/k=1.415 \tag{25}$$

as the internuclear distance in units of a_H.

The last two terms with negative signs in Eq. (22) represent the deviation from the Lamb formula. For the values of R and k in (24) we get

$$2kI/N=1.78279-0.28359=1.49920. \tag{26}$$

Putting $\frac{1}{3}\alpha^2=1.7752\times10^{-5}$, Eqs. (8) and (26) lead to the shielding constants

$$(-\Delta H/H)_{\text{He}}=3.3764\ (\tfrac{1}{3}\alpha^2)=5.9938\times10^{-5},$$
$$(-\Delta H/H)_{\text{H}_2}=1.49920(\tfrac{1}{3}\alpha^2)=2.6614\times10^{-5}. \tag{27}$$

For these values the ratio of nuclear gyromagnetic constants $\gamma_{\text{He}^3}/\gamma_p=0.7617866$ as obtained by Anderson by direct measurement must be corrected to

$$\gamma_{\text{He}^3}/\gamma_p=0.7617866$$
$$\times[1+(5.9931-2.6614)\times10^{-5}]=0.7618120 \tag{28}$$

instead of 0.7618081 by the Lamb formula.

The first-order correction $0.28359(\frac{1}{3}\alpha^2)=0.5034\times10^{-5}$ to the Lamb formula is very near to the correction 0.53×10^{-5} found by Ramsey[6] on the basis of measurements[5] of the spin-rotational interaction constant. Hence, if the latter value is to be identified with the sum of first- and second-order effects, the second-order effect should be small.

VI. SECOND-ORDER CORRECTION TO THE MAGNETIC SHIELDING IN HYDROGEN

Denoting by $\mathcal{H}_1$ the second term of Eq. (15), the second-order perturbation energy can be written as

$$\Delta E=-\sum_n (\mathcal{H}_1)_{0n}^2/(E_n-E_0), \tag{29}$$

where E_n is the energy of the nth excited state and $(\mathcal{H}_1)_{0n}$ a matrix element of the operator $\mathcal{H}_n$, the ground state being denoted by 0. As is well known,

$$\sum_n (\mathcal{H}_1)_{0n}^2=\int \psi_0\mathcal{H}_1^2\psi_0 d\tau \tag{30}$$

for a normalized ground-state wave function. Hence, replacing all E_n in (29) by a single one, say, E_1 the series can be summed and yields an approximate value or, eventually, a lower limit to the negative perturbation energy. If we take $E_1-E_0=Rh$ as a reasonable value for the energy difference between the ground state and the bulk of higher energy states, we get the approximate perturbation energy

$$\Delta E=-\frac{1}{Rh}\int \psi_0\mathcal{H}_1^2\psi_0 d\tau. \tag{31}$$

This procedure of estimating a second-order perturbation energy or its lower limit is much better than the original method devised by Weinstein.[8] However, his method has been improved by Stevenson and Crawford[9,10] and lately by Kohn[11] so as to correspond to (29) with $E_n\to E_1$ for the lower limit. A similar simplification has been made use of by van Vleck[12] in the theory of atomic and molecular diamagnetism.

---

[8] D. H. Weinstein, Proc. Nat. Acad. Sci. **20**, 529 (1934).
[9] A. F. Stevenson, Phys. Rev. **53**, 199 (1938).
[10] A. F. Stevenson and M. F. Crawford, Phys. Rev. **54**, 374 (1938).
[11] W. Kohn, Phys. Rev. **71**, 902 (1947).
[12] J. H. van Vleck, and A. Frank, Proc. Nat. Acad. Sci. **15**, 539 (1929); J. H. van Vleck, *Electric and Magnetic Susceptibilities* (Oxford University Press, London, 1932).

Squaring the second term $\mathcal{H}_1$ of Eq. (15) we need consider only product terms in $\mathbf{H}$ and $\boldsymbol{\mu}_a$ and $\boldsymbol{\mu}_b$. Also product terms in $\mathbf{p}_1$ and $\mathbf{p}_2$ disappear on integration according to (30). Putting $Rh=e^2/2a_H$ and replacing $\mathbf{p}$ by $(h/2\pi i)\nabla$ and considering $a_H/2k$ as unit of length, the second-order energy affecting our problem is approximately

$$\Delta E=32\alpha^2k^3\int\psi_0\Big\{[\tfrac{1}{2}\mathbf{H}\cdot(\mathbf{r}_{1a}\times\nabla_1)]\times\Big[\boldsymbol{\mu}_a\cdot\Big(\frac{\mathbf{r}_{1a}}{r_{1a}^3}\times\nabla_1\Big)+\boldsymbol{\mu}_b\cdot\Big(\frac{\mathbf{r}_{1b}}{r_{1b}^3}\times\nabla_1\Big)\Big]+[\tfrac{1}{2}\mathbf{H}\cdot(\mathbf{r}_{2b}\times\nabla_2)]\Big[\boldsymbol{\mu}_a\cdot\Big(\frac{\mathbf{r}_{2a}}{r_{2a}^3}\times\nabla_2\Big)+\boldsymbol{\mu}_b\cdot\Big(\frac{\mathbf{r}_{2b}}{r_{2b}^3}\times\nabla_2\Big)\Big]\Big\}\psi_0 d\tau. \quad (32)$$

To obtain a reasonably good value of this expression we use the former approximate wave function (18) and (19). To avoid an incorrect sign of the effect we must keep in mind that for first-order differential operators A and B we have

$$\int\psi_0AB\psi_0d\tau=-\int(A\psi_0)(B\psi_0)d\tau.$$

In this way we get, taking account only of the nucleus a

$$\Delta E=-(2\alpha^2k^3/N)\int\Big\{[\mathbf{H}\cdot(\mathbf{r}_{1a}\times\mathbf{r}_{1b})]\times[\boldsymbol{\mu}_a\cdot(\mathbf{r}_{1a}\times\mathbf{r}_{1b})]\frac{\bar\psi^2}{r_{1a}^3r_{1b}^2}-[\mathbf{H}\cdot(\mathbf{r}_{2a}\times\mathbf{r}_{2b})][\boldsymbol{\mu}_a\cdot(\mathbf{r}_{2b}\times\mathbf{r}_{2a})]\frac{\psi\bar\psi}{r_{2a}^4r_{2b}}\Big\}d\tau. \quad (33)$$

In the second term we can replace 2 by 1 and carry out the integration over the coordinates of one of the electrons. Further, by rotation of the nuclear axis the vector factor transforms into $\frac{1}{3}(\mathbf{H}\boldsymbol{\mu}_a$ times the square of the vector product which is equal to $4R^2(x^2+y^2)$, x and y being electron coordinates perpendicular to the molecular axis. The net result is an energy corresponding to a diminution of the magnetic field of

$$(-\Delta H/H)_2=\tfrac{1}{3}\alpha^2\frac{8k^3}{N}\int\frac{(x^2+y^2)R^2}{r_a^3r_b}\times\Big\{\bar N\frac{\exp[-\frac{1}{2}(r_a+r_b)]}{r_a}-\frac{\exp(-r_b)}{r_b}\Big\}d\tau, \quad (34)$$

the volume element being of the same form as in (20).

The integrals are elementary except for the exponential integral. We obtain

$$(-\Delta H/H)_2=\tfrac{1}{3}\alpha^2\frac{8k^3}{N}\Big[e^{-R}(1+R+\tfrac{1}{3}R^2)\Big\{(1+\tfrac{1}{2}R)e^{-R}-\frac{1}{2R}[(1+R)e^{-R}(C+\ln 2R)-Ei(-2R)]\Big\}-\frac{1}{3}\Big\{\frac{1}{4R}[1-e^{-2R}(1+2R+2R^2)]-R^2Ei(-2R)\Big\}\Big]. \quad (35)$$

For the values of R and k in (25) the difference of the two integrals in (35) corresponding to $\psi\bar\psi$ and $\bar\psi^2$ is $0.0591139-0.0404615=0.0186524$. Multiplied with $8k^3/N$ this yields

$$(-\Delta H/H)_2=1.61343(\tfrac{1}{3}\alpha^2)=0.2864\times10^{-5}. \quad (36)$$

Hence the result of the whole calculation is

Lamb formula	3.1648×10^{-5}
First-order correction	-0.5034×10^{-5}
	2.6614×10^{-5}
Second-order correction	0.2864×10^{-5}
Total $(-\Delta H/H)_{H_2}=$	2.9478×10^{-5}.

The above figures with four decimals presented as they result from well-defined calculations must not be taken too seriously. We do not expect the two first figures to change very much by introduction of a more accurate wave function. Nevertheless, even though the difference $(3.24-3.16)\times10^{-5}$ is appreciable, it is practically not so important that on this stage we should try to decide whether the Anderson-Nordsieck value 3.24×10^{-5} from the Lamb formula is too high or not.

Much less confidence, however, must be put in the figure for the second-order correction, which is merely a rough estimation and essentially an upper limit. It may be smaller and our decision to perform the rather intricate calculation was partly based on the hope that it would turn out to be comparatively negligible. It is, however, on this stage of the calculations difficult to understand how it could be small enough as to agree with the Ramsay value 2.71×10^{-5} of the shielding constant.

The application of a more accurate ground-state wave function of H_2 will probably not alter the above figures very much. Since a more handy accurate wave function

than that used by James and Coolidge[13] in their fundamental investigation of the H_2 molecule often is needed, the authors intend to repeat the energy calculations (eventually the magnetic shielding) for the H_2 molecule by the aid of the wave function

$$\psi_0=\psi\{1+c_1r_{12}+c_2(r_{1a}-r_{2b})^2\} +\bar{\psi}\{1+c_1r_{12}+c_2(r_{1b}-r_{2a})^2\} \quad (37)$$

which should be at least as good as the corresponding third-order wave function of the He atom.

[13] H. M. James and A. S. Coolidge, J. Chem. Phys. **12**, 825 (1933).

PHYSICAL REVIEW VOLUME 79, NUMBER 1 JULY 1, 1950

On the Energy-Momentum Tensor of the Electron

F. VILLARS
Institute for Advanced Study, Princeton, New Jersey
(Received March 8, 1950)

The first-order radiative correction to the energy-momentum tensor of the electron is investigated. In order to avoid the ambiguities connected with the occurrence of divergent integrals a regulization with auxiliary masses is introduced. It is shown that a procedure which is in accordance with the conservation laws necessarily has some of the features of an auxiliary field theory. The method of the present calculation corresponds to an introduction of an auxiliary neutral vector-meson field which is coupled to the electron-positron field with an imaginary coupling constant.

I. INTRODUCTION

ON investigating the effects of the vacuum field fluctuations on the field source, difficulties arise due to ambiguities in the interpretation of divergent integrals. The possibility of obtaining a non-vanishing photon self-energy, in contradiction to the gauge invariance of the underlying theory, illustrates this situation.[1] Since these ambiguities occur within the framework of a covariant formalism, there is some hope that on insisting on the formal properties of the theory: covariance, gauge invariance, and the validity of conservation laws, we might find a way to get rid of these difficulties.

On the other hand, one can argue that since these ambiguities are connected with the occurrence of divergent expressions, an invariant limiting process that makes these expressions finite should resolve these ambiguities. The first point of view, supported especially by Schwinger,[2,3] furnishes a set of rules of interpretation; thus, for instance, gauge invariance implies the invariance of a certain integral in momentum space under translations of the integration variable. (For further detail we refer to a forthcoming paper by S. Borowitz and W. Kohn.)

An investigation along the lines of the second point of view[4] exhibits the remarkable fact that the postulates of gauge invariance and conservation laws strongly reduce the possible number of different regularization procedures. A common feature of all of the admissible regularization methods seems to be their "realistic" aspect; this means, more precisely, that apart from the condition of a hermitian interaction, which in general is violated,[5,6] these methods can be interpreted as auxiliary field theories in the sense of Pais' f-field.[7]

In the present paper the second point of view is applied to the problem of the radiative corrections to the energy-momentum tensor of the electron. A straightforward calculation may lead to results in contradiction to the conservation laws, which require that

$$\partial T_{\mu\nu}(x)/\partial x_\nu=0.$$

An equivalent expression of this fact is the result of Pais and Epstein.[8] The difficulty of this special problem was first resolved by Rohrlich.[9] His results are contained in the present calculation as a special case.

Section II will be concerned with the establishment of the expression for the first-order radiative correction to the one-particle part of $\bar{T}_{\mu\nu}$. In Section III the regularization will be discussed, and finally in Section IV the actual form of $\bar{T}_{\mu\nu}(p'p)$ will be determined.

II. CALCULATION OF THE FIRST-ORDER RADIATIVE CORRECTION

The symmetrized gauge-invariant energy-momentum tensor of the interacting photon and electron-positron fields can be written as

$$T_{\mu\nu}(x)=\tfrac{1}{2}(F_{\mu\lambda}F_{\nu\lambda}+F_{\nu\lambda}F_{\mu\lambda}-\tfrac{1}{2}\delta_{\mu\nu}F_{\lambda\sigma}{}^2) +\tfrac{1}{4}(\bar{\psi}\gamma^{(\mu}\partial_{\nu)}\psi-(\partial_{(\nu}{}^*\bar{\psi})\gamma^{\mu)}\psi). \quad (1)$$

[1] G. Wentzel, Phys. Rev. **74**, 1070 (1948).
[2] J. Schwinger, Phys. Rev. **76**, 790 (1949), Appendix.
[3] Borowitz, Kohn, and Schwinger, Phys. Rev. **78**, 345 (1950).
[4] W. Pauli and F. Villars, Rev. Mod. Phys. **21**, 434 (1949).
[5] D. Feldman, Phys. Rev. **76**, 1369 (1949).
[6] W. Jost and J. Rayski, Helv. Phys. Acta **22**, 457 (1949).
[7] A. Pais, Verh. Ned. Akad. Amsterdam **XIX**, No. 1 (1947).
[8] A. Pais and S. Epstein, Rev. Mod. Phys. **21**, 445 (1949).
[9] F. Rohrlich, Phys. Rev. **77**, 357 (1950).

$A_{(\mu}B_{\nu)}=A_\mu B_\nu+A_\nu B_\mu$ and $\partial=\partial/\partial x-ieA(x)$; $\partial^*=\partial/\partial x+ieA(x)$. For the purpose of the present investigation it is convenient to express (1) in terms of operators which describe the physical electron, that is, satisfy a free particle equation, in which the original mass m_0 is replaced by the total mass m. In terms of these operators, the interaction between the two fields is

$$\mathfrak{H}'=-\int d^3x(j_\mu(x)A_\mu(x)+h_s(x))$$
$$=\int d^3x(h_I(x)-h_s(x)). \quad (2)$$

Expression (1) does not refer to a definite representation as long as $i(\partial/\partial x_4)$ has the signification of the total time derivative

$$\partial\Omega/\partial x_4=\partial'\Omega/\partial x_4+[\mathfrak{H}',\Omega].$$

In introducing the above mentioned representation into (1), $T_{\mu\nu}$ acquires the form

$$T_{\mu\nu}=T_{\mu\nu}^P+T_{\mu\nu}^E+\delta_{(\nu 4}\theta_{\mu)}, \quad (3a)$$

$$T_{\mu\nu}^P=\tfrac{1}{2}(F_{\mu\lambda}F_{\nu\lambda}+F_{\nu\lambda}F_{\mu\lambda}-\tfrac{1}{2}\delta_{\mu\nu}F_{\lambda\sigma}^2),$$

$$T_{\mu\nu}^E=\tfrac{1}{4}\left(\bar\psi\gamma^{(\mu}\frac{\partial'\psi}{\partial x_{\nu)}}-\frac{\partial'\bar\psi}{\partial x_{(\nu}}\gamma^{\mu)}\psi\right)-\tfrac{1}{2}ic(\bar\psi\gamma^{(\mu}\psi\cdot A_{\nu)}), \quad (3b)$$

$$\theta_\mu=\tfrac{1}{4}ic\bar\psi(x)(\gamma^\mu\gamma^4\gamma^\lambda+\gamma^\lambda\gamma^4\gamma^\mu)\psi(x)\cdot A_\lambda(x)$$
$$-\tfrac{1}{32}ie^2\int d^4x'(\bar\psi(x)\gamma^\mu\gamma^4M_F(x-x')\psi(x')+(\leftarrow))$$
$$-\tfrac{1}{32}e^2\int\int d^4x'd^4x''\delta(t-t')$$
$$\times(\bar\psi(x')\gamma^\mu S(x'-x'')M_F(x''-x)\psi(x)+(\leftarrow)). \quad (3c)$$

$(\leftarrow)$ indicates the reversed expression:

$$\bar\psi(x)M_F(x-x'')S(x''-x')\gamma^\mu\psi(x)$$

The e^2—self-energy density $h_s^{(2)}(x)$ in the above expression has been written as

$$-\tfrac{1}{8}ie^2\int d^4x'(\bar\psi(x)M_F(x-x')\psi(x')$$
$$+\bar\psi(x')M_F(x'-x)\psi(x)), \quad (4)$$

$$M_F=\gamma^\lambda S_F\gamma^\lambda\cdot D_F,$$

that is, in the form which follows directly from its definition (see below).

The variation in time of the state vector Ψ in the representation chosen above obeys the Schroedinger equation

$$i(\partial\Psi/\partial t)=\mathfrak{H}'\Psi.$$

Write $\Psi(t)=S(t)\Psi_0$. Then

$$S(t)=P\left[\exp\left(-i\int^t dt'\mathfrak{H}(t')\right)\right],$$

where P is the operator of ordering in time introduced by Dyson.[10]

The self-energy operator is defined by the requirement that a one-particle state must be an eigenstate of the system, which implies that

$$\langle S(\infty)\rangle_1=1. \quad (5)$$

This furnishes a recursive definition of the self-energy corrections of different orders. In first order in $\alpha=e^2/4\pi$ Eq. (5) yields

$$\tfrac{1}{2}(-i)^2\int\int dx_1dx_2\langle P(h_I(x_1),h_I(x_2))\rangle_1$$
$$-(-i)\int d^4xh_s^{(2)}(x)=0$$

from which (4) can be extracted as the operator representing the self-energy density.

If we adopt the definition $S_F=S^{(1)}-2i\bar S$, $D_F=D^{(1)}-2i\bar D$, it follows that

$$\epsilon(t-t')\langle P(\psi(x),\bar\psi(x'))\rangle_0=-\frac{1}{2}S_F(x-x'), \quad (6a)$$

but

$$\epsilon(t-t')\left\langle P\left(\frac{\partial\psi(x)}{\partial x_\nu}\bar\psi(x')\right)\right\rangle_0$$
$$=-\frac{1}{2}\frac{\partial S_F(x-x')}{\partial x_\nu}+i\delta_{\nu 4}\gamma^4\delta(x-x'). \quad (6b)$$

The energy-momentum tensor representing the physical electron: $\bar T_{\mu\nu}(x)$, may be written as

$$\bar T_{\mu\nu}(x)=\left\langle P\left[T_{\mu\nu}(x),\exp\left(-i\int_{-\infty}^{+\infty}\mathfrak{H}(t')dt'\right)\right]\right\rangle_1. \quad (7)$$

(This expression actually represents $S(\infty)\cdot\bar T_{\mu\nu}$ (where $\bar T_{\mu\nu}$ is the transformed operator in the sense[11] of Schwinger). This however reduces to $\bar T_{\mu\nu}$ in view of the mass renormalization. See Eq. (5).)

In the following we confine ourselves to the first-order radiative correction: $\bar T_{\mu\nu}^{(1)}$. This expression includes non-covariant parts by θ_μ, (3), and through (6b), but these are easily shown to cancel.

Let us write $\bar T_{\mu\nu}^{(1)}=\bar T_{\mu\nu}^P+\bar T_{\mu\nu}^E$, representing the parts that arise from the photon field and electron field

[10] F. J. Dyson, Phys. Rev. **75**, 486 (1949).
[11] J. Schwinger, Phys. Rev. **76**, 790 (1949).

tensors, respectively. From (7) it follows that

$$\tilde{T}_{\mu\nu}{}^{P}(x)=-\frac{1}{2}\int\int dx_1dx_2\langle P(T_{\mu\nu}{}^{P}(x),\, h_I(x_1),\, h_I(x_2))\rangle_1.$$

Introducing

$$I_{\alpha\beta;\epsilon\xi}=\int\int dx_1dx_2\bar{\psi}(x_1)\gamma^{\alpha}S_F(x_1-x_2)\gamma^{\beta}\psi(x_2)$$
$$\times(\partial D_F(x_1-x)/\partial x_\epsilon)(\partial D_F(x_2-x)/\partial x_\xi),$$

we can write this as

$$\tilde{T}_{\mu\nu}{}^{P}=-\tfrac{1}{8}e^2(I_{\lambda\lambda,\,(\mu\nu)}+I_{(\mu\nu),\,\lambda\lambda}-I_{\lambda(\mu,\,\nu)\lambda}-I_{(\mu\lambda,\,\lambda\nu)}$$
$$-\delta_{\mu\nu}(I_{\lambda\lambda,\,\sigma\sigma}-I_{\lambda\sigma,\,\sigma\lambda})). \quad (8)$$

In a similar manner we get

$$\tilde{T}_{\mu\nu}{}^{E}=\frac{e^2}{32}\int\int dx_1dx_2\Big(\bar{\psi}(x_1)\gamma^{\lambda}\Big[S_F(x_1-x)\gamma^{(\mu}\frac{\partial S_F(x-x_2)}{\partial x_{\nu)}}$$
$$-\frac{\partial S_F(x_1-x)}{\partial x_{(\nu}}\gamma^{\mu)}S_F(x-x_2)\Big]\gamma^{\lambda}\psi(x_2)\Big)D_F(x_1-x_2)$$
$$+\frac{e^2}{32}\int\int dx_1dx_2\Big(\bar{\psi}(x_1)M_F(x_1-x_2)$$
$$\Big[S_F(x_2-x)\gamma^{(\mu}\frac{\partial\psi}{\partial x_{\nu)}}-\frac{\partial S_F(x_2-x)}{\partial x_{(\nu}}\gamma^{\mu)}\psi(x)\Big]+\text{h.c.}\Big)$$
$$-\frac{ie^2}{8}\int dx_1(\bar{\psi}(x_1)\gamma^{(\mu}S_F(x_1-x)$$
$$\times D_F(x_1-x)\gamma^{\nu)}\psi(x)+\text{h.c.}). \quad (9)$$

In this last formula the second line is not quite correct insofar as it represents the expression omitting the terms appearing through the mass renormalization:

$$\frac{1}{4}\int dx_1\Big\langle P\Big(\bar{\psi}\gamma^{(\mu}\frac{\partial\psi}{\partial x_{\nu)}}-\frac{\partial\bar{\psi}}{\partial x_{(\nu}}\gamma^{\mu)}\psi,\, h_s{}^{(2)}(x_1)\Big)\Big\rangle_1$$

and the second and third line of (3c). If we include these terms, then in the second line of (9), $S_F(x_2-x)$ and $\partial S_F(x_2-x)/\partial x_\nu$ are to be replaced by

$$-i(\bar{S}(x_2-x)+\tfrac{1}{2}\epsilon(x_1-x)S(x_2-x)) \quad (10)$$

and its derivative

$$-i(\partial/\partial x_\nu)(\bar{S}(x_2-x)+\tfrac{1}{2}\epsilon(x_1-x)S(x_2-x)).$$

III. THE CONDITIONS FOR VANISHING DIVERGENCE OF THE REGULARIZED TENSOR

Let us introduce the two "force densities" f_ν, defined by

$$f_\nu{}^{P}=\partial\tilde{T}_{\mu\nu}{}^{P}/\partial x_\nu,\quad f_\nu{}^{E}=(\partial\tilde{T}_{\mu\nu}{}^{E}/\partial x_\nu). \quad (11)$$

These f_ν can be determined by a straightforward calculation, making use only of the equations

$$\Box^2D_F(x)=2i\delta(x),\quad (\gamma^{\lambda}(\partial/\partial x^{\lambda})+m)S_F(x)=2i\delta(x) \quad (12)$$

and some integrations by parts. The result is[12]

$$f_\nu{}^{E}=-f_\nu{}^{P}=\tfrac{1}{4}i\int dx_1\Big[(\bar{\psi}(x_1)\gamma^{\lambda}S_F(x_1-x)$$
$$\times\gamma^{\lambda}\psi(x)+(\leftarrow))\frac{\partial D_F(x_1-x)}{\partial x_\nu}-(\bar{\psi}(x_1)\gamma^{\nu}$$
$$\times S_F(x_1-x)\gamma^{\lambda}\psi(x)+(\leftarrow))\frac{\partial D_F(x_1-x)}{\partial x_\lambda}\Big]. \quad (13)$$

Thus the divergence of the complete tensor apparently vanishes. It should be observed, however, that f_ν is represented by a quadratically divergent integral in momentum space. A direct computation in momentum space will therefore in general not give zero for $f_\nu{}^{E}+f_\nu{}^{P}$, since all we can expect for $f_\nu{}^{E}$ and $f_\nu{}^{P}$ are two integrals that differ by a translation of the integration variables.[3]

From this situation it does not follow that any invariant regularization process that makes the expressions for $f_\nu{}^{P}$ and $f_\nu{}^{E}$ finite would yield automatically zero for the divergence of $\tilde{T}_{\mu\nu}$. The result (13) is based essentially on the wave equations (12), and any regularization of the D_F or the S_F function destroys the validity of the corresponding equation. If for instance we introduced individually regularized D-functions

$$(D_F(x))_R=D_F(x)-D_F{}^{(M)}(x)$$
$$=\frac{-2i}{(2\pi)^4}\int_0 d^4k e^{ikx}\int_0{}^{1}du\frac{M^2}{(k^2+M^2u)^2},$$

$f_\nu{}^{E}$ would go over into the corresponding regularized expression, but this is not the case for $f_\nu{}^{P}$ which takes the form

$$-\frac{M^2}{8}\int\int dx_1dx_2(\lambda,\lambda)[D_F{}^{(M)}(x_1-x)(\partial D_F(x_2-x)/\partial x_\nu)_R$$
$$+(\partial D_F(x_1-x)/\partial x_\nu)_R D_F{}^{(M)}(x_2-x)]+\textit{a similar term.}$$
$$(\lambda_1,\lambda)=\bar{\psi}(x_1)\gamma^{\lambda}S_F(x_1-x_2)\gamma^{\lambda}\psi(x_2)$$

Another still purely formal device would consist in regularizing $\tilde{T}_{\mu\nu}{}^{(1)}$ itself and defining the regularized expression by

$$(\tilde{T}_{\mu\nu}{}^{(1)})_R=\tilde{T}_{\mu\nu}{}^{(1)}(S_F,\, D_F)-\tilde{T}_{\mu\nu}{}^{(1)}(S_F,\, D_F{}^{(M)}). \quad (14)$$

Again $f_\nu{}^{E}$ is then replaced by the corresponding regularized expression. In the calculation of $(f_\nu{}^{P})_R$ the wave equation for $D_F{}^{(M)}$ comes into play which intro-

[12] To derive expression for $f_\nu{}^{E}$, Eq. (9) has been used without corrections (10). It is easy to verify that the term affected by (10) gives no contribution to $f_\nu{}^{E}$.

duces an additional term $\sim M^2$; in this way $(f_\nu{}^P)$ goes over into

$$(f_\nu{}^P)_R - M^2\frac{1}{8}\int\int dx_1dx_2\{(\bar\psi(x_1)\gamma^\lambda S_F(x_1-x_2)\times\gamma^\nu\psi(x_2)+(\leftarrow))D_F{}^{(M)}(x_1-x)[\partial D_F{}^{(M)}(x_2-x)/\partial x_\lambda] - \text{a term with } (\lambda,\nu) \text{ interchanged}\}. \quad (15)$$

To get rid of this additional term we are guided by the statement that this regularization has already some features of an "auxiliary field theory," but with the "unrealistic" feature of an imaginary coupling, *i.e.*, of this auxiliary (neutral vector-meson) field to the electron field.[5] This fact suggests the inclusion of the complete energy-momentum tensor of this auxiliary field into the system considered, and the discarding for the moment of the non-hermitian character of the interaction with the electron field. This procedure changes the situation in two respects: (a) The components ϕ_ν of the auxiliary field can no longer be quantized as independent scalars[12] and instead of $\delta_{\mu\nu}D_F{}^{(M)}(x)$ we have to put $(\delta_{\mu\nu}-M^{-2}\partial_\mu\partial_\nu)D_F{}^{(M)}(x)$. It is easy to show however that the terms arising from $M^{-2}\partial_\mu\partial_\nu$ never contribute to $\tilde T_{\mu\nu}$, which is just an expression of the gauge invariance of this operator.[13] (b) The energy-momentum tensor of the vector meson field differs from $T_{\mu\nu}{}^P$ by a term

$$M^2(\phi_\mu\phi_\nu-\tfrac{1}{2}\delta_{\mu\nu}\phi_\lambda\phi_\lambda),$$

which contributes

$$\frac{1}{8}M^2\int\int dx_1dx_2(\bar\psi(x_1)\gamma^\mu S_F(x_1-x_2)\gamma^\nu)\psi(x_2) - \delta_{\mu\nu}\bar\psi(x_1)\gamma^\lambda S_F(x_1-x_2)\gamma^\lambda\psi(x_2))\cdot D_F{}^{(M)}(x_1-x)\cdot D_F{}^{(M)}(x_2-x). \quad (16)$$

to the first-order radiative correction $\tilde T_{\mu\nu}{}^{(1)}$. One immediately sees that the divergence of (16) and the additional term in (15) cancel.

Such a device can no longer be called a purely formal prescription. The aim of such a formal method would have consisted in providing a generally applicable rule which should be formulated in such a way as to be in accordance with the conservation laws and gauge-invariance, which are both formal properties of the non-regularized theory. Apparently this program has not yet been carried through in a satisfactory way, and the actual situation seems to indicate that only a realistic theory (f-field)[7] will be able to re-establish a satisfactory situation.

IV. CALCULATION OF $\tilde T_{\mu\nu}(p',p)$

Let $\bar\psi(p')\exp(-ip'\cdot x)$ and $\psi(p)\cdot\exp(+ip\cdot x)$ be Fourier-components of $\bar\psi(x)$ and $\psi(x)$, respectively. $\tilde T_{\mu\nu}{}^{(1)}(x)$ may then be written as an integral over terms of the form

$$\bar\psi(p')e^{-ip'x}\tilde T_{\mu\nu}(p'p)e^{ipx}\psi(p). \quad (17)$$

The operator $\tilde T_{\mu\nu}(p'p)$ thus introduced has the general form

$$\Delta p_\mu\Delta p_\nu f(\Delta p^2)+\delta_{\mu\nu}g(\Delta p^2) + (i\gamma^{(\mu}P_{\nu)})h(\Delta p^2)+P_\mu P_\nu k(\Delta p^2), \quad (18)$$
$$(\Delta p=p'-p;\quad P=p'+p).$$

The symmetry of $\tilde T_{\mu\nu}(p'p)$ in p and p' is a necessary condition for the validity of the conservation laws

$$\Delta p_\mu\tilde T_{\mu\nu}(p'p)=0. \quad (19)$$

(Non-symmetrical terms

$$\sim i(\gamma^{(\mu}\Delta p_{\nu)})H(\Delta p^2)+\Delta p_{(\mu}P_{\nu)}K(\Delta p^2)$$

would contribute

$$i\gamma^\nu\Delta p^2H(\Delta p^2)+P_\nu\Delta p^2K(\Delta p^2)$$

to the divergence (19), which is $\neq 0$ unless $H=K\equiv 0$.)

In the symmetrical expression (18), $g(\Delta p^2)$ will be written as

$$S+\Delta p^2\cdot\tilde g(\Delta p^2).$$

The conservation laws then require that

$$S=0,\quad \tilde g(\Delta p^2)=-f(\Delta p^2).$$

It is the purpose of this paragraph to show anew how the regularization device which proved to be successful in Section III leads to a result satisfying (19). But furthermore it will be explicitly shown that the final result is now finite and independent of the auxiliary mass M up to terms $O(M^{-2}\log M)$. Finally the actual form of the functions $f(\Delta p^2)$, $h(\Delta p^2)$ and $k(\Delta p^2)$ may be of some interest.

Contribution of $\tilde T_{\mu\nu}{}^P(x)$

This part is expressed in terms of

$$I_{\alpha\beta;\epsilon\zeta}(x)=\int\int d\xi d\eta\bar\psi(x+\xi)\gamma^\alpha S_F(\xi-\eta)\gamma^\beta\psi(x+\eta) \times\partial D_F(\xi)/\partial\xi_\epsilon\cdot\partial D_F(\eta)/\partial\eta_\zeta.$$

The corresponding $I_{\alpha\beta;\epsilon\zeta}(p'p)$, defined through (17), reads

$$I_{\alpha\beta;\epsilon\zeta}(p'p)=\frac{8i}{(2\pi)^4}\int d^4k\gamma^\alpha(i\gamma k-m)\gamma^\beta \times\frac{(k_\epsilon-p_\epsilon')(k_\zeta-p_\zeta)}{(k^2+m^2)(k-p')^2(k-p)^2}. \quad (20)$$

(It should be noticed that in the terms $(\mu\lambda,\lambda\nu)$, $(\lambda\mu,\nu\lambda)$ and $(\sigma\lambda,\lambda\sigma)$ a part containing (k^2+m^2) in the numerator may be isolated. These parts are easily shown to give a vanishing contribution, their removal

[13] This argument is of purely formal character, since the expressions involved are divergent. A proof which avoids the divergences must make use of Stueckelberg's B-field formalism (see W. Pauli, Rev. Mod. Phys. 13, 203 (1941), Part II/2) to describe the neutral vector meson.

in this stage of the calculation however is an essential simplification of the results.)

To regularize these expressions in the manner outlined, we write

$$\frac{1}{a\cdot b\cdot c}-\frac{1}{a(b+M^2)(c+M^2)}=\frac{1}{a}\left\{\frac{M^2}{b\cdot c\cdot(c+M^2)}+\frac{M^2}{b(b+M^2)(c+M^2)}\right\},$$

$$a=k^2+m^2;\quad b=(k-p')^2;\quad c=(k-p)^2.$$

On introducing properly chosen Feynman parameters, this can be written as

$$3!M^2\int_0^1 du\int_0^u dv\int_0^u dw[(k-p(u-v)-p'v)^2+m^2(1-u)^2+\Delta p^2(u-v)v+M^2w]^{-4}.$$

If $k'=k-p(u-v)-p'v$ is introduced as new variable the numerator in (20) takes the form

$$k'^2\Gamma_1+\Gamma_2$$

and a straightforward integration yields

$$I_{\alpha\beta;\mu\xi}(p'p)=\frac{-2}{(2\pi)^2}\int_0^1 du\int_0^u dv\left[2\Gamma_1\log\frac{C+M^2u}{C}+\Gamma_2\left(\frac{1}{C}-\frac{1}{C+M^2u}\right)\right],$$

$$C=m^2(1-u)^2+\Delta p^2(u-v)v.$$

For the purpose of the following discussion it is convenient to introduce the variables

$$z=u,\quad zt=2v-u.$$

With (8) it follows now that

$$\bar{T}_{\mu\nu}{}^P(p'p)=\frac{-e^2}{8}\sum I(p'p)=\frac{e^2}{4(2\pi)^2}\int_0^1 dt\int_0^1 zdz\times\left[I\cdot\log\frac{C+M^2z}{C}+II\left(\frac{1}{C}-\frac{1}{C+M^2z}\right)\right],\quad(21)$$

where

$$I=2\sum\Gamma_1=2z[m\delta_{\mu\nu}+(i\gamma^{(\mu}P_{\nu)})],$$

$$II=\sum\Gamma^2=m\Delta p_\mu\Delta p_\nu[(z-2)z^2t^2+z]-2m^3\delta_{\mu\nu}[(z-1)^2+\epsilon^2z^2(1-t^2)]+mP_\mu P_\nu(z-1)^2z-m^2(i\gamma^{(\mu}P_{\nu)})[(z-1)^2(z+2)+\epsilon^2z^3(1-t^2)],\quad(21a)$$

$$C=m^2[(z-1)^2+\epsilon^2z^2(1-t^2)],\quad\epsilon^2=\Delta p^2/4m^2.$$

It is easy to verify that the traces of I and II vanish separately. In the following we shall omit the contributions from II. $(C+M^2\cdot z)^{-1}$, which are of the order $M^{-2}\cdot\log M$. A partial integration with respect to t splits the logarithmic term into a part independent of Δp^2 and a part proportional to Δp^2. Thus

$$\bar{T}_{\mu\nu}{}^P(p'p)=\frac{e^2}{2(2\pi)^2}\int_0^1 dz\left[z^2(m\delta_{\mu\nu}+(i\gamma^{(\mu}P_{\nu)}))\times\log\frac{C_0+M^2z}{C_0}-mz\delta_{\mu\nu}\right]+\frac{e^2}{4(2\pi)^2}\int_0^1 dt\int_0^1 zdz\times\{m^2(\Delta p_\mu\Delta p_\nu-\Delta p^2\delta_{\mu\nu})z^3t^2-m^2(i\gamma^{(\mu}P_{\nu)})[(z-1)^2(z+2)+\epsilon^2z^3(1+3t^2)]+mP_\mu P_\nu(z-1)^2z+m\Delta p_\mu\Delta p_\nu(z-2z^2t^2)\}\cdot 1/C,\quad(22)$$

$$(C_0=C(\epsilon=0)).$$

An explicit calculation shows that the last term $\sim\Delta p_\mu\Delta p_\nu$ vanishes. The constant (that is, Δp^2-independent) terms are easily shown to give $(\mu=M/m)$:

$$\frac{+e^2}{2(2\pi)^2}\left[m\delta_{\mu\nu}\left(\frac{1}{3}\log(1+\mu^2)+\frac{11}{18}\right)+(i\gamma^{(\mu}P_{\nu)})\left(\frac{1}{3}\log(1+\mu^2)+\frac{10}{9}\right)\right].\quad(23)$$

Contribution to $\bar{T}_{\mu\nu}(p'p)$ from $\bar{T}_{\mu\nu}{}^E(x)$

From (9) it follows that

$$T_{\mu\nu}{}^E(p'p)=\frac{e^2}{32(2\pi)^4}\left[\int d^4k\gamma^\lambda S_F(p'-k)\times(i\gamma^{(\mu}\cdot P_{\nu)}-2k_{\nu)})S_F(p-k)\gamma^\lambda\cdot D_F(k)+\int d^4q\int d^4\xi\left(e^{-i(p'-q)\xi}M_F(q)\left(-i\bar{S}(q)-\frac{i}{2}\epsilon(\xi_0)S(q)\right)\times\left(\gamma^{(\mu}\overleftarrow{\frac{\partial}{\partial\xi_{\nu)}}}+i\gamma^{(\mu}p_{\nu)}\right)+(p'\rightleftarrows p)\right)\right]-\frac{ie^2}{8}(\gamma^{(\mu}(S_FD_F)(p)\gamma^{\nu)}+\gamma^{(\mu}(S_FD_F)(p')\gamma^{\nu)}).\quad(24)$$

Introducing

$$M_F(q)=(i\gamma q+m)\cdot F(\rho)+G(\rho),\quad\rho=q^2+m^2,$$

the second line becomes

$$\int d^4q\int d^4\xi\left(e^{-i(p'-q)\xi}\left(-F(\rho)+(i\gamma q-m)\frac{G(\rho)-G(0)}{\rho}\right)\times(i\gamma^{(\mu}p_{\nu)})+(p'\rightleftarrows p)\right)=-2(2\pi)^4(F(0)+2mG'(0))(i\gamma^{(\mu}P_{\nu)}).$$

Before performing the k space integrations we substitute $D_F - D_F^{(M)}$ for D_F. We have then

$$M_F(q)=\frac{2i}{(2\pi)^2}\int_0^1 dz(i\gamma p(1-z)+2m)\times\log\frac{m^2z^2+M^2(1-z)+\rho(z-z^2)}{m^2z^2+\lambda^2(1-z)+\rho(z-z^2)}, \quad (25a)$$

and

$$(S_F D_F)(q)=\frac{-i}{(2\pi)^2}\int_0^1 dz(i\gamma p(1-z)-m)\times\log\frac{m^2z^2+M^2(1-z)+\rho(z-z^2)}{m^2z+\lambda^2(1-z)+\rho(z-z^2)}. \quad (25b)$$

For the first line of (24) the technique already outlined yields

$$\frac{-e^2}{8(2\pi)^2}\int_0^1 dt\int_0^1 zdz\left[I'\cdot\log\frac{C'+M^2(1-z)}{C'}+II'\left(\frac{1}{C'}-\frac{1}{C'+M^2(1-z)}\right)\right]. \quad (26)$$

Here a small "photon mass" λ has been introduced to avoid difficulties at the lower limit of the k-integration. We have also

$$I'=4m(z+1)\delta_{\mu\nu}+(z-1)(i\gamma^{(\mu}P_{\nu)}),$$

$$II'=(1-z)[(2-4z+z^2)m^2+(1-z+\tfrac{1}{4}z^2(1-t^2))\Delta p^2](i\gamma^{(u}P_{\nu)})+2m(z-1)^2zP_\mu P_\nu+2m(z+1)z^2t^2\Delta p_\mu\Delta p_\nu, \quad (26a)$$

$$C'=m^2[z^2(1+\epsilon^2(1-t^2))+\eta^2(1-z)],$$

$$\epsilon^2=\Delta p^2/4m^2, \quad \eta=\lambda/m.$$

The second and third lines of (24) are, by (25)

$$\frac{-e^2}{8(2\pi)^2}\int_0^1 dz\left[(3(1-z)(i\gamma^{(\mu}P_{\nu)})-4mz\delta_{\mu\nu})\times\log\frac{C_0'+M^2(1-z)}{C_0'}-2m^2z(1-z^2)(i\gamma^{(\mu}P_{\nu)}\left(\frac{1}{C_0'}-\frac{1}{C_0'+M^2(1-z)}\right)\right], \quad (27)$$

In (27) and also in the factor multiplying II', the terms $\sim(C'+M^2(1-z))^{-1}$ will be dropped again. By a partial integration with respect to t we get:

$$T_{\mu\nu}^E(p'p)=\frac{-e^2}{8(2\pi)^2}\int_0^1 dt\int_0^1 zdz\{2m(z+1)z^2t^2\times[\Delta p_\mu\Delta p_\nu-\Delta p^2\delta_{\mu\nu}]+2m(z-1)^2zP_\mu P_\nu+(1-z)[(2-4z+z^2)m^2+(1-z+\tfrac{1}{4}z^2(1-t^2))\Delta p^2]\times(i\gamma^{(\mu}P_{\nu)})\}\cdot\frac{1}{C'}-\frac{e^2}{8(2\pi)^2}\int_0^1 dz\Big[(4mz^2\delta_{\mu\nu}+(3-z)(1-z)(i\gamma^{(\mu}P_{\nu)}))\log\frac{C_0'+M^2(1-z)}{C_0'}-2m^2z(1-z^2)(i\gamma^{(\mu}P_{\nu)})\cdot\frac{1}{C_0'}\Big]. \quad (28)$$

The constant terms contribute the quantity

$$\frac{-e^2}{2(2\pi)^2}\left[m\delta_{\mu\nu}\left(\frac{1}{3}\log(1+\mu^2)-\frac{7}{18}\right)+(i\gamma^{(\mu}P_{\nu)})\left(\frac{1}{3}\log(1+\mu^2)+\frac{65}{72}-\frac{1}{2}m^2\int_0^1 dz(1-z^2)/C_0'\right)\right]. \quad (29)$$

By comparison of this result with (23) it is seen that all contributions proportional to $\log(1+\mu^2)$ cancel. There remains, however, a finite part containing $\delta_{\mu\nu}$:

$$S=\frac{e^2}{2(2\pi)^2}m\delta_{\mu\nu}\frac{11+7}{18}=\frac{\alpha}{2\pi}m\delta_{\mu\nu}. \quad (30)$$

This corresponds just to the result of Pais and Epstein,[8] where it is deduced by calculating the so-called stress that

$$S=\tilde{T}_{11}^{(1)}(pp)=\tfrac{1}{3}(\tilde{T}_{\mu\mu}^{(1)}-\tilde{T}_{44}^{(1)}).$$

But $\tilde{T}_{44}^{(1)}=0$ (this result is due to our representation, compare Section II, in contradistinction to the situation in references 2 and 9). Since $\tilde{T}_{\mu\mu}^{P}=0$, we should have

$$S=\tfrac{1}{3}\cdot\tilde{T}_{\mu\mu}^{E}(pp) \quad (31)$$

and this can indeed be verified from (28) and (29):

$$\tilde{T}_{\mu\mu}^{E}(pp)=\frac{e^2m}{2(2\pi)^2}\left\{\int_0^1 dz(-4+3z+z^2)+4\left(\frac{7}{18}+\frac{65}{72}\right)\right\}=\frac{\alpha}{2\pi}m\left(-4+\frac{3}{2}+\frac{1}{3}+\frac{31}{6}\right)=3\cdot\frac{\alpha}{2\pi}m.$$

The stress vanishes, as was shown in Section III, Eq. (16), if one includes the additional term arising

through the energy-momentum tensor of the auxiliary field

$$M^2(\phi_\mu\phi_\nu-\tfrac{1}{2}\delta_{\mu\nu}\phi_\lambda{}^2). \tag{32}$$

Its contribution to $\bar{T}_{\mu\nu}{}^{(1)}(p'p)$ is

$$\frac{-e^2M^2}{4(2\pi)^2}\int_0^1 dt\int_0^1 zdz[2m\delta_{\mu\nu}+z(i\gamma^{(\mu}P_{\nu)})]\cdot\frac{1}{C+M^2Z}. \tag{33}$$

The minus sign in (33) is due to the choice of an imaginary coupling ie of this auxiliary field.

Neglecting again terms of the order $M^{-2}\cdot\log M$, Eq. (33) gives

$$-(e^2/2(2\pi)^2)[m\delta_{\mu\nu}+\tfrac{1}{4}(i\gamma^{(\mu}P_{\nu)})]. \tag{34}$$

Thus the formerly remaining stress-part (30) is now cancelled and a divergence free energy-momentum tensor is obtained. There remains, however, an infra-red term in the third line of (28). Because of the factor Δp^2 this term plays no role in the energy-momentum four-vector $P_\mu=\int T_{\mu 4}d^3x$. It indicates, however, that as soon as we try to localize energy and momentum and to build up wave packets, the well-known failure of the power series approach in constructing of the physical electron becomes manifest. Expressed in terms of the operators of the present approximation, the physical electron carries still a cloud of virtual low energy photons with itself, the effect of which is discarded on going to the one-particle, no-photon part of $\bar{T}_{\mu\nu}$. Thus, to investigate the energy-momentum density distribution, the above calculation would have to be completed by a sort of Bloch-Nordsieck treatment, but which is not within the scope of the present investigation.

The discussion of the energy-momentum four vector P_μ displays again the necessity for the inclusion of (32) into the system, in a way which, of course, is connected with the self-stress difficulty. Since the change in the physical properties of the electron due to its interaction with the radiation field vacuum consists only in a change of its mass, and since this change has already been included in the representation of the electron field, $\bar{T}_{\mu\nu}{}^P+\bar{T}_{\mu\nu}{}^E$ should give no contribution at all to P_μ. From this statement it follows that the coefficients of $(i\gamma^{(\mu}P_{\nu)})$ and $P_\mu P_\nu$ should vanish too for $\Delta p^2=0$. This fact is easily verified from (22), (23), (28), (29), and (34). The inclusion of the contribution $\sim(i\gamma^{(\mu}P_{\nu)})$ in (34) is essential and exhibits again the failure of a purely formal mass regularization.

In conclusion I would like to express my gratitude to Dr. J. R. Oppenheimer for the privilege of a stay at the Institute for Advanced Study, and also for helpful criticism.

PHYSICAL REVIEW VOLUME 79, NUMBER 1 JULY 1, 1950

Microwave Collision Diameters I. Experimental*

RAYDEEN R. HOWARD† AND WILLIAM V. SMITH
Department of Physics, Duke University, Durham, North Carolina

(Received February 24, 1950)

The diameters of fifteen polar and non-polar gases for collisions with ammonia are obtained from measurements of the pressure broadening of the ammonia 3–3 inversion line in the mixed gases at low pressures. The design of the spectroscope used and the experimental technique involved are discussed.

I. INTRODUCTION

PRESSURE broadening of spectral lines has been studied for many years in the optical and infra-red regions. In 1936 a review of work done up to that time was given by Margenau and Watson.[1] The difficulties encountered in this region are great. A large Doppler breadth and insufficient resolution hamper measurements at low pressures while at high pressures multiple collisions complicate the process. Because of these and other difficulties the problem suffered from neglect and never was brought to satisfactory completion.

More recently, the expansion of microwave spectroscopy has caused new interest to arise and a number of theoretical and experimental papers have appeared.[2] In the microwave region, resolution is high and Doppler breadth is only about 70 kc. At breadths of the order of a megacycle, the more intense lines, especially the ammonia 3–3 inversion line, may easily be displayed on an oscilloscope for observation.

In the case of collision broadening in a pure gas, the

* The research reported in this document has been made possible through support and sponsorship extended by the Geophysical Research Directorate of the Air Force Cambridge Research Laboratories under Contract No. W(19-122) ac-35. It is published for technical information only and does not represent recommendations or conclusions of the sponsoring agency.

† The material in this paper is a part of the author's thesis submitted in partial fulfillment of the requirements for the degree of Doctor of Philosophy at Duke University.

[1] H. Margenau and W. W. Watson, Rev. Mod. Phys. 8, 22 (1936).

[2] H. Margenau, Phys. Rev. 76, 121 (1949); J. H. Van Vleck and V. F. Weisskopf, Rev. Mod. Phys. 17, 227 (1945); P. W. Anderson, Phys. Rev. 76, 647 (1949); H. M. Foley, Phys. Rev. 69, 616 (1946); B. Bleaney and R. P. Penrose, Proc. Phys. Soc. London LIX, 418 (1947); LX, 83 (1948).

line breadth constant $\Delta\nu$ is given by

$$2\Delta\nu_1 = N_1\sqrt{2}\bar{V}_1 b_1^2,$$

while in a mixture of two gases

$$2\Delta\nu_2 = N_1'\sqrt{2}\bar{V}_1 b_1^2 + N_2\bar{V}_{12} b_{12}^2,$$

where N_1, $\bar{V}_1$, and b_1 are the molecular density, average velocity and collision diameter, respectively, of the absorbing gas. The relative velocity $\bar{V}_{12}$ is equal to $(\bar{V}_1^2+\bar{V}_2^2)^{\frac{1}{2}}$ and b_{12} is the collision diameter for mixed collisions. In our measurements, pressures were so adjusted that $\Delta\nu_1=\Delta\nu_2$ and, with the intensity ratio $I_2/I_1=N_1'/N_1=I$, the cross-section ratio becomes

$$b_{12}^2/b_1^2 = (\sqrt{2}\bar{V}_1/\bar{V}_{12})(1-I)/[(P_2/P_1)-I],$$

where pressures have been substituted for molecular densities.

The measurements needed, then, for determining the cross-section ratios are the pressure of pure ammonia, the pressure of the mixture, and the relative intensity of absorption.

II. EXPERIMENTAL

Figure 1 is a block diagram of the spectroscope used. The Type 2K50 klystron was chosen because of its unusually broad mode. It was found that with intensities of absorption 10 percent of that of pure ammonia no correction for curvature of the mode was necessary.

The klystron is reflector-tuned through 3 to 4 Mc to either side of the absorption line by a 60-cycle sawtooth voltage and is frequency modulated[3,4] by a 100-kc sinusoidal voltage of small amplitude. Upon detection, the 100-kc component is amplified and redetected by a communications receiver tuned to 100 kc. The envelope obtained (the absolute magnitude of the first derivative of the absorption line) is displayed on an oscilloscope as in Fig. 2.

The modulated output from the klystron is fed into two X-band absorption cells (labeled "measurement cell" and "comparison cell") four meters long by a magic tee and transition sections. The measurement cell is terminated by a Type 1N26 crystal rectifier whose output is connected to the grid of a cathode follower. The load on the crystal, the grid resistor, was adjusted to give a square law response at the power level used.[5]

To avoid non-linearities it is desirable to have a constant signal in the signal channels of the communications receiver and oscilloscope. Accordingly, the output from the cathode follower is connected to an attenuator. In order that relative intensities might be read from the attenuator setting, it was calibrated under "use" conditions with a 100-kc signal at 0.01 volt applied to the input of the cathode follower and an oscilloscope in parallel with the input to the receiver. Signal heights as a function of attenuator setting were then photographed on a linear portion of the oscilloscope screen to give the calibration. A second-cathode follower was used to match the high output impedance of the attenuator to the low impedance input of the receiver.

The crystal calibration was obtained by introducing ammonia into the cell and tuning to the 3–3 line. Input to the crystal was then varied over a range of 14 db by means of a calibrated microwave attenuator and the output measured as the corresponding change of the 100-kc attenuator necessary to maintain the oscilloscope display at constant height.

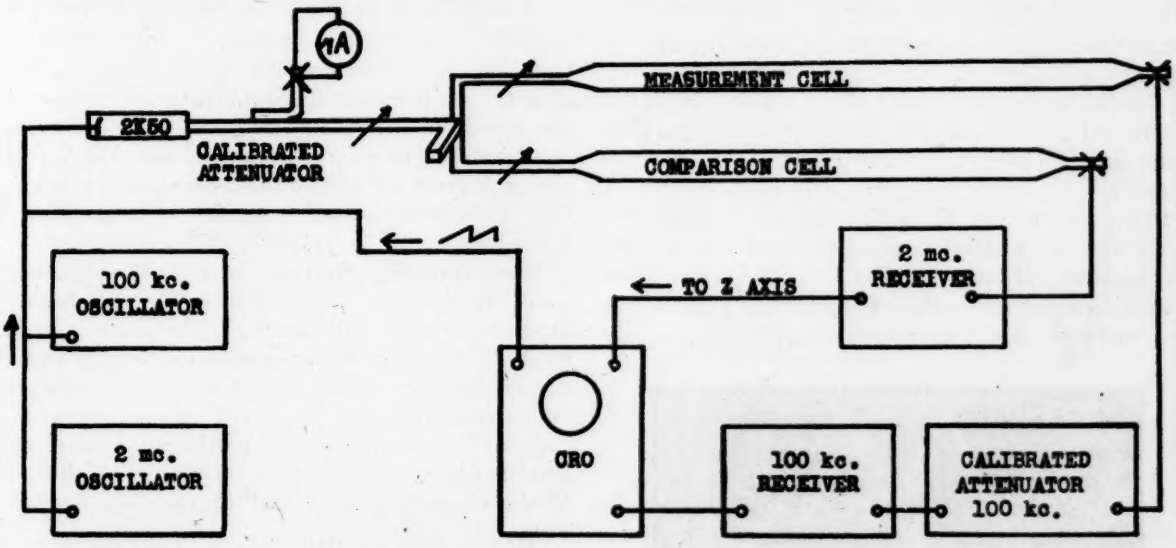

FIG. 1. Block diagram of spectroscope.

[3] W. Gordy and M. Kessler, Phys. Rev. 72, 664 (1947).
[4] Robert Karplus, Phys. Rev. 73, 1027 (1948).
[5] H. C. Torrey and C. A. Whitmer, *Crystal Rectifiers*, M.I.T. Radiation Laboratory Series V, 15 (McGraw-Hill Book Company, Inc., New York, 1948), p. 333.

III. CORRECTIONS AND MONITOR DEVICES

The power absorbed in the guide is given by $P=Po(1-e^{-\gamma x})$, where the absorption coefficient γ is given by

$$\gamma=\gamma_0(\Delta\nu)^2/[(\nu-\nu_0)^2+(\Delta\nu)^2].$$

Thus the line breadth, as measured between points of maximum $dP/d\nu$, must be corrected for the decrease of γ in the mixture as compared to pure ammonia. Experimental values of γx were used to make the correction. This amounts to a decrease of the measured ratio P_2/P_1 of 5 to 7 percent, depending on the concentration of ammonia in the mixture.

In order to insure that the frequency scale remained unchanged during the course of a measurement, the comparison cell and a third reflector modulation were introduced to give markers of known frequency spacing. The comparison cell was filled with ammonia at low pressure to give a narrow absorption line. The amplitude of the modulating signal must be kept low to avoid distorting the signal in the measurement cell. The modulation frequency, however, may be varied over a wide range and was usually set at 2 Mc. The cell is terminated by a crystal detector connected to a communications receiver and the redetected signal is applied to the intensity grid of the oscilloscope. The receiver was usually tuned to 200 kc less than the modulation frequency as the markers obtained here appear somewhat sharper than those at the oscillator frequency. Figure 2 is a photograph of the ammonia line with frequency scale markers at an ammonia concentration of about 30 percent. The unsymmetrical marker presentation is due primarily to the different response of the two detection systems involved. This is considered to be fortunate since it permits intensity measurement without the necessity of turning off the markers, as would be the case if the central marker fell on the display center. Symmetry is not necessary to the determination of a constant frequency scale or of line shifts since, in any case, the markers are of constant position.

Input power level was monitored by a crystal detector and microammeter on a directional coupler near the klystron. It was required that the power level remain constant within a few percent during the course of a run and a small correction, assuming square law response of the monitor crystal, was made when necessary. The power was maintained at such a level that the small variations noted would not contribute to saturation broadening. The intensity measurement requires also that the amplitude of the 100-kc modulating signal be held constant. This was done by means of the self-contained meter in the Hewlett-Packard Type 650-A oscillator used.

FIG. 2. Typical absorption line with frequency markers.

IV. GASES AND VACUUM SYSTEM

Commercial compressed gases of high purity or reagent grade chemicals were used with the following exceptions: CH_3Cl was prepared by the action of concentrated HCl and CH_3OH in the presence of $ZnCl_2$ as a catalyst.[6] ClCN was prepared by chlorination of a suspension of KCN in CCl_4.[7] HCN was prepared by the reaction of dilute sulfuric acid and KCN.[8] COS was prepared by the action of dilute sulfuric acid on NH_4CNS.[8]

A glass reservoir of 12 liter capacity was connected to the measurement cell so that the system would "hold" to better than 10^{-4} mm Hg for a 12-hour period. Pressures were measured with a McLeod gauge and the possible presence of condensable vapors was checked with a Pirani gauge. None were present.

V. PROCEDURE

Each "run" comprises measurement of line breadth, pressure and intensity for pure ammonia and for one mixture of ammonia with a foreign gas. For the first point, ammonia is admitted into the evacuated measurement cell at a pressure of 0.02 to 0.04 mm Hg. Ammonia adsorbs very strongly onto the walls of the system. At these pressures and for this system, somewhat more than 24 hours are required to reach full equilibrium, at which time the pressure is about one-fourth of the original pressure. At about one-half hour after the gas is admitted, however, the adsorption rate has slowed to the extent that pressure and intensity measurements may be considered instantaneous, with negligible error. Because of this adsorption it is essential that both breadth and intensity of absorption be measured.

After adsorption processes have slowed sufficiently, gains are adjusted to give the oscilloscope display a fixed height and width (Fig. 2). The pressure is then measured and the 100-kc attenuator setting and the various monitor readings noted. For the mixture point measurement 70 to 90 percent of the ammonia is pumped from the system and sufficient foreign gas is admitted to return the line to its original breadth. The 100-kc attenuation is reduced to restore the display to

[6] James F. Norris and Hazel B. Taylor, J. Am. Chem. Soc. **46**, 753 (1924).

[7] *Inorganic Syntheses II*, W. C. Fernelius, Editor (McGraw-Hill Book Company, Inc., New York, 1946), p. 90.

[8] A. Farkas and H. W. Melville, *Experimental Methods in Gas Reactions* (The Macmillan Company, New York, 1939), pp. 161, 168.

its former height, and pressure and monitor readings again recorded.

Seven or more such runs were made for each of the gases reported. The time allowed for clearing the system of the foreign gas between runs varied from 2 hours for the rare gases to more than 12 hours for the adsorbing polar gases.

VI. RESULTS

Our measured collision diameters and typical experimental values of the pressure ratio and relative intensity are given in Table I. Collision diameters as measured by Bleaney and Penrose[9] are given for certain of the non-polar gases. With the exception of CS_2 their values are higher by about 20 percent. Bleaney and Penrose deduce their diameters from intensity measurements only, assuming their gas mixtures to be known. Unknown relative adsorption of gases on the container walls or non-linearities in the detector may introduce errors in this approach. We measure two parameters, line width and intensity ratio. The accuracy of our line width measurement limits our over-all accuracy to two to three percent, as indicated by our statistical probable error. Our intensity measurements are not only carefully calibrated, but in any case enter into our results only as a correction factor of some ten to twenty percent. We should note, however, that Bleaney and Penrose's measurement of the self-broadening of ammonia does not involve these experimental difficulties, and presumably is accurate to a few percent. (Townes,[10] however, reports a line breadth for the 3–3 line 10 percent higher than given by Bleaney and Penrose.) Correlations of our measurements with other molecular data and estimates of molecular quadrupole moments may be found in the following paper.[11]

TABLE I. Experimental values of the collision diameters.

Mixture gas	Number of measurements	P_2/P_1 typical	I values	$b\times10^8$ cm (average)	Probable error (percent)	$b\times10^8$ cm (reference 9)
NH_3						13.8
He	7	19.0	0.306	2.00	2.3	2.35
A	7	13.5	0.181	3.73	1.7	4.6
H_2	7	7.70	0.202	2.95	1.9	3.50
N_2	11	5.74	0.190	5.54	1.4	6.4
O_2	7	12.1	0.170	3.86	2.3	4.85
CO_2	8	3.54	0.190	7.59	1.7	
COS	7	3.58	0.194	7.54	3.7	
CS_2	7	3.55	0.163	7.72	1.9	7.5
HCN	7	1.99	0.097	9.95	2.3	
ClCN	14	1.49	0.202	11.9	1.6	
CH_3Cl	7	1.71	0.140	11.3	0.9	
CH_2Cl_2	7	2.20	0.117	10.3	1.3	
$CHCl_3$	7	1.24	0.163	13.7	2.8	
CCl_4	7	3.87	0.300	7.20	2.4	
SO_2	7	2.15	0.100	10.4	1.4	

No shifts of absorption line frequency were observed. Particular care was taken in the case of self-broadening of the ClCN line at 23885 Mc and in the case of broadening of the NH_3 3–3 line by Argon. Observations on ClCN were made relative to a marker 10 Mc from the ammonia 3–3 line in the comparison cell. In these cases we estimate that the ratio of shift to line breadth was less than 0.03.

We wish to express our appreciation to Mr. Louis Moose of the Bell Telephone Laboratories for technical advice concerning operation of 2K50 klystrons and to Dr. Ralph Trambarulo for the necessary chemical preparations.

[9] B. Bleaney and R. P. Penrose, Proc. Phys. Soc. London LX, 540 (1948).

[10] C. H. Townes, Phys. Rev. 70, 665 (1946).

[11] William V. Smith and Raydeen R. Howard, Phys. Rev., following paper.

Microwave Collision Diameters II. Theory and Correlation with Molecular Quadrupole Moments*

WILLIAM V. SMITH AND RAYDEEN HOWARD†
Department of Physics, Duke University, Durham, North Carolina
(Received February 24, 1950)

Observed microwave collision diameters are interpreted as arising exclusively from transitions induced during the collision. Collision diameters greater than kinetic theory values arise from dipole-dipole or dipole-quadrupole interactions. The former case affords a quantitative test of the theory. In the latter case measurements of collision diameters yield quadrupole moment measurements which are correlated with molecular structure.

INTRODUCTION

THE line widths of microwave spectra at low pressures can be described adequately by the concept that collisions initiate and terminate the molecular radiation or absorption. The Fourier analysis of the resulting wave trains gives a Lorentz or resonance type variation in intensity of absorption with frequency[1] with the half-power half-width $\Delta\nu$ of the absorption line related to the mean time τ between collisions by

$$\Delta\nu = 1/2\pi\tau. \quad (1)$$

Although the collision time is in general shorter than would be derived from kinetic theory cross sections, it is useful to define a cross section σ for microwave collisions by

$$\tau = 1/n\bar{v}\sigma, \quad (2)$$

where $\bar{v}$ is the relative velocity of impact.†† The problem then arises of evaluating σ in terms of the known intermolecular forces.

A number of partially contradictory, partially complementary theories of pressure broadening exist.[2–4] Their applicability to microwave spectra has so far been tested almost exclusively by Bleaney and Penrose's data on the self-broadening of the ammonia inversion spectrum centered near 24,000 megacycles.[2] While all theories manage to explain these data reasonably well, extension of the data to include the variation in line width with temperature serves to eliminate one of the theories.[5] These and other considerations finally lead to a verification of Anderson's theory of impact broadening. A simplified version of this theory is then applied to the broadening of ammonia absorption lines by polar symmetric tops, polar linear molecules, and non-polar linear molecules with permanent quadrupoles. The self-broadening of polar linear molecules is also analyzed. Less extensive data and more qualitative analysis are presented for the broadening of the ammonia lines by asymmetric tops and spherical tops.

ELEMENTARY IMPACT THEORY

The simplest form of impact theory states that a radiation interrupting collision between two molecules occurs whenever their interaction energy, governed by their distance of separation r (center to center), exceeds a certain, perhaps arbitrarily assigned, quantity. When applied to the self-broadening of ammonia, a single interaction energy, W, of 2 to 3×10^{-16} erg (depending on the assumptions made in averaging the collisions) yields the observed cross sections for all the lines.[2] As these cross sections vary by a factor of almost three, the agreement between theory and experiment is quite good. Furthermore, the best figure for the interaction energy corresponds to W/hc equal to 1 cm^{-1}, almost exactly the energy separation of the inversion doublets. This coincidence of interaction energy with doublet separation implies that every microwave collision redistributes the relative population of the inversion doublets —a conclusion already experimentally confirmed by data on the saturation effect[6] where a high energy density of microwave radiation at the resonance frequency is observed to disturb the thermal distribution of the inversion doublet state. Indeed, in interpreting this saturation data, it is necessary to assume that, to the accuracy of the experimental data, every "line broadening" collision is also an energy redistributing collision.‡

Bleaney and Penrose's theory is formulated on a "hard ellipsoid" assumption in which the collision

* The research reported in this document has been made possible through support and sponsorship extended by the Geophysical Research Directorate of the Air Force Cambridge Research Laboratories under Contract No. W19-122-ac-35. It is published for technical information only and does not represent recommendations or conclusions of the sponsoring agency.

† The material in this paper is a part of the author's thesis submitted in partial fulfillment of the requirements for the degree of Doctor of Philosophy at Duke University.

[1] J. H. Van Vleck and V. F. Weisskopf, Rev. Mod. Phys. **17**, 227 (1945).

†† $\bar{v}=[\bar{v}_1^2+\bar{v}_2^2]^{\frac{1}{2}}$ where $\bar{v}_1$ and $\bar{v}_2$ are the mean velocities of the two molecules involved in the collision.

[2] B. Bleaney and R. P. Penrose, Proc. Phys. Soc. **LX**, 540 (1948).

[3] H. Margenau, Phys. Rev. **76**, 121 (1949).

[4] P. W. Anderson, Phys. Rev. **76**, 647 (1949).

[5] R. Howard and W. V. Smith, Phys. Rev. **77**, 840 (1950).

[6] R. Bleaney and R. P. Penrose, Proc. Phys. Soc. **LX**, 83 (1948); R. L. Carter and W. V. Smith, Phys. Rev. **73**, 1053 (1948); Robert Karplus, Phys. Rev. **73**, 1120 (1948); R. Karplus and J. Schwinger, Phys. Rev. **73**, 1020 (1948).

‡ Margenau however considers this coincidence of the interaction energy at the collision radius with the doublet separation to be a weak point in the elementary impact theory (see reference 3).

radius is assumed independent of the impact velocity. As the interaction energy varies with r^{-3} this assumption seems unreasonable, and is, indeed, found to be experimentally invalid,[5] since the observed cross section varies with v^{-1}. The elementary theory also ignores rotational resonance interactions which are shown by Anderson to be important for molecules whose component K of total angular momentum J along the symmetry axis is low. When the theory is modified in these respects, it becomes indistinguishable from Anderson's theory.[4]

STATISTICAL THEORY

A radically different approach to the line breadth problem is the statistical theory.[3] The idea here is, essentially, to analyze an instantaneous picture of the molecular distribution in space. A given radiating or absorbing molecule will have its energy levels perturbed by interactions with neighbor molecules. At low pressures the interaction will be predominantly with one nearest neighbor. If the frequency shift $\nu-\nu_0$ is weighted according to the probabilities of the appropriate intermolecular distances, it is found that the intensity varies inversely as $(\nu-\nu_0)^2$. The assumptions made in this derivation are known to break down near $\nu=\nu_0$, so that the mathematical infinity here is not serious. A quantitative agreement with the experimental data for ammonia is obtained by assuming that the true intensity distribution near $\nu-\nu_0$ is given by a resonance type curve

$$I(\nu)=C\frac{\Delta\nu}{(\nu-\nu_0)^2+\Delta\nu^2} \qquad (3)$$

and normalizing (3) to agree with the statistically derived expression in the wings of the curve. Inasmuch as (3) has been derived as a specific result of the impact theory, this step would seem to constitute a mathematical acceptance of the impact theory in the face of a physical denial of it. There is clearly no mechanism explaining saturation effects inherent in the statistical theory. We should note, however, that the theory predicts line widths independent of molecular velocities, in agreement with observation.[5] Fortunately, the more rigorous version of the impact theory also yields line widths independent of molecular velocity.

RIGOROUS IMPACT THEORY

A rigorous quantum mechanical treatment of collision broadening in the microwave region, with particular emphasis on the ammonia problem, has been given by Anderson.[4] We shall merely summarize his results and indicate where simplifications are possible.

In essence, a "collision" occurs in either of two limiting cases. If the collision perturbation induces transitions between states j and k, with a total probability a_{jk} integrated over the path of the perturbing molecule, then if $|a_{jk}|=\frac{1}{2}$, a collision has occurred, with complete interruption of radiation.¶ This is the non-adiabatic case. On the other hand, even if no transitions are caused, the energy levels j and k will be displaced by the perturbing molecule. If the two displacements are not equal, the radiation frequency will vary continuously during a collision. Although both before and after the impact $\nu=\nu_0$, there will be a phase shift in the emitted radiation. Weisskopf assumed that if the magnitude of the phase shift is unity, a "collision" has occurred in the sense that an arbitrarily large phase shift is the equivalent of a complete interruption of radiation.[7] This is the adiabatic case.

TABLE I.

Broadening gas (2)	Temperature	μ_2 Static Debye units	$\bar{\mu}_2$ Debye units	Arbitrary $P/\Delta\nu$	$\frac{T\Delta\nu}{\bar{\mu}_2 P}$
NH_3	300°K	1.44	0.78	1±0.02	385
NH_3	195°K	1.44	0.775	0.66±0.02	396
$CHCl_3$	300°K	0.95	0.57	1.33±0.04	396
CH_3Cl	300°K	1.87	0.47	1.83±0.02	349

It should be emphasized that the above development is historically in reverse—i.e., in optical spectra, non-adiabatic collisions are the exception—hence the necessity for a phase shift theory. An implication of this theory is that frequently these phase shifts do not average to zero so that there is an over-all frequency shift accompanying pressure broadening. We have seen in considering the ammonia example that in this case most collisions are non-adiabatic. Qualitative observations on saturation effects indicate that most microwave collisions are non-adiabatic. Furthermore, no microwave transition has shown a frequency shift accompanying line broadening at low pressures.[8] (The frequency shifts in ammonia at high pressures are another phenomenon of a much smaller order of magnitude than those predicted by the phase shift theory.) To be sure, no net shift would be expected for the best observed absorption —ammonia—even on the phase shift theory. On the other hand, for linear molecules, a frequency shift is predicted on this theory—but not observed. For these reasons, then, we shall ignore the phase shift terms in computing microwave collision broadening.

Anderson, in his rigorous theory, has made no assumption so crude as to merely set $|a_{jk}|$ equal to $\frac{1}{2}$ for a collision. Rather, he has averaged the contributions to line broadening arising from different impact parameters (distance of closest approach) b. The end result of this averaging, however, is to arrive at a collision cross section σ depending on the parameters of the problem in the same manner as with the crude assumption—only the constant of proportionality is slightly different. To

¶ We choose a value $|a_{jk}|=\frac{1}{2}$ rather than the apparently more logical choice $|a_{jk}|=1/\sqrt{2}$ (which populates both states equally). This yields eventual agreement with Anderson's rigorous theory, without the necessity of carrying an adjustable constant.

[7] V. Weisskopf, Zeits. f. Physik **75**, 287 (1932).

[8] R. Howard and W. V. Smith, Phys. Rev. **78**, 128 (1950).

TABLE II. Collision diameters (b) of NH_3 with various colliding molecules.

Colliding molecule (2)	μ_2 ($\times 10^{18}$)	$\bar{\mu}_2$ ($\times 10^{18}$)	$b\times 10^8$ microwave 3–3 line[a]	$b\times 10^8$ kinetic theory[b]	$Q\times 10^{16}$
NH_3	1.44[c]	0.775	13.8	4.43	
H_2	0	0	2.00	3.31	0
A	0	0	3.73	4.04	0
H_2	0	0	2.95	3.59	<0.10
N_2	0	0	5.54	4.09	0.27
O_2	0	0	3.86	4.02	<0.09
CO_2	0	0	7.59	4.46	0.65
COS	0.720[d]	0	7.56		0.61
CS_2	0	0	7.72		0.64
HCN	2.96[e]	0	10.0		1.6
ClCN	2.80[f]	0	11.9		2.4
CH_3Cl	1.87[g]	0.47	11.3	5.14	—
CH_2Cl_2	1.59[h]	0	10.3		1.5
$CHCl_3$	0.95[h]	0.57	13.7		—
CCl_4	0	0	7.20		0
SO_2	1.7[h]	0	10.4		1.6

[a] See reference 8 except for NH_3, which is from reference 2.
[b] E. H. Kennard, *Kinetic Theory of Gases* (McGraw-Hill Book Company, Inc., New York, 1938). (Value for CH_3Br used for CH_3Cl.)
[c] A. Van Itterbeek and K. de Clippelier, Physica **14**, 349 (1948).
[d] Dakin, Good, and Coles, Phys. Rev. **70**, 560 (1946).
[e] R. G. Shulman and C. H. Townes, Phys. Rev. **78**, 347 (1950).
[f] Townes, Holden, and Merritt, Phys. Rev. **74**, 1126 (1948).
[g] Dailey, Mays, and Townes, Phys. Rev. **76**, 136 (1949).
[h] P. Debye, *Polar Molecules* (Chemical Catalog Company, Inc., 1929).

arrive at a convenient working formula, then, we will consider the case of dipole-dipole broadening in an elementary fashion, comparing our results to Anderson's.

The transition probability a_{jk} is given by[9]

$$a_{jk}=-i\int\frac{H_{jk}\exp(-i\omega_{jk}t)}{\hbar}dt, \tag{4}$$

where H_{jk} is the collision perturbation Hamiltonian (Anderson's $H_i=-iH_{jk}$), and $\omega_{jk}=(E_k-E_j)/\hbar$ is the unperturbed angular frequency. Anderson has shown that if $K=(b\omega_{jk})/v$ is less than unity, the exponential term can be set equal to one with only a few percent error. Since for the ammonia inversion spectrum at room temperature $K=0.2$, and in general in the microwave region $K<1$, this approximation is valid. When $K>1$, as in most optical spectroscopy, non-adiabatic collisions are unimportant.

Anderson's Eq. (7) then yields for dipole-dipole broadening, ignoring rotational resonance terms which are important only for the special case of ammonia‖ (and then only for low K values).

$$|a_{jk}|=\left(\frac{8}{9}\right)^{\frac{1}{2}}\left(\frac{\mu_1\bar{\mu}_2}{b^2v\hbar}\right).$$

[9] H. M. Foley, Phys. Rev. **69**, 616 (1946).

‖ For other microwave transitions the population of rotational states differing by $J=1$ from the "struck" molecules is usually too small to be important.

We have included an r.m.s. average over the polar and azimuthal angles with respect to the impact parameter b. μ_1 and $\bar{\mu}_2$ are the magnitudes of the components of the dipole moment along the angular momentum axis. An average of μ_2 over the states of the colliding molecule has been included. Setting (5) equal to $\frac{1}{2}$ and solving for $\sigma=\pi b^2$

$$\sigma=\frac{2\pi\mu_1\bar{\mu}_2}{v\hbar}\left(\frac{8}{9}\right)^{\frac{1}{2}}. \tag{6}$$

This expression may be compared with Anderson's Eq. (11), rewritten as

$$\sigma=\frac{2\pi\mu_1\bar{\mu}_2}{v\hbar}\left(\frac{8}{9}\right)^{\frac{1}{2}}C, \tag{7}$$

where C is a constant whose value, depending on the averaging assumption, lies between 1.11 and 0.885. Clearly to the accuracy of the theory, the simpler Eq. (6) is satisfactory. Substituting (6) in (1) and (2), then, for symmetric top dipole broadening

$$\Delta\nu=\frac{n\mu_1\bar{\mu}_2}{\hbar}\left(\frac{8}{9}\right)^{\frac{1}{2}}. \tag{8}$$

The final result is seen to be independent of the molecular velocity. Formula (8) however is not valid over extreme ranges of velocity, as at very low velocity the assumption $K<1$ becomes invalid. Table I summarizes the experimental test of Eq. (8) for variations in temperature and foreign gas. The NH_3 3, 3 line is chosen, both because it is the strongest and because, even for self-broadening, rotational resonance terms are negligible in this case. The last column of Table I, with n proportional to P/T, should be a constant for verification of the theory. It is seen to be constant to within ± 9 percent, which is about the combined inaccuracies of the experimental parameters (including dipole moments).

It should be stressed at this point that a general acceptance of Bleaney and Penrose's elementary impact theory has led to the assumption that the line breadth, for constant pressure, is inversely proportional to the square root of the temperature. Thus many of the "engineered" intensity formulas current in the literature give an incorrect temperature dependence. It is also evident that only for symmetric top dipole broadening, with its interaction energy proportional to the inverse cube of the distance, will the line breadth be strictly independent of the velocity. For dipole-quadrupole broadening, only a small error is introduced in neglecting the velocity dependence. When the colliding molecules obey "harder" force laws involving higher inverse powers of r, the line width approaches proportionality to $T^{-\frac{1}{2}}$ as in the elementary impact theory.

HIGHER ORDER INTERACTIONS

When the colliding molecule 2 possesses no permanent dipole moment, averaged over the rotational motion, a

number of interactions that can be neglected when dipole-dipole forces are prominent now must be considered. Firstly, if the colliding molecule is linear and polar, there is the Keesom alignment interaction, resulting from the tendency of two rotating dipoles to "lock in" their rotation to a common frequency. This interaction is small when the dipole moment is small as in OCS. For an experimental confirmation, the observed microwave collision diameters given in Table II differ negligibly among the molecules CO_2, CS_2, and OCS despite the fact that OCS is polar and the other two are not. For dipole moments greater than about 2×10^{-18} e.s.u., this interaction is no longer negligible. The moderate size of the ammonia dipole however makes the interaction somewhat smaller than for the case of self-broadening of the linear molecules discussed in a subsequent section.

A second possible interaction is that arising from the polarization of molecule 2 by the dipole of molecule 1. This interaction varies as $\cos^2\theta$, where θ is the angle which μ_1 makes with the distance of closest approach b. Since the period of a microwave oscillation is long compared with the duration of a collision, μ_1 may be considered stationary during the collision. The torque exerted on the dipole thus averages to zero over the collision and, as a first approximation, the interaction vanishes. By considering collision-induced transitions other than the pure inversion discussed above, Anderson[4] calculated some finite collision diameters which are, however, considerably smaller than either kinetic theory ones, or observed microwave values.**

DIPOLE-QUADRUPOLE BROADENING

From Table II, we observe that many microwave diameters greatly exceed the kinetic theory diameters, implying the operation of some long range forces. We suggest that the important interactions in these cases are between the ammonia dipole moment and the quadrupole moment Q of the colliding molecule. Since these interactions vary as the inverse fourth power of the radius, they can give rise to large collision diameters. We should note that collision broadening differs from Van der Waal's interactions in that the former, in the microwave region, involves only the anisotropic part of the interaction potential,[4] as the isotropic part cannot induce transitions. Thus, it is possible for the largely isotropic polarization energies to play so important a role in Van der Waal's forces that quadrupole contributions can be neglected[10] while, conversely, quadrupole interactions sometimes assume the major role in microwave collision broadening.

If the colliding molecule 2 possesses no permanent dipole moment, averaged over the rotational motion, but does possess a permanent quadrupole moment†† Q, then the interaction energy of this quadrupole with a dipole is given by [11]

$$H=\tfrac{3}{4}\mu_1(Qe/r^4)[\cos\theta_1'(1-3\cos^2\theta_2') +2\cos\theta_2'\sin\theta_2'\sin\theta_1'\cos(\phi_1'-\phi_2')], \quad (9a)$$

where θ_1', θ_2', ϕ_1', and ϕ_2' are the polar and azimuthal angles of dipole and quadrupole with respect to the r axis. In terms of the polar angles θ and ϕ with respect to the impact parameter b (constants of the motion), then

$$H=\tfrac{3}{4}\mu_1(Qe/r^4)\cos\psi[(1-3\cos^2\theta_2) +2\cos\theta_2\sin\theta_2\sin\theta_1\cos(\phi_1-\phi_2) +5\sin^2\psi\{\cos\theta_1(\cos^2\theta_2-\sin^2\theta_2\cos^2\phi_2) -2\cos\theta_2\sin\theta_1\sin\theta_2\cos\theta_1\cos\phi_2\}] \quad (9b)$$

plus terms in $\sin\psi\cos\psi$. Here $r^2=b^2+\bar{v}^2t^2$; $\sin\psi=\bar{v}t/r$. Substituting (9b) in (4), integrating, and averaging the magnitude of the interaction over the angles yields‡‡

$$|a_{jk}|=\frac{0.42\mu Qe}{\hbar b^3\bar{v}}=\frac{1}{2}. \quad (10)$$

For the ammonia 3,3 line, $Q=2.09b^3\bar{v}$.

Quadrupole moments evaluated from the microwave values of b are given in Table II. The values appear to be consistent with the molecular structure, although an independent check from other physical data, unfortunately, is not possible in most cases. The self-broadening of HCN, ClCN, and OCS, however, furnish corrobatory evidence, as discussed in the next section.

SELF-BROADENING OF LINEAR MOLECULES

The self-broadening of linear molecules in the infrared region has been the subject of much experimental and theoretical investigation.[4, 9, 12] In this region, the important interactions are rotational resonance and second-order Keesom alignment forces. We have already seen that, except for the special case of ammonia self-broadening, rotational resonance is relatively unimportant in the microwave region owing to the scarcity of colliding molecules with low J values. The general formula for the alignment interactions may be specialized to the case where J_2 of the colliding molecule is much greater than J_1 of the radiating molecule. In

** Anderson has recently considered the interactions between the ammonia quadrupole moment (arising from the displacement of the dipole moment from the molecular center of gravity) and induced dipole moments. These interactions give close agreement with theory for argon, helium, hydrogen, and oxygen—with, however, slight disagreements suggesting the presence of quadrupole moments for oxygen and, less definitely, hydrogen (private communication).

[10] F. London, Zeits. f. Physik **63**, 245 (1930).

†† For a linear rotating molecule this is equal to ½ the amount of the static molecule, and is perpendicular to the plane of the motion. Our Q is twice Margenau's Θ/e.

[11] H. Margenau, Rev. Mod. Phys. **11**, 1 (1939).

‡‡ We note that with increasing "hardness" of the interaction, agreement between our simple assumptions and Anderson's averaging should become better. Since we have fitted our constants to agree with an inverse cube interaction, however, this means they will not agree quite so well with an inverse fourth power law, as is the case for dipole-quadrupole interactions. The over-all effect will be that our calculated Q values will be too small by a few percent. This error is approximately compensated by neglect of other interactions in computing Q.

[12] E. Lindhohn, Zeits. f. Physik **109**, 223 (1938).

TABLE III. Calculated and observed microwave collision diameters for linear molecules.

Molecule	[b] microwave $\times 10^8$ [a]	[b] theoretical $\times 10^8$
OCS	8.6	6.3
ClCN	17.7	16.8
HCN	14.7	12.7

[a] Townes, Holden, and Merritt, Phys. Rev. **74**, 1113 (1948). Smith, Gordy, Simmons, and Smith, Phys. Rev. **75**, 260 (1949).

this case, the second-order interaction $\langle H_2\rangle_{Av}$ is given by

$$\langle H_2\rangle_{Av}=\tfrac{1}{3}(\mu^4/r^6E_{J2}), \tag{11}$$

where E_{J2} is the average rotational energy of the colliding molecule $=kT=4.1\times10^{-14}$ erg. The interaction energy calculated from Eq. (11) may be compared with that from Eq. (9b) averaged to be $H=\frac{1}{3}(\mu_{jk}Qe/r^4)$. For OCS the dipole-quadrupole interaction at 7.5 angstroms is a factor of 18 greater than the alignment interaction. For HCN at 14 angstroms, the discrepancy is reduced to a factor of 2.6. For dipole moments of 3×10^{-18} or more the alignment interactions become predominant.

In Table III, experimental collision diameters (calculated from the published line widths) are compared with the theoretical ones from Eq. (10), using the dipole and quadrupole moments listed in Table II. The theoretical collision diameters are somewhat smaller than the observed values. We interpret this to mean that for low dipole moments the neglected higher order interactions are important, and for high dipole moments the Keesom alignment interactions are important. For HCN and ClCN however, the dipole-quadrupole interactions are a satisfactory first approximation to the interaction energy.

CORRELATION OF QUADRUPOLE MOMENTS WITH MOLECULAR STRUCTURE

In interpreting our quadrupole moment data, we shall visualize a non-rotating linear molecule as having point charges at the nuclei, and a uniform negative charge density ρ (depending on the bond) between the nuclei. Thus our observed Q value for the rotating molecule is equal to $\Theta/e=\sum \rho_i x_i^2$ for the stationary molecule, as compensating factors of two cancel in the definition of Q and the transition from linear to rotating molecule. For nitrogen, with $Q=0.27\times10^{-16}$ cm^2 (nuclear separation $=1.10$A) this model gives positive charges of $0.6e$ on each nitrogen nucleus—i.e., the distortion from spherical symmetry is equivalent to $0.4e$ per bond. Our upper bound for the quadrupole moments of hydrogen and oxygen is about 0.1×10^{-16} cm^2—one-third the observed value for nitrogen. This bound is of the same magnitude as London's estimate[10] of Q for $H_2=0.08\times10^{-16}$ cm^2. Furthermore the small Q for oxygen suggests that its bond more closely resembles a single bond than a double bond.¶¶ This single bond hypothesis for oxygen was originally suggested by London in interpreting the paramagnetism and reactivity of oxygen.[13]

Interpretation of the quadrupole moments of CO_2 and CS_2 is a little more complex as the bond dipole moments of these molecules can also contribute to the quadrupole moment of the rotating molecule. The slight difference in electronegativity between carbon and sulfur should permit us to ignore the dipole moment contributions here however. Thus calculations similar to those for nitrogen, utilizing the C−S deparation of 1.55A, gives positive charges of $0.4e$ on each sulfur nucleus and $0.8e$ on the carbon nucleus—i.e., the distotion per bond is the same for CS_2 as for N_2. Lest we extrapolate this simple picture too far, however, we note that this model gives for hydrogen a Q of only 0.04×10^{-16} cm^2, a value consistent with our measurements, but only half the theoretical value. Also, we may note that calculations for CO_2 show approximate cancellation of the homopolar and the bond dipole contributions to the over-all quadrupole moment. Thus our present picture is to be considered as qualitative only, but the observed moments should serve as valuable checks on more quantitative theories.

It is possible to deduce from the observed quadrupole moments of simple molecules the homopolar quadrupole moment per bond. Our data indicates a proportionality of bond quadrupole moment to bond order N times the square of the bond length, so that

$$Q\cong0.07r^2N. \tag{12}$$

This relation gives quadrupole moments about a factor of five smaller than those proposed by Lassettre and Dean to explain internal rotation phenomena.[14]

We wish to thank Professors W. O. Gordy and W. M. Nielsen for their interest and encouragement in this problem. We have benefited from conversations and correspondence with many people, especially P. W. Anderson, B. Bleaney, and J. H. Van Vleck.

¶¶ The prevalent interpretation is that oxygen possesses essentially a double bond. Our quadrupole observations do not constitute a disproof of this picture, but do cast some doubt on it.

[13] F. London, Zeits. f. Physik **50**, 24 (1928).

[14] E. N. Lassettre and L. B. Dean, Jr., J. Chem. Phys. **17**, 317 (1949).

Polarization of Neutrons and Protons by Scattering*

JOSEPH V. LEPORE
Institute for Advanced Study, Princeton, New Jersey
(Received January 23, 1950)

Neutrons and protons can be polarized by scattering provided there is a spin-orbit interaction between the incident particle and the scattering nucleus. The polarization effect has been found for a nucleus of spin zero allowing for the possibility of resonance scattering. Particular attention has been paid to the resonance scattering of neutrons by He^4 where almost full polarizations can be obtained, together with large cross sections. The polarization can be detected by a double scattering experiment, since the second scattering will be axially asymmetric with respect to the direction of the first scattered neutron. The existence of this effect and a preliminary treatment of it was first pointed out by Schwinger.

The scattering of polarized neutrons by protons has been studied for potentials suggested by the symmetrical, charged and neutral meson theories. The polarization effect on the differential cross section is negligible for the symmetrical theory, but is significant for the other two.

I. INTRODUCTION

THE scattering of neutrons by He^4 has been studied by various investigators[1] who have shown that there is an anomaly in the scattering in the region of 1 Mev (incident neutron energy). This anomaly has been attributed to the existence of a P-resonance associated with the formation of an unstable He^5 nucleus. Recently, Koontz and Hall[2] measured the differential cross section for various neutron energies in the region 0.8 to 1.6 Mev and thus established the existence of strong P-scattering. This confirmed the earlier conclusions[1] that the anomaly is due to a P-resonance. Under the assumption that P-resonant scattering but only ordinary S-scattering is involved[3] Koontz and Hall were able to show that the P-resonance must be split into $^2P_{3/2}$ and $^2P_{1/2}$ components. This splitting must therefore arise from some spin-orbit interaction.[4] The scattering can be qualitatively accounted for on the basis of the following parameters.

$$E_{1/2}=1.0 \text{ Mev} \quad \sin^2\delta_0=0.5$$
$$E_{3/2}=1.3 \text{ Mev} \quad \Gamma=0.3 \text{ Mev}, \quad \delta_0<0.$$

Here $E_{1/2}$, $E_{3/2}$ are the relevant resonance energies, Γ is their common width, and δ_0 is the S phase shift.

In consequence of the large splitting between the levels, the incident neutron is effectively subjected to a strong spin-orbit force which manifests itself in a polarization of neutrons scattered through a definite angle. The spin-orbit force can cause a neutron incident with a given spin direction to reverse this direction upon being scattered. The scattered wave will thus consist of two parts which represent those particles which have reversed their spin and those scattered with spin direction unchanged. The amplitudes of these two parts of the scattered wave will be different in their angular dependence so that for a given angle of scattering there will be some net spin direction.

The polarization effect can be detected by a double scattering experiment. Thus a beam polarized by scattering can be scattered again by a second nucleus and the polarization can be detected, since the differential cross section for the second scattering will now be axially asymmetric with respect to the direction of the first scattered neutron. This asymmetry arises since the scattering is now dependent upon two space vectors of the system, i.e., the beam direction and the polarization, so that the axial arbitrariness of the first scattering is absent. This effect and a preliminary treatment of it was first given by Schwinger.[5] Other discussions of polarization effects have been given by Wolfenstein[6] and Hammermesh.[7]

II. THE POLARIZATION FORMULA

Although the foregoing remarks were directed toward the case of helium scattered neutrons, it is clear that the same type of polarization effect can be expected for any nucleus of spin zero which shows a resonance of arbitrary angular momentum for the scattering of either neutrons or protons.

The polarization resulting when charged particles of spin $\frac{1}{2}$ are scattered by a nucleus with charge Z will now be calculated. The differential cross section for this process was first found by Bloch.[8] The method to be used here is somewhat different from his, however, since the polarization effect is of primary importance. This can be most easily treated by representing the wave functions describing the scattering directly in terms of the vectors $\boldsymbol{\sigma}$, $\mathbf{k}_0$ and $\mathbf{k}$ which are the Pauli spin vector of the incident particle, and its direction of incidence and scattering, respectively. This permits an elegant derivation of the polarization formula.[9]

* The first section of this paper constituted part of a thesis submitted to Harvard University (May, 1948).

[1] Williams, Shepherd, and Haxby, Phys. Rev. **52**, 390 (1937); H. Staub and W. E. Stephens, Phys. Rev. **54**, 236 (1938) and **55**, 131 (1939); H. Staub and H. Tatel, Phys. Rev. **58**, 822 (1940).

[2] P. G. Koontz and T. A. Hall, Phys. Rev. **72**, 196 (1947).

[3] L. Eisenbud, Phys. Rev. **74**, 1206 (1948) throws doubt on this conclusion.

[4] S. M. Dancoff, Phys. Rev. **58**, 327 (1940).

[5] J. S. Schwinger, Phys. Rev. **69**, 681 (1946).

[6] L. Wolfenstein, Phys. Rev. **75**, 1664 (1949).

[7] M. Hammermesh, Phys. Rev. **75**, 1281 (1949).

[8] F. Bloch, Phys. Rev. **58**, 829 (1940).

[9] This method was kindly pointed out to me by Professor Schwinger.

The incident beam may be taken as

$$\psi_{\text{inc}}=\exp i[\mathbf{k}_0\cdot\mathbf{r}-\alpha\ln 2kr]\cdot\chi_{\text{inc}}. \quad (1)$$

Here χ_{inc} is a spin function which represents the polarization of the incident beam

$$\mathbf{P}_{\text{inc}}=(\chi_{\text{inc}},\,\boldsymbol{\sigma}\chi_{\text{inc}}). \quad (2)$$

The constant α is

$$\alpha=(Ze^2\mu)/(kh^2). \quad (3)$$

It is now necessary to find a solution of the Schroedinger equation which satisfies the boundary condition of asymptotically representing an incoming wave of the form (1) together with a diverging spherical wave

$$\psi\sim\psi_{\text{inc}}+\frac{\exp i[kr-\alpha\ln 2kr]}{r}f(\theta)\chi_{\text{inc}}. \quad (4)$$

In virtue of the spin-orbit interaction which we wish to include in the description the vector, $\mathbf{L}$, of the orbital angular momentum is no longer a constant of the motion so that the motion must be described in terms of the total angular momentum

$$\mathbf{J}=\mathbf{L}+\tfrac{1}{2}\boldsymbol{\sigma}. \quad (5)$$

The required set of commuting constants of the motion is

$$\mathbf{J}^2,\ J_z,\ \mathbf{L}^2,\ \boldsymbol{\sigma}^2. \quad (6)$$

The incident beam (1) can now be decomposed, asymptotically, into its constituent orbital angular momenta

$$\psi_{\text{inc}}\sim\sum_{l=0}^{\infty}(2l+1)^{\frac{1}{2}}i^l\frac{\sin(kr-l\pi/2-\alpha\ln 2kr)}{kr}\times Y_l^0(\cos\theta)\chi_{\text{inc}}. \quad (7)$$

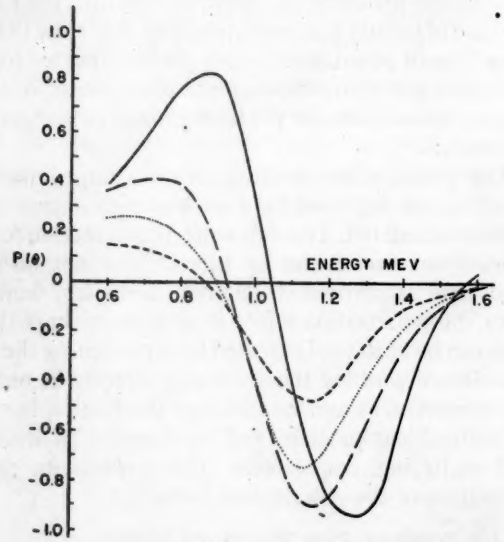

FIG. 1. The calculated degree of polarization, $P(\theta)$, as a function of the incident neutron energy, for scattering angles. $\theta=30°$, 45°, 60°, 90°. ——— Polarization at $\theta=90°$; — — Polarization at $\theta=60°$; ····· Polarization at $\theta=45°$; – – – – Polarization at $\theta=30°$.

It is now necessary to express this incident beam in terms of the proper functions of the operators (6). This resolution is most easily accomplished through the medium of the following projection operators.

$$\Pi_l^+=\frac{l+1+\boldsymbol{\sigma}\cdot\mathbf{L}}{2l+1},\quad \Pi_l^-=\frac{l-\boldsymbol{\sigma}\cdot\mathbf{L}}{2l+1}. \quad (8)$$

Π_l^+ is so constructed that when applied to a function of the type $Y_l^0\chi_{\text{inc}}$ it destroys all those states within this function for which $J=l-\frac{1}{2}$ and selects out only those states with $J=l+\frac{1}{2}$. Π_l^- similarly destroys all states with $J=l-\frac{1}{2}$. These operators clearly satisfy the condition

$$\Pi_l^++\Pi_l^-=1. \quad (9)$$

We can now attempt to find a solution to the scattering problem by writing the wave function for the system in the asymptotic form

$$\psi\sim\sum_{l=0}^{\infty}(2l+1)^{\frac{1}{2}}i^l\left[A_l^+\Pi_l^+\frac{u_l^+(kr)}{kr}+A_l^-\Pi_l^-\frac{u_l^-(kr)}{kr}\right]Y_l^0\chi_{\text{inc}}. \quad (10)$$

Here A_l^+ and A_l^- are constants to be determined by the condition that ψ have the form (4). The radial functions are

$$u_l^\pm(kr)=\sin(kr-l\pi/2-\alpha\ln 2kr+\delta_l^\pm), \quad (11)$$

where $\delta_l^\pm$ is a phase shift which describes the effect of Coulomb, nonresonance, and resonance scattering and may be written in this order as

$$\delta_l^\pm=\alpha_l+\beta_l^\pm+\gamma_l^\pm. \quad (12)$$

α_l is the ordinary phase shift due to the Coulomb field

$$\alpha_l=\arg\Gamma(l+i\alpha). \quad (13)$$

$\beta_l^\pm$ is the shift due to ordinary potential scattering and $\gamma_l^\pm$ is that due to the presence of the resonance which may be taken into account by writing

$$\tan\gamma_l^\pm=\Gamma_l^\pm/(E_l^\pm-E). \quad (14)$$

E is the energy of the incident particle, $E_l^\pm$ is the resonance energy and $\Gamma_l^\pm$ is its width.

After the coefficients $A^\pm$ of Eq. (10) have been determined the scattered wave

$$\psi_{\text{scatt}}=\psi-\psi_{\text{inc}} \quad (15)$$

is given by

$$\psi_{\text{scatt}}\sim\frac{\exp[i(kr-\alpha\ln 2kr)]}{kr}\sum_{l=0}^{\infty}\frac{1}{(2l+1)^{\frac{1}{2}}}\times\{[(l+1)\exp(i\delta_l^+)\sin\delta_l^++l\exp(i\delta_l^-)\sin\delta_l^-]Y_l^0+(\exp(i\delta_l^+)\sin\delta_l^+-\exp(i\delta_l^-)\sin\delta_l^-)\boldsymbol{\sigma}\cdot\mathbf{L}Y_l^0\}\chi_{\text{inc}}. \quad (16)$$

If $\mathbf{k}$ is the direction in which the scattering is observed it can easily be verified that the term $\boldsymbol{\sigma}\cdot\mathbf{L}Y_l^0$ can be written as

$$-i\sin\theta\frac{\partial}{\partial(\cos\theta)}Y_l^0\boldsymbol{\sigma}\cdot\mathbf{n}. \tag{17}$$

The vector $\mathbf{n}$ is the normal to the plane in which the scattering occurs defined by

$$\mathbf{k}\times\mathbf{k}_0=\mathbf{n}k^2\sin\theta. \tag{18}$$

The angular function $f(\theta)$ defined by (4) may now be written as

$$f(\theta)=A(\theta)+\boldsymbol{\sigma}\cdot\mathbf{n}B(\theta), \tag{19}$$

where

$$A(\theta)=\frac{1}{k}\sum_{l=0}^{\infty}\frac{1\sqrt{4\pi}}{(2l+1)^{\frac{1}{2}}}$$
$$\times[(l+1)\exp(i\delta_l^+)\sin\delta_l^++l\exp(i\delta_l^-)\sin\delta_l^-]Y_l^0$$
$$B(\theta)=-\frac{i\sin\theta}{k}\frac{\partial}{\partial(\cos\theta)}\sum_{l=0}^{\infty}\frac{1\sqrt{4\pi}}{(2l+1)^{\frac{1}{2}}}$$
$$\times[\exp(i\delta_l^+)\sin\delta_l^+-\exp(i\delta_l^-)\sin\delta_l^-]Y_l^0. \tag{20}$$

From (19) we determine the differential cross section to be

$$\sigma(\theta)=(AA^*+BB^*)\left[1+\frac{A^*B+B^*A}{AA^*+BB^*}\mathbf{P}_{\text{inc}}\cdot\mathbf{n}\right]. \tag{21}$$

The second term within the bracket gives the effect of a polarized incident beam.

The polarization of the scattered beam is given by

$$\mathbf{P}=\frac{(f(\theta)\chi_{\text{inc}},\ \boldsymbol{\sigma}f(\theta)\chi_{\text{inc}})}{(f(\theta)\chi_{\text{inc}},\ f(\theta)\chi_{\text{inc}})}. \tag{22}$$

Using (19) this becomes

$$\mathbf{P}=\frac{AA^*\mathbf{P}_{\text{inc}}+(AB^*+B^*A^*)\mathbf{n}+i(A^*B+B^*A)\mathbf{P}_{\text{inc}}\times\mathbf{n}+BB^*(2\mathbf{P}_{\text{inc}}\cdot\mathbf{n}\mathbf{n}-\mathbf{P}_{\text{inc}})}{AA^*+BB^*+(A^*B+B^*A)\mathbf{P}_{\text{inc}}\cdot\mathbf{n}}. \tag{23}$$

If the incident beam is unpolarized this reduces to

$$\mathbf{P}=\frac{AB^*+BA^*}{AA^*+BB^*}\mathbf{n}=P(\theta)\mathbf{n}. \tag{24}$$

Thus in this case the resulting polarization is directed along the normal to the scattering plane and is dependent upon the interference between the two parts of the scattered wave. Large polarizations can come about only when this interference term is comparable to the cross section itself.

III. DOUBLE SCATTERING

The question of a double scattering experiment is easily treated by comparing (24) and (21). If the first scattering takes place at an angle θ_1 and in a plane defined by $\mathbf{n}_1$ and if θ_2, $\mathbf{n}_2$ are the corresponding quantities for the second scattering the differential cross section becomes

$$\sigma(\theta)=(AA^*+BB^*)[1+P(\theta_1)P(\theta_2)\mathbf{n}_1\cdot\mathbf{n}_2] \tag{25}$$

for an originally unpolarized beam.

The asymmetry of the second scattered beam can be clearly shown by considering the case when both scatterings take place in the same plane. Then either $\mathbf{n}_1=\mathbf{n}_2$ or $\mathbf{n}_1=-\mathbf{n}_2$ and the ratio R of the scattered intensities for these two cases is

$$R=\frac{1+P(\theta_1)P(\theta_2)}{1-P(\theta_1)P(\theta_2)}. \tag{26}$$

Thus, if large polarizations can be obtained R can be quite large.

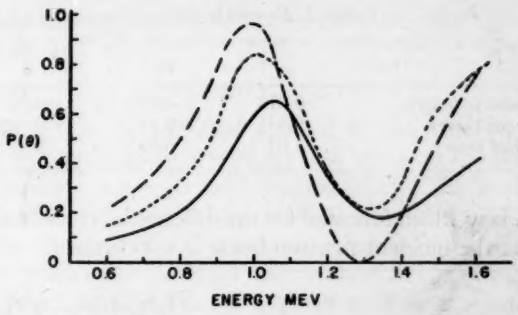

FIG. 2. The calculated degree of polarization, $P(\theta)$, as a function of the incident neutron energy, for scattering angles $\theta=120°$, 135°, 150°. — — Polarization at $\theta=120°$; - - - - Polarization at $\theta=135°$; ——— Polarization at $\theta=150°$.

IV. APPLICATION TO SCATTERING OF NEUTRONS BY HELIUM

If we apply our results to helium scattered neutrons, assuming resonant P scattering and ordinary nonresonant S scattering, the functions A and B of Eq. (20) become

$$A(\theta)=\frac{1}{k}\Big[\exp(i\delta_0)\sin\delta_0$$
$$+\left(\frac{\Gamma}{E_{3/2}-E-\frac{1}{2}i\Gamma}+\frac{1}{2}\frac{\Gamma}{E_{1/2}-E-\frac{1}{2}i\Gamma}\right)\cos\theta\Big]$$
$$B(\theta)=\frac{\sin\theta}{2ik}\left(\frac{\Gamma}{E_{3/2}-E-\frac{1}{2}i\Gamma}-\frac{\Gamma}{E_{1/2}-E-\frac{1}{2}i\Gamma}\right). \tag{27}$$

If we substitute these expressions in (21) they yield the

TABLE I. P—phase shifts.

	η_0	η_1	η_2
Symmetric theory	0.074	−0.054	−0.017
Charged theory	0.531	−0.114	−0.046
Neutral theory	−1.02	0.995	0.073

ordinary Bloch formula[6] for the differential cross section when the incident neutron beam is unpolarized.

The polarization to be expected for an initially unpolarized beam can be obtained from (24). If we introduce the abbreviations

$$x=(E_{3/2}-E_{1/2})/\Gamma,\quad x_{1/2}=(E_{1/2}-E)/\Gamma,\quad x_{3/2}=(E_{3/2}-E)/\Gamma \tag{28}$$
$$d_{1/2}=x_{1/2}^2+\tfrac{1}{4}\quad d_{3/2}=x_{3/2}^2+\tfrac{1}{4}$$

the degree of polarization[10] $P(\theta)$ can be written as

$$P(\theta)=\frac{\left[\left(\frac{1}{d_{1/2}}-\frac{1}{d_{3/2}}\right)\frac{\sin 2\delta_0}{4}-\left(\frac{x_{3/2}}{d_{3/2}}-\frac{x_{1/2}}{d_{1/2}}\right)\sin^2\delta_0-\frac{3}{4}\frac{x}{d_{1/2}d_{3/2}}\cos\theta\right]\sin\theta}{\left\{\sin^2\delta_0+\frac{1}{4}\left(\frac{1}{d_{1/2}}+\frac{1}{d_{3/2}}\right)-\frac{1}{2}\left(\frac{x_{1/2}x_{3/2}+\frac{1}{4}}{d_{1/2}d_{3/2}}\right)+\left[\left(\frac{x_{3/2}}{d_{3/2}}+\frac{1}{2}\frac{x_{1/2}}{d_{1/2}}\right)\sin 2\delta_0\right.\right.}$$
$$\left.\left.+\left(\frac{1}{d_{3/2}}+\frac{1}{2}\frac{1}{d_{1/2}}\right)\sin^2\delta_0\right]\cos\theta+3\left[\frac{1}{4}\frac{1}{d_{3/2}}+\frac{1}{2}\frac{(x_{1/2}x_{3/2}+\frac{1}{4})}{d_{1/2}d_{3/2}}\right]\cos^2\theta\right\}. \tag{29}$$

This expression has been used to calculate the polarization effects due to helium scattering of neutrons for the following parameters

$$x=1,\quad \sin^2\delta_0=0.5,\quad E_{1/2}=1.0,\quad E_{3/2}=1.3\ \text{(Mev)}. \tag{30}$$

The results are indicated in Figs 1 and 2. It is to be noted that there are regions of almost full polarization where the polarization does not vary too rapidly with energy and angle.

The effects of a double scattering experiment can be estimated directly from the graphs provided that the energy loss of the neutron at the first encounter

$$E_{\text{loss}}=[2m_nm_\alpha/(m_n+m_\alpha)^2]E(1-\cos\theta) \tag{31}$$

is taken into account. The result for the intensity ratio R can be determined from Eq. (26). Thus, for the case of neutron energy 1.2 Mev and scattering angle $\theta_1=90°$ (c.g. system) $P(\theta_1)=-0.85$. The energy loss at this angle of scattering is $E_{\text{loss}}=0.385$ Mev so that if the neutron is scattered again through $\theta_2=90°$, $P(\theta_2)=0.8$ the ratio R becomes

$$R=\frac{1+(0.85)(0.8)}{1-(0.85)(0.8)}=5.25. \tag{32}$$

V. SCATTERING OF POLARIZED NEUTRONS BY PROTONS

The scattering of neutrons by protons at 15.3 Mev has been discussed by Rarita and Schwinger[11] for various types of meson theories. It is of some interest to investigate the effect on their results if the incident neutrons were polarized. The results of their paper can be taken over almost completely, except that in performing averages over the spin we must average only over the spin direction of the scattering nucleus. Determination of the polarization effect can also be simplified by neglecting the states $^3D_1$ and $^3F_1$ and the variation of the $^3S_1$ phase shift with the magnetic quantum number. Neglect of the $^3D_1$ state is permissible for, on averaging over the spin of the nucleus, all polarization effects due to $S-D$ interference vanish. Polarization effects due to $P-D$ interference are, of course, very small compared with those arising from $S-P$ interference.

According to reference 11 the $^3P_0$ and $^3P_1$ components of the incident beam

$$3i\frac{g_1(kr)}{kr}\frac{\mathbf{k}_0\cdot\mathbf{r}}{kr}\chi_1^m \tag{33}$$

can be written as

$$^3P_0:\ \frac{1}{2}\frac{g_1(kr)}{kr}\frac{1}{2}(\boldsymbol{\sigma}_1-\boldsymbol{\sigma}_2)\cdot\frac{\mathbf{r}}{r}(\boldsymbol{\sigma}_1-\boldsymbol{\sigma}_2)\cdot\frac{\mathbf{k}_0}{k}\chi_1^m$$
$$^3P_1:\ \frac{3}{2}\frac{g_1(kr)}{kr}\frac{1}{2}(\boldsymbol{\sigma}_1+\boldsymbol{\sigma}_2)\cdot\frac{\mathbf{r}}{r}(\boldsymbol{\sigma}_1+\boldsymbol{\sigma}_2)\cdot\frac{\mathbf{k}_0}{k}\chi_1^m. \tag{34}$$

The $^3P_2$ component can be expressed as the difference between (33) and the sum of these two expressions.

The result for the scattering amplitude is, after the inclusion of $^3S_1$ scattering,

$$f(\theta)=\frac{1}{k}\left[S+A\frac{1}{2}(\boldsymbol{\sigma}_1-\boldsymbol{\sigma}_2)\cdot\frac{\mathbf{r}}{r}\frac{1}{2}(\boldsymbol{\sigma}_1-\boldsymbol{\sigma}_2)\cdot\frac{\mathbf{k}_0}{k}+B\frac{1}{2}(\boldsymbol{\sigma}_1+\boldsymbol{\sigma}_2)\cdot\frac{\mathbf{r}}{r}\right.$$
$$\left.\times\frac{1}{2}(\boldsymbol{\sigma}_1+\boldsymbol{\sigma}_2)\cdot\frac{\mathbf{k}_0}{k}+C\frac{\mathbf{k}_0\cdot\mathbf{r}}{kr}\right]\chi_{\text{inc}}{}^T, \tag{35}$$

[10] This expression was originally found by Schwinger and was applied to the case of 90° scattering (reference 5). I wish to thank Professor Schwinger for letting me see his result in this case.

[11] W. Rarita and J. Schwinger, Phys. Rev. **59**, 556 (1941).

where $\chi_{inc}{}^{T}$ is the triplet part of the incident spin function

$$\chi_{inc}{}^{T}=\tfrac{1}{4}(3+\boldsymbol{\sigma}_1\cdot\boldsymbol{\sigma}_2)\chi_{inc}. \tag{36}$$

The coefficients S, A, B, C depend on the phases η_0, η_1, η_2 due to ${}^3P_0$, ${}^3P_1$, ${}^3P_2$ scattering respectively and the S phase shift δ.

$$\begin{aligned} A&=(e^{i\eta_0}\sin\eta_0-e^{i\eta_2}\sin\eta_2)\\ B&=\tfrac{3}{2}(e^{i\eta_1}\sin\eta_1-e^{i\eta_2}\sin\eta_2)\\ C&=3e^{i\eta_2}\sin\eta_2 \quad S=e^{i\delta}\sin\delta. \end{aligned} \tag{37}$$

The differential cross section for triplet scattering can now be found from the relation

$$\sigma(\theta)=(f(\theta)\chi_{inc}{}^{T},\quad f(\theta)\chi_{inc}{}^{T}). \tag{38}$$

Insertion of $f(\theta)$ in this expression yields:

$$\begin{aligned} \sigma(\theta)=\sigma_0(\theta)+&\frac{\mathbf{P}_{inc}\cdot\mathbf{n}\sin\theta}{4k^2}\\ &\times\{[\tfrac{3}{2}\sin\eta_2\sin\eta_1\sin(\eta_2-\eta_1)\\ &+\sin\eta_2\sin\eta_0\sin(\eta_2-\eta_0)\\ &+3\sin\eta_1\sin\eta_0\sin(\eta_1-\eta_0)]\cos\theta\\ &+\sin\delta[-5\sin\eta_2\sin(\eta_2-\delta)\\ &+3\sin\eta_1\sin(\eta_1-\delta)\\ &+2\sin\eta_0\sin(\eta_0-\delta)]\}. \end{aligned} \tag{39}$$

Here $\sigma_0(\theta)$ is the ordinary cross section for unpolarized neutrons given in reference 11. The effect of the polarization is represented by the term in (39) proportional to the incident polarization, $\mathbf{P}_{inc}$.

The values for the P phase shifts calculated in reference 11 are indicated in Table I. The value of the ${}^3S_1$ phase shift δ has been taken as the average of the real parts of the ${}^3S_1$ phase shifts for magnetic quantum numbers $m=\pm1$ and 0. This value is $\delta=-1.67$. The contribution of the polarization to the cross section has been calculated from (39) and added to the ordinary unpolarized cross section found in reference 11 for ${}^3S_1+{}^3D_1$, ${}^1S$, and ${}^1P$ and ${}^3S_1$, ${}^3P$ interference. The results are:

Symmetric Theory

$$\begin{aligned} \sigma(\theta)d\omega=&0.606[(1-0.080\cos\theta+0.77\cos^2\theta)\\ &+\mathbf{P}_{inc}\cdot\mathbf{n}\sin\theta(0.017+0.001\cos\theta)]d\omega/4\pi. \end{aligned}$$

Charged Theory

$$\begin{aligned} \sigma(\theta)d\omega=&0.657[(1+0.126\cos\theta+0.042\cos^2\theta)\\ &+\mathbf{P}_{inc}\cdot\mathbf{n}\sin\theta(-0.183+0.030\cos\theta)]d\omega/4\pi. \end{aligned} \tag{40}$$

Neutral Theory

$$\begin{aligned} \sigma(\theta)d\omega=&0.852[(1+0.932\cos\theta+0.457\cos^2\theta)\\ &+\mathbf{P}_{inc}\cdot\mathbf{n}\sin\theta(0.047-0.513\cos\theta)]d\omega/4\pi. \end{aligned}$$

Thus the asymmetry is appreciable only for the two latter cases.

VI. CONCLUSION

Although the formulas derived in the first sections of this paper have not been applied to the case of proton scattering, a few general remarks can be made about this effect, since it is fully covered by our results. The large background scattering provided by the Coulomb field will tend to block the realization of full polarization. This can be achieved for neutron scattering, since the denominator of (24) (which is proportional to $\sigma(\theta)$) can become comparable to its numerator. For charged particles $\sigma(\theta)$ will contain the Rutherford scattering term and its interference with the specifically nuclear scattering so that full polarization may not be conveniently realized.

Polarization effects can come about regardless of whether a scattering resonance exists (e.g., $N-P$ scattering). One can expect such effects for He^4 scattering of neutrons in the region of 2.5 to 3.1 Mev since Barschall and Wheeler[12] have shown that the scattering at these energies can only be understood on the basis of a spin-orbit interaction which splits the P phases. Of course, the presence of a resonance is desirable, since it insures large cross sections.

The large intensity ratios which can be expected for the case of scattered neutrons in a double scattering experiment come about because in some of the cases (e.g., 90°), the polarization roughly reverses direction as one passes from one resonance level to the next, so that if the level splitting is comparable to the energy loss at the first encounter large polarizations occur at both scatterings and R is large.

Finally, it may be remarked that similar results might be expected for neutron scattering from carbon which appears to exhibit a resonance[13] of the helium type at energies of 3.6 and 4.1 Mev. For this nucleus, the energy loss for 90° scattering is $\frac{1}{6}$ of the energy of the incident neutron, so that for an incident neutron of energy 4.1 Mev the scattered neutron's energy is 3.4 Mev. Thus, one might hope that carbon exhibits effects similar to that of helium.

In conclusion, I wish to acknowledge my indebtedness to Professor Schwinger for suggesting the general problem of the production and detection of polarized neutrons and protons by helium scattering, as well as for showing me some of his earlier results and for his kind advice.

Note:† The referee has kindly called to my attention recent work[14,15] on helium scattered neutrons which casts serious doubt on its interpretation in terms of a doublet resonance with splitting comparable to the widths involved, and hence on the applicability

[12] J. A. Wheeler and H. H. Barschall, Phys. Rev. **58**, 682 (1940).
[13] Goldsmith, Ibser, and Feld, Rev. Mod. Phys. **19**, 266 (1947).
† This note was added March 16, 1950.
[14] T. A. Hall, Phys. Rev. **77**, 411 (1950).
[15] Bashkin, Petree, Mooring and Peterson, Phys. Rev. **77**, 748 (1950).

of the polarization curves herein presented. These results were prepared, however, not only to exhibit the effects to be expected in this case but were intended also to be illustrative of the general behavior of the polarization in the neighborhood of such a resonance.

The author does believe, however, that the situation in regard to helium scattering is still fluid in spite of the careful work of Bashkin *et al.* on the total cross section and will so remain until crucial experiments on the differential cross section have been performed.

PHYSICAL REVIEW VOLUME 79, NUMBER 1 JULY 1, 1950

Electrical Resistance of Thoria

W. E. DANFORTH AND F. H. MORGAN
Bartol Research Foundation of The Franklin Institute, Swarthmore, Pennsylvania
(Received March 6, 1950)

Measurements of the electrical conductivity of thoria were taken in vacuum at temperatures up to 2073°K. Activation by passage of current resulted in values of resistance as low as 1 ohm-cm at 1900°K and 10 ohm-cm at 1000°K. Activation energies between 3.2 volts and 0.58 volt were found. The density of impurity centers was computed as 10^{18} per cc and was found to be independent of the degree of activation by current, a result which is inconsistent with the hypothesis of the electrolytic origin of impurity centers.

I. INTRODUCTION

STUDIES of the electrical conductivity of thoria have obvious practical interest as regards cathode design and performance. In addition, there are several objectives of a theoretical nature. An understanding of the conduction mechanism is a necessary step in the understanding of the mechanism of thermionic emission and also of the causes of the disintegration of cathode material by passage of current. Previous investigations have been made by Foex[1] whose values of resistance are much higher than those we have found and by Wright[2] who briefly reported some data which have been found to fit satisfactorily into the general pattern of our observations.

II. EXPERIMENTAL PROCEDURE

Our measurements have been taken on sintered sleeves of thoria, mounted between molybdenum end pieces as indicated in Fig. 1. The material was molded to size and sintered. It was not pressed. The density was approximately 7 g/cm². Currents up to 7.6 amp./cm² were passed through the specimens and potentials were were measured at the probe leads, by oscilloscope for pulsed data, and high resistance voltmeter for the dc runs. Pyrometer readings were made on the inside of the specimen through a hole in one of the end pieces.

The specimens were mounted in a small vacuum furnace whose main features are shown in Fig. 2. The thoria piece, whose length was about 2 cm and outside diameter 3 mm, was supported within a coil of 60 mil tungsten.

The data to be presented were taken with this furnace mounted in a water-cooled copper jacket which was continuously pumped on a mercury system. Since the system contained one soft-soldered joint, it could not be baked at high temperature but was maintained at 100°C for 24 hours. Pressures were below 10^{-7} mm with a cold specimen but would rise to 5×10^{-6} mm at a specimen temperature of 1800°C, the maximum used at present.

III. RESULTS

Figure 3 shows the results of measurements taken on a specimen prepared from C.P. thoria from Eimer and Amend. Before any current was passed through the thoria it was outgassed at 1800° for several hours. Then runs of resistance *vs.* temperature were taken using single pulses, produced by a simple condenser discharge arrangement, and an oscilloscope.

For each one of these curves, several runs were taken, a smooth curve was drawn through the data, and points from this average curve were transferred to the logarithmic plot. The probable error estimated from the spread of the data is about 10 percent.

As shown in Fig. 3a, it was found that the data from pulse measurements require two exponential components, one with activation energy of 0.86 volt and the other of 3.2 volts. Activation energy is here defined as the quantity E in the Eq. $\sigma=\sigma_0 e^{-E/kT}$.

One must remember, of course, that we have a porous, sintered, specimen and not a crystal. It is perhaps appropriate, therefore, (following Loosjes and Vink[3]) to ascribe the low activation energy, the one predominant at the low temperature, to conductance through the solid particles, and the high temperature portions of the curve with a work function of 3.2 to thermionic emission across the interstices.

The pore-conduction hypothesis, however, is by no means established in the present case. It would, in fact,

[1] M. Foex, Comptes Rendus **215**, 534 (1942).
[2] D. A. Wright, Proc. Phys. Soc. London **B62**, 188 (1949).
[3] R. Loosjes and H. J. Vink, J. App. Phys. **20**, 884 (1949).

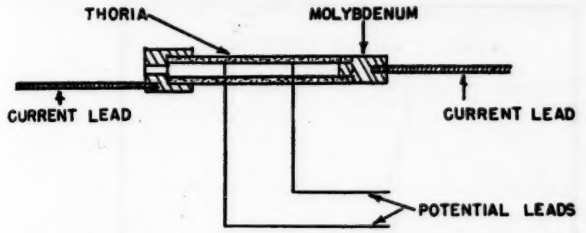

FIG. 1. Arrangement of conductivity specimen.

be just as plausible to assign the 3.2 volt activation to an intrinsic excitation. Spectroscopic evidence for the required intrinsic level is being sought.

Passage of 0.076 amp./cm² dc through the specimen causes immediate increase of conductivity by a large factor, after which the situation appears to be dominated by a single activation energy of 1.0 volt.

It is interesting to notice that the data of Wright[2] happen to fall within the probable error on this curve which we find as an activation state corresponding to a current density of 0.076 amp./cm².

Increasing the dc density further to values of 0.76 amp./cm² and then to 7.6 amp./cm² produced successive increases of the conductivity until values of resistivity as low as 1 ohm-cm at 1900°K and 10 ohm-cm at 1000°K were obtained. A specimen thus activated may be directly heated from room temperature by passage of current.

One naturally cannot take too seriously the application of semi-conductor theory to these sintered specimens. However, it may be of interest to note the following: As Wright has pointed out, if one uses the relation $n=\sigma/ev$ where σ is the conductivity, n the number of conduction electrons, e their charge, and v their mobility, and if one assumes a mobility of 10 cm/sec. per volt/cm one finds 10^{16} conduction electrons per cc at 1900°K. Then using the Fowler equation[4] with the observed activation energies one computes a density of impurity centers of 10^{18} per cc.

If we apply this same calculation to our most highly activated state we have the interesting result that the increase in conductivity produced by this increase of current is not accompanied by an increase in the number of impurity centers but would follow entirely from the observed decrease of activation energy. Otherwise stated, different conditions of activation by current show different values of E but the coefficient σ_0 tends to remain constant.

This result, that the activation by a current does not increase the number of impurity centers, is of course contrary to the view that the activation is caused by electrolysis of the material. Also it is questionable whether the electrolysis theory can explain the fact that the increase of activation takes place very quickly, in a few seconds. The time required to produce 10^{18} atoms even with our highest current of 7.6 amp./cm² will be several minutes if the percent ionic conduction is as low as we believe it to be; that is, 10^{-4} ion per electron. With our lowest current (0.076 amp./cm²) the calculated time exceeds the observed time by a factor of more than one thousand.

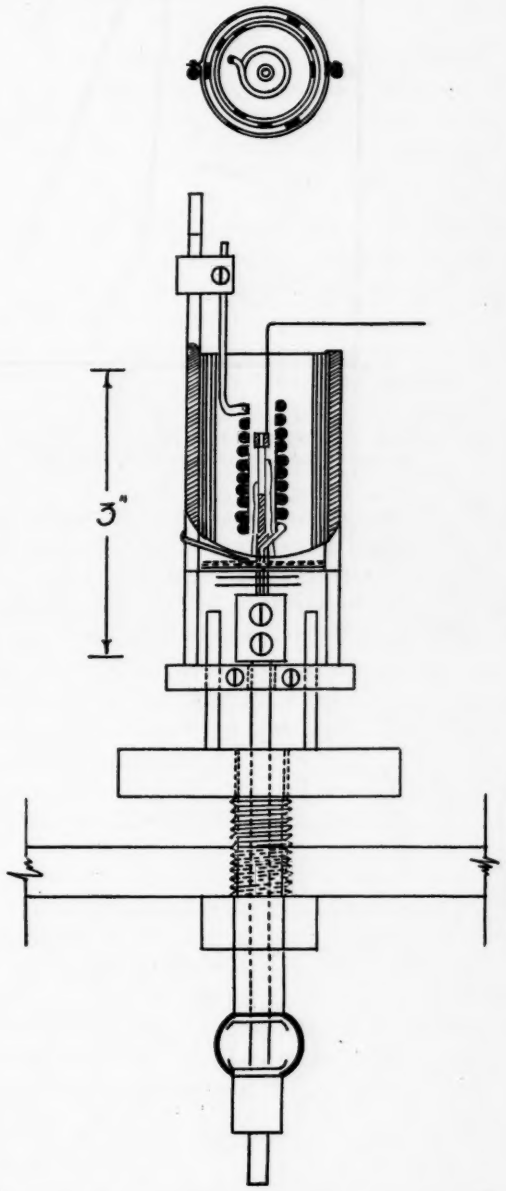

FIG. 2. Vacuum Furnace. The specimen is mounted within a tungsten coil which is surrounded by five coaxial molybdenum heat shields.

[4] $n=n_0^{\frac{1}{2}}\{(2\pi mkT)/h^2\}^{\frac{3}{4}}\exp(-U/2kT)$, where n=density of impurity centers. The quantity $U/2$, one half of the energy band separation, is equal to the observed slope of the curve of $\log\sigma$ *vs.* $1/T$ and is thereby empirically determined. There is admittedly some question as to whether the above equation is appropriate for analysis of this data or whether one should use the other limiting case in which the number of impurity centers is in excess of the number of available electrons (see N. F. Mott and R. W. Gurney, Electronic Processes in Ionic Crystals (Clarendon Press, 1940), Chapter V, Section 2). Pending further evidence in this matter, the simpler expression was chosen.

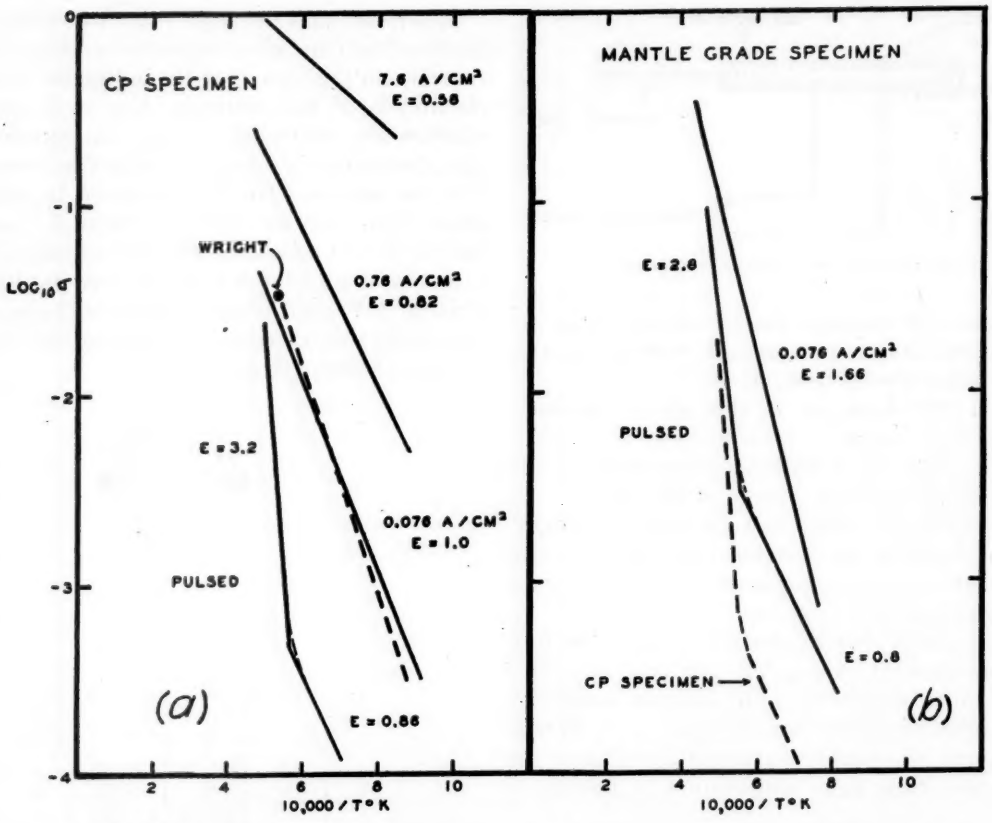

FIG. 3. Conductivity (σ) in (ohm-cm)$^{-1}$ for different states of activation-by-current. The curves marked *pulsed* represent data before any dc was permitted to flow. Values of E are activation energies in electron-volts.

On Fig. 3b we have data taken with mantle grade thoria, the dashed lines representing C.P. data from the preceding figure. As one might expect, the initial conductivity before activation by current is less for the purer material. A higher temperatures, where perhaps some intrinsic phenomen are occurring, the two materials give more nearly equal values of conductivity.

It is a pleasure to acknowledge the skilled services of Harry Bleecher, who constructed the apparatus and assisted in taking the measurements.

PHYSICAL REVIEW VOLUME 79, NUMBER 1 JULY 1, 1950

On Field Theories with Non-Localized Action

A. PAIS
Institute for Advanced Study, Princeton, New Jersey

AND

G. E. UHLENBECK
H. M. Randall Laboratory of Physics, University of Michigan, Ann Arbor, Michigan

(Received February 14, 1950)

It is investigated whether suitable generalizations of the field equations of current field theories to equations of higher order may be of help in eliminating the divergent features of the present theory. It turns out to be difficult, if feasible, to reconcile in this way the requirements of convergence, of positive definiteness of the free field energy, and of a strictly causal behavior of the state vector of a physical system. Progress may perhaps be made by relinquishing the condition of unlimited localizability of any space time event.

I. INTRODUCTION

CONSIDERABLE progress has been made during the last two years in our understanding of the scope and limitations of the present picture of systems of interacting particles and fields. Thus, noting that a theoretical subdivision of the experimental mass and experimental charge of the electron so far seems unwarranted from any observational point of view, a "renormalization program" has been worked out for the interaction of electrons and electromagnetic fields. This scheme has had great success in making such effects as the Lamb-Retherford shift of lines in the hydrogen atom and subtle anomalies in the magnetic moment of the electron amenable to theoretical interpretation.[1] Nor is the applicability of this evaluation technique limited to any power in a development in terms of the fine structure constant.[2]

Much less satisfactory, however, has been the outcome of investigations on the application of renormalization ideas to other systems of particles and fields.[3] In the domain of nuclear phenomena in particular one still encounters many difficulties. Not only do calculations of certain so-called reactive effects still yield divergent results,[4] but even if finite, one often finds results which are quantitatively inconsistent with experimental data. A striking instance is, for example, the ratio of the "extra" magnetic moment of the proton to the difference between this moment and the magnetic moment of the neutron.[5] It is true that such results cannot be considered definitive in view of the dubiousness of the power series approximation underlying these theoretical derivations. Yet the generally unsatisfactory situation in the theory of nuclear interactions makes it difficult to escape the conclusion that the Maxwell-Yukawa analogy, however suggestive in many of its qualitative predictions, is inadequate and that in the region of small distances (presumably starting at ranges of the order of the nucleon Compton wave-length) novel theoretical features must be anticipated.

It has often been suggested that the typical divergent features of present theories may well be due to overlooking intimate relations between elementary particles of various kinds.[6] However this may be, the apparent lack of connections between such particles as well as between the various dimensionless constants representative of interaction strengths calls for more compact methods of formulation, with the ultimate ideal of the predictability of particles from deeper lying principles.

Now, whether or not the answer to such questions will eventually lead us outside the domain of concepts embodied by relativity and complementarity, it seems worth while at this stage to ask for models which lead to convergent answers. An apparently appealing model of this type can be obtained as follows.

The electromagnetic as well as the meson field equations are generally of the prototype

$$(\Box-\kappa^2)\psi=\rho, \tag{1}$$

where ρ is the source creating a field described by ψ. Depending on the transformation properties of ψ and ρ one has scalar, vector fields, etc.; $\kappa=0$ corresponds to photon, and $\kappa\neq 0$ to meson fields. Finally, the reality properties of ψ determine the charged or neutral character of the field. Now consider instead of (1) an equation of the prototype

$$F(\Box)\psi=\rho \tag{2}$$

[1] S. Tomonaga *et al.*, Prog. Theor. Phys. **1**, 27 (1946); **2**, 101 (1947); **4**, 47, 121 (1949). J. Schwinger, Phys. Rev. **74**, 1439 (1948); **75**, 651 (1949); **76**, 790 (1949). R. Feynman, Phys. Rev. **74**, 1430 (1948); **76**, 749, 769 (1949).

[2] F. J. Dyson, Phys. Rev. **75**, 486, 1736 (1949).

[3] See P. T. Matthews, Phys. Rev. **76**, 1254 (1949); Phil. Mag. **41**, 185 (1950); also D. Feldman, Phys. Rev. **76**, 1369 (1949) for electromagnetic properties of vector mesons.

[4] As, e.g., the nucleon magnetic moment calculated on the basis of the vector meson theory [see K. Case, Phys. Rev. **75**, 1440 (1949)]. In our present state of limited knowledge it seems premature to conclude from the occurrence of such infinities to the non-existence of certain particles or certain interactions concerned.

[5] K. Case, Phys. Rev. **76**, 1 (1949); J. Luttinger, Helv. Phys. Acta **21**, 483 (1948); M. Slotnick and W. Heitler, Phys. Rev. **75**. 1645 (1949); S. Borowitz and W. Kohn, Phys. Rev. **76**, 818 (1949),

[6] See attempts to eliminate divergences by compensation: A. Pais, Phys. Rev. **68**, 227 (1945); Verh. Kon. Ac. Wetenschappen, Amsterdam **19**, 1 (1947); S. Sakata and O. Hara, Prog. Theor. Phys. **2**, 30, 145 (1947).

where

$$F(\Box)=\prod_{i=1}^{N}(\Box-\kappa_i^2). \tag{3}$$

That this is a model of the type we want is clear. First, (2) describes quanta of rest mass[7] κ_i and thus in a trivial way unites particles of various kinds. Second, these particles are all bound with the same strength to the source ρ. Third, an equation like (2) leads to a less divergent behavior of ψ at points near the source ρ than (1) does: take, for example, for ρ a point source with strength g: $\rho=g\delta(\mathbf{x})$. Then the static potential following from (2) and defined by

$$F(\Delta)\psi=g\delta(\mathbf{x})$$

is

$$\psi(r)=\frac{g}{2\pi^2 r}\int_0^\infty kdk\frac{\sin kr}{F(-k^2)},$$

where r is the distance from the source. The strong increase of F with increasing k leads to a decrease of ψ for small r. In fact, taking in (3) $N=2$, $\kappa_1\neq\kappa_2$, we have

$$\psi(r)=(g/4\pi r)[\exp(-\kappa_1 r)-\exp(-\kappa_2 r)] \tag{4}$$

which is already singularity free at the origin.

It is the aim of this paper to develop the quantum field theory of equations of the type (2). Clearly Eq. (2) can, in the absence of sources, be derived from the following action integral

$$L=\int\psi F(\Box)\psi d_4x, \tag{5}$$

the integration being extended over the whole four-dimensional space-time (volume element d_4x). Equivalently (5) can be written as

$$L=\int\mathfrak{L}d_4x,\quad \mathfrak{L}(x_\mu)=\int\psi(x)\epsilon(x-x')\psi(x')d_4x' \tag{6}$$

where

$$\epsilon(x_\mu)=\frac{1}{(2\pi)^4}\int d_4k\,\exp(ik_\mu x_\mu)F(-k_\mu^2) \tag{7}$$

is essentially the Fourier transform of F. For a general F containing arbitrarily high powers of $\Box$—we will in fact admit that N in (3) may tend to infinity provided the infinite product thus arising is mathematically well defined—it is readily seen from (6) that the Lagrangian density $\mathfrak{L}(x_\mu)$ will generally depend on the field variables at finite distances $x_\mu'-x_\mu$ from the world point under consideration. Following a terminology introduced by Dirac[8] we can thus say that the present type of theory is characterized by a non-localized action.[9] The relativistic invariance of L guarantees the existence of a symmetric divergence free energy momentum tensor.[10] Thus, energy and momentum densities can be constructed which, like $\mathfrak{L}$, have non-localized characteristics.

Various investigations have been made of theories of this kind from a classical point of view. In particular, the work of Bopp[11] should be noted; this author studied especially the following generalization of the electromagnetic theory:[12]

$$\Box(\Box-\kappa^2)A_\mu=-j_\mu \tag{8}$$

and showed that it leads to a classical theory which is not only singularity free and goes over into the conventional theory for distances $\gg\kappa^{-1}$ (κ can be chosen conveniently large), but also does not exhibit the so-called runaway solutions which so often occur in attempts to eliminate classical infinities.[13] Thus if one considers, for instance, a harmonically bound particle to be the source of the field A_μ, the net radiation reaction on the particle always leads to a damping, notwithstanding the fact that the radiation field corresponding to (8) consists of an electromagnetic field and of a mesonic field, the latter having the disagreeable property of being negative definite. One would expect that such negative energy radiation would somehow lead to trouble and it has indeed been shown by Feynman[14] that situations may arise in which this is the case.

The quantum-mechanical radiation field (8) consists of an assembly of photons of positive definite and of neutral vector mesons with a negative definite energy. The negative quanta lead to even graver difficulties in quantum theory than in classical theory.[15] In Section III-A-2 we will discuss this aspect for the general Eqs. (2) and (3), and it will turn out that while formally any such equation leads to a finite self-energy for the electron in the hole theory as long as $N>1$, the non-definiteness makes such equations inacceptable. The same

[7] Throughout this work we put $\hbar=c=1$.

[8] P. A. M. Dirac, Phys. Rev. **73**, 1092 (1948).

[9] The function $\psi(x)$ itself is, however, still perfectly localized. The recent suggestion of Yukawa [Phys. Rev. **76**, 300 (1949); **77**, 219 (1950)] to consider non-localized fields, i.e., systems in which $\psi(x)$ itself is replaced by a non-localized entity, thus constitutes a departure of a different nature from equations like (1); see however M. Fierz, Phys. Rev. **78**, 183 (1950).

[10] See F. Bopp, Zeits. f. Naturforschung **1**, 237 (1946); T. Chang, Proc. Camb. Phil. Soc. **42**, 132 (1946); **44**, 76 (1948); J. deWet, Proc. Camb. Phil. Soc. **44**, 546 (1948); Proc. Roy. Soc. **A195**, 365 (1949); H. S. Green, Proc. Roy. Soc. **A197**, 73 (1949).

[11] F. Bopp, Ann. d. Physik **38**, 345 (1940); **42**, 572 (1943); Zeits. f. Naturforschung **1**, 53 (1946).

[12] This equation has also been proposed by A. Landé and L. Thomas, Phys. Rev. **60**, 121, 514 (1940); **65**, 175 (1944); by B. Podolski *et al.*, Phys. Rev. **62**, 68 (1942); **65**, 228 (1944); by D. Montogomery, Phys. Rev. **69**, 117 (1947); and by A. Green, Phys. Rev. **72**, 628 (1947). See also B. Podolski and P. Schwed, Rev. Mod. Phys. **20**, 40 (1948). Recently, a discussion along similar lines has been given by L. deBroglie, Comptes Rendus **229**, 157, 269, 401 (1949).

[13] See P. A. M. Dirac, Proc. Roy. Soc. **A167**, 148 (1938); W. Wessel, Ann. d. Physik **43**, 565 (1943).

[14] R. P. Feynman, Phys. Rev. **76**, 939 (1948); see especially p. 945.

[15] See A. Pais, reference 6, Chapter II. §7; P. T. Matthews, Proc. Camb. Phil. Soc. **45**, 441 (1949).

holds *mutatis mutandis* for "multi-meson equations" of the types (2) and (3) involving coupling with nucleons (see III-A-2).

The final results for self-energies on the basis of (2) and (3) are essentially equivalent to those obtained by Pauli and Villars[16] by means of the "regulator-procedure" with the single difference however that the "regulator condition" for the self-energy here follows automatically (see III-A-2).

It should also be noted that (see III-A-4) the negative energy difficulties remain the same whether all κ_j in (3) are different or whether some of them are equal. Thus, for example, the equation

$$(\Box-\kappa^2)^2\psi=\rho \tag{9}$$

recently discussed by Bhabha,[17] which leads to an exponential instead of a Yukawa static potential, still has the non-definiteness as a stumbling block. Nor will it turn out to lead to any improvement in this respect to take some κ_j to be complex. In fact additional complications now occur as will be explained in Section III-A-3.

It may be pointed out here that the occurrence of such energies can only constitute a difficulty in the case of fields of the Bose-Einstein type (of any integer spin). Generalizations of the Dirac equation to equations like

$$\prod_{j=1}^{N}(\gamma_\mu\partial_\mu+\kappa_j)\psi=0, \quad \partial_\mu=\partial/\partial x_\mu \tag{10}$$

do not lead to such complications (III-A-5) because here an appropriate definition of the vacuum, taking into account the exclusion principle, can help out. We have investigated whether the use of (10) can be of help in eliminating the divergences occurring in the charge renormalization of the electron. Such an attempt was suggested by the "regularization" of the charge renormalization by means of auxiliary fields of the Fermi-Dirac type.[18] It will be shown, however, that the use of (10) sheds no new light on this problem. It seems, in fact, that the construction of a model which might conceivably correspond to reality and which leads to a finite vacuum polarization is much more difficult than finding a model yielding finite self-energies (cf. also III-B-4).

As a next step in the discussion of "model theories," one might try to study equations like (2) where F is a *general* integral function of $\Box$. On the basis of Weierstrass' product theorem, this means that we now have to envisage the presence of exponential functions of the dalembertian. It will be shown in Section III-B-1 that the new features we now have to consider are all exhibited by an equation of the type

$$e^{f(\Box)}(\Box-\kappa^2)\psi=\rho. \tag{11}$$

A special case of this, with $f(\Box)=-\Box$, has been proposed and investigated by Born and Green within the framework of reciprocity theory.[19] Here one encounters problems of a new type; *viz.*, the lack of "propagation character." By this the following is meant: consider a space-time point P and its light cone. Now, on the basis of our present conceptions, physically meaningful differential and integral equations must be such that knowledge of any physical quantity in P must be obtainable from these equations by specifying sufficient initial conditions inside the past light cone only. It will be shown in Section III-B-2 that this condition is satisfied if $F(\Box)$ in (2) is a polynomial in $\Box$ with arbitrary constant coefficients. On the other hand, we shall see in III-B-3 that (11) does not have propagation character whenever $f(\Box)\neq 0$. However, the situation is radically different for the cases that f is an odd or is an even function of its argument. In the latter case deviations from orthodox theory show the suggestive feature that they seem to average out over space-time regions of the order of a universal length λ, the magnitude of which so far remains arbitrary.[19a] Some aspects of the situation in this case are discussed in III-B-4 and in the concluding Section IV.

As in conventional problems, we shall first study uncoupled systems. Now, in the same sense as the equation $(\Box-\kappa^2)\psi=0$ has the harmonic oscillator as its mechanical model, knowledge of the properties of the latter essentially determining all characteristics of the former, so the general equation $F(\Box)\psi=0$ will have its mechanical model too. We shall discuss these models in the next section.

II. THE MECHANICAL MODELS

A. Equations of Motion of Finite Order

1. Introductory Remarks

We consider one-dimensional mechanical systems (coordinate q) whose equation of motion, although involving time derivatives higher than the second, is still of finite order $2N$ so that it can be written as

$$F(D)q=0, \quad D=d/dt \tag{12}$$

where F is a polynomial of degree $2N$. We shall deal exclusively with reversible motions so that F is an even function of its argument. In this case (12) is derivable from an action principle with the Lagrangian

$$L=-qF(D)q. \tag{13}$$

---

[16] W. Pauli and F. Villars, Rev. Mod. Phys. **21**, 434 (1949).

[17] H. Bhabha, Phys. Rev. **77**, 665 (1950). We are indebted to Professor Bhabha for communicating his results.

[18] See reference 16 and also D. Feldman, reference 3.

[19] For a survey and references see M. Born, Rev. Mod. Phys. **21**, 463 (1949). We have been greatly stimulated by this article which we had an opportunity to see prior to publication. Also, we are much indebted to Dr. H. S. Green for many useful discussions on this subject.

[19a] In this respect the theory shows relationships with the modifications of classical electrodynamics as proposed by R. Peierls and H. McManus, Proc. Roy. Soc. **A195**, 323 (1948); see also J. Irving, Proc. Phys. Soc. London **A62**, 780 (1949).

In conventional mechanical problems the transition to the quantum theory is made by first putting the classical equations into Hamiltonian form. We shall show in what follows that the quantization by means of Hamiltonian methods is always possible in case F in Eq. (12) is of finite degree. The first question thus is to hamiltonize the system described by (13) and we must ask especially how this can be done in a way most suitable for subsequent quantization.

A procedure for deriving a Hamiltonian corresponding to (13) was given long ago by Ostrogradski[20] in case F is a polynomial: One defines quantities Q_i, P_i by the relations

$$\left.\begin{aligned} Q_i &= D^{i-1}q, \\ P_i &= \delta L/\delta(D^i q), \end{aligned}\right\} i=1,\cdots,N, \tag{14}$$

where $D^N q$ is the highest derivative of q occurring in L;[21] $\delta L/\delta x$ denotes a variational derivative:

$$\frac{\delta L}{\delta x}=\frac{\partial L}{\partial x}-D\frac{\partial L}{\partial(Dx)}+D^2\frac{\partial L}{\partial(D^2x)}-\cdots.$$

Then the Hamiltonian is

$$H=P_1Q_2+P_2Q_3+\cdots+P_{N-1}Q_N+P_N(DQ_N)-L, \tag{15}$$

where DQ_N is to be expressed in terms of the P's and Q's by means of[21] Eq. (14) for P_N. The Hamiltonian equations of motion derived from (15) reduce to (12) and a number of identities.

It is now possible to quantize (15) in the usual way, but this method meets with two objections:

(1) Since the method works only for finite N one can at best hope to master the quantization problem for transcendental F by approximating F by a finite number of terms of a power series, the development of F around the origin. In the methods to be discussed approximations of this kind can actually always be avoided.

(2) Even for finite N the method is clumsy as can be seen, for example, from the non-separable character of the Schrödinger equation in N variables corresponding to (15).

One expects however that for finite polynomials the problem should be separable since by writing[22]

$$F=\prod_{i=1}^{N}(1+D^2/\omega_i^2), \tag{16}$$

the solution of (12) is a linear combination of oscillations with frequencies ω_i. At least for the case that all ω_i are real and distinct one would expect the Hamiltonian to be some linear combination of oscillator Hamiltonians which would make the quantization trivial. Actually we will see that the restriction on the ω_i just mentioned is in no way necessary to achieve separability. Thus instead of following the Ostrogradski method, which is essentially based on a power series representation of F, we shall use only product representations and then have only to distinguish between the cases of real or complex, single or multiple frequencies ω_i.

2. *Real and Distinct Frequencies*

We start from the Lagrangian (13) where F is given by (16) and the ω_i are real and distinct. It is natural to define N coordinates Q_i by

$$Q_i=\prod_{j=1}^{N}{}'(1+D^2/\omega_j^2)q \tag{17}$$

where the prime on the product sign denotes that the ith factor is missing. According to (12) and (16) the Q_i satisfy the equation

$$(D^2+\omega_i^2)Q_i=0, \tag{18}$$

while there are clearly no constraints among the Q_i as their number just corresponds to the number of independent solutions of (12).

Now instead of describing our system by the Lagrangian (13) we try to use another form:

$$\bar{L}=-\sum_{j=1}^{N}\eta_j Q_j(D^2+\omega_j^2)Q_j. \tag{19}$$

We are entitled to do so if we can fix the N constants η_j in such a way that $\bar{L}$ differs from L by at most a time-derivative of a function of q and its derivatives. We shall show that this is possible, and that the η_j are uniquely determined.

Denoting by the symbol $\approx$ an equality apart from an additive time-derivative, and using (16) and (17), we have in fact:

$$\bar{L}\approx -q[\sum_k \eta_k\{\prod_j{}'(1+D^2/\omega_j^2)\}^2(D^2+\omega_k^2)]q$$

$$=-qF^2(D)\sum_k\frac{\eta_k\omega_k^2}{1+D^2/\omega_k^2}q,$$

which is equal to L provided that

$$\sum_k\frac{\eta_k\omega_k^2}{1+D^2/\omega_k^2}=\frac{1}{F(D)}. \tag{20}$$

As the roots of $F(D)$ are simple we can perform a partial fraction decomposition of F^{-1} with constant

[20] M. Ostrogradski, *Mémoires sur les équations differentielles relatives au problème des isopérimètres*, Mem. Ac. St. Petersbourg, VI 4, 385 (1850). See also Whittaker, *Analytical Dynamics* (1937), (Cambridge University Press, London, 1937), fourth edition, p. 265.

[21] When using Ostrogradski's method, it is most convenient to perform partial time differentiations on L such that it contains $D^N q$ as highest derivative instead of $D^{2N}q$, as is the case for (13). In this alternative form for L, $D^N q$ will occur quadratically which ensures that DQ_N can be eliminated from the Hamiltonian (15), while also there will then be no constraints between coordinates and momenta, in contradistinction to what would happen if one were to start from L in its form (13).

[22] This is always possible apart from a trivial multiplicative constant. We will never have to deal with any ω_i being zero.

(D-independent) numerators. Hence it follows that

$$\eta_k = 1/\omega_k{}^4 F'(-\omega_k{}^2),$$

where

$$F'(-\omega_k{}^2) = (dF/d(D^2))_{D^2=-\omega_k{}^2}. \tag{21}$$

Thus we have found the η_k and thereby have obtained a Lagrangian $\bar{L}$ dynamically equivalent to L.

It is important to note that as F is a single-valued function, the quantities $F'(-\omega_k{}^2)$, and therefore η_k, alternate in sign. Thus if we normalize F so that $F'(-\omega_1{}^2)$ is positive, then all η_k (k odd) are positive and all η_k (k even) are negative.

For future reference we mention two further types of relations involving the η_k. In the first place one verifies that q is connected with the Q_j by

$$q = \sum_{j=1}^{N} \eta_j \omega_j{}^2 Q_j. \tag{22}$$

Second, there exist N simple identities between the η_j which are easily obtained from (20):

$$\sum_{1}^{N} \eta_k \omega_k{}^2 = 1, \tag{23}$$

$$\sum_{1}^{N} \eta_k \omega_k{}^{2n} = 0, \quad n = 2, \cdots, N. \tag{24}$$

The first of these follows from (20) by putting $D=0$, while the others are proved by developing both sides of (20) in a series in D^{-2}. Next, putting $\bar{L}$ in the form

$$\bar{L} \approx \sum \eta_j \{(DQ_j)^2 - \omega_j{}^2 Q_j{}^2\},$$

we can immediately write down the Hamiltonian

$$H = \sum_j [(P_j{}^2/4\eta_j) + \eta_j \omega_j{}^2 Q_j{}^2]. \tag{25}$$

Performing the contact transformation

$$P_j \to P_j \cdot (2|\eta_j|)^{\frac{1}{2}}, \quad Q_j \to Q_j \cdot (2|\eta_j|)^{-\frac{1}{2}} \tag{26}$$

and remembering the sign properties of the η_j mentioned above, Eq. (25) becomes, in these new variables,

$$H = \tfrac{1}{2} \sum_{j=1}^{N} (-1)^{j-1} (P_j{}^2 + \omega_j{}^2 Q_j{}^2). \tag{27}$$

This shows that our system consists of a linear combination of harmonic oscillators, some with positive-definite energy (j odd) and some with negative definite energy (j even). Quantization yields the eigenvalues

$$E_{n_1, \cdots, n_N} = \sum_{1}^{N} (-1)^{j-1} \cdot (n_j + \tfrac{1}{2}) \omega_j; \quad n_j = 0, 1, \cdots. \tag{28}$$

Clearly, the "oscillator coordinates" Q_i given by (17) and their conjugate momenta ought to be related to the "Ostrogradski variables" (3) for the corresponding problem by a linear contact transformation. This can be shown in the usual way by verifying that the difference $\sum P_i dQ_i$ for the oscillator and for the Ostrogradski variables is a perfect differential.

Finally, it may be noted that whereas we can write down an L as well as an H in terms of the oscillator variables, we have only a Hamiltonian, Eq. (15), in terms of the Ostrogradski variables. An Ostrogradski Lagrangian does not exist, since (15) is linear in the momenta.

3. *Real and/or Complex Distinct Frequencies*

If we admit some of the ω_i in (16) to be complex, the reality of quantities like L and H necessitates the occurrence of complex conjugate pairs of frequencies. Irrespective of reality properties the formal introduction of the Q_i by means of (17) is still possible with the Q_i satisfying (18). Likewise, one can define an $\bar{L}$ by (19) with η_k given by (21). As the problem is still separable in the various Q_i, η_i will be real if ω_i is real, while if ω_m and ω_n are complex conjugates the same is true for η_m and η_n. The Hamiltonian is again given by (25). We will now pick from (25) a pair of terms corresponding to a pair of "complex conjugate oscillators." Clearly then, if we know how to quantize the Hamiltonian describing such a pair we will have solved the question of quantizing the entire Hamiltonian (25).

Let $j=1$, 2 in (25) denote such a pair. We thus consider the Hamiltonian

$$H = [(P_1{}^2/4\eta_1) + \eta_1 \omega^2 Q_1{}^2] + [(P_2{}^2/4\eta_2) + \eta_2 \omega^{*2} Q_2{}^2],$$
$$\omega = \omega_1 = \omega_2{}^*, \quad \eta_2 = \eta_1{}^*, \tag{29}$$

We consider first some classical features of our system. From (29) it follows that

$$(D^2 + \omega^2) Q_1 = (D^2 + \omega^{*2}) Q_2 = 0 \tag{29a}$$

as expected. Further, the part of q corresponding to Q_1 and Q_2 is according to (22) given by

$$q = \eta_1 \omega^2 Q_1 + \eta_2 \omega^{*2} Q_2; \quad (D^2 + \omega^2)(D^2 + \omega^{*2}) q = 0. \tag{29b}$$

Consider a solution of (29b) of the form

$$q = R_1 e^{-\alpha t} \cos(\nu t + \theta_1) + R_2 e^{\alpha t} \cos(\nu t + \theta_2), \tag{29c}$$

where we have put

$$\omega = \nu + i\alpha.$$

In contrast to the case of two real roots the motion (29c) is in general unbounded in time. Moreover, considering the two terms on the right side of (29c) as two rectangular coordinates in a plane, the orbit will not densely cover a portion of the plane, as in the case of the Lissajous motion with incommensurable real frequencies, and therefore the motion is degenerate in the classical sense.

With the help of (29a, b) we can express Q_1 and Q_2 in terms of the constants R_1, R_2, θ_1, θ_2 and then calculate

the energy using (29). The result is (we put $\eta_1=\eta\exp i\varphi$)

$$H=(2R_1R_2/\eta)[(\nu^2-\alpha^2)\cos(\theta_1-\theta_2-\varphi) -2\nu\alpha\sin(\theta_1-\theta_2-\varphi)]. \quad (30)$$

Again in contrast to the real frequencies the energy depends on the phases and can thus have either sign. In the quantum theory we will find the counterparts of the unboundedness of the motion and the indefiniteness of the energy.

Performing the contact transformation[23]

$$P_1\to P_1(2\eta_1)^{\frac{1}{2}},\quad P_2\to P_2(2\eta_1^*)^{\frac{1}{2}}$$
$$Q_1\to Q_1/(2\eta_1)^{\frac{1}{2}},\quad Q_2\to Q_2/(2\eta_1^*)^{\frac{1}{2}},$$

Eq. (29) becomes

$$H=\tfrac{1}{2}(P_1^2+\omega^2Q_1^2)+\tfrac{1}{2}(P_2^2+\omega^{*2}Q_2^2). \quad (31)$$

For purposes of quantization it is important to note that here the P's and Q's are non-Hermitian operators. In fact, taking q in (29b) to be Hermitian, we must have

$$Q_1^\dagger=Q_2,\quad P_1^\dagger=P_2. \quad (31a)$$

One can go over to Hermitian variables by the canonical transformation[24]

$$\begin{aligned}P_1&=\tfrac{1}{2}\omega^{\frac{1}{2}}[(p+iq)+i(P-iQ)],\\ P_2&=\tfrac{1}{2}\omega^{*\frac{1}{2}}[p-iq)-i(P+iQ)],\\ Q_1&=-\frac{1}{2i\omega^{\frac{1}{2}}}[(p-iq)+i(P+iQ)],\\ Q_2&=\frac{1}{2i\omega^{*\frac{1}{2}}}[(p+iq)-i(P-iQ)].\end{aligned} \quad (32)$$

In terms of these variables H becomes

$$H=-\alpha(PQ+pq)-\nu(Pq-pQ),$$

where the first bracket has to be properly symmetrized to make H Hermitian. Thus the Schrödinger equation is

$$\left[-\alpha\left(Q\frac{\partial}{\partial Q}+q\frac{\partial}{\partial q}\right)+\nu\left(Q\frac{\partial}{\partial q}-q\frac{\partial}{\partial Q}\right)\right]\Psi=(iE+\alpha)\Psi.$$

Putting

$$q=r\cos\theta,\quad Q=r\sin\theta,$$

we get

$$[-\alpha r(\partial/\partial r)-\nu(\partial/\partial\theta)]\Psi=(iE+\alpha)\Psi$$

with eigenvalues

$$E_{n,\lambda}=n\nu+\lambda\alpha \quad (33a)$$

and wave functions

$$\Psi_{n,\lambda}=(1/2\pi)e^{-in\theta}\cdot(1/r)e^{i\lambda\ln r}. \quad (33b)$$

[23] This is not a real transformation, but that does not matter as the dynamical variables in (29) are not real to begin with.

[24] This transformation is essentially a transition to Fock-like variables [see P. Dirac, *Quantum Mechanics* (Oxford University Press, New York, 1949), third edition, Oxford, 1949, p. 136] with a subsequent splitting in Hermitian and anti-Hermitian parts.

Here n can be any positive or negative integer or zero, while λ is continuous and ranges from $-\infty$ to $+\infty$. The energy spectrum is therefore indefinite, continuous, and each level is infinitely degenerate. $\Psi_{n,\lambda}$ has been normalized in the λ-scale.[25]

Let us now consider the matrix elements for the operators Q_1, Q_2, P_1, P_2 occurring in (31). We have, for example,

$$Q_1\Psi_{n,\lambda}=(1/2r\omega^{\frac{1}{2}})[(n-1-i\lambda)\Psi_{n-1,\lambda}+r^2\Psi_{n+1,\lambda}],$$

so

$$\begin{aligned}(m,\lambda'|Q_1|n,\lambda'')=\frac{1}{4\pi\omega^{\frac{1}{2}}}\Big[&(n-1-i\lambda)\delta(m-n+1)\\ &\times\int_{-\infty}^{\infty}dz\exp[i(\lambda'-\lambda)z-z]+\delta(m-n-1)\\ &\times\int_{-\infty}^{\infty}dz\exp[i(\lambda'-\lambda)z+z]\Big],\end{aligned} \quad (34)$$

where $z=\ln r$. The z integrals are badly divergent. Thus, corresponding to the classically observed unbounded motion the representation for Q_1 (and likewise for the other variables) is unbounded. This does not mean that the matrix elements of all functions of p and q are unbounded, as is already clear from the finite expression (33) for the energy. Indeed, one verifies also that

$$\begin{aligned}(m,\lambda'|\tfrac{1}{2}(P_1^2+\omega^2Q_1^2)|n,\lambda'')&=\tfrac{1}{2}\omega(n-i\lambda'')\delta(m-n)\delta(\lambda'-\lambda''),\\ (m,\lambda'|\tfrac{1}{2}(P_2^2+\omega^{*2}Q_2^2)|n,\lambda'')&=\tfrac{1}{2}\omega^*(n+i\lambda'')\delta(m-n)\delta(\lambda'-\lambda''),\end{aligned}$$

so that the energy of each of the complex oscillators separately is also finite, although complex.

In conclusion, it may be pointed out that for the reality of H the relations (31a) are not strictly necessary; one could also have taken

$$Q_1^\dagger=-Q_2,\quad P_1^\dagger=-P_2, \quad (31b)$$

corresponding to anti-Hermitian q. In the case of a real oscillator, one chooses either a Hermitian or an anti-Hermitian q in order to obtain a (positive or negative) definite energy; the same holds for the case of the distinct real frequencies discussed in the previous section. For complex frequencies, however, each choice leads to an energy which is indefinite to begin with, and therefore (31a) and (31b) cannot be distinguished from each other.

4. *Presence of Multiple Frequencies*

We first consider the case that only a double real frequency is present, so that L is

$$L=-q(D^2+\omega_0^2)^2q.$$

[25] This is meant in the customary sense of the continuous spectrum, i.e., one takes $m=n$ and integrates over λ'' from $\lambda'-\epsilon$ to $\lambda'+\epsilon$ where ϵ is a small quantity.

The general solution of the equation of motion is

$$q=R_1\cos(\omega_0 t+\theta_1)+R_2 t\cos(\omega_0 t+\theta_2), \tag{35}$$

which in general is again not bounded and degenerate. For the energy one finds[26]

$$4\omega_0^2 R_2[R_1\omega_0\sin(\theta_1-\theta_2)-R_2]$$

which as in the complex case is indefinite. For the Hamiltonization process the partial fraction method of the previous two sections is clearly inapplicable, while the Ostrogradski method though feasible is again inconvenient. It is natural, however, to try here to consider the double frequency as the confluence of two distinct real frequencies. For the latter one has

$$\begin{aligned} L&=-q(D^2+\omega^2)(D^2+\omega_0^2)q \\ &\approx[Q_1(D^2+\omega^2)Q_1-Q_0(D^2+\omega_0^2)Q_0]/(\omega^2-\omega_0^2), \end{aligned} \tag{36}$$

with

$$\begin{aligned} Q_1&=(D^2+\omega_0^2)q, \quad Q_0=(D^2+\omega^2)q, \\ q&=(Q_1-Q_0)/(\omega^2-\omega_0^2). \end{aligned}$$

The occurrence of a factor $(\omega^2-\omega_0^2)^{-1}$ in (36) indicates already that the transition $\omega\to\omega_0$ has to be performed with some care. We put

$$\omega=\omega_0+\epsilon$$

where ϵ is considered infinitesimally small, and also

$$Q_0=Q_1+\epsilon Q_2.$$

Then L becomes in the limit $\epsilon\to 0$

$$\begin{aligned} L&=Q_1^2-(1/\omega_0)Q_2(D^2+\omega_0^2)Q_1 \\ &\approx Q_1^2+(1/\omega_0)(DQ_1\cdot DQ_2-\omega_0^2 Q_1Q_2), \end{aligned} \tag{37}$$

and in the same limit

$$q=-Q_2/2\omega_0.$$

One easily verifies that (37) leads to the same general motion (35) for q, which justifies the procedure. From (37) one finds for the Hamiltonian

$$H=\omega_0(P_1P_2+Q_1Q_2)-Q_1^2$$

which, on performing the canonical transformation,

$$\begin{aligned} &Q_1\to Q_1, && P_1\to P_1-Q_2/2\omega_0, \\ &Q_2\to -P_2+Q_1/2\omega_0, && P_2\to P_2, \end{aligned}$$

becomes

$$H=\omega_0(P_1Q_2-P_2Q_1)-\tfrac{1}{2}(Q_1^2+Q_2^2).$$

Put

$$Q_1=r\cos\theta, \quad Q_2=r\sin\theta,$$

then the Schrödinger equation is

$$-i\omega_0\partial\Psi/\partial\theta=(E+\tfrac{1}{2}r^2)\Psi,$$

so that

$$E=n\omega-r'^2/2, \quad \Psi_{n,r'}(r,\theta)=\delta(r-r')e^{in\theta}/(2\pi r')^{\frac{1}{2}},$$

with n a (positive, negative, or zero) integer while r' ranges continuously from 0 to ∞. Thus, as in the complex case, the energy spectrum is continuous, indefinite and each level is infinitely degenerate.

The general procedure for dealing with a mixture of single and multiple frequencies of arbitrary multiplicity is now clear: dissolve first each n-fold root ω into n neighboring ones $\omega+\epsilon_i$, $i=1,\cdots,n$, with $\epsilon_i\neq\epsilon_j$. Then develop in L with respect to the ϵ_i and pass to the limit. As for our further discussions a detailed analysis of this procedure seems hardly necessary, we will not pursue this question any further. However some additional comments regarding multiple frequencies will be found in the Appendix.

To recapitulate the results of Section A: if L contains more than one frequency the energy is always indefinite, both classically and quantum mechanically. For the case of real frequencies we saw that this follows immediately from the alternating signs of the η_k. In the other cases this simple argument cannot be taken over, but from the analysis of the Schrödinger problems it was found that the same conclusion holds. It is this indefiniteness which will constitute a grave difficulty in field theoretical applications.

B. Equations of Motion of Infinite Order

1. Introductory Remarks

If $F(D)$ contains derivatives of infinite order we have essentially to do with integral equations. It is therefore often more convenient in this case to use instead of (12) the following form for the equations of motion

$$\int K(t-t')q(t')dt'=0, \tag{38}$$

where the time reversibility is now expressed by the requirement of the evenness of K as function of its argument. Corresponding to (38) L has the form

$$L=-q(t)\int K(t-t')q(t')dt'. \tag{39}$$

The connection between (12) and (13) on the one hand and (38) and (39) on the other is expressed by

$$K(t)=(1/2\pi)\int_{-\infty}^{\infty} dk e^{ikt}F(ik). \tag{40}$$

We will restrict ourselves to functions F which are integral functions in the sense of complex function theory. It is known that according to Weierstrass such functions can be represented in the form

$$F(D)=e^{f(D)}\prod_i(1+D^2/\omega_i^2), \tag{41}$$

provided $\sum\omega_i^{-2}$ converges. Equation (41) expresses F in terms of its zeros and of an exponential factor; $f(D)$

[26] As can, e.g., be shown from the Ostrogradski form of the Hamiltonian.

is again an (even) integral function determining the behavior of F at the point at infinity. The motivation for the choice of functions of the type (41) is that in corresponding field problems the zeros will each correspond to quanta of a certain mass whereas the exponential is suggestive of a cut-off factor.

Again the question arises of the quantization. It is clear that if no exponential is present (i.e., $f=0$), the methods of the previous chapter can be applied immediately. We illustrate this with a simple example: If $F(D)=\cosh\alpha D$ we have the product representation

$$F(D)=\prod_1^\infty(1+D^2/\omega_i^2),\quad \omega_i=\pi(2i-1)/2\alpha.$$

Thus in our terminology we have an infinite number of distinct real frequencies. Now we can define an infinite number of Q_i by using (17) (for $N=\infty$) and an $\bar{L}$ as in (19). From (20) one sees that the η_k are to be determined from the relation

$$\sum\eta_k\omega_k^2/(1+D^2/\omega_k^2)=1/\cosh\alpha D.$$

The partial-fraction series for $\cosh^{-1}\alpha D$ is well known to be[27]

$$\operatorname{sech}\alpha D=\frac{4}{\pi}\sum_1^\infty\frac{(-1)^{k-1}}{2k-1}\cdot\frac{1}{1+D^2/\omega_k^2},$$

so

$$\eta_k=\frac{4}{\pi}\cdot\frac{(-1)^{k-1}}{(2k-1)\omega_k^2}=\frac{16\alpha^2}{\pi^3}\cdot\frac{(-1)^{k-1}}{(2k-1)^3}.$$

One notes again the sign alternation of the η_k. The identity (23) is easily verified.[28]

If there is an exponential present in F, the problem can still be reduced greatly by the above method of decomposition. In fact it is readily verified that for the Lagrangian (13) with F given by (41) we can introduce an $\bar{L}\approx L$, where

$$\bar{L}=\sum\eta_kQ_ke^{f(D)}(1+D^2/\omega_k^2)Q_k,$$

with the same Q_k and η_k as before. Therefore the quantization problem will be mastered if we can deal with a system whose Lagrangian is

$$L=-qF_1(D)q,\quad F_1(D)=\tfrac{1}{2}e^{f(D)}(D^2+\omega^2),\qquad(42)$$

i.e., for a system with only one frequency and an exponential factor.

For a system of this kind the generalization of the various methods described above for finding a Hamiltonian becomes awkward since one would always have to approximate the exponential either by a power series of finite order (in the Ostrogradski method) or by a finite product representation (in the oscillator method), and then in some way have to pass to the limit. However, one can circumvent the use of the Hamiltonian for quantization by following a method advocated especially by Heisenberg.[29] The idea here is to start from (1) the equations of motion, (2) the expression of the energy E in terms of q and its time derivatives, (3) the quantum-mechanical definition of time derivation which follows from attributing to E the rôle of time-displacement operator, thus

$$[E,\varphi(q,\dot{q},\ddot{q},\cdots)]=-i\dot{\varphi}\qquad(43)$$

for any function φ. From these three requirements the eigenvalues of the energy must be determined and the representation of q must be found.

We will now apply Heisenberg's method to the system (42). First of all, we need an expression for the energy, to the derivation of which we now turn.

2. Classical Theory—General Expression for the Energy

From the general definition of E as the integral of the motion for a time displacement, one readily finds that

$$E=\sum_{n=1}^\infty D^nq\cdot[\delta L/\delta(D^nq)]-L$$

$$=\sum_{n=1}^\infty D^nq\sum_{m=0}^\infty(-1)^mD^m[\partial L/\partial(D^{m+n}q)]-L.$$

We will consider the Lagrangian to be of the general form (13). Its value then is zero in virtue of the equations of motion (which are supposed to be given and thus may be used freely in contradistinction to the situation in the Hamiltonian method). It is convenient to introduce the Fourier transforms of the various quantities. Writing

$$F(D)=\sum_0^\infty\lambda_nD^n,$$

$$q(t)=(1/2\pi)\int_{-\infty}^\infty R(k)e^{-ikt}dk,$$

$$E(t)=(1/2\pi)\int_{-\infty}^\infty\mathcal{E}(s)e^{-ist}ds,$$

one finds

$$\mathcal{E}(s)=-\frac{1}{2\pi}\sum_{n=1}^\infty\sum_{m=0}^\infty(-1)^m\lambda_{n+m}$$

$$\times\int_{-\infty}^\infty dk\cdot(-ik)^m\cdot\{-i(s-k)\}^nR(k)R(s-k).$$

[27] See Whittaker-Watson, *Modern Analysis* (Cambridge University Press, London, 1940), fourth edition, p. 136. Quite generally the possibility of decomposing $F^{-1}(D)$, F given by (41) with $f=0$, and $\Sigma\omega_i^{-2}$ convergent, in a partial fraction series is a consequence of the Mittag-Leffler theorem of complex function theory.

[28] The identities corresponding to (24) now are

$$\sum_1^\infty\eta_k\omega_k^{2n}=0,\quad n\geq 2$$

which are divergent series but by the known methods can be summed to zero.

[29] W. Heisenberg, Zeits. f. Physik **123**, 93 (1944).

Putting $m+n=p$ and retaining m, one can carry out the summation over m. The subsequent summation over p can be expressed in terms of F. The result is

$$\mathcal{E}(s)=(1/2\pi s)\int_{-\infty}^{\infty}dk(k-s)R(k)R(s-k) \times[F\{i(k-s)\}-F(ik)] \quad (44)$$

and we note that as the equation of motion in Fourier form is $F(-ik)R(k)=0$ and as F is an even function of its argument, $s\mathcal{E}(s)$ clearly is zero as a consequence of the equation of motion; this expresses the energy conservation. For the L given by (42) we have

$$q=A\cos\omega t, \quad R=\pi A[\delta(k+\omega)+\delta(k-\omega)].$$

One finds that $\mathcal{E}(s)$ is proportional to $\delta(s)$ and eventually that

$$E=\tfrac{1}{2}A^2\omega^2 e^{f(i\omega)}. \quad (45)$$

If

$$F(D)=\tfrac{1}{2}\chi(D)\prod_i(1+D^2/\omega_i^2), \quad (46)$$

where χ is any function without zeros one may conveniently write

$$q=\sum_n \eta_n A_n\cos\omega_n t, \quad R=\pi\sum_n \eta_n A_n[\delta(k+\omega_n)+\delta(k-\omega_n)],$$

where the η_k are the constants given by (20) for $\chi=1$. One then finds

$$E=\tfrac{1}{2}\sum_k \eta_k\chi(i\omega_k)\omega_k^2 A_k^2. \quad (47)$$

This additivity of the energy follows immediately from the corresponding additivity of the Lagrangian as found in the previous section.

3. *Quantum Theory—Diagonalization of the Energy*

We will discuss now the quantization of the system described by (42), making use of Fourier transforms throughout. Then (43) is clearly satisfied if

$$[R(k), E]=kR(k).$$

In the representation in which E is diagonal this means that the matrix elements of R must be of the form

$$(E'|R(k)|E'')=\delta(E'-E''-k)(E'|R|E''). \quad (48)$$

As the equation of motion is $F_1(ik)R(k)=0$, it follows that $R(k)$ is zero except for $k=\pm\omega$ so that we may write for (48)

$$(E'|R(k)|E'') =\delta(k^2-\omega^2)\delta(E'-E''-k)(E'|R_0|E''). \quad (49)$$

With this form of R all requirements are fulfilled apart from the diagonalization of the energy, the condition for which is

$$\frac{1}{2\pi}\int_{-\infty}^{\infty}ds(E'|\mathcal{E}(s)|E'')e^{-ist}=E'\delta(E'-E'')$$

where $\mathcal{E}(s)$ is given by (44) with $F=F_1$. From (44) and (49) one readily finds

$$E'=\frac{1}{16\pi^2}e^{f(i\omega)}\{|(E'|R_0|E'+\omega)|^2 +|(E'|R_0|E'-\omega)|^2\}. \quad (50)$$

This equation should determine both the spectrum of E and the explicit form of the matrix elements $(E'|R_0|E'\pm\omega)$. In the case of an ordinary oscillator ($f=0$) a solution clearly is[30]

$$E'=(n'+\tfrac{1}{2})\omega,$$
$$(E'|R_0|E'')=2\pi\sqrt{2}[(n'\omega)^{\frac{1}{2}}\delta(n'-n''-1) +(n''\omega)^{\frac{1}{2}}\delta(n'-n''+1)].$$

For our system with the exponential factor one therefore must have

$$E'=(n'+\tfrac{1}{2})\omega e^{f(i\omega)}$$

while $(E'|R_0|E'')$ is the same as for the ordinary oscillator. Thus q_{mn}, the matrix element of q in the energy representation is the same as in the case $f=0$.

It should be noted that if f is of the form $(D^2+\omega^2)^k$, both the eigenvalues of the energy and the matrix elements of q are exactly the same as for an ordinary oscillator. Hence in this case the exponential factor has no effect whatsoever, both classically and quantum mechanically, as long as one confines one's attention to the homogeneous problem, i.e., to the case that no outside forces act.

As soon as such forces are present the exponential factor has a profound effect, however. Consider, for example, the problem of an "exponential oscillator" coupled to an ordinary one as described by a Lagrangian

$$L=-\tfrac{1}{2}q\exp[\lambda^{2k}(D^2+\omega^2)^k](D^2+\omega^2)q -\tfrac{1}{2}q_0(D^2+\omega_0^2)q_0+\epsilon q_0 q,$$

where λ has the dimensions of an inverse frequency. The equations of motion are

$$\exp[\lambda^{2k}(D^2+\omega^2)^k]\cdot(D^2+\omega^2)q=\epsilon q_0, \quad (D^2+\omega_0^2)q_0=\epsilon q.$$

Now solve in the usual way by putting

$$q\sim e^{i\nu t}, \quad q_0\sim e^{i\nu t}$$

where ν must satisfy the condition

$$\exp[\lambda^{2k}(\omega^2-\nu^2)^k]\cdot(\omega^2-\nu^2)(\omega_0^2-\nu^2)=\epsilon^2.$$

In contrast to the conventional problem with $\lambda=0$ one does not find two solutions for ν, one near ω and one

[30] The uniqueness of the solution for the harmonic oscillator has been studied by E. P. Wigner, Phys. Rev. **77**, 711 (1950). Wigner finds that for this case the results of the present method are not necessarily the same as those obtained by the Hamiltonian method. It has kindly been pointed out to us by Professor Pauli that uniqueness can be obtained by requiring the commutator of q and $\dot{q}$ to be independent of the particular choice of E (a result already implicit in the last paragraph of Wigner's paper). We are indebted to Professors Wigner and Pauli for interesting discussions on this topic.

near ω_0, but rather an infinity of solutions,[31] so that as soon as $\epsilon \neq 0$ the motion becomes a great deal more complicated. In field theoretical applications this distinction between the homogeneous and the inhomogeneous problem will turn out to be of great importance.

III. FIELD THEORETICAL APPLICATIONS

A. Absence of Exponentials

1. *Introductory Remarks*

With the help of the methods developed in Section II we are now in a position to discuss a number of questions concerning field equations of the general type (2). For the function F we first limit our choice to expressions like (3) (with a finite or an infinite number of factors) and defer until Section III-B the discussion of more general types of integral functions F which include exponential functions of the dalembertian $\Box$.

We begin with the case that ψ in (2) is the electromagnetic field and the ρ is the current vector due to the presence of electrons, thus

$$f(\Box)\Box A_\mu = -j_\mu, \quad f(\Box) = \prod_i (1-\Box/\mu_i^2), \tag{51}$$

where j_μ is the conventional Dirac current operator. It is thereafter pretty straightforward to see what will happen for other choices of ψ and ρ in (2). Some comments on the application to the coupling of mesons with nucleons are made in the following subsection.

In an analogous manner to the developments in Section II we shall make increasingly general assumptions about the μ_i: at first that they are real and distinct and later that there are also pairs of complex conjugate μ_i and multiple occurring μ_i. In subsection 5 we discuss generalized equations of the Dirac-type (10).

We now start with the discussion of (51) for real μ_i.

2. *Real Masses—The Self-Energy of the Electron*

The Lagrangian density from which the generalized electromagnetic Eqs. (51) as well as the wave equation for the electron can be derived is

$$\mathfrak{L} = -\frac{1}{2}\frac{\partial A_\mu}{\partial x_\nu} f(\Box) \frac{\partial A_\mu}{\partial x_\nu} - j_\mu A_\mu - \bar{\psi}(\gamma_\mu \partial_\mu + \kappa)\psi, \tag{52}$$

$$j_\mu = i\epsilon \bar{\psi}\gamma_\mu \psi.$$

Here ψ is the wave function of the electron, $\bar{\psi}$ its adjoint; κ is the electron mass, ϵ its charge. We impose on A_λ the supplementary condition

$$\partial A_\mu/\partial x_\mu = 0. \tag{53}$$

Following the procedure of II-A-2, $\mathfrak{L}$ can be split by introducing the following set of field variables

$$A_\mu^{(0)} = f(\Box) A_\mu$$

$$A_\mu^{(i)} = \prod{}' (1-\Box/\mu_k^2)\cdot(\Box/\mu_i^2) A_\mu, \quad i = 1, 2, \cdots$$

With the convention $\mu_0 = 0$ and using partial space-time differentiations we can replace (52) by

$$\mathfrak{L} \approx -\frac{1}{2}\sum_i \zeta_j \left(\frac{\partial A_\mu^{(j)}}{\partial x_\nu} \frac{\partial A_\mu^{(j)}}{\partial x_\nu} + \mu_j^2 A_\mu^{(j)2} \right) - j_\mu \sum_k \zeta_k A_\mu^{(k)} - \bar{\psi}(\gamma_\mu \partial_\mu + \kappa)\psi, \tag{54a}$$

with

$$\zeta_0 = 1, \quad \zeta_k = 1/\mu_k^2 f'(\mu_k^2); \quad k = 1, 2, \cdots. \tag{54b}$$

The transformation from (52) to (54a, b) has been made by following step by step the derivation of (19) from (13). The coupling term in (54a) is obtained from that in (52) by using the analog of (22); i.e.,

$$A_\mu = \sum \zeta_k A_\mu^{(k)}.$$

As to the derivation of the values (54b) for the ζ_k, one readily verifies that the determining equation (which here plays the same rôle as (20) for the mechanical model) now is

$$1/\Box \prod_i (1-\Box/\mu_i^2) = (\zeta_0/\Box) - \sum_i \zeta_i/(1-\Box/\mu_i^2).$$

In particular one finds $\zeta_0 = 1$ by multiplying by $\Box$ and then putting $\Box = 0$. The identities which are the counterpart of (24) now turn out to be

$$\sum_{i=0}^{N} \zeta_i \mu_i^{2n} = 0, \quad n = 0, 1, \cdots, N-1. \tag{55}$$

Also the sign alternation of the constants ζ_k is of course found here again as in II-A-2. We have normalized our definitions of the $A_\mu^{(k)}$ so that $\zeta_0 = 1$ which means that the part of (54a) which contains $A_\mu^{(0)}$ has precisely the structure of the standard electromagnetic field Lagrangian with interaction, so that we now identify $A_\mu^{(0)}$ with the electromagnetic potential. Similarly, for $k \neq 0$, $A_\rho^{(k)}$ is now a neutral vector meson field with meson mass μ_k. Following the reasoning which led up to (28) one sees that for even (odd) k the field energy is positive (negative) definite.

From (54) it follows that, for all k,

$$(\Box - \mu_k^2) A_\mu^{(k)} = -j_\mu$$

which means that each field is coupled to the electron with the same strength ϵ. Further it follows from (53) and from the independence of the fields that[32]

$$\partial A_\mu^{(k)}/\partial x_\mu = 0, \quad \text{all } k. \tag{56}$$

[31] This is an immediate consequence of the Picard theorem. Roughly speaking, one might say that for $\epsilon = 0$ an infinity of roots have collapsed to the point in infinity but are "drawn back" from there as soon as ϵ differs from zero. Clearly, the transition $\epsilon \to 0$ is highly non-uniform.

[32] It is well known that the essential role of relations of the type (56) is to insure the definiteness of the energy for the field concerned. In view of the fact that (56) is still insufficient for obtaining a positive definite energy for the assembly of fields under consideration, one may ask whether the supplementary

For the quantization of the fields it is important to note that the momentum conjugate to $A_\mu^{(k)}(\mathbf{x}, t)$ is $\zeta_k \dot{A}_\mu^{(k)}(\mathbf{x}, t)$. Consequently the covariant commutation relations are

$$[A_\mu^{(k)}(x), A_\nu^{(m)}(x')] = i\delta_{\mu\nu}\delta_{km}\cdot(1/\zeta_k)\Delta_k(x-x'), \quad (57)$$

where $\Delta_k(x)$ is the well-known four-dimensional "δ-function" involving the mass μ_k.[33] To each Δ_k we can adjoin functions $\bar{\Delta}_k$ and $\Delta_k^{(1)}$ in the manner indicated by Schwinger.[33] In addition, we will assume in parallel with (57) that the vacuum expectation value of the anticommutator of $A_\mu^{(k)}(x)$ and $A_\nu^{(m)}(x')$ is given by

$$\langle\{A_\mu^{(k)}(x), A_\nu^{(m)}(x')\}\rangle_{\text{vac}} = \delta_{\mu\nu}\delta_{km}\cdot(1/\zeta_k)\Delta_k^{(1)}(x-x'). \quad (58)$$

To the interpretation of (58) we will return presently and will now first consider the self-energy of the electron in the order ϵ^2 as it can be calculated by means of the formal relations (57) and (58).

We note first that it will consist of a sum of terms each being the contribution of a separate field $A_\mu^{(k)}$. Evidently such a term contains a factor ζ_k^2 since we deal with an effect of the second order in the interaction energy which according to (54a) is weighted with ζ_k. Furthermore it follows directly from (57) and (58) that the term we consider contains another factor ζ_k^{-1}. Hence the total self-energy will be of the form:

$$\delta m = \sum_k \zeta_k W(\mu_k), \quad (59)$$

where $W(\mu_k)$ is the standard expression for the self-energy of an electron coupled to a neutral vector meson field with meson mass μ_k; therefore

$$\delta m = \frac{\epsilon^2\kappa}{8\pi^2}\int_0^1 du(1+u)\sum_n \zeta_n[(C-\ln\eta) - \ln(u^2\kappa^2+\mu_n^2(1-u))],$$

where $C=0.577\cdots$, and η is a cut-off which ultimately tends to zero. Now according to the first of our identities (55) we have

$$\sum_n \zeta_n = 0 \quad (60)$$

and we see therefore that this relation guarantees the finiteness of δm.

Thus theories of this type automatically lead to the finiteness of the self-energy but this result has been obtained at the cost of an unreasonable assumption. In fact the use of (58) for the vacuum expectation value of functions of the $A_\mu^{(k)}$ implies that for *all* fields one has chosen as vacuum definition

$$A_\mu^{+(k)}\Psi = 0, \quad (61)$$

where Ψ is the vacuum state vector and $A_\mu^{+(k)}$ denotes the positive frequency part of $A_\mu^{(k)}$. For even k, ($\zeta_k>0$), this means that no annihilation of quanta of positive energy is possible. For odd k, ζ_k is negative so that the rôle of creation and annihilation is interchanged. Hence for odd k (61) means that no creation of quanta of negative energy is possible. This condition formally ensures that the vacuum is a state of minimum energy. However, a definition of the vacuum which forbids creation processes is certainly completely unphysical and, since the quanta obey Bose-statistics, a reinterpretation by means of a filling-up of the negative energy states is impossible. Alternative interpretations with the help of an indefinite metric in Hilbert space are equally unsuccessful (see Matthews[15]). Theories of this kind therefore are physically inconsistent.

The procedure here described for obtaining finite self-energies is closely connected with the regularization procedures developed by Pauli and Villars[16] and others. As has been emphasized by these authors, the use of "regulators" is a computational device which amounts to making certain divergent expressions finite. An essential step in this procedure is the introduction of certain parameters, called c_i and M_i in the cited paper. Between these, certain relations must be postulated to achieve the desired convergence. On closer comparison of the above results with the regulators one readily sees that the c_i and M_i just correspond to our ζ_i and μ_i. Thus there are two differences between the regulator procedure and the models of the present section. First, the "auxiliary masses" M_i formally introduced in an advanced stage of the calculation, here correspond to actual masses μ_i introduced from the outset and linked with fields. Second, the regularization condition $\sum c_i = 0$ which has to be postulated in reference 16 is equivalent to the identity (60) which here follows automatically. Thus the formalism in this section may be said to be a realization of the regulator type of theory, but as we have just seen, it is not an acceptable scheme.

Actually (60) is only one of the many identities which are given by (55) (for suitably large N). In the present case only the first of the relations (60) is needed for convergence (which amounts to saying that the self-energy is finite for any $N\geq 1$), but in related problems further similar relations come into play. Thus it is clear that the formalism here developed is immediately adaptable to the case where ψ in (2) is some meson field and ρ the corresponding nucleon source. Also in this case one will have identities closely analogous to (60). Now it is well known that for all couplings involving derivatives of the meson field potential (like the tensor coupling in the vector theory) the self-energy of the nucleon in the first non-vanishing order exhibits a quadratic and a

condition (53) is the most appropriate one for the problem on hand. It would seem most unlikely, however, that the indefiniteness can be avoided in such a way that the ultimate aim of obtaining convergent self-energies can still be reached.

[33] The conventions followed in the definition of Δ_k, as well as $\bar{\Delta}_k$ and $\Delta_k^{(1)}$ to be introduced below are those of J. Schwinger, Phys. Rev. 75, 651 (1949), Eqs. (A.29), (A.21), and (A.37).

For $k\neq 0$ one has strictly speaking to add to the right of (57) terms involving second derivatives of Δ. As those terms can effectively be transformed away (see P. T. Matthews, Phys. Rev. 76, 1254 (1949)) we have not bothered writing them down here.

logarithmic divergence. We leave it to the reader to verify that in such a situation the first *two* identities of the type (60) suffice to obtain convergence.[34]

3. *Complex μ_i—Unbounded Interactions*

In the previous section we have seen how the occurrence of negative energy states for the uncoupled system prohibits a logical physical interpretation of a formalism based on (52) and (51) with real masses μ_i. These negative energy states were encountered already in the corresponding real frequency model of II-A-2. In II-A-3 it was shown that for complex frequencies such negative energies also occur. Now the latter model will play the same role for the case of complex μ as the real frequency model did for real μ. It is therefore clear that we will run into the same negative energy trouble whether or not we admit complex conjugate pairs of μ_i to occur in (51). In certain respects the situation gets even worse, however, when complex μ_i are present. It is this qualitative difference between the cases of real and of complex μ_i which we want to comment on now.

Also if there are some pairs of complex conjugate μ_i in (51) we can still write down the Lagrangian density (52) and can again perform the decompositions leading to (54a, b). Let us first consider the case of the absence of interactions ($\epsilon=0$). The field quantization does not differ in any essential from that of more conventional situations. By performing a spatial Fourier development one can show by standard methods that the total Hamiltonian referring to a pair of complex conjugated μ_i is a linear superposition of pairs of complex conjugated oscillators of the type (31):

$$H=\tfrac{1}{2}\sum_{\mathbf{k}}[P_1^2(\mathbf{k})+\omega_k^2Q_1^2(\mathbf{k})+P_2^2(\mathbf{k})+\omega_k^{*2}Q_2^2(\mathbf{k})],$$

where

$$\omega_k^2=\mu^2+|\mathbf{k}|^2, \tag{62}$$

with complex μ. According to (33) the eigenvalues for the kth mode are

$$n\nu_k+\lambda\alpha_k,$$

where, as in (29c), we put $\omega_k=\nu_k+i\alpha_k$. According to (62) the dispersion law of the modes of the fields is of an inherently complex nature so that no particle attributes can be ascribed to these modes in the manner used for real μ.

When dealing with the problem of interaction we must be prepared for a queer situation. For the interaction energy is according to (54a) linear in the A_ρ, and hence, as far as the contribution from complex μ_i is concerned, linear in field amplitudes which according to (62) are unbounded as a function of time. It is therefore clear that a coupling like $j_\mu A_\mu^{(c)}$, where $A_\mu^{(c)}$ stands for the contribution to A_μ of the complex μ_i, cannot be treated as a time dependent *perturbation* notwithstanding the fact that it is proportional to a small parameter, because the coupling is not periodic in t. If the coupling had only exponentially decreasing modes, one might try to use much the same methods as are employed in problems of line-breadth and resonance fluorescence. However the modes which increase exponentially with time and which are of course the real source of complication, make this impossible.

Rather than discuss in detail the field theoretical applications we shall exemplify with the help of a simple model what may happen under such circumstances.

Consider a pair of complex conjugated oscillators (31) coupled to an ordinary oscillator in the following manner:

$$H=\tfrac{1}{2}(P_1^2+\omega^2Q_1^2)+\tfrac{1}{2}(P_2^2+\omega^{*2}Q_2^2)+\tfrac{1}{2}(P_0^2+\omega_0^2Q_0^2)+g(Q_1+Q_2)Q_0, \tag{63}$$

where all quantities with the subscript $_0$ refer to the real oscillator; the coupling is proportional to a constant g which we may take as small as we like. Hence it must be possible to transform away the coupling in H by means of a point-transformation in such a way that, in terms of the new variables, H represents an uncoupled system, again consisting of one real oscillator and a pair of complex conjugated oscillators, where the real as well as the complex frequencies have undergone a small shift from their original values. By expressing P_0 and Q_0 in the new variables one can calculate the expectation value of the "old" real oscillator energy for a given state of the new system. It is then readily seen that part of this expectation value comes from the diagonal elements of

$$\text{const.}(P_1'P_2'+Q_1'Q_2'), \tag{64}$$

where the primed quantities are the new variables in the sense just explained. Using the eigenfunctions (33a), one easily shows that the diagonal elements of (64) are infinite.[35]

Infinities of this type have, of course, nothing to do with the divergences of present field theories which are due to the infinite number of degrees of freedom of the fields. They rather remind one of the pathological runaway solutions in electron theory which are well known to occur if we attribute to the electron an infinite sink of mechanical energy.

Thus the introduction of complex μ_i has brought us farther from, rather than nearer to, an acceptable field theoretical model. We will not pursue this line of attack further.

3. *Multiple Real Masses*

From the results of II-A-4 we infer that again the negative energy difficulty prevails. We also met in the

[34] In this case ρ in (2) is proportional to a coupling constant of the dimensions charge × length. This length should be considered to be independent of the κ_i occurring on the left-hand side of (2).
Added in proof. See also W. Thirring, Phys. Rev. **77**, 570 (1950).

[35] All other contributions to the expectation value of the energy of the old real oscillator are finite and thus of no interest for the argument.

corresponding mechanical model with the feature of unbounded motion, although the increase of the motion with t is not so rapid as in the complex case. The multiple masses thus will occupy a position somewhat intermediate between the real and the complex case. We have not investigated this category in any further detail.

Recapitulating the results of the last three sections we may state that any generalization of the electromagnetic or mesonic field equations of the kind (2) where F is an arbitrary polynomial in $\Box$ may lead to an elimination of divergences but only at the cost of other unnatural features.

4. *Multi-Mass Dirac Equations*

The partial fraction method can also be applied to equations of the type (10). Let us start from a Lagrangian

$$\mathfrak{L}_m = -\bar{\psi}F(-\kappa_0)F(\gamma_\mu\partial_\mu)(\gamma_\mu\partial_\mu+\kappa_0)\psi, \tag{65}$$

with

$$F(x)=\prod_{j=1}^{N}(1+x/\mu_j).$$

The constant factor $F(-\kappa_0)$ has been introduced for reasons of convenience which will presently be clear. Define now

$$\Psi_0=F(\gamma_\mu\partial_\mu)\psi,$$

$$\Psi_j=(1+\gamma_\mu\partial_\mu/\kappa_0)\prod_k{}'(1+\gamma_\mu\partial_\mu/\kappa_k)\psi, \quad j=1,\cdots,N,$$

and the adjoint quantities accordingly. Now replace $\mathfrak{L}_m$ by

$$\bar{\mathfrak{L}}_m=-\sum_0^N\xi_j\bar{\Psi}_j(\gamma_\mu\partial_\mu+\kappa_j)\Psi_j. \tag{66}$$

The ξ_j are to be determined from

$$\xi_0+\sum_1^N\xi_j\frac{\kappa_j}{\kappa_0}\frac{1+y/\kappa_0}{1+y/\kappa_j}=\frac{F(-\kappa_0)}{F(y)}. \tag{67}$$

Hence, putting $y=-\kappa_0$:

$$\xi_0=1, \tag{68a}$$

while, after developing $F^{-1}(y)$ in partial fractions, one readily finds that

$$\xi_j=-\frac{\kappa_0^2}{\kappa_j^2}\frac{F(-\kappa_0)}{(\kappa_j-\kappa_0)F'(-\kappa_j)}, \quad j>0. \tag{68b}$$

One also verifies that

$$\psi=[1/\kappa_0F(-\kappa_0)]\sum\xi_k\kappa_k\Psi_k.$$

From (68a, b) it follows again that $\xi_k>0$ for even k and <0 for odd k. Here of course the occurrence of negative ξ_k does not lead to the negative energy complications of the previous sections, as we have now to do with Fermions. Hence by interchanging the rôles of particle and antiparticle for the fields with odd k as compared with the even ones one has obtained a reasonable formulation for an assembly of $N+1$ fields of the Fermi-Dirac type. The normalization of (65) with a factor $F(-\kappa_0)$ led to $\xi_0=1$ and we can therefore directly identify the term of (66) with $j=0$ with the Lagrangian for free electrons (mass κ_0).

The quantization can now be performed by putting[36]

$$\{\Psi_k(x),\,\bar{\Psi}_1(x')\}=i(-1)^{k+1}\xi_k^{-1}\delta_{k1}S_k(x-x')$$

where the index k on S indicates that this quantity refers to the mass κ_k. A factor $(-1)^k$ has to be introduced to obtain positive probabilities for such quantities as the number of particles in a given volume. The main formula for computing vacuum expectation values becomes

$$\langle[\Psi_k(x),\,\bar{\Psi}_l(x')]\rangle_{\text{vac}}=(-1)^{k+1}\xi_k^{-1}\delta_{kl}S_k^{(1)}(x-x') \tag{66a}$$

where the factor $(-1)^k$ expresses the effect of the interchange of particles and antiparticles for odd k on the definition of the vacuum.

In introducing the electromagnetic interaction one will first of all try to replace ∂_μ in (65) by

$$D_\mu=\partial_\mu-i\epsilon A_\mu$$

and add the Lagrangian $\mathfrak{L}_{elm}$ of the electromagnetic field. We express this by

$$\mathfrak{L}=\mathfrak{L}_m(\partial_\mu\to D_\mu)+\mathfrak{L}_{elm}. \tag{69}$$

Next one may also in the definition of Ψ_k replace ∂_μ by D_μ so that the matter fields would depend implicitly on A_μ. It is not difficult to see, however that then

$$\bar{\mathfrak{L}}=\bar{\mathfrak{L}}_m(\partial_\mu\to D_\mu)+\mathfrak{L}_{elm} \tag{70}$$

is *not* equivalent to $\mathfrak{L}$ because it leads to different electromagnetic field equations than does $\mathfrak{L}$. Therefore the decomposition method (which in the case of multi-mass equations of the Bose-Einstein type also works when an interaction is present) here breaks down. This arises from the fact that according to (69) the coupling would no longer be linear in A_μ. It is an open question whether a theory based on (69) leads to an improved situation with regard to such questions as the vacuum polarization.

Alternatively, one might try to use (70) itself as a starting point for the description of a system of spin $\frac{1}{2}$-fields coupled with the electromagnetic field, i.e., one might, so to say, forget the way (66) was obtained from (65). There is no objection to this, but no advantage either. For it is readily seen that in the computation of the charge renormalization the ξ_k drop out entirely; therefore the vacuum polarization is essentially unaffected.

[36] We define $S(x)$ and $S^{(1)}(x)$ in the same way as J. Schwinger, see esp. Phys. Rev. **74**, 1439 (1948), Eq. (2.29) and Phys. Rev. **75**, 651 (1949), Eq. (1.68).

B. Field Equations of the Exponential Type

1. Introductory Remarks

We now turn to a discussion of the main features of equations of the type

$$e^{f(\Box)}\prod_i(\Box-\kappa_i^2)\psi=-\rho.$$

From the remarks made at the beginning of II-B-1, it follows that the problem is separable up to the stage at which one has to deal with

$$e^{f(\Box)}(\Box-\kappa^2)\psi=-\rho. \tag{71}$$

In view of applications to electromagnetic phenomena we put $\kappa=0$; none of the essential new features we shall meet presently are affected by this specialization.

Equations of type (71) go so far beyond the partial differential equations usually encountered in field theory that it seems necessary to investigate first whether the basic mathematical problems and results pertaining to differential equations of the wave equation (hyperbolic) type have their counterpart in the present case. It may therefore be well to recapitulate briefly what the two fundamental problems and the two principal results are for the ordinary wave equation

$$\Box\psi=-\rho: \tag{72}$$

(α) *The initial value or Cauchy problem.*—A solution of the homogeneous wave equation is sought when ψ and its normal derivative are given on some space-like surface.

(β) *The source problem.*—A solution of the inhomogeneous equation is asked for, such that ψ and $\partial\psi/\partial t$ are zero at $t=-\infty$. These initial conditions correspond to the requirement that the source ρ exerts a retarded action.

It is well known that (α) and (β) have a unique solution and that they are intimately related to each other. This relation can, in the language of present day field theory, be stated in terms of the connection between the $\bar{D}$- and the D-function[37]

$$\bar{D}(x)=-\tfrac{1}{2}\,\mathrm{sign}(t)\cdot D(x) \tag{73}$$

with $\mathrm{sign}(t)=\pm1$ for $t\gtrless0$. The solution of (α) is:

$$\psi(x)=\int d\sigma\left[D(x-x')\frac{\partial\psi}{\partial n}-\psi(x')\frac{\partial}{\partial n}D(x-x')\right], \tag{74}$$

where $\partial/\partial n$ denotes differentiation normal to the surface on which the initial values are specified and over which the integral (74) is extended. The solution of (β) is

$$\psi(x)=\int d_4x'\,\bar{D}_{\mathrm{ret}}(x-x')\rho(x'). \tag{75}$$

[37] See e.g., J. Schwinger, Phys. Rev. **75**, 651 (1949), Eq. (A.1). The explicit representations for D and $\bar{D}$ given in reference 33, Eq. (A.29) (with $\kappa_0=0$) and (A.23), are also used here.

Here $\bar{D}_{\mathrm{ret}}$ is the Green function for the retarded type of solution. It is given by

$$\bar{D}_{\mathrm{ret}}=\frac{1}{(2\pi)^4}\int d\mathbf{k}\int d\omega\frac{\exp[i(\mathbf{kx}-\omega t)]}{\mathbf{k}^2-\omega^2}$$

$$=\frac{1}{4\pi r}\delta(t-r),\quad (r=|\mathbf{x}|) \tag{76}$$

with the specification that in the complex ω-plane one shall integrate over a path parallel to and above the real axis. By integrating below the real axis one gets the Green function $\bar{D}_{\mathrm{adv}}$ for the advanced solution. We have

$$\bar{D}(x)=\tfrac{1}{2}(\bar{D}_{\mathrm{ret}}+\bar{D}_{\mathrm{adv}}); \tag{77}$$

all three functions in (77) satisfy

$$\Box\bar{D}=-\delta(x). \tag{78}$$

After this connection between (α) and (β) a second fundamental aspect may be recalled; *viz.*, that for both problems the solutions do not depend on *all* initial values or values of the source but only on the values in a *finite domain of dependence.* [In fact for (β) this domain is the past light cone, and for (α) the part of the space-like surface bounded by that cone.] This is the mathematical expression for the *propagation character* of hyperbolic equations. For the wave equation (72) the propagation character is physically obvious and can also be stated as

$$\left.\begin{aligned}D(x_\mu)=0,\\ \bar{D}(x_\mu)=0\end{aligned}\right\}x_\mu{}^2>0, \tag{79}$$

i.e., both D and $\bar{D}$ vanish outside the light cone.

The suitable generalization of the problems (α) and (β) to linear partial equations of higher order and with constant coefficients and the characteristic features of their solutions have been extensively treated in the mathematical literature. We mention especially the work by Herglotz[38] and a recent investigation by Gårding.[39] It seemed worth while to us to present a short account of some of Gårdings results, since from these it follows that for all equations studied in III-A we have the same kind of relations between the initial value problem and the source problem as for (72), while moreover all these equations have propagation character. In subsection 3 we will see that for equations of the exponential type (71) the situation is radically different.

[38] G. Herglotz, Ber. Sachs. Akad. Wiss, Math.-Phys. Klasse **78**, 41, 287 (1926); **80**, 69 (1928).

[39] L. Gårding, "Linear partial hyperbolic differential equations with constant coefficients," Acta Math. (to be published). See also Comptes Rendus **228**, 731 (1949). It is a pleasure to thank Dr. Gårding for making available to us a copy of his manuscript and for many instructive discussions on these topics.

2. *On the Propagation Character of Equations of Finite Order*

Gårding considers polynomials $q(\xi_1, \cdots, \xi_n)$ in n variables ξ_i and with complex coefficients and associates with them partial differential equations of the form

$$q(\partial/\partial x_1, \cdots, \partial/\partial x_n)\psi = -\rho. \tag{80}$$

The first question is whether it is possible to determine solely from the structure of the polynomial the main characteristics of the solutions of (80). Especially one would like to know for what polynomials the equation is of hyperbolic character. Here it should be pointed out that an equation is of hyperbolic type only with respect to certain directions in the space $\xi_1, \cdots, \xi_n$. That is to say, only for surfaces perpendicular to these directions are the problems (α) and (β) correctly set and only with respect to these directions do the solutions have propagation character.[40] Thus for the wave equation these directions are the time-like vectors and correspondingly the surfaces on which initial conditions are specified are space-like surfaces.

More precisely, one has therefore to find a criterion for a polynomial $q(\xi_1, \cdots, \xi_n)$ to be hyperbolic with respect to a fixed direction $(\bar{\xi}_1, \cdots, \bar{\xi}_n)$. Gårding's criterion is: Put $q=p+r$, where p is the principal part of q, i.e., the homogeneous part of q of highest degree. Then if for a direction $\bar{\xi}_i$ we have

$$p(\bar{\xi}_i) \neq 0, \quad q(\tau\bar{\xi}_i + i\eta_i) \neq 0, \tag{81}$$

for all τ which are larger than a real number τ_0 and for any real vector η_i, then the polynomial $q(\xi_i)$ is said to be hyperbolic with respect to $\bar{\xi}_i$. Gårdings main theorem is: a necessary and sufficient condition for the solutions of (80) to have propagation character with respect to $\bar{\xi}_i$ is that $q(\bar{\xi}_i)$ is hyperbolic with respect to $\bar{\xi}_i$.[41]

It is easy to apply (81) to the wave equation (72). In fact (72) can be considered as the equation adjoined to the polynomial

$$q = \xi_1^2 + \xi_2^2 + \xi_3^2 - \xi_4^2.$$

taking $\bar{\xi}_i = (0, 0, 0, 1)$; i.e., the direction of the time axis, one verifies (81) with $\tau_0 = 0$. The same is true for

$$q = \xi_1^2 + \xi_2^2 + \xi_3^2 - \xi_4^2 - \kappa^2 \rightarrow (\Box - \kappa^2)\psi = -\rho$$

for real κ. If κ is complex the time axis is again a hyperbolic direction, but for τ_0 we now have to take

$$\tau_0 = \{\tfrac{1}{2}((\alpha^2+\beta^2)^{\frac{1}{2}} - \alpha)\}^{\frac{1}{2}}, \quad \kappa^2 = \alpha + i\beta.$$

The significance of τ_0 will become clear presently when we will deal with the source problem (see reference 43).

It may be remarked finally that also the polynomial to which we can adjoin

$$\prod_i (\Box - \kappa_i^2)\psi = -\rho \tag{82}$$

is a hyperbolic polynomial for real or complex, single or multiple occurring κ_i. This is true because (for suitably chosen τ_0) each factor of the product is hyperbolic with respect to the time-axis.

Consider now the source problem for (80). It is clear that a solution in terms of Fourier integrals can be given in the form

$$\psi(t, \mathbf{x}) = \frac{1}{(2\pi)^4} \int\int \frac{d\mathbf{k}d\omega}{q(-i\omega, i\mathbf{k})} \exp[i(\mathbf{kx} - \omega t)]$$

$$\times \int\int dt' d\mathbf{x}' \rho(t', \mathbf{x}') \exp[-i(\mathbf{kx}' - \omega t')] \tag{83}$$

$$= \int\int dt' d\mathbf{x}' \rho(t', \mathbf{x}') K(t - t', \mathbf{x} - \mathbf{x}'), \tag{84}$$

$$K(t, \mathbf{x}) = \frac{1}{(2\pi)^4} \int\int \frac{d\mathbf{k}d\omega}{q(-i\omega, i\mathbf{k})} \exp[i(\mathbf{kx} - \omega t)], \tag{85$_1$}$$

where in view of the physical applications, we consider from now on polynomials q in the four variables[42] $\mathbf{x}, t$, which are hyperbolic with respect to the time direction, i.e. $\bar{\xi}_i = (0, 0, 0, 1)$. It is also well known how to take care of the retarded action of the source by taking the path of the ω-integration above the real axis in the ω-plane such that all the zeros of $q(-i\omega, i\mathbf{k})$, the latter considered as a polynomial in ω, lie below this path. This recipe can also be expressed otherwise; *viz.*, by

[40] The other main property mentioned above, *viz.*, the existence of a relation between the solutions of (α) and (β), is well known [see e.g., Courant-Hilbert, *Methoden der mathematischen Physik* (Dover Publications, New York), Vol. II, p. 165] and is of a much more elementary nature. Suppose (80) to be of mth order in $\partial/\partial t$ where the t axis is the hyperbolic direction. Consider then the initial value problem $q\varphi = 0$ with initial conditions that for $t = -\infty$ all φ and all its time derivatives, up to the $(m-2)$nd one are zero, while $\partial^{m-1}\varphi/\partial t^{m-1} = \rho(s, \mathbf{x})$ where s has to be considered as a parameter. Let the solution be $\varphi(t, \mathbf{x}; s)$. Then the solution of the source problem for (80) is $\psi(t, \mathbf{x}) = \int_{-\infty}^{t} \varphi(t - s, \mathbf{x}; s)ds$.

[41] This is stated very loosely. More explicitly we mean by propagation character of (80) in the direction $\bar{\xi}_i$ the fact that for planes perpendicular to this direction one can suitably generalize the problems (α) and (β) and that the solutions have again a finite domain of dependence. Gårding defines propagation character still more rigorously as follows: Take a sequence $\psi_k(x_1 \cdots x_n)$ of solutions of (80) which is such that for $k \rightarrow \infty$, $\psi_k(x_i)$ tends strongly to zero in a plane $\bar{\xi}_1 x_1 + \cdots + \bar{\xi}_n x_n = 0$. (By "strongly" is meant that ψ_k as well as all its derivatives tend uniformly to zero on every finite domain in the plane). If from the fact that ψ_k tends strongly to zero in this plane it follows that ψ_k tends strongly to zero everywhere, then (80) is said to have propagation character with respect to $\bar{\xi}_i$. It is intuitively clear that if the solution of (80) has a finite domain of dependence the above-mentioned limit property is true. The converse is not so obvious and is shown by Gårding by explicitly constructing the domain of dependence, to which question we will return presently.

[42] We have followed the customary physical convention of taking opposite signs in the Fourier development in $\mathbf{x}$ and t. This is contrary to what is done in reference 39, and as a result certain differences in sign between our account and Gårding's paper appear.

We have also with the usual lack of qualms interchanged orders of integration in going from (83) to (84). $K(t, \mathbf{x})$ is the solution corresponding to a source $\delta(x) = \delta(t) \cdot \delta(\mathbf{x})$. The careful justification of the result (84) is dealt with extensively in reference 39.

putting

$$K(t,\mathbf{x})=\frac{1}{(2\pi)^4}\int d\mathbf{k}\int_{-\infty}^{\infty}d\omega\frac{\exp[i\mathbf{kx}+(\tau-i\omega)t]}{q(\tau-i\omega,i\mathbf{k})}, \quad (85_2)$$

where τ is an arbitrary quantity larger than some fixed real number τ_0 and where we now integrate along the real ω-axis.[43] Since $K(t,\mathbf{x})$ is independent of the value of τ, one sees from this form immediately that $K(t,\mathbf{x})=0$ if $t<0$ by letting $\tau\to\infty$.

The essential step in the derivation by Gårding of the domain of dependence lies in a generalization of the form (85_2) to

$$K(t,\mathbf{x})=\frac{1}{(2\pi)^4}\int_{-\infty}^{\infty}d\mathbf{k}\times\int_{-\infty}^{\infty}d\omega\frac{\exp[(\tau\xi+i\mathbf{k})\mathbf{x}+(\tau\xi_0-i\omega)t]}{q(\tau\xi_0-i\omega,\tau\xi+i\mathbf{k})}, \quad (85_3)$$

where again $\tau>\tau_0$ and where moreover a four-vector (ξ_0,ξ) has been introduced which satisfies the requirement that the zeros of q *still* lie below the real ω-axis and all paths of integration are now taken along the real axis. From Cauchy's theorem it is then clear that (85_3) is equivalent to (85_2) and that therefore the integral in (85_3) is independent of the vector ξ_i and of the magnitude of τ. By letting again $\tau\to\infty$ one now sees that in all points t, $\mathbf{x}$ for which

$$\xi_0 t+\xi\mathbf{x}\leqslant 0 \quad (86)$$

we shall have $K(t,\mathbf{x})=0$. To find therefore the domain of dependence of the solution of (80) one only has to determine the set of directions ξ_i which satisfy the condition stated above. For the equation $(\Box-\kappa^2)\psi=\rho$ one readily finds, whether κ is real or complex, that the ξ_i-domain is

$$\xi_0>0,\quad \xi_0^2-\xi^2>0,$$

i.e., the inner part of the future light cone. Then it follows from (86) that the domain of dependence is

$$t\geqslant 0,\quad t^2-\mathbf{x}^2\geqslant 0.$$

Clearly the same is true for a product of factors $(\Box-\kappa_i^2)$ so that we may state: The equation $F(\Box)\psi=\rho$, where F is an arbitrary polynomial with complex coefficients, is a hyperbolic equation with respect to the time direction. Its domain of dependence is the past light cone and its interior.

Gårding has succeeded in expressing these results in a much more general way. He associates with the polynomial q which is hyperbolic with regard to the direction $\bar{\xi}_i$ a cone $\Gamma(\bar{\xi}_i)$ generated by the direction $\bar{\xi}_i$. $\Gamma(\xi)$ is defined as follows. Consider the principal part p of q and put

$$p(\tau\xi+\bar{\xi})=p(\xi)\prod_i(\tau+u_i(\bar{\xi},\xi)). \quad (87)$$

For real ξ, the roots $u_i(\bar{\xi},\xi)$ can be shown to be real if q is hyperbolic. From the homogeneity of p one easily sees that

$$u_i(\bar{\xi},a\xi)=au_i(\bar{\xi},\xi);\quad u_i(a\bar{\xi},\xi)=(1/a)u_i(\bar{\xi},\xi) \quad (88)$$

and

$$u_i(\bar{\xi},\bar{\xi})=1. \quad (89)$$

The cone $\Gamma(\xi)$ is defined by the assembly of all directions ξ for which the *smallest* of the roots u_i is still >0. From (88) it follows that we really have to do with a cone determined by the direction of $\bar{\xi}$ only, while from (89) and the continuity of $u_i(\bar{\xi},\xi)$ one infers that such a cone must exist and that the direction $\bar{\xi}$ belongs to it. The importance of the cone $\Gamma(\xi)$ lies in its following two main properties: (1) If q is hyperbolic with respect to $\bar{\xi}$ then it is also hyperbolic with respect to any direction ξ in $\Gamma(\xi)$; and any direction in $\Gamma(\xi)$ generates the same cone. (2) The cone $\Gamma(\xi)$ contains all vectors for which (85_3) is identical with (85_2) and therefore according to (86), $\Gamma(\xi)$ determines the domain of dependence.

3. *Remarks on the Propagation Problem for Equations of Infinite Order*

Little is known about equations of the type (71). However, it can readily be seen that there are essential differences from the hyperbolic differential equations discussed above.

In the first place it is clear that in the homogeneous equation the exponential factor does not play any rôle so that the initial value problem is the same as for $f=0$. Thus with regard to the Cauchy problem the equation has propagation character. Another way of expressing this is to say that the D-function in (74) and (79) is unaffected by the introduction of an exponential.

Just as for the exponential case in the mechanical problems (see II-B-3) the situation is quite different for the inhomogeneous problem. The solution of

$$e^{f(\Box)}\Box\psi=-\rho \quad (90)$$

can still be written down in a form analogous to (83):

$$\psi(t,\mathbf{x})=\frac{1}{(2\pi)^4}\int\int\frac{d\mathbf{k}d\omega}{\mathbf{k}^2-\omega^2}\exp[-f(\omega^2-\mathbf{k}^2)+i(\mathbf{kx}-\omega t)]\times\int\int dt'd\mathbf{x}'\rho(t',\mathbf{x}')\exp[-i(\mathbf{kx}'-\omega t')] \quad (91)$$

where one would be inclined, as in subsection 2, to perform the ω-integration along a path parallel to and above the real axis. However, the argument that this choice will give a retarded action breaks down since one clearly may never close the path by a big half circle, so that one cannot conclude that $\psi=0$ for $t<0$.

Nevertheless it is of interest to discuss the formal solution (91) for this choice of path. For the case that $f(\Box)$ is a polynomial one still must make an important distinction, *viz.*, that between odd and even functions f. This will be clear enough from the two cases we will now discuss separately:

$$\text{(a) } f(\Box)=-\lambda^2\Box,\quad \text{(b) } f(\Box)=\lambda^4\Box^2,$$

[43] Clearly, the meaning of this transformation is that since the number of zeros of q is finite we can push them all below the real ω-axis by adding an imaginary part to ω; the quantity τ_0 which we have encountered in Eq. (81) and in the examples discussed above is simply the imaginary part of that root of $q(-i\omega,i\mathbf{k})=0$ which lies highest above the real ω-axis.

where λ is a quantity with the dimensions of a length. The signs have been chosen such that for the static point source problem, (90) always gives a ψ finite at the origin.

Case a.—If ρ is the δ-function $\delta(t)\delta(\mathbf{x})$, the ω-integral is divergent so that the analog to $\bar{D}_{\text{ret}}(x)$ does not exist. This does not mean that (91) always leads to a divergent ψ, but it implies a severe restriction on the admissible source functions ρ. This can also be illustrated as follows. For the case considered (90) becomes

$$\exp(-\lambda^2\Box)\cdot\Box\psi(t,\mathbf{x},\lambda^2)=-\rho(t,\mathbf{x}), \tag{92}$$

where the dependence of ψ on the parameter λ has been written down explicitly. Hence differentiating with respect to λ^2 and omitting the plane wave solutions for ψ which do not interest us at the moment, we get

$$\partial\psi/\partial(\lambda^2)-\Box\psi=0. \tag{93}$$

Equation (93) has to be solved with the initial value $\psi(t,\mathbf{x},0)$ satisfying the ordinary wave equation

$$\Box\psi(t,\mathbf{x},0)=-\rho(t,\mathbf{x}).$$

Equation (93) is of the heat conduction type in the variables λ^2 and $\mathbf{x}$ but with respect to λ^2 and t it is the analog of the equation of heat conduction toward negative time. Now it is well known that for the ordinary heat conduction equation

$$\partial u/\partial t=\partial^2 u/\partial x^2$$

the solution is an analytic function of x for any $t>0$, whatever function the given initial value $u(x,0)$ is. Clearly therefore, in order to get a solution for an equation of the type

$$\partial u/\partial t=-\partial^2 u/\partial x^2,$$

one can only allow initial values which are analytic functions of x, and even this may not be enough.

Case b.—Here (91) exists even for a δ-function source. To evaluate it further one conveniently cuts up the path of the ω-integration into: (1) two small half-circles over the poles $\omega=\pm|k|$, (2) a principal-value integral along the real axis. One easily sees that, as in the case $\lambda=0$, the contribution of the half-circles is

$$-(1/8\pi r)\{\delta(t+r)-\delta(t-r)\}. \tag{94}$$

The principal value integral I becomes, after some angular integrations,

$$I=\frac{1}{16i\pi^3}\cdot\frac{1}{r}\int_{-\infty}^{\infty}kdk\cdot P\int_{-\infty}^{\infty}d\omega\frac{\exp[-\lambda^4(k^2-\omega^2)^2]}{k^2-\omega^2}$$
$$\times[\exp[i(kr-\omega t)]-\exp[-i(kr+\omega t)]].$$

To evaluate this further, one has to distinguish several cases. Consider first $t>0$, $t^2>r^2$ and put

$$t=\rho^{\frac{1}{2}}\cosh\alpha,\quad r=\rho^{\frac{1}{2}}\sinh\alpha,\quad \rho=t^2-r^2. \tag{95}$$

Now divide the (k,ω)-domain in two regions and make the following substitutions:

$k^2>\omega^2$: $k=R\cosh\varphi$, $\omega=R\sinh\varphi$; $-\infty<R<+\infty$
$k^2<\omega^2$: $k=R\sinh\varphi$, $\omega=R\cosh\varphi$; $-\infty<\varphi<+\infty$.

One then obtains after some calculation

$$I=-\frac{1}{4\pi^3}\cdot\frac{1}{\rho^{\frac{1}{2}}}\int_{-\infty}^{\infty}\frac{|R|}{R}dR\exp(-\lambda^4R^4)\int_0^{\infty}d\vartheta$$
$$\times\{\sinh\vartheta\sin(\rho^{\frac{1}{2}}R\sinh\vartheta)-\cosh\vartheta\sin(\rho^{\frac{1}{2}}R\cosh\vartheta)\}$$
$$=\frac{1}{\pi^3}\frac{\partial}{\partial\rho}\int_0^{\infty}\frac{dR}{R}\exp(-\lambda^4R^4)\int_0^{\infty}d\vartheta$$
$$\times\{\cos(\rho^{\frac{1}{2}}R\sinh\vartheta)-\cos(\rho^{\frac{1}{2}}R\cosh\vartheta)\},$$

or finally[44]

$$I=\frac{1}{\pi^3}\frac{\partial}{\partial\rho}\int_0^{\infty}\frac{dy}{y}\exp(-\lambda^4y^4\rho^{-2})\left[K_0(y)+\frac{\pi}{2}Y_0(y)\right].$$

One proceeds likewise in the other parts of the r,t-plane. Adding the contribution (94), the final result for ψ is:

$$\psi=-\frac{1}{8\pi r}[\delta(t+r)-\delta(t-r)]+\varphi_\lambda(\rho) \tag{96}$$

$$\varphi_\lambda(\rho)=\frac{1}{\pi^3}\frac{\partial}{\partial\rho}\left\{\operatorname{sign}(\rho)\cdot\int_0^{\infty}\frac{dy}{y}\exp(-\lambda^4y^4\rho^{-2})\right.$$
$$\left.\times\left[K_0(y)+\frac{\pi}{2}Y_0(y)\right]\right\}. \tag{97}$$

For $\lambda=0$, φ can be written as[44]

$$\varphi_0(\rho)=\frac{1}{\pi^3}\left(\frac{\partial}{\partial\rho}\operatorname{sign}(\rho)\right)\cdot\int_0^{\infty}\frac{dy}{y}\left[K_0(y)+\frac{\pi}{2}Y_0(y)\right]$$
$$=\frac{2}{\pi^3}\delta(\rho)\int_0^{\infty}\frac{dy}{y}\int_0^{\infty}\frac{du}{u}\sin u\sin\frac{y^2}{4u}$$
$$=\frac{1}{\pi^3}\delta(\rho)\int_0^{\infty}\frac{du}{u}\sin u\int_0^{\infty}\frac{dv}{v}\sin\frac{v}{u}=\frac{1}{4\pi}\delta(\rho).$$

Therefore, remembering the definition (95) of ρ, we have verified that for $\lambda=0$, ψ becomes the function $\bar{D}_{\text{ret}}$ of (76).

For $\lambda\neq0$, $\varphi_\lambda(\rho)$ is zero for $\rho=0$ and has two peaks symmetrically around $\rho=0$ at a distance $\sim\lambda^2$, with height $\sim\lambda^{-2}$ and width $\sim\lambda^2$. For decreasing λ the peaks will move nearer together and become higher, but will remain separated by the zero value of φ at the origin,

[44] K_0 and Y_0 are defined as in Watson, *Theory of Bessel Functions* (1944), second edition, Eq. (4), p. 78, and Eq. (2), p. 64, respectively; see also Eq. (14), p. 183, Eq. (13), p. 180, and Eq. (3), p. 184.

however small λ may be. Therefore the limit at which the two peaks coalesce to the δ-function is reached in a highly non-uniform manner.

Thus according to (96) the ψ corresponding to a pulse (δ-source) at the time $t=0$ is for $t>0$ not strictly zero outside the sphere $r=t$, although for $\rho>\lambda$ the excitation function ψ drops rapidly to zero. Moreover it follows from (96) that for times prior to the occurrence of the pulse there is already an excitation. For all these reasons the notion of propagation therefore now loses its meaning.

If, however, we average ψ over a region of the order λ around the light cone this average value is vanishingly small for $t>0$, while for $t<0$ one approaches rapidly the same value $\bar{D}_{\text{ret}}$ for ψ as in the conventional theory. In this sense we can therefore say that the equation

$$\exp(\lambda^4\Box^2)\cdot\Box\psi=-\rho \tag{98}$$

exhibits a *propagation character in the mean.*

From the examples discussed it is clear that for the exponential type of Eqs. (90)—or, for that matter, for Eq. (71)—the propagation character in the sense discussed in subsection 2 does not seem to exist. On our request Dr. Gårding has kindly investigated this problem along the lines mentioned in reference 41 and has given a mathematically rigorous proof of the non-existence of the propagation character for the Eqs. (71).

For the purposes of the next section we note that it is still possible to define a function $\bar{D}_\lambda$ for Eq. (98) in much the way that was done in (77) for $\lambda=0$. One can, in fact, determine the solution of the equation

$$\exp(\lambda^4\Box^2)\cdot\Box\psi=-\delta(x) \tag{99}$$

which corresponds to the advanced solution for $\lambda=0$ by integrating below instead of above the poles on the real ω-axis. Defining then $\bar{D}_\lambda(x)$ as half the sum of this solution and of (96), one obtains

$$\bar{D}_\lambda(x)=\varphi_\lambda(\rho). \tag{100}$$

Finally one can integrate (99) below the pole at $\omega=-|\mathbf{k}|$ and above the pole $\omega=+|\mathbf{k}|$. This mode of integration has been used extensively by Feynman in his version of quantum electrodynamics. For this integration the result is

$$\psi=\varphi_\lambda(\rho)+\frac{i}{4\pi^2}\cdot\frac{1}{r^2-t^2},$$

or

$$\psi=\bar{D}_\lambda(x)+\tfrac{1}{2}iD^{(1)}(x), \tag{101}$$

where $D^{(1)}(x)$ is the same function as occurs in the customary formulation of quantum electrodynamics.[45] Mathematically speaking, the reason that $D^{(1)}$ comes out unchanged is that it is a contribution from the poles at $\omega=\pm|\mathbf{k}|$ and is not affected by the behavior of ψ at the point at infinity in the ω-plane.

[45] See reference 37, Eq. (A.40).

4. On Exponential Modifications of Quantum Electrodynamics

In this section we shall discuss some of the novel features which arise if we modify the electromagnetic field equations in the manner indicated by Eq. (90), so that we start from a Lagrangian density

$$\mathfrak{L}=-\frac{1}{2}\frac{\partial A_\mu}{\partial x_\nu}e^{f(\Box)}\frac{\partial A_\mu}{\partial x_\nu}-j_\mu A_\mu-\bar{\psi}(\gamma_\mu\partial_\mu+\kappa)\psi, \tag{102}$$

where all quantities are defined as in Eq. (52). We will again impose the supplementary condition (53) on A_μ. As $\mathfrak{L}$ exhibits all conventional invariance properties it is clear that an energy-momentum tensor density must exist which satisfies the usual conservation laws. (The most suitable way to find this tensor is by means of an elegant method recently developed by Green.[46])

We consider first the case in which there is no interaction. It follows directly from the results in subsection 3 on the initial value problem that classically the situation is unchanged; i.e., it is the same as for $f=0$. This is true also quantum mechanically.

First of all we can make a spatial Fourier decomposition of the electromagnetic field quantities, as a result of which the electromagnetic field Lagrangian becomes a superposition of harmonic oscillator Lagrangians each modified by an extra exponential factor $\exp[f(-D^2-\omega^2)]$, where ω is the frequency of the wave considered and D again stands for d/dt. From the argument given in II-B-3 it then follows that the result of quantizing each Fourier component is in all respects identical with that of an oscillator without exponential factor. Hence it follows also that the commutation relations between two field quantities taken at the same time but at different points in space remain unchanged. But, as according to subsection 3 the propagation character for the homogeneous problem is unaffected by the presence of exponentials, the commutation relations are also unchanged if we take the field variables at different times, so that we may state that

$$[A_\mu(x),\, A_\nu(x')]=i\delta_{\mu\nu}D(x-x'),$$

where D is the D-function of ordinary quantum electrodynamics.

As further consequences of the absence of any influence of the exponential on problems in which no interactions are involved, we mention that Planck's radiation law is unaffected and also that the vacuum expectation value of any function of the A_μ remains unchanged. In particular,

$$\langle\{A_\mu(x),\, A_\nu(x')\}\rangle_{\text{vac}}=\delta_{\mu\nu}D^{(1)}(x-x')$$

in which the conventional $D^{(1)}$-function occurs. This is in harmony with the result quoted in Eq. (101) where in other context we met an unmodified $D^{(1)}$.

[46] H. S. Green, Proc. Roy. Soc. **197**, 73 (1949), Section 4.

Turning now to problems of interaction, a remark on the classical theory is in order. Calling φ the modified Coulomb potential, it is seen from (102) that for a point electron at rest

$$\varphi(r)=\frac{\epsilon}{2\pi^2 r}\int_0^\infty \frac{dk}{k}\sin kr\,\exp[f(-k^2)].$$

For both cases a and b discussed in subsection 3, the k-integral is convergent and φ is finite for $r=0$. Therefore the classical self-energy of a point charge is finite, and this is true in any Lorentz frame of reference. For $f=-\lambda^2\Box$ this has been discussed by Born.[19] Thus for such static and quasi-static effects there is no essential difference between the cases a and b. On the other hand, the truly dynamical features have been shown there to be quite different, and for the reasons given in that section we will from now on confine our attention to the case of even functions f and will choose again especially $f=\lambda^4\Box^2$.

For this case we have given in subsection 3 the formal solution of the pulse problem, i.e., the excitation which is generated by a δ-function source acting at $t=0$, $\mathbf{x}=0$ has been computed. It was found that such pulses act in such a peculiar way, *viz.*, "before they start", and giving an excitation which partly moves with velocities greater than that of light, that it is out of the question to consider without further ado the application to actual physical situations. In particular the integrability conditions of the Tomonaga-Schwinger theory which express the unambiguous causal development with time of the state vector of a system can no longer be expected to be satisfied.

On the other hand, we have been stimulated by the reasonable behavior in an average sense explained in the previous section to make some conjectures as to the possible use of such exponential equations in a situation where one no longer insists on the unlimited localizability of space-time events. The tentative and incomplete nature of the remarks made hereafter need, of course, hardly be stressed.

First of all, it is clear that the effect of the modifications may be quite different for virtual as compared to real processes. In the latter case the lack of propagation character is such a drastic change of our fundamental physical notions that one can only hope to obtain an interpretable scheme by renouncing a strictly causal description. This will be the subject of further investigation.

On the other hand, one may expect that the effect on virtual processes will simply be the replacement of the ordinary $\bar{D}$- and $\bar{\Delta}$-functions by the corresponding exponential modifications of these propagation functions, while the $D^{(1)}$- and $\Delta^{(1)}$-functions remain unchanged. In fact, this procedure can be justified by means of the S-matrix methods recently developed by Källén and by Yang and Feldman.[47] Their idea is to stay in the Heisenberg representation throughout the calculations and in this representation to solve by iteration the equations describing the behavior of sources and fields.

We consider first the electron self-energy integral which in the notation of Schwinger is given by[48]

$$\delta m=-\frac{e^2}{2}\int d_4\xi\cdot\gamma_\mu[S^{(1)}(\xi)\bar{D}(\xi)+\bar{S}(\xi)D^{(1)}(\xi)]\gamma_\mu\exp(-ip_\mu\xi_\mu).$$

In keeping with the foregoing, one will retain the $D^{(1)}$-function but must now replace $\bar{D}$ by $\bar{D}_\lambda$ given by (97) and (100). This would make the first term in the square brackets finite, but would not alter the second which still diverges. Thus, exponential modifications of the electromagnetic field do not yield a finite self-energy in contrast to the polynomial modifications studied in previous sections. This is essentially because the exponentials do not affect the vacuum fluctuations, whereas in the polynomial case new fluctuations occur due to the presence of new types of quanta.

It would seem plausible, however, that once one gives up the localizability of the electromagnetic field quantities, the same should be done with the electron field. Thus, one will keep again the expression for $\Delta^{(1)}$ but may let $\bar{\Delta}$ satisfy

$$\exp[\lambda^4(\Box-\kappa^2)^2]\cdot(\Box-\kappa^2)\bar{\Delta}(x)=-\delta(x), \quad (103)$$

where the exponent has been so chosen that according to a similar argument as given above the free electron states are unaffected. This implies a modification of the last term of (102) by the exponential factor $\exp\lambda^4(\Box-\kappa^2)^2$. Thus, the matter equations now are

$$\exp[\lambda^4(\Box-\kappa^2)^2]\cdot(\gamma_\mu\partial_\mu+\kappa)\psi=ie\gamma_\mu A_\mu\psi. \quad (104)$$

Doing this, one obtains an absolutely convergent integral for δm which can be readily seen to be

$$\delta m=\frac{e^2\kappa}{8\pi^2}\int_0^\infty y^2dy\left[\frac{1}{(1+y^2)^{\frac{1}{2}}}\left\{\frac{2-(1+y^2)^{\frac{1}{2}}}{-1+(1+y^2)^{\frac{1}{2}}}\times\exp[-4\lambda^4\kappa^4(1-(1+y^2)^{\frac{1}{2}})^2]-\frac{2+(1+y^2)^{\frac{1}{2}}}{1+(1+y^2)^{\frac{1}{2}}}\times\exp[-4\lambda^4\kappa^4(1+(1+y^2)^{\frac{1}{2}})^2]\right\}+\frac{2}{y}\exp(-4\lambda^4\kappa^4y^2)\right].$$

Once the $\bar{\Delta}$-function has been modified according to (103) the question arises as to how this will affect the

[47] G. Källén, "Mass and charge renormalizations in quantum electrodynamics without use of the interaction representation Arkiv. f. Mat. Astr. o. Fys. (to be published); C. N. Yang and D. Feldman (to be published). We are indebted to Professor Pauli for making Dr. Källén's manuscript available to us as well as for instructive discussions on this point.

[48] See reference 37, Eq. (3.78).

vacuum polarization. The integral representing the current $\delta(i\epsilon\bar{\psi}\gamma_\mu\psi)$ induced by an external field A_μ^e is, according to Schwinger,[49]

$$\delta(i\epsilon\bar{\psi}\gamma_\mu\psi)=-4\epsilon^2\int d_4x' K_{\mu\nu}(x-x')A_\nu^e(x'), \tag{105}$$

$$K_{\mu\nu}(x)=\frac{\partial\bar{\Delta}}{\partial x_\mu}\cdot\frac{\partial\Delta^{(1)}}{\partial x_\nu}+\frac{\partial\bar{\Delta}}{\partial x_\nu}\frac{\partial\Delta^{(1)}}{\partial x_\mu}$$
$$-\delta_{\mu\nu}\left(\frac{\partial\bar{\Delta}}{\partial x_\lambda}\frac{\partial\Delta^{(1)}}{\partial x_\lambda}+\kappa^2\bar{\Delta}\Delta^{(1)}\right).$$

If instead of the ordinary $\bar{\Delta}$-function one again employs the expression following from (103) it is not surprising that the charge renormalization will be finite. The more interesting question is what will now happen with gauge invariance and charge conservation. The decisive quantity here is the divergence of $K_{\mu\nu}$ for which one has

$$\partial K_{\mu\nu}/\partial x_\mu=(\partial\Delta^{(1)}/\partial x_\nu)\cdot(\Box-\kappa^2)\bar{\Delta}$$
$$=-(\partial\Delta^{(1)}/\partial x_\nu)\cdot\exp[-\lambda^4(\Box-\kappa^2)^2]\delta(x). \tag{106}$$

This is not equal to zero as one would like it to be. Nor could this be expected since (104) is not gauge invariant. This of course makes it questionable to call $i\epsilon\bar{\psi}\gamma_\mu\psi$ a current and the quantity (105) an induced current. It can be asked, however, whether (106) could be zero "in the mean"; i.e., in some way similar to the manner in which we obtained an average propagation of an electromagnetic excitation with light velocity. For this purpose we study

$$\chi(x)=\exp[-\lambda^4(\Box-\kappa^2)^2]\delta(x).$$

By the same methods used to derive Eq. (97) one finds

$$\chi(x)=\frac{1}{\pi^3}\frac{\partial}{\partial\rho}\cdot\frac{1}{\rho}\int_0^\infty ydy\left[\exp\left[-\lambda^4\left(\frac{y^2}{\rho}+\kappa^2\right)^2\right]K_0(y)\right.$$
$$\left.+\exp\left[-\lambda^4\left(\frac{y^2}{\rho}-\kappa^2\right)^2\right]\cdot\frac{\pi}{2}Y_0(y)\right].$$

We note the following main properties of χ: First it is ≈ 1 when integrated over a space-time domain $\sim\lambda^4$ around the origin and in this sense behaves approximately like a δ-function. Second it vanishes very strongly for $t=0$, $\mathbf{x}=0$. In fact, the product of $\chi(x)$ and the derivative of $\Delta^{(1)}$ occurring in (106) is zero at this point, notwithstanding the singular behavior of $\Delta^{(1)}$ for $\rho=0$. Thus one can give an unambiguous meaning to the right-hand side of (106), in contradistinction to the case that $\lambda=0$. As $\chi(x)$ is an even function of its argument while $\partial\Delta^{(1)}/\partial x_\nu$ is odd, it follows that the average of (106) over a small space-time domain around the origin vanishes. In this sense we can speak of a conservation of the induced charge in the mean.

[49] See reference 37, Eq. (2.20).

The preceding remarks would seem to indicate that the assumption of non-localizability should be made for all kinds of fields once it is made for one kind, and that "macroscopic" conservation laws may perhaps have to be considered as valid only in some average sense.

IV. OUTLOOK

From the investigations described in this paper we have seen that it is very difficult, if it is at all feasible, to reconcile the three requirements of convergence, positive-definiteness and strict causality in dealing with field equations which are partial differential equations of high order or are integral equations. It may be asked whether the restriction to integral functions made in this paper has been unduly narrow and whether more general functions might be better suited for the purposes outlined in the introduction. We have not made a systematic exploration of such possibilities. A further study may be of interest, but it seems to us that the main physical consequences of the use of finite distance operators have been laid bare by the present investigation. However one point which we still wish to mention is that by using meromorphic functions or rational fractions for F in (2) it is possible to obtain multi-mass equations without having negative-energy troubles. From Eq. (47) the reader will in fact verify that if between each two zeros of F there lies a simple pole, one gets an assembly of fields with quanta of various masses and all with positive-definite energy. On the other hand, the introduction of fractions leads again to loss of convergence.[50]

The multi-mass equations studied in this paper are, generally speaking, connected with the idea of compensation (see Introduction). As we have seen, the various fields whose contribution to the self-energy etc. tend to balance each other are all of the same relativistic transformation type. Other compensation schemes (see reference 6), are not covered by the present work. On the whole it seems however that all attempts made so far to achieve convergence by compensation are inadequate. This is in our opinion not so much a criticism of the underlying idea as well an indication that one should look for still more intimate connections between fields of various types.

All in all, it seems to us that the most hopeful approach which the present investigation possibly indicates is one, where, as for example in the case of the exponentials studied here, the possibility of an ordering of space-time events is no longer a strict requirement. But it should again be emphasized that here we have

[50] To quote an example: consider

$$\Box^{\frac{1}{2}}\tan\lambda\Box^{\frac{1}{2}}\cdot A_\mu\equiv F(\Box)A_\mu=-\lambda j_\mu.$$

For $\lambda\to 0$ (or for low frequencies in the Fourier development) $F(\Box)\simeq\lambda\Box$. F has zeros κ_n^2, where $\kappa_n=n\pi\lambda^{-1}$, $n=0, 1, 2, \cdots$ are quantum rest masses. Also F has singularities at $\Box=\alpha_n^2$, $\alpha_n=(n-\frac{1}{2})\pi\lambda^{-1}$. Thus, all quanta have positive definite energies. Convergence is lost as is already clear from the singular nature of the modified Coulomb potential which is $(4\pi r)^{-1}\coth\pi r/2\lambda$ and is $\sim r^{-2}$ for $r\to 0$.

come to the limits of the foundations of our present picture of the physical world. An attempt at loosening up these foundations by relinquishing the "causality in the small" might throw more light on the situation.

The present work was begun during the stay of one of the authors (G.E.U.) at the Institute for Advanced Study. He wishes to express his appreciation for this stimulating experience and for the hospitality shown to him. He is also indebted to the Institute for having supported his research in part by a grant of AEC funds. Both authors also wish to thank the staff of the Brookhaven National Laboratory for working facilities provided them last summer.

APPENDIX

Some Further Comments on Multiple Frequencies

We wish to indicate here briefly the treatment of a mixture of single and multiple frequencies, and that of frequencies with multiplicity higher than two. For this purpose we consider first the situation in which three distinct real frequencies are present:

$$L=-q\prod_{i=0}^{2}(D^2+\omega_i^2)q, \tag{A1}$$

$$\approx\sum_{0}^{2}\eta_j Q_j(D^2+\omega_j^2)Q_j; \tag{A2}$$

$$Q_j=\prod_{i}{}'(D^2+\omega_i^2)q,$$

$$\eta_0=\{(\omega_1^2-\omega_0^2)(\omega_2^2-\omega_0^2)\}^{-1},$$
$$\eta_1=\{(\omega_2^2-\omega_1^2)(\omega_1^2-\omega_0^2)\}^{-1},$$
$$\eta_2=\{(\omega_2^2-\omega_1^2)(\omega_2^2-\omega_0^2)\}^{-1}.$$

From this we get the case of one single plus one double root by putting $\omega_2=\omega_1+\epsilon$, $Q_1=Q_2+\epsilon Q_3$ and going to the limit $\epsilon\to 0$ in the same way as described in II-A-4. Obviously the Q_0-dependent part of (A2) remains unaffected apart from $\eta_0\to(\omega_1^2-\omega_0^2)^{-2}$. The generalization to the case of more than one simple frequency plus multiple frequencies is obvious. We can also get from (A2) the case of a triple frequency by putting

$$\begin{aligned}&\omega_1=\omega_0+\epsilon_1,\quad \omega_2=\omega_0+\epsilon_2,\\ &Q_0=R_0+(\epsilon_1+\epsilon_2)R_1+\tfrac{1}{2}(\epsilon_1+\epsilon_2)^2R_2,\\ &Q_1=R_0+\epsilon_2R_1+\tfrac{1}{2}\epsilon_2^2R_2,\\ &Q_2=R_0+\epsilon_1R_1+\tfrac{1}{2}\epsilon_1^2R_2.\end{aligned} \tag{A3}$$

The transformed L then becomes (after multiplication with a trivial constant factor $-4\omega_0^2$)

$$L=\dot R_0\dot R_2-\omega_0^2R_0R_2-R_0^2+\dot R_1^2-\omega_0^2R_1^2+4\omega_0R_0R_1,$$

which can be shown to give the same equations of motion in terms of q as (A1) does. The Hamiltonian is

$$H=P_0P_2+\omega_0^2R_0R_2+\tfrac{1}{4}P_1^2+\omega_0^2R_1^2+R_0^2-4\omega_0R_0R_1.$$

Performing the contact transformation

$$P_0\to\omega_0^{\frac{1}{2}}\left(P_0-\frac{1}{\omega_0(2\omega_0)^{\frac{1}{2}}}P_1\right),\quad R_0\to\frac{1}{\omega_0^{\frac{1}{2}}}R_0$$

$$P_1\to\sqrt{2}\left(P_1+\frac{1}{(2\omega_0)^{\frac{1}{2}}}R_2\right),\quad R_1\to\frac{1}{\sqrt{2}}\left(R_1+\frac{1}{\omega_0(2\omega_0)^{\frac{1}{2}}}R_0\right)$$

$$P_2\to\omega_0^{\frac{1}{2}}\left(P_2+\frac{1}{(2\omega_0)^{\frac{1}{2}}}R_1\right),\quad R_2\to\frac{1}{\omega_0^{\frac{1}{2}}}R_2$$

H becomes

$$H=\omega_0(P_0R_2-P_2R_0)+\frac{1}{4\omega_0}(R_0^2+R_2^2)+\frac{1}{2}(P_1^2+\omega_0^2R_1^2).$$

Comparison with (37) shows that a triple frequency is equivalent to a double one plus a single oscillator with the same frequency which of course introduces a new degeneracy.

The generalization of relations like (A3) to the case of n-fold multiplicity is straightforward. We have not investigated this further but conjecture that a $2n$-fold root is equivalent to a degenerate system of n double roots and that a $(2n+1)$-fold root is equivalent to a $2n$-fold root degenerate with a single oscillator.

Letters to the Editor

PUBLICATION of brief reports of important discoveries in physics may be secured by addressing them to this department. The closing date for this department is five weeks prior to the date of issue. No proof will be sent to the authors. The Board of Editors does not hold itself responsible for the opinions expressed by the correspondents. Communications should not exceed 600 words in length.

Wave-Length of the Transauroral Line of Oxygen

N. D. SAYERS AND K. G. EMELEUS
Queen's University, Belfast, Ireland
April 24, 1950

THERE is an interesting discrepancy between the wave-lengths of the transauroral line $^3P_1-{}^1S_0$ of OI, as determined directly by L. and R. Herman,[1] and indirectly from Kvifte and Vegard's measurements[2] of the green and red forbidden lines $^1D_2-{}^1S_0$ and $^3P_1-{}^1D_2$. The wave-length obtained by R. and L. Herman is 2972.25±0.01A. From Kvifte and Vegard's best values of 5577.346 and 6363.854A for the visible pair, the wave-length of the ultraviolet line should be 2972.35A. We have recently succeeded in photographing the transauroral line on a Hilger large quartz instrument, with exposures of 2 to 3 days, using as source a larger version of a positive column tube described previously[3] containing argon and oxygen at a total pressure of about 4 mm Hg. Using an iron arc reference spectrum, the wave-length has been recorded as 2972.325±0.02A. With exposures of this duration it is difficult to be sure that no small shift has occurred, but the results obtained from the four best exposures lie between 2972.305 and 2972.34A. In view of the interest attaching to the exact values of the separations of the low terms of OI, an interferometric determination of the wave-length of the transauroral line is much to be desired. This may not be easy to obtain, as, apart from the question of intensity, the forbidden lines of oxygen are frequently associated with continua or diffuse bands, at least when the oxygen is diluted with an inert gas.[1,4] These could produce an apparent broadening or asymmetrical displacement of the line. It is possible that the differences in wave-length which have been reported have some such origin. On our plates there is no sign of a continuum or of diffuse bands in the immediate neighborhood of 2972.3A, the nearest feature of this kind being a small patch of continuum extending for about 1.5A around 2974, on one plate only.

We are indebted to M. and Mme. Herman for discussion of this work.

[1] L. Herman and R. Herman, Ann. de Géophys. **1**, 165 (1944).
[2] G. Kvifte and L. Vegard, Geofys. Publ. Oslo **17**, No. 1 (1946).
[3] Emeleus, Sloane, and Cathcart, Proc. Phys. Soc. London **51**, 978 (1939).
[4] R. Herman and L. Herman, J. de phys. et rad. **11**, 69 (1950).

Neutron-Proton Capture and Coherent Scattering Amplitudes

LAMEK HULTHÉN
Royal Institute of Technology, Stockholm, Sweden
April 26, 1950

THE theoretical calculations of the neutron-proton capture cross section, σ_c, reported earlier[1] have been repeated with improved numerical accuracy, using the present best values for the deuteron binding energy and the epithermal neutron-proton scattering cross section. We assume a central Yukawa potential in the ^3S as well as in the ^1S state with the same range in both cases, so that

$$V(^1S)=-Ae^{-\kappa r}/r, \quad V(^3S)=-Be^{-\kappa r}/r, \tag{1}$$

with

$$\kappa=mc/\hbar.$$

The constant B is determined from the deuteron binding energy[2] $|E_0|=2.23_7$ Mev, and A is then fixed by the epithermal scattering cross section[3] $\sigma_0=20.3_8$ barns, together with the condition that the ^1S state be virtual.

The calculations were carried out for two different values of the meson mass, m. The errors in the theoretical cross sections, due to the approximate wave functions used, are believed not to exceed a few parts per thousand.[4] The results are indicated in Table I.

TABLE I. σ_c (barns) at a neutron velocity of 2200 meters/sec.

Meson mass	Theoretical	Experimental[a]
$200m_e$	0.303	0.313±0.013
300	0.311	

[a] Quoted from M. Ross and J. S. Story, *Reports on Progress in Physics* (The Physical Society, London, 1948–49), Chapter XII, p. 293. The measurement is by W. J. Whitehouse and G. A. R. Graham, Can. J. Research **A25**, 261 (1947).

This agreement could perhaps be considered to be satisfactory, but it does not permit quantitative conclusions concerning the range of the potential.

Turning now to the scattering amplitudes, we can calculate a_t (triplet amplitude) and a_s (singlet amplitude) once A, B, and m are fixed. The coherent scattering amplitude is then obtained from the relation

$$f=\tfrac{3}{4}a_t+\tfrac{1}{4}a_s. \tag{2}$$

The results of this calculation are shown in Table II.

TABLE II. Scattering amplitudes.

Meson mass	Theoretical values (units of 10^{-13} cm)			Experimental value[a]
	a_t	a_s	f	f
$200m_e$	5.58	−23.54	−3.40	−3.75±0.03
300	5.34	−23.72	−3.85	

[a] Hughes, Burgy, and Ringo, Phys. Rev. **77**, 291 (1950).

It is, of course, tempting to interpolate to see what meson mass gives the "correct" value of f. The answer is $m=277\pm7m_e$, while the present best Berkeley value[5] for the π-meson mass is $276\pm6m_e$. Here it is appropriate to warn against rash conclusions. We must remember that non-central forces and charge exchange effects have not been taken into account in these calculations, and these might change the picture.

A closer consideration shows that a value for f, however accurate it may be, does not allow of independent conclusions concerning the singlet range. Starting from the experimental f-value quoted in Table II and the epithermal cross section $\sigma_0=20.36\pm0.10$ barns, we obtain[6] the values $a_s=(-23.70\pm0.06)\cdot10^{-13}$ cm and $a_t=(5.40\pm0.03)\cdot10^{-13}$ cm. From a_s we only get a relation between the range, $1/\kappa$, and the "depth," A, of the potential. On the other hand, combining the value just given for a_t with the value of the deuteron binding energy $|E_0|=2.237\pm0.005$ Mev, and assuming a pure central Yukawa potential in the triplet state, we can fix certain limits for the range, and obtain $m=275\pm13m_e$, the error arising almost entirely from the uncertainty in a_t. A similar calculation for the singlet state would be possible only if σ_c could be measured with an accuracy of the order of one part in a thousand.

It remains to be seen whether a Yukawa potential with this range can account for the neutron-proton scattering in the energy region up to about 6 Mev, where the contribution from the P-states can be neglected safely. Calculations to this effect are in progress, and it appears that the earlier discrepancy between theory and experiment[7] will at least be reduced, thanks to the new f-value.

This work has been supported financially by the Swedish Atomic Energy Committee. The ready assistance of Mr. B. Nagel and Mr. S. G. Nilsson is gratefully acknowledged.

[1] L. Rosenfeld, *Nuclear Forces* (North Holland Publishing Company, Amsterdam, 1948), p. 180.
[2] R. E. Bell and L. G. Elliott, Phys. Rev. **74**, 1552 (1948).
[3] E. Melkonian, Phys. Rev. **76**, 1744 (1949).
[4] The values of a_t and a_s given in Table II are much more accurate, being closely connected with the eigenphases, which are stationary in the variational method used. See L. Hulthén, Kgl. Fysiograf. Sällsk. Lund Förhandlingar **14**, No. 21 (1944); Arkiv f. Mat. Astr. o. Fys. **35A**, No. 25 (1948). Smith, Barkas, Bishop, Bradner, and Gardner, Phys. Rev. **78**, 86 (1950).
[6] In addition to Eq. (2) we have the well-known relation

$$\sigma_0 = 3\pi a_t^2 + \pi a_s^2.$$

[7] L. Hulthén and S. Skavlem (unpublished manuscript, 1949).

The Hyperfine Structure of Ni^{61}

KARL G. KESSLER
National Bureau of Standards, Washington, D. C.
May 5, 1950

INTERFERENCE spectrograms of nickel[1] enriched to 80 percent in Ni^{61} have been made with a liquid-nitrogen-cooled beryllium hollow cathode discharge tube filled with helium and argon. Fabry-Perot interferometers having 15, 25, 50, and 67 mm Invar separators were used with aluminum-coated quartz plates. No clear hyperfine structure splitting has been observed, but certain lines in the spectrum, especially those involving the $d^9s\ ^3D_3$ level, show definite broadening in excess of that caused by the Doppler effect.

The lines involving transitions to the $^3D_3$ level, in the region 3300 to 3600A, show a half-width of approximately 0.06 cm^{-1}. This is very nearly double the half-width of the sharpest lines from other transitions in the same region. The approximate half-width of these sharpest lines, 0.03 cm^{-1}, is very nearly equal to the limit of 0.025 cm^{-1} determined by Doppler broadening at liquid nitrogen temperatures. The resolution was insufficient to determine the spin, but the upper limit of the magnetic moment appears to be of the order of 0.25 nuclear magneton. Further study of this isotope by using liquid hydrogen cooling is contemplated.

[1] Produced by the Y-12 plant, Carbide and Carbon Chemicals Corporation, Oak Ridge, Tennessee, and obtained by allocation from the United States AEC.

On the Origin of the Sodium *D* Lines during Twilight

F. D. KAHN
Department of Mathematics, University of Manchester, Manchester, England
May 1, 1950

PENNDORF[1] has recently proposed a new mechanism to explain the twilight luminescence of atmospheric sodium. This was done mainly in order to account for certain experimental results, found by Vegard and Kvifte,[2] which are hard to interpret on the usual theory. Unfortunately the new process itself raises great difficulties.

According to Bricard and Kastler[3] the intensity of the *D* line emission at twilight is about 1.5×10^{10} photons/cm^2 column/sec., or 10^4 photons/cm^2/sec. in a 15 km layer. To account for this Penndorf has suggested the following series of reactions, supposed to take place near 100 km height:

$$Na + N_2O = NaO + N_2, \quad (1)$$
$$NaO + Na_2 = Na(^2P) + Na_2O, \quad (2)$$
$$Na(^2P) = Na(^2S) + h\nu(\lambda = 5890A), \quad (3)$$
$$Na_2O + h\nu = Na_2 + O. \quad (4)$$

The rate of (2) must be $\alpha[NaO][Na_2] = 10^4$ reactions/cm^3/sec., in order to give the observed intensity of emission. The value of α is probably 10^{-10} cm^3/sec.

The four reactions quoted are to be considered together with (5) and (6):

$$Na_2 + h\nu = Na + Na, \quad (5)$$
$$Na + Na + X = Na_2 + X. \quad (6)$$

Equation (5) denotes the photo-dissociations of Na_2 by light of wave-length $\lambda = 3500A - \lambda = 2900A$. The rate of this reaction is $\delta[Na_2]$; here $\delta = (\pi e^2\lambda^2/mc^3)fI$, where f is the oscillator strength of the transitions leading to the dissociation, and $I(\sim 4\times10^{20}$ photons/cm/cm^2/sec.) stands for the intensity of solar radiation in the spectral region concerned. Thus $\delta \sim 3.6\times10^{-1}f$; even with f as small as 10^{-3}, $\delta > 10^{-4}$.

Three-body recombination (6) of Na atoms seems to be faster than radiative association; with a local particle density $[X] = 10^{14}$ its rate would be about $10^{-16}[Na]^2$. For equilibrium between (5) and (6)

$$\delta[Na_2] = 10^{-16}[Na]^2,$$

or

$$[Na_2] \leqslant 10^{-12}[Na]^2,$$

and by the conditions for reaction (2)

$$[NaO] \geqslant 10^4/\alpha \cdot 10^{-12} \cdot [Na]^2 = 10^{26}/[Na]^2.$$

Table I lists some possible values of [Na] and corresponding minimum values of [NaO].

TABLE I. Possible values of [Na], and corresponding minimum values of [NaO].

[Na]	$[NaO]_{min}$
10^6	10^{13}
10^5	10^{16}
10^6	10^{15}
2×10^6	2.5×10^{13}

By consideration of the Na^+:Na equilibrium in an ionized region it has been shown by the writer[4] that the greatest possible value of [Na] is 2×10^9 atoms/cm^3 at the heights concerned. Thus, in order to make Penndorf's process work, the concentration of NaO must be impossibly high (at least 25 percent).

Some of the values adopted in the calculation may be rather unfavorable to the new process, but it is clear that the ratio [NaO]:[Na] will always be very large. This again would be hard to explain, as NaO is probably dissociated not only by reaction (2), but also by sunlight, and by its reaction with atomic oxygen

$$NaO + O = Na + O_2.$$

[1] R. Penndorf, Phys. Rev. **78**, 66 (1950).
[2] L. Vegard and G. Kvifte, Geofys. Publ. Oslo, **16**, No. 7 (1945).
[3] J. Bricard and A. Kastler, Ann. de Geophys. **1**, 53 (1944).
[4] F. D. Kahn, Thesis, Oxford University (January, 1950).

Zero-Point Vibrations and Superconductivity

J. BARDEEN
Bell Telephone Laboratories, Murray Hill, New Jersey
May 22, 1950

A THEORY of superconductivity which depends on interaction of the valence electrons with the zero-point vibrations of the crystal lattice is proposed. This approach was stimulated by the recent finding of Reynolds, Serin, Wright, and Nesbitt[1] and of E. Maxwell[2] that the critical temperature, T_c, of mercury depends on the isotopic mass. The theory is a modification of one proposed some years ago by the writer.[3] It gives a natural explanation of the isotope effect and the energies and critical temperatures are of the correct order.

It is assumed that the vibrational modes of the superconducting state differ from those of the normal state in that the vibrations are such as to lower the energy of electrons in states near the

surface of Fermi distribution, $E=E_0$. The normal modes in the superconducting state are assumed to consist in part of wave groups which extend over distances of the order of 10^{-6} cm and which have average wave vectors which connect electron states with energies near E_0. This implies a correlation between the displacements of ions from their equilibrium positions which extends over distances of this order. It will be shown below that it is reasonable to expect that coherence over distances of $\sim 10^{-6}$ cm will give a lower energy for the electrons than coherence over larger or smaller distances. Interaction with these modes gives rise to new states which are linear combinations of the ψ_k with E near E_0 and which have energies which differ from the old by $\sim\Delta E$. If the interactions are such as to depress the levels just below E_0 and raise those just above, there will be a net decrease in electron energy if $kT\sim\Delta E$ or less. We therefore assume that $kT_c\sim\Delta E$. The normal modes of the superconducting state have a lower zero-point energy than those of the normal state.

It is presumed that the motion of the electrons is sufficiently rapid so that the wave functions are those appropriate to a fixed position of the ions at any moment and that they follow the motion of the ions adiabatically.[4]

Superconductivity follows as in the earlier theory.[5] Electrons in the superconducting states near the Fermi surface have a small effective mass. These states are linear combinations of ψ_k with small net current, but which are easily modified by an external field to give a large current. That superconductivity follows from the model is also suggested by Slater's theory.[6] The wave functions of the electrons in the superconducting state extend over the region of coherence of the lattice vibrations. Slater showed that wave functions extending over $\sim$137 atom diameters may be expected to give a large diamagnetism and lead to superconductivity.

To get a rough estimate of the nature of the normal modes and of the interaction energies involved, we consider a volume V which contains only a small number p of states with energies within $\Delta E\sim kT_c$ of E_0. The usual normal modes for a volume of this size will presumably be similar to the normal modes of the superconducting state. It is necessary to take the volume small because the amplitude of the zero-point motion varies as $V^{-\frac{1}{2}}$, but if the volume is taken too small one cannot confine the wave functions of the electrons to the region of coherence without an increase of Fermi energy. If $N(E)\Delta E$ is the number of states/cm^3 in ΔE, we take

$$V\sim p/[N(E)\Delta E]. \tag{1}$$

The energy changes, ΔE, resulting from the interactions are of the order of the matrix element

$$\Delta E\sim|M_{kk'}|_{Av}=|\int_V\psi_{k'}{}^*U\psi_k d_\tau|_{Av}, \tag{2}$$

where U, the interaction potential for a mode which connects k and k', is proportional to the displacement of the ions. We can estimate the magnitude from conductivity theory. For a mode with zero-point energy $\frac{1}{2}h\nu=\frac{1}{2}\kappa\Theta$ in the volume V:

$$|M_{kk'}|_{Av}{}^2=(\Theta/2TV)(e^2/3\pi\hbar)[dE/dk]^2\rho. \tag{3}$$

The resistivity ρ is taken at a high temperature such that ρ/T is a constant.[7] Using (1) for V, and setting $|M_{kk'}|_{Av}=\Delta E$, we find from (3) that

$$\kappa T_c\sim\Delta E\sim(\Theta N(E)/2Tp)(e^2/3\pi\hbar)[dE/dk]_m{}^2\rho. \tag{4}$$

A high density of electrons in a wide energy band and a large interaction between electrons and lattice are favorable for superconductivity. The theory gives T_c proportional to Θ, as observed empirically by Serin, Reynolds, and Nesbitt[8] in Hg isotopes.

An estimate of T_c can be obtained by expressing $N(E)$ and dE/dk in terms of the concentration of valence electrons, n_e, in the free electron approximations. The result is:

$$T_c\sim(\hbar e^2/4\pi m)(\Theta\rho n_e/\kappa Tp)\sim 1.5\times 10^{-4}(n_e\Theta\rho/Tp). \tag{5}$$

This gives the right order of magnitude for T_c for the "soft" superconductors if we take $p\sim$10 to 20, which is a reasonable value. The volume V is then $\sim 10^{-18}$ cm^3 for $n_e\sim 10^{23}$/cm^3.

The decrease in electron energy per unit volume at $T=0$ is of the order

$$W_e\sim N(E)\Delta E\times\Delta E=N(E)(\Delta E)^2\sim 3n_e(\Delta E)^2/2E_0. \tag{6}$$

For $n_e\sim 10^{23}$/cm^3, $\Delta E\sim 5\times 10^{-16}$ erg, $E_0\sim 5\times 10^{-12}$ erg, Eq. (6) gives $W_e\sim 7.5\times 10^3$ which corresponds to $H_c\sim$400 oersteds. The theory predicts that H_c at $T=0$ should vary in the same way with isotopic mass as T_c.

The writer is indebted to Dr. B. Serin for communicating the data of the Rutgers group in advance of publication and to Dr. C. Herring for a critical reading of the manuscript.

[1] Reynolds, Serin, Wright, and Nesbitt, Phys. Rev. **78**, 487 (1950).
[2] E. Maxwell, Phys. Rev. **78**, 477 (1950).
[3] J. Bardeen, Phys. Rev. **59**, 928(A) (1941). Zero-point displacements replace the small periodic distortion of the former theory.
[4] The time taken for an electron with a velocity $\sim 10^8$ cm/sec. to go $\sim 10^{-6}$ cm is $\sim 10^{-14}$ sec.; about one-tenth of usual vibrational periods.
[5] Peierls' modification of the Landau theory gives a large diamagnetism for electrons of very small effective mass. It will be shown in a subsequent publication that such a model leads to a theory of superconductivity of the London type.
[6] J. C. Slater, Phys. Rev. **51**, 195 (1937); **52**, 214 (1937).
[7] For the theory on which (4) is based, see, for example, N. F. Mott and H. Jones, *Theory of the Properties of Metals and Alloys* (Oxford University Press, New York), Chapter VII.
[8] Serin, Reynolds, and Nesbitt, Phys. Rev. **78**, 813 (1950).

On the Production of Penetrating Showers in Lead and Carbon

L. Mezzetti and R. Querzoli*
Instituto de Fisica dell' Università,
Centro di Studio per la Fisica Nucleare del C.N.R., Roma, Italy
April 21, 1950

An experiment has been performed at the Laboratorio della Testa Grigia, Cervinia (3500 m) to study the dependence of the mean free path for production of penetrating showers (p.s.) on the atomic number of the generating layer, and the total number of ionizing particles in the shower. The counter arrangement is sketched in Fig. 1. The counter telescope ABC (active

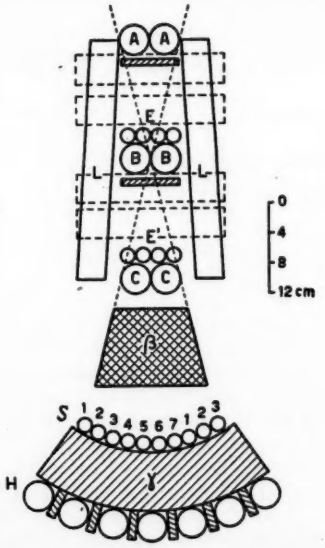

Fig. 1. Counter arrangement.

surface of each counter 4×10 cm^2, distance between the axes of counters A and $C=32$ cm) defined the solid angle of the incident radiation. The counters of the trays S, H, E, E', were connected to four addition circuits; in the set S counters indicated with the same number were connected in parallel; in the set H the counters were separated from each other by a thickness of about 1 cm Pb, and from the counters S by an absorber $\gamma=7.5$ cm Pb; the 14 counters L, which surrounded the telescope ABC on all sides, were all connected in parallel. Two lead absorbers α and α', 1 cm

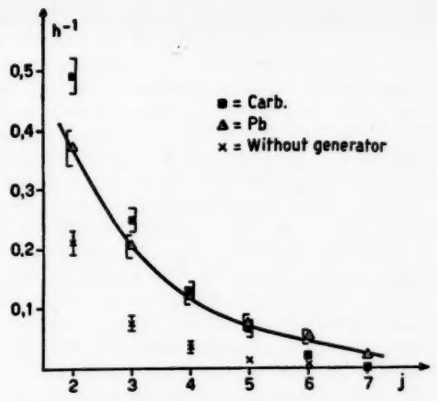

FIG. 2. Measured frequencies of the events (H_2S_j).

thick each, were placed above the counter trays E and E', at a distance of about 10 cm. The diameter of the counters E and E', as well as of the counters S, was 2 cm.

The event recorded was a coincidence ABC accompanied by the discharge of a number ≥ 2 of the counters H, with the condition that not more than one counter was discharged in each of the two trays E and E', and no counter discharged in the group L. This event will be referred to by the symbol H_2. A seven-channel discriminator was triggered by the events H_2 and recorded simultaneously the frequencies of the H_2 events which were accompanied by the discharge of j or more of the counters $S(j=1, 2\cdots 7)$; such an event will be indicated by the symbol (H_2S_j).

The producing layers β ("generators") were placed above the counters S, and measurements were made alternatively with $\beta=0$, $\beta=46$ g/cm² Pb, and $\beta=17$ g/cm²C. The thicknesses of lead and carbon were so chosen as to give the same total geometrical cross section, on the assumption that the radius of a nucleus of atomic weight A is proportional to $A^{\frac{1}{3}}$. The two thicknesses were also approximately equivalent for the absorption of mesons and protons of not too high energies.

TABLE I. Frequencies of the events of the type (H_2S_j) in (100 hr.)$^{-1}$.

Generator β	$j=1$	2	3	4	5	6	7
0	168±6	21±2	7.5±1.2	3.4±0.8	1.2±0.5	0.6±0.3	0
17 g/cm² C	176±6	49±3	24.8±2.3	12.9±1.6	6.5±1.3	2.0±0.6	0
47 g/cm² Pb	164±6	37±3	20.4±2.1	12.1±1.6	7.5±1.3	5.3±1.1	1.9±0.6

The experimental frequencies of the events (H_2S_j) are given in Table I, and plotted in Fig. 2 *vs.* j, for $j\geq 2$. The events of the type (H_2S_j) are clearly due mainly to hard ionizing particles crossing all of the apparatus and giving rise to knock-on secondaries in the lead absorber γ.

The frequencies of the events (H_2S_j) for $j\geq 2$ can be due to: (a) p.s. generated in the layer β; (b) p.s. generated in the counter walls or in the material above counters C; (c) cascade showers; (d) double knock-ons; (e) lateral showers; (f) random coincidences; and (g) p.s. produced in the lead γ and having some backward-emitted particles. The contribution due to the cascade showers has been carefully investigated and shown to be completely negligible. The contributions of the spurious effects (b), (d), and (f) have been either measured or calculated and subtracted from the observed frequencies. A discussion of the effects (e) and (g) shows that their contribution is very approximately the same in the measurements with and without generator; therefore we have assumed that the differences between the frequencies obtained with and without the lead or carbon generator, corrected for effects (b), (d), and (f), represent the actual number of p.s. produced in the layer β.

With these assumptions, from the frequencies with $j=2$ (representing the total number of showers with at least two ionizing particles penetrating 7.5 cm Pb) we have obtained for the ratio of the mean free paths (in g/cm²) for generation of the p.s. recorded in lead and carbon the value $\lambda_{Pb}/\lambda_C=4.4\pm1.0$. This result is not incompatible with the assumption that the ratio of the generation cross sections is equal to the ratio of the nuclear geometrical cross sections, as found by Tinlot and Gregory,[1] but deviates from the result of Cocconi[2] and particularly from that of Lovati, Mura, Salvini, and Tagliaferri,[3] who found $\lambda_{Pb}/\lambda_C=0.30\pm0.14$.

The dependence of the production rate on the total number of ionizing particles in the shower has been investigated also and compared with the theoretical distributions as given by the plural production and multiple production theories,[4] but the results obtained do not allow a choice to be made between the two theories.

Thanks are due Professor G. Bernardini and Professor B. Ferretti for helpful discussions.

* Now at the Laboratorio di Fisica dell'Istituto Superiore di Sanità, Roma, Italy.

[1] J. Tinlot and B. Gregory, Phys. Rev. **75**, 519 (1949).
[2] G. Cocconi, Phys. Rev. **75**, 1074 (1949).
[3] Lovati, Mura, Salvini, and Tagliaferri, Nuovo Cimento **7**, 36 (1950).
[4] W. Heitler and L. Jánossy, Proc. Phys. London **A62**, 669 (1949). W. Heisenberg, Zeits. f. Physik **126**, 569 (1949).

Beta-Gamma and Gamma-Gamma Angular Correlation Experiments on Sb^{124}

J. R. BEYSTER AND M. L. WIEDENBECK
Department of Physics, University of Michigan, Ann Arbor, Michigan
May 1, 1950

THE decay scheme of Sb^{124} has been discussed by many investigators.[1-3] The level scheme shown in Fig. 1 is a tentative proposal of the Indiana group.[2] The angular momenta and parity assignments are those of Segrè and Helmholz.[3] At first, this scheme appears complicated for use in a coincidence experiment. However, if the lower energy beta-groups are stopped with

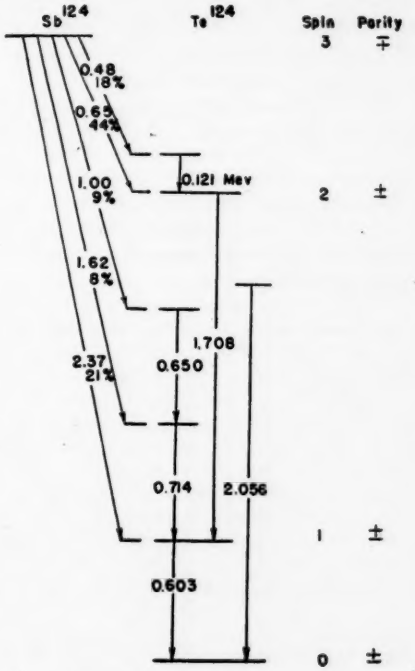

FIG. 1. Disintegration scheme of Sb^{124} as proposed by the Indiana group.

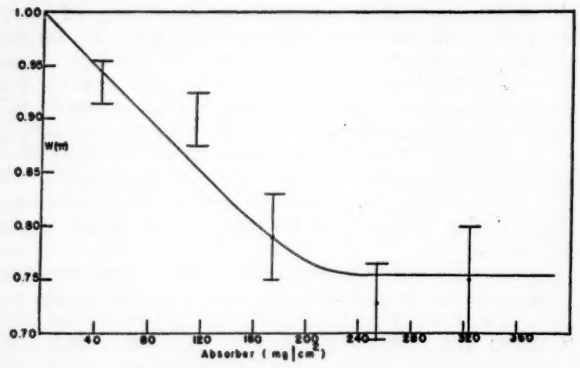

FIG. 2. Observed angular correlation as a function of absorber thickness.

absorber, the beta-gamma-coincidence rate will involve only the 2.4-Mev beta-transition and the 0.6-Mev gamma-transition. The gamma-gamma-coincidence rate should consist primarily of coincidences between the 1.7-Mev gamma and the 0.6-Mev gamma.

In the beta-gamma-correlation experiment scintillation detectors employing 931-A photo-multipliers were used. The phosphor for gamma-detection was a 2-cm thickness of stilbene, and the phosphor for beta-detection a thin crystal of anthracene. The source was mounted on a zapon backing and was less than 1 mg/cm² in thickness. A baffle was employed with the beta-detector to minimize the probability of detecting scattered betas. Counter solid angles were about one percent. The correlation experiment was performed with various thicknesses of absorber intercepting the betas. Figure 2 shows $W(\pi)$ as a function of absorber. It appears that 260 mg/cm² of aluminum is sufficient absorber to cut out most of the lower energy components. Using 260 mg/cm² of aluminum the shape of the correlation function was run. This is shown in Fig. 3. Curve A is the observed function and curve B is the final curve after a correction for gamma-gamma-coincidences is made to the observed data. Several other activities have been tested with this apparatus. In most cases we have observed symmetry, but in K^{42} there appears to be a small asymmetry. The experiments are as yet not completed.

The gamma-gamma-correlation experiment was performed with essentially the same apparatus. The thin anthracene crystal was replaced by a stilbene crystal 2 cm thick. Solid angles were again one percent. Precautions were taken to prevent secondary gamma-scattering between counters. The experiment was performed at three angles and the function seemed to be essentially symmetric. Correlation experiments on Co^{60} and other radioactive isotopes with cascade gamma-rays were carried out and in general confirm previous work.[4]

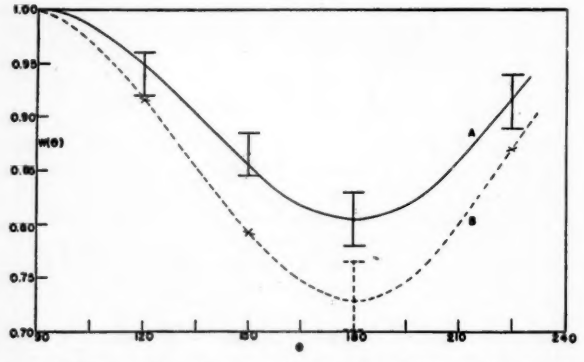

FIG. 3. (A) Observed angular correlation function. (B) Correlation function obtained after correcting curve A for gamma-gamma-coincidences.

The lack of a noticeable asymmetry in the gamma-gamma-coincidence rate is not inconsistent with the angular momenta assignments of Segrè and Helmholz. The upper gamma-transition could be a mixture of magnetic dipole and electric quadrupole radiations such that the angular asymmetry is very small.

Fitting the observed beta-gamma-correlation function with any one assignment of angular momenta and interaction appears to be difficult at present. All of the correlation functions have been calculated theoretically for single matrix elements (no interference) in the first-forbidden case. The scalar interaction will not work nor will unambiguous cases in the other interactions. For example, the data cannot be explained by the assignments of angular momenta 4, 2, 0; 0, 2, 0; and 3, 1, 0 using the matrix element B_{ij}. There are ways of accounting for the observed asymmetry however. For example, if it is assumed that matrix element B_{ij} is the dominant element present, the observed correlation seems to be fit reasonably well with angular momenta assignments 1, 1, 0 or 3, 2, 0. These are not the only two possibilities. A careful theoretical investigation of the significance of this function is being carried on. If the beta-gamma-correlation function could be observed as a function of the beta-energy, the interpretation might be simplified. An analysis of the shape of the high energy beta-spectrum would also be very valuable.

[1] Der Mateosian, Goldhaber, Muehlhause, and McKeown, Phys. Rev. **72**, 1271 (1947).
[2] Kern, Zaffarano, and Mitchell, Phys. Rev. **73**, 1142 (1948); C. S. Cook and L. M. Langer, Phys. Rev. **73**, 1149 (1948); E. T. Jurney and A. C. G. Mitchell, Phys. Rev. **73**, 1153 (1948).
[3] E. Segrè and A. C. Helmholz, Rev. Mod. Phys. **21**, 294 (1949).
[4] E. L. Brady and M. Deutsch, Phys. Rev. **74**, 1541 (1948).

Angular Correlation in the Reaction $F^{19}(p, \alpha)O^{16*}(\gamma)O^{16}$

W. R. ARNOLD*
State University of Iowa, Iowa City, Iowa
May 8, 1950

BOTH the alpha- and gamma-particles from the 330-kev resonance in the reaction $F^{19}(p, \alpha)O^{16*}$ have been found to be spherically symmetric with respect to the incoming proton beam.[1] This indicates that only S-wave protons are involved, and that the compound nucleus Ne^{20*} will have a spin of 0 or 1 and the same parity as F^{19}. The angular momentum of the emitted alpha-particle will be even or odd, depending on whether the parity of O^{16*} is the same or opposite to Ne^{20*}. If an angular correlation is taken only of alpha-particles in coincidence with gamma-rays, angular momentum of the alpha-particles would lead to an anisotropic angular correlation which will in most cases be unique for given spin and parities[2] of Ne^{20*} and of O^{16*}.

This angular distribution has been measured in two planes and found to fit only the theoretical curve $W(\theta)=A(1+111\cos^2\theta-305\cos^4\theta+225\cos^6\theta)$ corresponding to a spin of 1 for Ne^{20*}, an angular momentum of 3 for the alpha, a spin of 3 for O^{16*}, and a spin of 0 for the O^{16} ground state. This means that if the parity of F^{19} is even, Ne^{20*} has even parity, and O^{16*} has odd parity. (Even parity for both the excited state of Ne^{20} and the ground state of O^{16} with a spin difference of 1 would account for the absence at this resonance of long range alphas.) Theoretical curves were calculated for Ne^{20*} spins of 0 and 1, and for spins of O^{16*} up to and including 5; from general trends in the shapes of the curves and because of longer lifetimes for the excited state, a spin of 6 or more seems unlikely.

This experiment was suggested by R. E. Holland, who also did the calculations on the modification of Hamilton's theory[3] necessary for application to this problem. Full details will be published shortly.

* Now at Los Alamos Scientific Laboratory.
[1] Van Allen and Smith, Phys. Rev. **59**, 501 (1941).
[2] C. N. Yang, Phys. Rev. **74**, 764 (1948).
[3] D. R. Hamilton, Phys. Rev. **58**, 122 (1940).

Photo-Conductivity in Amorphous Selenium

PAUL K. WEIMER
RCA Laboratories, Princeton, New Jersey
May 18, 1950

IN contrast to the vast number of papers[1] which have appeared on the photo-conductivity of gray metallic selenium, very little attention has been given to the possibility of photo-conductivity in the red amorphous form. Although Gudden and Pohl used red monoclinic crystals of selenium for their classic studies of primary and secondary photo-currents,[2] the usual statement in the literature concerning the amorphous form of selenium is that it is an insulator showing no photo-conductivity.[3] The work described in this letter has indicated that amorphous selenium is a photo-conductor[4] possessing markedly different properties from those of either the common metallic form or the red monoclinic crystals.

Thin films of amorphous[5] selenium were deposited by distillation or by evaporation on to glass targets which had been previously covered with a transparent conducting coating. The second electrode on top of the selenium film was obtained by evaporating a thin metal coating on to the selenium or by scanning the selenium directly with an electron beam.[6] The selenium films prepared in the above manner are a deep red in color and have a dark resistivity of greater than 10^{12} ohm-cm, as compared to 10^{5} ohm-cm for the metallic form. They exhibit the following photo-conductive properties measured through the film.

(1) Sensitivities approaching unity quantum efficiency have been obtained for those wave-lengths in the visible giving highest response.

(2) The excessive time lags associated with the secondary currents in gray selenium have been absent.

(3) The spectral response in general is peaked in the blue-green portion of the spectrum (clearly on the short wave-length side of the absorption edge[7]) with very low response in the red (Fig. 1). This may be contrasted with the gray form of selenium for which the sensitivity is a maximum to red light.[3]

(4) The range of the carrier of the photo-current in amorphous selenium exceeds the range of penetration of the blue and green light by a factor of 10 to 100.

(5) Space-charge effects owing to trapped charges are encountered with thick films or weak applied fields.

These observations suggest that the blue sensitive photo-conductivity in amorphous selenium is largely of primary nature.[8] Item (4) allows one to determine the sign of the carrier by adjusting the polarity of the illuminated electrode. Higher response is obtained by illuminating the positive electrode indicating hold

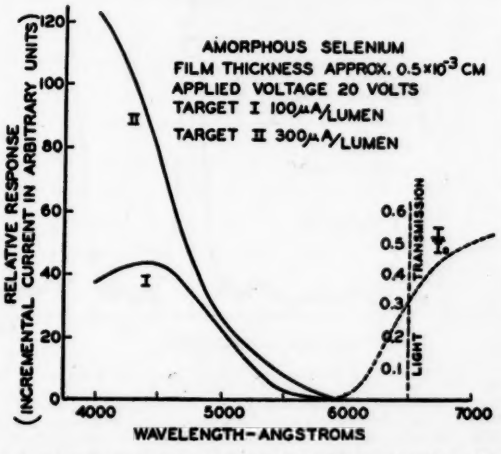

FIG. 1. Spectral sensitivity characteristics for equal values of radiant flux at all wave-lengths. Spectral response curves for photo-conductivity in amorphous selenium measured through a thin film of selenium with a low velocity scanning beam serving as one electrode.

conduction in amorphous selenium to be predominant over electron conduction. This result has been confirmed by Pensak[9] for conductivity induced by high voltage electron bombardment.

The range of the holes is found in some samples to exceed 10^{-3} cm. Ranges of this length in insulators have been previously verified only in crystals such as diamond or carefully annealed silver chloride.

[1] G. P. Barnard, *The Selenium Cell* (Richard R. Smith, Inc., New York, 1930).
[2] B. Gudden and R. Pohl, Zeits. f. Physik. 35, 243 (1926).
[3] Hughes and DuBridge, *Photoelectric Phenomena* (McGraw-Hill Book Company, Inc., New York, 1932).
[4] During the course of the work described here, a paper has appeared by R. M. Schaffert and C. D. Oughton, entitled "Xerography: A new principle of photography and graphic reproduction," J. Opt. Soc. Am. 38, 991 (1948). Although it is not stated directly, it is probable that the selenium used in this process is amorphous selenium.
[5] Electron diffraction photographs by E. G. Ramberg showed only faint rings corresponding to the red monoclinic crystals. It was concluded that the evaporated films are primarily amorphous with a very slight amount of monoclinic crystallinity.
[6] Weimer, Forgue, and Goodrich, Electronics, 70 (May, 1950).
[7] Becker and Schaper, Zeits. f. Physik, 122, 49 (1944).
[8] This statement is no longer true when a slight impurity is added to the selenium. Under these conditions, the greatly increased sensitivity and time lag along with an altered spectral response indicates a strong secondary photo-effect.
[9] L. Pensak, Phys. Rev. 78, 171 (1950), following letter.

Electron Bombardment Induced Conductivity in Selenium

L. PENSAK
RCA Laboratories, Princeton, New Jersey
May 18, 1950

MEASUREMENTS of bombardment induced conductivity were taken on films of red, amorphous selenium obtained by evaporation in vacuum. This work is an extension of that described earlier[1] on measurements on silica. Although there are reports on the bombardment of selenium,[2-4] there has been no indication of it having been other than the gray, metallic form.

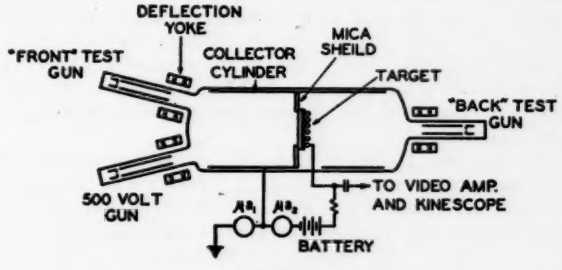

FIG. 1. Experimental tube.

The experimental data were obtained using a three-beam cathode-ray assembly in a demountable vacuum system as shown in Fig. 1. One beam at 500 volts and approximately 2 μa is scanned in a television raster. The other beam on the same side is also scanned over the same area but with different voltages, and is called the front bombarding beam. The third beam is called the back bombarding beam. The target was a sheet of fine mesh of approximately 50 percent transmission on which was picked up a very thin film of collodion to form the base for an evaporated layer of aluminum. The selenium was evaporated onto the aluminum and the target faced toward the two-gun side of the test chamber and bounded by suitable shields. A video signal was taken out as shown, to check the location of the beams in the target and a d.c. connection was made to apply various voltages to the aluminum.

Figure 2 shows typical data where the conduction ratio (ratio of increase in target current to bombarding beam current) is plotted against the test beam voltage while the selenium surface potential is held by the secondary emission of the 500-volt beam.

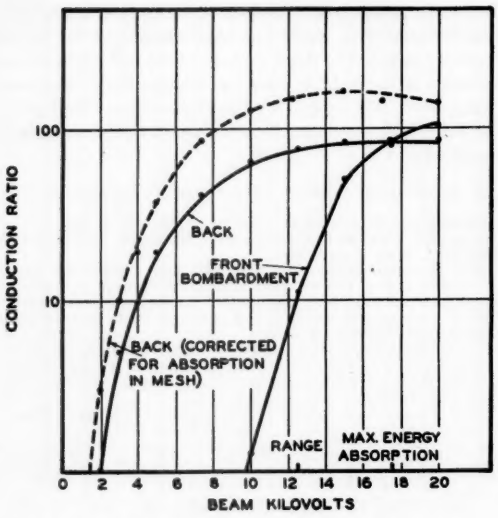

FIG. 2. Induced conductivity in amorphous selenium.

The film was 9000A thick and the aluminum was set at +10 volts. Calculations were made as described in reference 1 on the range voltage and that at which the maximum energy is absorbed and these values are indicated on the graph.

The data indicates that, with "front" bombardment, no appreciable bombardment induced conductivity occurs till the beam voltage approaches the value where complete penetration begins. However, with "back" bombardment, the effect occurs at much lower values. If this latter curve is corrected for a 50 percent absorption of the beam by the mesh and, at the low end, for absorption of beam energy by the aluminum backing layer, it can be seen that a penetration of only a few percent of the film thickness is sufficient to produce an appreciable effect. Therefore, effects in the selenium-aluminum interface region can permit current to flow through the entire film thickness. This has not been true for other insulators tested this way, such as silica and magnesium fluoride. The polarity of the aluminum requires that the current be primarily due to hole conduction. Similar conclusions had been drawn by Weimer[5] from photo-conductive measurements.

The fact that the front bombardment curve apparently does not maximize at the maximum energy absorption value, as is true for most insulators, may indicate a barrier at the selenium-aluminum interface and that it requires some excitation in order for current to flow. Yet, the back bombardment curve shows that the volume effect can predominate even when the barrier is excited.

[1] L. Pensak, Phys. Rev. **75**, 472 (1949).
[2] E. S. Rittner, Phys. Rev. **73**, 1212 (1948).
[3] R. de L. Kronig, Phys. Rev. **24**, 377 (1924).
[4] Becker and Kruppke, Zeits. f. Physik **107**, 474 (1937).
[5] P. K. Weimer, Phys. Rev. **78**, 171 (1950), preceding letter.

Gamma-Ray Spectra from B^{10}, B^{11}, and Be^{9} under Proton Bombardment*

R. L. WALKER†
Cornell University, Ithaca, New York
May 12, 1950

THE spectra of gamma-rays emitted by B^{10}, B^{11}, and Be^{9} when bombarded by protons have been measured with a gamma-ray pair spectrometer which is described in a previous paper.[1] Figure 1 shows the spectrum obtained from B^{11} (in the form of B_4C with normal isotopic mixture) bombarded by 1.2-Mev protons from the Cornell cyclotron. The energies and relative intensities of the gamma-ray lines given in the caption of Fig. 1 have been obtained in the manner described in reference 1. The three gamma-ray lines observed were found in 1938 with different relative intensities by Fowler, Gaerttner, and Lauritsen[2] using the technique of measuring pairs in a cloud chamber. They suggested that the 16.7-Mev gamma-ray is emitted in a transition to the ground state of the product nucleus, C^{12}, whereas the 12.1- and 4.4-Mev lines arise from a double transition, first to a 4.4-Mev level in C^{12}, and then to the ground state.[3] This origin of the gamma-ray lines, which is still accepted,[4] means that the 12.1- and 4.4-Mev lines should be present in equal intensities. The data of Fig. 1 are consistent with this, even though the 4.4-Mev line appears to be much weaker than the 12.1-Mev line. The apparent weakness of the 4.4-Mev radiation illustrates the rapid decrease in the efficiency of the pair spectrometer at low energies. The sensitivity falls off at lower energies not only because of a decrease in the pair cross section, but also because of greatly increased multiple scattering of the pair electrons in the radiator.[1]

The difference in the relative intensities of the 16.7- and 12.1-Mev lines found by Fowler, Gaerttner, and Lauritsen (approximately 1 to 7 at low bombarding energies) and in the present experiment indicates that the relative intensity depends upon the bombarding proton energy. Some data were taken at a proton energy of 0.51 Mev to investigate this point. Weak lines were observed at 16.34±0.25 and 11.76±0.18 Mev, with relative intensities 1 to 4.

The spectra of gamma-radiation from the capture of protons by B^{10} is shown in Fig. 2. The single line at 9.47±0.12 Mev has not been previously observed, presumably because of its low intensity compared with the 12.1-Mev B^{11} line. The data of Fig. 2 were taken with a thick target of separated B^{10} bombarded with 1.2-Mev protons. The gamma-rays at 12.1 and 16.7 Mev arise, of course, from residual B^{11} in the B^{10} sample.

The spectrum of gamma-rays produced by 1.2-Mev protons striking a thick target of Be^{9} consists mainly of a strong line at 7.37±0.07 Mev as shown in Fig. 3a. According to Fowler, Lauritsen, and Lauritsen,[4] 7.4-Mev radiation is produced from the broad proton resonance at 988 kev, whereas the sharp resonance at 1077 kev leads to a double transition involving first the emission of a 6.7-Mev gamma-ray, followed by one of 0.7 Mev. A slight indication of the 6.7-Mev line may be seen in Fig. 3a, but in order to

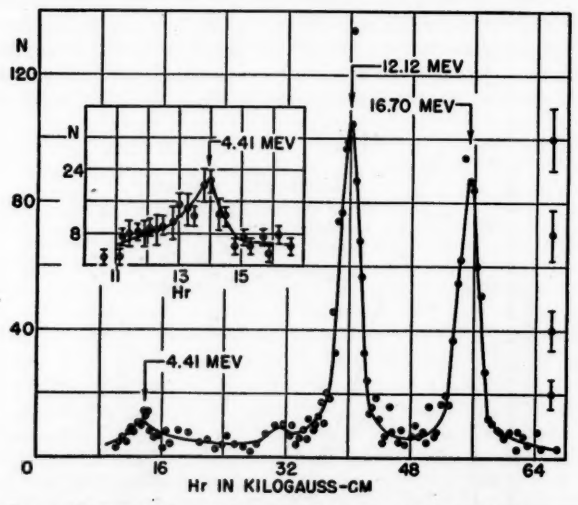

FIG. 1. Spectrum of gamma-rays emitted by a thick target of normal B_4C when bombarded with a 1.2-Mev protons. The number of pair coincidences, N, obtained is plotted against Hr in kilogauss-cm, where r is the *sum* of the radii of the two electrons of a pair. These data were taken with a 0.002-in. Cu radiator in the spectrometer, except that the data shown in the insert were obtained with a 0.003-in. Pb radiator. The relative intensities of the lines at 16.70±0.17 Mev and 12.12±0.12 Mev are approximately 1 to 2.1. The relative intensity of the line at 4.41±0.15 Mev cannot be obtained with accuracy from this data, but is of the same order of magnitude as the other two lines.

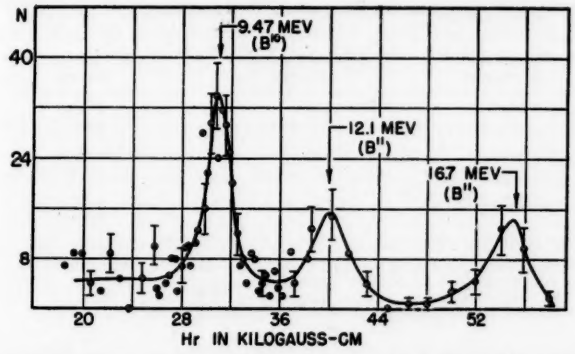

FIG. 2. Spectrum of gamma-rays emitted by a thick target of separated B^{10} isotope when bombarded by 1.2-Mev protons. In addition to the single line at 9.47±0.12 Mev from B^{10}, lines at 12.1 and 16.7 Mev from residual B^{11} are observable. The spectrometer radiator was 0.003-in. Pb.

obtain further information about the radiation from the 1077-kev resonance data were taken with a thin Be target (approximately 0.9 mg/cm²) and a proton energy of 1.21 Mev. The results are shown in Fig. 3b, where a gamma-ray of energy 6.82±0.10 Mev is resolved from the 7.48-Mev line.

TABLE I. Order of magnitude of the relative yields of gamma-radiation from thick targets of Li^7, B^{10}, B^{11}, and Be^9.[a] (An estimate of the probable error is perhaps a factor of 2.)

Target	Proton energy (Mev)	Gamma-ray energy (Mev)	Relative yield (gamma-rays/proton)
Li metal	0.460	17.6 ±0.2 14.8 ±0.3	1.0 0.5
B^{10}	1.2	9.47±0.12	0.018
B_4C (normal boron)	1.2	16.70±0.17 12.12±0.12	0.11 0.23
B_4C (normal boron)	0.51	16.34±0.25 11.76±0.18	0.0022 0.009
Be metal	1.2	7.37±0.07 6.71	1.5

[a] The absolute yield of Li gamma-rays is given by W. A. Fowler and C. C. Lauritsen [Phys. Rev. **76**, 314 (1949)] as 1.90×10^{-4} gamma-ray per proton.

No attempt was made to measure accurately the yield of gamma-rays from B^{10}, B^{11}, and Be^9, but since the order of magnitude may be of interest, rough estimates of the yields relative to that of the 17.6-Mev lithium gamma-rays are given in Table I.

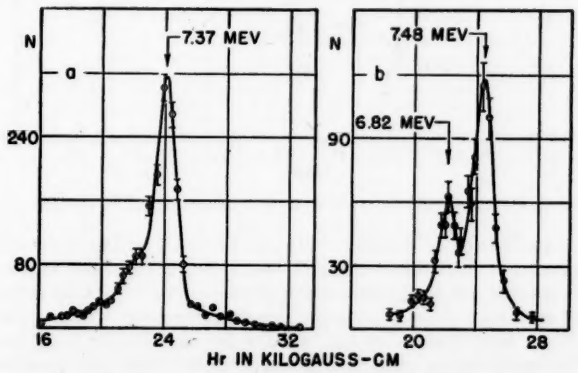

FIG. 3. (a) Gamma-ray spectrum from a thick Be target bombarded with 1.2-Mev protons. (b) Spectrum from a thin Be target (approximately 0.9 mg/cm²) bombarded with protons of energy 1.21 Mev. Both curves were obtained with a 0.002-in. Cu radiator in the spectrometer. The slight increase in the energy of the "7.4-Mev" gamma-ray seen in curve b can be ascribed to an increase in the effective proton energy. Curve a shows radiation produced mainly by protons at the 0.99-Mev resonance, while the protons for curve b have an energy near 1.08 Mev.

I am indebted to Mr. Robert Rochlin for help in taking the data and to the AEC for loaning the B^{10} sample.

* This work was supported in part by the ONR.
† Now at the California Institute of Technology, Pasadena, California.
[1] R. L. Walker and B. D. McDaniel, Phys. Rev. **74**, 315 (1948).
[2] Fowler, Gaerttner, and Lauritsen, Phys. Rev. **53**, 628 (1938).
[3] W. F. Hornyak and T. Lauritsen, Rev. Mod. Phys. **20**, 191 (1948).
[4] Fowler, Lauritsen, and Lauritsen, Rev Mod. Phys. **20**, 236 (1948).

Superconductivity of Sn^{124}*

EMANUEL MAXWELL
National Bureau of Standards, Washington, D. C.
May 19, 1950

OUR measurements[1] of the critical fields and superconducting transition temperatures of mercury isotopes are being extended to the isotopes of tin and thallium. We have obtained preliminary results with an enriched sample of Sn^{124}. This sample, kindly loaned to us by the AEC, contained 83.4 percent of Sn^{124} by weight, and had an average atomic mass, M, of 123.1. (The atomic mass of natural tin is 118.7.) Spectrochemical analysis revealed a total chemical impurity content of less than 0.01 percent. Elements detected were Mg, Pb, Si, Ag, Al, B, Cu.

The experimental method was essentially the same as that employed with the mercury[1] and consisted in observing magnetically the destruction of superconductivity. The specimen was about 50 mg in weight and was in the form of a wire cast in a Pyrex capillary.

TABLE I. Transition temperature of Sn.

Sample	M	T_c°K
Natural	118.7	3.715
Enriched in Sn^{124}	123.1	3.662

The results are given in Table I. The data for natural tin are taken from Laurmann and Shoenberg.[2]

It is seen that the effect of increasing the mass is to shift the transition temperature to lower temperatures, exactly as was found in the case of mercury.[1,3] On the basis of these meager data the shift in temperature is apparently 0.012°K per mass unit. In the case of mercury it was about 0.007°K per mass unit, obtained by using our data[1] and that of Serin, Reynolds, and Nesbitt.[4]

These measurements are being extended and will be reported in detail later.

* Supported by ONR.
[1] E. Maxwell, Phys. Rev. **78**, 477 (1950).
[2] E. Laurmann and D. Schoenberg, Proc. Roy. Soc. **A198**, 560 (1949).
[3] Reynolds, Serin, Wright, and Nesbitt, Phys. Rev. **78**, 487 (1950).
[4] Serin, Reynolds, and Nesbitt, Phys. Rev. **78**, 813 (1950).

Measurement of the Gamma-Ray Energy of K^{40}

P. R. BELL AND JUDITH M. CASSIDY
Oak Ridge National Laboratory, Oak Ridge, Tennessee
May 1, 1950

THE energy of the gamma-ray accompanying K-capture of K^{40} has been measured by a scintillation spectrometer in which NaI-Tl has been substituted for the usual anthracene so that the photo-electrons rather than Compton electrons are used to produce the light pulse in the phosphor.

Anthracene and the other organic phosphors give substantially only the Compton process with gamma-rays from 100 kev to 2 Mev and pair formation within the phosphor is very small even at 2.76 Mev.

Sodium iodide, thallium activated, on the other hand gives strong photoelectric effect in the iodine even at 2.76 Mev and pair production at this energy is prominent and can be seen as

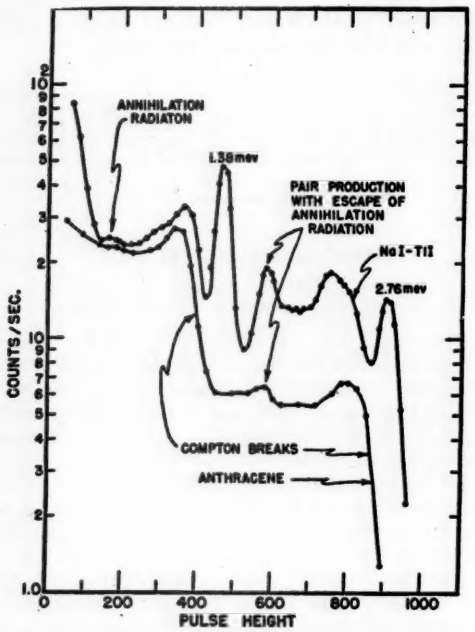

FIG. 1. Pulse-height distribution from the gamma-rays of Na^{24} in anthracene and NaI-TlI.

low as 1.5 Mev. Figure 1 shows the pulse distributions obtained both with anthracene and with NaI-TlI for the gamma-rays of Na^{24}. Pairs produced in the phosphor largely stop in it due to the large thickness of crystal (anthracene—2.4 g/cm², NaI—9.3 g/cm²). If the quanta from the annihilation of the positron escape from the crystal a peak is produced at 1.02 Mev lower energy than the gamma-ray. This peak is large in the NaI curve; it is still visible on the anthracene curve but is about nine times smaller as expected.

The single gamma-ray of K^{42} at 1.51 Mev is shown in Fig. 2.

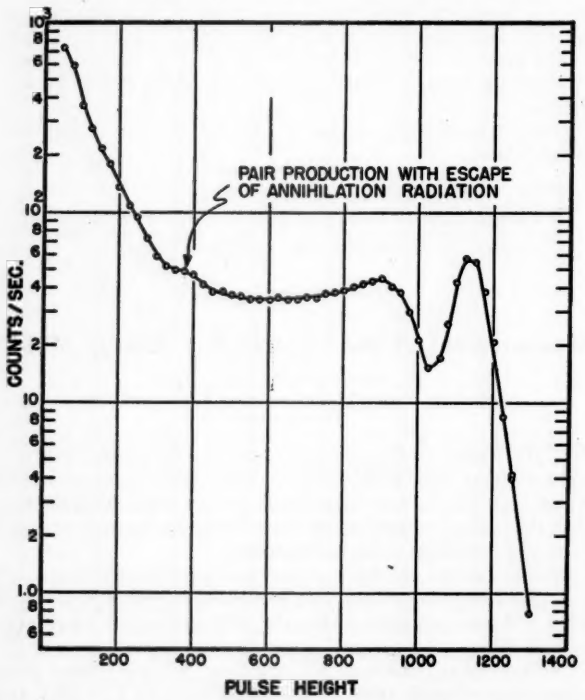

FIG. 2. Pulse-height distribution from the gamma-rays of K^{42} in NaI-TlI.

TABLE I. Comparison of gamma-rays.

Comparison substance	Reported gamma-energy	K^{40} gamma-energy
Na^{24}	1.380[a] 1.74[b](2.765)	1.464 1.47
K^{42}	1.51[c]	1.460 1.456
Zn^{65}	1.118[d]	1.466 1.461

[a] Robinson, Ter-Pogossian, and Cook, Phys. Rev. **75**, 1099 (1949).
[b] Pair production peak from upper gamma-ray.
[c] K. Siegbahn, Arkiv. f. Mat. Astr. o. Fys. **34B**, No. 4 (1947).
[d] Jensen, Laslett, and Pratt, Phys. Rev. **76**, 430 (1949).

This gamma-ray is very close in energy to that of K^{40}. The pair production peak at 0.49 Mev can barely be seen.

About 500 g of KCl was placed around the NaI crystal and a typical pulse distribution produced is shown in Fig. 3.

Table I shows the comparison of the K^{40} gamma-ray with that of Zn^{65}, Na^{24} and K^{42}. The mean energy is 1.462±0.01 Mev. The mean value agrees well with our previous report[1] and that of Pringle, Standil, and Roulston.[2]

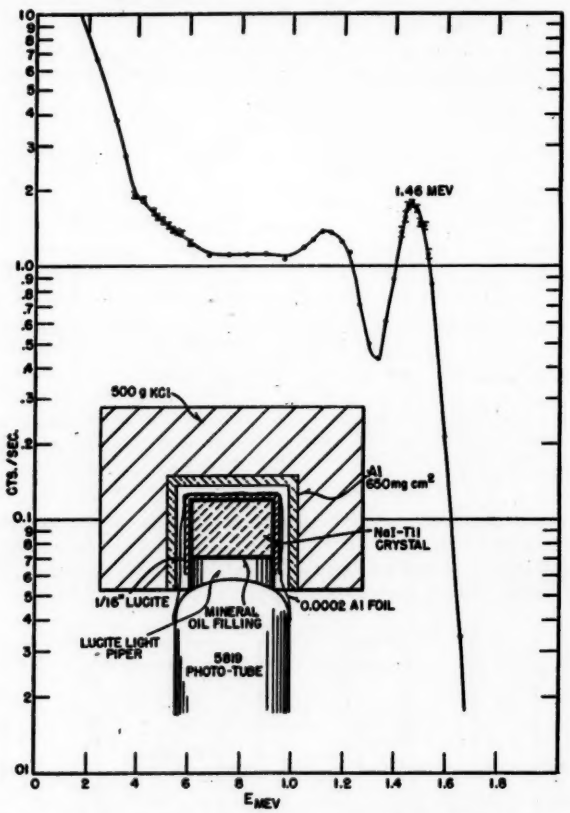

FIG. 3. Pulse-height distribution from the gamma-rays of K^{40} in NaI-TlI.

Examination of the curve between 0.4 and 0.6 Mev shows the presence of two weak overlapping peaks. One of them at 0.44 Mev is expected due to the production of pairs in the crystal as in the K^{42} spectrum. After subtracting this expected peak, a peak about 0.1 *c/s* high remains at the location for annihilation radiation. This annihilation radiation probably comes from the positron member of pairs produced in the 500 g sample and the shield walls and not from positron emission in K^{40}. It appears therefore that the ratio of positrons emitted to beta-rays is less than 2×10^{-5} for K^{40}.

[1] P. R. Bell and J. M. Cassidy, Phys. Rev. **77**, 409 (1950).
[2] Pringle, Standil, and Roulston, Phys. Rev. **77**, 841 (1950).

The Nuclear Magnetic Moment of Scandium[45]

ROBERT E. SHERIFF* AND DUDLEY WILLIAMS
Ohio State University, Columbus, Ohio
May 8, 1950

THE nuclear magnetic resonance due to Sc^{45} has been located in a magnetic field of 5000 gauss at 5.14 Mc/sec. by means of the super-regenerative detection method.[1,2] A strong signal of the same order of intensity as for the Br^{79} signal in saturated aqueous NaBr was found in a saturated aqueous solution of $ScCl_3$. Our preliminary value of the ratio of the resonance frequency of the Sc^{45} signal to that of the Br^{79} signal in the same magnetic field is:

$$\nu(Sc^{45})/\nu(Br^{79})=0.96954\pm0.00006.$$

Using Zimmerman and Williams' value[1] for the ratio of the Br^{79} and proton resonance frequencies in the same magnetic field, we find:

$$\nu(Sc^{45})/\nu(H^1)=0.24296\pm0.00005.$$

Making a diamagnetic correction[3] of 0.260 percent and using the value 2.79255 nuclear magnetons for the proton's magnetic moment[4] we find for the nuclear g-value of Sc^{45}:

$$g(Sc^{45})=1.3605\pm0.0003.$$

The spin of Sc^{45} is known to be 7/2 from hyperfine structure studies.[5,6] Thus the magnetic moment is:

$$\mu(Sc^{45})=4.7617\pm0.0010 \text{ nuclear magnetons.}$$

This value agrees very closely with the best spectroscopic value[7] of 4.8 nuclear magnetons.

* AEC Research Fellow.
[1] J. R. Zimmerman and D. Williams, Phys. Rev. **76**, 350 (1949).
[2] W. H. Chambers and D. Williams, Phys. Rev. **76**, 638 (1949).
[3] W. E. Lamb, Phys. Rev. **60**, 817 (1941).
[4] Hipple, Sommer, and Thomas, Phys. Rev. **76**, 1877 (1949).
[5] H. Schuler and T. Schmidt, Naturwiss. **22**, 758 (1934).
[6] H. Kopfermann and E. Rasmussen, Zeits. f. Physik **92**, 82 (1934).
[7] H. Kopfermann and H. Wittke, Zeits. f. Physik **105**, 16 (1937).

The Half-Life of Strontium[90]*

RUTH I. POWERS AND A. F. VOIGT
Institute for Atomic Research and Chemistry Department, Iowa State College, Ames, Iowa
May 11, 1950

THE long-lived strontium isotope, Sr^{90}, one of the nuclides resulting from uranium fission, is important because of its high yield in fission, about five percent, as well as its long half-life. In any fission product mixture more than a few years old, this nuclide and its daughter, the 62-hr. Y^{90}, together constitute a large fraction of the total activity. Consequently the half-life of the parent Sr^{90} assumes some importance in calculations dealing with long term use or storage of the fission products.

This nuclide was first reported in this country by Nottorf,[1] of this laboratory,[2] in 1943. The decay of several samples which he prepared have now been followed for seven years, by means of a Lauritsen electroscope, and the half-life resulting from these measurements is sufficiently different from that currently used to warrant its publication at this time. The currently accepted value of 25 yr. is an average between the 23±3-yr. value reported by Nottorf[3] as a result of measurements over two and one-half years, and the value of 24 to 30 yr. estimated by Glendennin,[4] and Coryell[5] from fission yield data.

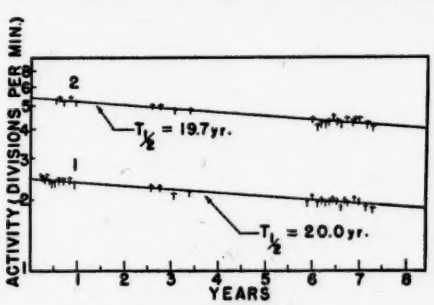

FIG. 1. Decay curve of Sr^{90}.

The original samples, after separation from cyclotron bombarded uranyl nitrate, were purified by repeated carbonate precipitations, and mounted as strontium carbonate.

In order not to measure any of the 55-day Sr^{89}, which was originally present, sample 1 was read with 746 mg/cm² of aluminum absorber, while sample 2 was read with 714 mg/cm². The beta-ray from Sr^{89} has an energy of 1.5 Mev and a range of 680 mg/cm² of aluminum. Before each reading the stability of the electroscope was checked with a uranium standard. Noteworthy is the fact that the Lauritsen electroscope has remained stable over this period of seven years.

The method of least squares[6] was used to draw the best possible straight line through each set of data (Fig. 1). From this, a half-life of 20.0 yr. was obtained with sample 1, while sample 2 gave 19.7 yr. Therefore the half-life of Sr^{90} may be taken as 19.9±0.3 yr.

* This work was performed at the Ames Laboratory of the U. S. AEC.
[1] R. W. Nottorf, Metallurgical Project Report, CC-521 (March 15, 1950).
[2] Present address, E. I. du Pont de Nemours and Company, Parlin, New Jersey.
[3] R. W. Nottorf, National Nuclear Energy Series, M.P.T.S., Div. IV, Vol. 9, Paper No. 77.
[4] L. E. Glendennin and C. D. Coryell, National Nuclear Energy Series, M.P.T.S., Div. IV, Vol. 9, Paper No. 78.
[5] C. D. Coryell, Metallurgical Project Report, CC-1112 (December, 1943).
[6] A. G. Worthing, and J. Geffner, *Treatment of Experimental Data* (John Wiley and Son Inc., New York, 1946), Chapter XI.

The Angular Distribution of Protons from the $B(\alpha, p)C$, C^* Reaction

J. L. PERKIN
Wheatstone Laboratory, King's College, London, England
May 8, 1950

USING a 5-mc polonium α-particle source and a cloud chamber, Roy[1] examined the angular distribution of protons from the reaction $B(\alpha, p)C$, C^*. The angular distributions of the two groups with Q-values of 0.42 and 0.09 Mev were found to be roughly isotropic within the wide limits of statistical fluctuation imposed by the small number of protons recorded.

Creagan[2] examining the emission of protons at 0° and 90° found the intensity of protons from transitions to the ground state (Q=4.07 Mev) in the forward direction to be small compared with that observed at 90°.

The present experiments were performed using a 1.4-mc polonium α-particle source, unbacked boron targets, and Ilford C2 photographic plates to record the emitted protons.

The photographic plates were held in a frame by retaining screws such that the plane of the emulsion lay 3 mm below the line joining the source and target.

Boron targets were made by smearing a suspension of boron powder in a collodion-ether solution on glass plates. In this way unbacked and fairly uniform tagets could be obtained with thicknesses as low as 0.2 mg/cm². Microscopic examination showed that the relative amount of collodion in the film could be reduced to quite small proportions before the target became too fragile.

The source holder and collimating arrangement were designed so that the spread of the α-beam at the target was ±10°, and so that the maximum angle at which the plate could see all the target was as much as 170° in one case.

Non-resonance experiment. For the first exposure (14 days) the energy of the α-particles at the target was set at 4.3 Mev. This corresponded to the top of the potential barrier of the B^{10} nucleus. A target of thickness 0.35 mg/cm² was used.

About 4000 proton tracks were measured and groups corresponding to Q-values of 4.08±0.12, 3.35±0.25, 0.65±0.15, 0.15±0.15, and −0.57±0.15 Mev, were observed. The over-all intensities of the first four of these groups were in the ratio 10:1:100:50. Comparison of the Q-values found with the more precise ones obtained by Creagan[3] since this work was completed,

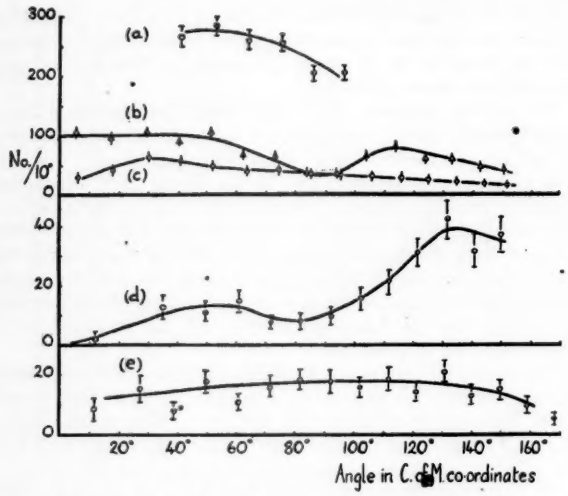

FIG. 1. Angular distribution of protons from the reaction $B(\alpha, p)C$, C^*.
(a) $E=4.3$ Mev $Q=-0.57$ Mev.
(b) $Q=0.65$ Mev.
(c) $Q=0.15$ Mev.
(d) $Q=4.08$ Mev.
(e) $E=2.9$ Mev $Q=4.08$ Mev.

indicates that the group observed at 0.15 Mev is probably the superposition of two groups at $Q=0.31$ and 0.07 Mev. The weak group observed at $Q=3.35$ Mev was not found by Creagan.

The angular distributions of the protons from the groups with Q-values 4.08, 0.65, 0.15, and -0.57 Mev, are shown in Fig. 1.

The vertical lines indicate the statistical error. The groups at $Q=0.65$ and 0.15 Mev were only partially resolved and are subject to an additional error ($\sim$10 to 20 percent) due to the empirical method of dividing these groups at any angle. Contamination by recoil protons in the forward direction and by α-particle background at higher angles severely restricted the distribution of the group at $Q=-0.57$ Mev.

All the angular distributions for this non-resonance experiment show some degree of anisotropy and asymmetry. The ground state group in particular has a very low minimum at 0° and a pronounced maximum in the backward direction confirming the results of Creagan discussed earlier. An examination of Roy's results for the groups at 0.42 and 0.09 Mev corresponding to the groups found at 0.65 and 0.15 Mev shows that his results are not in contradiction to those observed. The statistical accuracy of the cloud-chamber work was not sufficient however to establish the shape of these distributions with any certainty.

Resonance experiment. The α-particle energy at the target for the second exposure (28 days) was reduced to 3.4 Mev. (i.e., below the energy necessary to penetrate through the top of the barrier of the B^{10} nucleus as found by Miller *et al.*[4] The target was replaced with one of stopping power 1.4 mg/cm². One high energy proton group was observed which, if it is assumed to be due to ground state protons, gives a value of 2.9 Mev for the α-particle resonance energy.

It is energetically impossible for this group to be formed in a reaction with the heavier boron isotope B^{11}. Miller *et al.*[4] using an ionization chamber were the first to find this resonance level. Their experiments, however, were not decisive as the proton groups they were able to observe ($Q=0.4$ and -0.1 Mev) could have been assigned to the $B^{11}(\alpha, p)C^{14}$, C^{14*} reaction.

Examination of the distribution (*e*) in Fig. 1 shows that the distribution of this ground state group at resonance is practically isotropic between the limits 30 to 150°.

My thanks are due Dr. F. C. Champion for useful discussions and the Department of Scientific and Industrial Research for financial support.

[1] R. Roy, Phys. Rev. **75**, 1775 (1949).
[2] R. Creagan, Phys. Rev. **75**, 1292 (1949).
[3] R. Creagan, Phys. Rev. **76**, 1769 (1949).
[4] Miller, Duncanson, and May, Proc. Camb. Phil. Soc. **30**, 549 (1934).

Theoretical Hall Coefficient Expressions for Impurity Semiconductors*

V. A. JOHNSON AND K. LARK-HOROVITZ
Purdue University, Lafayette, Indiana
May 15, 1950

IN the analysis of impurity semiconductors, the carrier density n (per cm³) and the Hall coefficient R (cm³/coulomb) are assumed to be related by

$$R=\pm 3\pi/(8ne), \tag{1}$$

where e is the electronic charge in coulombs. The derivation of Eq. (1) assumes that the mean free path of a conduction electron is independent of its kinetic energy and that the applied magnetic field is weak. The effects upon Eq. (1) of certain deviations from these assumptions have been calculated.

The theory of the Hall effect yields a general expression for the ratio

$$r=\frac{|R|}{(1/ne)}=\frac{3n}{4\pi m}\frac{I_2}{I_1^2+(eH/m)^2I_2^2} \tag{2}$$

where H is the magnetic field, m is the effective electron mass, and

$$I_1=\int_0^\infty \frac{lv^3}{1+(eHl/mv)^2}\frac{\partial f_0}{\partial \epsilon}dv; \quad I_2=\int_0^\infty \frac{l^2v^2}{1+(eHl/mv)^2}\frac{\partial f_0}{\partial \epsilon}dv,$$

in which l is the mean free path, f_0 the unperturbed distribution function, and $\epsilon=mv^2/2$. If one uses classical statistics and replaces ϵ/kT by x, then

$$r=(3\pi^{\frac{1}{2}}/4)J_2(J_1^2+\alpha J_2^2)^{-1} \tag{3}$$

where

$$J_1=\int_0^\infty lx^2e^{-x}(x+\alpha l^2)^{-1}dx; \quad J_2=\int_0^\infty l^2x^{\frac{3}{2}}e^{-x}(x+\alpha l^2)^{-1}dx;$$

$$\alpha=e^2H^2/(2mkT).$$

In the weak field approximation ($\alpha\approx 0$) Eq. (3) leads to Eq. (1) if l is independent of the energy ϵ. However, if l is proportional to ϵ^s, as in the Rutherford-type scattering by impurity ions,[1] Eq. (3) yields $r=315\pi/512$. It has been found that the resistivity ρ of impurity semiconductors can be explained[2] as the sum of ρ_L, resistivity due to scattering by lattice ions, and ρ_I, resistivity due to scattering by impurity ions. The mean free path l_L associated with ρ_L is independent of ϵ, while l_I is proportional to ϵ^2. The effective mean free path l is found by reciprocal addition

$$l=l_Ll_I/(l_L+l_I). \tag{4}$$

From resistivity theory one obtains

$$l_L=3(2\pi mkT)^{\frac{1}{2}}(4ne^2\rho_L)^{-1} \tag{5a}$$

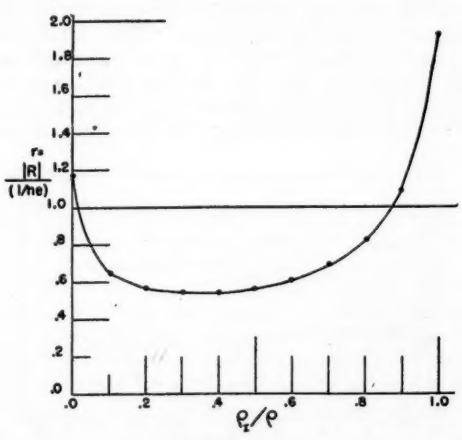

FIG. 1. The dependence of $r=|R|/(1/ne)$ on the ratio of ρ_I, resistivity due to Rutherford-type scattering by impurity ions, to ρ, the total resistivity.

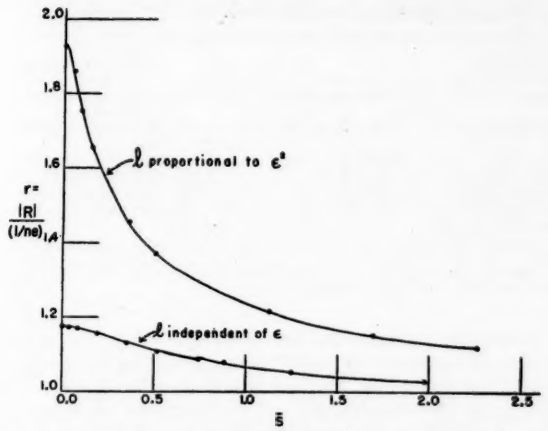

FIG. 2. The dependence of r on $\bar{s}$, the mean value of the ratio of mean free path to radius of curvature in the magnetic field.

and

$$l_I = a\epsilon^2 = (\pi m)^{\frac{1}{2}}\epsilon^2(2kT)^{-\frac{1}{2}}(2ne^2\rho_I)^{-1}. \quad (5b)$$

The use of these equations in Eq. (3) gives an expression for r in terms of ρ_I/ρ

$$r = \pi^{\frac{1}{2}}\rho^2(48\rho_I^2)^{-1}\int_0^\infty x^{9/2}e^{-x}\{1+(1/6)(\rho/\rho_I-1)x^2\}^{-2}dx. \quad (6)$$

Figure 1 shows the dependence of r on ρ_I/ρ. The deviation of r from the value $3\pi/8$ has an important bearing on the computation of the carrier mobility from measured Hall coefficient and resistivity values, since the mobility $b=(ne\rho)^{-1}=R/(r\rho)$.

The effect of the magnetic field on the Hall coefficient has been calculated by Harding[3] for l independent of ϵ. When $l=a\epsilon^2$, Eq. (3) becomes

$$r = (3\pi^{\frac{1}{2}}/4)K_1(\beta)/\{K_2^2(\beta)+\beta K_1^2(\beta)\}, \quad (7)$$

where

$$K_1(\beta)=\int_0^\infty x^{9/2}e^{-x}(1+\beta x^3)^{-1}dx; \quad K_2(\beta)=\int_0^\infty x^3e^{-x}(1+\beta x^3)^{-1}dx;$$
$$\beta = a^2e^2H^2(kT)^3/2m.$$

Figure 2 shows the dependence of the Hall coefficient on the magnetic field; r is plotted as a function of $\bar{s}$, the mean value of the ratio of mean free path to radius of curvature in the field H. Values of $\bar{s}$ are found from

$$\bar{s}=3\pi\times10^{-8}H/(8ne\rho_L) \quad \text{for constant } l$$
$$\bar{s}=4\beta^{\frac{1}{2}}\pi^{-\frac{1}{2}}=10^{-8}H/(2ne\rho_I) \quad \text{for } l=a\epsilon^2,$$

with H in gauss, n in cm^{-3}, e in coulombs, and ρ in ohm-cm. As $\bar{s}$ becomes comparable with unity, the r values computed in this treatment are no longer reliable because the assumptions made in the Lorentz solution of the Boltzmann equation lose their validity.

* Work assisted in part by a Signal Corps Contract.
[1] E. Conwell and V. F. Weisskopf, Phys. Rev. **69**, 258 (1946); **77**, 388 (1950).
[2] K. Lark-Horovitz and V. A. Johnson, Phys. Rev. **69**, 258 (1946); K. Lark-Horovitz (unpublished material).
[3] J. W. Harding, Proc. Roy. Soc. **A140**, 205 (1933).

Cosmic-Ray Intensity in the Upper Atmosphere

M. PANETTI AND G. WATAGHIN
Physical Institute of the University of Turin, Turin, Italy
April 19, 1950

THE present note concerns the possibility of representing the observed variation of cosmic-ray intensity with depth in the upper atmosphere[1] by means of the following formula:

$$I(x)=I_1(x)+A\int_0^x I_1(x')dx'+BxI_1(x), \quad (1)$$

where

$$I_1(x)=[0.8+0.2(b_1/b^*)]f(\eta)+0.2[1-b_1/b^*]f(\bar{\eta}).$$

Here $f(\eta)=e^{-\eta}+\eta Ei(-\eta)$, $\eta=x/l=(b-b^*)x$, $\bar{\eta}=bx$, x is the atmospheric depth, $l=120$ g cm^{-2} is the value of the absorption path of energetic nucleons determined from experimental data, data, $b\sim1/60$ and $b^*\sim1/120$ g^{-1} cm^2 are respectively the coefficient of absorption and production of the nucleons and b_1 is the coefficient of production of nucleons by α-particles. The first, second, third terms of (1), as discussed below, correspond respectively to the nucleons intensity, meson intensity and intensity of particles (nucleons and mesons) produced locally. Electron and photon intensities are taken into account also. The parameters A, B, b_1 can be chosen in order to fit the experimental data. From Fig. 1 it appears that curve I is in accord with the observations made by J. A. Van Allen and H. E. Tatel with a Geiger counter on a rocket for atmospheric depth $x\lesssim200$ g cm^{-2}, if one assumes: $A=1.1$ g^{-1} cm^2, $B=0.08$ g^{-1} cm^2, $b_1=1/100$ g^{-1} cm^2. The following arguments justify the choice of (1).

The spectrum of primary particles is composed[2] of energetic protons ($\sim$79 percent) and of α-particles ($\sim$20 percent); the contribution of the heavier nuclei with $Z>2$ is unessential. The Geiger counter used in the measurements will be considered as an isotropic detector of the charged particles.

The variation with depth of the intensity of the primary protons (0.8 of the number of primaries) and secondary energetic nucleons is given by $I_1'(x)=0.8f(\eta)$. Similarly, the intensity of the primary α-particles is $I_\alpha(x)=0.2f(\bar{\eta})$, since the value corresponding approximately to the geometric cross section of the air nuclei can be assumed as the cross section of the α-particles. The production of the secondary energetic nucleons by collision of a primary particle is evaluated introducing the coefficient, b_1, of production which appears to be greater than the corresponding value b^* for protons, as is plausible. For the intensity of the energetic nucleons originated by α-particles, the formula $I_1''(x)=0.2(b_1/b^*)[f(\eta)-f(\bar{\eta})]$ is easily deduced. Hence the intensity of nucleons and of α-particles together gives the first term of (1):

$$I_1'(x)+I_\alpha(x)+I_1''(x)=I_1(x). \quad (2)$$

Referring to the meson intensity, $I_2(x)$, the usual method of a diffusion equation[3] can be applied. If meson decay is not considered (since the recorder reveals equally $\pi^\pm$-mesons, $\mu^\pm$-mesons, $e^\pm$ electrons), and if ionization is neglected, the equation becomes:

$$[\partial I_2(x)]/\partial x = AI_1(x).$$

Thus:

$$I_2(x)=A\int_0^x I_1(x')dx'. \quad (3)$$

The Geiger counter records with a greater probability a nucleon or a meson produced locally, than a nucleon or a meson produced

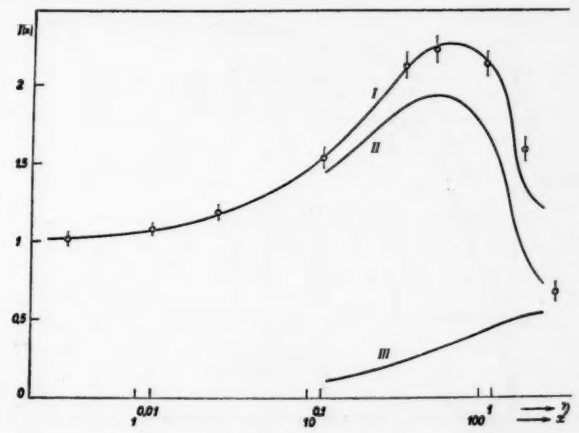

FIG. 1.—Curve I represents intensity of cosmic rays calculated by the formula (1), as a function of the atmospheric depth x (g/cm^2) or of $\eta=x/120$. Circles indicate experimental data. Curves II and III represent respectively $I_1(x)+I_2(x)$ and $I_2(x)$.

in a distant collision. This effect[4] is obviously proportional to the local density of air and to the incident nucleon intensity:

$$I_3(x) = BxI_1(x). \quad (4)$$

Expressions $I_1(x)+I_3(x)$ and $I_2(x)$ are respresented in curves II and III respectively. Formula (1) or curve I is obtained by adding the two mentioned expressions.

The influence of the production of secondary particles in the mass of the rocket is approximately proportional to the total intensity of the incident particles and does not affect the given formula.

[1] J. A. Van Allen and H. E. Tatel, Phys. Rev. **73**, 245 (1948).
[2] H. L. Bradt and B. Peters, Phys. Rev. **77**, 50 (1950).
[3] B. Rossi and K. Greisen, Rev. Mod. Phys. **13**, 240 (1941).
[4] A. Wataghin, Anais de Academia Brasileira de Ciencias **21**, 353 (1949).

Rise Times of Voltage Pulses from Photo-Multipliers*

O. Martinson, P. Isaacs, H. Brown, and I. W. Ruderman
Pupin Physics Laboratories, Columbia University, New York, New York
May 1, 1950

A METHOD has been devised for measuring fast rise times of voltage pulses from photo-multiplier tubes without using high speed oscillographs.

1P21 tubes were operoted at voltages high enough (about 1600 v) to give 25-volt pulses from a radium source, when used in conjunction with a 6AG7 cathode follower. The time constant of the RC circuit on the last dynode from which the pulses are taken is $\sim 10^{-6}$ sec. The pulse is fed into a variable length of shorted RG63U cable, thus subtracting from it a delayed pulse of equal height. The maximum height reached by the resulting difference pulse is the height of the original pulse at a time after its start equal to the delay. The clipped pulse then is fed through a discriminator and scaler. By varying the length of the shorted delay line and adjusting the discriminator setting so that a constant counting rate is obtained from a given source, the shape of the pulse can be accurately plotted if the cathode follower and crystal diode responses are known (measurements showed them to be quite linear in the region used).

Plots of the rise of the pulses have been made for pulses from various organic phosphors, and for noise pulses (using both thermionically emitted electrons and those knocked out of the photo-cathode by gamma-rays). With slight deviations which are undoubtedly due to limiting or curvature of cathode follower or crystal diode characteristics, logarithmic plots of the curves in Fig. 1 show them to be of the form $V = V_0(1-e^{-t/\tau})$. The value of τ for the noise pulse is 5 to 6×10^{-9} sec., of which an unknown, but probably not the major, fraction is due to delay in the circuit following the photo-multiplier, and the remainder represents the spread of transit time through the photo-tube for the secondary electrons from a primary noise electron emitted at the photo-cathode.

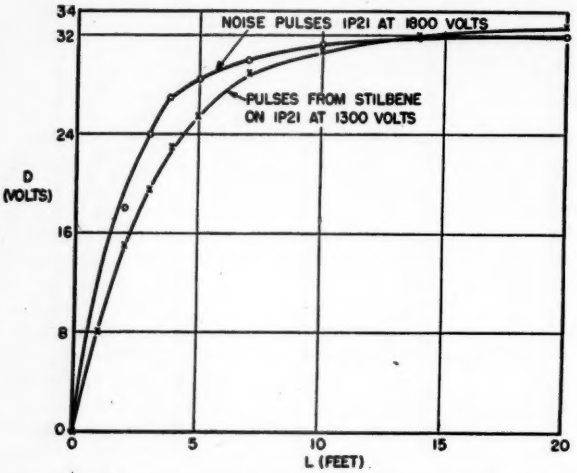

FIG. 1. Rise of noise pulses and pulses from stilbene. D is the discriminator reading corresponding to a constant counting rate. L is the length of shorted delay cable (4 feet of which correspond to a time delay of 10^{-8} sec.).

TABLE I. Rise time of voltage pulses from 1P21 at 1500 v.

Crystal	τ	Quality of crystal
Stilbene	$(0.85\pm0.05)\times10^{-8}$ sec.	Single crystal, colorless, transparent.
Phenanthrene	$(1.0\pm0.1)\times10^{-8}$ sec.	Microcrystalline, pale yellow.
Anthracene	$(2.1\pm0.2)\times10^{-8}$ sec.	Single crystal, colorless.
o-Phenylphenol*	0.9×10^{-8} sec.	Microcrystalline, pinkish
p-Phenylphenol*	2.0×10^{-8} sec.	Microcrystalline, colorless.
5-*sec*-butyl-2-hydroxy-α^1,α^3-xylenediol*	1.6×10^{-8} sec.	Microcrystalline, colorless.

* These rough measurements probably good to 0.4×10^{-8} sec., were taken with larger 1P21 voltages ($\sim$1700 v).

Table I summarizes results on organic phosphors. The figures given are averages of a number of crystals, which show some variation in τ. For these experiments, the rise time of the voltage pulse differs from that of a noise pulse due to the decay time of the fluorescence of the phosphor.

These results show fair agreement with those of other investigators.[1] The three last ones have not been previously covered in the literature.

* We should like to thank the AEC which aided materially in this research.
[1] For example, Hofstadter, Liebson, and Elliot, Phys. Rev. **78**, 81 (1950); J. R. Bell, unpublished results.

Altitude Dependence of Neutron Production by Cosmic-Ray Particles*

W. B. Fowler
Physics Department, Washington University, St. Louis, Missouri
May 8, 1950

THE counters and circuits used in the cloud-chamber study of neutron coincidences[1] (carried out jointly with the Harvard cosmic-ray group) have been employed in a preliminary study of the changes in neutron coincidence rates between Climax, Colorado (3400 meters) and St. Louis, Missouri (170 meters). The experimental arrangement is shown in Fig. 1. The crossed four-fold G-M tube telescopes[2] are placed between a 10.16-cm Pb filter and a 10.16-cm Pb absorber. The double anticoincidence tray C more than covers the cone defined by the telescopes. Below C is a large paraffin thermalizer containing five thermal neutron counters, proportional counters filled with enriched BF_3.[3]

The following events were recorded: telescope coincidences (AB), anticoincidences ($AB-C$), neutron counts (N), and neutron counts in delayed coincidence (3 to 150 μsec.)[4] with AB events (AB:N) and $AB-C$ events ($AB-C$:N). The neutron counters were, in addition, in prompt anticoincidence (± 1 μsec.) with the C tray; this feature discriminated against pulses due to showers.

TABLE I. Neutrons associated with stoppings (AB-C:N).

	Climax	St. Louis
With absorber (115 g/cm² Pb)	$7.02\pm0.48/h$	$1.16\pm0.09/h$
	Expected $\pm0.15/h$ Casuals	Expected $\pm0.005/h$ Casuals
	Corrected rate $6.87\pm0.48/h$	Corrected rate $1.15\pm0.09/h$
Sans absorber (0.69 g/cm² brass in counter walls)	$0.16\pm0.09/h$	$0.051\pm0.01/h$
	Expected $\pm0.19/h$ Casuals	Expected $\pm0.002/h$ Casuals

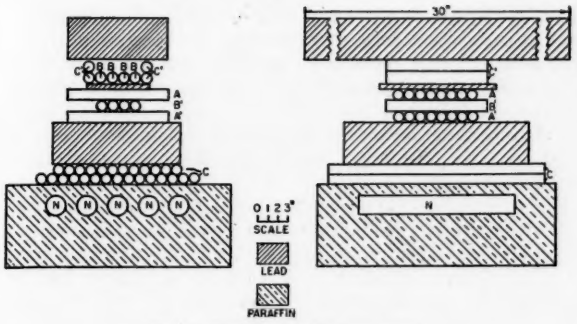

FIG. 1. Experimental arrangement.

It had no effect at St. Louis. At Climax it changed the N rate little; however, when 1 mm Cd sheaths were slipped over the neutron counters, the anticoincidence feature reduced the rate 40 percent. The "with Cd" rate at Climax was less than 5 percent of the "without Cd" rate. Certain refinements were found necessary at Climax' higher elevation. We added four anticoincidence C' counters in the top of the telescopes and also placed one cm of Pb in the telescopes. This discriminated against side showers and low energy stars in the telescope and filter.

Data were taken with and without the absorber. The results are given for neutrons coincident with apparent stoppings in the absorber $(AB-C:N)$ and neutrons coincident with apparent penetrations of the absorber $(ABC:N)$. The $(AB-C:N)$ results are shown in Table I, the $(ABC:N)$ results in Table II. The uncertainties given are the estimated statistical standard errors. The expected casuals are computed from the measured rates and neutron coincidence resolving time. The corrected rates are found[5] by subtracting the expected casual rates from the measured rates. The observed $(AB-C:N)$ rates without absorber may be attributed to accidentals. Previous experience has shown that the observed rates with Cd are always of the order of magnitude of the expected casuals. The factor of increase of the $(AB-C:N)$ coincidences from St. Louis to Climax is seen to be 6.0 ± 0.6. The factor of increase of the $(ABC:N)$ coincidences from St. Louis to Climax is seen to be 16.3 ± 1.2 with absorber and 18.9 ± 1.7 without absorber. These two factors are equal within the statistical uncertainty. The rate of apparent stoppings $(AB-C)$, corrected for the zero effect, increases 2.8 times, in agreement with Kraushaar's[6] results for μ-mesons. The intensity of the hard component (ABC), increases 2.1 times.

Three possible causes of $(AB-C:N)$ events are known, μ^--capture, π^--capture, and low energy proton stars (type 0_p in the Bristol notation[7]). The first should increase by a factor of 2.8. We consider the second and third together as events of nucleonic origin. It is known[8] that the factor of increase for both low and high energy nuclear interactions is greater than 10. It is unlikely that the nucleonic component giving rise to $(AB-C:N)$ events increases less rapidly. If we use the factor of increase for the $(ABC:N)$ events (17.3), we find 75 percent for the fraction of $(AB-C:N)$ events at sea level due to μ^--mesons, and 35 percent at Climax.

TABLE II. Neutrons associated with penetrations $(ABC:N)$.

	Climax	St. Louis
With absorber (115 g/cm² Pb)	$33.7\pm1.1/h$	$2.04\pm0.13/h$
	Expected $\pm1.1/h$ Casuals	Expected $\pm0.04/h$ Casuals
	Corrected rate $32.6\pm1.1/h$	Corrected rate $2.00\pm0.13/h$
Sans absorber (0.69 g/cm² brass in counter walls)	$19.4\pm1.2/h$	$1.02\pm0.07/h$
	Expected $\pm0.7/h$ Casuals	Expected $\pm0.03/h$ Casuals
	Corrected rate $18.7\pm1.2/h$	Corrected rate $0.99\pm0.07/h$

The author wishes to express his thanks to Professor R. D. Sard for his advice and guidance during the course of this work.

* Work supported by the joint program of the ONR and the AEC.
[1] Fowler, Sard, Fowler, and Street, Phys. Rev. 78, 323 (1950).
[2] Cool, Fowler, Street, Fowler, and Sard, Phys. Rev. 75, 1275 (1949).
[3] The enriched BF_3 was made available by the Isotopes Division of the Atomic Energy Commission. The counters were made by the N. Wood Counter Laboratory, Chicago, Illinois.
[4] Sard, Conforto, and Crouch, Phys. Rev. 76, 1134 (1949).
[5] Sard and Sard, Rev. Sci. Inst. 20, 526 (1949).
[6] W. L. Kraushaar, Phys. Rev. 76, 1054 (1949).
[7] R. H. Brown *et al.*, Phil. Mag. 40, 862 (1949).
[8] For example, B. Rossi, Echo Lake Cosmic-Ray Symposium, 307 (1949).

On the Shift of the Nuclear Magnetic Resonance in Paramagnetic Solutions*

N. BLOEMBERGEN**
Harvard University, Cambridge, Massachusetts
AND
W. C. DICKINSON
Research Laboratory of Electronics, Massachusetts Institute of Technology, Cambridge, Massachusetts
May 18, 1950

IN the measurement of gyromagnetic ratios of nuclear spins, paramagnetic ions are often added to the liquid sample in order to reduce the relaxation time.[1] The resonance frequency depends, however, on this addition, because the effective magnetic field at the nucleus is given by

$$H_{eff}=H_0+(4/3\pi-\alpha)M+qM. \quad (1)$$

Here H_0 is the externally applied field. The second term represents the contribution to the local field from the magnetization of the sample outside a spherical cavity around the nucleus under consideration, α being the demagnetizing factor and depending on the shape of the sample. For a sphere the second term vanishes.

The last term is the contribution to the local field at the nucleus from the paramagnetic ions inside a small sphere around the nucleus. This term has heretofore been put equal to zero. This is theoretically correct for pure dipole-dipole interaction in a liquid or in a solid with cubic symmetry.[2]

Experiments show, however, that this term cannot be neglected and represents an important correction in the comparison of gyromagnetic ratios. The value of q depends strongly on the type of chemical compounds used in the liquid sample. An example of the effect is shown in Fig. 1. More detailed experimental results covering different paramagnetic ions will be published in a subsequent paper by one of us (W.C.D.). Although q is usually positive, several cases of negative values of q have been observed.

The effect must not be confused with the chemical binding effect arising from the second-order paramagnetic correction in diatomic or polyatomic molecules.[3-5] The purpose of this letter is to present a possible explanation of the interaction factor q.

The paramagnetic ion in the liquid is subjected to strong varying electric fields. These are responsible for the quenching of the orbital momentum so that the effective magnetic moment of the ion is close to the "spin only" value.[6] Although the average electric field in the liquid will have spherical symmetry, the field at any instant will deviate from the average. Let us consider as a specific example the resonance of a F^{19} nucleus in a solution containing both fluorine ions and paramagnetic ferrous ions. The electric field produced by the F^- ion at the position of a neighboring Fe^{++} ion will have cylindrical symmetry around the radius vector connecting the two ions. Let us take the overall effect of the other particles in the liquid into account by a dielectric polarization, which reduces the field of the F^- ion by a factor ϵ, where ϵ is the dielectric constant of the solution. Now the effective g-value of the paramagnetic ion will depend on the angle between the axis of the electric field and the magnetic field H_0.

$$g^2=g_{\parallel}^2\cos^2\theta+g_{\perp}^2\sin^2\theta. \quad (2)$$

The values of $g_{\parallel}$ and $g_{\perp}$ may be different by a considerable amount, as is well known from observations of the magnetic susceptibility

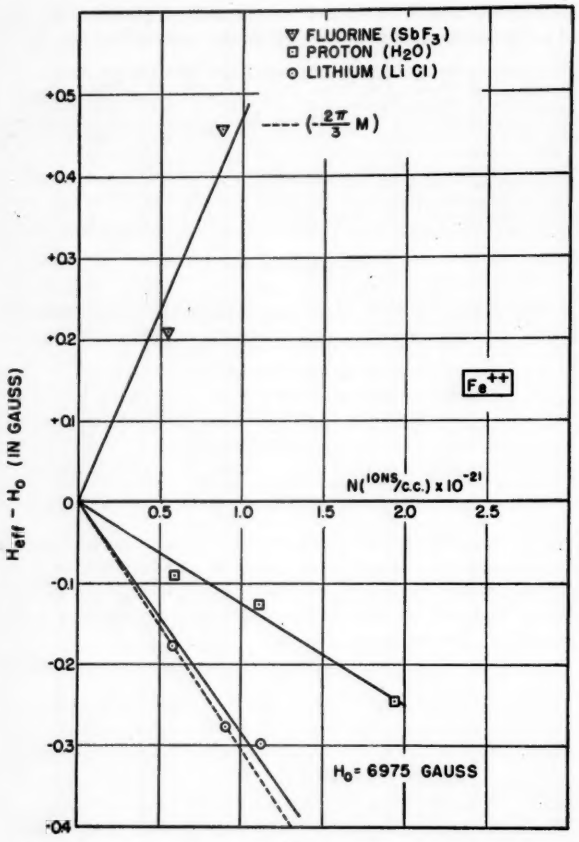

FIG. 1. The shift of the magnetic resonance of F^{19}, H^1, and Li^7 in aqueous solutions containing various amounts of $FeCl_2$. The samples have the shape of a long cylinder with the axis perpendicular to H_0. For $q=0$ the dotted line would result.

in single crystals.[7,8] A static calculation of $g_{\parallel}$ and $g_{\perp}$ is permissible if the motion in the liquid, and therefore the change in the electric field, is described by frequencies which are small compared to the multiplet splitting of the paramagnetic ion. This is a reasonable assumption. The magnetic moment of 1 cc of the solution, containing N ions, is then given by averaging the Langevin formula over all angles

$$M=Ng^2\beta^2H_0S(S+1)/3kT=N(g_{\parallel}^2+2g_{\perp}^2)\beta^2H_0S(S+1)/9kT. \quad (3)$$

The time average local magnetic field at the position of the F^{19} nucleus is obtained by first multiplying the moment of a single paramagnetic ion averaged over the spin orientations by $(-1+3\cos^2\theta)a^{-3}$, where a is the distance between the two ions in the ion pair. Then we take the average over all angles, and finally multiply by the probability $4\pi Nb^3/3$ to find a paramagnetic ion in the sphere of attraction of the F^{19} nucleus. The result, which in general will not vanish, is

$$qM=4\pi Nb^3a^{-3}(4/15)(g_{\parallel}^2-g_{\perp}^2)\beta^2H_0S(S+1)/9kT. \quad (4)$$

Dividing Eq. (4) by Eq. (3) an expression for q is found. The experimental value of q for the F^{19} resonance in a solution of $FeCl_2$ can be explained by giving $g_{\parallel}^2-g_{\perp}^2$ a value which is comparable to those observed in crystals. Of course, there is considerable uncertainty in the geometrical factor b^3a^{-3}, which was introduced in a rather crude way. One must expect, however, that the q value for the Li^7 resonance is much smaller, as has been observed experimentally. The average distance of approach between a Li^+ and a Fe^{++} ion will be much larger and consequently not only the factor a^{-3} is smaller, but also the anisotropic electric field at the Fe^{++} ion, and therefore the anisotropy factor $g_{\parallel}^2-g_{\perp}^2$. In the case of protons, bound in water molecules, more elaborate considerations would be necessary. Even for single ions the geometrical situation has been oversimplified. It seems fruitless to attempt to calculate the detailed configurations of ions and molecules in these concentrated solutions. An experimental determination of the shift for each different type of solution seems necessary. But the order of magnitude of the experimental shift can be understood from the theoretical model, which also leaves room for negative q-values.

It is conceivable that other effects of the same order of magnitude also contribute to the shift. An exchange effect between the F^- and Fe^{++} ion, in which an unbalanced electron spin has a small but finite probability to be found on the fluorine ion, has been suggested by Purcell.[9] The unbalanced spin would create a very large magnetic field at the F^{19} nucleus for a small fraction of the time. This exchange effect would also depend strongly on the distance a, and a much smaller shift for Li^7 is again expected.

* This work has been supported in part by the Signal Corps, the Air Materiel Command, and the ONR.
** Society of Fellows.
[1] Bloembergen, Purcell, and Pound, Phys. Rev. **73**, 679 (1948).
[2] H. A. Lorentz, *Theory of Electrons* (Teubner, Leipzig, 1909), p. 138.
[3] W. C. Dickinson, Phys. Rev. **77**, 736 (1950).
[4] E. M. Purcell and N. F. Ramsey, Phys. Rev. **78**, 807 (1950).
[5] W. G. Proctor and F. C. Yu, Phys. Rev. **77**, 717 (1950).
[6] J. H. Van Vleck, *Electric and Magnetic Susceptibilities* (Oxford University, Press, New York, 1932), p. 285.
[7] D. Polder, Physica **9**, 709 (1942).
[8] B. Bleaney and D. J. E. Ingram, Nature **164**, 116 (1949).
[9] Private communication.

Coincidence Studies of the Disintegration of Sc^{44}*

WILLIAM H. CUFFEY
Department of Physics, Indiana University, Bloomington, Indiana
May 10, 1950

INVESTIGATIONS of the radioactivity of Sc^{44} have been made by Smith[1] and by Hibdon, Pool, and Kurbatov.[2] These authors showed that the disintegration of Sc^{44} involves an isomeric transition in the parent nucleus since two periods, 52 and 4.1 hr. were found. Smith showed that the 52-hr. state lies higher than the 4.1-hr. state and feeds the lower state by an internally converted gamma-ray of 0.27 Mev energy. The 4.1-hr. state emits positrons of 1.45 Mev energy. Hibdon, Pool, and Kurbatov showed that an additional gamma-ray was emitted and determined its energy, by lead absorption, as 1.33 Mev.

In the present experiments coincidence and absorption techniques have been employed in order to get further information on the decay scheme of this element. The sources were prepared by

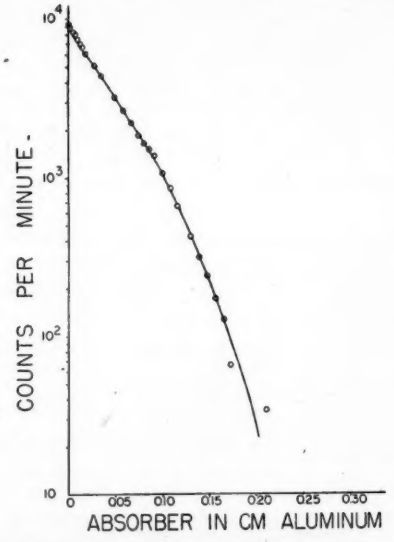

FIG. 1. Absorption of positrons in aluminum.

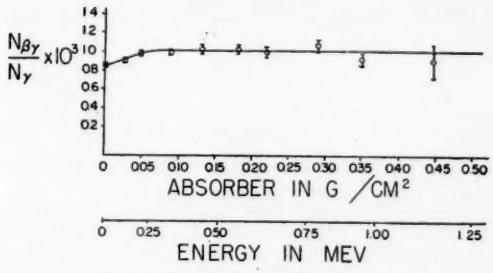

FIG. 2. Beta-gamma-coincidences in Sc^{44}.

bombarding separated K^{41}, obtained from the Y-12 plant of Oak Ridge, by 23-Mev α-particles with the cyclotron. The scandium was separated chemically and enough time was allowed to elapse before the beginning of the experiments so that the decay followed the 52-hr. period of the isomeric state.

A beta-ray absorption curve was taken using an end-window counter with a mica window of surface density 4 mg/cm². The absorption curve is shown in Fig. 1, in which the logarithm of the intensity is plotted against absorber thickness in centimeters of aluminum. An analysis of the data by the method of Bleuler and Zunti[3] yields a value of 1.54 Mev for the positron end point. In addition, the slight rise in the curve at 0.015 cm of aluminum shows the presence of the internal conversion electrons from the gamma-ray at 0.27 Mev.

The energy of the gamma-rays was determined by measuring the coincidence absorption of Compton electrons. The curve shows an "end point" corresponding to a gamma-ray of 1.2 Mev energy, with a break at lower energies corresponding to annihilation radiation. A Bleuler-Zunti analysis of the data gives 1.18 Mev for the energy of the harder gamma-ray.

Beta-gamma-coincidences were measured in the usual manner using a lead cathode counter as the gamma-counter and an end-window counter as the beta-counter. The results are shown in Fig. 2 in which $N_{\beta\gamma}/N_\beta$ is plotted against the range of the positrons. The number of beta-gamma-coincidences per disintegration is independent of the energy of the positrons from 0.25 to 1.2 Mev, indicating that there is only one positron group. The decrease in $N_{\beta\gamma}/N_\beta$ from 1.01×10^{-3} at 0.25 Mev to 0.85×10^{-3} at the lowest energies obtained is caused by the internal conversion electrons of the 0.27-Mev line. From a knowledge of the efficiency of the counter[4] and the value for $N_{\beta\gamma}/N_\beta=1.01\times10^{-3}$, one obtains a value of about 1.0 Mev for the energy of the coincident gamma-ray in Sc^{44}. It would appear, therefore, that, following the isomeric transition, the 4.1-hr. state disintegrates by the emission of one positron group of about 1.5 Mev energy followed by a 1.18-Mev gamma-ray.

The author wishes to thank Professor A. C. G. Mitchell for his interest in this work.

* This research was assisted by the joint program of the ONR and AEC.
[1] G. P. Smith, Phys. Rev. **61**, 578 (1942).
[2] Hibdon, Pool, and Kurbatov, Phys. Rev. **67**, 289 (1945).
[3] E. Bleuler and W. Zunti, Helv. Phys. Acta **19**, 375 (1946).
[4] E. T. Jurney and F. Maienschein, Rev. Sci. Inst. **20**, 932 (1949).

Ferromagnetic Resonance in Manganese Ferrite and the Theory of the Ferrites

CHARLES GUILLAUD
C.N.R.S. Laboratoires, Bellevue (S. et O.), France
AND
W. A. YAGER, F. R. MERRITT, AND C. KITTEL
Bell Telephone Laboratories, Murray Hill, New Jersey
May 17, 1950

WE have observed microwave ferromagnetic resonance absorption at room temperature at a frequency of 24,164 Mc/sec. in polycrystalline specimens of manganese ferrite $Fe(MnFe)O_4$ in the form of spheres ranging from 0.035 to 0.060 cm in diameter. Typical results are shown in Fig. 1. The observed g-value in the resonance equation $\hbar\omega=g\mu_B H$, as deduced from the average of runs on four separate spheres of various sizes, is found to be 1.99(7) with a mean deviation of ±0.003. The half-width at half-power of the resonance line is about 240 oersteds. The field intensities were measured by proton resonance.

On the simplest picture of the electronic structure of manganese ferrite the carriers of the magnetic moments are to be found among the Mn^{++} and Fe^{+++} ions. Each of these ions has a half-filled $3d$ shell and a ^6S ground state, leading to a predicted g-value very close to the free spin value 2.00. It is to be noted that our experimental results are in good agreement with the theory.

Measurements of the saturation magnetization were made earlier by one of us[1] on the specimen employed in the microwave work, and give σ_∞ (0°K) = 110.6 for the moment per gram extrapolated to infinite fields at 0°K. From this value we calculate

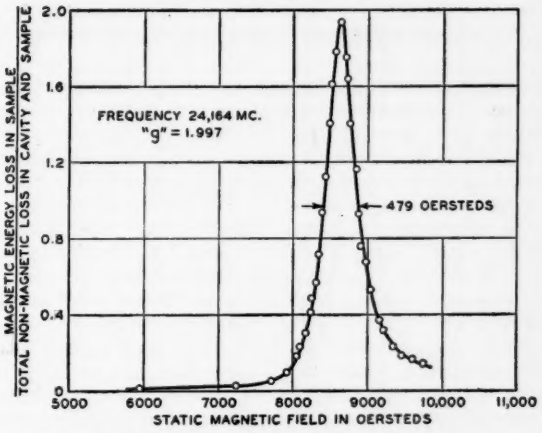

FIG. 1. Resonance absorption in polycrystalline manganese ferrite (0.024-in. diameter sphere).

that the contribution of each manganous ion is $4.6\mu_B$, where we have used Néel's hypothesis[2] that only the manganous ions Mn^{++} contribute to the magnetization, the Fe^{+++} ions being in an antiferromagnetic arrangement. Other measurements by Gorter[3] give $5.0\mu_B$.

This type of hypothesis had been anticipated by Guillaud[4] in the case of the ferromagnetic alloy Mn_2Sb, where one imagines that two types of manganese ions on two different sites are oriented antiparallel. Since, however, in manganese ferrite the Mn^{++} and Fe^{+++} ions are isoelectronic, the predicted g-value of 2.00 is independent of the particular way in which component ions are coupled together. It is in any case a satisfying confirmation of the simple ionic model of the electronic structure of ferrites that the observed g-value is in agreement with expectation.

[1] C. Guillaud, Comptes Rendus **230**, 1256 (1950).
[2] L. Néel, Ann. de physique **3**, 137 (1948).
[3] E. W. Gorter, Comptes Rendus **230**, 192 (1950).
[4] C. Guillaud, thesis, Strasbourg (1943).

Isomerism in Pb^{204} and "Memory" in Angular Correlation*

A. W. SUNYAR, D. ALBURGER, G. FRIEDLANDER, M. GOLDHABER,** AND G. SCHARFF-GOLDHABER**
Brookhaven National Laboratory, Upton, New York
May 3, 1950

THE only even-even nucleus for which a fairly long-lived metastable state is known is Pb^{204}. Here a lifetime of 65 to 68 minutes has been reported[1] for an isomeric transition with an energy of about 1 Mev. It seemed to be of interest to investigate this rather unique case further. In order to do so we obtained Pb^{204m} as a daughter of Bi^{204} (12 hr.) which in turn was produced by a $(d, 2n)$ reaction from lead in the M.I.T. cyclotron. In some experiments, lead enriched in the Pb^{204} isotope was used.[2] The lead

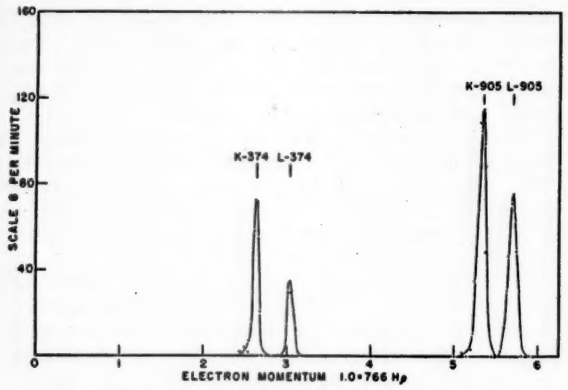

FIG. 1. Spectrum of internal conversion electrons from Pb^{204m}.

target was dissolved in nitric acid, most of the lead removed as $PbCl_2$ and bismuth separated from the remainder by chemical plating on nickel powder. The Pb^{204m} was then separated from bismuth by one of a number of procedures involving combinations of several of the following steps: precipitations of $BiPO_4$, $PbSO_4$, $Bi(OH)_3$ and $PbCrO_4$, and plating of bismuth on nickel.

From gamma-ray coincidence studies it was found that the isomeric transition takes place in two steps.[3] To obtain the exact energies of the transitions, the internal conversion electrons of Pb^{204m} were studied in a lens spectrometer. The electron spectrum is shown in Fig. 1. The K and L lines of gamma-rays of 374 kev and 905 kev were observed. No further electron lines were found in the region from 70 kev to 1.7 Mev. The K/L ratio for the 374-kev line is 2.1 ± 0.2 and for the 905-kev line it is 1.5 ± 0.2. Approximate values of the internal conversion coefficients were obtained from an absorption curve of the internal conversion electrons and gamma-rays taken with an end window G-M counter. The values found for the internal conversion coefficients are ~5 percent for the 374-kev line and ~10 percent for the 905-kev line.

Delayed coincidences between the conversion electrons were found with Geiger counters, and between the gamma-rays with scintillation counters as detectors. The half-life of the second step is 3×10^{-7} second (Fig. 2.). Absorption measurements showed

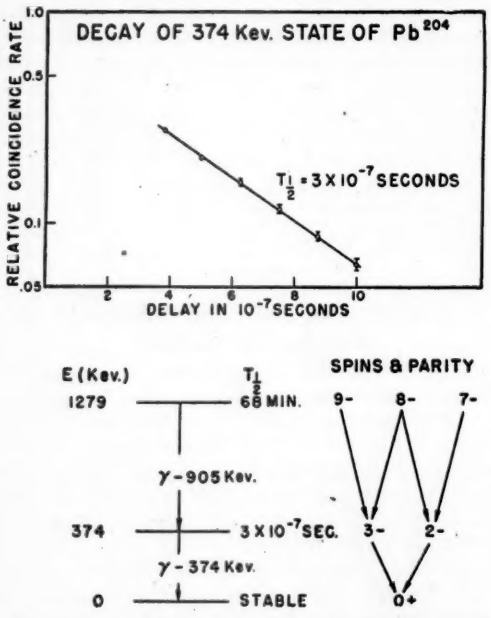

FIG. 2. Decay curve of 374-kev state of Pb^{204} (delayed $\gamma-\gamma$-coincidences taken with scintillation counter) and proposed decay scheme.

that the 905-kev transition precedes the 374-kev transition. The combination of half-lives, energies, K/L ratios and conversion coefficients is best compatible with the interpretation that the 68-minute transition is of multipole order 6 and the 3×10^{-7}-second transition is of multipole order 3, though multipole orders lower by one unit cannot be excluded in either transition. A decay scheme and some possible spin and parity assignments are shown in Fig. 2.

Because of the high spin changes involved, the angular correlation between the two gamma-rays would not be expected to show spherical symmetry, except if "memory" of spin orientation were not retained for a measurable time by the 3×10^{-7}-second state. In order to decide this question the angular correlation between the 905-kev and the 374-kev gamma-rays was measured with a 5×10^{-7}-second delay and a resolving time of 2×10^{-7} second. Tl-activated NaI scintillation counters were used as detectors. The Pb^{204m} was in the form of an aqueous lead acetate solution (~0.2 cc). The gamma-rays defined within a half-angle of 8°. The ratio of coincidences at 180° to those at 90° was found to be 1.22 ± 0.05. Thus we have definitely established the existence of "memory" of spin orientation for a time at least as long as 5×10^{-7} second. How well the "memory" is retained in different compounds and to what extent it can be affected by an applied magnetic field is being investigated at present. It is hoped in this way to decide the feasibility of measuring the gyromagnetic ratio of the 3×10^{-7}-second state.

Drs. Falkoff[4] and Hamilton[5] have kindly communicated to us the following results of calculations of the $\gamma-\gamma$-correlation functions to be expected for a number of possible spin assignments for Pb^{204m}. The multipole order of the transition assumed is indicated above each arrow.

A^3 $9\overset{6}{\rightarrow}3\overset{3}{\rightarrow}0$ $W(\vartheta)=1+0.755\cos^2\vartheta+0.210\cos^4\vartheta-0.064\cos^6\vartheta$

B^3 $8\overset{5}{\rightarrow}3\overset{3}{\rightarrow}0$ $W(\vartheta)=1+0.770\cos^2\vartheta+0.095\cos^4\vartheta-0.003\cos^6\vartheta$

$C^{3,4}$ $8\overset{6}{\rightarrow}2\overset{2}{\rightarrow}0$ $W(\vartheta)=1+0.636\cos^2\vartheta-0.198\cos^4\vartheta$

$D^{3,4}$ $7\overset{5}{\rightarrow}2\overset{2}{\rightarrow}0$ $W(\vartheta)=1+0.555\cos^2\vartheta-0.148\cos^4\vartheta$

E^4 $7\overset{6}{\rightarrow}2\overset{2}{\rightarrow}0$ $W(\vartheta)=1-1.088\cos^2\vartheta+0.873\cos^4\vartheta$

Our experimental value for $W(180°)$ excludes case E. Any one of the cases A–D which give values of $W(180°)$ between 1.41 and 1.90 would be compatible with the experimental result if there is some "loss of memory" of the angular correlation.

Our thanks are due Drs. M. Deutsch and J. W. Irvine, and J. Bulkley of the M.I.T. cyclotron group whose kind cooperation made this work possible, and E. der Mateosian and Miss Elizabeth Wilson for valuable help.

* This work was carried out under the auspices of the AEC.
** On leave from the University of Illinois.
[1] K. Fajans and A. F. Voigt, Phys. Rev. **58**, 177 (1940); W. Maurer and W. Ramm, Zeits. f. Physik 119, 602 (1942); Templeton, Howland and Perlman, Phys. Rev. **72**, 766 (1947).
[3] The enriched material was supplied by the Y-12 Plant, Carbide and Carbon Chemicals Corporation through the Isotopes Division, U. S. AEC.
[3] Sunyar, Alburger, Friedlander, Goldhaber and Scharff-Goldhaber, Phys. Rev. **78**, 326 (1950).
[4] D. L. Falkoff, private communication.
[5] D. R. Hamilton, private communication.

The Ejection of Li^8 Nuclei by Gamma-Rays

C. H. MILLAR AND A. G. W. CAMERON
Atomic Energy Project, National Research Council of Canada, Chalk River, Ontario, Canada
May 5, 1950

AN Ilford type E1 nuclear research emulsion, 100 microns thick, was exposed to 240 roentgens of γ-rays from the University of Saskatchewan betatron operating at 26.7 Mev. The method of exposing the plate and of developing it by the "grain gradation" process has been described previously.[1]

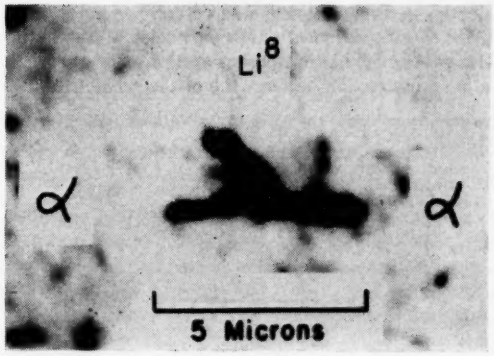

FIG. 1. Photo-micrograph of γ-ray induced "hammer" track in Ilford E1 emulsion.

In a search of 12 cm² of this plate 5 "hammer" tracks were found, of which one is shown in Fig. 1. The two equal and opposite tracks have the grain density characteristic of α-particles, while the third track is considerably denser. Such a configuration, which is well known in cosmic-ray work, is here attributed to the photo-disintegration of a constituent of the emulsion with the ejection of a Li^8 nucleus. After coming to rest, the Li^8 decays by β-emission to the broad C Mev excited level of Be^8, which then breaks up into two α-particles.

From mass considerations the emission of a Li^8 nucleus in any photo-nuclear reaction involving the light elements (carbon, nitrogen, oxygen, and sulfur) in the emulsion requires an energy of 29 Mev or greater, and such reactions are therefore ruled out by the fact that this exceeds the maximum γ-ray energy available. The simple photo-emission of Li^8 from any of the heavy elements (silver, bromine, and iodine) in the emulsion is, however, energentically possible, and Table I shows the threshold energies for such reactions as calculated from the semi-empirical mass formulas of Weizsaecker[2] and Feenberg.[3] Though the emission of neutrons or singly charged ions simultaneously with the Li^8 ion would not be seen, these reactions would require 8 Mev or more of additional energy, and hence are energetically impossible.

Certain considerations favor silver as the probable source of the Li^8 nuclei. The energies of the Li^8 ions in the 5 events were estimated from the general range-energy relationship for charged particles[1] and two range-energy values for Li^7 obtained by Farragi.[4] The energies obtained were 1.0, 2.8, 4.0, 4.9, and 5.7 Mev; thus, on an energy basis, only one of these events could be attributed to bromine (Table I). While all events are energetically possible if silver or iodine is involved, the occurrence of iodine in the emulsion is only 2.5 percent of that of silver, and therefore the cross section for the photo-disintegration of iodine would have to be more than one order of magnitude greater than that for the corresponding reaction in silver in order to have a comparable yield. Thus silver is regarded as the most probable origin of the Li^8 nuclei.

Assuming that silver isotopes are the parent nuclei, and that the range of γ-ray energies effective in causing this reaction is 22 to 26.7 Mev, the cross section for the reaction is of the order of 10^{-30} cm².

TABLE I. Calculated energy thresholds for (γ, Li^8) reactions.

Reaction	Threshold energy (Mev) Feenberg's formula	Weizsaecker's formula
$Br^{79}(\gamma, Li^8)Ge^{71}$	25.2	25.8
$Br^{81}(\gamma, Li^8)Ge^{73}$	25.0	25.0
$Ag^{107}(\gamma, Li^8)Ru^{99}$	22.3	22.0
$Ag^{109}(\gamma, Li^8)Ru^{101}$	21.4	21.5
$I^{127}(\gamma, Li^8)Sn^{119}$	19.1	19.0

We should like to thank Dr. R. N. H. Haslam and his coworkers at the University of Saskatchewan for making the betatron irradiations, Dr. B. W. Sargent for his interest and advice, and Mr. R. G. Hayman for his assistance in searching the plate.

[1] C. H. Millar and A. G. W. Cameron, Phys. Rev. **78**, 78 (1950).
[2] E. Feenberg, Rev. Mod. Phys. **19**, 239 (1947).
[3] As quoted by E. Fermi in *Nuclear Physics* (University of Chicago Press, Chicago, 1950) p. 7.
[4] H. Farragi, Comptes rendus **229**, 1223 (1949).

The Hydromagnetic Equations

WALTER M. ELSASSER
Randal Morgan Laboratory of Physics, University of Pennsylvania, Philadelphia, Pennsylvania
May 18, 1950

COSMIC fluids, being electrical conductors, can carry electric currents and their magnetic fields. These phenomena are of interest for solar, stellar and sunspot magnetism, geomagnetism, magnetic fields in stellar atmospheres and in interstellar space and the related problems of galactic radio noise and the origin of cosmic rays.

In this note as previously[1] we confine ourselves to "Maxwellian" electrodynamics where the relations between the vectors **D**, **E** and **B**, **H** have the familiar scalar and isotropic form; this excludes certain classes of phenomena in rarefied gases. The interaction between the velocity field **V** and the magnetic field **B** is described by the hydrodynamic equations together with the electromagnetic field equations, both containing proper coupling terms.[2] In the field equations the displacement current is omitted; the hydrodynamic equations are simplified by assuming incompressibility. We have,

$$d\mathbf{V}/dt+(\mathbf{V}\cdot\nabla)\mathbf{V}=-\nabla p/\rho-\lambda\mathbf{B}\times(\nabla\times\mathbf{B})+\nu\nabla^2\mathbf{V}$$
$$d\mathbf{B}/dt=\nabla\times(V\times\mathbf{B})+\nu_m\nabla^2\mathbf{B}$$

where ν is the conventional specific viscosity and

$$\lambda=(4\pi\mu\rho)^{-1},\quad \nu_m=(4\pi\mu\sigma)^{-1}.$$

(μ susceptibility, ρ density). The quantity ν_m is the "magnetic" viscosity.[1] We now transorm these equations as follows: (a) take their sum and difference, respectively; (b) introduce new variables defined by the equations

$$\mathbf{P}=\mathbf{V}+\lambda^{\frac{1}{2}}\mathbf{B},\quad \mathbf{Q}=\mathbf{V}-\lambda^{\frac{1}{2}}\mathbf{B},$$
$$\nu_1=\nu+\nu_m,\quad \nu_2=\nu-\nu_m,$$
$$q=p/\rho+(\mathbf{P}-\mathbf{Q})^2/8;$$

(c) by virtue of some straightforward transformations using known vectorial identities the new equations can be written

$$d\mathbf{P}/dt+(\mathbf{Q}\cdot\nabla)\mathbf{P}=-\nabla q+\nabla^2(\nu_1\mathbf{P}+\nu_2\mathbf{Q})$$
$$d\mathbf{Q}/dt+(\mathbf{P}\cdot\nabla)\mathbf{Q}=-\nabla q+\nabla^2(\nu_2\mathbf{P}+\nu_1\mathbf{Q}).$$

For vanishing field, $\mathbf{P}=\mathbf{Q}$, the two equations become identical and go over into the Stokes-Navier equations of hydrodynamics.

The remarkable symmetry of these equations and their analogy to the ordinary hydrodynamic equations is apparent. One might, in particular, expect that phenomena of turbulence will occur in hydromagnetic systems, similar to those in ordinary hydrodynamics and at mechanical or "magnetic"[1] Reynolds numbers of comparable magnitude. They will no doubt give rise to a "turbulent" magnetic field coupled with the mechanical motion.

The case of compressible fluids is of considerable physical interest. Truesdell[3] has recently shown that the conservation theorem of the magnetic flux can be extended to compressible fluids on replacing **B** by $\mathbf{B}/\rho$ throughout. In the above equations, however, there appears the combination $\mathbf{B}/\rho^{\frac{1}{2}}$, and this is necessary on dimensional grounds; we have thus been unable to ascertain whether similarly simple, symmetrized equations exist for the compressible case.

[1] W. M. Elsasser, Rev. Mod. Phys. **22**, 1 (1950).
[2] Reference 1, Eqs. (35) and (41).
[3] C. Truesdell, Phys. Rev. **78**, 823 (1950).

Latitude Effects for Stars. I. Production Rates and Prong Distributions*

E. O. SALANT, J. HORNBOSTEL, C. B. FISK, AND J. E. SMITH
Brookhaven National Laboratory, Upton, New York
May 19, 1950

WE present here certain features of some 1500 stars in minimum ionization emulsions, flown to 15 g/cm² at 31° and 57° geomagnetic north.[1]

The plates, 200–300μ Ilford G5, Eastman NTB3 and laminated emulsions, were exposed, with emulsion planes vertical, for about six hours at ceiling, as recorded by barograph. All data given are corrected for events accumulated below ceiling. Data involving minimum ionization tracks are taken only from plates with satisfactory grain density histograms, which are peaked at about 20 grains per 100μ.

Minimum tracks mean 1.3 minimum grain density or less (kinetic energy $\geq$0.75 rest energy). Denser tracks are called heavy prongs. Proton-induced stars are called p-stars, examples of which have been shown.[2] Stars without minimum tracks in the hemisphere above are called q-stars, those showing outgoing minimum tracks q', those showing no such tracks q''; the fraction caused by relativistic alpha-particles is being measured.

The number of heavy prongs H will characterize a star's size, regardless of the star's minimum tracks. Fowler reports that 90 percent of shower particles are mesons, almost all of the heavy prongs being due to protons or heavier particles.[3]

Table I records the stars observed. Only about one percent of p-stars have $H=1$. The distributions of p-stars according to heavy-prong number appear substantially the same at the two latitudes, hence do not vary appreciably with the energy of the incident proton.

In laminated plates, we find no stars with $H>5$ and few with $H>4$ originating in the thin gelatine layers, the light nuclei C, N, O giving the small stars. This is similar to Harding's observations at mountain altitude.[4]

Light nuclei take up 0.28 of the geometric cross section of emulsion nuclei. In unlaminated emulsions, the fraction of p-stars with $H\leq4$ is less than 0.28 at each latitude, and for $H\leq5$ is 0.30 at the southern and 0.40 at the northern latitude. Thus, the fractions are compatible with disintegrations proportional to geometric cross sections, small stars coming predominantly from light nuclei. Large stars, $H\geq9$, come from the heavy nuclei (Ag, Br, I), the medium $6\leq H\leq8$, coming, possibly, from both light and heavy nuclei.

The efficiency for detection of minimum tracks was determined, (1) by successfully following long tracks parallel to the emulsion surface, and (2) for steeper tracks, by comparing the measured dip-angle distribution of minimum shower tracks with the probability curve for this distribution, which gave an average efficiency of 75 percent.

With the measured correction for inefficiency, and by measuring emulsion shrinkages and other relevant factors, production rates for p-stars, per gram per day, are 300 at the northern and 70 at the southern latitude, a ratio of 4.3±1.0.

Recently, Winckler *et al.*[5] found the same ratio 5.0±0.3 for the flux of ionizing particles at the same latitudes and altitude. It follows that the cross sections for disintegration of the emulsion nuclei by protons are essentially the same at the two latitudes. Magnetic cut-offs are 8 Bev at 31° and 1 Bev at 57°, median proton kinetic energies being 14 Bev and 3 Bev, respectively.[5,6]

TABLE I. Star distributions, $H\geq2$

Type of star H		p 2,3,4	p 5	p 6,7,8	p ≥9	p Totals	q'	q'' Totals
31°	Number	51	16	43	107	217	158	480
	Fraction	0.24	0.07	0.20	0.49	1		
57°	Number	39	29	26	72	166	90	342
	Fraction	0.24	0.17	0.16	0.43	1		

Production rates and Rossi's flux value[7] give a geometric cross section for disintegration of emulsion nuclei. With the fluxes of Winckler *et al.*, allowing for mesons and primary alphas, the disintegration cross section becomes 0.6 of the geometric.

* Research carried out at the Brookhaven National Laboratory under the auspices of the AEC.
[1] Balloon flights by courtesy and arrangement of ONR.
[2] J. Hornbostel and E. O. Salant, Phys. Rev. **76**, 859 (1949).
[3] P. H. Fowler, Phil. Mag. **41**, 169 (1950).
[4] J. B. Harding, Nature **163**, 440 (1949).
[5] Winckler, Stix, Dwight, and Sabin, Phys. Rev. (to be published).
[6] M. S. Vallarta, Phys. Rev. **74**, 183 (1948).
[7] B. Rossi, Rev. Mod. Phys. **20**, 537 (1948).

Latitude Effects for Stars. II. Shower Particles*

E. O. SALANT, J. HORNBOSTEL, C. B. FISK, AND J. E. SMITH
Brookhaven National Laboratory, Upton, New York
May 19, 1950

IN this study we consider shower particles in p-stars only.

We use the term "multiplicity" only for minimum tracks. A multiplicity increasing with star size has already been suggested[1] for the south (31°) and shown for the north.[2]

Histograms of observed multiplicities are given in Fig. 1, for large stars ($H\geq9$) and for small stars ($H\leq5$), that is, for heavy and light nuclei. Small northern stars are omitted, their histogram being indistinguishable from that of the small southern stars (but lacking the three events of multiplicity >4).

Mean multiplicity is defined as $\bar{m}=L/N$, where L is the total number of minimum tracks in N stars. Adopting the Bristol notation[3] Op for p-stars with no shower particles, then $\bar{m}_0$ is a measure of the average number of shower particles per proton collision, when N includes the Op events; $\bar{m}_1$ is the average multiplicity in a shower when N excludes the Op events. Since one-fifth of the protons at 57° are above[4] 8 Bev and have essentially the same intensity and spectral distribution as do the protons at 31°, the mean multiplicities caused by protons in the 1- to 8-Bev range are easily calculated to be $\frac{1}{4}[5\bar{m}(\text{north})-\bar{m}(\text{south})]$.

Mean multiplicities for different proton energies and star sizes appear in Table I, observed multiplicities having been corrected for missed steep tracks.[5] It is seen that, at each latitude, the multiplicity increases with star size, which, with the latitude-independence of prong distribution shown in reference 5, indicates plural production of shower particles.

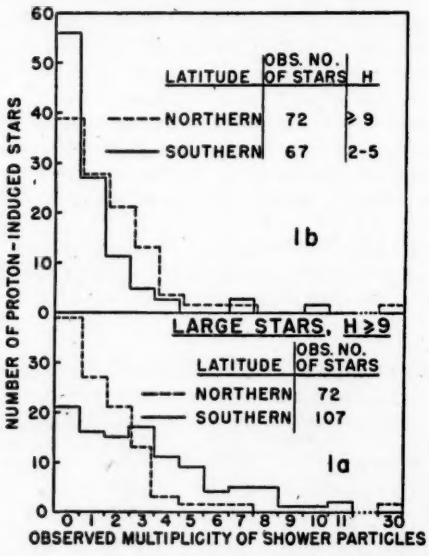

FIG. 1. Histograms of the observed multiplicities. The areas of all histograms are normalized to the area of the solid graph of Fig. 1a.

TABLE I. Mean multiplicities of shower particles, $\bar{m}_0$ and $\bar{m}_1$.

	2–5H $\bar{m}_0$	6–8H $\bar{m}_0$	≥9H $\bar{m}_0$	2–5H $\bar{m}_1$	6–8H $\bar{m}_1$	≥9H $\bar{m}_1$
31°	1.4±0.3	2.4±0.4	4.2±0.3	3.0±0.5	3.4±0.4	5.2±0.4
57°	1.4±0.2	1.7±0.3	2.0±0.3	2.6±0.3	2.7±0.5	3.2±0.4
1 to 8 Bev	1.3±0.3	1.5±0.4	1.5±0.4	2.5±0.4	2.4±0.6	2.7±0.5

For small stars (light nuclei), the mean multiplicities do not vary with the incident proton energy; such an energy-insensitivity would be expected if a single relativistic particle were produced in a nucleon-nucleon encounter. Multiple production is not excluded, but is rare.

Figure 1a and Table I show that the higher proton energies raise the multiplicities of large stars (heavy nuclei). An increase of energy of the incident proton can produce more relativistic particles by cascade within large nuclei, and so, in view of the energy-independence of light-nuclei multiplicities, the latitude effect for heavy nuclei is interpreted as the result of plural collisions. Furthermore, Table I shows that heavy nuclei struck by 1- to 8-Bev (median 2.5 Bev) protons give as high mean multiplicities as do light nuclei struck by protons of energy >8 Bev (median 14 Bev); the same situation is pictured in Fig. 1b. Accordingly, it seems to be inescapable that there is plural production of shower particles in heavy nuclei.[6]

The 1- to 8-Bev protons give the same multiplicity for all star sizes, which implies that they produce their maximum number of shower particles in a 12 to 16 nucleon system.

Sands estimates that six charged mesons are created in the atmosphere for every primary proton;[7] $\bar{m}_0$ for emulsion nuclei C, N, O is 1.4 (which includes outgoing relativistic protons), making it difficult to account for the six mesons. In these light nuclei, half of the p-stars are Op; the energy balance requires that neutral radiation (fast neutrons or other particles or both) be produced. It is, perhaps, not impossible that enough neutral mesons are created by energetic protons to supply, by decay, the required charged mesons.

A full report of these and other observations will appear later.

* Research carried out at the Brookhaven National Laboratory under the auspices of the AEC.

[1] E. O. Salant and J. Hornbostel, ONR Proc. Echo Lake Cosmic-Ray Symposium, p. 65 (November, 1949).
[2] Camerini, Coor, Davies, Fowler, Lock, Muirhead, and Tobin, Phil. Mag. **40**, 1073 (1949).
[3] Brown, Camerini, Fowler, Heitler, King, and Powell, Phil. Mag. **40**, 862 (1949).
[4] Winckler, Stix, Dwight, and Sabin, Phys. Rev. (to be published).
[5] Salant, Hornbostel, Fisk, and Smith, Phys. Rev. **78**, 184 (1950) preceding letter.
[6] W. Heitler and L. Jánossy, Proc. Phys. Soc. (London) **62**, 669 (1949).
[7] M. Sands, Phys. Rev. **77**, 180 (1950).

On High Energy Nucleon-Nucleon Scattering*

K. M. CASE AND A. PAIS
Institute for Advanced Study, Princeton, New Jersey
May 16, 1950

THE recent Berkeley experiments on high energy nucleon-nucleon scattering would seem at first sight to indicate a sizable difference between the $n-p$ and $p-p$ interactions, in contrast to the charge independence found at low energies. Thus the 350 Mev $p-p$ cross section is, at 90°, from 2 to 4 times larger than the corresponding quantity for $n-p$ scattering at 260 Mev. Also at 350 Mev $\sigma_{p-p}(\theta)$ is rather isotropic from 90° down to about 20° in contrast with the 260 Mev $n-p$ data over the same angular region.

It is the aim of this note to point out that, nonetheless, it seems at least qualitatively possible to obtain a charge-independent phenomenological theory. This can be achieved by introducing the simplest kind of velocity dependent force, *viz.* a spin-orbit interaction of the type familiar from atomic phenomena:

$$V(r)\mathbf{L}\cdot(\boldsymbol{\sigma}^1+\boldsymbol{\sigma}^2). \tag{1}$$

This coupling, superposed on an interaction of the kind proposed by Christian and Hart in their analysis of the $n-p$ data, gives a fair account of the $p-p$ experiments. Considering first the 30 Mev $p-p$ scattering, the interaction (1) gives a ^3P-state contribution at such an intermediate energy

$$\sigma(\theta)\sim(18/k^2)\eta^2\sin^2\theta \tag{2}$$

where η is the $^3P_2$ phase. Therefore the principal puzzling feature of $\sigma(\theta)$ at this energy, *viz.* its rise (after a rapid decrease away from small angles due to the Coulomb force) to a rather flat maximum around 90°, can be interpreted as a spin-orbit effect. For this purpose it suffices that $\sigma(90°)$ as given by (2) is ~2 mb, corresponding to $\eta\sim3.7°$.

To see the main features of this coupling at still higher energies one can examine its effects in the Born approximation. It is readily seen that the cross section due to (1) is proportional to $\sin^2\theta$, thus favoring large angle scattering. The LS-contribution to the $n-p$ cross section at 90° is only one-fourth of that for $p-p$ scattering. (Indeed, by an appropriate choice of the exchange dependence of (1) it is possible to have this ratio hold for all angles.) The effect on $n-p$ scattering thus is rather small. Somewhat more detailed considerations actually show that, with the dearth of experimental data, it is hardly possible to draw any quantitative conclusions about spin-orbit coupling from the available high energy $n-p$ experiments.

Also for low energies the LS-term has little effect on the $n-p$ system. In particular it vanishes in S-states. From considerations on bound neutron proton states the sign of the spin-orbit interaction is determined to be such that states of highest total angular momentum lie lowest.

The main characteristics of the spatial dependence of the LS-coupling are rather closely determined by the $p-p$ experiments. The high 90° cross section at 350 Mev (~4 mb) shows that large momentum transfers are involved. Hence the potential must be quite singular at small distances. The flatness of the cross section at 350 Mev requires that the potential have a relatively small tail.

It seems possible to fit all $p-p$ data with various radial forms of the potential. The form yielding the most reasonable values for the parameters is

$$V=V_0\frac{1}{x}\frac{d}{dx}\frac{e^{-x}}{x}, \quad x=r/r_0. \tag{3}$$

In this case rough estimates indicate that $V_0\sim12$ Mev, $r_0\sim1$, 1×10^{-13} cm, are adequate. It should be noted that the r^{-3} singularity need not be taken too seriously since regions smaller than the nucleon Compton wave-length are not explored by particles of the energies considered thus far. The form (3) is also suggestive in that derivations of spin-orbit couplings from field theory, or as a Thomas term, usually yield this type of radial dependence.

If an interaction (1) with a radial dependence (3) is used to explain the $p-p$ data, a further conclusion about $p-p$ scattering can be deduced. This is that $\sigma_{p-p}(90°)$ should be approximately constant for energies greater than about 150 Mev up to energies (not much larger than 350 Mev) where relativistic effects start to play a preponderant role. Here the r^{-3} dependence of (3) up to small distances is decisive. This conclusion is probably also valid for any alternative interpretation using such singular potentials.

Summarizing, it would seem possible to give a charge independent description of nuclear force, in that the $p-p$ experiments can all be accounted for on the basis of an interaction involving (1), while previous interpretations of $n-p$ scattering are not drastically modified.

We note finally a possible connection with the spin orbit interaction postulated by Mrs. Mayer in her interpretation of the shell model of heavy nuclei. In fact, simple estimates indicate that a two-body spin-orbit interaction of the above type may lead to intramultiplet energy differences of the order of a Mev.

A fuller account of this work is in preparation.

* One of us (K.M.C.) is indebted to the Institute for Advanced Study for having supported his research by a grant of AEC funds.

Supersonic Wind at Low Pressures Produced by Arc in Magnetic Field

H. C. Early and W. G. Dow
Department of Electrical Engineering, University of Michigan, Ann Arbor, Michigan
January 20, 1950

THE properties of a low pressure discharge are greatly modified by the presence of a transverse magnetic field of several thousand gauss. The over-all behavior, here described, is believed to be unique to values of gas concentration for which the mean free time of the electrons is much greater than their cyclotron periodicity, and the mean free time of the ions much less than their cyclotron periodicity. The experiments were performed inside a large vacuum chamber having a volume of approximately one cubic meter. When the arc is in a large unconfined region, wind effects are observed which are not present when the discharge is in a small glass tube.

Figure 1 illustrates the general appearance of an arc at 0.5 millimeter pressure, transverse to a magnetic field of 6000 gauss. The voltage gradient is approximately 100 volts/cm, and the power input and the current density are many times larger than when the magnetic field is not present. The arc column, in air or nitrogen, is pale blue and quite transparent. Although the power dissipated in the positive column of the arc is more than one-half kw/cm of arc length, the gas temperature is surprisingly low because of the cooling effect of the wind. This temperature is greatly dependent on the manner in which the wind is circulating inside the chamber, and to what extent it is cooled during the recirculating process. Observations based on the melting point of chemical salts indicate that in most cases the arc temperature is less than 600 degrees centigrade.

When the air flow is blocked by placing a ceramic sheet on the "downwind" side of the discharge, the arc flattens out against the sheet and forms a white hot surface layer. If the sheet is placed on the "upwind" side of the arc, so as to block the air from entering the region, the arc then spreads out in all directions. Under such conditions, manometer pressure measurements show that the discharge is acting like an air pump. The air pressure on the side of the ceramic sheet which is adjacent to the arc is about 20 percent of the pressure on the opposite side of the sheet.

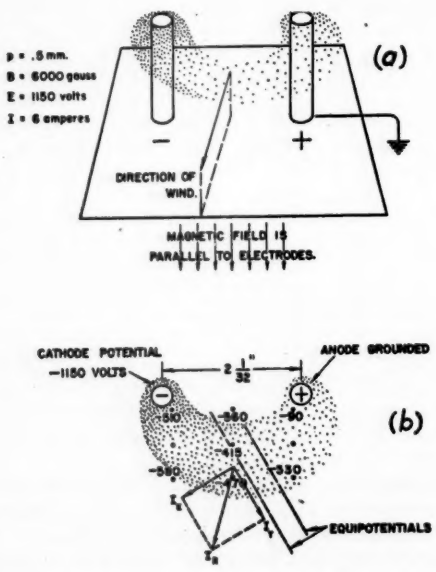

FIG. 1. (a) Arc between two copper rods. (b) Section of arc taken perpendicular to electrodes and probe measurements of potentials with respect to anode. I_E = component of ion drift velocity in direction of electric field. I_T = component of ion drift velocity transverse to electric field. I_R = resultant velocity in direction of wind.

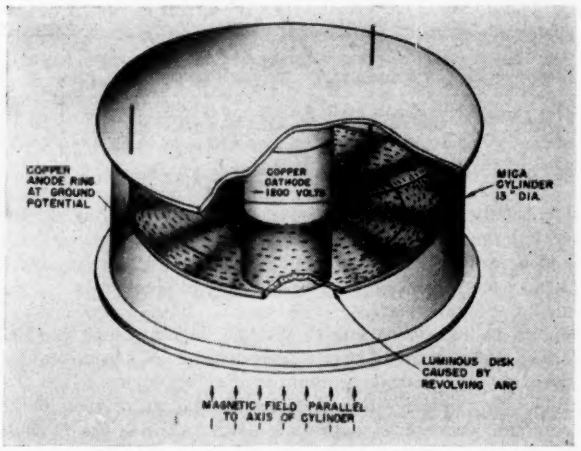
COPPER ANODE RING AT GROUND POTENTIAL
COPPER CATHODE −1800 VOLTS
MICA CYLINDER 15" DIA.
LUMINOUS DISK CAUSED BY REVOLVING ARC
MAGNETIC FIELD PARALLEL TO AXIS OF CYLINDER

FIG. 2. Revolving arc inside a transparent mica cylinder.

A significant factor in this type of discharge is the low mobility of the electrons. It is believed that during each mean free path any electron makes many rotations about the magnetic flux lines and that its drift movement is almost entirely at right angles to the electric gradient. In contrast, an ion apparently does not follow a rotational or cycloidal path, because a collision will always occur before a fraction of one rotation is completed. As a result the ion mobility is not greatly reduced by the magnetic field. Available information as to the ion mobility to be expected under these conditions indicates that an assumption of nearly 100 percent ion conduction is quite consistent with the observed values of current density and electric gradient. For the conditions in Fig. 1, calculations predict that the component of the ion drift velocity, transverse to the electric gradient, has approximately the same magnitude as the component in the direction of the gradient. Because of the skewed position of the equipotentials, Fig. 1(b), the resultant ion current is believed to be perpendicular to the plasma boundary and in the same direction as the wind. This wind is presumably caused by the ion drift movement and the resultant interchange of momentum with neutral molecules. Since a substantial part of the energy which the ions receive from the field is utilized in producing directed momentum of gas molecules, this device appears to be a fairly efficient wind generator.

The electrons which are formed by the ionization processes throughout the discharge also move to the downwind edge of the plasma where they recombine with the ions. This electron drift is probably nearly parallel to the equipotential lines. A more detailed study of these experiments, now in progress, promises to provide a satisfactory explanation for the skewed position of these equipotentials.

Figure 2 is a sketch of an arc between a copper cylinder and a surrounding ring. An axial magnetic field causes this arc to revolve like a spoke in a wheel. The rate of rotation can be measured by means of a plasma probe connected to an oxcilloscope. When the air pressure and other variables are similar to those shown in Fig. 1, the rate of rotation is about 17,000 r.p.s. The air inside the cylinder also revolves, but its velocity is less than that of the arc. Measurement of the wind velocity is difficult because the air density is too low for the usual techniques. One method of measurement involved the sudden injection into the cylinder of a chemical vapor which colored the discharge. Stroboscopic observations of this experiment indicated that the color, caused by this vapor, spread downstream at a rate of at least 4500 miles/hr. Another experiment involved the measurement of the force on a small tungsten vane which was deflected by the air stream. On the basis of this latter data, the air speed was estimated to be approximately 3000 miles/hr.

The Production of Neutral Mesons by Photons*

K. A. Brueckner and K. M. Watson
Radiation Laboratory, University of California, Berkeley, California
May 15, 1950

A NUMBER of recent experiments at Berkeley have given independent and strong support for the hypothesis that there exists a neutral meson which is strongly coupled to nucleons. Of particular interest are the experiments of Steinberger, Panofsky, and Steller[1] which seem to indicate that neutral mesons can be produced by photons with a cross section which is not less than that for charged mesons.

Photo-meson production is among the simplest of phenomena involving mesons; and it might therefore be hoped that some of its general features can be understood on the basis of our admittedly very incomplete theoretical knowledge of the properties of mesons. In particular, we are interested in seeing whether a photo-production cross section for neutral mesons as large as that for charged mesons can be understood theoretically.

For the photo-production of charged mesons Brueckner[2] found that of the four types of meson fields only the pseudoscalar theory gave satisfactory agreement with experiment. For such a theory as the scalar theory with charged meson currents extending about the nucleon over a region of the order of the meson Compton wave-length, the angular (dipole) distribution of the ejected photo-mesons arising from the coupling of the electromagnetic field to the meson currents is incompatible with the observed,[3] flat angular distribution for charged mesons. Such a coupling of the charged meson field to the electromagnetic field would also lead one to expect the ratio of cross sections for neutral to charged mesons to be of the order of $(\mu/M)^2$ (where μ is the meson mass and M is the nucleon mass), since for neutral meson production the electromagnetic field coupling is to the nucleon. This is in contradiction to the observed largeness of the neutral meson cross section.

Assuming that neutral meson production takes place through the interaction of the electromagnetic field with the magnetic moment of the nucleon, both classical and lowest order perturbation calculations for scalar mesons and pseudoscalar mesons with pseudovector coupling lead to a ratio of the neutral to charged meson cross section (near threshold) of the order of $(\mu/M)^2$, in agreement with the above qualitative arguments.

Such semiclassical arguments are not necessarily applicable in the case of the pseudoscalar field, however, where relativistic quantum-mechanical effects are likely to be important. Here the matrix element for neutral meson production for a γ-ray striking a proton is proportional to

$$(F|H|I)\simeq\boldsymbol{\mu}\cdot\boldsymbol{\xi}(\rho)\left\{\left[\frac{1}{(P_{I\mu}\rho_\mu)}-\frac{1}{(P_{F\mu}\rho_\mu)}\right]M_{\rho 0}\right\}. \qquad (1)$$

Here μ is the Dirac magnetic moment of the proton, $(P_{I\mu})$ and $(P_{F\mu})$ are its four-momenta in the initial and final states, respectively, (ρ_μ) is the four-momentum of the incident photons, and $\boldsymbol{\xi}$ is the electric field strength. Equation (1) differs from that for charged meson emission by the factor in brackets, which is non-vanishing only because of retardation effects and is of order (μ/M) near threshold. This is because the magnetic moment is relatively undisturbed by the process of neutral meson emission, causing phase cancellation between initial and final states. Thus, again the ratio of neutral to charged meson cross sections is of order $(\mu/M)^2$. Similar results are obtained for vector and pseudovector theories. (The experimental evidence is against the neutral mesons having spin one, because of their apparent annihilation into two photons.[4])

It is seen, therefore, that neither classical considerations nor lowest order perturbation theory provide a clue to the largeness of the cross section for neutral photo-mesons. We note, however, that the factor in the brackets in Eq. (1) is small only when the nucleon recoil is small. Due to the very close binding of the meson field to the nucleon for pseudoscalar theory, high energy virtual recoils are expected and it might be thought that these will remove the near cancellation of the two terms in the brackets. To investigate this possibility, we have calculated the first-order radiative corrections to Eq. (1). The corresponding radiative corrections for charged meson production have been calculated by Brueckner.[2] Combining lowest order and first-order radiative corrections for both charged and neutral meson production and choosing the coupling constant as $g^2/4\pi\simeq 10$ (a reasonable value obtained from other considerations), we obtain about equal cross sections for the two processes, in reasonable agreement with experiment. With this choice of coupling constant, the radiative corrections to charged meson production are not qualitatively important, while for neutral meson production the lowest order terms are small.

Since the validity of large radiative corrections is open to considerable doubt, we feel justified in concluding only that the large observed cross section for neutral meson production is not necessarily incompatible with conclusions that can be drawn from pseudoscalar meson theory.

We would like to express our appreciation to Dr. Steinberger and his co-workers for dicussion of their experiments.

* This work was sponsored by the AEC.
[1] J. Steinberger, W. Panofsky, and J. Steller, Phys. Rev. **78**, 802 (1950).
[2] K. Brueckner, Phys. Rev., in press. His calculations of radiative corrections did not include effects from virtual neutral mesons, but it does not seem that this would change his results in a qualitative manner.
[3] J. Steinberger and A. S. Bishop, Phys. Rev. **78**, 493, 494 (1950).
[4] C. N. Yank, Phys. Rev. **77**, 242 (1950).

Neutron Spectrum for Protons on Be^9*

V. R. Johnson, F. Ajzenberg, and M. J. Wilson Laubenstein
University of Wisconsin, Madison, Wisconsin
May 18, 1950

WITH the observation of two energy groups of neutrons in the Li(p, n) spectrum,[1,2] it has become of considerable interest to find a more satisfactory source of monoenergetic neutrons. Since the inelastically scattered protons from Be^9 indicate only one level at 2.4 Mev in the range[3] up to 5.0 Mev, one can expect from mirror nuclei arguments that B^9 also has only one level at about 2.4 Mev in the same range. Thus, it seemed likely that the $Be^9(p, n)B^9$ reaction would produce monochromatic neutrons in the region below 2.5-Mev neutron energy. Additional interest in this reaction arises from the suggestion by Guth and Mullin[4] that a level may occur in Be^9 at about 1.6 Mev, a level which did not show up clearly in the proton scattering work of Davis and Hafner. Again from mirror nuclei arguments, it would be expected that a level in B^9 would also occur in the neighborhood of 1.5 Mev, if this postulate were correct.

The measurement of the neutron spectrum was accomplished by the photographic plate technique in essentially the same way

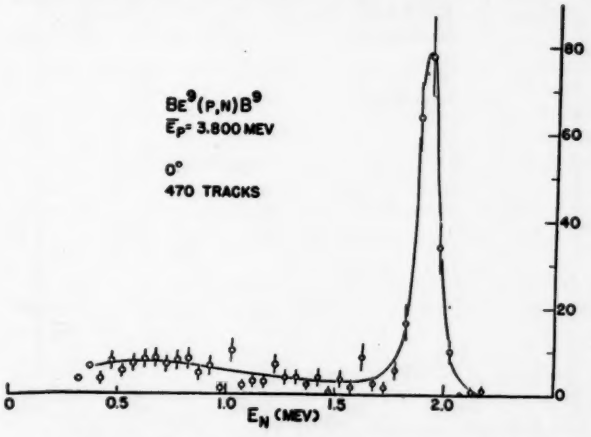

FIG. 1. Number of neutrons per 50 kev interval *versus* neutron energy for $\bar{E}_p$ =3.800 Mev at 0°

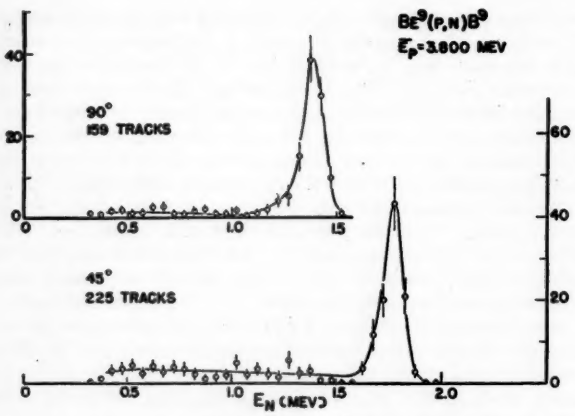

FIG. 2. Number of neutrons per 50 kev interval *versus* neutron energy for $\bar{E}_p = 3.800$ Mev at 45° and 90°.

as was described earlier.[1] In this case, the targets were approximately 30 kev thick foils of beryllium mounted on a tantalum backing. Eastman NTA 100 micron emulsions were mounted 4 inches away at angles of 0, 45, and 90 degrees. The first exposure was made with a bombarding energy of 3.817 Mev. The data plotted in 50 kev intervals and corrected for variation of $n-p$ scattering cross section is shown in Fig. 1 and Fig. 2. Because of the large uncertainty in the determination of the angle of recoil for tracks from low energy particles, 0.4 Mev was arbitrarily set as the lower limit of measurements. Applying the criteria for acceptance of tracks becomes increasingly difficult below 1.0 Mev, so that the actual uncertainty in the region between 0.4 and 1.0 Mev is somewhat greater than the indicated statistical uncertainty.

The data show clearly the group from the transition to the ground state of B^9. Below this there occurs a continuous energy distribution of neutrons. Comparison with the earlier $Li(p, n)$ data[1] under similar conditions indicates that this continuous distribution does not result from background neutrons and scattering. The low intensity of the continuum in the region between 0.4 and 1.0 Mev on the 90° plate also excludes the possibility of the intensity in this region on the 0 and 45 degree plates from being due to an isotropic background in the room. To check the results of the first experiment a somewhat different target arrangement was constructed and a second exposure was made. The bombarding energy was 3.940 Mev. The 0 degree data are shown in Fig. 3.

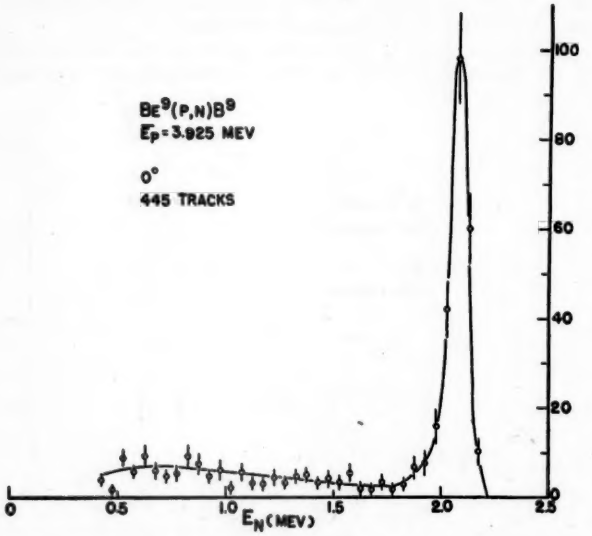

FIG. 3. Number of neutrons per 50 kev interval *versus* neutron energy for $\bar{E}_p = 3.925$ Mev at 0°.

Several possible origins of the continuum were considered. Cascade processes, in which the 2.41 Mev excited state[3] of Be^9 is formed and subsequently breaks up into either Be^8 and a neutron or into He^5 and He^4, are not able to give the observed data. The continuum could arise from the break-up of the compound nucleus either into Be^8, a proton, and a neutron, or into Be^8 and a deuteron in the singlet state. Another quite different possibility is that the continuum results from the interaction of the incident proton chiefly with the very loosely bound neutron in Be^9 without the formation of a compound state. The relatively low intensity of the continuum on the 90 degree plates might favor this possibility. Finally, one cannot rule out the possibility of the existence of a very broad level in B^9.

In regard to the use of the $Be^9(p, n)$ reaction as a neutron source, it is of interest to note that the thin target neutron yield *versus* energy curve does not show an observable yield of neutrons for proton bombarding energies between the (p, pn) threshold and the (p, n) threshold.[5] If the continuum is due to the (p, pn) reaction, one can probably expect the yield of the continuum to remain at a low value throughout a useful range of energies.

We wish to extend our sincere appreciation to Professor H. T. Richards, who suggested this problem and with whom we have had many invaluable discussions.

* This work was supported partly by the AEC and partly by the Wisconsin Alumni Research Foundation.

[1] Johnson, Laubenstein, and Richards, Phys. Rev. **77**, 413 (1950).
[2] B. Hammermesh and V. Hummel, Phys. Rev. **78**, 73 (1950).
[3] K. E. Davis and E. M. Hafner, Phys. Rev. **73**, 1473 (1948.
[4] E. Guth and C. J. Mullin, Phys. Rev. **74**, 833 (1948).
[5] Browne, Smith, and Richards, Phys. Rev. **77**, 754 (1950).

Masses of Si^{30}, Co^{59}, Ni^{60}, Zr^{90}, Mo^{96} and Mo^{100}*

HENRY E. DUCKWORTH, RICHARD S. PRESTON, AND KARL S. WOODCOCK**
Scott Laboratory, Wesleyan University, Middletown, Connecticut
May 1, 1950

THE mass spectrographic mass determinations recently reported have been extended to include Si^{30}, Ni^{60}, Zr^{90}, Mo^{96} and Mo^{100}. From the mass of Ni^{60} that of Co^{59} can be deduced, using disintegration data.

Si^{30}, Ni^{60} and Co^{59}. With an ion source consisting of a spark between two silicon electrodes, photographs were taken of the CH_3-Si^{30} doublet appearing at mass number 15. From eight photographs, the CH_3-Si^{30} packing fraction difference[1] was found to be $\Delta f = 24.53 \pm 0.05$. Assuming the packing fraction of CH_3 to be[2] 18.83 ± 0.015, that of Si^{30} is found to be -5.70 ± 0.05. This is in satisfactory agreement with the value -5.64 ± 0.02 listed by Mattauch and Flammersfeld,[3] and by Alburger and Hafner.[4]

The $Si^{30}-Ni^{60}$ packing fraction difference has been found in this laboratory[5] to be $\Delta f = 2.90 \pm 0.01$. This, when combined with the above value for Si^{30}, gives for Ni^{60}, $f = -8.60 \pm 0.05$. This is in satisfactory agreement with Shaw's[6] value of -8.69 ± 0.08, but does not agree very well with the value of -8.37 ± 0.06 obtained by Okuda *et al.*[7]

The packing fraction of Co^{59} can be computed from Ni^{60} by use of the Q-value for the $Co^{59}(d, p)Co^{60}$ reaction, recently measured by Bateson and Pollard.[8] Their Q of 5.19 Mev, together with values of 0.308 Mev and 2.40 Mev for the beta- and gamma-rays from Co^{60}, as listed by Mattauch and Flammersfeld,[3] gives a packing fraction for Co^{59} of $f = -8.43$. In this computation, Bainbridge's recommended values[2] for the masses of H^1 and H^2 were used.

Zr^{90}. With a spark between a silicon and a zirconium electrode, the $Si^{30}-Zr^{90}$ doublet was photographed at mass 30. The packing fraction difference was found from five photographs to be $\Delta f = 1.88 \pm 0.04$. This, combined with the above Si^{30} value, gives the packing fraction of Zr^{90} as $f = -7.58 \pm 0.07$.

Mo^{96} and Mo^{100}. With a spark between two molybdenum electrodes, the C_2-Mo^{96} and C_2H-Mo^{100} doublets were photographed at mass numbers 24 and 25. From eleven photographs, the C_2-Mo^{96} packing fraction difference was found to be $\Delta f=9.88\pm0.03$. From seventeen photographs of the C_2H-Mo^{100} doublet, $\Delta f=12.47\pm0.03$. Assuming the packing fractions of C_2 and C_2H to be 3.213 ± 0.016 and 6.336 ± 0.016, respectively, that of Mo^{96} is found to be $f=-6.67\pm0.04$ and that of Mo^{100} $f=-6.14\pm0.04$.

Table I gives the new mass values found in this work.

TABLE I. New mass values.

Nuclide	Packing fraction	Mass
Si^{30}	-5.70 ± 0.05	29.98290 ± 0.00015
Co^{59}	-8.43	58.95029
Ni^{60}	-8.60 ± 0.05	59.94840 ± 0.00030
Zr^{90}	-7.58 ± 0.07	89.93178 ± 0.00063
Mo^{96}	-6.67 ± 0.04	95.93597 ± 0.00039
Mo^{100}	-6.14 ± 0.04	99.93860 ± 0.00040

The authors were assisted in some of these experiments by Mr. Howard A. Johnson, Mr. Clifford Geiselbreth and Mr. Richard F. Woodcock. They are grateful to the Astronomy Department for the use of the comparator.

* This letter is based on work done at Wesleyan University under contract with the AEC.
** On leave from Bates College.
[1] The factor $\times10^{-4}$ will be understood and not written in expressing the numerical value of the packing fraction.
[2] K. T. Bainbridge, Isotopic Weights of the Fundamental Isotopes, Preliminary Report No. 1, National Research Council, June, 1948.
[3] J. Mattauch and A. Flammersfeld, "Isotopic Report—1948," Verlag d. Zeits. f. Natur., Tübingen, Germany, 1949.
[4] D. E. Alburger and E. M. Hafner, The Properties of Atomic Nuclei—III. Nuclear Energy Levels, $Z=11$–20 (Brookhaven National Laboratory, July 1, 1949).
[5] Duckworth, Johnson, Preston, and Woodcock, Phys. Rev. **78**, 386 (1950).
[6] A. E. Shaw, Phys. Rev. **75**, 1011 (1949).
[7] Okuda, Ogata, Kuroda, Sima, and Shindo, Phys. Rev. **59**, 104 (1941).
[8] W. O. Bateson and E. Pollard, Phys. Rev. (to be published).

The Microwave Rotational Spectrum and Structure of Bromogermane

A. HARRY SHARBAUGH, BENJAMIN S. PRITCHARD, AND VIRGINIA G. THOMAS
General Electric Research Laboratory, Schenectady, New York

AND

JOHN M. MAYS* AND BENJAMIN P. DAILEY
*Columbia University, New York, New York***

May 18, 1950

WE have measured and identified about one hundred lines arising from the fourth, fifth, and sixth pure rotational transitions of Ge^{70}, Ge^{72}, Ge^{74}, and Ge^{76} in the eight possible combinations with Br^{79} and Br^{81} in GaH_3Br. In addition, the dipole moment of SiH_3Br has been determined to be 1.31 ± 0.03 Debye units. The measured and derived constants for GeH_3Br are listed in Table I. Although the absolute accuracy of the quoted frequencies is about ±1 Mc/sec, the isotopic frequency differences were measured considerably more accurately (±0.1 Mc/sec).

TABLE I. Molecular constants for GeH_3Br.

Species (Ge and Br mass numbers)	Frequencies ±1 (Mc/sec.) $J=4$–5	B_0 average (Mc/sec.)
70–79	24385.54	2438.57
70–81	24101.61	2410.17
72–79	24064.35	2406.42
72–81	23780.11	2378.01
74–79	23758.99	2375.88
74–81	23474.75	2347.46
76–79	23468.0	2346.84
76–81	23183.8	2318.37

Within the allowable experimental error, the B_0 values computed from the different transition frequencies for a given isotopic species may be considered constant, as they should be if the centrifugal distortion correction is negligible.

The theoretical hyperfine structure to be expected for a nuclear spin of $\frac{3}{2}$ for bromine was found to be in excellent agreement with the observed spectra, indicating zero spin for the even isotopes of Ge. Lines due to $Ge^{73}H_3Br^{79}$ and $Ge^{73}H_3Br^{81}$ were observed in the predicted positions. As was expected, they had very complex structure because of the further splitting due to the quadrupole coupling of the Ge^{73} nucleus found by Townes *et al.*[1] in GeH_3Cl. The quadrupole coupling constants $eQ(\partial^2V/\partial z^2)$ were determined from measurements involving the $J=3\rightarrow4$ transition where the pattern was least complicated.

The dipole moment of SiH_3Br was determined by analysis of the movement of Stark components of the $J=2\rightarrow3$, $K=2$, $F=7/2\rightarrow(5/2,\ 7/2,\ 9/2)$ line. Because of experimental and theoretical difficulties the dipole moment of GeH_3Br is not available at this time.

The structure of this molecule was determined using the average moments of inertia obtained for the three transitions of $Ge^{70}H_3Br^{79}$, $Ge^{70}H_3Br^{81}$, and $Ge^{74}H_3Br^{81}$ and checked against the remaining species. Since accurate values of the isotopic masses of germanium have not been measured, these were computed using a packing fraction[2] of -6.7×10^{-4} mass unit. The structural data and quadrupole coupling constants for this molecule are compared with the corresponding quantities for CH_3Br and SiH_3Br in Table II. Although not stated explicitly, the limits of error on the

TABLE II. Structural parameters for CH_3Br, SiH_3Br, and GeH_3Br.

Molecule	CH_3Br[a]	SiH_3Br[b]	GeH_3Br
X-Br(A)	1.932 (1.93)	2.209 ± 0.001 (2.31)	2.297 ± 0.001 (2.36)
H-X(A)	1.11 (1.09)	1.57 ± 0.03 (1.47)	1.55 ± 0.05 (1.52)
H-X-H	109°22′	111°20′ ±1°	112°0′ ±1°
Dipole moment (Debye)	1.797°	1.31 ± 0.03	
	$eQ(\partial^2V/\partial z^2)$(Mc/sec.)		
Br^{79}	577	336	380
Br^{81}	482	278	321

[a] Gilliam, Edwards, and Gordy, Phys. Rev. **75**, 1014 (1949).
[b] Sharbaugh, Bragg, Madison, and Thomas, Phys. Rev. **76**, 1419 (1949).
[c] Shulman, Townes, and Dailey, Phys. Rev. **78**, 145 (1950).

CH_3Br structural parameters are of the same order, or slightly greater, than those quoted for the other two molecules, since the CH_3Br structure determination was based partially on less accurate infra-red data. The numbers in parentheses are the sums of the covalent radii of the respective atoms. Within the limits of experimental error, the angle $\angle HXH$ must be considered to be the same for these three molecules and very nearly tetrahedral (109°28′).

As in the corresponding series of chlorides[3] there is a marked shortening of the Si−Br and Ge−Br bonds. This is attributed to contributions from a double bond structure of the sort $H_3Si^-=Br^+$ involving use of a d-orbital which is not available in carbon. On the basis of quadrupole coupling constants[4] and bond shortening one can make the following semiquantitative assignment of bond characters: CH_3Br, 18 percent ionic; SiH_3Br, 40 percent ionic, 25 percent double bond; GeH_3Br, 40 percent ionic, 15 percent double bond.

Thanks are due Dr. John R. Ladd of General Electric Research Laboratory for preparing the bromogermane used at that laboratory.

* Eastman Kodak Fellow 1949–50.
** Work at Columbia University supported jointly by the Signal Corps and Office of Naval Research.
[1] Townes, Mays and Dailey, Phys. Rev. **76**, 700 (1949).
[2] J. Mattauch, *Nuclear Physics Table* (Interscience Publishers, Inc., New York, 1940), p. 113.
[3] Dailey, Mays, and Townes, Phys. Rev. **76**, 136 (1949).
[4] C. H. Townes and B. P. Dailey, J. Chem. Phys. **17**, 782 (1949).

Preliminary Analysis of the Microwave Spectrum of Ketene

B. Bak, E. Stenberg Knudsen, E. Madsen, and J. Rastrup-Andersen
Department of Chemistry, University of Copenhagen, Denmark
May 5, 1950

MICROWAVE spectra of $CH_2=CO$, $CHD=CO$ and $CD_2=CO$ were taken at a pressure of 0.1 mm Hg in a 23-foot brass wave guide (X-band) with central steel electrode using Hughes-Wilson modulation technique. The oscillator was a 2K33 Klystron which, by proper adjustment of its largest screw (not the ordinary turning screw) and correct matching, oscillates between 16,000 to 21,200 and 22,000 to 25,800 Mc/sec. Wave-lengths were measured by a wave meter, carefully calibrated against well-determined $N^{14}H_3$ and $N^{15}H_3$ absorption frequencies. The frequencies obtained seem good to 2 to 3 Mc/sec.

A solution of $CH_2=CO$ in acetone was prepared by cracking of acetone. A solution of the deuterated species was prepared by cracking a mixture of deuterated acetones which were obtained by leaving a mixture of 18 g D_2O, 0.2 g NaOD and 16 g acetone for 36 hours and afterwards distilling off the acetones through an efficient column. In this way 15.2 g deuterated acetones were prepared. Density determination of the H_2O-D_2O mixture, subsequently distilled off, showed that exchange equilibrium had been reached The various ketene species used for the absorption experiments were admitted to the gas cell from their acetone solution which was kept at $-70°C$.

$CH_2=CO$ absorbed at 20,200 Mc/sec. (middle intensity) and at 20,257 (weak), near[1,2] $N^{15}H_3$ at[3] 20,272.3 and[1,4] $N^{14}H_3$ at[4] 20,371.4.

By cooling of the gas cell to about $-60°C$ it was seen that the intensity of the stronger line increased about 3 times while the weak line remained of constant intensity. The 20,200 Mc frequency thus must be assigned to the ground state of the molecule, 20,257 to an excited level. Both Raman spectrum[2] and infrared measurements[5] show the existence of a vibrationally excited level at 510 (Raman) or 529 cm^{-1} (infra-red). The next level apparently lies at 600 cm^{-1}. The weak line, 20,257, may therefore be assigned to a molecule, excited by 510 cm^{-1}, but it remains unexplained why another, slightly weaker line, corresponding to 600 cm^{-1} excitation was not observed.

The strong line showed a Stark affect (at $\sim$500 volts $\Delta\nu\sim 6$ Mc/sec.) which is in agreement with the molecular dipole moment[1] (1.45 D.U.). Ketene prepared from acetone contains CH_4, $CH_2=CH_2$, CO and acetone as impurities. It was shown by experiment that acetone does not absorb at the frequencies assigned to ketene.

Correspondingly $CHD=CO$ showed weak absorption at 18,892, stronger at 18,825 (close to[4,6] $N^{14}H_3$ at 18,884.9 and[1,7] $N^{14}H_3$ at[3] 18,808.7. $CD_2=CO$ absorbed with middle strength at 17,690 (close to[6,8] $N^{15}H_3$ at 17,548.4 and[1,7] $N^{15}H_3$ at[3] 17,855.3). No weak line was observed in the case of $CD_2=CO$.

From the interatomic distances determined by election diffraction[6] ($d_{CC}=1.35\pm0.02$A, $d_{CO}=1.17\pm0.02$A) and the selection rules[9] it follows that the absorption frequencies found must correspond to a $0_0\rightarrow 1_{-1}$ transition. $CH_2=CO$ has 3 different moments of inertia $I_a\ll I_b<I_c$, where $I_c=I_a+I_b$. In units of chemical molecular weight times angstrom squared I_a may be assumed to vary between 1.49 and 1.97 corresponding to $d_{CH}=1.05$A, $\angle HCH=110°$ resp. $d_{CH}=1.09$A, $\angle HCH=130°$. This gives $I_b=49.28$, resp. 49.08, $I_c=50.77$ and 51.05.

The geometry of the molecule is somewhat better determined (although not completely) than has hitherto been the case. The results for $CH_2=CO$ and $CD_2=CO$ are easy to handle as here the dipole moment lies in the axis of least moment of inertia. The geometry of the molecule has 4 unknowns: d_{CH}, d_{CC}, d_{CO} and $\angle HCH(=2\varphi)$. If reasonable values of d_{CH}(1.05–1.09A) and $2\varphi(110°–130°)$ are assumed a number of corresponding d_{CC} and d_{CO} values can be calculated. For $d_{CC}=1.07$A fine agreement with the election diffraction data is obtained at $2\varphi=123°.7\pm1°.0$. For $d_{CH}=1.05$A $2\varphi=120°.3\pm1°$. For $d_{CH}=1.09$A $2\varphi=127°.1\pm1.0$. We thus know that $119°<2\varphi<128°$. The electron diffraction pattern was analyzed by assuming $2\varphi=110°$, but the analysis is only slightly influenced by a change in the position of the hydrogen atoms. At the same time it is found that $d_{CC}=1.330$–1.340A and $d_{CO}=1.140$–1.170A.

The results for $CHD=CO$ can be utilized preliminarily by assuming that the moments of inertia of $CHD=CO$ are close to those for an imaginary molecule $CX_2=CO$, where the mass of X is the average of H and D. If this is done the values $d_{CH}=1.06$, $d_{CC}=1.333$, $d_{CO}=1.150$ and $2\varphi=122°.5$ must be favored. This means that d_{CO} comes close to the CO distance in CO_2 and in[7] OCS (1.162A) and d_{CC} close to 1.353A from ethylene.[8] Likewise $\angle HCH=122°.5$ is near the ethylene value[8] 120° and the formaldehyde value[10] (123°.5).

Further calculations are being postponed until better frequency determinations can be carried out.

[1] Hanney and Smith, J. Am. Chem. Soc. **68**, 1357 (1946).
[2] Kopper, Zeits. f. physik Chemie **B34**, 396 (1935).
[3] Sharbaugh, Madison, and Bragg, Phys. Rev. **76**, 1529 (1949).
[4] W. E. Good and D. K. Coles, Phys. Rev. **71**, 383 (1949).
[5] F. Halvorsen and Van Zandt Williams, J. Chem. Phys. **15**, 552 (1947).
[6] J. Y. Beach and D. P. Stevenson, J. Chem. Phys. **6**, 75 (1938).
[7] Townes, Holden, and Merritt, Phys. Rev. **74**, 1117 (1948).
[8] W. S. Gallaway and E. F. Barker, J. Chem. Phys. **10**, 88 (1942).
[9] G. Herzberg, *Infrared and Raman Spectra* (D. Van Nostrand Company, Inc., New York, 1945).
[10] G. H. Dicke and G. B. Kistiakowsky, Phys. Rev. **45**, 4 (1934).

Current Fluctuations in D.C. Gas Discharge Plasma*

P. Parzen and L. Goldstein
Federal Telecommunication Laboratories, Inc., Nutley, New Jersey
April 21, 1950

RADIOFREQUENCY energy produced in a d.c. gas discharge plasma has been measured in the microwave region.[1,2] The use of gas discharge tubes as microwave noise standards has recently been indicated.[2] This noise power can be accounted for by a study of the electron current fluctuations in the plasma as follows.

An electron whose thermal speed lies between V and $V+dV$ will on the average suffer Z_VT collisions in a time T. Actually there will be fluctuations in this number, and the probability $p(K)$ that it experiences K collisions in a time T is:

$$p(K)=[(Z_VT)^K/K!]\exp(-Z_VT). \tag{1}$$

The probability $q(\theta)$ that the time of consecutive collisions of an electron lies between θ and $\theta+d\theta$ is:

$$q(\theta)=Z_V\exp(-Z_V\theta)d\theta. \tag{2}$$

Now making the usual assumptions that the electron current exists only between collisions, the current i_x measured between the electrodes due to an electron which has collided at time t_k with a subsequent free time θ_k is:

$$i_x(t-t_k;\theta_k)=e/d[V_x+a(t-t_k)] \text{ for } t_k\leq t\leq t_k+\theta_k, \tag{3}$$

where d=length of tube parallel to direction of applied electric field E_x, $a=eE_x/m$, and V_x=thermal velocity of electron parallel to x axis.

There are similar expressions for the current in the Y and Z directions, except that a is set equal to zero. The total electron current $I(t)$ will be a function of the random variables t_k and θ_k and it is possible to find its fluctuations and spectrum by the usual methods.[3] Under the assumptions that the electron distribution is Maxwellian with an electron temperature T_e and that the collision rate Z_V is independent of velocity, the spectrum $W(f)$ of the current fluctuations is given by:

$$\langle(I-\bar{I})^2\rangle_{Av}=\int_0^\infty W(f)df \tag{4}$$

$$W(f)=4kT_eG(\omega)+4\frac{\bar{I}^2}{N}\frac{Z}{Z^2+\omega^2}\left[2+\frac{Z^2-\omega^2}{Z^2+\omega^2}\right], \tag{5}$$

where $\bar{I}=\langle I(t)\rangle_{Av}$=average electron current, $\omega=2\pi f$=angular frequency of observation, $G(\omega)$=a.c. conduction of gas discharge plasma, N=total number of electrons in the plasma.

The available noise power P_ω from a gas discharge plasma placed in the transverse plane of a rectangular wave guide propagating only in its lowest mode is

$$P_\omega=|I_E|^2/4G(\omega). \tag{6}$$

Here I_E=a.c. electron current in the direction of the E vector of the wave guide. Hence in this case,

$$P_\omega=\left\{kT_e+\frac{P_0}{NZ}\cos^2\theta\left[2+\frac{Z^2-\omega^2}{Z^2+\omega^2}\right]\right\}df, \tag{7}$$

where θ=angle between E vector and axis of gas tube, and P_0=d.c. power dissipated in tube. For ordinary gas tubes that are used as microwave noise standards, the contribution of the frequency sensitive term is of the order of a few percent of the total noise power output. This calculation does not account for noise power due to other fluctuations.

* This development was sponsored by the Signal Corps Engineering Laboratories, Fort Monmouth, New Jersey.
[1] L. Goldstein and N. Cohen, Phys. Rev. 73, 83 (1948).
[2] W. W. Mumford, Bell Sys. Tech. J. 28, 608 (1949).
[3] S. O. Rice, Bell Sys. Tech. J. 23, 282 (1949).

Nuclear Magnetic Resonance of Sb^{121} and Sb^{123}*

V. W. Cohen, W. D. Knight,** and T. Wentink, Jr.
Brookhaven National Laboratory, Upton, Long Island, New York
and
W. S. Koski
Johns Hopkins University, Baltimore, Maryland
May 11, 1950

We have made attempts to find the nuclear resonance of Sb in Sb_2O_3 and $SbCl_3$ without success. On the supposition that this failure was due to a large interaction between the electric quadrupole moment of the Sb nucleus and the non-uniform electric field of the above molecules a search was made in an ion in which the electric field would be symmetrical. This requirement is fulfilled in the $SbCl_6^-$ ion in which the Cl atoms are believed to be arranged in a regular octahedral configuration about the Sb.

A search was made in a solution of $HSbCl_6$ in HCl guided roughly by the spectroscopic values of the magnetic moments as given by Crawford and Bateson[1] using a radiofrequency magnetic resonance spectrometer.[2] Distinct resonances were observed in the vicinity of 9800 kc and 5300 kc which from the spectroscopic information would presumably be associated with Sb^{121} and Sb^{123} respectively. Repeated series of readings were taken comparing the Sb^{121} resonance to that of Na in solid NaCl, and the Sb^{123} resonance to that of D in D_2O. The frequencies of resonance were measured by means of a U. S. Signal Corps frequency meter type EC 221–Q, calibrated at 100 kc intervals against harmonics generated by a General Radio crystal controlled oscillator operating at 100 kc and in turn standardized against Station WWV. The magnetic field was electronically controlled to a constancy of about one part in 50,000.

The average values of the ratios of the observed frequencies are:

$$[\nu(Sb^{121})/\nu(Na^{23})]=0.90469\pm0.00004$$

and

$$[\nu(Sb^{123})/\nu(D^2)]=0.8442\pm0.0001.$$

If we take Bitter's[3] value of the observed ratio of $\nu Na/\nu H=0.26450\pm0.01$ percent, and used a first-order atomic diamagnetic correction for Sb of 1.00517 as calculated from the Hartree-Fock functions[4] and the value[5] for H^2 of 1.000027, we get for the ratio $g(Sb^{121})/g(H^1)=0.24052\pm0.00003$. Taking the spectroscopic value of 5/2 for the spin of Sb^{121} and the value for μ_H as measured by Taub and Kusch,[6] we get

$$\mu(Sb^{121})=3.3595\pm0.0004.$$

One must note that this value of the magnetic moment may possibly be in error as a result of second-order molecular effects which we are unable to evaluate at this time.

Similarly, taking Bloch's[7] value of

$$\mu(P)/\mu(D)=3.257195\pm0.00002,$$

we get $[g(Sb^{123})/g(H)]=0.13025\pm0.00002$, and taking the value 7/2 for the spin, we get for the magnetic moment

$$\mu=2.5470\pm0.0003 \text{ nuclear magnetons.}$$

It is of interest to compare the ratio of the g-values of the two Sb isotopes as obtained spectroscopically by Crawford and Bateson,

$$[g(Sb^{121})/g(Sb^{123})]=1.82\pm0.02 \text{ to our } 1.8466.$$

* Work performed under contract with AEC.
** Present address Trinity College, Hartford, Connecticut.
[1] Crawford and Bateson, Can. J. Research 10, 693 (1934).
[2] Pound and Knight, Rev. Sci. Inst. 21, 219 (1950).
[3] F. Bitter, Phys. Rev. 75, 1326 (1949).
[4] W. C. Dickinson, private communication; W. E. Lamb, Jr., Phys. Rev. 60, 817 (1941).
[5] N. Ramsey, Phys. Rev. 77, 567 (1950).
[6] Taub and Kusch, Phys. Rev. 75, 1481 (1949).
[7] Bloch, Levinthal, and Packard, Phys. Rev. 72, 1125 (1947).

Effect of Magnetic Fields on Conduction—"Tube Integrals"

W. Shockley
Bell Telephone Laboratories, Murray Hill, New Jersey
May 18, 1950

The effect of a magnetic field $\mathbf{H}$ on electrical conduction can be reduced to integrals by using "tubes." Choose parallel to $\mathbf{H}$ an axis $\mathbf{P}_H$ in the $\mathbf{P}=\hbar\mathbf{k}$ space of the Brillouin zone. Then the region lying between planes $\mathbf{P}_H$ and $\mathbf{P}_H+d\mathbf{P}_H$ and energy surfaces $E(\mathbf{P})=E$ and $E+dE$ is a "tube." For spherical energy surfaces the tube is a torus with a parallelogram cross section. For more complex surfaces and for energies for which the surfaces reach the boundary of the Brillouin zone the tube may possibly take a helical path and eventually fill most of the space between E and $E+dE$. We shall discuss only simple closed tubes of interest for semiconductors.

For any tube α an angle variable θ and a tube mass m_α are defined by equations

$$m_\alpha\theta=\int_0^{P_l} dP_l/v_l, \quad 2\pi m_\alpha=\oint dP_l/v_\alpha, \tag{1}$$

where P_l is the distance in the $\mathbf{P}$-space along the tube from an arbitrarily selected fixed point and v_α is the scalar magnitude of the component perpendicular to $\mathbf{H}$ of the group velocity $\mathbf{v}=\nabla E(\mathbf{P})$. $\mathbf{H}$ produces incompressible flow along the tube α with

$$\begin{gathered}d\mathbf{P}/dt=(-e/c)\mathbf{v}\times\mathbf{H}, \quad \dot{P}_l=(-e/c)v_\alpha H \\ \dot{\theta}=\dot{P}_l/v_\alpha m_\alpha=-eH/m_\alpha c=\omega_\alpha,\end{gathered} \tag{2}$$

so that $\dot{\theta}$ is constant and the period is given by the classical formula with a mass m_l.

If we assume that after one transition, due to thermal vibration for example, an electron will have average velocity zero, then the current produced by a given tube can be reduced to closed form as follows. When an electric field $\mathbf{E}$ is applied each element dV_P of volume in $\mathbf{P}$-space becomes a source of electrons of strength

$$(-eV/kTh^3)f(1-f)\mathbf{E}\cdot\mathbf{v}dV_P, \tag{3}$$

where V is the volume of the crystal, f the Fermi-Dirac distribution function and e, k, T, h are as usual. If $v(\varphi)=1/\tau(\varphi)$ is the probability of being scattered per unit time at tube position φ, the total current density $d\mathbf{I}_\alpha(=(-e/V)\mathbf{e}v(\varphi))$ due to electrons brought into tube α by $\mathbf{E}$ is

$$\begin{gathered}d\mathbf{I}_\alpha=(e^2/kTh^3)f(1-f)dEdP_H(m_\alpha/\omega_\alpha). \\ \int_\theta^{2\pi} d\theta\int_0^\infty d\varphi\mathbf{E}\cdot\mathbf{v}(\theta)\mathbf{v}(\varphi)\exp\left[-\int_\theta^\varphi v(\varphi')d\varphi'/\omega_\alpha\right].\end{gathered} \tag{4}$$

(Note that $dV_P = m_\alpha dE dP_H d\theta$.) The total current **I** is to be obtained by integration over dE and dP_H. This leads to an expression for **I** as a linear function of **E** where the coefficients are integrals involving **H** through ω_t so that in principle the relationship of **I** to **E** is reduced to quadratures for all values of **H**.

This result is formally more general than that of Davis[1] which extends to terms in H^2 and that of Wilson[2] which is restricted to eliptical surfaces and $\tau = \tau(E)$.

Equation (4) can be evaluated for large values of **H** for various assumed forms of $v(\theta)$ and $v(\theta)$. It is hoped that by these means the energy surface parameters[3] for germanium can be determined from magnetoresistance measurements on single crystals.[4,5]

The writer is indebted to G. L. Pearson and H. Suhl for stimulating discussions of their data, to J. Bardeen, I. Estermann, and F. Seitz for several discussions and to the last for the opportunity to see his manuscript dealing with spherical surfaces but varying τ.

[1] L. Davis, Phys. Rev. **56**, 93 (1939).
[2] A. H. Wilson, *The Theory of Metals* (Cambridge University Press, Cambridge, 1936), Chapter V.
[3] W. Shockley, Phys. Rev. **78**, 173 (1950).
[4] G. L. Pearson, Phys. Rev. **78**, 646 (1950).
[5] H. Suhl, Phys. Rev. **78**, 646 (1950).

The Question of Isomerism in Ca^{49}

E. DER MATEOSIAN* AND M. GOLDHABER†
Argonne National Laboratory, Chicago, Illinois
May 5, 1950

IN the course of a systematic investigation of isomers produced by slow neutron bombardment it seemed to us of interest to study in greater detail the case of isomerism in Ca($Z=20$), the element of lowest charge for which isomerism has been reported. Walke[1] had assigned periods of 30 min. and 2.5 hr. to Ca^{49}. In view of the connection between isomers of the even-odd type and nuclear shell models recently discussed by Feenberg, Nordheim, and Mayer, this problem takes on added interest.

To our surprise, we were unable to confirm the existence of either of the reported activities when Ca enriched in the isotope of mass 48 (62 percent Ca^{48}) was exposed to slow neutrons from the Argonne heavy water reactor. Instead, we noticed two activities of 8.5 min. and 1 hr. half-life as shown in Fig. 1, upper curve. By chemical separation we could show that the 8.5-min. activity was due to a Ca isotope, Ca^{49}, and the 1-hr. activity due to a Sc isotope, Sc^{49}. The relative intensities of the 8.5 min. and 1 hr. activities were compatible with the interpretation that the 1-hr. Sc^{49} is the daughter of 8.5-min. Ca^{49}. A 57-min. Sc^{49} was also observed by Walke[1] in the Sc fraction after neutron or deuteron bombardment of Ca. The isotopic activation cross section of Ca^{48} was found to be 1.1×10^{-24} cm^2 and the cadmium ratio ~35, similar to that of Al, which behaves approximately like a 1/v absorber.

The energy of the beta-rays of Ca^{49} as determined by absorption in Al in a calibrated arrangement, was found to be ~2.7 Mev. Hard gamma-rays capable of producing photo-neutrons from Be and D were also present, with an intensity comparable to that of the beta-rays (see Fig. 1, lower curve). The beta-rays of Sc^{49} were found to have an energy of ~2.4 Mev. The assignment of the 8.5-min. activity to Ca^{49} was further checked by bombarding ordinary Ca, and Ca enriched in the isotope of mass number 46.

In the spin-orbit coupling model of nuclear shell structure the onset of isomerism involving reasonably long lifetimes should not take place until $g_{9/2}$ and $p_{1/2}$ levels start competing for the lowest level. This occurs for 39 odd nucleons.[2] From the point of view of this model which has been remarkably successful in predicting the spins of the ground states of the nuclei—though not so successful in predicting parity changes in isomeric transitions—it is satisfactory that of the reported cases of isomerisms for nuclei with 29 neutrons that of Ca^{49} could not be substantiated. However, another case of isomerism is believed to exist for 29 neutrons, that of Ti^{51} where a 72-day and a 6-min. period have been reported.[3] We were able to confirm the 6-min. activity in Ti of high purity bombarded with slow neutrons, but the intensity of the 72d activity, if present, was at least 10 times smaller than ex-

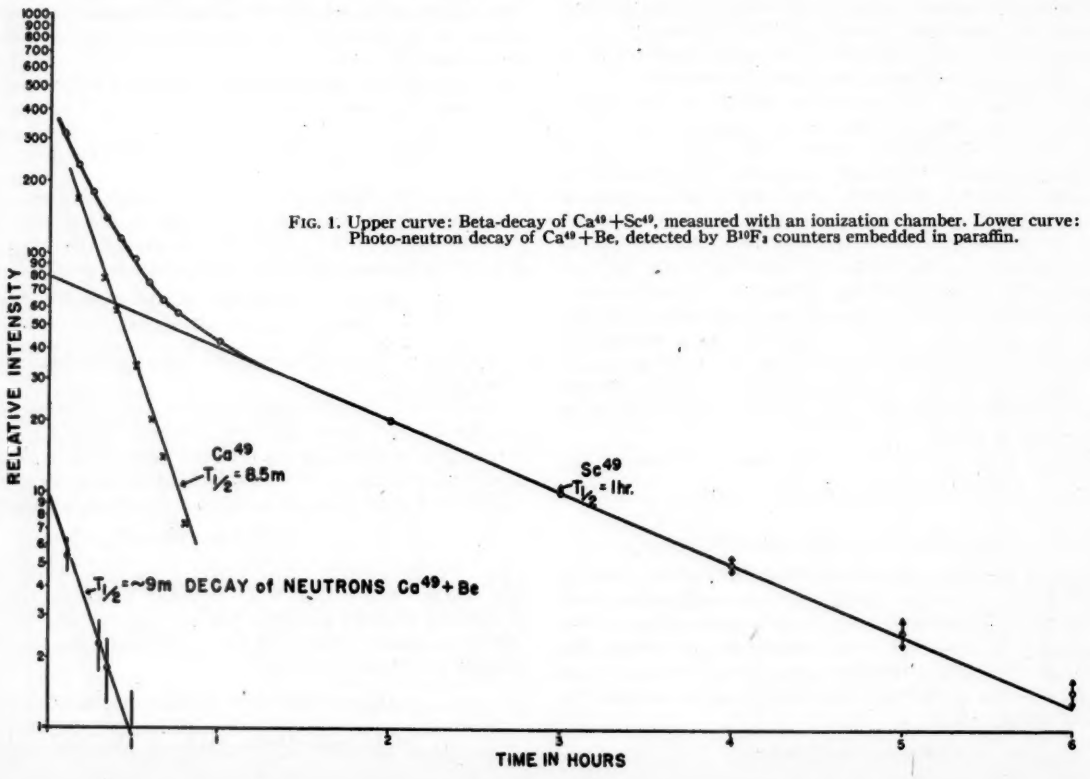

FIG. 1. Upper curve: Beta-decay of $Ca^{49}+Sc^{49}$, measured with an ionization chamber. Lower curve: Photo-neutron decay of $Ca^{49}+Be$, detected by $B^{10}F_3$ counters embedded in paraffin.

pected from the cross section reported by Seren *et al.*[4] A detailed search for the 72-day activity is reported in the succeeding note by Miskel, der Mateosian, and Goldhaber.[5]

Our thanks are due Dr. Keim's group at Oak Ridge who supplied the enriched calcium isotopes.

* Now at Brookhaven National Laboratory.
† Department of Physics, University of Illinois, Urbana, Illinois.
[1] H. W. Walke, Phys. Rev. **52**, 777 (1937).
[2] M. G. Mayer, Phys. Rev. **78**, 16 (1950).
[3] See E. Segrè and A. C. Helmholz, Rev. Mod. Phys. **21**, 271 (1949).
[4] Seren, Friedlander, and Turkel, Phys. Rev. **72**, 888 (1947).
[5] Miskel, der Mateosian, and Goldhaber, Phys. Rev. **78**, 193 (1950).

The Question of Isomerism in Ti^{51}

J. A. Miskel, E. der Mateosian, and M. Goldhaber*
Brookhaven National Laboratory,† Upton, Long Island, New York
May 5, 1950

IT was shown in the preceding note[1] that of the two reported cases of isomerism for 29 odd neutrons in even-odd nuclei, *viz.*, Ca^{49} and Ti^{51}, the first case could not be confirmed. In the second case, some doubt was thrown on the existence of the 72-day activity[2] of Ti^{51}, isomeric with 6 min. Ti^{51}. To investigate this activity further we obtained a source of Ti^{51} (72d) of nominally 0.5 millicurie intensity, from Oak Ridge, where it had been produced by slow neutron bombardment of TiO_2.

To find clues for possible chemical impurities in the sample the photon component was studied with the help of physical devices of fairly specific response, which were in use here for other work: a proportional counter for low energy photons[3] and a photo-neutron detector for high energy photons.[4] In this way the presence of Hf^{181} (46d) was established with the help of the L radiation accompanying its decay and that of Sb^{124} (60d) with the help of the photo-neutrons which its gamma-rays produce in Be. The spectroscopic analysis accompanying the TiO_2 sample had revealed neither Hf nor Sb. After precipitation of Sb as sulfide, the titanium was purified by repeated distillation of $TiCl_4$ (b.p. 136.4°C) prepared from the irradiated TiO_2. Carriers were added for suspected impurities during the purification. After purification a sample of ~200 mg TiO_2 spread over an area of about 10 cm^2 showed an activity of only 4 counts/min. when measured with a thin end window counter (3 mg/cm^2 of mica). This activity was not studied further. It represented a reduction in intensity from the original activity by a factor of $\sim 10^5$. It is therefore probable that no 72d Ti^{51} exists, and that previous observers were measuring an apparent activity caused by a number of impurities of comparable half-life. In agreement with expectations from the spin orbit coupling model[5] of nuclear shell structure, no case of isomerism for less than 39 odd nucleons is now established for even-odd nuclei.

We wish to thank Maria Mayer for stimulating discussions.

* On leave from the University of Illinois.
† Work carried out under the auspices of the AEC.
[1] E. der Mateosian and M. Goldhaber, Phys. Rev. **78**, 192 (1950).
[2] See E. Segrè and A. C. Helmholz, Rev. Mod. Phys. **21**, 271 (1949) for references to earlier work on this activity.
[3] Scharff-Goldhaber, der Mateosian, McKeown and Sunyar, Phys. Rev. **78**, 325 (1950).
[4] E. der Mateosian and M. Goldhaber, Phys. Rev. **78**, 326 (1950).
[5] M. G. Mayer, Phys. Rev. **78**, 16 (1950).

Neutron-Induced Radioactivity in Palladium

A. Storruste
Physics Department, University of Birmingham, England
May 12, 1950

NEUTRON capture in Pd^{110} gives radioactive Pd^{111} which decays by beta-emission with a half-life of 26 min. to Ag^{111}. The 7.5-day activity of Ag^{111} has been studied by several investigators. Helmholz and others[1] found the beta-ray spectrum to be simple with an upper energy limit of 1.06 Mev. Steinberg[2] reports for the beta-rays energy limits of 0.24 Mev and 1.0 Mev. Kraus and Cork[3] report little or no gamma-radiation, and other investigators report no gamma-rays.

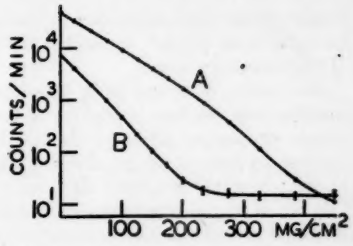

FIG. 1. Absorption of Ag^{111} beta-rays, A, and corresponding beta-gamma-coincidence rate, B.

The neutron-induced radioactivity in palladium has here been investigated with a sensitive scintillation counter. Palladium from Johnson, Matthey & Co., London, of purity 99.995 percent was irradiated in the Harwell pile. The irradiated palladium was dissolved and a small amount of inactive $AgNO_3$ added. The silver was precipitated as the chloride and then redissolved in ammonium hydroxide and reprecipitated.

In addition to the well-known beta-rays, the silver precipitate was found to emit gamma-rays of weak intensity. The activities were followed for six weeks with special attention toward any difference in half-life between the beta- and gamma-activities. The half-lives were found to be equal, both being in agreement with the 7.5 days previously reported for Ag^{111}. An absorption measurement of the gamma-rays gave an absorption coefficient in lead of 0.31 g^{-1} cm^2 which corresponds to an energy of 0.33 Mev. The gamma-rays were found to be in coincidence with the beta-rays. Curve A in Fig. 1 shows the counting rate of the total beta-radiation *versus* thickness of the aluminium absorbers, curve B is the corresponding coincidence rate multiplied by a factor of 100. The upper energy limit of the main beta-spectrum and the upper energy limit of the beta-rays giving rise to coincidences differ roughly by the energy 0.33 Mev of the gamma-rays, though the weak intensity of the gamma-radiation prevents an accurate determination. The intensity of the gamma-rays was found to be 6.5 gamma-rays per 100 beta-particles. No gamma-gamma-coincidences were recorded.

The conclusion is that 6.5 percent of the beta-decay of Ag^{111} has an upper energy limit of 0.73 Mev and leads to an excited state of Cd^{111} at 0.33 Mev. Both this and the 1.06-Mev beta-transition to the ground state appear to be once forbidden. These facts and the conversion coefficients for the transitions[1] in Cd^{111} may be explained by assuming that the 0.33-Mev excited state and the ground state both have the same parity and spin equal to 1/2, while the excited states at 0.247 Mev, 0.396 Mev and 0.420 Mev have spins of 5/2, 13/2 and 9/2 respectively, with parities opposite to that of the ground state.

From the solution the palladium was precipitated with dimethyl-glyoxim. This precipitate showed the 87 kev gamma-rays following the 13-hour activity of Pd^{109} and the very soft components of the 17-day activity of Pd^{103}, but, except for the internal bremsstrahlung no harder component was found in the precipitate.

[1] Helmholz, Hayward and McGinnis, Phys. Rev. **75**, 1469 (1949).
[2] E. P. Steinberg, Plutonium Project Report CC-1331, Feb. 23, 1944.
[3] J. D. Kraus and J. M. Cork, Phys. Rev. **52**, 763 (1937).

The Bohr Formula for the Rydberg Constant

Raymond T. Birge
University of California, Berkeley, California
April 24, 1950

THE first great triumph of the Bohr theory for the hydrogen atom was the derivation of the Rydberg constant for infinite mass in terms of certain atomic constants. For the past third of a

century it has been customary to *assume* the correctness of Bohr's formula, in all critical investigations on the most probable values of the atomic constants.

As a result of recent work in quantum electrodynamics some question has now been raised[1] as to the theoretical validity of the simple expression given by Bohr. Hence it is of considerable interest to make a direct check of the formula in terms of the atomic constants involved. Fortunately there is now available a number of high precision results in quite new fields of work, each of which involves one or more of the atomic constants. A careful study of the various constants and especially of their assigned uncertainties has led to an expression, Eq. (9), which is believed to give the most accurate calculated value of the Rydberg constant. This final formula results from the combination of three alternative expressions for R_∞, each of which alone yields a far less reliable value.

From among the new experimental results, the following four appear to be most suitable for our present purpose:

$$\gamma_P=\omega_P/H=(2.67524\pm0.00020)\times10^4 \text{ gauss}^{-1}\text{ sec.}^{-1}$$
$$=\text{gyromagnetic ratio of the proton.}^2 \quad (1)$$

$$\mu_P=\omega_P/\omega_e{}^c=(15.2100\pm0.0002)\times10^{-4}$$
$$=\text{magnetic moment of the proton in terms of Bohr magnetons.}^3 \quad (2)$$

Here $\omega_e{}^c$ = orbital resonance frequency of the electron in the magnetic field of the cyclotron, and ω_P = nuclear precession frequency of the proton in the same magnetic field.

$$\omega_P{}^c/\omega_P=0.358106\pm0.000010. \quad (3)$$

In this measured ratio[4] $\omega_P{}^c$ is the proton frequency corresponding to $\omega_e{}^c$ for the electron.

$$\Delta\nu_H=(4c/3)\frac{2I+1}{I}(m_\tau/m)^3(\mu_e/\mu_0)(1+\tfrac{3}{2}\alpha^2)R_\infty\cdot\alpha^2\cdot\mu_P$$
$$=(1420.410\pm0.006)\times10^6 \text{ sec.}^{-1}. \quad (4)$$

The measured value of $\Delta\nu_H$ (the hyperfine splitting of the $^2S_{\frac{1}{2}}$ level of hydrogen) is due to Nafe and Nelson[5] and Eq. (4) has been used by Taub and Kusch, who obtained the precision value $1/\alpha=137.043\pm0.003$, where only the error in μ_P was considered.[6] Without further explanation, we give the assumed numerical value of the following factors in Eq. (4)

$c=(2.99776\pm0.00004)\times10^{10}$ cm/sec.,
$I=1/2$,
$m_\tau/m=1/1.0005445$, with negligible error.

$\mu_e/\mu_0=1+\alpha/2\pi=1.0011617$. A third term $(-2.973\alpha^2/\pi^2)$ has, however, been suggested and I, therefore, take its value, 0.000016, as the *probable error* of the simpler expression.

Taub and Kusch,[6] in order to evaluate α, naturally used the known *spectroscopic* value[7]

$$R_\infty=109{,}737.30\pm0.05 \text{ cm}^{-1}$$

but this is just the magnitude we are trying to check. Hence Eq. (4) is of no value to us except in combination with other equations.

Bohr's original equation is

$$R_\infty=2\pi^2e^4m/h^3c \quad (5)$$

but e is now best determined from F/N_0 and h and m can be measured precisely only in combinations like e/m and h/e. Hence we transform Eq. (5) into

$$R_\infty=2\pi^2(F/N_0)^2/(h/e)^3(e'/m), \quad (6)$$

where F (Faraday) and e' are in e.m.u., and e in e.s.u.

Now F has been evaluated[4] from

$$F=(\gamma_P)(H^+)(\omega_P{}^c/\omega_P), \quad (7)$$

with $H^+=1.007580\pm0.000003$ (atomic weight of the proton),[4] and with the values of the other two factors already quoted. Furthermore, e'/m has been evaluated[3] from

$$e'/m=\gamma_P/\mu_P. \quad (8)$$

Combining Eqs. (6 and 7), one gets

$$R_\infty=2\pi^2(H^+)^2(\gamma_P)(\mu_P)(\omega_P{}^c/\omega_P)^2/(h/e)^3N_0{}^2. \quad (9)$$

Finally, we may use the definition

$$\alpha=2\pi e^2/hc \quad (10)$$

to transform Eq. (2) into

$$1/R_\infty=2(1/\alpha)^2(e'/m)(h/e), \quad (11)$$

with e'/m given by Eq. (5).

We now have three expressions for R_∞, namely Eqs. (4), (9), and (11), which can be combined to eliminate two quantities. Since there is no precision value of α aside from that *calculated* from Eq. (4), it is obvious that α is one of the two quantities to be eliminated. Various trial combinations, whose details will not be given here, have shown that h/e is predominantly responsible for the final error in R_∞, in any expression in which it occurs. Hence Hence h/e is the second quantity to be eliminated.

The result of thus eliminating α and h/e from Eqs. (4), (9), and (11) is

$$R_\infty{}^5=\frac{(\Delta\nu_H)^3\cdot N_0{}^2}{16\pi^2(H^+)^2\cdot K^3\cdot T^3\cdot\gamma_P{}^4\cdot\mu_P(\omega_P{}^c/\omega_P)^2}, \quad (12)$$

where K stands for

$$4c/3(2I+1/I)(m_\tau/m)^3(\mu_e/\mu_0)=(15.98053\pm0.00033)\times10^{10} \text{ cm/sec.}$$

and $T=1+3\alpha^2/2=1.00007987$, with no appreciable error.

For N_0 (physical scale) I use the 1945 value[8]

$$N_0=(6.02502\pm0.00023)\times10^{23} \text{ mole}^{-1}.$$

All of the numerical values needed in Eq. (12), together with their probable errors, have now been listed. The result of the substitution is

$$R_\infty=109{,}733.61\pm7.03 \text{ cm}^{-1},$$

and the discrepancy with the direct spectroscopic value is thus only -3.69 ± 7.03 cm^{-1}.

If all probable errors in Eq. (12) are ignored, *except* that in γ_P, the resulting probable error in R_∞ is reduced only to 6.56 cm^{-1}. Hence this amazingly accurate verification of Bohr's formula (to *less* than one part in 10^4) rests primarily upon the assigned accuracy of γ_P, which in turn depends upon the accuracy of the measurement[2] of a certain magnetic field in absolute units.

Finally, if the spectroscopic value of R_∞ is used in Eq. (9) to calculate h/e one obtains $(1.379466\pm0.000056)\times10^{-17}$ erg·sec./e.s.u. and, conversely, unless the direct experimental value of h/e has a probable error less than ±0.0001, it cannot lead to an indirect calculation of R_∞ as trustworthy as that given by Eq. (12).

[1] F. J. Belinfante, private communication. See also Bull. Am. Phys. Soc. **25**, No. 3, 10 (1950).
[2] Thomas, Driscoll, and Hipple, Phys. Rev. **75**, 902 (1949). The fifth decimal is as quoted in reference 4.
[3] J. H. Gardner and E. M. Purcell, Phys. Rev. **76**, 1262 (1949).
[4] Hipple, Sommer, and Thomas, Phys. Rev. **76**, 1877 (1949).
[5] J. E. Nafe and E. B. Nelson, Phys. Rev. **73**, 718 (1948).
[6] H. Taub and P. Kusch, Phys. Rev. **75**, 1481 (1949). With the more accurate μ_P value of reference 3, and with *all* sources of probable error considered, one gets $1/\alpha=137.0446\pm0.0017$.
[7] R. T. Birge, *Reports on Progress in Physics* VIII, 90 (1941).
[8] R. T. Birge, Am. J. Phys. **13**, 63 (1945). The quoted value is 1.000272 times the published value of 6.02338 on the chemical scale.

Erratum: Measurement of a 1.6×10^{-9} Second Half-Life in Yb^{170}

[Phys. Rev. **78**, 490 (1950)]

R. E. Bell and R. L. Graham
Atomic Energy Project, National Research Council of Canada, Chalk River, Ontario, Canada

Through an editorial error the figures "1.6×10^{-9}" were omitted in the title to this Letter to the Editor as printed. The correct title is as given above.

Proceedings of the American Physical Society

Minutes of the Meeting at Washington, April 27–29, 1950

THE 299th meeting of the American Physical Society, being the 1950 Spring Meeting, was held at Washington, D. C., on Thursday, Friday, and Saturday, April 27, 28, and 29, 1950. Most of our recent meetings have been unique in one important feature or another; this one comprised the greatest number of contributed (ten-minute) papers on record, amounting to 273. Since—more through accident than through design—the number of invited papers was unusually small and there were no symposia, the total number of papers did not set a new record, and the available halls were ample for our meetings. We are grateful to the Local Committee, headed as in recent previous years by Claire Marton and Hugh Odishaw, who did an immense amount of work for our benefit and did it very well; to the National Bureau of Standards for intervening with various Departments of Government to obtain the privilege of using their lecture halls, to these Departments themselves, and to the Bureau for welcoming us to its excellent East Building Lecture Room; to George Washington University for lending us its Lisner Auditorium, and to the National Academy of Sciences for the repeated favor of its own Auditorium. The only drawback to these arrangements is the wide dispersion of the halls. It will be interesting to our members to be told that owing to the initiative of Mrs. Marton and Mr. Odishaw, we expect to be able to confine next year's meeting to the halls of a prominent hotel and those of the National Bureau of Standards. The registration this year was about fifteen hundred. It is taken for granted that many of those in attendance failed to register; but even with all reasonable allowance for this factor it appears that our Washington meetings do not match our New York meetings in respect to total attendance.

The twelve invited papers were given by Felix Bloch (T1), J. W. M. DuMond (H1), Maurice Goldhaber (Y1), J. A. Hipple (A3), R. B. Holt (A1), Hans Kopfermann (I1), D. H. Menzel (T3), J. R. Pierce (A4), Grote Reber (T2), William Shockley (J14), H. S. Taylor (A2), and Herbert York (F12). The letters and numbers after these names indicate where in the following pages the titles of these papers will be found; for, as already twice announced in the *Bulletin*, the pages of the *Bulletin* which carry the abstracts and the intervening material are now and henceforth will be reproduced in *The Physical Review* without the least alteration, except for the renumbering of the pages. Preceding these pages are printed the "errata" which the contributors of abstracts have sent to the American Institute of Physics since the *Bulletin* appeared.

The banquet of the Society was held on the Friday evening in the Grand Ballroom of the Mayflower Hotel, and was adorned by after-dinner speeches by W. V. Houston and H. D. Smyth.

The Council met on the Wednesday preceding the meeting of the Society, and selected to Membership one hundred and five candidates whose names appear hereinafter. It will be of interest to our members to learn that the work of preparing a thirty-year Author and Subject Index of *The Physical Review* is well under way. Since the Index is to extend through 1950, it can scarcely be published before the autumn of 1951.

According to reports reaching the office of the Society, we have lost through death D. Coster (Groningen, Holland).

The Nominating Committee met on the Thursday afternoon, and reported that the following Fellows of the Society will be candidates for office in the election to be held next January: C. C. Lauritsen for President, J. H. Van Vleck for Vice-President, K. K. Darrow for Secretary, G. B. Pegram for Treasurer; R. F. Bacher, J. B. Fisk, E. M. Purcell, and H. K. Schilling for Councillor (four-year term, two vacancies to be filled); Maurice Goldhaber, Robert Serber, and C. H. Townes for membership in the Board of Editors (three-year term, three vacancies to be filled).

Elected to Membership: Carl D. Baumann, Raymond E. Benenson, John P. Benkard, Kurt Berman, William M. Boggs, Francis G. Boyle, Pierce A. Brennan, Karl W. Brockman, Jr., Bjorn Bruno, Nestor Cadorette, William F. Cartwright, Joses Jen Lieh Chen, Calvin M. Class, Julius Cohen, George E. Comstock, III, E. N. Dacus, Alcides R. Da Silva, Raymond L. Dickeman, John E. Dougherty, Joseph Dresner, Leonard Norman Eselson, Frederick C. Essig, John J. Floyd, Michael J. Forster, Meyer Garber, Robert W. Gelinas, Desmond A. George, James F. Goff, C. Herbert Grauling, Jr., Thomas C. Hall, Jr., John C. Hubbs, Leslie E. Johnson, Geoffrey Jones, Malvin H. Kalos, Harvey Kaplan, Robert W. Keyes, Charles H. Klane, Jack Kliger, Nobuo J. Koda, John W. Kunstadter, Wilbur Lakin, Erkki A. Laurila, Herbert N. Leifer, John L. Levy, C. H. Long, Stefan Machlup, Jose M. Malpica, John A. McCarthy, T. King McCubbin, Jr., Robert E. McDonald, Francis D. McDonough, George F. Mechlin, Clarence R. Mehl, William H. Metten, Richard A. Montgomery, George J. Moshos, H. Motz, Michael J. Neumann, Kaworu C. Nomura, James O'Day, Paride A. Ombrellaro, Wilfred E. Osberg, Jr., William Oshinsky, Paul G. Pallmer, Jr., Charles S. Peet, Martin L.

Perl, Robert H. Phillips, Roy Pietsch, George Edgar Reis, Howard Reiss, Fred L. Ribe, David C. Rich, Carl J. Rigney, Alfred C. Robinson, William G. V. Rosser, Kenneth Rubin, Donald H. Rusling, Stephen F. Samojeden, John E. Setzko, Henry Shenker, Henry B. Silsbee, Charles H. Skeen, Beatrice Anne Slater, John K. Sloatman, Jr., Curtiss A. Smith, William Spindel, D. Arthur Spohr, Henry L. Stadler, William E. Stein, Richard K. Steinberg, Robert M. Sugarman, Robert G. Sutherland, Nils Svartholm, Robert K. Swank, Chuan Tseng Tai, Theodorus A. M. Van Kleef, Henry Viervoll, Charles F. Wahlig, John C. Wahr, Gordon W. Wares, Gabriel Weinreich, Roger P. Wellinger, Norman M. Wolcott, Roger D. Woods, Miss Tosiko Yuasa, and George W. Ziegler, Jr.

With immeasurable regret we announce that John T. Tate, most wise, able, and diligent servitor of the Society for twenty-four years in the office of Managing Editor, departed this life on May 27, 1950.

KARL K. DARROW, *Secretary*
American Physical Society
Columbia University
New York 27, New York

Errata Pertaining to Papers C1, D11, I3, I8, J1, J8, M6, M7, O4, O7, P2, P3, R8, V2, W10, W13, and Y6

C1, by Leitner and Spence. The word "approximate" in the sixth line should read "appropriate."

D11, by Sumner Mayburg. The quantity $\partial \ln\epsilon/\partial p$ for KCl should be -1.05×10^{-5} bar^{-1} instead of -1.03×10^{-5} bar^{-1}.

I3, by O. H. Arroe. Beginning should read: "In hyperfine structure studies with separated isotopes^{++} of Mo^{96} and Mo^{97}, certain lines, including $4d^5\,5s\,{}^7S_3-4d^5\,5p\,{}^7P_{2\,3\,4}$ and $4d^5\,5s\,{}^5S_2-4d^5\,5p\,{}^5P_{1\,2\,3}$, show clearly. . . ."

I8, by William M. Conn. Line 7: Change "exposition" to "explosion." Add at end of abstract: Assisted by the ONR.

J1, by W. F. G. Swann. Line 5: The expression $e^{-\alpha x}$ should read $e^{-\alpha t}$. Lines 13 and 14: Delete the words: "and that the time constant $1/\alpha$ is greater than RC." Line 18: "τ_2 with a week" should read "τ_2 with two weeks."

J8, by H. Ekstein and T. Gilbert. Line 14: Replace $t_n = t_{d/6P}$ by $t_n = t_d/P$.

M6, by R. E. Marshak and A. S. Wightman. Line 2: "A. S. Whitman" should read "A. S. Wightman." Lines 13 and 14: $g^2/\hbar c$ should be equated to $0.25^{+0.2}_{-0.1}$ instead of $0.55^{+0.3}_{-0.1}$, and $g^2/\hbar c$ should be equated to $0.03^{+0.02}_{-0.01}$ instead of $0.07^{+0.04}_{-0.01}$.

M7, by Stephen Tamor. The next to last sentence should read: "For pseudoscalar mesons the radiative and non-radiative absorption probabilities are comparable."

O4, by John Sheridan and Walter Gordy. The moments of inertia should be 537.417×10^{-40} g/cm^2 and 541.121×10^{-40} g/cm^2.

O7, by Quitman Williams and Walter Gordy, "$678._1\times10^{-40}$ g/cm^2 and 683.7×10^{-40} g/cm^2" should read "672.5×10^{-40} g/cm^2 and 689.4×10^{-40} g/cm^2.

P2, by J. Brossel, P. Sagalyn, and F. Bitter. Footnotes should be added at the end of the abstract as follows: (a) M. H. L. Pryce, Phys. Rev. **77**, 136 (1950), and (b) J. Brossel and A. Kastler, Comptes Rendus **229**, 1213, (1949). These footnotes were present in the manuscript submitted by the authors but were removed by the editor to reduce the abstract to the stipulated length.

P3, by T. L. Collins. The value quoted for the magnetic moment of Sb^{121} is incorrect. Subsequently to submission of the abstract, the observed signal was identified as due to Cu^{63} in the metallic copper of the detector coil. The resonance due to Sb^{121} has been observed in agreement with Proctor (private communication).

R8, by A. H. Van Tuyl. Line 11: $\epsilon(1-\sigma)$ in place of ϵ. Line 12: $\epsilon(1-\sigma)^2$ in place of $\epsilon(1-\sigma)$. Line 13: $\epsilon(1-\sigma)^{5/2}$ in place of $\epsilon(1-\sigma)^2$. Line 19: $\epsilon(1-\sigma)$, $\epsilon(1-\sigma)^2$ in place of ϵ, $\epsilon(1-\sigma)$. Line 20: $\epsilon(1-\sigma)^{5/2}$ in place of $\epsilon(1-\sigma)^2$.

V2, by Joseph A. Bruner and Lawrence M. Langer. The first names of both authors were omitted from the abstract.

W10, by James Terrell. In line four, the reaction is $Be^9(\alpha n,\gamma)C^{12}$.

W13, by W. W. Buechner and D. M. Van Patter. Q-value, line 6, read: 9.232. Q-values, line 7, read: 7.091; 4.775; 2.480; 2.430; 1.935; 0.667; and 0.311 Mev. Q-value, line 15, read: 2.430 Mev. Q-value, line 16, read: 2.480 Mev.

Y6, by Robert Stump and Sherman Frankel. The title should read "$\beta-\gamma$-Angular Correlation Measurements." In footnote 2 "Carwin" should read "Garwin."

PROGRAMME

THURSDAY MORNING AT 10:00

Lisner Auditorium

(J. E. MAYER presiding)

Invited Papers

A1. High-speed Spectroscopic and Electron-Density Measurements on Gas-Discharge Plasmas. R. B. HOLT, *Harvard University.* (40 min.)

A2. Adsorption, Catalysis, and the Physics of Surfaces. H. S. TAYLOR, *Princeton University.* (40 min.)

A3. Recent Developments in Precision Mass-Spectroscopy and the Present Status of the Method of Magnetic Resonance. J. A. HIPPLE, *National Bureau of Standards.* (30 min.)

A4. Physical Aspects of Postwar Microwave Amplifiers. J. R. PIERCE, *Bell Telephone Laboratories.* (35 min.)

THURSDAY MORNING AT 10:00

Departmental Auditorium

(L. R. HAFSTAD presiding)

Fission; Nuclear Masses; Miscellany in Nuclear Physics

B1. Fission of Liquid Drop Nuclear Model. DAVID L. HILL, *Vanderbilt University.*—The computed trajectory of the liquid drop model undergoing fission will be discussed. Particular attention will be paid to an oscillatory motion which is spontaneously generated as the nuclear model departs from the critical form of unstable equilibrium and which causes a cyclic swelling and shrinking of the equatorial portion, coupled with pauses or even recessions in the elongation of the drop. Several cycles of this quadrupole oscillation are observed in each fission act and seem to accumulate energy from the primary fission mode. A dynamic instability of the elongating form is thus indicated; its possible contribution to the pronounced asymmetry of nuclear fission will be discussed. The asymmetric oscillations deriving from the zero-point excitation of the model and previously reported,* appear likewise to gather some energy as fission proceeds. The fact that a possible charged meson field may be expected to adjust to minimum energy rapidly in comparison with the adjustment of the inertial field suggests that preferred nucleon configurations in the nascent fragment nuclei may be readily formed, contributing to a possible early rupture of the nucleonic bonds at a transient constriction produced by the above mentioned ripples of the elongating form.

* A.P.S., New York meeting (February, 1950).

B2. Ionization Yields of Fission Fragments.* R. B. LEACHMAN, *Iowa State College.*—Ionization chamber measurements for fission fragments are difficult to interpret in terms of kinetic energies because the energy-ionization conversion ratio, w, is not accurately known. In order to determine the relative variation of w with fragment mass, a comparison has been made between fission fragment mass[1] and ionization distributions.[2] It appears that for the most probable mass ratio of U^{235} slow neutron fission the value of w for the light fragment is about three percent less than for the heavy fragment, which is in agreement with an estimate that about 6 Mev of kinetic energy is lost through nuclear collisions not producing ionization. In the course of this determination it is found that the total energy dispersion, which represents a combination of instrumental errors and recoil energy from neutron emission, has a distribution width at half-maximum of roughly 10½ Mev. This width is about one-half as large as the distribution width observed in the total energy for a fixed fission mass ratio.

* Work performed in the Ames Laboratory of the AEC.
[1] Plutonium Project, Rev. Mod. Phys. 18, 513 (1946).
[2] D. C. Brunton and G. C. Hanna, Phys. Rev. 75, 990 (1949).

B3. Ionization Yields of Heavy Particles.* J. K. KNIPP, *Iowa State College.*—A heavy particle which is stopped in a substance of about the same atomic number loses energy predominantly in nuclear collisions after its velocity falls below $(Z/20)^{\frac{1}{2}}e^2/\hbar$. Since the recoiling nuclei are of lower velocity and hence themselves lose energy predominantly to nuclei, this is a critical velocity below which ionization yields are relatively small. More generally, particle losses to atomic nuclei predominate below $(Z^{4/3}Z_a^{5/3}m/\mu)^{\frac{1}{2}}e^2/\hbar$, where μ/m is the reduced mass of particle and atom in units of the electron mass and Z and Z_a are the atomic numbers of particle and atom, respectively. For $Z<Z_a$ this is also the critical velocity and for $Z>Z_a$ it is very nearly so except for the extreme case in which the recoiling nuclei are on the average of sufficient velocity to be effective in ionization. The energy associated with the critical velocity is largely undetected in the usual ionization measurements.

* Work performed at the Ames Laboratory of the AEC.

B4. Delayed Neutrons From U^{238} and Th^{232} Fission.* K. H. SUN, R. A. CHARPIE, F. A. PECJAK, AND B. JENNINGS, *Westinghouse Research Laboratories,* AND J. F. NECHAJ AND A. J. ALLEN, *University of Pittsburgh.*—The half-lives of the delayed neutrons from U^{238} and Th^{232} fission were found to be 0.4, 1.7, 5.8, 22.6, and 55, and 0.4, 1.4, 4.4, 20, and 56 sec., respectively, by using fast neutrons from 15-Mev cyclotron deuterons on a thick carbon target. These may be compared

with 1.1, 4.5–5.2, 22.6, and 55–55.2 and 0.36–0.43, 1.1–1.8, 4.4–5.5, 22–23, and 55–56 sec. from slow neutron fission of Pu^{239} and U^{235}, respectively, found by various investigators.[1] Evidently the delayed neutron emitters from Pu^{239}, U^{235}, Th^{232}, and U^{238} fission are identical in the life region indicated. The delayed neutron yield after 300 sec. of bombardment was about eight per 100 fissions. A preliminary survey indicated that the 23- and 56-sec. half-lives were also present when LiF or B_4C instead of carbon was used as the cyclotron target for the neutron source.

* Assisted by the joint program of the AEC and ONR.
[1] E.g., Phys. Rev. **72**, 541, 570, 567 (1947); **73**, 111 (1948); **74**, 1330 (1948).

B5. Fission Excitation Functions for Charged Particles. J. JUNGERMAN, *University of California, Berkeley.**—Absolute fission excitation functions have been measured using an ionization chamber to detect the pulse of a recoiling single fragment. In the experiment performed using the 60-in. Crocker cyclotron deuterons and alpha-particles were used with Th^{232}, U^{235}, and U^{238} targets. Thresholds of these reactions were also observed. The maximum alpha-particle energy used was 33.5 Mev and the maximum deuteron energy was 17.5 Mev. Beam current was integrated using both a Faraday cup and an ionization chamber. The 184-in. synchrocyclotron was used to extend the fission excitation functions to alpha-particle energies of 390 Mev and deuteron energies of 193-Mev Bi^{209} and Au^{197} targets were also added. Preliminary results with protons of 340-Mev maximum energy will also be reported.

* Present address: Floyd Newman Laboratory of Nuclear Studies, Cornell University, Ithaca, New York.

B6. The $Ca^{40}-A^{40}$ Mass Difference and the Radioactivity of K^{40}.* T. R. ROBERTS AND ALFRED O. NIER, *University of Minnesota.*—The mass difference, $Ca^{40}-A^{40}$, has been measured as $(3.2\pm0.8)\times10^{-4}$ AMU by comparing the mass doublets $C_3^{13}H_4-Ca^{40}$ and $C_4^{13}H_4-A^{40}$ in a double-focusing mass spectrometer. This is to be compared with the value $(2.7\pm2.1)\times10^{-4}$ AMU obtained by Sailor[1] from disintegration data. The present results combined with 1.41 ± 0.02 and 1.54 ± 0.1 Mev for the end point of the beta-spectrum and gamma-ray, respectively, as given by Hirzel and Wäffler[2] indicate an excited state of A^{40} 0.17 ± 0.13 Mev below the ground state of K^{40}. This precludes positron emission to the excited state of A^{40}. A determination of the $K^{40}-A^{40}$ mass difference now under way will furnish additional independent data for making comparisons. The Ca^{40} and A^{40} packing fractions as found from the above doublets were -6.11 ± 0.02 and -6.19 ± 0.02, respectively.

* Supported by the joint program of the ONR and AEC.
[1] V. L. Sailor, Phys. Rev. **75**, 1836 (1949).
[2] O. Hirzel and H. Wäffler, Phys. Rev. **74**, 1553 (1948).

B7. Integral Relationships between Atomic and Nuclear Quantities. ENOS E. WITMER, *University of Pennsylvania.*—The writer has pointed out before that one-eleventh of the electron mass appears to be a natural unit for nuclear masses. Designating this unit *the prout*, the accurate data on light nuclei are in harmony with the idea that *the masses of all nuclei in the ground state, provided it is not subject to β-decay, are an integral number of prouts. Some of the nuclear masses excluded by this statement follow the integral rule.* In prouts the masses of the nuclei up to and including C^{12} contain an unusual number of powers of 2 as factors. Thus the neutron mass is $(2^8\times79)$ prouts. This may be significant. In a recent abstract the writer pointed out that the fundamental atomic constants may be calculated very accuretely from $R\infty$, N, and c and the assumptions that (hc/e^2) is 861 and (M_p/m) is 1836 exactly. It is interesting to note that the value of e obtained in this way, namely $(4.80290\pm0.00020)\times10^{-10}$ e.s.u., is in excellent agreement with the value calculated from a recent value of the Faraday,[1] namely $(4.80277\pm0.00080)\times10^{-10}$ e.s.u.

[1] Hipple, Sommer, and Thomas, Phys. Rev. **76**, 1877 (1949).

B8. Evidence from Nuclear Masses on Proposed Closed Shells at 20 Nucleons.* C. H. TOWNES AND W. LOW, *Columbia University.*—Microwave measurement of the mass differences $S^{34}-S^{36}$, $Cl^{35}-Cl^{37}$, and $Cl^{35}-Cl^{36}$ together with a series of nuclear reactions permit the evaluation of masses between $A=31$ and $A=43$ and with neutron numbers $N=17$ to $N=22$. Nuclear shell structure suggests that nuclei with 20 neutrons or 20 protons should be particularly stable and that after subtracting the odd-even mass variation a plot of the isotopic masses *versus* number of neutrons should show a change in slope at 20 neutrons. However, such plots for $Z=16$, 17, 18, and 19 show no difference in binding energy greater than ½ Mev between the 20th and 21st neutron due to shell structure. On the other hand, for $Z=20$ (Ca^{40}) this difference appears to be 3.5 Mev. Similarly there is no evidence of a closing of proton shells at 20 protons for various N's except in the case $N=20$ (Ca^{40}). Hence the shell which is expected to be closed at 20 particles does not produce a major change in binding energy, and is not simply connected with the well-known stability of Ca^{40}. The Ca^{40} binding appears rather to be peculiar to this nucleus instead of being due to the closing of shells at 20 nucleons.

* Work supported jointly by the Signal Corps and ONR.

B9. The Packing Fraction Curve in the Neighborhood of the Magic Number $n=50$.* HENRY E. DUCKWORTH, KARL S. WOODCOCK,† AND RICHARD S. PRESTON, *Wesleyan University.*—A large Dempster-type double-focusing mass spectrograph has been used to photograph the following doublets $C_2H_2-Pd^{104}$, $C_2H_3-Pd^{103}$, $C_2H_2-Cr^{52}$, $C_2H_3-Fe^{54}$, $Cr^{52}-Pd^{104}$, $Fe^{54}-Pd^{108}$, CH_3-Si^{30}, $Si^{30}-Zr^{90}$, C_2-Mo^{96}, and C_2H-Mo^{100}. Precision masses, obtained from the measurement of these photographs, will be reported for Zr^{90} (50 neutrons), Mo^{96} (54 neutrons), Mo^{100} (58 neutrons), Pd^{104} (58 neutrons), and Pd^{108} (62 neutrons). Preliminary measurements from these photographs, made at the time of the writing of this abstract, indicate a sudden break in the packing fraction curve at, or in the neighborhood of, Zr^{90}. Photographs of typical doublets will be shown.

* This work was supported by the AEC.
† On leave from Bates College.

B10. A Technique for Measuring Meson Production Cross Sections in the Forward Direction.* H. A. WILCOX, W. F. CARTWRIGHT, C. RICHMAN, AND M. N. WHITEHEAD, *University of California, Berkeley.*—In a previous communication[1] a method was described for measuring the positive and negative π-meson production cross sections of various nuclei when bombarded by 345-Mev protons in the external beam of the synchro-cyclotron. The method was successfully applied to mesons produced at 90° to the beam in carbon[1] and in lead.[2] For observations in the extreme forward direction, however, the heavy proton background has made it necessary to extend this technique by introducing a magnetic field in the region about the target. Negative mesons are deflected in this field to one side and positive mesons and protons are deflected to the other. Curved channels in large shielding blocks are arranged so as to select roughly equimomenta particles which then enter and stop in absorber blocks containing embedded nuclear emulsions. A complete spatial separation is obtained between the protons and the positive mesons since the mesons penetrate much more deeply into these blocks than do the heavier protons having the same momenta. Preliminary results on the

forward production from carbon and hydrogen will be presented.

* This work was supported by the AEC.
[1] C. Richman and H. A. Wilcox, Phys. Rev. (to be published).
[2] M. Weissbluth, Phys. Rev. (to be published).

B11. Energy Loss of Million-Volt Electrons. ROBERT D. BIRKHOFF,* EARL E. HAYS,† AND S. A. GOUDSMIT,† *Northwestern University.*—A line source of a beta-active substance was placed parallel to the lines of force in a vertical homogeneous magnetic field. The electrons were restricted by baffles to move along helical paths of 10.75 to 11.25 cm radius. Thin foils were placed in their path at 180° from the source. The displacement of the linear focus at 360° was measured photographically and with counters. A counter was placed 12.8 cm below the source along the lines of force. It could be moved radially and the position of maximum intensity was observed. These measurements give the most probable, rather than the usual, average energy loss. By varying the field, the kinetic energy of the selected electrons was varied from 0.25 to 1.5 Mev. The following foils were used: Be (16.0 mg/cm²), Al (4.7, 14.0, and 37.0 mg/cm²), Ag (5.35 and 10.5 mg/cm²), Ta (10.0 mg/cm²). Comparison with the theory of Landau for the most probable energy loss shows reasonable agreement. Facilities of Argonne National Laboratory were kindly put at our disposal for this work.

* Now at the University of Tennessee, Knoxville, Tennessee.
† Now at Brookhaven National Laboratory, Upton, Long Island, New York.

B12. Search for Gamma-Rays from Nuclei Exposed to Synchrotron Radiation.* J. C. KECK, M. STEARNS, AND R. R. WILSON, *Cornell University.*—An investigation is being made of the production of energetic gamma-rays by nuclei in the photon beam of the synchrotron. Two scintillation counters so placed that the beam passes between them are used as the energy sensitive detectors. The counters consist of activated NaI crystals, each 4 cm in diameter and 5 cm long, facing photo-multiplier tubes. The crystals can be surrounded by 2 r.l. of lead to increase the efficiency at high energies. By adjusting a discriminator bias, the energy threshold can be changed from about 10 to 100 Mev. Calibration has been made against the γ-rays of Co, Th C″, and the Li(p,γ) reaction. A pulsed light source is used to extend the calibration to higher energies. Good collimation of the primary γ-ray beam results in very low backgrounds at large angles. Individual counts, coincidences, and delayed coincidences (assumed casuals) are recorded. Preliminary measurements at 220 Mev indicate that the cross section for emission of energetic gamma-rays in coincidences from Be is $<10^{-29}$ cm² per nucleus per photon per logarithmic energy interval. More sensitive measurements extending to higher energies are in progress. Single high energy particles are observed but positive identification has not been made.

* Supported by ONR.

B13. Coincidence Efficiency of Gamma-Rays. J. M. BARNOTHY AND M. FORRO, *Barat College.*—Several years ago the authors[1] found at great depth a scarcely ionizing radiation of local origin. Later measurements[2] were also not able to settle definitely the question whether this local radiation is a decay product of the penetrating cosmic radiation, or the gamma-radiation of the surrounding materials. To clear this point, investigations were carried out to determine the dependency of the coincidence efficiency of gamma-rays from the energy of the gamma-rays, from the aperture of the coincidence equipment, from the material and wall thickness of the G-M counters, and from the circumstance that the gamma-ray source emits one or two gamma-rays simultaneously. The experiments were sponsored by a grant of Research Corporation.

[1] J. Barnothy and M. Forro, Phys. Rev. **55**, 870 (1939).
[2] J. Barnothy and M. Forro, Phys. Rev. **74**, 1300 (1948) and Miesowicz Jurkiewicz, and Massalski, Phys. Rev. **77**, 380 (1950).

THURSDAY MORNING AT 10:00

National Academy

(E. P. WIGNER presiding)

Theoretical Physics

C1. Effect of a Finite Groundplane on Antenna Radiation.* ALFRED LEITNER, *New York University* AND R. D. SPENCE, *Michigan State College.*—The field of a quarter-wave dipole antenna over a circular groundplane is calculated exactly. The Green's function is represented in terms of the oblate spheroidal wave functions, and satisfies approximate boundary conditions on the conducting circular disk of zero thickness and radius a. Thus both the current on the groundplane and the radiation at large distances are found. (Alternatively, one may calculate the current on the groundplane by applying the reciprocity theorem, after Papas and King.[1]) As a is increased, the radiation resistance and the surface current oscillate about the values which characterize a quarter-wave antenna above an infinite groundplane. The radiation pattern, however, is entirely different. The results are in good quantitative agreement with those of recent experiments by Meier and Summers.[2]

* Supported in part by Geophysical Research Directorate, Air Force Cambridge Research Laboratories, A. M. C.
[1] Papas and King, J. App. Phys. **19**, 808 (1948).
[2] Meier and Summers, Proc. I. R. E. **37**, 609 (1949).

C2. Finite Wiener-Hopf Equations. RICHARD LATTER, *Rand Corporation.*—The Wiener-Hopf technique has been applied to obtain solutions for a class of integral equations of the form:

$$\text{(i)} \quad f(x)=\lambda\int_0^a dy K(x-y)f(y)$$

$$\text{(ii)} \quad f(x)=g(x)+\lambda\int_0^a dy K(x-y)f(y).$$

Solutions have been obtained for those cases in which the Generalized Fourier transform* of the kernel $K(x)$ has no essential singularities or branch points. A general class of kernels consistent with these conditions is that in which $K(x)$ is a sum of polynomials times exponentials. The more important problems wherein the transform of the kernel has essential singularities or branch points (as for diffraction by a finite slit or diffusion through a finite slab) have not yet been solved.

* Titchmarsh, Fourier Integrals.

C3. Quantum Mechanical Resonance between Identical Big Molecules. HERBERT JEHLE, *University of Nebraska.*—A macromolecule which has a rigid structure will perform thermally excited vibrations of the type of an orchestra. This term is meant to imply that the molecule has several commensurable modes which, due to anharmonic terms in the vibrators' potential energy, are coupled. In correspondence terms this coupling causes statistically preferred phase relations in between the phases of the modes. A pair of molecules will interact with each other through their vibrating electric dipole moments. If the molecules are identical, both molecules prefer to perform the same phase-related vibration and will then interact very strongly. They will tend to orient themselves so that they are parallel in the z direction and antiparallel in the x and y directions. Some simplified models of this situation have been calculated by straightforward quantum mechanics. The previous qualitative correspondence arguments are justified by the quantum mechanical calculations. This attractive interaction is seen to be a quantum effect proportional to R^{-7} whose essential features are given by first-order perturbation theory; the second-order theory brings out the relation to Londons dispersion forces. Self-duplication of genes and viruses depends on this attraction which is very specific, depending on identical structures.

C4. On the Theory of Van der Waals Forces. FRANKLIN C. BROOKS, *Yale University.*—The usual method of calculating Van der Waals forces employs the classical electrostatic interaction energy between the molecules as a perturbation on the unperturbed state of the compound system. The shift in energy caused by this interaction is evaluated using the Schrödinger perturbation theory or the variation method. For this purpose the interaction is frequently expanded in inverse powers of the internuclear distance, R. This expansion does not converge everywhere in the configuration space of the compound system, and its use causes the Van der Waals energies, expressed as a series in inverse powers of R, to be divergent for all values of R. These series are, in fact, asymptotic in the sense of Poincaré to the true interaction. As such they are satisfactory for determining the true interaction at large internuclear distances providing they are cut off after an appropriate number of terms. For small R, however, they greatly overestimate the true polarization force. At intermediate values of R, for instance the position of the Van der Waals minimum in helium, a rough calculation of the maximum possible error caused by the use of the divergent expansion gives an upper bound for the helium atom interaction energy curve which is in good (although perhaps accidental) agreement with recent low temperature determinations.

C5. On the Notion of Pressure in a Canonical Ensemble. R. J. RIDDELL, JR., *University of Michigan.*—A discussion will be given with regard to a recent controversy between J. de Boer[1] and H. S. Green[2] concerning the notion of pressure in a canonical ensemble. The question is whether the pressure as derived from the partition function (thermodynamic pressure) is always identical with the "kinetic" pressure as derived from the virial theorem. De Boer's answer is in the affirmative, and we will confirm his view. The origin of the discrepancy which Green finds between the kinetic and the thermodynamic pressure lies, in our opinion, in the treatment of the boundary conditions due to the potential of the wall of the vessel in which the system is enclosed. Green (and also de Boer) represents the vessel by a sudden infinite potential jump, and it is well known that with such potentials the formulas of the transformation theory have to be used with caution.

[1] J. de Boer, Physica **XV**, 843 (1949).
[2] H. S. Green, Physica **XV**, 882 (1949).

C6. Irreversibility and the Statistical Mechanical Derivation of the Equations of Hydrodynamics. JOHN M. RICHARDSON, *Bureau of Mines.*—A general classical theory of irreversible processes recently developed by the author is applied here to the derivation of the hydrodynamical equations of a one-component system involving pair interactions between spherical molecules. The first step is to define functions of coordinates and momenta which, when averaged, will be densities of mass, momentum, and momentum-momentum, respectively. The general theory requires that mass density in pair-space be considered in addition to that in ordinary space in order that the Hamiltonian can be represented as a linear superposition of the observables. Exact expressions for the time derivatives of the above observables are obtained. Certain approximations are applied to reduce these to the familiar form of the hydrodynamical equations. However, the results thus obtained are completely non-statistical and, even after ensemble averaging, leave no room for dissipation and irreversibility. According to the general theory, irreversibility is appropriately treated in a manner automatically satisfying the second law if the time derivatives of the observables are replaced by finite differences over a certain interval τ (of sufficient duration to establish approximate equilibrium with respect to degree of freedom not defined by the observables). Then the resulting expressions are ensemble averaged with a "coarse-grained" phase density equal to an exponential function of a linear combination of observables.

C7. Removal of Degeneracy in Any Order. MELVIN LAX, *Syracuse University.*—The vanishing (or small) energy denominators in a conventional perturbation expansion associated with exactly (or approximately) degenerate states may be avoided by treating perturbation-wise only the part of the interaction matrix V not involving these states in *either* index. If P is a projection operator selecting the subspace of hilbert space associated with the degenerate states and $Q=1-P$ the Schrödinger equation $(E-H)\Psi=(P+Q)V(P+Q)\Psi$ may be split into a pair: $(E-H-QVQ)(Q\Psi)=QV(P\Psi)$ and $(E-H-PVP)(P\Psi)=PV(Q\Psi)$. The "external" wave function $(Q\Psi)$ may be eliminated in favor of $(P\Psi)$ the part of Ψ appropriate to the degeneracy box: $(Q\Psi)=(QS)(P\Psi)$ where $(QS)=[1-(E-H)^{-1}QVQ]^{-1}(E-H)^{-1}QV$. The resulting equation for the exact "starting approximation" is $(E-H-PKP)(P\Psi)=0$ where $K=V+VQS$. Thus the energy levels, and the correct linear combinations $(P\Psi)$ of (almost) degenerate states are obtained by diagonalizing $H+PKP$, i.e., solving a finite set of linear equations. K and QS are equivalent to the usual perturbation expansions for energy and wave function with all degenerate indices removed from the summations. This procedure has the advantage (1) that any group of states, possibly non-degenerate, may be treated in semi-exact fashion. (2) Only one secular change of base need be made regardless of the order of accuracy desired.

C8. The Uncertainty Principle for an Arbitrary Number of Variables. RONALD L. REED AND M. DRESDEN, *University of Kansas.*—For two variables the uncertainty principle is an immediate formal consequence of Schwartz' inequality. A similar derivation for an arbitrary number of variables requires a generalization of this inequality. To obtain this one utilizes the known expression of the Schwartz inequality for two vectors in a space, which itself is the direct sum of a countable number of identical unitary spaces. The resulting inequality is

$$|\Sigma_i (f_i, g_i)|^2 \leqslant \Sigma_{ij} \|f_i\|^2 \|g_j\|^2.$$

Here f_i and g_i are vectors in a unitary space. If now R_i and S_i represent a set of observables as well as their corresponding Hermitean operators, it is possible to deduce from this inequality, the uncertainty principle for an arbitrary number of variables

$$\Sigma_{ij} (\Delta R_i)^2 (\Delta S_j)^2 \geqslant [\Sigma_i \tfrac{1}{2}\langle [R_i, S_i]_+ \rangle_{Av} - \bar{R}_i \bar{S}_i]^2 - \tfrac{1}{4}[\Sigma_i \langle [R_i, S_i]_- \rangle_{Av}]^2.$$

It is interesting to observe that in general the lower limit will depend explicitly on the state of the system. This will be exemplified by applying this inequality to a system consisting of an infinite set of oscillators.

C9. On the Role of the Subsidiary Condition in Quantum Electrodynamics. F. COESTER AND J. M. JAUCH, *The State University of Iowa.*—The S-matrix in quantum electrodynamics may be calculated alternatively from the Hamiltonian density $-j^{\mu}(x)A_{\mu}(x)$ and a Hamiltonian in which the Coulomb interaction of the charges and the interaction of the currents with the transverse field are separated. Both procedures lead to identical S-matrices if proper care is taken in defining the initial state, in particular the initial vacuum state. It is essential that the initial state is taken at the time $\tau=-\infty$. Only then is the definition of the vacuum state the same in both representations.

C10. Conservation Laws in Einstein's Theory of Gravitation with Electromagnetic Field.* ROBERT PENFIELD AND HENRY ZATZKIS, *Syracuse University.*—In a fully covariant theory, the energy and momentum contained in a three-dimensional domain can always be converted into an integral over its two-dimensional surface. This representation is particularly important when the domain contains singularities; it is analogous to the surface integral over **D** in Maxwell's theory that measures the amount of charge inside. Freud[1] has given the correct integrands for the purely gravitational case. We have added to Freud's expressions the contributions of the electromagnetic field, so that we are able to determine the energy and the linear momentum associated with a system of charged mass points. These expressions obey conservation laws in every possible coordinate system and gauge frame in that their rates of change are determined by flux expressions through the bounding surface. But they are not covariant quantities: Under certain conditions all components may vanish in one coordinate system, but not in another. As an illustration, we have computed the total energy of a Schwarzchild singularity with electric charge at rest in two different coordinate systems; the two results differ significantly.

* Supported by ONR.

[1] Ph. v. Freud, Annals of Mathematics **40**, 417 (1939).

C11. Equations of Motion in the Covariant Canonical Formulism.* PETER G. BERGMANN, ROBERT PENFIELD, RALPH SCHILLER, AND HENRY ZATZKIS, *Syracuse University.*—Using the expression for the Hamiltonian of the General Theory of Relativity presented at the New York meeting, we have derived the expression for the rate of change of linear momentum for a field singularity corresponding to an electrically charged mass point, i.e., the "force" acting on it. The mass and the linear momentum are defined as the surface integrals described in the preceding abstract. At a time t_0 the field variables and the momentum densities must be chosen so that all the constraints between them are satisfied. Then the canonical equations determine uniquely the values of all time derivatives of finite order of any dynamical variable, including integrals. The calculations are lengthy, but lead to the desired result, showing that the force is the combined electrostatic and gravitational force. This derivation leads to rigorous expressions insofar as nowhere do we introduce power series expansions in c^{-2}. Otherwise, our method is equivalent to that of Einstein, Infeld, and Hoffman.

* Supported by ONR.

C12. Gravitational Radiation and Motion. A. E. SCHEIDEGGER AND L. INFELD, *University of Toronto.*—It is known[1] that one can set up an approximation procedure for obtaining the equations of motion from the field equations in relativity theory. In such a scheme there is an ambiguity which can be restricted by choosing a set of co-ordinate conditions. Changing those co-ordinate conditions alters the equations of motion. We show that there exist co-ordinate transformations which change the usual equations of motion of (1) into equations whose analogues in linear theories describe radiation damping. Conversely, all relativistic radiation damping effects hitherto calculated are shown to be due to a particular choice of the co-ordinate system. They have no physical meaning if the approximation procedure is adopted. Furthermore, we show that it is always possible to find such a co-ordinate system that the form of the equations of motion is Newtonian. Then, the relativistic effects are described by the metric field alone. This yields a new version of the approximation method where co-ordinate transformations play the same role as dipoles in (1) toward the vanishing of certain surface integrals and the fulfilment of the integrability conditions.

[1] A. Einstein and L. Infeld, Can. J. Math. **1**, 209 (1949).

C13. Stability of Systems and General Principles. ROBERT E. BASS, *University of Toledo.*—The earth's velocity and position at any time are so that from these conditions and from laws connecting cause and effect ("causal laws") continued existence of the orbit follows; Newton remarked that the stars have such mutual distances that they will not collide;—Einstein[1] rejected the hypothesis that the stellar universe is a finite island in infinite space, since such an island would irretrievably lose energy. Such highly differentiated systems as the solar system, star systems, and the stellar universe are "stable" which means they are fit for continued existence. This property is rooted in simultaneously existing conditions which have, in some cases, been proved to follow from certain earlier simultaneous conditions. Fitness for continued existence involves a relation between simultaneous facts. Causal laws alone cannot establish such a relation. Such fitness contains, therefore, an element irreducible to causal laws and is, in this sense, a basic property. In the author's view this result applies to the whole of nature, also to fitness for continued existence of single organisms, species, and life as a whole.

[1] A. Einstein, *Relativity* (New York, 1921), p. 169.

C14. Self-Energy of Moving Free Electron. F. J. BELINFANTE, *Purdue University.*—Assuming that integration over angles gives $\int d^3\mathbf{k}(\boldsymbol{\alpha}\cdot\mathbf{k})/k^3=0$, French and Weisskopf proved that the free-electron self-energy S calculated separating longitudinal electromagnetic fields equals the self-energy C obtained using a quantized covariant potential four-vector. Umezawa and Kawabe[1] recently defined a covariant cut-off enabling them to obtain by ordinary perturbation theory Schwinger's expression for the **C**-self-energy of a free moving electron $C=(3\ln Z-\frac{1}{2})K\beta$ with $2\pi K=(e^2/\hbar c)mc^2$ and $mc^2Z=$cut-off in electron rest-system for (cp_i+E_i) of electronic intermediate state. Using the same method we find for the **S**-self-energy $S=C+T-(K/3mc)(\boldsymbol{\alpha}\cdot\mathbf{p})$ with $T=[p^2\beta-mc(\boldsymbol{\alpha}\cdot\mathbf{p})]\cdot f(p)=0$. This apparent discrepancy with French and Weisskopf's result is due to $S-C=(-e^2/4\pi^3)\int d^3\mathbf{k}(\boldsymbol{\alpha}\cdot\mathbf{k})/k=(-e^2/6\pi\hbar)(\boldsymbol{\alpha}\cdot\mathbf{p})\neq 0$ by this cut-off method. After formal "mass-renormalization" this leaves in the **S**-theory a small finite negative "self-energy of motion" of a free moving electron $S-C\approx(-1/1291)(mv^2/2)(1-v^2/c^2)^{-\frac{1}{2}}$.

[1] H. Umezawa and R. Kawabe, Prog. Theor. Phys. **4**, 420, 461 (1949).

THURSDAY MORNING AT 10:00

National Bureau of Standards

East Building Lecture Room

(F. SEITZ presiding)

Miscellany in Solid-State Physics

D1. The Heat Capacity of Liquid Mercury between 0° and 450°C. T. B. DOUGLAS, ANNE F. BALL, AND D. C. GINNINGS, *National Bureau of Standards* (Introduced by F. G. Brickwedde).—Using an improved ice calorimeter and furnace, the enthalpy referred to 0°C of a sample of highly purified mercury has been measured by a drop method at nine temperatures between 0° and 450°C (up to a saturation pressure of approximately five atmospheres). The precision obtained is equivalent to an average probable error of the mean relative enthalpy for a given temperature in this range of 0.02 percent. A check on the accuracy of the method was afforded by measuring the enthalpy of water between 0° and 250°, with a variation of 0.02 percent from the precise value obtained earlier in this laboratory by use of an adiabatic calorimeter. Values of entropy and specific heat were derived from the data. The probable uncertainty in the values of heat capacity, estimated to be less than 0.3 percent, is much smaller at the higher temperatures than the wide discrepancies among the results of the earlier workers who measured mercury. As has been found in this laboratory analogously for liquid sodium and potassium, mercury shows a shallow but definite minimum in its specific heat (C_p), as a function of temperature, somewhat below its normal boiling point.

D2. The Heat Capacity of Sodium between 0° and 900°C. D. C. GINNINGS, T. B. DOUGLAS, AND A. F. BALL, *National Bureau of Standards* (Introduced by F. G. Brickwedde).—In the measurements of heat capacities at high temperatures by the drop method, the furnace and ice calorimeter have been improved to give more accurate results with easier manipulation. The enthalpy of sodium has been measured from 0° to 900°C, and values of heat capacity and entropy have been derived. Liquid sodium was found to have a minimum heat capacity at about 600°C, in agreement with current theories that the metal does not acquire complete randomness on melting.

D3. Effect of Heat Treatment on the Electrical Properties of Platinum. ROBERT J. CORRUCCINI, *National Bureau of Standards* (Introduced by R. E. Wilson).—The average temperature coefficient of resistance over the interval 0° to 100°C, α, and the thermal e.m.f. are often used as criteria of the purity or freedom from strain of platinum. Ordinarily, both increase of purity and relief of strain (by annealing) result in increase of coefficient of resistance and decrease of thermal e.m.f. towards limiting values of, respectively, $\alpha=0.003927$ and $E_{0°}^{1200°}=-10$ microvolts (referred to Pt27, the platinum thermoelectric standard of the NBS). The relation between α and E for annealed samples of platinum of various degrees of purity has been found to be

$$\alpha=0.003922-0.5\times10^{-6}E_{0°}^{1200°} \text{ (vs. Pt27)}$$

provided the impurity, gold, is absent. In the present investigation it was found that quenching pure platinum wires from a temperature of 1450°C in various gaseous media caused a decrease in α and an increase in E relative to the annealed condition, the changes being greater, the more rapid the cooling of the wires. The effect, which is analogous to a strain, was removed by annealing at 500°C or above, followed by slow cooling. The relation between α and E for samples of pure platinum quenched at various rates was the same as the relation given above for variation due to impurity.

D4. On the Theory of Beta-Brass Structure. LOUIS GOLD, *University of Colorado.*—It is generally believed that beta-brass has the CsCl-type structure.[1] Studies of the order-disorder process in the alloy Cu Zn have been handicapped by the well-known limitation imposed by the similar x-ray scattering powers of the two elements[2] so that it has not been possible to estimate the degree of long range order at specified temperatures. The present paper is intended to show that on the basis of extant data it is reasonable to formulate a structure whose space group is O_h^5-$Fm3m$. There are two major consequences of the hypothesized structure: first, the superlattice lines ordinarily related to the ordered position of the copper and zinc atoms in the CsCl structure are associated with superlattice lines in the new structure which vanish for either complete order or disorder, and second, a new set of lines arise which have no analog in the conventional beta-brass structure. These lines having $\Sigma H^2=3, 11, 19, 27$—etc., do not conform to the transformation $4\Sigma h^2=\Sigma H^2$ between the two possible structures. Further experimental investigations are needed to resolve the situation.

[1] F. W. Jones and C. Sykes, Proc. Roy. Soc. **161**, 440–446 (1937).
[2] B. E. Warren and D. Chipman, Phys. Rev. **75**, 1629 (1949).

D5. A Dislocation Model of a Kink Band.* J. S. KOEHLER AND E. SALKOVITZ, *Carnegie Institute of Technology.*—Single crystals of hexagonal metals with a c/a ratio exceeding 1.732 can be deformed in compression by kinking providing the basal plane is nearly parallel to the specimen axis. In kinking a certain portion of the length of the specimen rotates about an axis in the basal plane and perpendicular to the slip direction which lies nearly along the specimen axis.[1] Ballistic pendulum measurements on pure zinc cylinders of dimensions 3 cm by 0.6 cm give the length of the kink to be from 0.1 cm to 0.6 cm, the angle of rotation to be from 6° to 14°, and the energy absorbed during kinking to be from 1 to 10×10^5 ergs. The rotated portion of the sample can be made to fit onto the undeformed ends by supposing that the interface contains a large number of edge type dislocations.[1] A theoretical calculation of the interface energy shows that the parallel line dislocations are not uniformly spaced on the interface. Instead they occur in clusters separated by 2 microns; each cluster contains about 1500 dislocations.

* This research was supported in part by ONR Contract.
[1] J. B. Hess and C. S. Barrett, Metals **1**, 599 (1949).

D6. Techniques for Measuring Sound Velocities and Elastic Constants. HENRY L. LAQUER AND WILLIAM E. MCGEE, *Los Alamos Scientific Laboratory.*—Resonance and pulse techniques for the measurement of the velocity of longitudinal and transverse sound waves in solid materials are described. The effects of various factors on the accuracy of the results are evaluated. With specimens of relatively low internal friction, such as most metals, the resonance technique offers precisions of 1 part in 10,000 or better, and is hence most suitable for the determination of the temperature coefficients.

The disadvantages of the resonance technique are that the cylindrical specimens have to be machined accurately, that the surface condition may affect the observed resonance frequencies, and that the methods of producing and observing resonance are somewhat involved. If Radar timing techniques can be taken for granted, the pulse technique is simple, fast and direct. The specimens need to have only two plane and parallel surfaces; however, the maximum pulse frequency is limited in polycrystalline materials and this in turn limits the precision to about 1 part in 2000. This is unfortunate since it is the only technique presently available for use with most plastics and for work on pressure coefficients using liquid pressure systems.

D7. The Structure of Lead Sulfide Films. J. DOUGHTY, K. LARK-HOROVITZ, L. M. ROTH, AND B. SHAPIRO, *Purdue University.*—Films of lead-sulfide, lead-selenide, and lead-telluride obtained by evaporation of the compound onto glass, mica or quartz, and lead-sulfide deposited on the same surfaces from solutions were investigated with x-rays, electron diffraction, and electron-microscope. X-ray diffraction patterns of the freshly deposited lead-sulfide, as well as lead-sulfide films heat treated in air, correspond primarily to PbS, whereas the electron diffraction pattern of the heat treated material corresponds primarily to Lanarkite ($PbO \cdot PbSO_4$). The orientation of the crystallites and their size varies with the type of substrate, the temperature of deposition, and heat treatment of the deposit. Formvar replicas can be made without impairing the light sensitivity of the treated films. Crystal size determined with the electron-microscope varies from $0.1\mu - 1\mu$, the larger crystallites showing well-developed edges. High resistance films show large isolated crystals with a smooth substrate in between. Films of lead-sulfide deposited from solution on Formvar show, also with x-rays additional lines besides PbS (probably $PbO \cdot PbSO_4$).

D8. Temperature Variation of Properties of Photo-Sensitive Lead Sulfide Films.* RAYMOND H. MCFEE, *Photoswitch Incorporated.*—Measurements have been made of dark current, photo-current and noise as functions of temperature between 90°K and 300°K of several typical sensitive lead sulfide cells. Response to 200°C black body radiation both unmodulated and modulated at 90 c.p.s. was measured by means of a special cooling system and high impedance input preamplifier. Dark currents show decrease of four orders of magnitude at 90°K relative to values at 300°K. Photocurrents are roughly constant at higher temperatures and become proportional to dark currents at low temperatures. Sensitivity, defined as the ratio of photo-current to dark current increases with decreasing temperature in some cases by a factor of a thousand over this temperature range. Response to 90 c.p.s. modulated radiation falls off below 180°K due to increase in time constant. Maximum signal-to-noise for this frequency occurs at around 180°K.

* Work performed under contract with the Air Materiel Command.

D9. Hydrogen Bond Energy from A.C. Conduction Data on Ice. E. J. MURPHY, *Bell Telephone Laboratories.*—The a.c. conductivity of ice approaches a limit value as the frequency increases. The limit value may be described as a polarization conductivity or local conductivity of the material because it characterizes the process of forming the polarization and depends upon local mobility rather than upon migration. This local conductivity is an exponential function of the reciprocal of the absolute temperature from which an activation energy can be calculated. Its value for ice is 11.5 kcal./mole. This is in agreement with the heat of sublimation of ice, 11.5 kcal./mole, as calculated by Bernal and Fowler and with the experimental value 11.8. Taking the process of activation as requiring the breaking of two hydrogen bonds, we obtain for the energy per bond 5.75 kcal./mole (or 0.5 electron-volt). This is a determination of the hydrogen bond energy (with an accuracy estimated to be at best ± 0.1 kcal.) from radiofrequency measurements of dielectric properties. It agrees with the value 5.8 ± 0.2 kcal./mole derived from the heat of sublimation of ice by Fox and Martin.

D10. A Phase Transition due to Dipole Interaction in a Simple Cubic Crystal.* JOHN S. THOMSEN AND T. H. BERLIN, *The Johns Hopkins University.*—A simple cubic crystal model with classical dipoles at each lattice point is investigated. The interaction matrix is set up and diagonalized, and an approximate partition function is evaluated by the technique of "sphericalization." This shows a phase transition at a finite temperature. This transition must represent a change from the non-magnetic state to an antiferromagnetic state. (It is noted that one- and two-dimensional models do not exhibit any such transition.) It is hoped that calculations can be made for the internal field in this model.

* Supported by the ONR.

D11. The Effect of Pressure on the Low Frequency Dielectric Constant of Ionic Crystals. SUMNER MAYBURG, *University of Chicago.*—The effect of hydrostatic pressure on the dielectric constant ϵ of MgO, LiF, NaCl, KCl, and KBr at 1000 c.p.s. and room temperature has been investigated to 8000 bars. The dielectric constants were determined from capacity measurement on single crystal slabs. The dielectric constant of these materials decreases linearly with pressure with slopes $\partial \ln\epsilon/\partial p$ of -0.32, -0.45, -0.98, -1.03, and -1.17×10^{-5} bar^{-1} respectively. The observed decrease of the dielectric constant can be qualitatively explained as being caused by the increase, at high pressure, in the resorting forces in the lattice which resist the action of an electric field in its attempt to displace the lattice of positive ions with respect to the lattice of negative ions. Consequently, the lattice polarizability decreases and, in fact, changes enough to outweigh the effect of density changes which tend to increase the dielectric constant. The change of lattice polarizability with pressure can be calculated and it is not found sufficient to explain the observed decrease in dielectric constant. The data can be explained if the inner field decreases with increasing pressure. This concept is consistent with the picture of Mott and Littleton.[1]

[1] N. F. Mott and R. W. Gurney, *Electronic Processes in Ionic Crystals* (Oxford University Press, New York, 1940), Chapter 1.

D12. Vector Functions for Uniform Spheres and Spherical Shells.* DOROTHY WRINCH, *Smith College.*—Let $g(r)$ represent a uniform sphere of radius a and density m from which a smaller concentric sphere of radius b and density n has been deleted and $T(R)$ the Fourier transform. The corresponding vector function $g_v(r)$ is then[1] the Fourier transform of $T^2(R)$ and it follows that

$$12g_v(r)/\pi = m^2(2a-r)^2(r+4a) + n^2(2b-r)^2(r+4b) - 2mn\{16b^3,(a+b-r)^2[r+2(a+b)-3(a-b)^2/r]\},$$

the various functions being taken from $r-0$ to $2a$, $r-0$ to $2b$, $r-0$ to $a-b$, and $r-a-b$ to $a-b$. It has already been shown[2] that the vector function for a crystal may be obtained from the vector function of the crystal reduced to any level, by suitably adjusting its level. Hence the result given for $g_v(r)$ yields the vector map of a crystal comprising a uniform sphere or shell of any densities repeated with any displacements in any constant medium. The bearing of this result on vector maps of hydrated protein crystals will be discussed.

* This work is supported by the ONR.
[1] D. Wrinch, Nature **137**, 226 (1946).
[2] D. Wrinch, Phil. Mag. **27**, 490 (1939).

D13. The Crystal Structure Problem. H. HAUPTMAN AND J. KARLE, *Naval Research Laboratory.*—A complete set of inequalities in the crystal structure factors based on the positiveness of the electron distribution function has been derived.[1] The relation between these inequalities and the equalities which result from the limiting case of the point atom approximation has been studied from the point of view of a set of algebraic equations. The equalities afford a basis for adjusting the observed magnitudes of the crystal structure factors which are known only approximately from experiment. The complex structure factors are also determined. In addition, the solution of the set of algebraic equations permits an evaluation of the coordinates of the atoms in a unit cell in terms of the observed magnitudes. This contrasts with Avrami's[2] formal solution to the problem which requires an exact knowledge of many more magnitudes than are usually determined.

[1] J. Karle and H. Hauptman, Acta Cryst. 3, 181 (1950).
[2] M. Avrami, Phys. Rev. 54, 300 (1938).

THURSDAY MORNING AT 10:15

Department of Commerce Auditorium

(E. P. NEY presiding)

Cosmic Rays. I

E1. Monte Carlo Calculations of Showers in Lead. ROBERT R. WILSON, *Cornell University.*—The Monte Carlo method has been applied to the calculation of showers in lead. The initial electron or photon and all degraded radiation are followed through successive distance intervals (0.2 radiation length). At each interval, the radiation or electron production is determined by spinning a wheel of chance. A graph is made for each shower showing the energy-distance history of the initial and secondary particles. From a few hundred such graphs, prepared for each kind of shower, pertinent averages can be taken. Calculations have been completed for 50-, 100-, 200-, and 300-Mev electron- and photon-initiated showers. The results, which differ significantly from those of Arley and from those given by standard shower theory, will be presented. The range and straggling of individual electrons in lead from 10 to 1000 Mev have also been calculated both analytically and by the above method. The mean range in radiation lengths is $\ln 2 \ln(\beta+E/\beta \ln 2)$ when E and β are the energy and critical energy in Mev. The calculations are being extended to include effects due to multiple scattering. On the basis of the above work, a high efficiency gamma-ray detector with a reasonably sharp high energy threshold has been developed.

E2. On Penetrating Showers and Meson Production.* K. SITTE, *Syracuse University.*—The local production of penetrating showers, both by single penetrating particles and by air shower particles, has been studied at an altitude of 3260 m. From the results, the following conclusions can be drawn: (1) The production in a nuclear collision of a shower containing several penetrating particles becomes probable only at very large primary energies. (2) For smaller primary energies, collisions result predominantly in the ejection of a small number of "knock-on nucleons." (3) The processes in which, directly or indirectly, electrons are released in nuclear collisions are either infrequent at all energies, or confined to very high primary energies.—A discussion of the differences between the geomagnetic latitude effects of the primary radiation and of the sea level hard component, and of the differences between the E-W effects of the sea level hard component between equator and moderate latitudes, shows that these effects are well compatible with the above conclusions.

* Supported in part by AEC contract.

E3. On the New Unstable Cosmic-Ray Particles.* A. J. SERIFF, R. B. LEIGHTON, C. HSIAO, E. W. COWAN, AND C. D. ANDERSON, *California Institute of Technology.*—Thirty-four "forked tracks" similar to two previously reported by Rochester and Butler,[1] have been observed in 11,000 cloud-chamber photographs of cosmic-ray penetrating showers, confirming their conclusion that new unstable neutral and charged particles exist. The neutral particles decay into two charged particles (and possibly into neutral particles also) and the charged particles into a charged particle and presumably at least one neutral particle. The unstable neutral particles have a mean rest life time of $(3\pm2)\times10^{-10}$ sec., and the unstable charged particles a mean life perhaps shorter, but of the same order of magnitude. The number of unstable neutral particles is about three percent of the number of charged particles in a penetrating shower. Of the two charged secondaries of the unstable neutral particles, curvature and ionization show that at least one has a mass between 150 m_e and 350 m_e, and large angle scattering and star production show that at least one has a strong nuclear interaction; the data also indicate that neither of the decay products is an electron.

* Supported in part by the joint program of the ONR and AEC.
[1] G. D. Rochester and C. C. Butler, Nature 160, 855 (1947).

E4. A Large Cloud Chamber for the Study of Penetrating Showers.* MELVIN B. GOTTLIEB AND ALFRED J. HARTZLER, *University of Chicago.*—A rectangular chamber with a sensitive volume of 24×16×7 in. has been constructed for the study of high energy nuclear events in which penetrating particles and electron cascades occur. The chamber was expanded on two sides. It thus could be illuminated through the rear glass wall resulting in relatively high light efficiency. About 300 g/cm² of gold in the form of 16 plates of 1 cm thickness were placed in the chamber and inclined toward the cameras. The expansion of the chamber was controlled by a fivefold coincidence between counters located inside of and below the chamber. The inside counters were located in a tray near the center of the chamber. The counters below the chamber consisted of two horizontal trays, one above the other, and were shielded by lead blocks. This counter arrangement proved to be highly selective for high energy nuclear events. Other counters at a distance from the chamber were used for the detection of extensive showers. Events occurring in the chamber were photographed by three cameras for stereoscopic observation. Some of the photographs obtained with this apparatus will be discussed in the following paper.

* Assisted by the joint program of the ONR and AEC.

E5. Cloud-Chamber Observations of Showers at an Altitude of 11,500 Ft.* ALFRED J. HARTZLER AND MELVIN B. GOTTLIEB, *University of Chicago.*—The cloud chamber and associated apparatus described in the previous paper were operated at Climax, Colorado (altitude 11,500 ft.) for a period of several months in the fall of 1949. Nine thousand stereoscopic pictures were taken. The gold plates used in this

experiment were particularly valuable for the study of several high energy phenomena. The large amount of material in the chamber (about 300 g/cm²) permitted the observation of a great number of cases in which successive production of nuclear events occurred. In the case of showers containing both penetrating particles and electron cores, the short radiation length in gold (0.3 cm) resulted in the rapid absorption of the soft cascade showers, thus making the penetrating component more easily observable. A number of pictures showed the complete development and absorption of very high energy electron showers. Photographs of typical events will be shown.

* Assisted by the joint program of the ONR and AEC.

E6. The Production of High Energy Photons in Nuclear Interactions of Cosmic Rays.* B. P. GREGORY AND J. H. TINLOT,† *M.I.T.*—Seventy-eight electronic showers produced in nuclear interactions occurring in the lead and aluminum plates of a cloud chamber were examined in order to determine whether they were electron- or photon-initiated. All these showers penetrated at least one lead plate (1.2 radiation lengths) and showed a multiplicity of more than four electrons. Under the assumption that the shower-initiating particles are produced at a distance from the origin of the nuclear interaction small with respect to the thickness of the plates, it was established that less than 20 percent of the showers were electron-initiated when the nuclear event occurred in an aluminum plate, and less than 30 percent when the nuclear event occurred in lead. In those two cases, the data were also consistent with all showers being photon-initiated. The possibility of interpreting these photons as the decay products of a neutral meson will be discussed.

* Assisted by the joint program of the ONR and AEC.
† Now at Columbia University.

E7. Cross Sections for Nuclear Collisions of Protons and π-Mesons.* J. H. TINLOT AND B. P. GREGORY,† *M.I.T.*—The cloud chamber described in the previous paper was, in one experiment, triggered by a simple counter telescope above. The observed nuclear collisions of ionizing particles (protons) indicated that the relative cross sections for aluminum and lead were compatible with the assumption of "geometric" cross sections. The energy of the majority of protons was estimated as less than 1 Bev. In a second experiment, the chamber was triggered by a counter telescope below, in anticoincidence with a large tray of counters above. Nuclear interactions of widely varying energies and multiplicity were observed. Of interest were the secondary collisions of the locally produced penetrating particles, which were presumably a mixture of protons and π-mesons. Events were tentatively classified as to multiplicity of penetrating particles, this being a crude measure of the energy transmitted in the collision. A preliminary survey indicated the following.

Multiplicity	Traversals (g/cm² Pb)	Nuclear collisions	M.F.P. (g/cm² Pb)
2–3	1150	3	~400
2–4	2500	12	~200
>4	2000	13	~160

The "geometric" mean free path in lead is 160 g/cm².

* Assisted by the joint program of the ONR and AEC.
† Now at Columbia University.

E8. Altitude and Latitude Dependence of Bursts in a Lead-Shielded Ion Chamber.* ALLEN J. MCMAHON AND BRUNO ROSSI,† *Brookhaven National Laboratory.*—The instrument used in this experiment consists of a cylindrical ionization chamber covered by a half cylindrical lead shell 15 cm thick and of six trays of G-M tubes, of which five are placed around the lead shield and one directly under the chamber. Various kinds of coincidences between bursts of the ionization chamber and pulses of the counter trays are recorded. These events are interpreted as due to nuclear interactions of cosmic rays. The instrument was installed aboard a B-29 and flown at the pressure altitudes of 273, 300, and 383 g cm^{-2} at 55°N geomagnetic latitude, and at the pressure altitudes of 300 and 383 g cm^{-2} at 20°N geomagnetic latitude. The experiment provided information on the altitude, latitude, and angular dependence of the radiation responsible for nuclear interactions. If one considers in particular penetrating ionizing particles capable of producing high energy nuclear events after traversing 15 cm of lead, one finds that the altitude dependence corresponds to an absorption thickness of about 124 g cm^{-2} both at 55° and 20° and that the intensity ratio between the two latitudes is about 1.14.

* Research carried out at Brookhaven National Laboratory under the auspices of the AEC.
† At M.I.T.

E9. Energetic Stars at Different Latitudes.* C. B. FISK, J. HORNBOSTEL, E. O. SALANT, AND J. E. SMITH, *Brookhaven National Laboratory.*—Eastman NTB3 emulsions were flown to an atmospheric pressure of 15 g/cm² at 57° and 31°N** geomagnetic latitudes, cut-offs 2.8 and 8 Bev, respectively. About 1000 stars were examined in plates verified as sensitive to minimum ionization tracks. Latitude effect for star production by incident singly charged, relativistic particles is about the same as reported for particle flux by Winckler *et al.* (private communication), implying approximately constant cross section, over relevant energy ranges, for proton disintegrations. No significant differences between the two latitudes are found for distribution in either numbers of heavy prongs or multiplicities of outgoing minimum tracks. Considering only stars of 3 or more heavy prongs, data at each latitude show: (a) about one-fourth of the stars are caused by relativistic protons, (b) two-thirds of the proton-induced stars have outgoing minimum tracks, presumably mostly relativistic mesons, with an average multiplicity of 3, (c) two-thirds of these stars have 6 or more and one-half have 9 or more heavy prongs, (d) one-half of all stars contain only heavy prongs, of which only one-fourth have 6 or more prongs. This distribution, contrasted with (c), suggests only moderately energetic neutrons as a cause. Angular spreads of minimum tracks will be discussed.

* Research carried out at Brookhaven National Laboratory under the auspices of the AEC.
** Flights by ONR.

E10. Further Experiments on Slow μ-Mesons Stopped at Thin Al Foils.* W. Y. CHANG, *Purdue and Princeton Universities.*—The cloud-chamber-counter arrangement for the more recent work on thin Pb foils[1] was used to continue study of meson absorption by thin Al foils. Eight 4/1000-in. and three 32/1000-in. Al foils were symmetrically placed inside the chamber. The total sensitive time was about 1500 hr. More than 60 mesons were stopped at the Al foils. About half of these are decaying mesons, and the other half do not give rise to an observable heavy charged particle or a decay electron and hence are negative mesons. About 12 of these latter events occur at the 4/1000-in. foils. If, from every negative meson captured by an Al nucleus, a proton with a 3-Mev kinetic energy was emitted, then six out of the 12 pictures should have shown proton tracks. Our results therefore support the view for Al too that the μ-meson gives up its negative charge to the Al nucleus and a much larger portion of its rest energy is emitted as a neutral meson or a neutrino. Since the potential barrier of Mg^{27} for a proton is much smaller than the binding energy of a nucleon, a neutron may escape from a Mg^{27} nucleus without much greater probability than a proton. Our results therefore indicate that the negative μ-meson imparts only about 15 Mev or much less to the Al nucleus, taking 3 Mev to change Al^{27} to Mg^{27}.

* Assisted by the joint program of the AEC and ONR.
[1] Phys. Rev. **76**, 170 (1949); Princeton Biennial Reports on Cosmic Rays, July 1, 1947 to July 1, 1949.

THURSDAY AFTERNOON AT 2:00

Department of Commerce Auditorium

(BRUNO ROSSI presiding)

Cosmic Rays. II

F1. Total Primary Cosmic-Ray Energy at the Geomagnetic Equator.* J. A. VAN ALLEN AND S. F. SINGER, *Johns Hopkins University.*—Our experimental measurements above the atmosphere at $\lambda = 0°$ have given the following results: (a) Vertical intensity 0.028 sec.$^{-1}$ cm^{-2} steradian^{-1}. (b) A marked increase in the intensity, averaged over all azimuths, with zenith angle. (c) Azimuthal asymmetry of the proper sign, but of much less magnitude than predicted for a radiation consisting only of positive primaries. (d) Bulk of the charged radiation singly charged, with specific ionization about minimum. Result (b) is inconsistent with geomagnetic theory for either all positive, all negative, or mixed positive and negative primary beams and, therefore, provides clear evidence for the importance of atmospheric albedo, particularly at large zenith angles. Thus, result (c) can be shown in accord with the assumption that the primaries are positive, but that the east-west asymmetry is diluted by the large contribution of albedo. If one takes the measured vertical intensity as consisting only of primary protons, then with the help of geomagnetic theory, the total energy brought in by the primary radiation can be easily computed. The result is 2.2 Bev (horizontal cm^2)$^{-1}$ sec.$^{-1}$ using a differential number spectrum of $dN = KE^{-2}dE$. A flatter spectrum, based on the latitude variation of vertical intensity above the atmosphere, yields an even larger value for the total energy. Such results can be harmonized with Millikan's value of the ionization energy integral of 0.94 Bev-cm^{-2}-sec.$^{-1}$.

* Supported by the Navy Bureau of Ordnance.

F2. The Daytime Azimuthal Effect for Heavy Nuclei.* E. P. NEY, J. LINSLEY, AND P. S. FREIER, *University of Minnesota.*—A device was constructed to maintain orientation of a plate stack during a high altitude balloon flight. A small sphere containing photographic plates was hung from a large cloud-chamber sphere by a suspension which contained a motor-driven rotating joint. The motor rotated the plate sphere relative to the big one so as to cancel the rotation of the big sphere relative to the ground. The motor was controlled by phototubes coupled with light beams to a compass. Photographic recorders in both spheres showed that during 190 minutes at altitude the orientation of the plate sphere was held constant within ±15° for 140 minutes and within ±35° for 184 minutes while the balloon and large sphere rotated considerably. The flux of heavy nuclei was measured as a function of zenith and azimuth and the results will be reported.

* This work was supported in part by the ONR.

F3. Nighttime Flux of Heavy Nuclei.* P. S. FREIER, E. P. NEY, J. NAUGLE, AND G. ANDERSON, *University of Minnesota.*—The nighttime flux and angular distribution of heavy nuclei were determined at a residual atmosphere of 25 g/cm^2. The values are compared to those from a daytime flight at the same altitude. The vertical flux at night is lower than the daytime flux by a factor of two to three. The rate of "star" production at night does not seem significantly different from the daytime rate. A recorder which worked for only part of the flight showed that the load was fortuitously oriented for at least one-fourth of the time at altitude. At large zenith angles the heavy nuclei flux shows an azimuthal asymmetry far beyond any expected statistical fluctuations.

* This work has been supported in part by the ONR.

F4. Preliminary Results of a Cloud Chamber Study of the Cosmic Radiation at an Altitude of 90,000 Feet.* R. RONALD RAU AND G. G. HARRIS, *Princeton University.*—A series of balloon flights have been made in which a Wilson cloud chamber was sent to an altitude of 90,000 feet. The balloons were the single cell plastic Project Skyhook type made available by the ONR. The cloud chamber was expanded at one minute intervals. The measured sensitive time of the chamber was 0.2 second. The chamber contained three plates, each 1 cm thick. During three flights the top plate was beryllium and the two lower ones were lead. During one flight all three plates were lead. A total of 1500 pictures were obtained. Preliminary results will be presented on two types of events: (a) events produced in beryllium by ionizing and non-ionizing radiations; (b) events designated as "sprays" by Oppenheimer and Ney.[1]

* Assisted by the joint program of the ONR and AEC.

[1] F. Oppenheimer and E. P. Ney, Phys. Rev. **76**, 1418 (1949).

F5. Absorption Measurements on Cosmic-Ray Particles Producing Nuclear Interactions at 10,600 Feet.* R. H. REDIKER AND H. S. BRIDGE.—The paper describes the results of an experiment designed to measure the *absorption* and the *collision* mean free paths in lead and carbon of ionizing cosmic-ray particles capable of producing different kinds of nuclear interactions. The detector consisted of a lead-shielded ionization chamber and of several trays of Geiger-Mueller tubes. The separation between the absorption and the collision mean free paths was achieved by investigating whether the particle responsible for the nuclear interaction came out of the absorber alone or accompanied by other particles. If one considers nuclear interactions in which penetrating particles are produced one finds that: (a) the absorption mean free path of the producing radiation is approximately the same in gram per cm^2 for lead and carbon (~500 g/cm^2); (b) the collision mean free path is, however, greater in lead (~300 g/cm^2) than in carbon (~120 g/cm^2) in approximate inverse-relation to geometric cross section; (c) the absorption mean free path in carbon is approximately four times the absorption mean free path in air. The last result suggests that some of the nuclear interactions under the carbon absorber are due to π-mesons produced in the carbon.

* Assisted by the joint program of the ONR and AEC.

F6. Analysis of the Cosmic Radiation at 3.4 Kilometers into Its Proton and Meson Components.* CHARLES E. MILLER, JOSEPH E. HENDERSON, DAVID S. POTTER, AND JAY TODD, *University of Washington.*—In previous work of this laboratory a momentum spectrum of the meson plus proton component of the cosmic radiation at 3.4 kilometers was obtained through a magnetic (8000 gauss) cloud-chamber analysis. Electrons were separated from the heavier particles through shower formation while the later were partially separated into protons and mesons through the increased density of the proton tracks of lower energy. Because of uncertainties and limitations to the ionization density criterion for protons an improved method of analysis has been employed. In this an arrangement of Geiger counters and absorbers was used to photograph selectively tracks of those non-shower producing particles lying in definite range intervals. Range intervals of 0–5, 5–15 and 15–25 cm of lead were used. In each case a plot of the momentum distribu-

tion of negative particles shows a single maximum at the momentum to be expected for mesons lying in the range interval selected. The distributions for positive particles show a second maximum at the momentum value to be expected for protons. It is interesting to note that, at this altitude, of those particles stopping in 5 cm of lead the number of protons is well in excess of the number of mesons.

* This work supported by the joint program of ONR and AEC.
** A division of the Department of Physics.

F7. On the Zenith Angle and Energy Dependence of Mesons at Sea Level.* JACOB L. ZAR AND M. H. SHAMOS, *New York University.*—Delayed coincidences have been observed with a telescope having threefold coincidence trays, with provision for the insertion of lead and iron moderators, a graphite absorber, an anti-coincidence tray, and side counters to detect decay electrons from the graphite. The apparatus tilts in the zenith direction and has an effective angular resolution of $\pm 7.3°$. The zenith dependence of mesons as determined by their characteristic decay was fitted by $I(\theta)=I(0)\cos^n\theta$; in which n, as determined for incident meson energies of 235, 550, and 890 Mev, was respectively 3.2, 2.3, and 2.0. Coincidence and anti-coincidence determinations of n gave values close to 2.0 and 3.0 respectively over the same energies. This work extends the measurements of Greisen[1] and Kraushaar[2] to higher energies. The results are in agreement in the region where comparisons can be made.

* Assisted by the joint program of the ONR and AEC, and by the Research Corporation.
[1] K. Greisen, Phys. Rev. **61**, 212 (1942).
[2] W. L. Kraushaar, Phys. Rev. **76**, 1045 (1949).

F8. Latitude Dependence of Atmospheric Neutrons at High Altitudes.* W. P. STAKER AND W. O. DAVIS,** *New York University.*—Atmospheric neutrons associated with the cosmic radiation have been measured to high altitudes at 30.4°N and 54.7°N geomagnetic latitudes using balloon-borne equipment. A system using one BF_3 counter enriched in the B^{10} isotope to 96 percent of the boron present and another counter depleted in the B^{10} isotope to 10 percent was developed. This method allows the calculation of the density of all neutrons in the energy range activating a BF_3 proportional counter. With similar physical characteristics, the counters can be assumed to contain identical star-producing materials, so it can be assumed that statistically the background will be the same for each counter. A maximum for the neutron density was found at approximately 100 g/cm² at 54.7°N and 120 g/cm² at 30.4°N. The relative counting rates at these two latitudes were about 3 to 1 at the maximum which is in good agreement with the data obtained at lower altitudes by Simpson[1] and Yuan.[2]

* Assisted by joint program of ONR and AEC.
** Major, USAF, now assigned to USAF Special Weapons Command, Kirtland AFB, Albuquerque, New Mexico.
[1] J. A. Simpson, Phys. Rev. **73**, 1389 (1948).
[2] L. C. L. Yuan, Phys. Rev. **76**, 1267 (1949).

F9. Measurements on Cosmic Radiation Far Underground. LOWELL M. BOLLINGER, *Cornell University.*—Properties of cosmic radiation in a salt mine at depths of approximately 1150, 1500, and 1790 meters water equivalent have been measured by means of a G-M counter hodoscope. The absolute vertical intensity and the angular distribution were measured at all three depths for the hard component. At 1790 m.w.e. the vertical intensity and angular distribution of the soft component were measured. Secondary events initiated both in the salt roof and in the lead of the apparatus by penetrating particles were recorded by the hodoscope. There are many events in which two counters are discharged simultaneously without a third counter being discharged. The ratio of the number of these twofold events relative to the single counter rate was measured for the natural radiation and for several γ-ray sources. The results support the view that the background twofold rate is caused by local γ-radiation.

F10. Cloud Chamber Triggered by Internal Scintillation Counter.* R. W. WILLIAMS, L. M. SPETNER, W. L. KRAUSHAAR, H. W. J. COURANT, *M.I.T.*—A magnet cloud chamber has been constructed which contains the fluorescent crystal of a scintillation counter, for observations on cosmic rays. The cloud chamber is 11¼ in. i.d., 3½ in. deep, and is supported between the poles of an electromagnet whose field, at 43 kilowatts, is 11,000 gauss. The 1 in.×3 in.×4 in. napthalene crystal is mounted approximately in the center of the cloud chamber, with the 3 in. edge parallel to the cloud chamber axis. Two 1 in. diameter quartz rods, one abutting against either free edge of the crystal, guide the fluorescent radiation out to regions of weak field, where it falls on RCA 5819 photomultipliers in heavy magnetic shields. The crystal is wrapped with aluminum foil and sealed with Vinylite tape. The degree of internal reflection in this system is such that coincidences between the photomultipliers are observed with nearly 100 percent efficiency for particles of minimum ionization passing anywhere through the crystal. The cloud chamber can be triggered whenever either a coincidence between pulses of more than a given size occurs or a coincidence between pulses is followed, within 5 microseconds, by another coincidence. Representative photographs of cosmic-ray events will be shown.

* This paper is supported in part by the joint program of the ONR and the AEC.

F11. The Emulsion Chamber—A New Photographic Tool for the Study of Ionizing Particle Tracks. HERMAN YAGODA, *National Institutes of Health.*—The processing of thick (400 to 600 micron) nuclear emulsion plates is slow and is attendant with dangers of stripping or cracking during prolonged cosmic-ray exposures. Spurious curvature of tracks are also introduced as a result of uneven drying of the residual gelatin. To overcome these difficulties, and to extend the thickness of the recording medium to 2 mm, a departure has been made from the traditional glass coated plate: A concentrated AgBr emulsion is melted at 40° in a stainless steel cup measuring 5 cm in diameter and 0.5 cm high. After setting and dehydration an emulsion casting about 2 mm thick results. This is clamped between Lucite or lead plates to prevent buckling, and is thus exposed. Development and fixation are comparatively rapid (30 hours). During washing the gelatin swells to about 6 cm by 0.5 cm, but is brought back to its original diameter by gradual dehydration with a series of graded alcohols (1). The circular, uniform, emulsion casting minimizes track distortion and the exceptional thickness of the medium increases the probability of detecting double stars, and recording the termination point of fast particles. Preliminary results on a casting weighing 10 grams, exposed to cosmic radiation at Climax, Colorado, will be described.

[1] H. Yagoda, *Radioactive Measurements with Nuclear Emulsions* (John Wiley and Sons, Inc., New York, 1949), p. 53.

Invited Paper

F12. Gamma-Rays from Nuclear Collisions. HERBERT YORK, *University of California, Berkeley.*

THURSDAY AFTERNOON AT 2:15

Departmental Auditorium

(M. A. TUVE presiding)

Apparatus of Nuclear Physics

G1. Ring Focusing in a Thin Lens Magnetic Spectrometer. W. W. PRATT, F. I. BOLEY,* AND R. T. NICHOLS, *Iowa State College.*†—The baffle system of a thin lens beta-ray spectrometer[1] has been modified to make use of ring focusing.[2] The region of ring focusing was located by means of photographic films placed in the spectrometer at various axial positions with the plane of the film perpendicular to the spectrometer axis. Ring images on these films, due to a monoenergetic source of electrons, mapped out the electron beam. An annular baffle was inserted in the spectrometer to make use of the constriction observed in the beam. Using a Geiger counter aperture large enough to admit all electrons passing through the annulus, it was found that for a line half-width of two percent the transmission with this type of focusing is twice that obtained with axial focusing.

* Socony-Vacuum Corporation, Research Fellow.
† This work was performed at the Ames Laboratory of the AEC.
[1] Jensen, Laslett, and Pratt, Phys. Rev. **75**, 458 (1949).
[2] Keller, Koenigsberg, and Paskin, Phys. Rev. **76**, 454 (1949).

G2. A Gamma-Ray Spectrometer Based on the Compton Effect.* J. A. MCINTYRE AND R. HOFSTADTER, *Princeton University.*—Using NaI(Tl) scintillation counters a rough spectrometer for determining gamma-ray energies has been developed. The operation depends on a measurement in one of the crystals of the energy of the recoil electron in the Compton effect. The energy has been measured as a pulse height with a single channel discriminator. The scattered gamma-ray corresponding to the recoil electron studied has been utilized as a coincidence gate to select the time when the discriminator is active. Two different arrangements have been examined in which the gate corresponds to forward and backward scattered gamma-rays. With this spectrometer the 1.17- and 1.33-Mev lines of Co^{60} have been resolved. Other cases will be discussed.

* This work received partial support from the U. S. Army Signal Corps and the joint program of the AEC and ONR.

G3. A Small Electrostatic Generator.* D. I. COOPER, D. H. FRISCH, C. L. STORRS, JR., AND C. J. STRUMSKI, *M.I.T.*—A 1-Mv Van de Graaff generator has been built primarily for low energy $p-p$ and for $n-p$ scattering experiments. Salient characteristics are: (1) A simple d.c. arc in an axial magnetic field[1] (Alnico) provides more total current than the charging current and accelerating tube can handle at present, at tube pressures of $\sim 10^{-6}$ mm. No pre-acceleration is used. (2) The two identical accelerating tubes are made of high dielectric constant ($\kappa = 9$), locally fabricated statite sections, 8 in. mean i.d., 9 in. mean o.d., 2 in. high, and are assembled with the $\frac{1}{16}$ radian inside slope arranged so as to repel electrons from the surface. The thin flat electrodes are 7 in. i.d. The focusing electrode next to the high voltage terminal is a 1 in. i.d. quasi-doughnut. At present the beam induces frequent tube breakdowns, especially when in poor focus. (3) A 600-kv unanalyzed beam makes a white hot spot on Vykor glass. (4) The other parallel accelerating tube is to have in it a control beam of electrons, operating on the signal from a time-of-flight analysis of the mass two ion beam.

* Assisted by the joint program of the ONR and AEC.
[1] Bailey, Drukey, and Oppenheimer, Rev. Sci. Inst. **20**, 189 (1949).

G4. Radiofrequency Ion Source for Electrostatic Generator.* K. R. MORE, R. H. CHOW, J. K. KINNEAR, AND S. B. WOODS, *University of British Columbia.*—Ion sources excited by radiofrequency electrodeless discharges have been described by Bayly and Ward,[1] Thonemann[2] and others. A proton source of this type has been constructed for the University of British Columbia electrostatic generator. Positive ions of hydrogen are formed in a low pressure electrodeless discharge in a Pyrex tube. Radiofrequency power, at a frequency of 200 Mc/sec., is fed into the discharge tube by means of external electrodes. An axial magnetic field reduces the diffusion of ions to the tube walls. An electric field maintained between a small tungsten anode and the exit canal accelerates and focuses the ions into the canal. The emerging ions are focused and accelerated to 50 kv before entering the main accelerating column of the generator. Differential pumping of the ion source is provided. On a test system, total beam currents of 800 μa have been achieved with a gas consumption of 15 cc per hr. Magnetic analysis showed that the beam consists of 45 percent protons.

* Supported by a grant-in-aid from the National Research Council of Canada.
[1] Bayly and Ward, Can. J. Research **26**, 69 (1948).
[2] Thonemann, Moffatt, Roaf, and Sanders, Proc. Phys. Soc. **61**, 483 (1948).

G5. Performance of 300-Mev Betatron.* G. D. ADAMS, D. W. KERST, AND C. S. ROBINSON, *University of Illinois.*—The first trail of the 300-Mev betatron was made February 15, 1950, and yield was observed immediately. The first measurements at 300 Mev showed 15,000 r per hr. at one meter in 0.125-in. Pb with 6 pps. and about 40-kev injection. Calculated orbital radiation loss is nine percent at 96.6 percent of peak field for 300 Mev and is compensated by a flux pulse. Field test results were similar to those for the 80-Mev model.[1] An orbit is established within 12 μsec. of the start of the flux through the 275-ton yoke. The azimuthal variation of field at injection is less than ± 0.13 gauss except at the six field magnet junctions where lags 5° wide and as much as 0.5 gauss exist, and except at the coil terminals where the field is 0.2 gauss early. Radial field at the orbit is less than 0.13 gauss except at the junctions. The residual field between 300-Mev pulses is 4.5 gausses. It is uniform within ± 0.15 gauss.

* This work assisted in part by the joint program of the ONR and AEC.
[1] Kerst, Adams, Koch, and Robinson, Phys. Rev. **75**, 330 (1949). Also "An 80-Mev model of a 300-Mev betatron," Rev. Sci. Inst. (to be published).

G6. Operation of the M.I.T. 350-Mev Electron Synchrotron.* I. A. GETTING, J. S. CLARK, J. E. THOMAS, JR., I. G. SWOPE, AND M. L. SANDS, *M.I.T.*—A combination of the betatron and synchrotron principles has been incorporated in the design of a ring type magnet, weighing approximately 55 tons, with a nominal tube radius of 1 meter. The machine operates on single cycle excitation with a peak voltage of 15,000 volts and a peak current of 4500 amp. Betatron operation is used to 4 Mev. Synchrotron operation employs a self-excited, class *C* oscillator feeding a quarter-wave line cavity which constitutes one section of the accelerator tube. The entire tube is made of slip-cast steatite. The output of the machine at 350 Mev is approximately 100 mr per pulse measured two meters from the target with a Victoreen thimble chamber embedded in $\frac{1}{4}$ in. of lead.

* Assisted by the joint program of the ONR and AEC.

G7. Electron Injection Gun for the M.I.T. 350-Mev Synchrotron.* ORVILLE STONE, *M.I.T.*—An electron gun employing a sintered cathode has been developed for the injection of electrons in the synchrotron. The cathode material, developed by the Raytheon Manufacturing Company, consists of thoria (75 percent) and molybdenum (25 percent), and may be sintered in any desired shape. With proper shaping much better focusing properties may be obtained than with coiled filaments. Other advantages are great rigidity, high emission, and long life, even when exposed periodically to air.

* Assisted by the joint program of the ONR and AEC.

G8. Design of Magnet Ends and Straight Sections for a Racetrack Synchrotron.* G. B. BEARD, J. L. LEVY, W. A. NIERENBERG, AND R. W. PIDD, *University of Michigan.*—In a racetrack type synchrotron, undesirable end effects in the transition region between a magnetic quadrant and a field-free straight section are caused by the leakage flux and by out-of-phase field components due to eddy currents in the end laminations. To determine their extent at injection time, when they are especially harmful, mappings of the field were obtained under various conditions by local measurements of the field amplitude and the phase shift relative to the main field. These end effects can be varied considerably by shaping the magnet ends and using different materials, particularly iron, in the straight sections. Data are presented on the use of iron straight sections to control stray magnetic fields and eddy current effects. A special peaking strip arrangement was devised to meet the required precision for these measurements.

* This work was supported by the Navy Bureau of Ordnance.

G9. Optimum Parameters for Particle Acceleration by TM 010 Cylindrical Cavities. B. L. MILLER, *Bartol Research Foundation.*—Several linear accelerator projects make use of cylindrical cavities operating in the TM 010 mode. The energy imparted to the beam is somewhat increased by using less than a full half-cycle, because in the shorter cavity a higher field is attained for the same power input. For particles injected at velocity c, the cavity length for maximum acceleration is 0.44λ and the optimum injection angle 11° after the zero field phase, independent of the r-f power level.[1] For initial velocities less than c, the optimum cavity length and injection angle depend both on the injection velocity and the r-f power available. Calculations of these optimum parameters have been made in the low energy case, for small relativistic correction, and in the far relativistic region where most of the orbit is traversed near velocity c. Because the optimum values do not vary widely (e.g., injection angle always less than 11°), they can be estimated, from the above calculations, for the intermediate region.

[1] W. Graffunder, Helv. Phys. Acta **22**, 239 (1949).

G10. 200-kv Accelerator with Gas Recovery System. E. ALMQVIST, K. W. ALLEN, J. T. DEWAN, T. P. PEPPER, AND J. H. SANDERS, *Chalk River Laboratory.*—A 200-kv accelerator has been built incorporating a gas recovery system. A radio-frequency ion source[1] with a $\frac{1}{16}$-in. diameter exit canal produces at the target a 200-μA beam for a gas consumption of 8 cc per hour (hydrogen). The beam is focused through a second canal into the accelerating tube; the gas flowing out of the ion source is pumped by mercury diffusion pumps into a suitable reservoir. More than 95 percent of the gas is recovered by this differential pumping system. Since very little gas enters the accelerating tube, the pressure in it is less than 2×10^{-5} mm with the beam on. This results in a steady well-focused beam. When hydrogen is to be recovered the gas issuing from the mercury pumps is absorbed in a spongy uranium reservoir.[2] It may be recovered quantitatively by heating the uranium hydride to 430°C.[3]

[1] Thonemann *et al.*, Proc. Phys. Soc. **61**, 483 (1948).
[2] Taschek *et al.*, Phys. Rev. **75**, 1361 (1948).
[3] Spedding *et al.*, Nucleonics **4**, No. 1 (1949).

G11. A New Method of Radioactivity Measurement.* W. GROSS AND G. FAILLA, *Columbia University.*—The method is based on the measurement of the charge carried away from the radioactive source by the beta-rays. The source consists of a thin deposit of the active material at the center of a thick conducting plate. Secondary electron effects are eliminated by "covering" the source plate with an identical but non-active plate parallel and very close thereto, and by the use of a weak magnetic field which curls back the very low energy electrons. Measurements are carried out in an evacuated chamber to remove all ionization effects. The method is independent of beta-ray energy and is more direct than the usual G-M counter methods. To express the results in disintegrations per second (or curies) it is not necessary to know the complete disintegration scheme of the isotope. Beta- plus gamma-ray emitters can also be measured. The apparatus is simple, small, and reliable. Measurements of P^{32}, S^{35}, and I^{131} show very close agreement with the results obtained by another absolute method developed in this laboratory.

* Performed under AEC contract.

G12. Electron Track Grain Densities in Nuclear Emulsions. DALE R. CORSON AND MARGARET R. KECK, *Cornell University.*—We have studied the grain density of electron tracks in electron-sensitive Ilford G-5 nuclear emulsions in an attempt to observe the increase of grain density with energy which might be expected at energies above that of minimum ionization. Using magnetically deflected pair-produced electrons from synchrotron radiation, we have recorded tracks of 180-Mev electrons at right angles to 40-Mev electrons on a single plate together with 10-Mev cyclotron produced pair electrons. An energy is assigned to a track according to the direction of the track and to its multiple scattering. The observed grain density on a single plate for all three energies is 36.6 ± 0.6 grains per 100 microns. A more refined experiment is necessary to detect the increase in grain density, if any, at high energies. There are significant differences, however, in grain density from plate to plate, probably depending on the temperature of exposure, development procedure, emulsion batch, etc. On different plates we have observed relativistic electron track densities as low as 25 and as high as 42 grains per 100 microns.

G13. The Measurement of Particle Energies with Scintillation Counters.* W. FRANZEN, R. PEELLE, AND R. SHERR, *Princeton University.*—The response of a scintillation counter to heavy particles has been investigated with respect to resolution and relationship of pulse height to energy. Protons from the Princeton cyclotron were scattered by a platinum foil into NaI, KI, and anthracene crystals mounted under good optical conditions on a RCA-5819 photo-multiplier tube. The incident proton energy was varied by interposing aluminum foils. Pulses were amplified by a Model 501 amplifier (rise time 0.15 μsec.; clipping time 5 μsec.) and analyzed by a single channel discriminator. Approximately Gaussian distributions having a width at half-maximum of three percent were obtained with NaI and KI. For these crystals, a plot of pulse height *vs.* energy yields a straight line which passes through the origin if the initial proton energy is taken to be 17.1 Mev. An air range measurement yielded 16.9 Mev for this energy. For anthracene, the pulse height per Mev decreases markedly with decreasing proton energy. For comparison, the relative pulse amplitudes (per Mev) were measured for 626-Kev electrons, 17-Mev protons, and 5.3-Mev alpha-particles, and were found

to be approximately 4.6:4.6:3.4 for NaI, 0.9:1.0:1.0 for KI, and 2.9:1.8:0.3 for anthracene.

* Supported by the ONR and AEC.

G14. A Versatile Delayed Coincidence Circuit.* W. R. KONNEKER, S. DEBENEDETTI,† AND F. K. MCGOWAN,‡ *Washington University.*—A versatile survey instrument has been constructed for the purpose of investigating short-lived isomeric states over a wide range of half-lives. The instrument consists essentially of a coincidence circuit with provision for introducing various amounts of time delay, together with a gate circuit arranged so that only pulses of sufficient amplitude to give positive operation of the coincidence circuit are counted. The gate circuit, when used with scintillation counters, suppresses random time fluctuations due to variations in pulse height. The incident pulses are applied to a pair of multivibrators, and the return pulse, rather than the leading edge, actuates the coincidence circuit. Delay may thus be introduced by varying the time constant of the multivibrator feed-back circuit. Provision is made for matching the coincidence circuit resolving time to the time delay in order to maintain optimum counting rate consistent with the attainable accuracy. Half-lives can be measured over the range 0.05 μsec. to 1 μsec. Results will be reported on about 30 isotopes that have been investigated to date.

* Assisted by the joint program of the ONR and AEC.
† Now at Carnegie Institute of Technology, Pittsburgh, Pennsylvania.
‡ Oak Ridge National Laboratory, Oak Ridge, Tennessee.

THURSDAY AFTERNOON AT 2:15

Lisner Auditorium

(J. A. BEARDEN presiding)

Invited Paper

H1. High Precision Methods for Absolute Determination of Nuclear Energy Levels. J. W. M. DUMOND, *California Institute of Technology.* (25 min.)

X-Rays; Cryogenics

H2. Pair Spectrometer for High Energy X-Rays.* J. W. DEWIRE, A. ASHKIN, AND L. A. BEACH, *Cornell University.*—An electron pair spectrometer has been constructed for studies using the x-ray beam from the Cornell synchrotron. The x-rays pass through a slit system and a clearing magnetic field before striking the thin pair-forming target in the gap of the spectrometer magnet. The pairs created in the target are detected by 18 groups of Geiger-Müller counters placed symmetrically on either side of the magnet. Pulses from the counters are fed into an electronic circuit in which coincidences corresponding to the various x-ray energies are recorded in appropriate output channels. The circuit is designed to reject ambiguous events involving triple coincidences. The electron orbits in the spectrometer magnet were determined by suspending in the magnetic field a flexible wire carrying a current. The shape of the wire describes the orbit of an electron whose momentum is given by the ratio of the tension to the current in the wire. Preliminary measurements have been made on absorption of 210-Mev x-rays in various materials. Results of these experiments will be given.

* Assisted by the joint program of the ONR and AEC.

H3. Angular Distribution and Intensity of 70-Mev X-Rays from Various Targets.* G. C. BALDWIN, F. I. BOLEY, AND H. C. POLLOCK, *General Electric Company.*—Measurements have been made of the angular distribution and intensity of x-radiation generated by 70-Mev electrons in Al, Cu, Mo, W, and Pt targets of various thicknesses. The synchrotron beam was alternately contracted and expanded respectively to an inner tungsten reference target and to an outer target carried by a mechanism with which the targets could be changed without breaking the vacuum. Two arrays of small ionization chambers were used to measure the intensity distribution in each of the resulting x-ray beams. The results are compared with theoretical beam shapes and intensities calculated from multiple scattering and bremsstrahlung theory.[1] Excellent agreement with theory is found for Al and Cu targets for thicknesses of the order of 10^{-2} radiation lengths. Similar targets of higher atomic number show increasing deviations, indicating that multiple scattering and radiation in these elements are less than predicted from theory. Aluminum targets of thickness below 10^{-3} radiation units show indication of multiple transits by the electron beam.

* Supported by ONR contract.
[1] L. I. Schiff, Phys. Rev. 70, 87 (1946).

H4. A Versatile Precision Bent Crystal Focusing Vacuum X-Ray Spectrometer.* E. L. JOSSEM AND L. G. PARRATT, *Cornell University.*—A focusing crystal x-ray spectrometer has been constructed for investigation of solid state problems. The instrument features high luminosity and high, adjustable, resolving power as well as versatility and precision. The x-ray source, crystal and detector are in a common vacuum envelope evacuated to $\sim 10^{-6}$ mm Hg, permitting study of long wave-lengths. Either transmission or surface reflection may be used and the shift from one method to the other can be made quickly and easily. This allows use of a variety of crystals and provides a very large wave-length range. The crystal, bent to a radius of 50 cm, is fixed and the source and detector are moved to vary the wave-length region studied. The source and detector positions can be simply interchanged for measurement of double Bragg angles. A precision worm-and-gear measures Bragg angles to about ±0.1 second of arc. Both photographic and electrical recording of x-ray intensity are used to provide the supplementary advantages of the two methods and a direct comparison between their results. Preliminary results obtained with this spectrometer will be reported.

* Work supported in part by the ONR.

H5. Interface Absorption by Evaporated Aluminum Films at 130 Angstroms. E. M. PELL AND D. H. TOMBOULIAN, *Cornell University.*—Absorption experiments in the soft x-ray region conducted by Skinner and Johnston[1,2] on Li, Mg, and Al have indicated the presence of an intense and relatively sharp band superimposed on the absorption curve of the

metallic lattice itself. In the case of Al at least, this band is missing from the absorption curves obtained in the neighborhood of the K-edge.[3] The present investigation confirms the results previously obtained by Johnston in the case of Al and reveals the origin of the additional absorption band. Evidence obtained from recent measurements show that the sharp absorption dip arises from the interface region of about 500A in thickness lying between the evaporated metal and the organic substrate. The presence of the band does not seem to depend on the choice of substrate materials such as celluloid, Zapon, or polystyrene. However, thin Al absorbers free from backing materials do not exhibit the narrow absorption observed in the case of absorbers prepared by evaporation. The research was supported by the ONR.

[1] H. W. B. Skinner and J. E. Johnston, Proc. Roy. Soc. London, **161**, 420 (1937).
[2] J. E. Johnston, Proc. Camb. Phil. Soc. **35**, 108 (1939).
[3] Munier, Bearden, and Shaw, Phys. Rev. **58**, 537 (1940).

H6. Average Electron Density Measurements by Low Angle X-Ray Scattering.* H. M. BARTON, JR., *Phillips Petroleum Company.*—According to Guinier[1] the low angle x-ray scattering of particles should disappear when they are immersed in a fluid of equal electron density. This furnishes a way of measuring the electron density of powders, providing a suitable impregnating fluid can be found. Experiments of this type have been carried out with carbon black. A method of calculating the low angle scattering coefficient defined by Warren is given for impregnated samples. Total low angle scattering measurements were made using a double crystal spectrometer and Geiger counter. No liquid was found that would give complete matching but approximate matching was obtained with phosphoric acid solution. The data extrapolate to show an electron density of $1.1N \pm 0.1N$ where N = Avogadro's number. This compares with a value of $0.99N$ as calculated from the helium immersion mass density measurement on the same sample.

* Work carried out at the Polytechnic Institute of Brooklyn.
[1] A. Guinier, J. Chim. Phys. **40**, 133 (1940).

H7. Resistance Minima in Metals at Low Temperatures.* M. P. GARFUNKEL, F. G. DUNNINGTON, AND B. SERIN, *Rutgers University.*—The work of Meissner[1] indicated that magnesium and aluminum might have minima in resistance at low temperatures. Thus resistance measurements were made on polycrystalline wires of these substances in the liquid helium temperature range. No minimum was found in aluminum. Magnesium showed a pronounced increase in resistance with decreasing temperature, below 4.2°K. The magnesium wire was 0.028 in. in diameter and 99.7 percent pure, the major impurities being aluminum, iron and silicon. Two polycrystalline samples of gold of different purity had resistance minima. The temperatures of the minima depended on the residual resistances in exact agreement with the work of de Haas and van den Berg.[2]

* This work has been supported by the ONR, by the Research Corporation, by the Rutgers University Research Council, and by the Radio Corporation of America.
[1] W. Meissner and B. Voight, Ann. d. Physik **7**, 761 (1930).
[2] W. J. de Haas and G. J. van den Berg, Leiden Comm. No. 241 d (1936).

H8. Experiment with Alternating Currents on Tin Superconductors. II.* B. SERIN, C. A. REYNOLDS, AND M. P. GARFUNKEL, *Rutgers University.*—The measurements reported last year[1] in which a.c. and d.c. are superimposed on a superconductor, and the average e.m.f. is measured as a function of the amplitude of the a.c., have been extended. The work was done with a variety of samples, differing in normal resistivity and diameter. The resistivity was changed by adding small quantities of lead to pure tin. The increase in average e.m.f. for high frequency a.c. over what is predicted by the Silsbee effect was again observed. This deviation increases roughly linearly with increasing values of ρ = (radius ÷ a.c. skin depth in normal conductor), until $\rho = 5$ and then begins to decrease. These results indicate that experiments of this type are unsatisfactory for determining the relaxation time for the transition from the superconducting to the normal state.[2]

* This work has been supported by the ONR, by the Research Corporation, by the Rutgers University Research Council, and by the Radio Corporation of America.
[1] Serin, Feldmeier, and Garfunkel, Abstract No. C 7, Phys. Rev. **76**, 167 (1949).
[2] Lasarev, Galkin, and Khotkevich, C.R. Acad. Sci. U.R.S.S. **55**, 805 (1947).

H9. The Rollin Film Creep Rate in He^4 and He^3–He^4 Mixture. HENRY A. FAIRBANK, ERNEST A. LYNTON, AND C. T. LANE, *Yale University.**—The previously used technique of Fairbank and Lane[1] for determining the flow rate of the Rollin Film has been applied to further study of He^4 and mixtures of He^3–He^4. The creep rate with pure He^4 was found to rise from zero at the λ-point to about 20×10^{-5} cm³/cm-sec. near 1.6°K. Below this temperature it remained nearly constant over a temperature range varying with the size of the leak, and then rose abruptly, reaching in some cases values as high as 50×10^{-5} cm³/cm-sec. at 1.2°K. Elaborate precautions ensured that this was not a contamination effect. With mixtures of He^3 and He^4 having λ-points in the vicinity of 2.0°K the creep rate was considerably lower, being about one-third to one-half the value found for pure He^4.

* Assisted by the ONR.
[1] H. A. Fairbank and C. T. Lane, Phys. Rev. **76**, 1209 (1949).

H10. Bloch's Theorem and Superconductivity. M. DRESDEN AND J. DELORD, *University of Kansas.*—The attempts to explain superconductivity in terms of a lowest state which carries a finite current, have been discredited to some extent[1] in view of a general result of Bloch, which asserts, that for a quantum mechanical system the lowest energy state is one of zero linear momentum. More precisely the quantum mechanical average of the linear momentum vanishes, thus leading to a zero total current. Bloch's result can be generalized considerably, one can prove that in the lowest state the quantum mechanical average of the linear momentum of every electron vanishes. A simple extension of Bloch's method, yields an infinite sequence of similar though somewhat more complicated results. It should be remarked that these results suffer essential modifications when exchange interactions are taken into account. However, the currents dealt with in superconductivity are not the quantum mechanical averages to which Bloch's results refer. One should distinguish the quantum average of the probability current, a locally, microscopically defined electric current,[2] a macroscopic average of this last current. Consequently Bloch's result does not imply that this latter current, necessarily vanishes.

[1] B. Bohm, Phys. Rev. **75**, 502 (1949).
[2] F. London, Phys. Rev. **74**, 562 (1948).

H11. Equation of the Magnetic Threshold Curve for Indium. G. PRESTON BURNS, *Mary Washington College of the University of Virginia.*—On the basis of the Gorter-Casimir expression[1] for the jump in atomic heat of a superconductor at its transition temperature and the assumption[2] that the specific heat of superconducting indium varies as T^4 it has been shown that the magnetic threshold curve for indium is given by

$$H=[H_0/(18\gamma_N T_c^2+D_N T_c^4)](18\gamma_N T_c^2+D_N T_c^4 - 30\gamma_N T^2-5D_N T^4+3KT^5)^{\frac{1}{2}},$$

where

$$T_c=1/9K\{[1458K^2\gamma_N+64D_N^3 +54K(729K^2\gamma_N^2+64\gamma_N D_N^3)^{\frac{1}{2}}]^{\frac{1}{3}} +[1458K^2\gamma_N+64D_N^3 -54K(729K^2\gamma_N^2+64\gamma_N D_N^3)^{\frac{1}{2}}]^{\frac{1}{3}}+4D_N\}.$$

K is the constant relating the specific heat of the superconducting body to T^4 and other symbols are as defined previously.[3]

[1] C. J. Gorter and H. Casimir, Physica 1, 306 (1934).
[2] A. D. Misener, Proc. Roy. Soc. 174, 266 (1940).
[3] G. P. Burns, Phys. Rev. 76, 999 (1949).

H12. Superconducting Properties of Columbium. D. B. Cook, M. W. Zemansky, and H. A. Boorse, *Columbia University.*—Various values of the superconducting temperature T_0 of columbium have been reported, ranging from 5.09° to 9.58°K; in addition transitions in magnetic fields have been observed in the helium temperature range. In view of the uncertainty of T_0 and the absence of magnetic field data above 4.2°K, we have measured transitions between 5° and 9° on analyzed columbium of the highest purity obtainable (99.8 percent or better). Changes from the superconducting to the normal state were observed by an a.c. induction method. Comparison measurements were made on columbium containing 0.4 percent tantalum as determined by neutron studies. Samples of the two materials, annealed and outgased at 1000°C, gave identical results. The $H-T$ curve may be represented approximately by the usual parabolic relation $H=H_0(1-T^2/T_0^2)$ with $H_0=7280$ oerst and $T_0=9.0$°K. This value of H_0 is more than twice as large as that corresponding to the earlier measurements in the helium range. These experiments were performed on cylinders 5 cm long and 2 mm in diameter in transverse fields and therefore yielded values of the ratio $\rho=H_i/H_f$, where H_i is the field necessary to initiate an $s-n$ transition and H_f is the field necessary to complete it. Observed values of ρ, which were in the range 0.65 to 0.71, showed a slight temperature dependence similar to that observed on tin and mercury. Work supported in part by ONR.

H13. Thermal Rayleigh Disk in Liquid Helium II. John R. Pellam, *National Bureau of Standards.*—The Rayleigh Disk[1] is employed to detect second sound mechanically and to examine the hydrodynamics of the internal convection of liquid helium II. A small disk-shaped mirror suspended at 45° to the wave propagation axis of a second sound system experiences a torque under conditions of resonance, thereby deflecting a light beam. The operation of this Rayleigh Disk depends upon its response to *presence* of particle velocity irrespective of sign (being a velocity squared effect) so that the net torque is the sum of the contributions by the two separate fluid components. Thus, whereas mechanical detectors of the microphone class do not recognize the internal convection peculiar to second sound, the present device (detecting *kinetic energy density*) resolves this internal motion. This experiment is regarded as an added confirmation of the two-fluid hypothesis for liquid helium II. Measurements of the wave velocity of second sound agree with previous determinations, and are being extended in the temperature region near the λ-point. The variation of observed torque with temperature is hoped to provide information on the relative roles (the hydrodynamics) of the normal fluid and the superfluid in their respective interactions with the disk.

[1] Lord Rayleigh, *The Theory of Sound* (Dover Publications, New York, 1945), Vol. II, p. 44.

Thursday Afternoon at 2:15

National Academy

(W. F. Meggers presiding)

Invited Paper

I1. Isotope Shift in Atomic Spectra of Heavy Elements. Hans Kopfermann, *University of Goettingen.* (30 min.)

Atomic Spectroscopy

I2. The Spectrum of He^3 I. Mark Fred, Frank S. Tomkins, and James K. Brody, *Argonne National Laboratory.*—Helium isotope shifts previously reported[1] have been extended and the He^3 hyperfine structure partially resolved. The h.f.s. of the ^3S levels is inverted, indicating a negative nuclear magnetic moment as expected. The splitting of the $2\,^3S$ level is 0.221 ± 0.005 cm^{-1} which is slightly smaller than given by hydrogenic wave functions with Anerson's[2] value for the magnetic moment; higher ^3S levels have a splitting of about 0.216 cm^{-1}. The stronger h.f.s. components of transitions to the ^3P and ^3D levels are not resolved but the structure must be considered in evaluating the isotope shifts. Including contributions from reduced mass and coupling effects the predicted and observed shifts differ by $\sim$0.1 cm^{-1} in the sense that the He^3 ^3S terms are higher and the ^1S, ^3D, and ^1D terms lower than expected with respect to the ^3P and ^1P levels. In addition, the trend of the differences for successive D series members indicates an increase in the repulsion of the ^3D and ^1D terms near the crossing at $n=8$ due to the fact that the He^3 ^3D h.f.s. is larger than the He^4 ^3D find structure.

[1] Fred, Tomkins, and Brody, Phys. Rev. 75, 1772 (1949).
[2] Herbert L. Anderson, Phys. Rev. 76, 1460 (1949).

I3. On the Nuclear Spin of Mo^{95} and Mo^{97}. O. H. Arroe, *University of Wisconsin.**—In hyperfine structure studies with separated isotopes** of Mo^{95} and Mo^{97}, certain lines, including $4d_{5s}{}^5\,{}^7S_3-4d_{5p}{}^5\,{}^7P_{234}$ and $4d_{5s}{}^5\,{}^5S_2-4d_{5p}{}^5\,{}^5P_{123}$, show clearly that the nuclear spin of each of these isotopes is different from the value $\frac{1}{2}$ previously listed[1] as probable.

* Supported by Navy contract.
** Supplied by the Y-12 plant, Carbide and Carbon Chemicals Division, on AEC allocation.
[1] N. S. Grace and K. R. More, Phys. Rev. 45, 166 (1934).

I4. The Isotope Shift in Pb II.* Felix E. Geiger, Jr., *University of Wisconsin.*—A new investigation of the isotope shift in PbII has been undertaken in the visible region of the spectrum with AEC allocated** lead samples enriched in the isotopes of Pb^{204} and Pb^{207} respectively. The ratio of the shift of Pb^{206} relative to Pb^{204} to the shift of Pb^{208} relative to Pb^{206}, i.e., $(\nu_{206}-\nu_{204})/(\nu_{208}-\nu_{206})=R$, has been measured for lines λ5608 $(7s\,{}^3S_{1/2}-7p\,{}^3P_{3/2})$, λ5544 $(7p\,{}^3P_{3/2}-7d\,{}^3D_{5/2})$, and λ5373 $(6s6p^2\,{}^4P_{5/2}-5f\,{}^3F_{7/2})$, and the following ratios have been obtained thus far: $R_{5506}=0.90$ (±0.01 limit of error), $R_{5544}=0.90$ (±0.05 limit of error). R_{5608} is in good agreement with results obtained earlier by Schüler and Jones.[1] Although

interconfiguration perturbations currently appear to make absolute determinations of the isotope shift virtually impossible, an attempt is being made to determine the shift in the $7s\ ^2S_{1/2}$ level previously reported to have no shift at all.[1]

* Work done under ONR contract.
** Produced by Carbide Carbon Chemicals Division, Y-12 Plant, Oak Ridge.
[1] Schüler and Jones, Zeits. f. Physik **75**, 563, 1932.

I5. Zeeman Effect in O_2.* A. F. HENRY, *Yale University.*—A general formula for the Zeeman levels in O_2 is derived. The calculation starts with a set of eigenfunctions corresponding to Hund's case (a); the external magnetic field and terms in the Hamiltonian leading to the rotational triplets are introduced as perturbations. The work proceeds in two stages. First eigenfunctions differing only in the value of Σ are combined. In the second stage three such combinations differing in the total angular momentum, J, are further combined. The energy levels which result from the last operation are in good agreement with the observations of Beringer and Castile.[1] Calculated line intensities are in tolerable agreement with preliminary measurements.

* This work was supported by the ONR.
[1] Robert Beringer and J. G. Castle, Jr., Phys. Rev. **75**, 1963 (1949).

I6. Spectroscopic and Extrapolated Ionization Potentials of Atoms and Ions. WOLFGANG FINKELNBURG, *Fort Belvoir.*—The accuracy and reliability of spectroscopic ionization potentials, particularly those of higher atomic ions, depends on the number of observed lines and the observability of combinations with the ground state. Therefore, interpolated or extrapolated values, if properly based on a sufficient number of reliable spectroscopic ionization potentials, may occasionally be more accurate than direct spectroscopic values with an insufficient basis. Consequently, there does not seem to be a reason to regard such extrapolated spectroscopic values more sceptically than so-called direct spectroscopic values based on an extrapolation from a small number of observed lines. The methods of interpolation and extrapolation of ionization potentials as presented in two recent Letters to the Editor (W. Finkelnburg and F. Stern, Phys. Rev. **77**, 303, 1950; W. Finkelnburg, Phys. Rev. **77**, 304, 1950) have been further extended and improved. The different available methods will be discussed with their inherent accuracy. 160 ionization potentials of the first 18 isoelectronic sequences have thus been calculated or corrected, making use of the direct spectroscopic values in C. E. Moore's book *Atomic Energy Levels.*

I7. Pressure Broadening of Spectral Lines and Frequency Modulation. HENRY MARGENAU AND STANLEY BLOOM, *Yale University.**—Under certain circumstances, the contour of a spectral line can be calculated by means of the so-called statistical theory, under others the impact theory is appropriate. Extreme conditions for the validity of either approximation are easily stated, but the manner in which the statistical distribution transforms itself into the impact distribution is difficult to investigate. We have chosen the solution of a well-known engineering problem, sinusoidal frequency modulation, as a simple instance of the transformation in question. The results to which it leads are physically meaningful and will be discussed in this paper. The "modulation index" determines the nature of the intensity distribution; if its value is large, statistical theory is applicable. Roughly, this index corresponds to the ratio of the maximum frequency shift during molecular impacts to the number of collisions per second. As for detail, however, the model is not sufficiently flexible to do justice to the line-broadening problem.

* Assisted by the ONR.

I8. A Coating Method Based on the Use of Electrically "Exploded" Wires. WILLIAM M. CONN, *Rockhurst College.*—Condensers of large capacitance are discharged through very thin wires, ribbons, or powdered metal in capillary tubes. Deposits are obtained which seem to be due to sputtering from the exploding wire and the cloud of disintegration products observed after the exposition. By exploding the wire in nitrogen or hydrogen metallic deposits are obtained on glass and other non-metallic objects, for example, as follows: Spark gaps 5 mm, length of wires 25 mm, diameter of wires 0.10 mm, pressure for silver 48 mm Hg, gold—140 mm, aluminum—350 mm. Deposits are of high reflectivity and good adherence; they may be used for partial mirrors for interferometer work, etc. The principal advantages of this method over well-known methods of coating—chemical deposition, spraying, cathode sputtering, and vaporizing—are the moderate low pressure and the short time required (10^{-5} to 10^{-6} second) for obtaining a layer on the object.

THURSDAY AFTERNOON AT 2:15

National Bureau of Standards

East Building Lecture Room

(R. M. BOZORTH presiding)

Ferroelectricity; Ferromagnetism; Electron Optics

J1. On Certain Matters Pertaining to Electrets. W. F. G. SWANN, *Bartol Research Foundation.*—Consider an electret of thickness L with surfaces perpendicular to the axis of x at $x=0$ and $x=L$, and polarized in the positive direction of that axis. Suppose that P_x decays with time through a factor $e^{-\alpha x}$ and that initially, as the result of the polarization and surface or volume charges, the potentials at $x=0$ and $x=L$ are V_0 and zero. Suppose the surfaces covered by foils joined by a resistance R which may be the internal resistance of the dielectric. Let C be the capacity. It results that if the disappearance of the charges is determined by Ohm's law, the variation of the potential V at $x=0$ *will be independent of the original distribution of charge.* Provided that V_0 is negative and that the time constant $1/\alpha$ is greater than RC, V will drop to zero in a time τ_1 of the order of RC. It will then rise to a positive maximum V_m in a time τ_2 and will finally decay to zero. Reasonable values of the quantities concerned are consistent with τ_1 being comparable with a day or two, τ_2 with a week, V_m of the order of 2000 volts with a decay to ½ of this value in three years.

J2. Electronic Theory of Ferroelectrics. E. T. JAYNES AND E. P. WIGNER, *Princeton University.*—Ferroelectrics of the $BaTiO_3$ type occur, according to Matthias,[1] whenever an ion

with a closed shell is surrounded by an octahedron of oxygen ions of a certain size. There is considerable evidence[2] that spontaneous polarization in $BaTiO_3$ is not due to displacement of the central Ti ion. Preliminary studies show that many of the properties of $BaTiO_3$ may be accounted for on the basis of a shift of electronic wave functions. Consider in first approximation each octahedron as possessing independent internal electronic states. If two states of opposite parity lie close together in energy, a large polarizability results. This leads to a spontaneous polarization in the usual Langevin-Weiss manner if we assume an effective internal field $E+\beta P$, and determine the Lorentz factor β by comparison with the experimental dielectric constant and polarization. By properly choosing the level scheme the rste at which polarization sets in below the Curie point can be made equal to the observed value.

[1] B. Matthias, Phys. Rev. 75, 1771 (1949).
[2] Danielson and Rundle, Phys. Rev. 75, 1630 (1949); Kay, Wellard, and Vousden, Nature 163, 636 (1949).

J3. Susceptibility Measurements Using the Moment Balance. J. A. OSBORN, *Naval Research Laboratory.*—A new type of null-reading balance has been designed for that type of susceptibility measurement using a specimen in a non-uniform magnetic field H. Instead of measuring the force on the specimen, as with the Faraday method, an equal and opposite vertical force is applied by a current-bearing coil wound on the capsule containing the specimen. The coil axis is in the applied field direction. The balance is thus returned to its null position. The average field applied to the sample is determined by reversing the magnet field and using the moment coil as a search coil. The coil moment M for a null balance position (known from the turns-area of the moment coil and its current) is determined with the sample in the coil M_i and out of the coil M_0. The total susceptibility χ of the sample is then given by: $\chi=(M_i-M_0)/H$. Advantages and sources of error of this balance will be discussed together with the results of initial measurements on specimens of known susceptibility.

J4. Properties of Single Crystals of Nickel Ferrite. J. K. GALT, B. T. MATTHIAS, AND J. P. REMEIKA, *Bell Telephone Laboratories.*—Single crystals of $NiFe_2O_4$ have been grown in a flux of borax by slow cooling from 1330°C. The amount of borax required is critical, and the oxides apparently dissolve in it, to be precipitated out later in the form of crystals as the charge cools and the borax sublimates. Measurements of dielectric constant and initial permeability have been made. The dielectric constant at liquid air temperature is approximately 20. High conductivity made satisfactory measurements above this temperature impossible. Initial permeability is approximately 100 at room temperature and 15 at liquid air temperature. Saturation magnetization is about 260 c.g.s. units. Data on magnetic anisotropy will be presented.

J5. Ferromagnetic Resonance in Single Crystals of Nickel Ferrite. W. A. YAGER, J. K. GALT, F. R. MERRITT, E. A. WOOD, AND B. T. MATTHIAS, *Bell Telephone Laboratories.*—Ferromagnetic resonance absorption has been observed in spherical samples of single crystals of nickel ferrite. The observations were made at a frequency of about 24,000 mc/sec. The anisotropy constant has been determined from the variation of resonance field as a function of crystallographic orientation using the equations first developed by Kittel.[1] The easy direction is found to be [111], as in magnetite,[2] and the anisotropy constant is $K_1=-6.0\times10^4$ ergs/cc. The g value after correction for anisotropy effects is 2.19. We have found that, if the spheres are as large as 0.039" diameter, structure occurs in the absorption line which we believe is due to a cavity type electromagnetic resonance in the sphere. This effect can produce an appreciable shift in the field for which maximum absorption occurs. In spheres of about 0.015" diameter only a single narrow line occurs, however. The width of this line is between 70 and 85 oersteds at all crystallographic orientations. Data on line width as a function of the position of the crystal in the r.f. field has also been obtained.

[1] C. Kittel, Phys. Rev. 73, 155 (1948).
[2] L. R. Bickford, Jr., Tech. Rpt. XXIII, Laboratory for Insulation Research, M.I.T. (October, 1949).

J6. Theory of Magnetic Dispersion in Ferrites. C. KITTEL, *Bell Telephone Laboratories.*—The a.c. magnetic susceptibility of ferromagnetic ferrites of high electrical resistivity will be composed of two parts: $\chi=\chi_{rot}+\chi_{disp.}$, where χ_{rot} is caused by domain rotation and $\chi_{disp.}$ by domain boundary displacement. The rotational susceptibility has a frequency dependence characterized by spin resonance in the anisotropy field near the frequency $\omega\approx g(e/2mc)(2K/I_s)$, with relaxation frequency Λ. The susceptibility caused by boundary displacement has a relaxation frequency dependence:

$$\chi_{disp.}=\chi_{disp.}{}^0/[1+j2\pi\chi_{disp.}{}^0\omega/nGB_s],$$

where n is the average number of boundaries intercepted by a line of unit length; G is the constant in the boundary velocity equation $v=GH$ and is shown by Landau and Lifshitz[1] to be given by $G=\gamma^2I_s(A/K)^{\frac{1}{2}}/\Lambda$, with magneto-mechanical ratio γ, wall thickness parameter $(A/K)^{\frac{1}{2}}$, and relaxation frequency Λ as above. The interpretation suggested here is in qualitative accord with measurements[2] on magnesium ferrite.

[1] L. Landau and E. Lifshitz, Physik. Zeits. Sowjetunion 8, 153 (1935).
[2] Welch, Nicks, Fairweather, and Roberts, Phys. Rev. 77, 403 (1950).

J7. Thin Ferromagnetic Films.* MARTIN J. KLEIN AND ROBERT S. SMITH, *Case Institute of Technology.*—A theoretical study of the magnetization of thin ferromagnetic films has been made using the method of spin waves. The magnetization is known to be of the form A minus B where A is a constant (the magnetization with spins parallel) and B is a sum over all spin wave vectors which gives the effects of out of line spins. We have evaluated the magnetization by replacing the sum B by an integral over λ_x and λ_y (corresponding to spin waves in the plane of the film), and summing explicitly on λ_z (corresponding to waves perpendicular to the plane). When the film is sufficiently thick the latter sum can be replaced by an integral and the film behaves as a three-dimensional crystal, showing spontaneous magnetization which obeys the Bloch $T^{\frac{3}{2}}$ law. When the film is too thin for this replacement, essentially two-dimensional behavior is obtained: B becomes of the order of A indicating no spontaneous magnetization. The thickness at which the transition in behavior occurs depends on the film area and the temperature in a manner which will be discussed.

* Research supported in part by ONR.

J8. Mechanism of Remagnetization in an Initially Saturated Ferromagnet.* H. EKSTEIN AND T. GILBERT, *Armour Research Foundation.*—The mechanism by which a perfect ferromagnetic crystal, magnetized to saturation by an external field, changes its magnetization when the field is reversed has been theoretically investigated, using a method which avoids the difficulty of taking the interaction between the ferroelectrons and the rest of the crystal (conduction electrons, lattice vibrations, etc.) explicitly into account. Reasoning from the results of the Sixtus-Tonks experiments, one can justify the assumption that remagnetization only occurs after the formation of a small nucleus of reversed magnetization. The time required for a nucleus to form after the field is reversed is found to be $t_n=t_d/\mathfrak{P}$, where t_d is the decay time of a nucleus before the field is reversed and P is the probability of a nucleus occurring before the field is reversed. P is found to be given by $\log P=-1.39n$, where $n\approx10^7$ is the minimum number of spins in a critical nucleus from which remagnetization can

proceed. Since $t_d \approx 10^{-8}$ sec., t_n is extremely large, and it appears that observed remagnetization is probably due to crystal irregularities, non-magnetic inclusions, or inhomogeneous demagnetization fields existing near sharp irregularities at the crystal boundary.

* Supported by ONR.

J9. Effect of Tension on Magnetic Properties in Iron-Cobalt. H. H. PLOTKIN AND J. E. GOLDMAN, *Westinghouse Research Laboratories.*—The influence of tension on the magnetic properties of iron-cobalt of various cobalt compositions has been investigated. Samples of Hiperco 35 and Hiperco 50 (iron-cobalt alloys containing 35 percent cobalt and 50 percent cobalt respectively with small chromium additions)[1] in the form of strips 28×3×.062 cm supplied by J. K. Stanley of this laboratory were measured on a Carr permeammeter.[2] Tensions up to 2000 lb./sq. in. were applied and the complete magnetization curve measured at each value of the tension. For the 35 percent alloy, the permeability increased at all inductions. This is thermodynamically consistent with the known positive slope of the magnetostriction curve of the alloy. In the 50 percent alloy, the permeability is decreased by tension at low inductions but increased at higher inductions. Measurements were extended to a 65 percent cobalt alloy. In the latter case the effect of tension is to increase the permeability at all inductions. An x-ray investigation of the crystal orientation in the 50 percent alloy shows two definite preferred orientations. An explanation of the effect of tension in such a non-random alloy based on the effective demagnetizing force normal to the plane of the sample will be given.

[1] J. K. Stanley, Trans. A.S.M. (1949).
[2] W. J. Carr, Technical Publication No. 85, American Society for Testing Materials (1949).

J10. Magnetostriction in Magnetic Alloys with Preferred Crystal Orientation. J. E. GOLDMAN, *Westinghouse Research Laboratories.*—In grain oriented iron-silicon alloys, the magnetostriction as measured on strip samples is negative at values of induction up to approximately $B_s/\sqrt{2}$. The magnetostriction as a function of induction for alloys of Fe—Co with pronounced grain orientation has also been investigated on samples of similar shape. The results for the 50 percent alloy show a similar negative region although smaller in magnitude. The single crystal magnetostriction constant λ_{100} in the case of Fe—Si is known to be positive. Moreover, the magnetostriction curve for an alloy of 65 percent cobalt-iron shows a positive slope at all inductions suggesting that the magnetostriction constants are likewise positive in the case of Fe—Co where no single crystal data are available. It is suggested that the negative magnetostriction in both cases is due to the large demagnetizing field normal to the plane of the sheet. If the magnetically preferred crystal direction is out of the plane of the sheet, the demagnetizing field causes some of the domains to be magnetized in directions of easy magnetization other than those nearest the field. This can be shown to give rise to a negative magnetostriction even in materials where the magnetostriction constants are positive.

J11. Quantitative Field Mapping by the Electron Optical Shadow Method. J. AROL SIMPSON, *National Bureau of Standards.*—The method described is applicable to electric or magnetic fields of from 1 to 100 microns in extent. It requires only that the field in question have a plane such that an electron ray initially in the plane remain in the plane. Such a plane will be referred to as an "equatorial plane." The data required is a series of shadowgraphs of the field, taken, as previously described,[1] as the field is rotated about an axis perpendicular to the equatorial plane. Measurements made on these shadowgraphs can be reduced by a simple formula involving the constants of the observing instruments to a plot of angular deflection as a function of beam incidence angle and distance from optical axis. A numerical integration method is then applied to obtain the field. The accuracy of the method is discussed as well as the possibility of extension to fields where no "equatorial plane" as defined, exists.

[1] L. Marton and S. H. Lachenbruch, J. App. Phys. 20, 1171 (1949).

J12. Fringe Field Observations of Domains. L. MARTON, J. A. SIMPSON, AND A. VAN BRONKHORST, *National Bureau of Standards.*—The change of the shadow patterns produced by the fringe fields of ferromagnetic domains of a cobalt single crystal are investigated as the crystal is rotated about one edge as an axis. The domains are oriented at approximately right angles to the axis. The shadow patterns show an axis of symmetry which is maintained throughout the rotation, showing an "equatorial plane" through this axis of symmetry. As a result, the actual field strength could be calculated in this plane. Numerical values will be communicated. The investigation of the fringe fields of ferroelectric domains has been continued. It was found that with the reduction of the observing beam intensity, the shadow patterns due to accumulated charge disappeared but small portions of the pattern remained at places where light optical observations indicated the presence of domain boundaries. These domain fields are so weak as to be completely masked by the field of accumulated charge.

J13. A Theorem on the Focusing of Electron Beams in Magnetic Fields of Certain "Mirror" Symmetry, with Two Corollaries, One on the Fringe Effect. P. A. STURROCK, *National Bureau of Standards* (Introduced by L. Marton).—Magnetic fields whose scalar potential has a plane of antisymmetry are considered. The theorem establishes ray equations in a form which displays the focusing properties of a beam traveling near to the plane. The first corollary states the condition that a proposed beam path and proposed focusing conditions should be physically realizable. The second corollary shows that the fringe effects of fields which have sharply defined boundaries may be characterized by a pair of focal lengths for which simple formulas are given.

Invited Paper

J14. Fundamental Processes of Magnetization Shown by Movies. W. SHOCKLEY, *Bell Telephone Laboratories.*

FRIDAY MORNING AT 10:00

National Bureau of Standards, East Building Lecture Room

(A. VON HIPPEL presiding)

Semi-Conductors; Photoelectric Phenomena in Crystals

K1. On the Theory of Noise in Semiconductors. R. L. PETRITZ AND A. J. F. SIEGERT, *Northwestern University.*—The contribution to the noise in semiconductors made by fluctuations in the number of conduction electrons has been calculated by Davydov and Gurevich,[1] Gisolf,[2] and by H. Snyder (unpublished) under the assumption that the probability of

losing a conduction electron by trapping is independent of the number of conduction electrons present. This is not the general case since the trapping probability is proportional to the number of unoccupied localized states and can thus depend on the number of conduction electrons. For the standard model of a semiconductor, where the number of empty localized states equals the number of conduction electrons, we obtain in the low temperature case the power spectrum

$$\frac{1}{2}\frac{euF^2}{R}\left\{\frac{\tau}{1+(\omega\tau/2)^2}+\frac{\tau/2}{1+(\omega\tau/4)^2}\right\}d\nu$$

(Gisolf's notation). We have also computed the general case of which the above and the corresponding term in Davydov's result are the limiting cases.

[1] B. Davydov and B. Gurevich, J. Phys. U.R.S.S. 7, No. 3, 138 (1943).
[2] J. H. Gisolf, Physica 15, 8–9, 825 (1949).

K2. Perturbed Periodic Wave Equation in Three Dimensions. PAULA FEUER AND HUBERT M. JAMES, *Purdue University.*—The three-dimensional Schrödinger equation with periodic potential modified by a slowly varying perturbation $V(\mathbf{r})$ has been discussed by Peckar and Slater. Slater[1] expresses solutions as sums of localized orthogonal functions with coefficients obtained by solving a wave equation wherein the potential energy term is a constant plus $V(\mathbf{r})$ and the Laplacian of the Schrödinger equation is replaced by a differential operator of high order, which is effectively the Laplacian when applied to solutions with energies sufficiently near a band edge. In this case Slater's approach can lead also to Peckar's solution. For other energies, Slater's high order differential equation is not easily discussed. A modification of Slater's approach shows that, for cubic lattices and energies not too far from a band edge, Slater's equation can be replaced by an ordinary Schrödinger equation involving an effective potential derived from $V(\mathbf{r})$. This equation corresponds to the effective wave equation found by James[2] in the one-dimensional case, or to a wave equation in which the potential energy is exactly $V(\mathbf{r})$, but the effective mass varies appropriately with $E-V(\mathbf{r})$.

[1] J. C. Slater, Phys. Rev. 76, 1592 (1949).
[2] H. M. James, Phys. Rev. 76, 1611 (1949), Eqs. (4.58), (4.59).

K3. Potential Fluctuations in Homogeneous Semiconductors.* HUBERT M. JAMES AND GUY W. LEHMAN, *Purdue University.*—Even in homogeneous semiconductors the random distribution of impurities produces potential fluctuations that may affect conductivity. A theory of these fluctuations has been developed, for impurities with zero or finite activation energies. Their importance is greater the higher the impurity density, the lower the activation energy, and the lower the temperature. They are particularly great in semiconductors with very nearly equal densities N_+ of p-type and N_- of n-type impurities. In Ge, with $N_+=N_-=10^{16}$ impurities/cc, the fluctuations at room temperature are of the order of kT, with range of the order of 10^{-4} cm; a five percent difference in N_+ and N_- reduces their magnitude to half this, and their range to one-fourth. With impurities of a single type, the fluctuations at room temperature range from 0.015 ev for $N=10^{18}$ to 0.0015 ev for $N=10^{14}$, for all activation energies up to 0.1 ev. At lower temperatures the activation energy becomes an important factor. The fluctuations eventually decrease much faster than kT if there is an activation energy, but remain almost constant if the activation energy is zero, becoming important at low temperatures for all N.

* This and the preceding paper were supported in part by a Signal Corps contract.

K4. Electrical Properties of Semiconductors with Macroscopic Discontinuities. J. C. M. BRENTANO AND D. H. DAVIS, *Northwestern University.*—We found that the d.c. conductivity of certain semiconducting materials (Al_2O_3, ZnO, BaO, SnO_2 not CuO, Cu_2O) possessing internal boundaries is time dependent: with a constant external e.m.f. the current decreases with time. This decrease is not exponential but follows approximately the relation $i=A-B\ln t$. After passing the current a reverse current is observed on closed circuit, which also falls off with time. The initial value of this reverse current is larger after the primary current was flowing for a shorter time, it is smaller after the primary current was flowing for a longer time. The d.c. current for small applied potentials ($eV<kT$) does not obey Ohm's law. The a.c. conductivity obeys Ohm's law; it is frequency dependent even for low frequencies. The observed phenomena cannot be interpreted on the ground of simple condenser or electrolytic action at the boundaries. A model accounting for them assumes two types of carriers with different signs and mobilities. The displacement of carriers of high mobility gives origin to space charges at the boundaries which reduce the current. The displacement of carriers of opposite polarity and small mobility establishes dipole layers which partly trap and neutralize the carriers of the first type.

K5. The Transition from Insulating to Metallic Behavior in Semiconducting Silicon. G. W. CASTELLAN* AND F. SEITZ, *University of Illinois.*—Pearson and Bardeen have found that the ionization energy of carriers in pure silicon to which phosphorus or boron are added decreases with increasing concentration and becomes zero for concentrations in the vicinity of $5\cdot10^{18}$ per cc. This result is obtained from a range of temperature in which the fraction of donator or acceptor levels that are ionized lies between 1 and about 0.1, the most accurate values of the ionization energy being derived for the latter end of the range. Pearson and Bardeen have suggested that the decrease in ionization energy arises from the attractive Coulomb interaction between the free carriers and the ionized impurity atoms. It is pointed out that if this is the important interaction its contribution should depend primarily upon the density of carriers and not upon the density of impurity atoms and should become very small when the density of carriers is small. In fact the agreement found by Pearson and Bardeen on the basis of their assumption diminishes when as few as a tenth of the centers are ionized. Moreover, the experimental evidence suggests that the ionization energy actually depends upon the total density of impurity atoms and not upon the density of free carriers.

* AEC postdoctoral fellow.

K6. Theory of Infra-Red Absorption in Silicon and Germanium. J. BARDEEN, *Bell Telephone Laboratories.*—Mobile carriers and those weakly bound to donors and acceptors contribute to the absorption in germanium and silicon in the infra-red.[1,2] The magnitude of this absorption is much larger than that given by the semiclassical Drude-Zener theory which expresses the absorption in terms of the relaxation time, τ_0, associated with the low frequency conductivity. In an attempt to resolve this discrepancy, we have made a quantum-theoretical calculation based on second-order transitions in which a carrier absorbs a photon and emits or absorbs a phonon. Direct absorption by mobile carriers is forbidden by selection rules and is small for bound carriers. The formula obtained is similar to the classical except that τ_0 is replaced by an average value corresponding to the excited electron. If only the acoustical modes are considered, the theory gives an increase in absorption which is insufficient to account for the discrepancy. It is suggested that the absorption results mainly from interaction of the carriers with higher vibrational modes which can be excited if the incident photons have sufficient energy. Such absorption is relatively temperature independent.

[1] M. Becker and H. Y. Fan, Phys. Rev. 76, 1531 (1949).
[2] H. B. Briggs, Phys. Rev. 77, 727 (1950).

K7. Metallographic Study of Germanium Point Contact Rectifiers. M. H. DAWSON AND B. H. ALEXANDER, *Sylvania Electric Products, Inc.*—Germanium point contact rectifiers were prepared and mounted in methyl methacrolate. These units were ground down parallel and perpendicular to the tungsten whisker. For those units ground in a direction perpendicular to the whisker, the peak inverse voltage and the forward current started to decrease when the thickness of the Ge became less than 8×10^{-3} in. An explanation for this phenomena is discussed. Those units ground down to reveal the nature of the whisker-germanium contact exhibited a characteristic pit immediately below the whisker contact. Little change was observed in the reverse current before and after pitting, but the forward current dropped markedly. These phenomena indicate that the forward current flows throughout the contact area whereas the reverse current flows only at the periphery of the contact. Upon pulsing the rectifier and watching the contact under high magnification, the germanium was observed to melt for a region within 2×10^{-3} cm of the contact.

K8. Photo-conductivity of Trapped Electrons in the Alkali Halides. J. J. OBERLY AND E. BURSTEIN, *Naval Research Laboratory.*—Data obtained at room temperature show a considerable difference in the relative response of the various color center bands—*F*, *R*, *M*, *N*[1]—and also in the relative response of the *F*-band itself following various treatments of the crystal. All of these bands were known to be bleached by monochromatic light and thus perhaps photo-conductive. In a KCl crystal colored by a short exposure to x-rays, only the *F*-band was present and it was quite photo-conductive as reported by others. On the other hand, in an additively colored KCl crystal which had all of the absorption bands present in strength, the *F*-band was much less photo-conductive; the *R*- and *N*-bands showed considerable response, but the *M*-band comparatively little. It was noted that weak *N*-band response was obtained when no appreciable *N* absorption band was present. This behavior of the *F*-band, as well as other of its properties, would appear to indicate that it is a superposition of bands due to different types of centers. Other mechanisms which could account for this behavior will be discussed. Measurements to be made at low and high temperatures should provide more conclusive evidence.

[1] E. Burstein and J. J. Oberly, Phys. Rev. **76**, 1254 (1949).

K9. The Nature and Properties of Trapped Holes in the Alkali Halides. E. BURSTEIN AND J. J. OBERLY, *Naval Research Laboratory.*—The trapping of positive holes by positive ion vacancies in the alkali halides should be closely analogous to the trapping of electrons by negative ion vacancies. Color centers associated with holes trapped at positive ion vacancies and aggregates of positive ion vacancies may be expected under appropriate conditions which are analogous to the *F*, *F'*, *R*, *M*, and *N* centers associated with trapped electrons. Further, the color centers due to trapped holes should exhibit optical properties similar to those of trapped electrons, and a number of these centers should be photo-conductive, yielding free holes either by direct optical excitation (as for *F'* centers) or indirectly by a combination of optical and thermal excitation (as for *F* centers). The stability of the various trapped hole centers at any given temperature will in general differ markedly from that of trapped electron centers as a result of differences in the thermal diffusion and rate of aggregation of trapped holes and electrons which are associated with differences in the thermal diffusion of positive and negative ion vacancies. Recent measurements on trapped hole color centers will be discussed in the light of these considerations.

K10. Constant Quantum Efficiency of Some Luminescent Materials in the Vacuum Ultraviolet. K. WATANABE, F. S. JOHNSON, AND R. TOUSEY, *Naval Research Laboratory.*—The quantum efficiency of fluorescence was found by Harrison and Leighton[1] to be constant from 2400 to 4000A for aesculin and certain oils. We have found constant quantum efficiency for pump oil and a few other materials from 2400 to 900A. A vacuum monochromator and hydrogen discharge tube source were used. The resolution was 16A or less. The energy emerging from the exit slit was known from measurements made by Packer and Lock[2] with a thermocouple. The phosphor studied was coated on the envelope of a photo-multiplier placed in vacuum an inch behind the exit slit, and an area approximately 10 mm^2 was irradiated. This result makes it possible to use a fluorescent material and a photo-cell for making energy measurements instead of a thermocouple, and extends to 900A the region over which heterochromatic photographic photometry can be carried out by Harrison and Leighton's method.[1] Materials were found with adequate response speed and stability and with linear intensity of fluorescence over the intensity range covered. Among other phosphors studied, were counting crystals such as $CaWO_4$, CaF_2, LiF, and anthracene.

[1] G. R. Harrison and P. A. Leighton, Phys. Rev. **38**, 899 (1931).
[2] D. M. Packer and C. Lock, Paper No. 65, Meeting of the Optical Society of America, March 11, 1950.

K11. Some Phenomena in Diamond Gamma-Ray Counters.* E. PEARLSTEIN† AND R. B. SUTTON, *Carnegie Institute of Technology.*—Gamma-ray counting diamonds have been studied with respect to polarization[1] and the effects of heat treatment. It is found that the counting rate decreases and then increases with time, for high field strengths (~10,000 volts/cm); for low field strengths the counting rate monotomically decreases. If a diamond is given a heat treatment of 400°C for ten minutes its counting properties are changed as follows: The counting rate is initially much lower than before heat treatment; while counting it further decreases, then slowly rises to its value before heat treatment. If the diamond is one which before heat treatment could be polarized with no irradiation it cannot become so polarized after treatment. Several hours' exposure to gamma-rays or a few seconds' exposure to ultraviolet light nullifies the heat treatment. To explain this behavior more than one set of impurity levels appears to be required. Data on electron range and mobility, measured with unpolarized samples, will be given.

* This work was supported by the Bureau of Ships and ONR.
† AEC predoctoral fellow.
[1] See R. K. Willardson and G. C. Danielson, Phys. Rev. **77**, 300 (1950) and the references quoted therein.

K12. Scintillation Spectra of Some Organic Crystals. W. S. KOSKI AND C. O. THOMAS, *Johns Hopkins University.*—Using a Hilger quartz spectrograph and Eastman 103-0 plates the scintillation spectra of a series of structurally related organic crystals was measured. The same spectra were obtained for any one crystal, regardless of whether the mode of excitation was due to α-, γ-, or x-rays. The data are as follows.

Crystal	Wave-length of center of band	Width at half-max.
Diphenylethane	3925±50 (weak) 3765 (strong) 3525 (strong) 3395 (weak)	— 400 —
Stilbene	3975 (strong)	375
Tolane	3775	315
Bistyryl	4585 (strong) 4395 (weak)	325

The apparent correlation between structure of the molecules and the intensity and spectra of the scintillations will be discussed.

FRIDAY MORNING AT 10:00

Department of Interior Auditorium

(E. T. BOOTH presiding)

Mostly Pertaining to Neutrons

L1. Nuclear Energy Levels in Lead.* R. K. ADAIR,† C. K. BOCKELMAN, AND R. E. PETERSON, *University of Wisconsin.*—Total cross-section measurements for fast neutrons have been made on Pb^{206}. Values of the cross section were determined by transmission experiments using neutron energy spreads of 5 kev and 3 kev. Resonances were observed, many of which took the form of dips rather than peaks. The average spacing between levels appears to be about 50 kev. Previous investigations of ordinary Pb had disclosed the presence of three resonances which were attributed to levels in Pb^{209}, the compound nucleus formed by the interaction of neutrons with Pb^{208}.[1] These peaks have been reinvestigated with a neutron energy spread of about 3 kev. The height of the peaks so measured, together with the knowledge of the variation of the part of the cross section attributed to Pb^{206}, allows a more reliable determination of the spins and widths of the levels in Pb^{209}.

* Work supported partly by the AEC, partly by the Wisconsin Alumni Research Foundation.
† AEC Predoctoral Fellow.
[1] Barschall, Bockelman, Peterson, and Adair, Phys. Rev. 76, 1146 (1949).

L2. Nuclear Energy Levels in Sulfur.* R. E. PETERSON, R. K. ADAIR, H. H. BARSCHALL, AND C. K. BOCKELMAN, *University of Wisconsin.*—The total neutron cross section of sulfur has been measured for neutron energies in the range 15 to 750 kev. Neutron energy spreads of from 4 to 9 kev were used in making a survey of the variation of cross section with neutron energy; certain energy regions were later re-investigated with an energy resolution of from 1.5 to 3 kev. Nine maxima in the cross section were observed in the energy interval studied. These are attributed to the effect of energy levels in S^{33} producing resonances in the elastic scattering. Maxima observed at 111, 375, and 700 kev are preceded by minima presumably caused by interference between resonance and potential scattering;[1] *s*-neutrons should be responsible for these resonances. *p*-neutrons, yielding compound nuclei of spin $3\hbar/2$, probably cause a resonance observed at 585 kev. The remaining maxima are believed to be due to neutrons of one unit of angular momentum also. Natural widths of the resonances at 111, 375, 585, and 700 kev are estimated to be 18, 12, 1.5, and 12 kev, respectively.

* This work was supported by the Wisconsin Alumni Research Foundation and the AEC.
[1] Adair, Bockelman, and Peterson, Phys. Rev. 76, 308 (1949).

L3. Neutron Capture-Radiation from Heavy Elements, G. A. BARTHOLOMEW, B. B. KINSEY, AND W. H. WALKER, *Chalk River.*—The spectra of the gamma-radiation produced by slow neutron capture in heavy elements have been measured with the aid of a pair spectrometer. Cu, Zn, Sr, Cd, In, Sn, W, and Au all produce anumber of homogeneous radiation superimposed on a continuous background of unresolved radiations (resolution 2 percent). The Pb spectrum contains two radiations only, which are emitted in direct ground state transitions of Pb^{207} and Pb^{208}. Bi emits radiations corresponding to transitions from the capturing state to low lying excited states in Bi^{210}. These simple spectra may be associated with closed neutron and proton shells. The spectrum of Sn (50 protons), on the other hand, is similar to those of other heavy elements.

L4. Fast Neutron Capture Cross Section of AL^{27} as a Function of Energy.* R. L. HENKEL AND H. H. BARSCHALL, *University of Wisconsin.*—The fast neutron capture cross section of Al^{27} has been measured by observing the 2.4-minute β-activity of Al^{28}. This activity was induced by neutrons of energies between 150 and 700 kev. Radiative capture is the only absorption process in this energy range. Neutrons of variable energy were produced by the $Li^7(p,n)Be^7$ reaction, using the Wisconsin electrostatic generator. Cross sections were determined by comparison with the known thermal capture cross section of aluminum. A BF_3 proportional counter was employed for monitoring the neutron flux during this comparison, making use of the known energy dependence of the disintegration cross section of boron. The aluminum capture cross section in the energy range studied has values between 1 and 6 millibarns and shows resonance levels corresponding reasonably well to those levels found in the total neutron cross section. A quantitative comparison between level energies is made difficult by the complicated level structure and the poor energy resolution (20 to 30 kev) used in this preliminary work.

* Work supported partly by the AEC, partly by the Wisconsin Alumni Research Foundation.

L5. Neutron Capture γ-rays from Mg, Si, P, and K. B. B. KINSEY, G. A. BARTHOLOMEW, AND W. H. WALKER, *Chalk River.*—Pair spectrometer measurements of the γ-radiation resulting from slow neutron capture in Mg^{24} and Mg^{25} have failed to reveal direct transitions from the capturing state to the ground state. Radiations emitted in transitions to excited states are observed. The direct ground state radiations produced by capture in Si^{28} and Si^{29} were found to be very weak. Those produced by capture in K^{39} and K^{41} are much stronger although they are weaker than radiations emitted in transitions to excited states. Two units of angular momentum must be radiated in the ground state transitions following capture in Mg^{24} and K^{39}, one or two units in P^{31} and possibly one unit only in Si^{28}. It will be shown that the intensities of these radiations relative to those producing excited states cannot be explained in terms of selection rules which depend only on changes in nuclear spin and parity.

L6. On the Scattering of Slow Neutrons by Solid Helium. L. GOLDSTEIN AND D. SWEENEY, *Los Alamos Scientific Laboratory.*—The theory of slow neutron scattering by crystals has been applied to solid heavy helium at temperatures less than about 4°K and at neutron kinetic energies larger than about twice the approximate Debye temperature (~35°K) of solid helium. The coherent scattering cross section per atom is found to be small in comparison with the free atom scattering cross section especially at higher neutron energies. This reduction is due to the very large zero-point energy term in the exponent of the exponential temperature factor. As a result the coherent scattering becomes practically temperature independent. The incoherent scattering is a multiphonon excitation process at the neutron energies considered here. The incoherent scattering cross section is also practically temperature independent and tends, at large neutron energies, toward the free atom scattering cross-section value. The theory is being extended to the extreme solid model of liquid helium, the latter being assumed to have also the ideal hexagonal close packed structure which appears to be the most probable structure of the solid.

L7. Neutron Scattering Resonance in Cl^{35} at −73 Ev. C. T. HIBDON AND C. O. MUEHLHAUSE, *Argonne National Laboratory.*—Using a 4π-BF_3 annular neutron scattering chamber and a resonance neutron beam from the Argonne heavy water reactor, the total neutron cross section of chlorine was measured at 120 ev, 345 ev, and 2700 ev by the resonance scattering detection of Co, Mn, and V respectively.[1] By subtracting the $1/v$ absorption term, the scattering cross sections were obtained at these energies. The coherent neutron scattering cross section and the thermal scattering cross section[2] for chlorine were used to evaluate the thermal scattering amplitude, $\lambda\Gamma/2E_0$, as $\simeq 1$. The data is consistent with the following expression for the one-level Breit-Wigner scattering cross section, σ_s, as a function of energy when $E-E_0 \gg \Gamma$:

$$\sigma_s = 1.37 + \frac{600}{E+73} + \frac{24500}{(E+73)^2}, \quad (E>0).$$

The resonance parameters for Cl^{35}, $(i=\frac{3}{2})$, have the following values:

$$J=2, \quad R=0.82\times 10^{-12}\ \text{cm}\ \frac{\Gamma n}{\Gamma} \simeq 0.9.$$

[1] C. T. Hibdon and C. O. Muehlhause, Phys. Rev. **76**, 100 (1949).
[2] E. O. Wollan and C. G. Shull, Phys. Rev. **73**, 830 (1948).

L8. Neutron Scattering Cross Sections of the Noble Gases. S. P. HARRIS, *Argonne National Laboratory.*—Using the annular BF_3 scattering chamber described previously,[1,2] the scattering cross sections of He, Ne, A, Kr, and Xe were measured for sub-cadmium and resonance neutrons. Only Kr and Xe showed cross sections high enough so that it was significant to measure their transmission in these regions by self-indication. A small aluminum cell having 2-mil aluminum windows and filled with the gas to be measured was placed in the center of the annular chamber. This served as detector by scattering neutrons from the beam. A[3], Kr, and Xe all indicated resonances via boron absorption. The greatest resonance effect was in Xe. Its effective scattering cross section (by comparison with graphite) was highest with only cadmium filtering (about 20 barns). Under the same conditions the self-indication transmission cross section was about 500 barns. Xe thus appears to have a resonance with a considerable portion of scattering in the energy region of a few electron volts. The resonance (or resonances) is probably associated with one of the even Z odd N isotopes (Xe^{129} or Xe^{131}).

[1] Harris, Langsdorf, and Seidl, Phys. Rev. **72**, 866 (1947).
[2] C. T. Hibdon and C. O. Muehlhause, Phys. Rev. **76**, 100 (1949).
[3] E. Melkonian, Phys. Rev. **76**, 1750 (1949).

L9. Capture γ-Ray Multiplicity. C. O. MUEHLHAUSE' *Argonne National Laboratory.*—The average number of γ-rays, $\nu\gamma$, per neutron capture was measured for about thirty isotopes. A thermal plus resonance neutron beam from the Argonne Heavy Water Reactor was made to pass through various thin neutron absorbing foils. Two anthracene scintillation counters in coincidence straddled the beam and foils. The ratio of coincidence to single counting rate, c/s, was recorded for each absorber. c/s is proportional to $\nu\gamma-1$, and calibration was effected with the γ-rays from Co^{60} and Na^{24}. In the cases of Mn^{55}, As^{75}, and Au^{197} $\nu\gamma$ was measured for both thermal and resonance neutrons, and found to be independent of neutron energy. Gamma-ray angular correlations were also investigated, but no significant effects were found. Correlations of $\nu\gamma$ with atomic weight, level density, and nuclear type (odd and evenness of protons and neutrons) will be presented.

L10. Angular Distribution of Neutrons from 15-Mev Deuterons on Thick Cyclotron Targets.* C.E. FALK, *Carnegie Institute of Technology.*—It has been reported at an earlier date that the angular distributions of neutrons resulting from the bombardment of thick targets by deuterons of about 15 Mev was very sharply peaked in the forward direction. With the help of a counter telescope, consisting of four proportional counters with variable aluminum absorbers in front of the first and fourth counter, anti-coincidence analyzer, and threshold detectors, the study of the above phenomena has been extended. It has been found that the distributions consist sometimes of a single peak in the direction of the deuteron beam and sometimes of double peaks symmetric about the direction of the deuteron beam. The distribution can possibly be explained by stripping, the double peaks being caused by the Coulomb interaction. Neutron spectra have been taken at several parts of the angular distributions. The interpretation of the spectra with respect to stripping theory will be discussed.

* This work was carried out with the assistance of ONR.

L11. The Inelastic Scattering of High Energy Neutrons by Deuterons and the Neutron-Neutron Interaction. GEOFFREY F. CHEW, *University of California, Berkeley.*—Because elastic scattering represents a considerable fraction of the total *n-d* cross section even at high energy,[1,2] it is dangerous to assume that the latter is composed additively of *n-p* and *n-n* cross sections. Non-additive effects are less important in inelastic scattering, however, and one may attempt to derive information about the high energy *n-n* cross section from an observation of the disintegration protons. A theoretical approach has been developed to relate *n-d* inelastic scattering to free *n-p* and *n-n* scattering cross sections at the same energy, *without reference* to the nature of nuclear forces. The method depends on the short range of nuclear forces and on the smallness of two-body cross sections compared to the size of the deuteron but is *not* a Born approximation. Analysis of Powell's[2] preliminary data on this basis indicate the 90-Mev *n-n* cross section to be *less* than 15 mb. Since the proton-proton cross section at 350 Mev is ~30 mb,[3] doubt is cast on the equality of *n-n* and *p-p* interactions at high energies. This work was sponsored by the AEC.

[1] G. F. Chew, Phys. Rev. **74**, 809 (1948).
[2] See Abstract by W. Hartsough, M. Hill, W. M. Powell.
[3] Chamberlain and C. Wiegand, Bull. Am. Phys. Soc. **25**, No. 1, H-6 (1950).

L12. Deuterons Bombarded by 90-Mev Neutrons.* WALTER HARTSOUGH, MILTON HILL, AND WILSON M. POWELL, *University of California, Berkeley.*—A deuterium filled Wilson cloud chamber with heavy water vapor in a 21,700-gauss field was bombarded by 90-Mev neutrons produced by 190-Mev deuterons bombarding a half-inch thick beryllium target. The deuterons in the cloud chamber are elastically scattered one-third of the time and show a sharp peak in the forward direction in accord with "pick-up" theory,[1] a valley at 30 degrees, and another peak at 80 degrees. The proton fragments show a broader peak forward reaching half-value at 35 degrees. A few protons go backward, and one might interpret these as the residue of neutron-neutron collisions.[2] They amount to about five percent of the total number of events and may be used to obtain a rough estimate of the total neutron-neutron cross section relative to that of the deuteron.[3] This work was supported by the AEC.

[1] G. F. Chew and M. L. Goldberger, Phys. Rev. **77**, 470 (1950).
[2] See Abstract by G. F. Chew.
[3] Cook, McMillan, Peterson, Sewell, Phys. Rev. **75**, 7 (1949).

FRIDAY MORNING AT 10:00

National Academy

(I. I. RABI presiding)

Theoretical Physics, Largely Nuclear

M1. Scattering of Light by Light. ROBERT KARPLUS AND MAURICE NEUMAN, *Institute for Advanced Study.*—Previous investigations of the interaction of light with an electromagnetic field were beset by difficulties due to the appearance of divergent integrals and non-gauge invariant expressions. The recent improvements in the perturbation techniques of field theory, however, have made the calculation of these effects feasible. Accordingly a convergent, gauge invariant, and closed expression for the non-linear terms in the Lagrangian responsible for this interaction in the lowest non-vanishing order has been obtained. It could serve as a basis for the calculation of the scattering of light by light or by a Coulomb field and of processes like the triple decay of a neutral vector meson into photons. The integrations were carried out for the scattering of light by light and the differential cross section evaluated in the center of gravity system for unpolarized photons. The exceedingly complicated formula, expressible in terms of Spence's transcendents and elementary functions, simplifies greatly in the limits of high and low energies. The cross section at the pair threshold for 90° scattering is $d\sigma = 2.73 \times 10^{-30}(d\Omega/4\pi)$ cm².

M2. Singular Potentials. K. M. CASE.—For a potential which is highly singular at the origin the conventional methods of solving the Schrödinger equation fail. Non-relativistically this occurs for a $1/r^n$ potential with $n \geq 2$. The relativistic wave equations for spin 0, ½, or 1 in a sufficiently strong Coulomb field are similarly "singular." In these cases the differential equations have too many rather than too few solutions quadratically integrable near the origin. This incompleteness in the specification of the Hamiltonian operator may be removed by giving one additional parameter which is most conveniently taken as a phase angle. Then the above problems all yield a complete set of quadratically integrable solutions. Since in the non-relativistic cases the point spectrum always extends to $-\infty$ such potentials are of little physical use except as an approximation in scattering problems. In relativistic problems the situation is different since the discrete spectrum is restricted to the interval between plus and minus mc^2. Solving the Dirac equation with $\alpha Z > 1$ gives two discrete sets of levels. One set approximates the levels for $\alpha Z < 1$ while the others cluster around plus and minus mc^2. The interpretation is that of positrons bound in a repulsive potential. An analysis of the situation indicates that the conjecture that real pairs are produced at $Z = 137$ is probably unfounded.

M3. Non-Linear Spinor Fields. R. FINKELSTEIN AND M. RUDERMANN, *University of California at Los Angeles, and California Institute of Technology.*—We have investigated certain classical theories described by non-linear spinor field equations. In one example both plane wave and localized solutions exist. A rigorous separation of the field equations into angular and radial parts is possible and the resulting radial equations can be integrated accurately. The corresponding particles have positive mass, spin, magnetic moment, and tensor interaction, and may have +, −, or 0 charge.

M4. Velocity Dependent Nuclear Interactions.* R. AVERY, C. H. BLANCHARD, AND R. G. SACHS, *University of Wisconsin.*—Mayer's considerations on the relationship between nuclear shell structure and strong spin-orbit coupling suggest that the velocity dependent interactions listed by Wigner should be investigated. These interactions introduce additions to nuclear magnetic moments over and above the spin and orbital moments. On the assumption that this "interaction moment" should vanish for H^2 and be equal and opposite in the ^2S states of H^3 and He^3, possible interactions are

$$J(|\mathbf{r}_j-\mathbf{r}_k|)[(\mathbf{r}_j-\mathbf{r}_k)\times(\mathbf{p}_j-\mathbf{p}_k)]\cdot\begin{cases}(\boldsymbol{\sigma}_j-\boldsymbol{\sigma}_k)(\tau_{j3}-\tau_{k3})\\ [\boldsymbol{\sigma}_j\times\boldsymbol{\sigma}_k][\boldsymbol{\tau}_j\times\boldsymbol{\tau}_k]_3.\end{cases}$$

The interaction moment due to either of these interactions, introduced with a strength comparable to that of the usual interactions, can account for the observed anomalies in the H^3 and He^3 moments. Both interactions vanish between like particles; they differ only by a space exchange factor. Neither would affect the low energy properties of the two-body system. They can, however, be expected to modify high energy NP (but not PP) scattering.

* This work was supported by the AEC.

M5. Non-Perturbation Calculation of the Nucleon-Meson Coupling Constant. S. D. DRELL, *University of Illinois.*—Equations of motion are derived from a Lagrangian describing the interaction between a Dirac spinor field (nucleon) and a Yukawa field (meson). The fields are not quantized. Elimination of the meson field variables yields a non-linear equation for the nucleon field. Because of this non-linearity there exist lumps in the field which can be interpreted as particles.[1] Quantized values for the nucleon-meson coupling constant, $g^2/4\pi\hbar c$, result when the nucleon field is normalized to unit charge. We introduce four component spinor trial wave functions into an integral which is constructed so as to assume a stationary value when the nucleon field amplitudes satisfy the non-linear equation. A variation with respect to parameters in the wave functions is performed. A stationary state of a localized nucleon is found to exist for scalar mesons, scalar coupling. A lower bound of $g^2/4\pi\hbar c \approx 0.6$ to 0.8 is obtained. Results are unchanged for treatment of nucleons as Yukawa particles. No stationary states are found for a localized nucleon under the influence of a pseudoscalar meson field with pseudoscalar coupling.

[1] R. J. Finkelstein, Phys. Rev. **75**, 1079 (1949).

M6. Absorption of π^--Mesons by Protons. R. E. MARSHAK, *University of Rochester,* AND A. S. WHITMAN, *Princeton University.*—Panofsky[1] has observed high energy gamma-rays resulting from the absorption of slow π^--mesons by protons. His data can be interpreted most simply in terms of a competition between γ and π^0 (neutral meson) emission.[2] The γ-emission leads to a line at 130 Mev whereas the π^0-emission gives a square pulse of γ's centered at about half this energy. The width w of the pulse yields a sensitive determination of the mass μ_0 of π^0 while the ratio h of the heights of the pulse and the line fixes the π^0-nucleon coupling constant g. Using Panofsky's admittedly crude values $w = 35 \pm 15$ Mev, $h = 10 \pm 2$, we find $\mu_0 c^2 = 135^{+2}_{-5}$ Mev, $g^2/\hbar c = 0.55^{+0.3}_{-0.1}$ (pseudoscalar theory for both π^- and π^0) or $g^2/\hbar c = 0.07^{+0.04}_{-0.01}$ (scalar theory[2] for both π^- and π^0). Opposite parities for π^- and π^0 (pseudoscalar for π^-, scalar for π^0 or conversely) can be excluded be-

cause the coupling constant would become unreasonably large ($g^2/\hbar c$ would be multiplied by a factor $(Mc^2/w)^2 \approx 500$ where M is the nucleon mass). Conclusions can be drawn about the relative sign of coupling of π^0 with neutron and proton.

[1] W. K. H. Panofsky, post-deadline paper at New York meeting (1950).
[2] R. E. Marshak and A. S. Wightman, Phys. Rev. 76, 114 (1949).

M7. The Absorption of π^--Mesons by Deuterons. STEPHEN TAMOR,* *University of Rochester.*—The non-radiative absorption of pseudoscalar π^--mesons by deuterons has been calculated.[1] There is a qualitative difference between scalar and pseudoscalar mesons. If absorption of the π^--meson from the K shell is considered, the Pauli principle applied to the final two neutron system forbids non-radiative absorption of scalar mesons. Instead, the absorption is accompanied by a continuous γ-ray spectrum with a peak at 135 Mev and a width of 10 Mev. For pseudoscalar mesons, the radiative absorption is slower by a factor of 10^3 compared to the non-radiative absorption. The absorption of π^--mesons accompanied by the emission of neutral mesons will also be discussed.[2]

* AEC Fellow.
[1] C. Marty and J. Prentki, J. de phys. et rad. 10, 156 (1949).
[2] See abstract M6.

M8. Scattering of Mesons by Nucleons. MURRAY PESHKIN.* *Cornell University.*—The scattering of scalar and pseudoscalar mesons by nucleons has been calculated to the lowest order in which it appears, using the field theoretic methods of Feynman. Charged and mixed theories have been considered, and the computations have been carried out exactly for all energies. For a given nucleon, two different Feynman diagrams are needed, one in the case of a positive meson, and the other for a negative meson.[1] Only one enters in each problem because the order (along the nucleon line) of absorption and emission depends upon the charges. These lead to nearly equal cross sections, the difference being negligible whenever the recoil energy of the nucleon can be ignored. The cross section for a charged meson to lose its charge to the nucleon in the scattering process receives contributions from both diagrams. In the pseudoscalar theory, this cross section is $a[(\sigma_1)^{\frac{1}{2}} - (\sigma_2)^{\frac{1}{2}}]^2$, where a depends upon the mixture, while in the scalar theory the interference is not destructive. This difference, if higher order terms bear it out, may provide an experimental method for distinguishing between the two theories.

* AEC predoctoral fellow.
[1] R. P. Feynman, Phys. Rev. 76, 775 (1949), Fig. 5.

M9. The Scattering of Gamma-Rays by Protons.* R. G. SACHS, *University of Wisconsin,* AND L. L. FOLDY, *Case Institute of Technology.*—The cross section for the scattering of gamma-rays with energy near the threshold for meson production has been calculated on the basis of the symmetrical scalar and pseudoscalar meson theories. The calculation was carried out in the non-relativistic, weak coupling approximation, neglecting nucleon recoil effects. No divergence difficulties were encountered. In the scalar theory, the total cross section is somewhat less than the Thompson cross section (σ_0) as a consequence of interference between the scattering by the nucleon and that by the meson cloud. In pseudoscalar theory the total cross section varies strongly with energy as a result of interference effects and attains a value as high as $4\sigma_0$. The angular distribution in the scalar theory is very similar to that given by the Klein-Nishina formula: $\frac{1}{2}(1+\cos^2\theta)$. The pseudoscalar theory gives a quite asymmetric distribution, the form of asymmetry depending strongly on energy. All results are rather sensitive to the choice of coupling constant. The results may be taken as a strong indication that observation of the process could yield, in a sensitive way, information concerning the structure of the proton.

* Supported in part by the AEC.

M10. Electric Processes Involved in Deuteron Reactions.* M. L. GOLDBERGER, *M.I.T.*—Recent experiments by Boyer and his collaborators[1] on nuclear reactions produced by 14 Mev deuterons have indicated that some of the phenomena involved in deuteron reactions may be attributed to electric processes. We have studied the elastic and inelastic scattering together with the electric stripping process. In connection with the latter, we have taken into account accurately the influence of the Coulomb field on the stripped protons. This feature has been neglected in previous investigations.[2] The effect of the smeared out charge distribution of the deuteron on the elastic and inelastic scattering processes will be discussed and will be related to the tendency of the deuteron to stick together after having undergone a given momentum transfer.

* This work was supported by the joint program of the ONR and AEC.
[1] To be reported at this meeting.
[2] J. R. Oppenheimer, Phys. Rev. 47, 845 (1935), S. M. Dancoff, Phys. Rev. 72, 1017 (1947).

M11. Effect of Tensor Forces on the Level Structure of Li^6 and Li^7. A. M. FEINGOLD AND E. P. WIGNER, *Princeton University.*—An investigation of the effect of tensor forces on the level structure of Li^6 and Li^7 has been made by treating the tensor force as a perturbation on the low lying level structure given by central forces. As far as the normal states are concerned, the effect of the tensor forces manifests itself only in the second order of the perturbation calculation. First only such excited states have been considered in which the s^4 configuration of the He^4 core remained unaffected. This gave consistently unsatisfactory results: the large energy difference between He^6 and Li^6 could not be accounted for, and the $J=\frac{1}{2}$ state of Li^7 fell below the $J=\frac{3}{2}$ state. These results were independent of the exchange character of the tensor forces. Taking into account the possibility of the excitation of the He^4 core gave, however, a splitting between the $P_{3/2}$ and $P_{\frac{1}{2}}$ states of a single p particle.

M12. The Effect of the Nuclear Charge and of Interference on Calculated $\beta-\gamma$ Correlations. M. FUCHS AND E. S. LENNOX, *University of Michigan.*—The many negative experimental attempts to find $\beta-\gamma$-correlations have led us to consider two effects which one might think tend to modify or destroy the correlation and which were not calculated by Falkoff:* (1) The influence of the nuclear charge. This is essentially an internal scattering which might make the angular distribution of the outgoing β-particle more isotropic. (2) Interference between matrix elements for a given β-interaction and degree of forbidenness. We have calculated the first effect using both non-relativistic and relativistic coulomb wave functions for the emitted β-particle. The indications are that the effect of the nuclear charge is different for different β-interactions but is generally quite small. Interference was calculated for the upper end of the β-spectrum and strongly affects the correlation in magnitude and sign. It takes, however, very special choices of relative amplitude and phase for the matrix elements to give zero correlation. Numerical results will be given for both these effects.

* D. L. Falkoff, dissertation, University of Michigan (1948).

FRIDAY MORNING AT 10:00

Department of Commerce Auditorium

(C. C. LAURITSEN presiding)

Papers Not Classed Elsewhere

N1. A High Constant Speed Rotating Mirror.* E. C. SMITH AND J. W. BEAMS, *University of Virginia.*—A magnetic stainless steel rotor with symmetrically spaced optically flat polished surfaces is freely suspended in vacuum by an improved magnetic suspension.[1] The mirror is spun by a rotating magnetic field, the frequency of which is controlled by a piezoelectric crystal. It accelerates like a high resistance armature of an induction motor and because of the low frictional torque, pulls into synchronism with the rotating field and spins without hunting. Consequently, its rotational speed is as constant as the frequency of the crystal. The mirror speed is limited only by its mechanical strength and is set by the frequency of the crystal (10^5 cycles/sec.) used or one of its submultiples. Lateral motion of the rotor is damped by freely suspending the core of the supporting solenoid as a pendulum in an oil dash pot. The period of the pendulum is made equal to the lateral period of the rotor. The mirror has no observable horizontal or lateral motion and is very stable. It was developed for use in the study of short time phenomena and for possible use in velocity of light measurements.

* This work was supported by the Navy Bureau of Ordnance.
[1] Beams, Young, and Moore, J. App. Phys. **17**, 886 (1946).

N2. The Velocity of Electromagnetic Waves and the Dielectric Constant of Dry Air.* J. V. HUGHES, *Queen's Univeristy.*—Essen[1] and Aslaskan[2] have pointed out a discrepancy between the accepted value of the velocity of light, 299,775 km/sec., and the mean of six recent values for the velocity of radio waves, 299,790. Five of the radio results were determined in air and corrected to vacuum using a dielectric constant of air obtained at 1 Mc/sec. The following table shows values for the dielectric constant of dry air at N.T.P., which would need to be 1.00048 to obtain agreement between velocities. The author's

Observer	Measurement freq.	k for dry air
Meggers and Peters	Visible light	1.000575
Englund, Crawford, and Mumford	1 Mc/sec.	1.000590
C. M. Crain	9000 Mc/sec.	1.000572
Author and Lavrench	3000 Mc/sec.	1.00060

results have rather a wide spread, so that the difference from Englund's result is probably not significant, but clearly a value of 1.00048 is impossible. The discrepancy between the velocities must lie elsewhere.

* This work was supported by a grant from the Defense Research Board of Canada.
[1] L. Essen, Nature **159**, 611 (1947).
[2] C. I. Aslaskan, Nature **164**, 711 (1949).

N3. Electromagnetic Waves in Bounded Magneto-Ionic Media. BENJAMIN LAX.—The behavior of high frequency electromagnetic waves in ionized gases in the presence of an external magnetic field presents a dual problem of which only one aspect has been discussed in the literature. The first, solved by Appleton,[1] Hartree[2] and others, concerns the derivation of the propagation constant or the complex index of refraction when the frequency is assumed. The second involves the determination of the complex frequency when the value of the propagation vector is fixed or limited as it might be when the ionized medium is in a finite cavity or in a waveguide. The anisotropic properties of the magneto-ionic medium are responsible for the ordinary and extraordinary modes of propagation in one case and give rise to multiple resonant frequencies for a given mode in the other. Suitable approximations of uniform and moderate electron densities together with small collision frequencies are assumed for mathematical simplicity in order to obtain the theoretical results.

[1] E. V. Appleton, U.R.S.I. Reports, Washington (1927).
[2] D. R. Hartree, Proc. Camb. Phil. Soc. **25**, 47 (1929).

N4. Diffusion in the Ionosphere. M. H. JOHNSON AND E. O. HULBURT, *Naval Research Laboratory.*—It is assumed that the balance between rate of production of ions by monochromatic solar radiation and loss of ions by recombination and diffusion determines the ionic density in the atmosphere. The resulting non-linear differential equations have been integrated on the NRL Reac computer. Diffusion broadens the ionic density curve and shifts its maximum downward. The first effect changes the relations between real and virtual heights, and the second effect modifies the dependence of the height of the ionized region on the solar zenith angle. It was of interest to find that the relation between maximum ionic density and solar zenith angle was practically unchanged by diffusion (less than 20 percent). The influence of the magnetic field of the earth is taken into account.

N5. Extrapolation of the Geomagnetic Potential. C. J. SWIFT, *University of Pennsylvania.*—Recent theories place the source of the earth's magnetic field inside the core.[1] If there are no sources between the boundary of the core and the outer surface, the extrapolation of the surface field down to the core is possible by potential theory. Using conventional spherical harmonic analysis of the surface field, the series converges slowly. If we express the surface field in a limited region by means of surface harmonics which have a prescribed circle as a nodal line, we obtain more rapid convergence. These may be extrapolated down using solutions of Laplace's equation for a conical region. By this method we were able to obtain a lower limit for the secular variation at the boundary of the core. This is quite large, about one-half gauss per century. When we know the field and its time variation at the surface of the core we can set up an equation connecting fluid velocity with these quantities. This gives no unique solution, but considerable information. We obtained a lower limit of 0.04 cm/sec. for the surface velocity, lower than expected from other estimates.

[1] W. M. Elsasser, Rev. Mod. Phys. **22**, 1 (1950).

N6. Rapid Scanning Mass Spectroscope. WILLARD H. BENNETT, *National Bureau of Standards.*—The non-magnetic radiofrequency mass spectrometer is being developed for the rapid scanning of mass spectra. Methods have been developed for sweeping twice a second through masses ranging from 10 to 50 and presenting the observed mass components on a cathode-ray oscilloscope. The radiofrequency potential is modulated 10 percent at 1 kc and the 1-kc a.c. current received at the collecting electrode is amplified with an a.c. amplifier tuned to the modulation frequency. A fixed radiofrequency is used and the principal d.c. ion accelerating voltage is swept from 50 to 250 volts twice a second. The large inherent sensitivity of this kind of mass spectrometer tube makes it possible to use a.c. current amplifiers with short enough

relaxation constants to permit the rapid scanning of any mass ranges extending over a factor of five.

N7. Mass Spectra of Isotopic Hydrogen Molecules. FRED L. MOHLER, VERNON H. DIBELER, E. J. WELLS, JR., AND R. M. REESE.—The mass spectra of H_2, HD, D_2, HT, and T_2 have been measured with a Consolidated mass spectrometer with 50 volts ionizing voltage and with a magnetic field requiring 3800 volts to focus H^+. For H_2, D_2, and T_2 the following ratios were obtained: $H^+/H_2^+=0.0201$, $D^+/D_2^+=0.0096$ and $T^+/T_2^+=0.0061$. Sensitivities (current per unit pressure) for the molecule ions were 20.0, 19.5, and 17.8. For HD and HT the ratios were $H^+/HD^+=0.0096$, $D^+/HD^+=0.0097$, $H^+/HT^+=0.0085$, and $T^+/HT^+=0.0068$. Sensitivities for the molecule ions were 21.2 and 20.9. The HD pattern is based on spectra of pure HD fractionated by A. Fookson, P. Pomerantz, and E. H. Rich and the ratio D^+/HD^+ is an upper limit assuming H_2^+ is absent. Patterns for T_2 and HT were computed from two samples containing 91 and 37 atomic percent T in equilibrium. Theoretical values for the ratios of atom ions to molecule ions can be computed for ionization into the lowest state of the molecule ion and values are lower than observed by amounts ranging from 0.0015 to 0.0036. This is because ionization at 50 volts produces some ions from the repulsive states of the molecule ion.

N8. Mass Spectra of $C^{13}O_2$ and $C^{13}O$. V. H. DIBELER, E. J. WELLS, JR., AND R. M. REESE.—Mass spectra of $C^{13}O_2$ and $C^{13}O$ were obtained with a Consolidated mass spectrometer using conventional procedures. The CO_2 was evolved by H_2SO_4 on Eastman Kodak $BaCO_3$ containing 54 atom percent C^{13}. A portion of the CO_2 was completely reduced to CO with zinc. The peaks due to the ions containing C^{12} and C^{13} atoms were nearly of equal size, consequently the mass spectra of the isotopic molecules could be obtained from the same record. Corrections were made for oxygen isotopes. For CO_2, the ratio of the ions $C^{13}/C^{13}O_2$ was 0.0542 compared with the $C^{12}/C^{12}O_2$ ratio of 0.0564. The $C^{13}O/C^{13}O_2$ ratio was 0.0824 compared with the $C^{12}O/C^{12}O_2$ ratio of 0.0868. For CO, the $C^{13}/C^{13}O$ ratio was 0.0514 compared with the $C^{12}/C^{12}O$ ratio of 0.0540. The sensitivities of the isotopic molecule ions agreed within one percent. Thus, the frequency of rupture of a $C^{12}-O^{16}$ bond is approximately five percent greater than that of a $C^{13}-O^{16}$ bond. This is in essential agreement with the isotope effect reported by Thode and co-workers in the decomposition of oxalic acid. A comparable but less accurate difference was observed between the $C^{12}-O^{16}$ and $C^{14}-O^{16}$ bonds in CO_2 containing four atom percent C^{14}.

N9. Degradation of Different Molecular Weight Polyisobutylenes on Shearing in Solution. A. B. BESTUL AND H. V. BELCHER, *National Bureau of Standards*.—Five, ten, and fifteen weight percent solutions, in *o*-dichlorobenzene, of ten different unfractionated polyisobutylenes ranging in viscosity average molecular weight from 50,000 to five million have been investigated for decrease of viscosity during repeated shearing through a capillary at 40°C and a nominal rate of shear of 66,000 sec.$^{-1}$. For average molecular weights below 400,000 no reduction was observed at any of these concentrations. For average molecular weights above 400,000, reductions were observed at all of these concentrations. At each concentration the apparent viscosity observed during the first pass of a solution through the capillary rose sharply with increasing average molecular weight. For average molecular weights above 400,000 the apparent viscosity observed suring the fiftieth pass of a solution through the capillary rose but little with increasing molecular weight. Viscosities of dilute (0.1 to 0.5 percent) solutions prepared from the 10 percent solution of two million average molecular weight polyisobutylene both before and after shearing the 10 percent solution indicate that the shearing resulted in an average molecular weight decrease of at least 20 percent in this case. These results support the view that the decrease of viscosity of shearing is associated with a degradation of the polymer molecules.

N10. Diffusivity of Water Vapor in Some Common Gases. F. A. SCHWERTZ AND JEANNE E. BROW, *Mellon Institute*.*—From the measured rates of diffusion of water vapor into pure hydrogen, helium, methane, ethylene, nitrogen, oxygen, and carbon dioxide, the mutual coefficients of diffusion have been determined. Measurements were made at 34°, 56°, and 80°C and at atmospheric pressure employing the technique of Stefan.[1] The experimental diffusion coefficients were all several percent larger than those calculated by means of the semi-empirical equations of Arnold[2] and Gilliland.[3]

* Work supported by Koppers Company, Inc.

[1] Stefan, Ann. d. Physik **41**, 723 (1890).
[2] Arnold, Ind. Eng. Chem. **22**, 1091 (1930).
[3] Gilliland, Ind. Eng. Chem. **26**, 681 (1934).

N11. On the State of Conductivity Created in a Liquid Isolator under the Action of an Electric Dispersive Field. OLEG YADOFF, *Columbia University*.—An electric current is produced in a circuit by a suitable voltage connected to a point form pole suspended in air, the other pole being a metallic flat-bottomed reservoir filled with isolating liquid. The magnitude of current is a function of: the kind of isolators, voltage applied, distance between poles and thickness of liquid. A very peculiar phenomenon is observed then on the surface of the isolator: on water a kind of turbulence is formed, physically resembling surface Hertzian waves. In mineral oils, whirlings of strictly polygon shape are formed. It is these whirlings which bridge the insulator. Many photographs of phenomena prove the physical reality of these whirlings, which have a peculiar likeness to the thermoconvective whirlings of Tyndall and Bernard. The whirlings can be replaced by surface extension by applying suitable voltage. A kind of star is then formed; it grows instantly and throws some of the oil from reservoir if its walls are slanted. If they are vertical, instead descending whirlings are formed. Only when electrostatic field is used is this phenomenon observed.

N12. Sitting Time of Molecules on a Hot Wire Detector. D. T. F. MARPLE AND HENRY LEVINSTEIN, *Syracuse University*.—The experiments[1] for the determination of the velocity distribution of molecules in a molecular beam have been modified to determine the sitting time of alkali halide molecules on a hot tungsten wire. Atoms from an oven are pulsed by a rotating shutter disk. Because of the velocity distribution of molecules in the beam the pulse widens in transit between shutter and detector. The voltage across a resistance in the detector circuit, permits observation of the widened pulse on a cathode-ray oscillograph. Simultaneously with the pulsing of the molecular beam, a light beam from a source directly below the oven is being pulsed and detected by a photo-cell. After amplification the photo-cell output, when applied to the *Z* axis of the oscilloscope, locates the time when atoms pass through the shutter. The time interval between hot wire detector pulse and photocell pulse thus gives the molecular transit time from shutter to hot wire plus the molecular sitting time on the wire. The sitting time of the molecules on the wire is then determined by varying the distance between shutter and detector and extrapolating this curve to zero distance.

[1] I. L. Kofsky and Henry Levinstein, Phys. Rev. **74**, 500 (1948).

N13. Thermal Properties of Diphenyl Ether. G. T. FURUKAWA, R. E. MCCOSKEY, R. S. JESSUP, AND R. A. NELSON, *National Bureau of Standards* (To be presented by G. T. Furukawa).—The specific heat of diphenyl ether was measured in the temperature range 14 to 360°K using an adiabatic

vacuum-type calorimeter. A Debye function was used to extrapolate the specific heat below 14°K. The entropy, free energy, and enthalpy with respect to the solid at absolute zero were calculated. The heat of fusion was found to be 17,210 ±5 abs. j./mole and the triple point 300.03±0.01°K. The heat of combustion was determined in a bomb calorimeter. The standard heat, free energy, and entropy of formation at 25°C were calculated. $\Delta H_c° = -6119$ abs. Kj./mole. $\Delta H_f° = -32.13$ abs. Kj./mole. $\Delta S_f° = -590.0$ abs. j./mole deg $\Delta F_f° = 143.8$ abs. Kj./mole.

FRIDAY MORNING AT 10:00

Lisner Auditorium

(D. M. DENNISON presiding)

Microwave Molecular Spectra and Pressure-Broadening

O1. The Microwave Absorption Spectrum of Oxygen at Low Pressures.* J. H. BURKHALTER, R. S. ANDERSON, W. V. SMITH, AND W. GORDY, *Duke University.*—Using a Zeeman modulation microwave spectrograph, we have observed 25 absorption lines of oxygen in the 5-mm wave region, 19 of which have been measured with a frequency standard. The line width parameter $\Delta\nu$ was observed for three of these, and found to be ~.021 cm^{-1}/atmosphere for high K, but to increase for low K, being .053 cm^{-1}/atmosphere for $\nu_-(3)$. The latter breadth agrees with theoretical predictions from polarizability interactions. If it is assumed that the collision duration is comparable to a rotational period for the higher K lines, the decrease of $\Delta\nu$ with increasing K is also explained. The data suggest a collision duration of about 10^{-12} sec. Schlapp's formulas[1] are found to be inadequate. The quantity $\nu_+(K) + \nu_-(K-2)$, or $2\lambda+\mu$ by Schlapp's formula, increases approximately quadratically with K. It appears that the correction factor applies to the $\nu_-(K)$ formula alone, and is not symmetrical in the two series.

* Supported by a contract with Air Force Cambridge Research Laboratories.
[1] R. Schlapp, Phys. Rev. 51, 342 (1937).

O2. Effect of Fermi Resonance on Rotation-Vibration Interaction in OCS and OCSe.* W. LOW AND C. H. TOWNES, *Columbia University.*—Rotational frequencies of a linear XYZ molecule for an excited vibrational state are usually written

$$\gamma = 2J[B_e - \alpha_1(v_1+\tfrac{1}{2}) - \alpha_2(v_2+1) - \alpha_3(v_3+\tfrac{1}{2})]$$

where the α's are the vibration-rotation constants and allow for changes in B due to vibrations. However, measurements of the α's for the various vibrational states in OCS and OCSe show little consistency. These discrepancies are explained within experimental accuracy as due to interactions between adjacent vibrational levels[1] with quantum numbers v_1, v_2, v_3, and $v_1\pm1$, $v_2\pm2$, v_3. This is the "Fermi resonance" first found in CO_2. The interaction energies W_{ni} and the unperturbed α's for OCS are $\alpha_1 = 20.55$, $\alpha_2 = -10.59$ Mc, $W_{ni} = 40$ cm^{-1} and for OCSe they are $\alpha_1 = 14.01$, $\alpha_2 = -6.88$ Mc, $W_{ni} = 45.7$ cm^{-1}. Resonance of this type in ICN has been found to be much smaller.

* Work supported jointly by the Signal Corps and ONR.
[1] We are grateful to Professor R. C. Lord for information on the OCSe vibrational frequencies, and to Dr. W. Benedict for a discussion of these effects.

O3. Microwave Spectra of the Methyl Mercuric Halides.* WALTER GORDY AND JOHN SHERIDAN,** *Duke University.*—Several rotational transitions have been observed for methyl mercuric chloride, bromide, and iodide. A large number of lines was found for each transition. These arise from the nuclear coupling of the halogen and from several different isotopic weights of mercury which are present. In the chloride the spectrum of these isotopes was readily identified, and the nuclear quadrupole splitting of Hg^{201} was observed. The absence of a hyperfine structure for the other Hg isotopes supports the spin value of ½ for Hg^{199} and the expected spin of zero for $Hg^{198, 200, 202, 204}$. The analysis of the data is not yet complete.

* Supported by contract with the Air Force Cambridge Research Laboratories.
** On leave from the Department of Chemistry, University of Birmingham, Birmingham, England.

O4. Microwave Spectrum of Methyl Bromo-Acetylene.* JOHN SHERIDAN** AND WALTER GORDY, *Duke University.*—The $J=8\rightarrow9$, $9\rightarrow10$, and $11\rightarrow12$ transitions of $H_3C-C\equiv C-Br^{79}$ and the $J=8\rightarrow9$ and $11\rightarrow12$ transitions of $H_3C-C\equiv C-Br^{81}$ have been observed. The moments of inertia, I_B, are 537.07×10^{-40} g/cm^2 and 540.96×10^{-40} g/cm^2 respectively. The spectra show a well resolved hyperfine structure which is being analyzed.

* Supported by contract with Air Force Cambridge Research Laboratories.
** On leave from the Department of Chemistry, University of Birmingham, Birmingham, England.

O5. Microwave Spectrum of Methyl Cyanide and its Isotopic Modifications. D. K. COLES, W. E. GOOD, AND R. H. HUGHES, *Westinghouse Research Laboratories.*—The $J=1\rightarrow2$ transitions of CH_3CN, which fall in the region of 37,000 Mc, were first studied by Ring, Edwards, Kessler, and Gordy. An intense triplet which they observed has recently been considered by Nielsen (in a paper on l-type doubling in polyatomic molecules) as due to the molecules in the first excited state of the ν_8 vibration. Our measurements of the first and second order Stark effects in this spectrum confirm Nielsen's theory. We were able to determine the l-type doubling for the states $J=1$ and $J=2$ separately, since the presence of an electric field allows the observation of lines which are ordinarily forbidden. A weak doublet, a triplet, and a single line, were also found. These are attributed to molecules in the vibrational states $V_8=2$, $V_7=1$, $V_4=1$. Three other isotopic species of this molecule have been prepared and studied. Preliminary measurements yield the following spectroscopic constants.

$B_0(CH_3CN) = 9{,}198.70$ mc	$\alpha_4 = 46.3$ mc
$B_0(C^{13}H_3CN) = 8{,}933.15$ mc	$\alpha_7 = 5.2$ mc
$B_0(CH_3C^{13}N) = 9{,}194.20$ mc	$q_7 = 4.5$ mc
$B_0(CH_3CN^{15}) = 8{,}921.81$ mc	$\alpha_8 = -22.5$ mc
$\mu = 3.97$ Debye units	$q_8 = 17.7$ mc.

O6. Microwave Spectra and Molecular Constants of CD_3NC and CD_3CN.* RALPH TRAMBARULO AND WALTER GORDY, *Duke University.*—The measurements of Kessler, Ring, and Gordy on the ordinary methyl isocyanide and aceto-

nitrile have been supplemented by measurements on deuterated samples and on the compounds containing C^{13}. As a result the structural determinations of these molecules have been completed as follows: For methyl isocyanide, $\angle HCN = 109°9'$, $d_{CH} = 1.094A$, $d_{CN} = 1.427A$, and $d_{NC} = 1.167A$. For acetonitrile, $\angle HCC = 109°49'$, $d_{CH} = 1.092A$, $d_{CC} = 1.460A$, and $d_{CN} = 1.158A$. The nuclear coupling is -4.40 mc in acetonitrile and $< |0.5|$ mc in methyl isocyanide.

* Supported by a contract with Air Force Cambridge Research Laboratories.

O7. Microwave Spectrum of Bromoform and Phosphorus Tribromide. QUITMAN WILLIAMS* AND WALTER GORDY, *Duke University*.—The 14th, 15th, and 16th rotational transitions of $CHBr_3^{79}$ and $CHBr_3^{81}$ have been observed, and their hyperfine structure has been partially resolved. Measurements with a cavity wave meter yield $678._1 \times 10^{-40}$ g/cm² and 683.7×10^{-40} g/cm² for the respective moments of inertia, I_B. Similar measurements on the 18th, 19th, 20th, and 21st rotational lines of PBr^{79} and on the 20th, 21st, and 22nd lines of PBr^{81} yield $841._9 \times 10^{-40}$ g/cm² and $860._9 \times 10^{-40}$ g/cm² for their respective moments of inertia. More precise measurements are being made.

* Texas Company Fellow.

O8. Microwave Collision Diameters.* RAYDEEN R. HOWARD AND WILLIAM V. SMITH, *Duke University*.—The diameters of fifteen polar and non-polar gases for collisions with ammonia are obtained from measurements of the pressure broadening of the ammonia 3−3 inversion line in the mixed gases at low pressures. A type 2K50 klystron and magic tee supply microwave power to two absorption cells. In addition to the usual sawtooth sweep, the klystron is modulated at 100 kc and 2 mc. Delection of the 100-kc component through one cell gives an oscilloscope display of the first derivative of the line-shape. From pressure and relative intensity measurements at constant line breadth in pure ammonia and dilute ammonia mixtures the collision diameters are obtained. The other cell contains ammonia at low pressure. Detection of the 2-mc component through this cell yields markers of constant spacing which were used to maintain a constant frequency scale and to look for pressure shifts of resonant frequency.

* Supported by a contract with the Air Force Cambridge Research Laboratories.

O9. The Pressure Shift of the Inversion Frequency of Ammonia. A. H. NETHERCOT, JR. AND C. W. PETERS, *University of Michigan*.—In order to fit the microwave line shape data at high pressures by the Van Vleck-Weisskopf pressure broadening formula, it has been assumed by Weingarten that the inversion frequency of ammonia approached zero for pressures above 115 cm.[1] The resolution of the ν_1 band at 3μ—which results from the same type of inversion frequency transition plus a vibrational transition—reveals no such large shift. The infra-red data are consistent with the assumptions that no change in the splitting of the inversion doublet (1.6 cm^{-1}) occurs and that the line breadth is roughly proportional to pressure up to one atmosphere ($\Delta\nu/p = 0.01$ cm^{-1}/cm) and then rises somewhat less rapidly with pressure at two atmospheres. The total absorption is proportional to pressure. Great accuracy in these constants is not attained, but the results clearly rule out a large shift in frequency such as that employed previously in the interpretation of the high pressure microwave line shape data.

[1] Irving R. Weingarten, Columbia Radiation Laboratory Report (May 1, 1948).

Post-Deadline Papers, if Any

FRIDAY AFTERNOON AT 2:15

Lisner Auditorium

(H. C. TORREY presiding)

Hyperfine Structure in Radiofrequency Region; Paramagnetic and Anti-Ferromagnetic Resonance.

P1. Radiofrequency Transitions in a Tapered Electric Field. JOSHUA GOLDBERG AND PETER G. BERGMANN, *Syracuse University*.—In an experiment measuring the nuclear quadrupole interaction in C_2F, J. W. Trischka observed a broadening of the spectral lines in strong fields which he attributed to inhomogeneities in the fields.[1] We have calculated the probability that a molecule in a tapered (inhomogeneous) electric field will undergo a transition between two states of different spatial quantization when stimulated by a radio frequency field. In the calculations we considered diatomic molecules with a molecular dipole moment but without a nuclear quadrapole moment. By taking a linear combination of the solutions for the zero taper case, we were able to obtain differential equations for the probability amplitudes, the solutions of which reduce to the usual ones in the absence of a taper. Using a linear taper and making the assumption that the taper does not alter the line shape very much, we obtained an expression for the probability amplitudes in closed form. The solution shows a broadened line profile, but any shift of the resonance peak was less than the accuracy of the approximation. The approximation is valid for tapers which cause a broadening up to 20 percent.

[1] J. W. Trischka, Phys. Rev. **74**, 718 (1948).

P2. The Optical Detection of Radio-Frequency Resonance.* J. BROSSEL,** P. SAGALYN,*** AND F. BITTER, *M.I.T.*—The measurement of Zeeman patterns in weak fields is accomplished most effectively by the resonance absorption of radio-frequency energy. Optical means of detecting resonance have recently been discussed.[1] The predicted effects have been shown to be smaller than originally calculated and not actually observable. We have used successfully a method, recently suggested.

Mercury vapor in a magnetic field of the order of 100 gauss is illuminated perpendicularly to the field with radiation $\lambda = 2537$, polarized parallel to the field: only the π component, corresponding to a transition with $\Delta m = 0$ from the ground state $^1S_0$ to the excited state $^3P_1$ is absorbed and re-emitted. When transitions are induced within the excited state to the levels $m = \pm 1$ by means of the radio frequency field of the

correct frequency (~150 megacycles in our experiment) the radiation re-emitted contains σ as well as π components—consequently the intensity emitted parallel to the field is increased.

Radio frequency resonance for the isotopes of even mass and for Hg^{199} were observed at the expected frequencies and fields.

* This work has been supported in part by the Signal Corps, the Air Materiel Command and ONR.
** Joint fellow of Spectroscopy Laboratory and Laboratory for Nuclear Science and Engineering.
*** A.E.C. predoctoral fellow.
[1] F. Bitter, Phys. Rev. **76**, 833 (1949).

P3. Nuclear Magnetic Moment of Sb^{121}.* THOMAS L. COLLINS,** *University of British Columbia* (Introduced by G. M. Volkoff).—Weak signals for Sb^{121} have been observed on a recording magnetic resonance spectrometer. The frequency relative to sodium is $\nu Sb^{121}/\nu Na^{23}=1.0041\pm.0003$ which gives a value for the magnetic moment $\mu Sb^{121}=3.730\pm.002\mu_N$ (with diamagnetic correction). This compares excellently with Crawford's spectroscopic value of $3.7\mu_N$.[1] The measurements were made at a frequency of 7 mc in a proton stabilized field of about 6000 gauss. The frequency of a weak oscillator-detector (autodyne) was swept by a mechanical drive over both signals. The antimony absorption has a signal to noise ratio of about ten and a width of 7 kc between points of maximum slope while the much larger sodium signal has a width of less than 1 kc. The antimony shows a slight asymmetry which is not present in the sodium signal. The sample was 1 ml of concentrated $SbCl_3$ solution with a small amount of NaCl added.

* Work supported by the National Research Council of Canada.
** Holder of National Research Council of Canada Fellowship.
[1] M. F. Crawford and S. Bateson, Can. J. Research **10**, 693 (1934).

P4. Microwave Measurements on the Stable Selenium Isotopes in OCSe.* S. GESCHWIND, H. MINDEN, AND C. H. TOWNES, *Columbia University*.—From a re-examination of the $J=2-3$ transition[1] in OCSe, the relative masses of the stable Se isotopes have been determined, and an upper limit of 0.002×10^{-24} cm^2 assigned to the quadrupole moments. Frequency differences of the six selenium lines in $O^{16}C^{12}Se$, corresponding to the six naturally occurring Se isotopes, were measured to an accuracy of 15 kc or better and from them the relative Se masses were obtained. The variation of mass defect with isotopic number is in good agreement with the Bohr-Wheeler formula. The odd-even mass variation found is 0.0018 m.u. Although the OCSe lines were obtained as narrow as 60 kc, no noticeable asymmetry or splitting suggestive of hyperfine structure was observed in Se^{77} or in any other Se isotopes, in agreement with earlier work.[1] This gives an upper limit of 1 mc to the quadrupole coupling constant or 0.002×10^{-24} cm^2 to the quadrupole moment. Such a small quadrupole moment is puzzling in view of the measurements on the optical hyperfine structure which indicate a spin for Se^{77} of 5/2 or greater.[2]

* Work supported jointly by the Signal Corps and ONR.
[1] Strandberg, Wentink, and Hill, Phys. Rev. **75**, 827 (1949).
[2] J. E. Mack and O. V. Arroe, Phys. Rev. **76**, 160 (1949) and private communication.

P5. Hyperfine Structure and Nuclear Specific Heat of Copper. J. A. BRINKMAN AND C. KIKUCHI, *Michigan State College*.—The h.f.s. energy levels of Cu^{++} for the lowest electronic state in a tetragonal crystalline electric field and zero magnetic field were calculated to the first approximations. Using the nuclear specific heat constant, $CT^2/k=1.1\times10^{-4}$ cm^{-1}, measured by Benzie and Cooke,[1] based on Gorter's[2] paramagnetic relaxation method, we have been able to infer a value of 0.019 cm^{-1} as an upper limit for the h.f.s. splitting factor, a. This is in fair agreement with Ritschl's[3] spectroscopic value of 0.022 cm^{-1} for the unionized $^2D_{5/2}$ state of Cu, but is somewhat larger than Penrose's[4] value of 0.005 cm^{-1}, obtained by microwave measurements. The temperature dependence of the nuclear specific heat was calculated down to about 0.001°K. If other effects are negligible or constant in this range, the maximum in the nuclear specific heat curve should occur at about 0.002°K.

[1] R. J. Benzie and A. H. Cooke, Nature **164**, 837 (1949).
[2] C. J. Gorter, *Paramagnetic Relaxation* (Elsevier Publishing Company, Inc., New York, 1947).
[3] R. Ritschl, Zeits. f. Physik **79**, 1 (1932).
[4] R. P. Penrose, Nature **163**, 992 (1949).

P6. Effective g-Values of Various Paramagnetic Ions.* YU TING, ROY C. WEIDLER, AND DUDLEY WILLIAMS, *The Ohio State University*.—The microwave magnetic resonance absorption spectra of several paramagnetic salts have been studied. The experimental method involved the measurement of the transmission of 3.2-cm radiation through a resonant cavity containing a single crystal or powdered sample of the salt being studied. The resonant cavity was placed between the pole pieces of a large electromagnet and the variation of transmitted power with variations of the magnetic field strength was observed. From the frequency of the radiation and the magnetic field strength corresponding to maximum absorption, it is possible to determine the effective g-value for the paramagnetic ion in each salt. The results obtained for Mn^{++}, Cu^{++}, Ni^{++}, Fe^{+++}, and Cr^{+++} are in essential agreement with calculated values for spin-only ions. From the peak shapes it is possible to estimate the effects of interaction between the neighboring paramagnetic ions and between the ions and the crystalline fields.

* This work is related to research work done under a contract between the Geophysical Directorate of the Air Force Research Laboratory, Cambridge, Mass. and The Ohio State University Research Foundation.

P7. Paramagnetic Resonance in Single Crystals of the Manganous Halides. ALDEN H. RYAN, *Naval Research Laboratory*.—Measurements of the paramagnetic resonance spectrum of $MnCl_2\cdot4H_2O$ and $MnBr_2\cdot4H_2O$ have been made on single crystals of these salts, as a function of orientation of the crystal with respect to the static magnetic field. The measurements were made at a wave-length of 3.2 cm, using a magic T microwave bridge and superheterodyne detector. The measurements were carried out over a temperature range from about 80°K to about 300°K. The results are discussed in terms of the spectrum predicted by Kittel and Luttinger (Phys. Rev. **73**, 162 (1948)) and in relation to the anisotropy of the static magnetic susceptibility of these salts, as discussed by Van Vleck and Penney (Phil. Mag. **17**, 961 (1934)) and Krishnan and Banerjee (Trans. Roy. Soc. **A235**, 343 (1936)).

P8. Magnetic Resonance Absorption in Chromium Sesquioxide.* E. P. TROUNSON, D. F. BLEIL, AND L. R. MAXWELL, *U. S. Naval Ordnance Laboratory*.—Magnetic resonance absorption at microwave frequencies (3.2 cm) has been measured for Cr_2O_3 in the temperature range from room temperature to 70°C which includes a transformation from an antiferromagnetic to a paramagnetic state; the Curie temperature is reported by two different authors to be 34°C[1] and 47°C.[2] At 70°C the absorption is strong showing a single maximum coming at a field strength of about 3300 oersteds, as expected on the basis of paramagnetic absorption. As the temperature is lowered there is no large change in the height of the absorption peak until about 37°C is reached where the height drops precipitously to a value slightly greater than the background at 30°C. This sudden decrease in height of the absorption peak is attributed to the change of Cr_2O_3 from paramagnetism to antiferromagnetism.

* Supported in part by the ONR.
[1] K. Honda and T. Sone, Sci. Rep. Tohoku Imp. Univ. **3**, 223 (1914).
[2] G. Foex and M. Graff, Comptes Rendus **209**, 160 (1939).

P9. Interpretation of Magnetic Resonance Absorption in Antiferromagnetic Materials.* D. F. BLEIL AND R. K. WANGSNESS, *U. S. Naval Ordnance Laboratory.*—The experimental result reported in the previous abstract can be understood in terms of the local fields existing in antiferromagnetic materials. Antiferromagnetic materials are characterized by an exchange coupling which prefers antiparallel alignment of the spins rather than the usual parallel alignment found in ferromagnetism. Above the Curie temperature the usual paramagnetic absorption should occur. Below the Curie temperature the effective field ($\mathbf{H}_{eff}^{\pm}$) at any one atom will be modified by the spontaneous magnetization ($\mathbf{S}_0$) of its nearest neighbors which are aligned antiparallel. In contrast to the ferromagnetic case the field due to the spontaneous magnetization need not be parallel to the direction of the magnetic vector ($\mathbf{M}$). We have, therefore, $d\mathbf{M}/dt=\gamma\mathbf{M}\times\mathbf{H}_{eff}$[1] where

$$\mathbf{H}_{eff}^{\pm}=\mathbf{H}_a+2Jsg^{-1}\beta^{-1}(\mp\mathbf{S}_0)+2Js\mathbf{M}/Ng^2\beta^2. \qquad (2)$$

At the Curie temperature the spontaneous magnetization is zero and increases rapidly as the temperature is decreased. The resonant frequency increases with the internal field and rapidly exceeds the range of microwave equipment. Therefore, one could not expect any appreciable absorption below the Curie temperature at microwave frequencies.

* Supported in part by the ONR.
[1] C. Kittel, Phy. Rev. 73, 155 (1948).
[2] J. H. Van Vleck, J. Chem. Phys. 9, 85 (1941).

FRIDAY AFTERNOON AT 2:15

Department of Interior Auditorium

(C. C. LAURITSEN presiding)

Nuclear and Electronic Scattering; Pair-Production

Q1. Energy Dependence of Proton-Proton Scattering over the Interval of 19 to 32 Mev.* BRUCE CORK, *University of California, Berkeley.*—Measurements have been made of the absolute differential cross section of proton-proton scattering at 90° in the center of mass system. The energy of the incident protons from the linear accelerator was varied from 32 Mev down to 19 Mev and an energy interval of ±0.5 Mev was selected by means of a deflecting magnet. Apparatus using proportional counters and a triple coincidence method was used to reduce the background. Measurements were made simultaneously using the apparatus[1] for measuring the angular distribution at 31.8 Mev, and a single charge integrator for collecting the incident proton beam. The cross section at 90° center of mass varies approximately as the reciprocal of the energy of the incident protons. Data will be presented to show this dependence.

* This work was sponsored by the AEC.
[1] Richman, Johnston, and Cork, UCRL-482.

Q2. Coherent Neutron-Proton Scattering by Liquid Mirror Reflection. D. J. HUGHES, *Brookhaven National Laboratory,* AND M. T. BURGY AND G. R. RINGO, *Argonne National Laboratory.*—An accurate determination of the coherent neutron-proton scattering amplitude, a_H, is important because of the direct connection between a_H and the fundamental nuclear force constants. We have recently[1] obtained a value for a_H of $(-3.75\pm0.03)\times10^{-13}$ cm by a comparison with carbon, involving critical reflection of neutrons from a liquid hydrocarbon ($C_{12}H_{18}$) mirror. The experiment has now been repeated, using various liquids and a range of neutron wavelengths, in order to search for systematic errors. With $C_{12}H_{18}$, the unbalanced coherent scattering amplitude (a_C is positive and slightly larger than $1.5a_H$) was determined from the measured wave-length at a fixed incident angle (about 5 minutes). The present method consists of a determination of the particular C−H ratio for which the amplitude is zero, at which ratio the reflected intensity is zero for all incident angles. The reflected intensities from liquids of different C−H ratios, some of which are mixtures, are measured at different angles, and it is then a simple matter to extrapolate to the C−H ratio corresponding to zero amplitude. The values of a_H obtained with different liquids and neutron wave-lengths are in agreement with the $C_{12}H_{18}$ result and make systematic errors unlikely.

[1] Hughes, Burgy, and Ringo, Phys. Rev. 77, 291 (1950).

Q3. Neutron-Proton Scattering at 27 Mev. J. E. BROLLEY, JR., J. H. COON, AND J. L. FOWLER, *Los Alamos.*—Neutrons of average energy of 27.4 Mev, and with a maximum spread in energy of one Mev, were produced by bombarding gaseous tritium with deuterons accelerated by the cyclotron. Recoil protons from a polyethylene radiator 0.02 in. thick were observed at 0, 15, 30, 37.5, 45, and 52 deg. in the laboratory system. Quadruple coincidence counting of the protons was performed with a fourfold proportional counter system. Sufficient aluminum absorber was inserted between the two remote counters to absorb low range background particles. The neutron yield was monitored by the charge incident on the target as measured by a condenser type integrator. Angular distributions were obtained with two series of runs: one with the radiator at 5.7 in., and the other at 15.3 in., from the center of the target. The two sets of data agree and show that the distribution is definitely anisotropic. The ratio of the differential scattering cross section at 180 deg. to that at 90 deg. in the center of mass system is 1.3.

Q4. D−P Scattering for 10.4-Mev Deuterons. J. C. ALLRED, AND LOUIS ROSEN, *Los Alamos.*—A nuclear multiple plate camera has been utilized to measure the differential cross section for D−P scattering at 10.35±0.10-Mev deuteron energy. The camera contains its own collimating system for the incident as well as the scattered particles and no windows are utilized from the time the beam enters the first collimating slit until it emerges from the camera to enter a faraday cup. The solid angle subtended by each detector at the reaction volume is determined by an accurately machined slit system. Data will be presented of tests on this camera using the well known differential cross sections for p−p and p−He^4 scattering in the 3-Mev proton energy region. The cross section in barns for some of the center of mass angles investigated are: 50°, 0.163±0.004; 60°, 0.141±0.004; 65°, 0.126±0.003; 70°, 0.112±0.003; 75°, 0.100±0.0026; 80°, 0.0902±0.0024; 85°, 0.0862±0.0021; 90°, 0.0707±0.0018; 100°, 0.0604 ±0.0015; 110°, 0.0543±0.0013; 120°, 0.0576±0.0015; 130°, 0.0742±0.0020; 135°, 0.0809±0.0025; 140°, 0.107±0.003.

Q5. Scattering of 250-Mev Protons from Nucleons within Nuclei.* G. M. TEMMER, *University of Rochester.*—The circulating 250-Mev proton beam of the Rochester cyclotron was made to impinge upon thin internal targets of aluminum, copper, and lead. The emerging protons were sorted according

to their momenta and scattering angles by the magnetic field of the cyclotron and detected by nuclear emulsions along a radial probe, a method used in elastic p−p scattering.[1] Since to a given position and given entrance angle into the emulsion there uniquely correspond a definite proton energy and scattering angle, it is possible to determine both an angular distribution of scattered protons and proton energy distributions at fixed scattering angles, both of which are expected to yield information concerning the behavior of nucleons in nuclei. Some preliminary qualitative results indicate that single "elastic" proton-nucleon encounters account for an appreciable fraction of protons scattered from aluminum for scattering angles between 45° and 60° (laboratory), but for less from the heavier elements. This is reasonable in view of the mean free paths in nuclear matter for both incident and "elastically" scattered protons (lowest energy observed ~60 Mev). Further measurements are in progress, especially at larger scattering angles where internal nuclear effects are expected to show up more decisively.

* This work was assisted by the joint program of the ONR and the AEC.
[1] O. A. Towler, Jr. and C. L. Oxley, Bull. Am. Phys. Soc. **25**, 1, 19 (1950) (New York Meeting).

Q6. Elastic and Inelastic Scattering* of 14-Mev Deuterons. KEITH BOYER AND HARRY GOVE, *M.I.T.*—Energy spectra of inelastically scattered deutrons have been obtained for thin targets of a number of elements and angular distributions determined for the elastic group and inelastic groups in several of the targets. The elastic group in gold was found to obey the Rutherford law closely for angles less than about 50 degrees, while at greater angles it falls more rapidly. Fair agreement was obtained between the differential cross section of the elastic peak in gold at 20° computed from the Rutherford formula and the value measured by counting all the elastically scattered deuterons for an integrated beam current. The differential cross section for a number of individual groups was integrated over angle to obtain total cross sections.

* Assisted by the joint program of the ONR and AEC.

Q7. Scattering and Capture of Protons by Aluminum. F. C. SHOEMAKER,* J. E. FAULKNER, S. G. KAUFMANN AND G. M. B. BOURICIUS, *University of Wisconsin.*—Thin films of aluminum were bombarded with protons from the Wisconsin pressure generator. By use of the techniques developed in preliminary work,[1] yield curves covering the region from 1.4 to 4.1 Mev were obtained for elastically scattered protons (resolution ~2 kev), alpha-particles (resolution ~6 kev), and gamma-radiation. These curves show a large number of resonance levels with widths ranging from ~30 kev to ~1.5 kev. The general level of the elastic scattering decreases from 1.4 to 2.0 Mev and then remains substantially constant. The alpha-yield, essentially zero between resonances, shows a general increase at resonance with increasing proton energy. The intensity of hard gamma-radiation at resonance apparently does not increase appreciably with increasing proton energy, but an intense, very soft (~1 Mev) component is found at high proton energies. Inelastically scattered protons and low energy alphas were found which, it is believed, account for this. All charged particle yields were observed at 165° in the laboratory system. This work was supported in part by the AEC and in part by the Wisconsin Alumni Research Foundation.

* Now at Princeton University, Princeton, New Jersey.
[1] Bender, Shoemaker, Kaufmann, and Bouricius, Phys. Rev. **76**, 273 (1949).

Q8. Electron-Electron Scattering. LORNE A. PAGE AND W. M. WOODWARD, *Cornell University.*—The differential cross section, for the scattering of negative β-rays by atomic electrons, has been measured for various values of the β-ray energy, E, and fractional-energy-transfer, v. A $Sr^{90}-Y^{90}$ source was used for the β-rays and thin foils of Nylon and collodion for the scatterer. A magnetic field is used to define the energy of the primary electron and the fractional-energy-transfer. Pairs of Geiger counters in coincidence are used to detect the scattered particles. Results to date for $\sigma(E, v)$ for $v=\frac{1}{2}$, in units of 10^{-24} cm^2 and per unit fractional-energy-transfer are:

E(Mev)	$(E, \frac{1}{2})$
0.47	3.4
0.85	1.5
1.16	1.1

The method will be extended to positron-electron scattering.

Q9. Elastic Scattering of 16.5-Mev Electrons.* E. M. LYMAN, A. O. HANSON, AND M. B. SCOTT, *University of Illinois.*—The electron beam from the 22-Mev betatron was focused to a 2-mm spot 4 meters from the betatron by a magnetic lens. It passed through a low pressure ion chamber and impinged upon thin foil targets at the center of an evacuated scattering chamber 20 in. in diameter. Scattered electrons were selected in angle by a Lucite aperture $\frac{3}{8}$ in.×2 in., analyzed and refocused by a 75° Nier type magnetic analyzer with 3 percent energy resolution, and detected by coincidence Geiger counters. Preliminary results for the scattering cross sections in barns per unit solid angle are shown in the table. R represents the ratios to values calculated by McKinley and Feshbach.

	Z	σ (30°)	R	σ (90°)	R	σ (150°)	R
C	6	0.13	0.94	0.0010	0.73	0.000044	0.77
Al	13	0.65	0.97	0.0051	0.75	0.00022	0.94
Cu	29	3.1	0.86	0.031	0.74	0.0013	0.86
Ag	47	9.6	0.92	0.104	0.75	0.0044	0.85
Au	79	30	0.88	0.37	0.45	0.021	0.38

The experimental values were corrected for the effect of small angle multiple scattering, (~10 percent at 30°). Absolute values are less accurate than relative values at the same angle.

* Supported in part by the joint program of the ONR and AEC.

Q10. Study of Electron-Electron Scattering.* GERHART GROETZINGER, LEWIS B. LEDER, FRED L. RIBE, AND MARTIN J. BERGER, *University of Chicago.*—In the course of various cloud-chamber investigations pictures of 98 electron-electron collisions were obtained, in which the primary electrons ranged in energy approximately from 0.05 to 1.7 Mev and the deflections (in the center of mass system) exceeded 32°. By means of a statistical test suitable for the systematic evaluation of rather heterogenous data, a comparison was made of our results with the theory of Møller (M), relativistic versions of the theories of Mott (MR) and Rutherford (RR) and the classical non-relativistic Rutherford theory (R). Our data discriminate definitely only against (R). When combined with 122 electron-electron collisions observed by Champion[1] they are consistent only with (M) or (MR), but insufficient to discriminate decisively between them.

* This research was assisted in part by the joint program of the ONR and AEC.
[1] F. C. Champion, Proc. Roy. Soc. **A137**, 688 (1932).

Q11. Correlation between the Polarization States of Annihilation Quanta. FRANK L. HEREFORD, *University of Virginia.*—Following the suggestion of Pryce and Ward[1] the polarization states of the two quanta emitted in annihilation of an electron-positron pair have been investigated by coincidence detection of the photoelectrons ejected by the quanta at various azimuths. Several workers[2] have performed similar experiments detecting the scattered quanta. In the experiment described a collimated beam of annihilation radiation was obtained from a Cu^{64} positron source mounted in an Al capsule at the midpoint of a $\frac{3}{4}$-in. hole through a large Pb cylinder. This radiation impinged axially upon two small thin-wall Pb cylinders. The photo-electrons ejected in directions perpendicular to the radiation beam were detected by two end window

G-M counters in coincidence and distinguished from Compton recoils and the background by an absorption method. Coincidences were recorded as each counter was rotated in azimuth. In preliminary data 56±5 percent of the coincidences verify the $\sin^2(\phi_2-\phi_1)$ azimuthal dependence expected for cross polarization of the two quanta and for K and L_I photoelectron ejection. This corresponds to the ejection of some 75 percent of the electrons from the K and L_I levels.

[1] M. H. L. Pryce and J. C. Ward, Nature **160**, 435 (1947).
[2] C. S. Wu and I. Shaknov, Phys. Rev. **77**, 136 (1950), previous results are reviewed here.

Q12. Pair Production by Electrons.* MARSHALL R. CLELAND, WILFRED R. KONNEKER, AND A. L. HUGHES.—The creation of positrons by collisions of energetic electrons with nuclei has been treated by Bhabha[1] and others. Previous attempts to verify this theory experimentally have not agreed. Cloud-chamber work[2] has indicated 10^{-2} to 10^{-3} positrons per incident electron. A search for $\gamma-\gamma$-coincidences using Geiger counters[3] has yielded negative results, indicating less than 10^{-4} positrons per electron. A $\gamma-\gamma$-method has been used in this research using anthracene scintillation counters and a short resolving time coincidence circuit. A definite peak of coincidences has been observed at the 180° position. The peak has the same shape as thst produced by Cu^{61} positrons in the same geometry. A source of one millicurie of P^{32} obtained from Oak Ridge was placed inside absorbers sufficiently thick to stop all the electrons. The coincidence rate for lead absorber was 5 times the rate for aluminum absorber. In our geometry this is consistent with the Z^2 dependence of the cross section predicted by Bhabha.

* Assisted by the joint program of the ONR and AEC.
[1] Bhabha, Proc. Roy. Soc. **152**, 559 (1935).
[2] Skobelyn U. Stepanowa, J. de phys. et read. **6**, 1 (1935).
[3] Bradt, Helv. Phys. Acta **XVII**, 59 (1944).

FRIDAY AFTERNOON AT 2:15

National Bureau of Standards

East Building Lecture Room

(H. L. DRYDEN presiding)

Fluid Dynamics and Ultrasonics

R1. Incompressible, Ideal, Subsonic Flow Past an Infinite Cone. KEEVE M. SIEGEL,* *University of Michigan.*—The streamfunction for flow around a cone is derived. This is compared with the corresponding streamfunction for a wedge. A comparison is then made between pressure distributions around an infinite cone and an infinite wedge.

* USAF Contract.

R2. Vorticity Averages. C. TRUESDELL, *Naval Research Laboratory.*—Recent studies of turbulent fluid motions have drawn attention to the transfer of vorticity. The present study, eschewing conjectures regarding turbulence, proves as exact consequences of the kinematical equations the vanishing or the conservation of certain types of vorticity averages in the continuous motion of any medium whatever. The conditions for the validity of the results are satisfied by a motion within finite boundaries to which the material adheres without slipping, or by a motion vanishing at ∞ to a sufficiently high order, but are never satisfied by a plane motion. These results may offer some encouragement to those who criticise plane models of turbulence, for they show an instance where three-dimensional motions are simpler in their average properties than are plane motions.

R3. Flow of a Gas Characterized by the Beattie-Bridgeman Equation of State and Variable Specific Heats. Part II. Shock Waves.* J. C. CROWN, *Naval Ordnance Laboratory.*—The aerothermodynamic relations across both normal and oblique shock waves have been re-derived using the Beattie-Bridgeman equation of state in place of the perfect-gas law and allowing for the component of specific heat due to the vibrational mode of freedom (for polyatomic molecules). Significant deviations from the classical solution were indicated by the calculations.

* Sponsored by the ONR.

R4. Investigation of the Efficiency of a Simple Diffuser for Supersonic Wind Tunnels.* J. L. DIGGINS, *Naval Ordnance Laboratory.*—Some results are presented from the first tests in a program to determine the most efficient diffuser configuration for use in a supersonic wind tunnel. Sufficient data have been obtained at $M=2.48$ and $M=2.83$ to make possible the design of a simple yet very efficient diffuser to be used at these Mach numbers in a supersonic wind tunnel with a square cross section. A plot of pressure recovery *versus* diffuser throat location reveals that the most efficient location, at the two above Mach numbers, is 42 percent of the diffuser length from the beginning of the diffuser. This corresponds to 6.7 diameters from the nozzle exit, considering a diameter to be one side of the square which forms the nozzle exit. These values are valid for the 18×18 cm wind tunnel with a closed jet. It is further shown that the use of a half-open jet has practically no influence on the pressure recovery in this diffuser. Other curves are presented which show the optimum starting and operational throat openings and the starting and operational pressure ratios required for the whole tunnel system.

* Sponsored by the ONR.

R5. Statistical Analysis of Turbulence Data With Computing Machines.* F. N. FRENKIEL, *Naval Ordnance Laboratory.*—Turbulence recording measured with a hot wire have been analyzed using IBM machines. Various statistical characteristics of the turbulence are obtained including second- and third-order correlation coefficients, microscale of turbulence, frequency distribution of turbulent velocities, etc. The possibilities of this method of analysis are discussed.

* Sponsored by the ONR.

R6. A Solution of Lagrange's Problem of Interior Ballistics by Means of its Characteristic Lines.* W. HEYBEY, *Naval Ordnance Laboratory.*—The one-dimensional non-steady motion set up in a highly compressed gas when it accelerates a piston in a cylinder represents a problem of long standing. The first rigorous and rather complete solution was given in 1922 by A. E. H. Love. His analysis, however, is restricted to

specific values of γ; it is intricate, and requires cumbersome computations of power series coefficients in the later stages where several expansion waves intermingle. The solving process becomes more lucid and considerably shorter when the characteristic net of the problem is developed which pictures quite naturally the interactions of the various waves and does not call for Love's separate treatment following each reflection at breech and piston. Also, any value of the ratio of the specific heats may be used. The integration is performed stepwise. Agreement was excellent with a numerical computation after Love's method.

* Sponsored by the ONR.

R7. An Electronic Method for Determining Gas Liquefaction in Shock Tubes by Light Scattering. G. A. Lundquist, *Naval Ordnance Laboratory.*—One of the serious problems in the operation of hypersonic wind tunnels is the possible liquefaction of components of air at high Mach numbers. The thermodynamic conditions under which this condensation may occur in wind tunnels can be duplicated in the shock tube in the cold air behind the contact surface. The exact time and place in the shock tube at which the desired conditions exist can be determined theoretically and experimentally. By using a suitable observation point also the transit time of a gas through a hypersonic wind tunnel can be duplicated. The condensation can be detected by Rayleigh light scattering on droplets. The amount of light scattered at right angles to a collimated light beam is measured with a photo-multiplier tube and oscilloscope. The above method has already been used at the Naval Ordnance Laboratory and proven successful for the detection of water vapor condensation in the shock tube. Experiments are now being carried out on liquefaction of components of air in regions of extremely low air temperatures.

R8. On Nearly Glancing Reflection of Weak Shocks.* A. H. Van Tuyl, *Naval Ordnance Laboratory.*—When a plane shock wave moving at right angles to a plane wall strikes slightly concave corner (the edge of the corner being parallel to the shock wave), a triple shock configuration results. We assume that the shock moves in a perfect gas which is initially at rest. V. Bargmann (National Defense Research Committee AMP Report 108.2R, March 1945) has studied the flow for a sufficiently flat corner and a sufficiently weak initial shock wave. The angle of the corner will be denoted by $\pi-\epsilon$, and the Mach number behind the original shock in the reference system in which it is stationary by σ. If terms of the orders of ϵ and $\epsilon(1-\sigma)$ are retained while neglecting those of the orders of ϵ^2 and $\epsilon(1-\sigma)^2$, Bergmann showed that the flow is irrotational. Assuming that the flow is similar at all times after impact of the shock wave on the corner, the potential in the coordinates y_1, y_2 in which the flow is steady is $\Psi=\Psi_0+\Omega(y_1, y_2, \sigma)\epsilon$, where $\Omega(y_1, y_2, \sigma)$ is given in terms of elementary functions. These results have been extended to show that if terms of the orders of ϵ, $\epsilon(1-\sigma)$, and ϵ^2 are retained while those of the orders of ϵ^3, $\epsilon^2(1-\sigma)$, and $\epsilon(1-\sigma)^2$ are neglected, the flow is irrotational.

* Sponsored by the ONR.

R9. I. Kerr Cell Photography of High Speed Phenomena—Detonation and Shock Phenomena.* R. Heine-Geldern, E. M. Pugh, and S. Foner, *Carnegie Institute of Technology.*—By synchronizing a Kerr cell camera with an exploding wire light source of peak intensity 3 to 5×10^8 candle power, a wide variety of non-luminous high speed phenomena can be photographed, using exposure times of approximately one microsecond. Photographs are presented showing explosive charges in the process of detonation, as well as certain interference phenomena produced by the simultaneous detonation of two charges. The technique has also been used to obtain photographs of phenomena not heretofore observed directly, such as the behavior of shock waves in transparent solids. Fairly direct observations can also be made on shock waves in non-transparent solids, such as metals, by submerging them in water; the passage of the shock wave through the metal gives rise to a shock wave in the surrounding water which in turn can be photographed. The velocity of propagation of the shock wave (and of cracking, if present) can be estimated in all cases. Thus it was found that, given a sufficiently intense shock, glass could propagate cracks at the velocity of the shock wave, which exceeds 6000 m/sec.

* Work performed under contract with the Office of the Chief of Ordnance.

R10. II. Kerr Cell Photography of High Speed Phenomena—Metal Jet Charges.* E. M. Pugh, R. Heine-Geldern, and E. C. Mutschler, *Carnegie Institute of Technology.*—The metal jets from high explosive charges with lined conical cavities have been successfully photographed traveling at very high speeds through air. Previous attempts to photograph these jets with visible light were unsuccessful because they are accompanied by an opaque shroud of luminous particles. To produce sharp jet silhouettes a background must have sufficient brilliance to penetrate this shroud and the camera shutter must expose less than a microsecond. The shroud can be eliminated by using liners with perfect conical apexes. Since these jets travel at speeds comparable to speeds of meteors, photographs of tips of jets passing through air furnish very clear pictures of meteoric phenomena. Photographs show that jet tips have color temperatures well above that of the background screen (lighted by an exploding wire). Evaporation of metal vapor from tip surfaces is clearly seen. Photographs are also presented which show jets penetrating water, Plexiglas, and glass as well as jets perforating steel plates.

* Work performed under contract with the Office of the Chief of Ordnance.

R11. III. Kerr Cell Photography of High Speed Phenomena—Instrumentation.* S. Foner, E. M. Pugh, R. Heine-Geldern, and E. C. Mutschler, *Carnegie Institute of Technology.*—The photography of non-luminous high speed phenomena (10^3 to 10^4 m/sec.) requires a rapid shutter (10^{-6} sec. or less) and an intense light source. This is accomplished by using a Kerr cell shutter synchronized electrically with the phenomenon and an electrically "exploded" wire light source, which has a peak intensity of approximately 5×10^8 candle power. In spite of this high intensity, very fast film must be used. To minimize the graininess, a large image size on the negative is desirable. This necessitates the use of a large aperture (f/2.5), long focal length (7 in.) lens which in turn requires a Kerr cell of correspondingly large aperture, operated at a high voltage (25 kv). Practical designs of large Kerr Cells, characteristics of exploding wires and the associated equipment and techniques are discussed in this paper.

* Work performed under contract with the Office of the Chief of Ordnance.

R12. Ultrasonic Absorption in Glycerol. T. A. Litovitz, *Catholic University of America* (Introduced by K. F. Herzfeld).—Using pulse techniques developed during the war the US absorption of glycerol is being studied in the temperature range of from plus 40°C to minus 25°C at the frequency 30.5 Mc. Tentative findings indicate the value of absorption in glycerol is 2 to 3 times the classical value. The temperature coefficient of absorption seems to be the same as the temperature coefficient of viscosity. At temperatures below −5°C the absorption reaches a peak and falls to values below even the classical value. This behavior at the lower temperatures indicates a relaxation time effect, as proposed by Eyring and Frenkel, associated with the viscosity as the liquid becomes "glasslike." The excess absorption appears to be a compressional viscosity effect such as found in water.

R13. Relative Velocities of Ultrasonic Waves in Liquids by Spark Shadow Photography.* CAVID ENER,† *Catholic University of America.*—Ultrasonic plane progressive waves of the same frequency are generated in a double optical cell containing two liquids. A shadowgraph of the two wave systems is taken by using a spark of the order of 10^{-7} sec. duration.[1] From such spark pictures the wave-lengths can be measured with a micrometer microscope, and the velocities are of course in direct proportion to wave-length. Distilled water is used as a reference liquid. The method has been checked by comparison of measurements of ultrasonic velocity in dextrose solutions with those of C. R. Randall[2] by the ultrasonic interferometer, and a good agreement is found.

* Assisted by contract with the ONR.
† From the Department of Experimental Physics, The University of Istanbul, Turkey.
[1] Hubbard, Larkin, and Zartman, J. Opt. Soc. Am. 37, 832 (1947).
[2] C. R. Randall, Tech. Pap. Bur. Stand. 8, 79 (1932).

R14. A Barium Titanate Coaxial Cable for the Production of a Short Duration Spark.* J. A. FITZPATRICK AND W. J. THALER, *Catholic University of America.*—A coaxial cable of barium titanate, having a dielectric constant of 1575,[1] has been used to make spark photographs of progressive ultrasonics waves in water at as high a frequency as seven megacycles per second. This cable has an over-all length of 16.5 centimeters and total distributed capacity of 0.02 microfarads thus permitting much higher energies to be used resulting in a more intense light source than has been previously employed.[2,3]

* Supported by ONR.
[1] B. H. Marks, Electronics (August 1948).
[2] J. W. Beams *et al.*, J. Opt. Soc. Am. 37, 868 (1947).
[3] Hubbard, Larkin, and Zartman, J. Opt. Soc. Am. 37, 832 (1947).

R15. The Maximum Pressure for Cavitation in Biological Suspensions.* EUGENE ACKERMAN, *University of Pennsylvania.*—Sonic destruction of biological cells occurs only in the presence of cavitation. Sonic fields for the experiments described here were generated by a magnetically driven, steel diaphragm which formed the bottom of a cup containing the aquaeous suspension being treated. The breakdown rate for most organisms becomes so small at intensities at which cavitation barely occurs, that a sharp pressure limit for cavitation cannot be found. Using the very sensitive G's strain of Paramecium aurelia, and also, using the optimum breakdown frequency of P candatum, a minimum effective intensity was found. This is estimated to be about ½-atmospheres pressure amplitude. These cavities do not grow to macroscopic bubbles until the system becomes sufficiently non-linear at plate velocity amplitudes three times the minimum necessary for cavitation, i.e., until the intensities in the suspension reach about 0.3 watts/cm². The cavities must be filled with dissolved gases and are probably initiated at the nuclei on the surfaces of the biological cells.

* Work supported by a grant from the Raytheon Manufacturing Company.

FRIDAY AFTERNOON AT 2:15

National Academy

(R. M. BOWIE presiding)

Discharges in Gases; Electron Emission

S1. Investigation of a Low Pressure Mercury Arc.* ROBERT M. HOWE, *M.I.T.* (Introduced by W. B. Nottingham).—The electron energy distributions in the plasma of a low pressure mercury arc have been obtained using the Langmuir-probe method of analysis. The electron energy distribution curves exhibit a double slope when plotted on a log scale, indicating a non-Maxwellian distribution characterized by a depletion of fast electrons. It is believed that this depletion is caused by inelastic collisions of high energy electrons with the walls of the tube, since a close correlation between wall potential and the potential at which the depletion sets in is evident. The tantalum probes were surrounded closely in each case by tantalum guard rings, and experiment shows that the probe currents are independent of guard potential over a very wide range.

* Supported in part by the Signal Corps, ONR, and the Air Force.

S2. Anode Phenomena in High Current Arcs. C. J. GALLAGHER, *General Electric Research Laboratory.*—The power dissipated at the anode of a high current d.c. arc (50–200 amp.) has been measured by a water-cooling method for arcs in He, A, and N_2 at atmospheric pressure. The measurements were made in a partially enclosed system with gas flowing at a very low rate. The arc burned vertically with the anode at the bottom. The power at the anode ranged from 50 to 90 percent of the total power into the arc, depending on the length of the arc, the kind of gas, and the shape of the anode. As the arc length increased, the ratio of anode power to total power decreased somewhat, although both quantities increased. The heating at the anode is due to electrons accelerated by the anode drop, which give up kinetic energy and also heat of condensation. There is also some heating due to high temperature gas near the surface, plus excited atoms or dissociated molecules returning to the ground state at the surface and radiation incident from the column. There is some cooling by radiation and evaporation of anode material. The importance of these factors as they affect the increase in anode heating with increased length will be discussed.

S3. Current Fluctuations in a D.C. Gas Discharge Plasma. P. PARZEN AND L. GOLDSTEIN, *Federal Telecommunication Laboratories, Inc.*—Radiofrequency energy produced in d.c. gas discharge plasmas, in different gases, has been measured by one of us.[1] Mumford[2] has recently indicated the use of such tubes as noise standards in the microwave region. This noise power may be accounted for by a study of the electron current fluctuations in a gas discharge plasma. In general, the electron current fluctuations can be divided into two parts. One depends upon the electron temperature and the other upon the d.c. current. Expressions will be given for the spectrum of the current $I(t)$ from which it follows that the available noise power per unit frequency band is kT_e for the case of Mumford. T_e is electron temperature. For the case where the axis of the gas tube is parallel to the E vector of the wave guide, the available noise power is:

$$P=\left(kT_e+\frac{P_0}{NZ}\left[2+\frac{Z^2-4\pi^2f^2}{Z^2+4\pi^2f^2}\right]\right)df,$$

P_0=d.c. power dissipated in plasma, N=total number of electrons in plasma, Z=collisional frequency, f=frequency of observation.

[1] L. Goldstein and N. Cohen, Phys. Rev. 73, 83 (1948).
[2] W. W. Mumford, B.S.T.J. 28, No. 4, 608 (October, 1949).

S4. Magnetically Controlled Ambipolar Diffusion. O. T. FUNDINGSLAND AND GEORGE E. AUSTIN.—Low pressure studies of volume deionization in decaying plasmas are obscured by excessive diffusion losses. The use of a toroidal-shaped tube with a co-annular magnetic field is proposed as a means for retarding diffusion to the container walls. The effectiveness of this control has been estimated by analyzing the simpler problem of a long circular cylinder with a uniform coaxial magnetic field, in which ambipolar flow to the walls is described by a single coefficient. An expression for the ambipolar diffusion coefficient as a function of energy, magnetic field B, and pressure p is derived by considering the average motion of electrons and ions in a quasi-static plasma. At high B/p it approaches the coefficient for free electron diffusion in a magnetic field, as B/p approaches zero it reduces to twice the free diffusion coefficient for positive ions, and when B is constant there is a pressure at which it has a maximum value. At 1 micron and 1000 gauss ambipolar diffusion in atmospheric gases is reduced by about 10^7 and is small compared to expected recombination. Determination of recombination coefficients by microwave techniques originating at M.I.T. will be attempted at low pressures, utilizing a coaxial cylindrical cavity with a co-annular magnetic field.

S5. The Role of Plasma Oscillations in the Description of Electron Interactions. DAVID PINES AND DAVID BOHM, *Princeton University.*—Because of the long range of the Coulomb force, the usual one-particle solutions are, for many purposes, a poor description of the interactions in a collection of electrons. As a first step in the development of a new description, we investigate classically the electron interactions in a plasma, and show that the transition from a single-particle to a collective description of the electron motion in terms of plasma oscillations can be obtained by a suitable series of canonical transformations. The complete Hamiltonian for a collection of interacting charges is re-expressed as a sum of three terms. One involves the collective field coordinates, which act like waves in an enclosure, and which express the degree of excitation of plasma oscillations. The other terms correspond to the kinetic energy of free electrons, and to the residual interparticle forces, which are found to be approximately screened Coulomb forces of very short range. This result shows that the effective collision cross-section between electrons in a dense assembly is much less than that calculated on the basis of the individual-particle approximation. A quantum-mechanical theory of plasma oscillations is now under investigation, and applications to the interactions between electrons in a metal, and to superconductivity, will be discussed.

S6. Electron Removal in Helium Afterglows.* B. T. MCCLURE, R. A. JOHNSON, AND R. B. HOLT, *Harvard University.*—Observations of the electron density, visible and near ultraviolet light intensity, and spectrum associated with a 3000-mc/sec. pulsed electrodeless discharge have been made. The techniques employed to obtain this data at various times relative to the discharge and results obtained on helium and other rare gases have been described previously.[1] Our electron density data indicated recombination-type electron removal with a constant $\alpha=1.5\times10^{-8}$ cm³/ion sec., in reasonably good agreement with previous data. During the discharge, the spectrum of atomic helium predominates. In the afterglow the band spectrum of He_2 predominates. The total energy radiated in the wave-length range 2300A to 8000A is estimated as 0.5 ev per electron removed. A maximum in the light intensity occurs a few hundred microseconds into the afterglow. The following mechanism is quantitatively consistent with all of our data: He^+ forms He_2^+ by undergoing a triple collision with two neutral atoms, after which the molecular helium ions combine with electrons.

* This work was supported by the ONR.
[1] M. A. Biondi and S. C. Brown, Phys. Rev. 76, 1697 (1949), and Holt, Richardson, Howland, and McClure, Phys. Rev. 77, 239 (1950).

S7. Formative Time Lags of Spark Breakdown in Oxygen.* G. A. KACHICKAS AND L. H. FISHER, *New York University.*—Measurements of formative time lags of spark breakdown in uniform fields in air[1] are being extended to oxygen. Time lags have been measured as a function of percent overvoltage (O.V.) and pressure for a plate separation of 1 cm. In air, the time lags are independent of pressure over a wide pressure range, and vary from about 100 μsec. at 0.01 percent O.V. to about 1 μsec. at 2 percent O.V. In oxygen, however, the time lag variation with pressure is very pronounced. The variation of time lags with percent O.V. is also quite different. For a given percent O.V., the formative time lags in oxygen are much longer than in air. For example, in oxygen near atmospheric pressure, the time lags vary from approximately 100 μsec. at 1 percent O.V. to about 1 μsec. at 2.5 percent O.V. Thus at 1 percent O.V., the lags are 100 times longer in oxygen than in air. (The present apparatus does not permit measurement of times greater than 100 μsec.) It is not yet clear whether a mechanism in addition to space-charge distortion of the field by positive ions is necessary to explain the results.

* Supported by the ONR and the Research Corporation.
[1] L. H. Fisher and B. Bederson, Phys. Rev. 75, 1324, 1615 (1949); Bulletin, Am. Phys. Soc., 1950 Annual Meeting.

S8. Electrical Oscillations in Spark Discharges.* HARRY S. ROBERTSON AND G. H. DIEKE, *University of Miami and The Johns Hopkins University.*—Several observers have reported the presence of unidentified oscillations in the current of a spark discharge in an LC circuit. The expected discharge current should be in the form of a damped sinusoid of frequency approximately $1/2\pi(LC)^{\frac{1}{2}}$. Two other oscillations have been isolated. One of these, called the parasitic, is due to a secondary resonance in the circuit formed by the lead and other stray inductances, together with the distributed capacity of the inductor. The parasitic oscillation is excited, along with the fundamental component of the current, at the initial breakdown. It is probably the component responsible for most of the radio interference. The second stray oscillation, tentatively called the spark oscillation, always originates during the transition from the glow form of the discharge to the so-called cold-cathode arc. The nature of the spark oscillations is not understood, but there is evidence that the oscillations originate in the gap and are not related to the external circuit.

* This work was supported through an ONR contract with The Johns Hopkins University.

S9. Production of High Current Electron Pulses by a Resonant Cavity Accelerator. G. W. CLARK AND L. B. SNODDY, *University of Virginia.*—A doubly reentrant cylindrical cavity operating at approximately 400 Mc is used in conjunction with a pulsed electron source to produce a high current beam of less than 10^{-7}-sec. duration. The cavity is driven by a 7 C 22 pulse-operated twin triode. Near the end of the 5 μsec. driving pulse a metal vapour arc is formed on the surface of one of the cavity electrodes by a high current pulse of short duration. Electrons are drawn from the arc plasma and accelerated by the cavity field across the space between the electrodes. With the present arrangement 2×10^{12} electrons with energies greater than 40 kev can be obtained in a single pulse lasting less than 10^{-7} sec. This current is about ten times that measured in previous experiments.[1]

[1] L. B. Snoddy and J. W. Beams, Phys. Rev. 75, 1324 (1949).

S10. Crystallographic Variations in Field Emission from Single Tungsten Crystals.* MICHAEL K. WILKINSON. *M.I.T.* (Introduced by W. B. Nottingham).—By means of a spherical projection tube with a point filament etched electrolytically from tungsten wire and mounted on a hairpin filament for heating, a field emission pattern is observed showing the relative emission from a tungsten crystal along the various crystallographic directions. With the latest techniques in high vacuum procedure, a vacuum is reached which is sufficiently good that the emission pattern of clean tungsten is stable for periods of about an hour. The photometry of the pattern produced on the spherical fluorescent screen yields data that give the relative emission currents as the electric field at the filament is varied. These data are then interpreted according to the theoretical field emission equation derived by Fowler and Nordheim. Data now available indicate that the dark areas of the emission pattern are crystallographic directions for which the slope of the plotted line is higher than that determined by direct electrical measurement for the point as a whole. The bright areas represent crystallographic directions for which the slope is lower than the average.

* Supported in part by the Signal Corps, ONR, and the Air Force.

S11. Deterioration of Oxide-Coated Cathodes Under Low Duty-Factor Operation.* J. F. WAYMOUTH, JR., *M.I.T.* (Introduced by W. B. Nottingham).—A study has been made of the effect of emission current duty-factor on oxide cathode life. End of life is identified either by failure to yield an arbitrary specified emission or by the presence of an excessive potential drop across the coating for a given pulsed emission. For cathodes coated on nickel cores containing relatively high percentages of impurities (Si, Mn, Fe, etc.) mounted in diodes in which especial care had been taken to eliminate spurious impurities from the remainder of the structure, zero duty-factor operation is found to cause a high incidence of the development of cathode interface resistance. The interface resistance is found to be consistent with the hypothesis of an insulating layer several thousand atom diameters in thickness located at the interface between coating and core.

* Supported in part by the Signal Corps, the ONR, and the Air Force.

S12. Effect of Patch Fields on Schottky Deviations.* E. A. COOMES, R. J. MUNICK, AND W. B. LA BERGE, *University of Notre Dame.*—Schottky deviations[1] have been observed for clean tantalum wires for fields from 50 to 300,000 volts/cm, and in a temperature range from 1100° to 1700°K. The slope of the Schottky plots agreed with measured temperatures at low and high fields, but had an anomalous value at intermediate fields, in accordance with patch theory.[2] The breaks in slope indicate a patch size in good agreement with microphotographic grain growth observations on tantalum ribbons.[3] Breaks in slope show that patches grow in size when the wire is heat treated. Using the Schottky slopes determined experimentally, computed deviations from the Schottky line are continuous in phase and amplitude over the entire range of measurement. The observed maxima and minima are in fair agreement with the Guth-Mullin theory,[4] and there are no indications that patch fields disturb the effect at low applied fields, even down to where space charge might become important.

* This work sponsored by U. S. Navy Bureau of Ships.
[1] R. L. E. Seifert and T. E. Phipps, Phys. Rev. **56**, 652 (1939).
[2] J. A. Becker, Rev. Mod. Phys. **7**, 95 (1935).
[3] B. A. Mrowca, J. App. Phys. **14**, 684 (1943).
[4] E. Guth and C. J. Mullin, Phys. Rev. **59**, 575 (1941).

S13. Low Frequency Fluctuations in the Tungsten-Lamp-Photo-Cell System. BRITTON CHANCE, *University of Pennsylvania.*—In the course of development of methods for detecting very small changes of optical density ($\log Io/I < 10^{-3}$) of enzyme solutions occurring in a time range 10 msec. to 10 min., several attempts have been made to achieve a signal to noise ratio limited only by the shot noise of the photo-current.[1] In the system, voltage-regulated tungsten lamp, double-grating monochromator, and differential caesium-antimony photo-cells, the light intensity fluctuations due to lamp voltage variations are reduced to the equivalent of 2×10^{-6} in the photo-current while the actual amplitude of low frequency fluctuations (~0.1 c.p.s.) corresponds to 2×10^{-5}. Shot noise would contribute 5×10^{-6}. This fluctuation is independent of the wave-length of light illuminating the photo-tube (4000 to 5600A), independent of the photo-cell anode voltage (5–150 v), independent of the total photo-current (0.05–0.25 μa), but decreases with decreasing lamp voltage or temperature. Thus this excess fluctuation does not appear to be attributable to the lamp regulation circuit or to the photo-cells and may be due to a property of the tungsten filament of the lamp.

[1] B. Chance, Rev. Sci. Inst. **18**, 601 (1947).

S14. New Type of High Speed Coincidence Circuit.* Z. BAY, *George Washington University* (Introduced by R. O. Wales).—A new principle for a high resolving coincidence device was tried and found successful. (1) We compare some characteristic quantity Q_A of the pulses measured in channel A with the same kind of quantity Q_{AB} measured simultaneously between the channels A and B. With a pulse in A only, Q_A and Q_{AB} are equal, while in the case of coincidence $Q_A - Q_{AB} \neq 0$. (2) With a pulse in B only, we can make Q_{AB} equal zero and thus $Q_A - Q_{AB} = 0$ by applying a rectifier characteristic to the measurement of Q_{AB}. In the actual performance we used crystal diodes for the measurements, Q_A and Q_{AB} being here the charges going through the diodes and collected in separate condensers. For the measuring of $Q_A - Q_{AB}$ we used either a differential amplifier, or a self-subtracting circuit developed for this purpose and an ordinary pulse amplifier. The circuit built by us will respond to unequal pulses and uses no vacuum tubes or voltage supplies in the coincidence device, which is small in size and is stable. Using electron multiplier pulses we have been able to get resolving times $<10^{-9}$ sec. and to detect and measure time delays $\sim10^{-10}$ sec.

* Supported by the ONR.

FRIDAY EVENING AT 7:00

Grand Ballroom, Mayflower Hotel

(I. I. RABI presiding)

Banquet of the American Physical Society

After-dinner speech by W. V. HOUSTON, *Rice Institute.*

SATURDAY MORNING AT 10:00

Lisner Auditorium

(I. I. RABI presiding)

Invited Papers

T1. Recent Developments of Nuclear Induction. FELIX BLOCH, *Stanford University.* (50 min.)

11:00 A.M.

T2. Galactic Radio Waves. GROTE REBER, *National Bureau of Standards.* (30 min.)

11:40 A.M.

T3. How to Write Scientific Papers. D. H. MENZEL, *Harvard University.* (45 min.)

SATURDAY MORNING AT 10:00

National Bureau of Standards

East Building Lecture Room

(R. S. MULLIKEN presiding)

Molecular Spectroscopy in the Infra-Red Region; Molecular Interactions

U1. The Spectrum of Water Vapor in the Region of 2.7μ. W. S. BENEDICT AND E. K. PLYLER, *National Bureau of Standards.*—Using a 15,000-line grating and a lead sulfide photo-conductive cell, spectra of water vapor between 2.4 and 2.9μ have been obtained with resolution considerably better than previously reported (H. H. Nielsen, Phys. Rev. 62, 422 (1942)). The spectral slit width varied between 0.08 and 0.2 cm^{-1} and lines as close as 0.2 cm^{-1} are partially resolved. The bands of CO_2 in this region also appear. A quite complete rotational analysis of the results has been possible, which does not confirm earlier work in all details. Practically all the intense lines belong either to the ν_3 fundamental, of which energy levels have been located up to $J=10$, or to CO_2; the ν_1 fundamental has also been found, with intensity relative to ν_3 about 1:15, and with ν_0(vac) at 3656.2 ± 0.4 cm^{-1}. There are numerous examples of rotational perturbations between ν_1 and ν_3. If the strongest line of ν_3 is assigned a calculated relative intensity of 100, all predicted lines of intensity greater than 1 have been found.

U2. The Effect of Aging and of Heat Treatment on the Infra-Red and Ultraviolet Spectra of Urea.* RUTH C. SHEA AND GLADYS A. ANSLOW, *Smith College.*—Infra-red spectra from 2.5 to 7.5μ were obtained with a Perkin-Elmer recording spectrophotometer, employing CaF optics and ultraviolet spectra with a Beckmann quartz spectrophotometer and Lyman vacuum spectrograph. Crystals were deposited from methanol solutions on CaF plates in a vacuum desiccator or suspended in Nujol. Water solutions were heat-treated as previsously described.[1] In the 3μ region the intensities of the two N−H stretching vibration bands for unassociated bonds exceed those for associated bonds in freshly deposited speciments; during a three day period the intensities of the associated bands increase, after which a stable state appears established with the 3216 cm^{-1} association stronger than the 3160 cm^{-1} association band. The ultraviolet spectra show similar variance with degree and type of association. Solutions of freshly purified crystals give bands indicating more unassociated amide groups than do solutions from aged crystals and indicate associated water. End absorption characteristic of dimers is obtained from rapidly cooled solutions, and of polymers from slowly cooled specimens. Comparison is made with the ultraviolet spectra of acetamide.

* Supported by the ONR.

[1] G. A. Anslow and R. C. Shea, Phys. Rev. **75**, 1318 (1949).

U3. The Origin of the Weak Absorption in the Near Ultraviolet Spectra of Hydrogen-Bridged Amides and Alcohols.* GLADYS A. ANSLOW, *Smith College.*—In previous discussions the end absorption in the ultraviolet spectra of hydrogen-bridged molecules has been attributed to the rupture of the bond and bridge, following electronic excitation. At lower photon energies weaker bands appear, some with structure, probably resulting from rupture of the bridge with excitation of the bond to the lower vibrational energy states of the excited level. In some instances negative absorption coefficients were obtained in this region, attributable to reassociation. Bands with onsets near 35000 cm^{-1} and 38000 cm^{-1} in cyclic amides, containing water of crystallization, and in alcohols may result either from the (0, 1) and (0, 2) electronic-vibrational transitions or from ground state vibrational dissociation of unassociated or associated hydroxyls, respectively. Since the 35000 cm^{-1} band appears in the water-bound amides and in those alcohols, for which boiling point and infra-red data indicate low polymerization, and the 38000 cm^{-1} band predominates in highly polymerized alcohols, and since transition probabilities for $G''(0)\rightarrow G''(v_{max})$ for the highly perturbed energy states of such molecules must be large, evidence supports the second hypothesis.

* Supported by the ONR.

[1] See paper No. U2; also G. A. Anslow *et al.*, J. Chem. Phys. **17**, 436 (1949); Phys. Rev. **77**, 423 (1950).

U4. Raman and Infra-Red Spectra of Pentaborane.* W. J. TAYLOR, C. W. BECKETT, J. Y. TUNG, R. B. HOLDEN, AND H. L. JOHNSTON, *Ohio State University.*—The Raman spectrum of liquid pentaborane (B_5H_9), and the infra-red spectrum of the gas from 3 to 25 microns, have been obtained. The Raman lines observed are: 470, vvw; 566, 596, 616, w, dp; 700, 738, 782, m, dp; 793, 803, s, p; 884, w, dp; 982, vs, p; 999, s, p;

1120, m, p; 1170, 1193, vw, p; 1350, 1387, 1440, vw; 1740–1840, w, dp, diffuse band; 1840, m, p; 1870–2300, ~10 vw lines; 2077, 2152, w, p; 2600 cm^{-1}, vs, dp.[1] The principal infrared absorption bands observed are: 570, m; 605, 619, 628, vs; 702, vw; 798, 807, m; 815, 820, w; ~900, vs, broad; 1035, 1045, m; 1125, w; 1143, 1187, 1210, 1230, vw; ~1415, vs, broad; 1500, w; 1620, m; 1800, s; 2100, 2250, 2460, vw; ~2600, vs; 2700–3300 cm^{-1}, 6 vw bands.[1,2] The interpretation of the spectral data is discussed for two models: the pyramidal structure (C_{4v} or C_{2v}), and the cyclopentadiene-like bridge structure (C_{2v}) suggested by Pitzer. The spectral data are not entirely conclusive; however, the pyramidal structure is strongly supported by the calorimetric entropy obtained in this laboratory, and is also more consistent with the published electron diffraction data than the bridge model.

* This work was supported in part by the ONR under contract with the Ohio State University Research Foundation.

[1] v = very; w = weak; m = medium; s = strong; p = polarized; dp = depolarized.

[2] The bands in the NaCl region are confirmed by an unpublished spectrogram from the General Electric Company.

U5. Absorption Spectra of the Xylene Vapors in the Near Ultraviolet.* C. D. Cooper and H. Sponer, *Duke University.*—The xylenes were studied using a 3-meter grating spectrograph and quartz absorption cells of different lengths. Discrete absorption occurs in the region between 2850 and 2375A for all three compounds. The *ortho*-spectrum is the sharpest of the three and the richest in bands while the *meta*-spectrum has the least number of bands and the most diffuse appearance. Rough intensity measurements indicate that the *para*-spectrum is about three times as strong as the meta- or *ortho*-spectrum. The 0,0 bands are located for ortho at 37308 cm^{-1}, for *meta* at 36955 cm^{-1}, and for *para* at 36733 cm^{-1}. Prominent upper state frequencies which appear in progressions and combinations are for *ortho* 1195, 939, 692, and 507; for *meta* 1245, 965, and 470; and for *para* 1186, 802, 775, and 552. Many bands must be explained as resulting from v−v transitions. These v−v transitions are more plentiful in *ortho* than in the other two spectra.

* This work was supported by ONR.

U6. The Infra-Red Spectrum of Crystalline Hydrogen Sulfide. J. B. Lohman and D. F. Hornig, *Brown University.*—The infra-red absorption of crystalline hydrogen sulfide at −195°C has been examined between 800 cm^{-1} and 2800 cm^{-1}. In contrast to water, the main absorption peaks are very sharp, indicating an ordered crystalline structure. Absorption peaks at 1170 cm^{-1}, 2517 cm^{-1}, and 2540 cm^{-1} have been tentatively assigned to components (arising from crystalline coupling) of ν_2, ν_1, and ν_3 of the free molecule, respectively; weaker peaks at 1184 cm^{-1}, 2622 cm^{-1}, and 2722 cm^{-1} appear to be combinations of fundamentals with lattice vibrations. Reported x-ray studies of the hydrogen sulfide[1] crystal indicated a face-centered cubic crystal structure which implied a linear molecule. The infra-red and Raman spectra[2] of the crystal are not consistent with a crystal of higher than tetragonal symmetry, a conclusion consistent with the accepted non-linear structure of the hydrogen sulfide molecule.

[1] L. Vegard, Naturwiss. **18**, 1098 (1930).

[2] G. M. Murphy and J. E. Vance, J. Chem. Phys. **6**, 426 (1938).

U7. Remarks on the Infra-Red Spectrum of Deuteronaphthalene.* L. Corrsin, *Duke University.*—The infra-red spectrum of a newly synthesized sample of deuteronaphthalene will be compared with a spectrum of very pure ordinary naphthalene. These spectra taken in carbon tetrachloride and carbon disulfide solutions at the U. S. Bureau of Standards by Dr. E. K. Plyler and Miss Mary A. Lamb cover almost the entire region of the fundamental vibrations. Tentative assignments will be given for a number of prominent bands which were identified because of their strength, spectral region and isotope shift.

* This work was supported by the ONR.

U8. Relaxation Times for Exchange of Vibrational Energy in Gas Molecules. Wayland C. Griffith,* *Harvard University.*—The fact that the internal energy states of molecules fail to keep up with sufficiently rapid changes in their environment has important implications in some flow problems. Relaxation times for exchange of energy among the various modes of motion have been studied for seventeen gases: H_2, N_2, SO_2, CO_2, N_2O, NH_3, CH_4, C_2H_6, C_3H_8, C_4H_{10}, C_2H_4, C_4H_6, CCl_2F_2, $CHClF_2$, CH_3Cl, $CH_2{:}CHCH{:}CH_2$, and C_2H_4O. The measurements are based on a steady flow technique devised by Kantrowitz.[1] The total head in a jet read with a small pitot tube differs from the stagnation pressure in the reservoir by an amount that can be related to the relaxation time through the jet velocity and the pitot tube diameter. An accurate solution for the flow pattern involved has been found numerically using Southwell's Relaxation Method. Experimental techniques were developed which gave quite accurate and consistent results with very small scale measuring equipment. It was thus economical to expend the gas as in a blow-down wind tunnel, and gain the advantage of easily studying many gases of high purity. For gases on which sound dispersion data is also available good agreement is found between the two methods.

* Present address; Princeton University.

[1] A. Kantrowitz, J. Chem. Phys. **14**, 150 (1946).

U9. Gaseous Data of State for Hydrogen between 1 and 200 Atmos. from 20 to 300°K.[1] Herrick L. Johnston, Irving J. Bezmann, Thor Rubin, Lyle Jensen, David White, and Abraham S. Friedman, *Ohio State University.*—An apparatus, patterned after that of Bartlett[2] but similar in design to a precision vacuum calorimeter, has been developed at the Ohio State University Cryogenic Laboratory for measuring gaseous PVT data at low temperatures to an accuracy of 1 part in 10,000. Approximately 30 PV isotherms have been determined for hydrogen at temperatures of 20 to 300°K for pressures up to 200 atmos., and have been used to calculate the second and third virial coefficients. The saturated vapor pressure curve has also been determined. The Boyle Point was found to be 104.0±0.5°K, and the critical temperature and pressure 33.24°K and 12.797 atmos., respectively.

[1] This work was supported in part by the Air Materiel Command under contract with the Ohio State University Research Foundation.

[2] Bartlett, J. Am. Chem. Soc. **49**, 687 (1927).

U10. Intermolecular Force Constants for Hydrogen and for Nitrogen. David White, Abraham S. Friedman, and Herrick L. Johnston, *Ohio State University.*—The intermolecular force constants of hydrogen and of nitrogen have been determined using the potential function:

$$\epsilon_{(r)} = \epsilon_0\left[\frac{n}{n-m}\left(\frac{r_0}{r}\right)^m - \frac{m}{n-m}\left(\frac{r_0}{r}\right)^n\right],$$

where n and m equal 12 and 6, respectively. The determinations make use of our own values of the second virial coefficients, obtained recently from low pressure data of state between room temperature and the boiling points of the respective gases. The values of r_0 and $\epsilon_0 - k$ are 3.35A and 30.69 degrees for hydrogen, and 4.15A and 95.93 degrees for nitrogen.

U11. The Forces of Interaction in a Solution of Two Non-Polar Gases: Hydrogen and Nitrogen. David White, Abraham S. Friedman, and Herrick L. Johnston, *Ohio State University.*—The intermolecular force constants for a hydrogen-nitrogen solution have been evaluated from experimental second virial coefficients. It is shown that the interaction virial coefficients B_{12} and the virial coefficients for mixtures

B_{mix} can be fitted to a 6–12 Lennard-Jones potential function. The values of ϵ_{12}/k and r_{12} are -50.81_6 deg. and 3.78A, respectively. The interaction constants obtained from the values of B_{mix} at various concentrations lead to the following simple combination rules:

$$(\epsilon_0/k)_{mix}=N_1(\epsilon_0/k)_1+N_2(\epsilon_0/k)_2$$
$$(r_0)_{mix}=N_1(r_0)_1+N_2(r_0)_2.$$

Thus, the intermolecular force constants and virial coefficients can be computed for any binary gas mixture from a knowledge of the force constants of the pure gases.

U12. Intermolecular Force Constants for Helium and for Deuterium. DAVID WHITE AND HERRICK L. JOHNSTON, *Ohio State University.*—The intermolecular force constants for helium and for deuterium have been evaluated from experimentally determined second virial coefficients using a Lennard-Jones 6–12 potential function. The constants namely ϵ_0/k and r_0 obtained for helium are 7.40 degrees and 2.65A, respectively, which differ considerably from previous values evaluated from data of state, especially in the case of ϵ_0/k. Our value of ϵ_0/k indicates that the Boyle point for helium is 25.4°K instead of 20.7°K, as would be obtained from the previous constants. The constants of the Lennard-Jones 6–12 potential functions for deuterium are 33.27 degrees and 3.39A for ϵ_0/k and r_0, respectively. The latter value agrees with the r_0 obtained earlier for hydrogen, but the ϵ_0/k value is slightly higher, indicating a deeper "well" and a higher Boyle point. The second virial coefficients for deuterium were found to be considerably different from those for hydrogen, and the difference can be ascribed to quantum effects as given by Shafer[1] and by de Boer and Michels.[2]

[1] K. Shafer, Zeits. f. Physik. Chem. **B38**, 187 (1937).
[2] J. de Boer and A. Michels, Physica **5**, 945 (1938).

U13. The Second Virial Coefficients of Non-Polar Binary Gas Mixtures. DAVID WHITE, *Ohio State University.*—A method recently suggested by White, Friedman, and Johnston[1] for predicting second virial coefficients of non-polar binary mixtures has been tested on a set of seven gaseous mixtures where experimental data of reasonable accuracy were available. The method implies that B_{mix}, the second virial coefficient for the mixture, fits a 6–12 Lennard-Jones potential function with intermolecular force constants

$$(\epsilon_0/k)_{mix}=N_1(\epsilon_0/k)_1+N_2(\epsilon_0/k)_2$$

and

$$(r_0)_{mix}=N_1(r_0)_1+N_2(r_0)_2.$$

Where $(\epsilon_0/k)_1(\epsilon_0/k)_2(r_0)_1(r_0)_2$ are the intermolecular force constants of the pure components 1 and 2 obtained from a Lennard-Jones potential function, and N_1 and N_2 the mole fractions. This combination rule reproduces the experimental values very well. The combination rule used by Hirschfelder and Roseveare[2] for evaluation of the interaction virial coefficients B_{12} for binary mixtures has also been compared with the experimental data. In nearly all the cases, this rule was also found to lead to values of B_{mix} which agree well with the experimental values.

[1] White, Friedman, and Johnston, to be published.
[2] J. O. Hirschfelder and W. E. Roseveare, J. Chem. Phys. **43**, 15 (1939)

SATURDAY MORNING AT 10:00

National Academy

(M. GOLDHABER presiding)

Beta-Emitters. I

V1. Beta-Ray Spectrum of K^{40}. DAVID E. ALBURGER, *Brookhaven National Laboratory.**—A measurement of the beta-ray spectrum of K^{40} has been made using a lens spectrometer at 17 percent resolution. The source was prepared under the direction of C. P. Keim by electromagnetic enrichment at the Oak Ridge Y-12 plant. The K^{40} content is 7.13 percent. Enriched KCl was deposited by precipitation over a 4 cm² area on 0.5 mg/cm² Nylon backing. The average thickness of the source was 2.4 mg/cm². A maximum net counting rate of 16 per minute was observed above a background of 18 per minute. Calculated correction for resolution was made by graphical integration. The Kurie plot, corrected by the 3rd forbidden axial vector or tensor interaction factor for spin change 4, is linear from about 500 kev to the end-point at 1.38±0.03 Mev. Other forbidden transition factors have been applied to the data. α appears to give a non-linear plot but a D_2 correction is linear above 500 kev and cannot be excluded with present data. Deviations below 500 kev are thought to be due to effects of source thickness and are being investigated by comparison studies using allowed beta emitters mixed in normal KCl.

* Work performed at Brookhaven National Laboratory under the auspices of the AEC.

V2. Beta-Disintegration of Sc^{44}.* A. BRUNER** AND M. LANGER, *Indiana University.*—In an attempt to understand the unusual positron spectrum shape reported by G. P. Smith, the Sc^{44} disintegration has been reinvestigated with a 15 cm radius of curvature shaped magnetic field spectrometer. The source was prepared by bombarding an enriched sample (91.6 percent) of K^{41} with 22 Mev alpha-particles in the cyclotron. A Fermi plot of the data indicates that there are two groups of positrons with end points at 1.478±0.005 and 0.955±0.010 Mev. All parts of the distribution are found to decay with the same composite period resulting from the initial activation of both isomeric states, with the subsequent feeding of the 4.0 hr. level by the 57 hr. level. The general shape is quite different from that found by Smith. An examination of the photoelectrons ejected from a uranium radiator indicates the existence of a 1.25 Mev gamma-ray which, from its intensity, apparently is associated with at least some *K*-capture. Displacement of the back edges of the annihilation radiation lines suggests a gamma-ray of 0.52 Mev corresponding to the difference between the beta-end points. From the measurement of conversion electrons, the energy of the gamma-transition between the isomeric states is found to be 271.3±0.7 kev.

* Assisted by a grant from the Frederick Gardner Cottrell Fund of the Research Corporation and by the joint program of ONR and AEC.
** AEC Predoctoral Fellow.

V3. Internal Conversion Coefficients in Co^{60}. M. A. WAGGONER, M. L. MOON, AND A. ROBERTS, *State University of Iowa.*—Using a two-coil, thin lens β-spectrometer we have measured internal conversion coefficients in Co^{60}. In integrating the β-spectrum we assumed an allowed shape, as indicated by our results and previous experiments.[1] The end point was

318.7±4.0 kev. We obtained for coefficients for conversion in K, L, M shells together (unresolved): $\alpha_{1.17}=(1.733\pm0.061)\times10^{-4}$, $\alpha_{1.33}=(1.286\pm0.035)\times10^{-4}$. Theoretical values[2] of conversion coefficients for K shell for electric quadrupole radiation are: $\alpha K_{1.17}=1.545\times10^{-4}$, $\alpha K_{1.33}=1.175\times10^{-4}$. Conversion coefficients for other types of radiation differ from EQ by a factor 2 or more. Supposing $L+M$ conversion and screening corrections to be about 10 percent, we may classify both gamma-rays as EQ. Angular correlation experiments[3] show both gamma-rays to be quadrupole transitions with $J=4\rightarrow2\rightarrow0$. Present results fix all parities as even. Quantitative comparison with internal conversion theory requires evaluation of L conversion and screening corrections.

[1] Deutsch, Elliott, and Roberts, Phys. Rev. **68**, 193 (1945).
[2] Rose, Goertzel, Spinrad, Harr, and Strong, Phys. Rev. **76**, 184 (1948).
[3] Brady and Deutsch, Phys. Rev. **74**, 1541 (1948).

V4. The Disintegration of Ga^{66}.* R. D. MOFFAT AND L. M. LANGER, *Indiana University.*—The radioactivity of Ga^{66} has been studied in the 180° focussing, 40 cm radius of curvature, shaped field spectrometer. The activity was produced by $Cu^{63}(\alpha,n)Ga^{66}$ in the cyclotron. The positron distribution is found to consist of four groups having end-point energies and relative intensities as follows: 4.14 Mev, 87.0%; 1.4 Mev, 4.3%; 0.88 Mev, 6.9%; 0.40 Mev, 1.7%. In spite of the high ft value ($\sim10^8$), the highest energy group has a spectrum shape characteristic of an allowed transition. Since the transition from Ga^{66} to the ground state of Zn^{66} presumably involves *no* change of parity, one might expect that the 4.14 Mev spectrum does not go directly to the ground state. From measurements on the photo and compton electrons ejected from a radiator, gamma-rays are found with energies of 4.8, 2.75 and 1.03 Mev. The 1.03 Mev gamma is the most intense—about 300 times that of the 2.75 Mev. One can propose a reasonable level scheme for Zn^{66} only if the 1.03 Mev gamma follows the 4.14 Mev beta-transition. Since no β-γ-coincidences are found associated with the 4.14 Mev group, it must be assumed that the lifetime of the 1.03 Mev level is longer than 10^{-6} sec. Excited states of Zn^{66} lie 1.03, 3.78, 4.29 and 4.8 Mev above the ground state.

* Assisted by a grant from the Frederick Gardner Cottrell fund of the Research Corporation and by the joint program of ONR and AEC.

V5. Radiations from As^{72} and As^{71}. J. Y. MEI, ALLAN C. G. MITCHELL, AND C. M. HUDDLESTON, *Indiana University.**—Gallium was irradiated by alpha-particles and the resulting arsenic radiations studied in a magnetic lens spectrometer. When 23 Mev alpha-particles were used As^{72} (26 hours), As^{74} (17.5 days), As^{73} (90 days), and As^{71} (60 hours), the latter from $(\alpha, 2n)$ reactions, were obtained. When the bombarding energy was reduced, the radiations from As^{73} and As^{71} disappeared. The radiations from As^{72} were similar to those of Ga^{72}. The photo-electron spectrum showed a gamma-ray of 0.835 Mev, together with many weaker ones extending out to around 3 Mev. The beta-ray spectrum shows an internally converted line corresponding to a gamma-ray energy of 0.702 Mev (not seen in the photo-electron spectrum) and five beta-ray groups at 3.38, 2.486, 1.849, 0.669 and 0.255 Mev. The levels correspond closely to those obtained in Ga^{72}. As^{71} decays by K-electron capture accompanied by an internally converted gamma-ray at 0.173 Mev. Information on As^{74} and As^{73} will be given.

* Assisted by the joint program of ONR and AEC.

V6. Radiations Emitted by Sr-85.* LIN-SHENG CHENG AND J. D. KURBATOV, *Ohio State University.*—Strontium 85, produced by activation of rubidium with deuterons was separated without addition of common strontium. The radiations emitted by carrier free Strontium 85 were studied by coincidence procedure. It was found that this species disintegrating by orbital electron capture emits converted gamma-rays of ~510 kev and ~185 kev, the latter highly converted. The electron-photon coincidence measurements showed that monochromatic electrons of ~170 kev are in coincidence with x-rays and not with 510-kev photons. Also, data were obtained for the existence of several groups of monochromatic electrons of higher energy and of low abundance. No evidence was secured for the 800-kev photons previously reported as emitted by Sr-85.

* Assisted by a grant of the Alumni Development Fund of the Ohio State University.

V7. Disintegration of Ru^{103}. J. Y. MEI, C. M. HUDDLESTON, AND ALLAN C. G. MITCHELL, *Indiana University.**—Ruthenium was irradiated in the Oak Ridge pile. After a separation consisting of a distillation of RuO_4, the beta- and gamma-radiations were studied with a magnetic lens spectrograph. The photo-electrons ejected from a lead radiator showed K and L lines for a gamma-ray of energy 0.494 Mev, belonging to Ru^{103} (42 days) and a K line for a gamma-ray of 0.217 Mev belonging to Ru^{97} (2.8 days). The beta-ray spectrum of an aged source gave two groups of beta-rays with end points at 0.684 Mev (10 percent) and 0.204 Mev (90 percent). An internal conversion line corresponding to the gamma-ray at 0.494 Mev and also a conversion line at 0.035 Mev emitted from the product Rh^{103m} were found. The disintegration scheme of Ru^{103} will be discussed.

* Assisted by the joint program of ONR and AEC.

V8. Beta-Spectrographic Investigation of Ru^{103} and Rh^{103m}.* A. J. SAUR,†, P. AXEL, L. G. MANN, AND J. OVADIA, *University of Illinois.*—A double thin-lens beta-ray spectrometer was used to investigate the beta-spectrum of Ru^{103} and its daughter Rn^{103m}. In agreement with the evidence from absorption measurements,[1] two beta-spectra were found. The low energy, relatively intense spectrum has an energy of 205 kev while the less intense, high energy spectrum has an energy of 670 kev. The intensity relations are such that at least part of the low energy beta-rays lead to the 52-minute isomeric state in Rh^{103}. A conversion peak was found at 37 kev which has been interpreted as the L conversion of a 40-kev gamma-ray in Rh^{103m}. This interpretation is dictated by the absence of an electron line at about 57 kev (where one would be found if the 37-kev line were a K conversion line). The expected intensity of a line at 57 kev was estimated using the $l=4$ assignment for Rh^{103m}.[2] The interpretation is consistent with the data of Gunlock and Pool[3] who resolved the L and M conversion lines. A discussion of the gamma-rays and a decay scheme will be given.

* Supported in part by the joint program of the ONR and the AEC.
† AEC Predoctoral Fellow.
[1] C. E. Mandeville and E. Shapiro, Phys. Rev. **77**, 439 (1950).
[2] P. Axel and S. M. Dancoff, Phys. Rev. **76**, 892 (1949).
[3] H. F. Gunlock and M. L. Pool, Phys. Rev. **74**, 1264 (1948).

V9. The 282-Day Radioactivity in Silver 110.* W. C. RUTLEDGE, A. E. STODDARD, C. E. BRANYAN, J. LEBLANC, AND J. M. CORK, *University of Michigan.*—In our earlier study of the long-lived radioactivity in silver associated with mass 110, obtained by the activation of silver in the pile, a half-life of 282 days was observed. Many electron lines were present due to internal conversion. The K–L–M differences for certain of these lines were characteristic of silver indicating the emission of a gamma-ray preceding beta-emission. Four gamma-rays were reported. A subsequent investigation by Siegbahn showed these four together with six additional gamma-rays. With longer photographic exposures and more efficient emulsions, using both internal conversion and photo-electrons from lead and uranium, an enormous number of previously unobserved electron lines are now visible. In total, there appear to be about 26 gamma-rays, only one of which (115.9 kev) has K–L–M differences characteristic of silver while the

others, where observable, have differences characteristic of cadmium as expected following beta-emission from silver. With so many gamma-energies, it is possible to propose several nuclear level schemes, no one of which is unique.

* This project was assisted by the joint program of the ONR and AEC.

V10. Radioactivity in Enriched Cadmium Isotopes.* J. M. CORK, W. C. RUTLEDGE, A. E. STODDARD, C. E. BRANYAN, AND J. LEBLANC, *University of Michigan.*—Isotopes of cadmium enriched in masses 108 and 114, produced by Carbide and Carbon Chemicals Division, Oak Ridge National Laboratory, were made available by the AEC and irradiated in the pile. Spectrometric and absorption studies on the different samples revealed many gamma-rays not previously observed, and allowed a positive isotopic assignment of the long-lived radioactivities. Cadmium 109, whose half-life has been reported as from 156 to 300 days, decays by K-capture to silver 109 with the subsequent emission of a highly converted gamma-ray of energy 87.5 kev, and probably another whose energy is 86.3 kev.

Cadmium 115 is isomeric with half-lives 2.4 days and a longer period reported as being from 40 to 44 days. The 2.4-day activity emits a beta-ray followed by several converted gamma-rays in indium 115, whose energies are 335.5, 343.7, 348.9, 369.3, 451.9, 559.1, and 713.1 kev. The longer-lived Cd 115 activity has a beta-upper limit of 1.53 Mev and probably a converted gamma-ray of energy 525.3 kev.

* This project was assisted by the joint program of the ONR and AEC.

SATURDAY MORNING AT 10:00

Department of Commerce Auditorium

(E. C. POLLARD presiding)

Reactions of Transmutation, I

W1. Investigation of the T(T,2n)He^4 Reaction.* *Los Alamos Scientific Laboratory.*—The T(T,2n)He^4 reaction is being investigated using the Los Alamos 2.5-Mev electrostatic generator to accelerate tritons. The total neutron yield as a function of laboratory angle has been measured between 0° and 100° for tritons having energies of 0.6 and 0.8 Mev. The cross section varies between 0.011 and 0.0075 barn in this range. The yield at 0° and 90° as a function of triton energies from 400 kv to 1.4 Mev has been measured. It is reasonable to imagine the T−T reaction as taking place by any of the following reaction mechanisms:

$$\begin{aligned} \mathrm{T+T} &= \mathrm{He^4}+2n_0+Q \\ &= \mathrm{He^5}+n_0+Q_2 = \mathrm{He^4}+2n_0+Q \\ &= \mathrm{He^4}+n_0{}^2+Q_3 = \mathrm{He^4}+2n_0+Q_4. \end{aligned}$$

In order to differentiate between the various possible reactions an analysis of the energies of the α-particles as a function of angle was made. The maximum α-energy possible at any angle is that obtained when the two neutrons come off in the same direction; either as separate particles or as a dineutron having zero binding energy. If the dineutron is produced an α-group is to be expected which should vary with angle in a predictable manner. Preliminary evidence for such a group has been observed.

* This paper is based on work performed under Government Contract at the Los Alamos Scientific Laboratory of the University of California.

W2. The T+T Reaction: II. Energy Distribution of the Neutrons. J. H. SANDERS, K. W. ALLEN, E. ALMQVIST, J. T. DEWAN, AND T. P. PEPPER, *Chalk River Laboratory.*—The spectrum of the neutrons from the T+T reaction has been measured by observation of the recoil protons in Ilford C2 emulsions. A 200-μA beam of 220-kev ions containing about 10 percent tritons was focused into a 5-mm diameter spot on a brass target (see previous abstract). Plates were placed at 0° and 90° to the beam direction and measurements on the plates were made under well-defined geometrical conditions to ensure a small error in the derived neutron energy. The neutron spectrum shows a continuous distribution of energies from below 1 Mev to an upper limit of 9.5 Mev. This corresponds to the production of neutrons from the reaction T(t,2n)He^4. There is evidence for a small peak on the spectrum between 8.5 and 9 Mev, which can be attributed to the formation of He^5 in its unstable "ground" state. Fewer than 10 percent of the neutrons are formed in this way. A few 14-Mev neutrons were detected, due presumably to the T(d,n)He^4 reaction. The maximum intensity of the neutrons from T(t,2n)He^4 lies at about 4 Mev and the shape of the continuous spectrum is in general agreement with the expected distribution from the three-body disintegration.

W3. The T+T Reaction: I. Energy Distribution of the α-Particles. K. W. ALLEN, E. ALMQVIST, J. T. DEWAN, T. P. PEPPER, AND J. H. SANDERS, *Chalk River Laboratory.*—A 90° magnetic analyzer[1] has been used to obtain the momentum distribution of α-particles from the reaction T+T = He^4+2n^1+11.4 Mev at a triton bombarding energy of 220 kev. Sufficient intensity was obtained by bombarding a brass plate with a 200-μA beam containing 10 percent tritons, some of which were absorbed on the brass and acted as a target. The resolution used was about three percent in momentum. The α-particles were detected by recording scintillations from a ZnS or KI screen with an RCA 5819 photo-multiplier. A continuous distribution of α-particles, extending up to 3.8 Mev, was obtained. The distribution showed a broad maximum at about 2.7 Mev. Superposed on this distribution was a 3.5-Mev group of α-particles from the D+T reaction. The presence of this group can be explained by the natural deuterium content of the gas used and the high yield of the D+T reaction at low energies.[2] The energy distribution of the α-particles was also studied with a thin window proportional counter. The results were in agreement with those obtained by magnetic analysis.

[1] Burcham and Freeman, Phil. Mag. **40**, 807 (1949).
[2] Allan and Poole, Nature **164**, 102 (1949).

W4. Yield of He^3 and Scattered Protons from Li^6+P.* S. BASHKIN, F. AJZENBERG, C. P. BROWNE, GERSON GOLDHABER, M. J. W. LAUBENSTEIN, AND H. T. RICHARDS, *University of Wisconsin.*—Ordinary lithium targets (10–50 kev thick) evaporated on 1/20 and 1/50 mil thick nickel foils have been bombarded by monochromatic protons with energies from 0.440 to 3.5 Mev. Particles at 164° to the beam were observed with a 90° magnetic analyzer having two percent momentum resolution. This resolution plus pulse-height discrimination in a thin window proportional counter permitted identification of protons scattered from Li^6, Li^7, C^{12}, O^{16}, and

the nickel foil, and He^3 particles from $Li^6(p,\alpha)He^3$. Elastically scattered protons from Li^6 showed an asymmetric resonance (450-kev width at half-maximum) at $E_p=1.8$ Mev. The He^3 particles showed a similarly broad resonance, but with the maximum at $E_p=1.9$ Mev. These resonances indicate a level in Be^7 at 7.1 Mev, probably corresponding to the 7.38-Mev state of the mirror nucleus, Li^7. The He^3 yield was observed down to $E_p=0.440$ Mev, but resolution problems limited the low energy proton observations to $E_p>850$ kev. There is some indication from the low energy He^3 and scattered proton data of another resonance at low proton energy.

* Work supported partly by the AEC, partly by the Wisconsin Alumni Research Foundation.

W5. Yield of Scattered Protons from Li^7.* H. T. RICHARDS, S. BASHKIN, D. S. CRAIG, D. DONAHUE, V. R. JOHNSON, AND D. MARTIN, *University of Wisconsin.*—The method and equipment described in the foregoing abstract was used to examine the yield at 164° of elastically and inelastically scattered protons from Li^7 for proton energies up to about 3.5 Mev. The elastically scattered protons could only be resolved satisfactorily for $E_p>850$ kev. The well-known resonance at $E_p=1.05$ Mev was observed, but no other structure was detected below $E_p=1.87$ Mev. A weak maximum (30 kev wide at half-maximum) occurred at this energy. This level, which is below the threshold for neutron emission, may be that suggested by Breit and Bloch[1] to explain the observed neutron yield from $Li^7(p,n)Be^7$. An intense and broad maximum is observed at $E_p\approx2.06$ Mev. After passing through a minimum at $E_p\approx2.25$ Mev, there is a rise until $E_p=2.5$ Mev, above which the yield is almost constant. The inelastically scattered protons could only get through the counter window for $E_p>1.5$ Mev. No structure was observed in the inelastic scattering yield up to $E_p=3.5$ Mev.

* This work supported partly by the AEC, partly by Wisconsin Alumni Research Foundation.
[1] G. Breit and I. Bloch, Phys. Rev. 74, 397 (1948).

W6. Neutrons from the Disintegration of Li^7 by Deuterons.* W. D. WHITEHEAD, *Bartol Research Foundation of The Franklin Institute.*—A thin target (~100 kev) of Li_2SO_4 (99.8 percent Li^7)† was bombarded with 1.1-Mev deuterons supplied by the Bartol Van de Graaff generator, and the reaction neutrons were recorded in 100μ Ilford C2 emulsions making an angle of 0 degrees with the beam and mounted 10 cm from the target. The range distribution of the recoil protons of less than 5.6 Mev gives evidence of two groups of neutrons with Q-values of 0.3 and 3.9 Mev superposed on the continuous group of neutrons from $Li^7(d,\alpha)He^5$, $He^5\rightarrow\alpha+n$. These neutron groups indicate levels in Be^8 at 14.7 and 11.1 Mev.

* Assisted by the joint program of the ONR and AEC.
† Obtained from Y-12, Carbide and Carbon Chemicals Corporation, Oak Ridge, Tennessee.

W7. The Excited Nuclear State of Be^7.* GEO. D. FREIER, L. ROSEN, AND T. F. STRATTON, *University of Minnesota and Los Alamos Scientific Laboratory.*—Ilford nuclear emulsion plates were exposed to neutrons from the $Li^7(p,n)Be^7$ reaction, produced by bombarding a 35-kev thick metallic Li target with 3.49-Mev protons from the Minnesota electrostatic generator. The plates were at 0° with respect to the proton beam. In the reading of the emulsions only those knockon proton tracks were accepted which made an angle of 10° or less with the direction of the incident neutron beam. The actual x, y, z coordinates of the tracks were measured, and the angle and track length were used to find the energy of the incident neutron. Two groups of tracks were found. The best estimate of the peak separation at this time is 460±15 kev, with 0.10±0.03 of the tracks falling into the lower energy group. The difference in the Q-values for the reactions leading to the ground state and the excited state of Be^7 is 428±15 kev, in agreement with previous experimenters.[1-3] The data will be presented in the form of curves.

* Work supported in part by ONR.
[1] Brown, Chao, Fowler, and Lauritsen, Bull. Am. Phys. Soc. 24, No. 8, 11 (1949).
[2] Lauritsen and Thomas, Bull. Am. Phys. Soc. 24, No. 8, 11 (1949).
[3] Johnson, Laubenstein, and Richards, Phys. Rev. 77, 413 (1950).

W8. Angular Yield of Deuterons and Alphas from the Proton Bombardment of Be^9. J. A. NEUENDORFFER, D. R. INGLIS,* AND S. S. HANNA, *The Johns Hopkins University.*†—A Be foil was mounted in a semicircular chamber with seven photographic plates arranged inside at positions 25° apart and 22 cm from the target. The product alphas and deuterons were separated from the scattered protons by passing through gaps in a semicircular yoke of an electromagnet. Thus, the method combines the advantages of magnetic deflection and simultaneous photographic recording. The deuteron distribution exhibits principally a $1+a\cos\theta$ dependence, especially between 600 and 1000 kev, the coefficient a increasing with energy. The alpha-distribution appears to be somewhat similar, which perhaps reflects the fact that the two final nuclei are 0^+ and 1^+. The strong interference term requires states of the compound nucleus of opposite parity. Identifying these with states previously observed[1] it seems reasonable to ascribe the strong resonance at 330 kev to entering s-waves, and the higher resonance to p-waves. Stopping powers of Ilford C2 emulsions for protons, deuterons, and Li^6 nuclei of energies up to 1 Mev, and for alphas up to 2 Mev, and equilibrium ratios of He^+ to He^{++} and of Li^+ to Li^{++} ions as they leave the target were also measured.

* Now at the Argonne National Laboratory.
† Assisted in part by the AEC.
[1] Thomas, Rubin, Fowler, and Lauritsen, Phys. Rev. 75, 1612 (1949).

W9. Neutron Spectrum from Proton Bombardment of Beryllium.* V. R. JOHNSON, M. J. W. LAUBENSTEIN, AND F. AJZENBERG, *University of Wisconsin.*—A thin foil of Be, 1.7 microns thick, was mounted on a tantalum backing and bombarded with 3.815-Mev protons produced by the Wisconsin electrostatic generator. Eastman NTA nuclear emulsion plates 100 microns thick were mounted four inches away from the target at angles of 0°, 45°, and 90° with respect to the incident beam. A total of 400 tracks have been measured on the 0° plate. A plot of this data, after being corrected for variation of the $n-p$ scattering cross section and for geometry, shows clearly the group from the ground state transition of the reaction $Be^9(p,n)B^9$ with a half-width of the curve of about 0.12 Mev. There is also observed a continuous distribution of neutrons extending from the ground state group down to low energies. The average ordinate of this continuous distribution is less than one-tenth the height of the ground state peak. Comparison with the earlier $Li^7(p,n)Be^7$ spectrum measurements under similar geometry indicates that this continuous distribution does not result from scattered neutrons. These low energy neutrons can be attributed to the $Be^9(p,pn)Be^8$ reaction. Measurements on the other plates are in progress.

* Work supported partly by the AEC, partly by the Wisconsin Alumn Research Foundation.

W10. Pair Spectrum of Gamma-Rays from Polonium-Beryllium.* JAMES TERRELL,† *Rice Institute.*—A pair spectrometer using 180° focusing has been used in the investigation of the polonium-beryllium gamma-ray spectrum from a two-curie source (on loan from Los Alamos). A single peak has been found, corresponding to a 4.3-Mev gamma-ray from the reaction $Be^9(\alpha n,\nu)C^{12}$. No indications of other gamma-rays have been found in the range 2 to 10 Mev. Since the sensitivity of the spectrometer increases rapidly with energy, and background counting rates (with no radiator) are low in the high energy region, there is good evidence that no important gamma-radiation exists above 4.3 Mev. Below the main peak

the sensitivity is lower and the background more important, so that lower energy gamma-rays have not been entirely ruled out. Previous investigators[1,2] have reported gamma-radiation of 2.7, 4.2, and 6.7 Mev. The 2.62-Mev gamma-ray from ThC″ has been used to check the operation of the spectrometer. Other high energy gamma-rays are to be investigated.

* Assisted by the joint program of the ONR and AEC.
† AEC predoctoral fellow.
[1] W. Bothe, Zeits. f. Physik 100, 273 (1936).
[2] B. S. Dzelepov, Comptes Rendus U.R.S.S. 23, No. 1, 24 (1939).

W11. Excitation Levels in B^{10}. T. W. BONNER, J. W. BUTLER, AND J. R. RISSER, *Rice Institute.**—Excited states in B^{10}, resulting from the reaction $Be^9(d,n)^*B^{10}$, have been studied by the method of neutron thresholds. The prominent level in B^{10} at 5.0 Mev was investigated with monoenergetic deuterons near the neutron threshold of 920 kev. The observed shape of the threshold curve shows that the width of this excited level is less than 2 kev although it usually breaks up into Li^6+He^4 +0.8 Mev, instead of returning to ground state with γ-emission.[1] Four additional thresholds were observed with deuterons of energies from 920 to 1070 kev. In contrast to these results no additional levels were found with deuteron energies of from 750 to 920 kev.

* Supported by the joint program of the ONR and AEC.
[1] Chao, Lauritsen, and Rasmussen, Phys. Rev. 76, 582 (1949).

W12. Excitation Curves for $B^{10}(d,p)B^{11}$. G. C. PHILLIPS, *Rice Institute.**—The excitation curves for the longest range proton group of the reaction $B^{10}(d,p)B^{11}$ have been determined in the bombarding energy range of 0.7 to 2.0 Mev at the three laboratory angles of 0°, 90°, and 135° to the direction of the bombarding deuterons. The deuterons, accelerated by the Rice Pressure Van de Graaff, bombarded thin targets of B_2O_3 evaporated in a vacuum onto thin silver foils ($\sim$15 mg/cm^2). The B_2O_3, enriched to 96 percent in B^{10}, was obtained from Oak Ridge. The protons were counted by a proportional counter-linear amplifier combination that was biased to count all protons passing through the counter. Aluminum foils placed between the target and the counter stopped all but the energetic group of protons. The excitation curves so obtained indicate at least two broad resonances in this energy region corresponding to excitation levels of C^{12} in excess of 25.5 Mev. The angular distributions of these protons are not spherically symmetrical.

* Assisted by the ONR and AEC.

W13. Energy Levels in B^{11} from the $B^{10}(d,p)B^{11*}$ Reaction.* W. W. BUECHNER AND D. M. VAN PATTER, *M.I.T.*—The proton groups from thin targets of B^{10} (96 percent enriched) were observed at 90° with a 180° focusing magnetic spectrometer, using 1.5-Mev deuterons. The proton groups assigned to the $B^{10}(d,p)B^{11}$ reaction gave corresponding Q-values of 9.279; 7.128; 4.804; 4.225; 2.500; 2.450; 1.95; 0.68; and 0.32 Mev with a probable error of less than 20 kv. The last five proton groups were assigned by comparison of the relative yield from enriched B^{10} with that from natural boron targets. This was necessary to eliminate the proton groups from surface contaminants of carbon, oxygen, and nitrogen, which in many cases were more intense than the proton groups from B^{10}. A doublet is indicated in B^{11} at 6.8 Mev with a separation of 50 ± 5 kv. However, the group with $Q=2.450$ was about one-fifth as intense as the group with $Q=2.500$ Mev, and its assignment is less certain. The possibility that other doublets may exist is being investigated. These results are in general agreement with those recently reported by Bateson[1] considering the increased resolution in these experiments.

* This work was assisted by the joint program of the ONR and AEC.
[1] Bateson, Bull. Am. Phys. Soc. 25, No. 1, 32 (1950).

W14. Ground State of B^{12} from the $B^{11}(d,p)B^{12}$ Reaction.* E. N. STRAIT, D. M. VAN PATTER, AND W. W. BUECHNER, *M.I.T.*—The proton groups from thin targets of natural boron bombarded by 1.5-Mev deuterons have been analyzed at 90° with a magnetic spectrometer. Two groups were found which disappeared when the natural boron target was replaced by an enriched B^{10} target (4 percent B^{11}). Assuming these arise from the $B^{11}(d,p)B^{12}$ reaction, the Q-values are 1.136 ± 0.004 and 0.189 ± 0.004 Mev, corresponding to the ground state of B^{12} and an excited state at 0.947 ± 0.006 Mev. The relative intensities of the proton groups are about 3:1. The assignment of the high energy group, which was just resolved from the more intense $O^{16}(d,p)O^{17*}$ group, was confirmed by observing that the Q-value remained constant to 1 kv, when the bombarding energy was changed from 1.5 to 0.7 Mev. This result does not agree with that of Hudspeth and Swann,[1] who assign a group with $Q=1.25$ Mev and 1/60 the intensity of the lower energy group to the ground-state reaction. Comparison of $Q_0=1.136$ Mev with Hornyak and Lauritsen's[2] measurement for the end point of the beta-spectrum from B^{12} indicates that the beta-decay of B^{12} occurs primarily between the ground states of B^{12} and C^{12}.

* This work was assisted by the joint program of the ONR and AEC.
[1] Hudspeth and Swann, Phys. Rev. 76, 1150 (1949).
[2] Hornyak and Lauritsen, Phys. Rev. 77, 160 (1950).

SATURDAY AFTERNOON AT 2:15

Department of Commerce Auditorium

(C. C. LAURITSEN presiding)

Reactions of Transmutation, II

X1. Nuclear Energy Levels in Nitrogen (14) and Aluminum (27).* C. P. SWANN AND C. E. MANDEVILLE, *Bartol Research* FOUNDATION.—Ilford C_2 emulsions, making an angle of zero degrees with the bombarding beam, were irradiated by neutrons from the reaction $C^{13}(D,n)N^{14}$. The incident deuterons were supplied with an energy of 1.43 Mev by the Bartol Van de Graaff statitron. The target of C^{13} (isotopic concentration 50 percent) had a thickness of 100 kev. Neutron groups were observed corresponding to Q-values of 0.27, 1.30, 1.68, and 5.24 Mev giving energy levels in N^{14} at 4.97, 3.94, and 3.56 Mev. The group of lowest Q has been previously reported by the Rice group.[1] The intermediate Q-values offer a possible explanation for recently observed gamma-rays.[2] When a thick target of isotopic Mg^{26} was irradiated by deuterons, eight groups of neutrons were observed corresponding to energy levels in Al^{27} at 0.88, 1.92, 2.75, 3.65, 4.33, 5.32, and 5.81 Mev.

The Q-value for the ground state is 5.68 Mev. The level structure closely resembles that obtained by other methods; e.g., proton scattering by aluminum.

* Assisted by the joint program of the ONR and the AEC.
[1] Bennett, Bonner, Hudspeth, Richards, and Watt, Phys. Rev. **59**, 781 (1941).
[2] R. G. Thomas and T. Lauritsen, Bull. Am. Phys. Soc. **24**, No. 8, 11 (1949).

X2. Formation of N^{17} by Gamma-Ray Bombardment of O^{18}.* R. SHER, J. HALPERN, AND W. E. STEPHENS, *University of Pennsylvania.*—Following the suggestion of Charpie *et al.*,[1] the reaction $O^{18}(\gamma,p)N^{17}$ has been investigated by irradiating 250 cc of normal water with bremsstrahlung from the University of Pennsylvania 25 Mev betatron. The sample was irradiated close to the betatron target for 15 sec. at a beam intensity of about 100 roentgens per minute (measured at three feet from the target). The betatron was then turned off and the pulses from an enriched $B^{10}F_3$ counter placed behind the sample were recorded. A delayed neutron activity of 4.25 ± 0.5 sec. was found, indicating the presence of N^{17} (half-life 4.14 ± 0.04 sec.).[2] The threshold energy was found to be 18.2 ± 0.3 Mev, whereas the calculated Q-value is -15.9 Mev.[1] The difference is ascribed to effects of the Coulomb barrier. Various tests confirmed the supposition that the reaction $O^{17}(n,p)N^{17}$ was not being observed here.

* Supported by the joint program of the AEC and ONR.
[1] Charpie, Sun, Jennings, and Nechaj, Phy. Rev. **76**, 1255 (1949).
[2] Knable, Lawrence, Leith, Moyer, and Thornton, Phy. Rev. **74**, 1217 (1948).

X3. Concentration of Argon 36 and Study of the $A^{36}(d,p)A^{37}$ Reactions.* A. ZUCKER AND W. W. WATSON, *Yale University.*—By means of a multi-stage thermal diffusion apparatus we have brought the concentration of argon 36 from its natural 0.35 percent to 95.9 percent. The apparatus consisted of six 2-meter concentric-cylinder columns, the first of which was used as a scrubber. The last concentric cylinder column was coupled convectively to a metal hot-wire column which had a 200 cc light end-volume. These 7 columns produced 200 cc of 20 percent A^{36} every 70 hours at a pressure of 1.1 atmospheres. This gas was transferred batchwise to a glass hot-wire column operating at 0.9 atmospheres and 1500°K. The light end-volume of the glass column contained 40 cc S.T.P. of 95.9 percent A^{36} at the end of each run. With this well-separated A^{36} we investigated the $A^{36}(d,p)A^{37}$ reactions previously studied by Davison *et al.*[1] The gas was bombarded with 3.9 Mev deuterons, and protons were counted at 90° with a proportional counter. We find a ground state Q at 6.49 Mev, and 7 excited states of the A^{37} nucleus with Q's of 5.05, 3.93, 2.95, 2.09, 1.86, 1.42, and 0.64 Mev.

* Assisted by the AEC.
[1] Davison, Buchanan, and Pollard, Phys. Rev. **76**, 890 (1949).

X4. Protons from the Deuteron Bombardment of Co^{59}. W. O. BATESON AND ERNEST POLLARD, *Yale University.**—In the lighter elements deuteron bombardment yields discrete groups of protons. This has not been extensively tested for more complex elements. A target of cobalt electrolyzed onto gold has been bombarded by deuterons and proton group structure looked for. It is clear that the group structure is complex and although several Q-values can be determined there are unquestionably many unresolved groups. The Q-values obtained are 5.19, 4.80, 4.38, 3.91, 3.46, 3.02 and 2.39 Mev. The yield of protons increases rapidly as the excitation increases. If the relation $D=C\exp(-BE^{\frac{1}{2}})$ is applied to the yield of protons on the assumption that the yield is proportional to the density of unresolved levels, a value for B of 1.5 ± 0.5 Mev results.

* Assisted by the joint program of the ONR and AEC.

X5. Energy Levels in Lead, Bismuth and Thallium.* J. A. HARVEY, *M.I.T.*—Using 14 Mev deuterons from the cyclotron differential proton and triton spectra have been obtained from enriched** lead targets and bismuth and thallium targets. The proton spectra from all targets look very similar. Tentative Q values of ground states and excited levels (in Mev) correct to 0.1 Mev. are:

$Pb^{206}(d,p)Pb^{207}$	4.5, 3.6 (double),	1.8,	0.9,	0.0,	−0.8
$Pb^{207}(d,p)Pb^{208}$	5.1$_5$	1.7		0.0	−0.8
$Pb^{208}(d,p)Pb^{209}$		1.7	0.9(?)	0.1	−0.3 −0.8
$Bi^{209}(d,p)Bi^{210}$		1.95		0.3	−0.3 −0.8

Note the repetition of several of the Q values in all of the targets. The triton spectra from the 3 lead isotopes and bismuth target also look very similar to each other except for ground peaks. The energy levels of Pb^{207} obtained from triton spectra from Pb^{208} are in fair agreement with those obtained from the proton spectra of Pb^{206}.

* Assisted by joint program ONR and AEC.
** Supplied by Carbide and Carbon Chemical Division, Oak Ridge National Laboratory, Oak Ridge, Tennessee.

X6. Energy Spectrum and Differential Cross Sections of (d,p) Reactions Using 14 Mev Deuterons.* HARRY GOVE AND KEITH BOYER, *M.I.T.*—The energy spectrum of protons emitted when thin targets are bombarded with 14 Mev deuterons was measured as a function of angle for several elements. From this an energy spectrum integrated over angle was obtained which will be compared with existing theories. The differential cross sections of (d,p) reactions has been measured as a function of angle and proton energy by measuring the total number of particles of a particular energy at a convenient angle. From the target thickness and the number of incident deuterons, absolute cross sections were calculated. The deuteron beam intensity was checked in three independent ways, by activity measurement, Faraday cup, and thermal heating. The total cross section for the (d,p) reaction was obtained by cutting the spectrum off at $Q=-2.2$ Mev and integrating over energy and angle. This was compared with (d,p) cross sections measured by activation techniques where they are known.

* Assisted by the joint program of the ONR and the AEC.

X7. Photo-Alpha-Reactions in Light Nuclei. T. A. WELTON, *University of Pennsylvania.*—If C^{12} is bombarded with x-rays there exists an energy region from 7.3 Mev to 16.0 Mev in which the only reaction possible is the disintegration of the nucleus into three α-particles. Similarly, with O^{16}, between 7.2 Mev and 12.1 Mev only the emission of a single α-particle is possible. If the O^{16} nucleus can be regarded approximately as a resonating structure of four α's, then the cross section for the reaction can be estimated simply, somewhat as is done for the deuteron photo-disintegration. The cross section is a product of the usual statistical factor, a barrier penetration factor, and the square of an electric quadrupole matrix element. The angular distribution is unambiguously given by $\sin^2\theta\cos^2\theta$, and the energy variation near threshold appears dependable also. Unfortunately, preliminary estimates indicate an implausibly high value, of the order of 10^{-24} cm^2, at 12 Mev. If the α-particle picture is not valid, then the quadrupole matrix element must be very greatly reduced to describe the difficulty of "assembling" the α-particle, so that careful experiments may give clear evidence on the structure of the nuclear wave function.

X8. Nuclear Reactions Induced by High Energy X-Rays. KARL STRAUCH, *University of California, Berkeley.*—Using the x-ray beam from the 335 Mev Berkeley synchrotron the average photon energy responsible for several nuclear reactions has been measured by the transition curve method previously described.[1,2] Results to date are: $C^{12}(\gamma,n)C^{11}$ 30 Mev;

$Cu^{63}(\gamma,n)Cu^{62}$ 20 Mev; $Zn^{64}(\gamma,n)Zn^{63}$ 21 Mev; $Ag^{107}(\gamma,n)Ag^{106}$ 18 Mev; $Zn^{64}(\gamma,2n)Zn^{62}$ 32 Mev; $Zn^{64}(\gamma,pn)Cu^{62}$ 34 Mev; $Ta^{181}(\gamma,2p\cdots)$ 70 minute rare earth 70 Mev. Unidentified short half lives are produced in bismuth and lead by 90 Mev photons. The relative yield of several reactions has been determined; taking the $C^{12}(\gamma,n)C^{11}$ yield as 1.0 we obtain: $Zn^{64}(\gamma,n)Zn^{63}$ 11; $Zn^{68}(\gamma,p)Cu^{67}$ 1.2; $Zn^{64}(\gamma,2n)Zn^{62}$ 0.7; $Zn^{64}(\gamma,pn)Cu^{62}$ 3.3; $Zn^{66}(\gamma,3n)Zn^{63}<0.4$; $Zn^{64}(\gamma,p2n)Cu^{61}$ 0.55. Further measurements will be presented and these results will be discussed with respect to the several models for x-ray induced reactions that have been proposed. This work was sponsored by the Atomic Energy Commission.

[1] K. Strauch, Bull. Am. Phys. Soc. 24 (No. 8), 8 (1949).
[2] L. Eyges, Bull. Am. Phys. Soc. 24 (No. 8), 8 (1949).

X9. Photo-Disintegration of Ag and Al.* B. C. Diven and G. M. Almy, *University of Illinois.*—Energy and angular distributions of photo-protons from Ag and Al have been studied. A metal foil was irradiated with a pencil of x-rays from a 22-Mev betatron. Protons from the foil were caught in two nuclear photographic plates at near-grazing incidence and at angles 20° to 160° from the beam. The proton spectrum from the Ag isotopes (proton thresholds near 6 Mev, barrier at 9.8 Mev), excited with x-rays of 20.8 Mev maximum energy, extends to 13 Mev with a peak at 6 or 7 Mev. The higher energy protons are emitted preferentially near 90°, as observed for Rh.[1] Comparison with theory shows that the observed spectrum is shifted to higher energies than predicted from a statistical level density[2] but lower than if all protons had the maximum available energy or than predicted from Schiff's "regular level" density.[3] The proton spectrum from Al (proton threshold at 9.2 Mev, barrier at 4.2 Mev) excited with 20.8 Mev x-rays, extends to 11 Mev with peak at 4 Mev and shows no angular asymmetry.

* Assisted by joint program of the ONR and AEC.
[1] Curtis, Hornbostel, Lee, and Salant, Phys. Rev. 77, 290 (1950).
[2] V. F. Weisskopf and D. H. Ewing, Phys. Rev. 57, 472, 935 (1940).
[3] L. I. Schiff, Phys. Rev. 73, 1311 (1948).

X10. Neutron Yields from Photo-Disintegration by 17.6 Mev Gamma-Rays. R. L. Walker,* B. D. McDaniel, and M. B. Stearns, *Cornell University.***—Measurements have been made of the relative yields of neutrons from 32 different elements when irradiated by gamma-rays from the $Li^7(p,\gamma)Be^8$ reaction. The absolute yield has been measured for copper. The neutrons emitted from each sample were detected by four BF_3 proportional counters embedded with the sample in a large block of paraffin. With the exception of Ca, Ni and U, the elements examined yield values which fall within 15 percent of a smooth curve. This curve increases rapidly with increasing Z up to Z equal 74, then begins to decrease slightly. Representative yields relative to Cu are: Al 0.096, Cl 0.25, Ca 0.027, Ti 0.54, Co 0.83 Ni 0.41, Mo 2.6, Ce 4.2, W 5.9, Hg 4.7, Pb 4.5, Bi 4.5, and U 9.0. A calibrated RaBe source was used to determine the counter efficiency. Absolute gamma-ray intensity was determined in two ways: (1) by using a gamma-ray pair spectrometer, (2) by using a thin walled Geiger counter located in a broad region of magnetic field. The counter measures the number of Compton and pair processes occurring in thin radiators located immediately ahead of the counter. The tentative cross section for Cu is 0.068 ± 0.012 barn. Indication of the relative energy spectra of neutrons was obtained.

* Now at California Institute of Technology.
** Assisted by ONR.

X11. Photo Neutron Thresholds for Pb^{206}, Pb^{207}, Pb^{208}.* H. Palevsky and A. O. Hanson, *University of Illinois.*—Separated lead isotopes obtained from Oak Ridge were irradiated by electrons from the 22 Mev betatron and the number of neutrons emitted was measured as a function of the electron energy. The experimental apparatus utilized the electron beam, focused on copper sample holders at about eleven feet from the betatron. This reduced the background neutrons from the betatron to a negligible amount. Gated BF_3 proportional counters were used to detect the neutrons after each electron burst. Two samples were rotated synchronously in front of the beam, so that each was irradiated on alternate bursts. The yield *versus* energy data could, in each case, be represented as a parabola with the vertex at the respective threshold. The analysis gave the following thresholds based on the $Cu^{63}(\gamma,n)$ threshold of 10.9 Mev: Pb^{206}, 8.25 ± 0.10 Mev; Pb^{207}, 6.95 ± 0.10 Mev; Pb^{208}, 7.44 ± 0.10 Mev. The relative (γ,n) cross sections near threshold were as follows: Pb^{206}, 1.00; Pb^{207}, 0.80 ± 0.02; Pb^{208}, 0.99 ± 0.02.

* Supported in part by the joint program of ONR and AEC.

Saturday Afternoon at 2:15

National Academy

(M. L. Pool presiding)

Invited Paper

Y1. Recent Work on Nuclear Isomers. M. Goldhaber, *University of Illinois.* (40 min.)

Beta-Emitters, II

Y2. Radiations of Sn^{123} and Sn^{125}.* B. H. Ketelle, C. M. Nelson, and G. E. Boyd. *Oak Ridge National Laboratory.*—Samples of electromagnetically enriched Sn^{124} (52.0 ± 1.0 percent) and Sn^{122} (70.7 ± 1.0 percent) have been activated by prolonged irradiations in high slow neutron fluxes. Chemical separations were performed to purify the tin and to remove radioactive antimony and tellurium daughters. The beta-distributions of the 9.9 d Sn^{125} and 136 d Sn^{123} were obtained with a thin magnetic lens beta-ray spectrometer which gave end-point energies of 2.33 ± 0.01 and 1.42 ± 0.01 Mev, respectively. Both beta-ray distributions differed markedly from that for an allowed transition. The spectrum shapes were shown to correspond to that for a once forbidden transition with a spin change of two and a change in parity. The only conversion electron peaks observed in both sources were attributed to the 390-kev gamma-ray of In^{113} and to the 152-kev gamma-ray of Sn^{117} formed by neutron capture by the small amounts of Sn^{112} and Sn^{116} in the enriched preparations. The foregoing radiation characteristics and energy values were confirmed by absorption techniques using Al, Cu, and Pb.

* This document is based on work performed under contract for the Atomic Energy Project at Oak Ridge National Laboratory.

Y3. Radiations from Cerium (144)$\xrightarrow{\beta}$Praseodymium (144)$\xrightarrow{\beta}$Neodymium (144).* C. E. MANDEVILLE AND E. SHAPIRO, *Bartol Research Foundation.*—Ce^{144}, in equilibrium with its 17-minute daughter activity, Pr^{144}, was separated from fission fragments at the Oak Ridge pile. After further chemical purification, coincidence, and absorption measurements were made of the emitted radiations. The beta-rays of the 300-day Ce^{144} were found to have a maximum energy of 0.36 Mev, and the very hard beta-rays of Pr^{144} have an end point at 2.87 Mev. A source of the two radionuclides in equilibrium emits x-rays at 36 kev and gamma-rays having a mean energy of 1.67 Mev as determined by absorption curves in lead and aluminum. A coincidence absorption curve indicated that a hard gamma-ray at 2.60±0.15 Mev is emitted in the disintegration of Pr^{144}. The beta-gamma-coincidence rate of Pr^{144} was observed to decrease from an extrapolated value of 0.02×10^{-3} coincidence per beta-ray at zero absorber thickness to zero at an approximate beta-ray energy of 0.42 Mev. The magnitude of the coincidence rate and the calibration of the gamma-ray counter indicate that two percent of the beta-rays of Pr^{144} are coupled with the hard gamma-radiation. Gamma-gamma- but no beta-beta-coincidences were found in $Ce^{144}-Pr^{144}$.

* Assisted by the joint program of the ONR and the AEC.

Y4. Disintegration of Yb^{169}. E. N. JENSEN, L. J. LASLETT, R. T. NICHOLS, AND W. W. PRATT, *Iowa State College.**—The 33-day Yb^{169} was produced by neutron bombardment of ytterbium oxide[1] in the Clinton pile. The radiations were examined in a magnetic lens spectrometer more than a month after the sample was irradiated in the pile. The internal conversion spectrum and the photo-electron spectrum with a Pb radiator were determined. The low energy end of the photo-electron spectrum was also determined, with Ag and Sn radiators. The data indicate that Yb^{169} decays by K-capture to Tm^{169}. Ten gamma-rays were found having energies of 63.7±0.3, 94.5±0.9, 110.4±0.6, 120.4±1.2, 132.6±1.3, 142.6±1.4, 160.0±1.6, 177.9±0.9, 198.3±2, and 308.0±1.5 kev. A tentative decay scheme will be discussed.

* This work was performed at the Ames Laboratory of the AEC.
[1] The ytterbium oxide was kindly furnished by Dr. F. H. Spedding, P. E. Porter, and J. M. Wright of this laboratory.

Y5. The Doubtful Decay of Au^{198}.* PHILIP S. JASTRAM, W. KONNEKER, AND MARSHALL R. CLELAND, *Washington University.*—Conflicting reports on the existence and half-life of a short-lived metastable state in the disintegration of Au^{198} suggested a repetition of the lifetime measurement in the hope of clearing up some of the fog. Samples of this isotope prepared from Au^{197}, either by slow neutron bombardment in the Oak Ridge pile or by deuteron-bombardment in the Washington University cyclotron, were examined by means of a delayed-coincidence technique using scintillation counters. All yielded a metastable state having a half-life of 0.04±0.01 microsecond. The parent of this activity was found to have a half-life of 4 hours rather than 2.7 days, and consequently after one or two days subsequent to activation of the source, the short-lived state had vanished in the background produced by the well-known beta-spectrum and gamma-radiation decaying at the 2.7-day rate. This effect may account for the failure of some observers to find the short-lived transition. Deuterons and fast neutrons on Au^{197} yield Hg^{197} as well as Au^{198}; however, investigation of proton-bombarded Au^{197}, which produces only Hg^{197}, yielded no short-lived metastable state. The decay scheme of Au^{198} will be discussed in the light of these results and of subsequent work.

* Assisted by the joint program of the ONR and AEC.

Y6. $\beta-\pi$-Angular Correlation Measurements.* ROBERT STUMP† AND SHERMAN FRANKEL, *University of Illinois.*—$\beta-\gamma$-angular correlation measurements on Au^{198} and Rb^{86} have been repeated and measurements on Cb^{95} and Cs^{134} carried out. The previously reported isotropy in Au^{198} [1,2] and Cs^{134} [2] is verified. (To accentuate any correlation effect in Cs^{134} we have also made measurements with the β-scintillation counter biased to accept only the upper 7 percent of the β-spectrum.) Isotropy is also found for Cb^{95}. These isotropies are consistent with the allowed shapes of the beta-spectra. With an improved arrangement the previously reported results[1] for Rb^{86} are shown to be in error. The correlation function for Rb^{86} was found to be compatible with a distribution $W(\theta)=1+R/Q\cos^2\theta$. Using this function as the basis for evaluating the data from the other isotopes as well, we obtain: R/Q (Rb^{86})$=0.057\pm0.01$; R/Q (Cs^{134})$=0.0016\pm0.006$; R/Q (Au^{198})$=-0.005\pm0.02$; R/Q (Cb^{95})$=0.0034\pm0.02$. The data for Rb^{86} are corrected for the finite solid angle of the detectors (β-counter$=0.03$ steradian; γ-counter$=0.07$ steradian). They are in essential agreement with recent M.I.T. data.[3] Probable errors indicated are statistical.

* Work supported in part by ONR and AEC.
† AEC Predoctoral Fellow.
[1] S. Frankel, BAPS 24–7 (1949).
[2] R. L. Carwin, Phys. Rev. **76**, 1876 (1949).
[3] M. Deutsch (private communication).

Y7. Beta-Gamma-Angular Correlation in Rb^{86}, Au^{198}.* S. L. RIDGWAY,† *Princeton University.*—Beta-gamma-angular correlation was investigated with anthracene scintillation counters, dry ice cooled 1P21's, Los Alamos 501 amplifiers, and tenth-microsecond coincidence circuit. The beta- and gamma-counters, 5 cm distant from the source, subtended solid angles 0.12 and 0.08 steradian respectively. They were enclosed in a large evacuated chamber, the gamma-counter being rotated. The coincidence rate was normalized by the single rate in each channel to correct for variation in solid angle of the gamma-counter and drifts (~1 percent) in counter efficiency. For Au^{198} C(180°)/C(90°)$=1.004$, standard deviation 0.015; for Rb^{86} these quantities were 1.019; 0.014. The result for Au^{198} agrees with those of Frankel[1] and Garwin.[2] That for Rb^{86} is consistent with isotropy, and disagrees with Frankel's 9.4 percent effect. Tests were made that ruled out the possibility of scattering from one counter to another having an appreciable effect.

* Assisted by the joint program of the ONR and AEC.
† NRC Predoctoral Fellow (1946–1949).
[1] Sherman Frankel, Phys. Rev. **77**, 747 (1950), Bulletin, American Physical Society **24**, No. 7, 14 (1949).
[2] Richard L. Garwin, Phys. Rev. **76**, 1876L (1949).

Y8. A Mass Spectrometric Investigation of Branching in Neutron Inducer Activities. JOHN H. REYNOLDS, *Argonne National Laboratory.*—An investigation of branching in several neutron induced activities has been made mass spectrometrically. The method consists in subjecting gram quantities of the elements under investigation to prolonged neutron irradiation, allowing the (n,γ) activities to decay, and determining the amounts of the transmuted elements present. By use of an isotope dilution technique, these amounts can be determined with precision. A carefully weighed amount of the daughter element, with isotopic constitution *different* from that of the radiogenic material, is added as a tracer to a solution of the irradiated sample. Once isotopic mixing has occurred, results are independent of the yield of a subsequent chemical separation of the parent and daughter elements. Yields are calculated, instead, from the change in the isotopic constitution of the tracer. The elements Cu, Br, and I were irradiated, requiring mass spectrometer observations on Ni, Zn, Se, Kr, Te, and Xe. Preliminary calculations give the following values for the branching ratio (ratio of $Z\rightarrow Z-1$ transitions to $Z\rightarrow Z+1$ transitions):

Cu^{64} 1.62±0.11; Br^{80} 0.090±0.002; $Br^{82}<0.0003$
I^{128} 0.053±0.002.

The transition $I^{128}\rightarrow Te^{128}$ has not been reported heretofore and

is probably due to K-capture accompanying the 25 minute negatrons. Results of final calculations will be presented and compared with theory.

Y9. System for the Study of Short-Lived Radioactive Gases.* MICHEL TER-POGOSSIAN, FRED T. PORTER, AND C. SHARP COOK, *Washington University.*—The study of low "Z," short-lived radioactive gases is of theoretical interest. A number of serious problems arise, both in the adequate control of production of the radioactivity and also in the analysis of the radiation emitted by such a radioactive source. To provide a suitable means for such studies a system has been constructed in this laboratory whereby a gas may be circulated continuously between the cyclotron and the 14-cm radius of curvature magnetic spectrometer. At the cyclotron end of this system is a large aluminum bombardment chamber. At the spectrometer end a specially constructed source holder allows magnetic analysis of the charged particle radiations from the radioactive gas. The gas under study is activated continuously in the bombardment chamber and circulated by means of two mechanical pumps through the system. Foils may also be mounted within the bombardment chamber in order that certain gaseous souces may be produced from solid target materials. In this case the radioactive gas is carried through the system by a flushing gas, this to date being helium.

* Assisted by the joint program of the ONR and AEC.

Y10. Measurements of the Relative Transmission of Beta-Particles Through Thin Zapon Windows.* C. SHARP COOK AND CHIA-HUA CHANG, *Washington University.*—It has been known for some time that the relative number of beta-particles that are transmitted through a foil is a function of the energy of the incident beta-particles. This transmission coefficient gradually rises from a value of zero at the low energy cut-off of the window to a value approaching 100 percent at an energy several times that of the cut-off energy. The transmission curves for various thicknesses of Zapon Geiger-Mueller counter windows as a function of energy are being prepared. The method in use measures the increase in counting rate at each point in the lower energy region of a continuous beta-spectrum when the beta-particles are electrostatically accelerated at the source. The fact that the slope of the transmission curve is the same for a given energy of emitted electron for all voltages applied to the source indicates that the application of voltage to the source in the current experiment does not distort the direction of emission of the beta-particles. Curves obtained thus far for Zapon are in relatively good agreement with the curves obtained for Nylon by the St. Louis University group.[1]

* Assisted by the joint program of the ONR and AEC.
[1] Sturcken, Heller, and Weber, Bull. Am. Phys. Soc., New York meeting (1950).

SUPPLEMENTARY PROGRAMME

SP1. A Fast Multiplying Circuit.* B. CHANCE AND J. BUSSER, *University of Pennsylvania* AND F. C. WILLIAMS, *University of Manchester.*†—In the course of the development of a fast analogue computer for displaying families of curves for the solutions of differential equations representing biochemical reactions, a new version of the "quarter-square" multiplication method[1] has been developed. A single parabolic characteristic is used to square the amplitudes of alternate half-cycles of an 82KC/sec. square wave which represent the quantities $A+B$ and $A-B$. The difference of the squares gives the desired product $4AB$. The parabolic characteristic itself covers a scale of more than 25 volts and consists of a series of fifteen or more segments approximating a true parabola with an error of less than 0.4 percent. The slope of the segments is determined by the value of the input voltage which in turn determines the number of diodes contributing to the output current. This segmented non-linear element is stable and predictable. The circuit gives the product of the inputs every 12 μsec. with an error of less than one percent.

* To be given after Session N if the Chairman rules that time permits.
† Supported by the ONR.
[1] D. J. Mynall, Electronic Engineering 19 (June-September 1947).

Author Index to Papers Presented at the Washington Meeting

Ackerman, Eugene—No. R15
Adair, R. K., C. K. Bockelman, and R. E. Peterson—No. L1
Adams, G. D., D. W. Kerst, and C. S. Robinson—No. G5
Alburger, David E.—No. V1
Allen, K. W., E. Almquist, J. T. Dewan, T. P. Pepper, and J. H. Sanders—No. W3
Allred, J. C., and Louis Rosen—No. Q4
Almqvist, E., K. W. Allen, J. T. Dewan, T. P. Pepper, and J. H. Sanders—No. G10
Anslow, Gladys A.—No. U3
Arroe, O. H.—No. I3
Avery, R., C. H. Blanchard, and R. G. Sachs—No. M4
Baldwin, G. C., F. I. Boley, and H. C. Pollock—No. H3
Bardeen, J.—No. K6
Barnothy, J. M. and M. Farro—No. B13
Bartholomew, G. A., B. B. Kinsey, and W. H. Walker—No. L3
Barton, H. M., Jr.—No. H6
Bashkin, S., F. Ajzenberg, C. P. Browne, Gerson Goldhaber, M. J. W Laubenstein, and H. T. Richards—No. W4
Bass, Robert E.—No. C13
Bateson, W. O. and Ernest Pollard—No. X4
Bay, Z.—No. S14
Beard, G. B., J. L. Levy, W. A. Nierenberg, and R. W. Pidd—No. G8
Belinfante, F. J.—No. C14
Benedict, W. S. and E. K. Plyler—No. U1
Bennett, Willard H.—No. N6
Bergmann, Peter G., Robert Penfield, Ralph Schiller, and Henry Zatzkis—No. C11
Bestul, A. B. and H. V. Belcher—No. N9
Birkhoff, Robert D., Earl E. Hays, and S. A. Goudsmit—No. B11
Bleil, D. F. and R. K. Wangsness—No. P9
Bloch, Felix—No. T1
Bollinger, Lowell M.—No. F9
Bonner, T. W., J. W. Butler, and J. R. Risser—No. W11
Boyer, Keith and Harry Gove—No. Q6
Brentano, J. C. M. and D. H. Davis—No. K4
Brinkman, J. A. and C. Kikuchi—No. P5
Brolley, J. E., Jr., J. H. Coon, and J. L. Fowler—No. Q3
Brooks, Franklin C.—No. C4
Brossel, J., P. Sagalyn, and F. Bitter—No. P2
Bruner, A. and M. Langer—No. V2
Buechner, W. W. and D. M. Van Patter—No. W13
Burkhalter, J. H., R. S. Anderson, W. V. Smith, and W. Gordy—No. O1
Burns, G. Preston—No. H11
Burstein, E. and J. J. Oberly—No. K9
Case, K. M.—No. M2
Castellan, G. W. and F. Seitz—No. K5
Chance, Britton—No. S13
Chance, B., J. Busser, and F. C. Williams—No. SP1
Chang, W. Y.—No. E10
Cheng, Lin-sheng and J. D. Kurbatov—No. V6
Chew, Geoffrey F.—No. L11
Clark, G. W. and L. B. Snoddy—No. S9
Cleland, Marshall R., Wilfred R. Konneker, and A. L. Hughes—No. Q12
Coester, F. and J. M. Jauch—No. C9
Coles, D. K., W. E. Good, and R. H. Hughes—No. O5
Collins, Thomas L. —No. P3
Conn, William M.—No. I8
Cook, C. Sharp and Chia-hua Chang—No. Y10
Cook, D. B., M. W. Zemansky, and H. A. Boorse—No. H12
Coomes, E. A., R. J. Munick, and W. B. La Berge—No. S12
Cooper, C. D. and H. Sponer—No. U5
Cooper, D. I., D. H. Frisch, C. L. Storrs, Jr., and C. J. Strumski—No. G3
Cork, Bruce—No. Q1
Cork, J. M., W. C. Rutledge, A. E. Stoddard, C. E. Branyan, and J. LeBlanc —No. V10
Corrsin, L.—No. U7
Corruccini, Robert J.—No. D3
Corson, Dale R. and Margaret R. Keck—No. G12
Crown, J. C.—No. R3
Dawson, M. H. and B. H. Alexander—No. K7
DeWire, J. W., A. Ashkin, and L. A. Beach—No. H2
Dibeler, V. H., E. J. Wells, Jr., and R. M. Reese—No. N8
Diggins, J. L.—No. R4
Diven, B. C. and G. M. Almy—No. X9
Doughty, J., K. Lark-Horovitz, L. M. Roth, and B. Shapiro—No. D7
Douglas, T. B., Anne F. Ball, and D. C. Ginnings—No. D1
Drell, S. D.—No. M5
Dresden, M. and J. Delord—No. H10
Duckworth, Henry E., Karl S. Woodcock, and Richard S. Preston—No. B9
DuMond, J. W. M.—No. H1
Ekstein, H. and T.Gilbert—No. J8
Ener, Cavid—No. R13
Fairbank, Henry, Ernest A. Lynton, and C. T. Lane—No. H9
Falk, C. E.—No. L10
Feingold, A. M. and E. P. Wigner—No. M11
Feuer, Paula and Hubert M. James—No. K2
Finkelnburg, Wolfgang—No. I6
Finkelstein, R. and M. Rudermann—No. M3
Fisk, C. B., J. Hornbostel, E. O. Salant, and J. E. Smith—No. E9
Fitzpatrick, J. A. and W. J. Thaler—No. R14
Foner, S., E. M. Pugh, R. Heine-Geldern, and E. C. Mutschler—No. R11
Franzen, W., R. Peelle, and R. Sherr—No'.G13
Fred, Mark, Frank S. Tomkins, and James K. Brody—No. I2
Freier, Geo. D., L. Rosen, and T. F. Stratton—No. W7
Freier, P. S., E. P. Ney, J. Naugle, and G. Anderson—No. F3
Frenkiel, F. N.—No. R5
Fuchs, M. and E. S. Lennox—No. M12
Fundingsland, O. T. and George E. Austin—No. S4
Furukawa, G. T., R. E. McCoskey, R. S. Jessup, and R. A. Nelson—No. N13
Gallagher, C. J.—No. S2
Galt, J. K., B. T. Matthias, and J. P. Remeika—No. J4
Garfunkel, M. P., F. G. Dunnington, and B. Serin—No. H7
Geiger, Felix E., Jr.—No. I4
Geschwind, S., H. Minden, and C. H. Townes—No. P4
Getting, I. A., J. S. Clark, J. E. Thomas, Jr., I. G. Swope, and M. L. Sands—No. G6
Ginnings, D. C., T. B. Douglas, and A. F. Ball—No. D2
Gold, Louis—No. D4
Goldberg, Joshua and Peter G. Bergmann—No. P1
Goldberger, M. L.—No. M10
Goldhaber, M.—No. Y1
Goldman, J. E.—No. J10
Goldstein, L. and D. Sweeney—No. L6
Gordy, Walter and John Sheridan—No. O3
Gottlieb, Melvin B. and Alfred J. Hartzler—No. E4
Gove, Harry and Keith Boyer—No. X6
Gregory, B. P. and J. H. Tinlot—No. E6
Griffith, Wayland C.—No. U8
Groetzinger, Gerhart, Lewis B. Leder, Fred L. Ribe, and Martin J. Berger—No. Q10
Gross, W. and G. Failla—No. G11
Harris, S. P.—No. L8
Hartsough, Walter, Milton Hill, and Wilson M. Powell—No. L12
Hartzler, Alfred J. and Melvin B. Gottlieb—No. E5
Harvey, J. A.—No. X5
Hauptman, H. and J. Karle—No. D13
Heine-Geldern, R., E. M. Pugh, and S. Foner—No. R9
Henkel, R. L. and H. H. Barschall—No. L4
Henry, A. F.—No. I5
Hereford, Frank L.—No. Q11
Heybey, W.—No. R6
Hibdon, C. T. and C. O. Muehlause—No L7
Hill, David L.—No. B1
Hipple, J. A.—No. A3
Holt, R. B.—No. A1
Howard, Raydeen R. and William V. Smith—No. O8
Howe, Robert M.—No. S1
Hughes, A. L., Marshall R. Cleland, Wilfred R. Konneker—No. Q12
Hughes, D. J., M. T. Burgy, and G. R. Ringo—No. Q2
Hughes, J. V.—No. N2
James, Hubert M. and Guy W. Lehman—No. K3
Jastram, Philip S., W. Konneker, and Marshall R. Cleland—No. Y5
Jaynes, E. T. and E. P. Wigner—No. J2
Jehle, Herbert—No. C3
Jensen, E. N., L. J. Laslett, R. T. Nichols, and W. W. Pratt—No. Y4
Johnson, M. H. and E. O. Hulburt—No. N4
Johnson, V. R., M. J. W. Laubenstein, and F. Ajzenberg—No. W9

Johnston, Herrick L., Irving J. Bezmann, Thor Rubin, Lyle Jensen, David White, and Abraham S. Friedman—No. U9
Jossem, E. L. and L. G. Parratt—No. H4
Jungerman, J.—No. B5
Kachickas, G. A. and L. H. Fisher—No. S7
Karplus, Robert and Maurice Neuman—No. M1
Keck, J. C., M. Stearns, and R. R. Wilson—No. B12
Ketelle, B. H., C. M. Nelson, and G. E. Boyd—No. Y2
Kinsey, B. B., G. A. Bartholomew, and W. H. Walker—No. L5
Kittel, C.—No. J6
Klein, Martin J. and Robert S. Smith—No. J7
Knipp, J. K.—No. B3
Koehler, J. S. amd E. Salkovitz—No. D5
Konneker, W. R., S. DeBenedetti, and F. K. McGowan—No. G14
Kopfermann, Hans—No. I1
Koski, W. S. and C. O. Thomas—No. K12
Laquer, Henry L. and William E. McGee—No. D6
Latter, Richard—No. C2
Lax, Benjamin—No. N3
Lax, Melvin—No. C7
Leachman, R. B.—No. B2
Leitner, Alfred and R. D. Spence—No. C1
Litovitz, T. A.—No. R12
Lohman, J. B. and D. F. Hornig—No. U6
Low, W. and C. H. Townes—No. O2
Lundquist, G. A.—No. R7
Lyman, E. M., A. O. Hanson, and M. B. Scott—No. Q9
McClure, B. T., R. A. Johnson, and R. B. Holt—No. S6
McFee, Raymond H.—No. D8
McIntyre, J. A. and R. Hofstadter—No. G2
McMahon, Allen J. and Bruno Rossi—No. E8
Mandeville, C. E. and E. Shapiro—No. Y3
Margenau, Henry and Stanley Bloom—No. I7
Marple, D. T. F. and Henry Levinstein—No. N12
Marshak, R. E. and A. S. Whitman—No. M6
Marton, L., J. A. Simpson, and A. Van Bronkhorst—No. J12
Mayburg, Sumner—No. D11
Mei, J. Y., C. M. Huddleston, and Allan C. G. Mitchell—No. V7
——Allan C. G. Mitchell, and C. M. Huddleston—No V5
Menzel, D. H.—No. T3
Miller, B. L.—No. G9
Miller, Charles E., Joseph E. Henderson, David S. Potter, and Jay Todd—No. F6
Moffat, R. D. and L. M. Langer—No. V4
Mohler, Fred L., Vernon H. Dibeler, E. J. Wells, Jr., and R. M. Reese—No. N7
More, K. R., R. H. Chow, J. K. Kinnear, and S. B. Woods—No. G4
Muehlhause, C. O.—No. L9
Murphy, E. J.—No. D9
Nethercot, A. H., Jr. and C. W. Peters—No. O9
Neuendorffer, J. A., D. R. Inglis, and S. S. Hanna—No. W8
Ney, E. P., J. Lindsley, and P. S. Freier—No. F2
Oberly, J. J. and E. Burstein—No. K8
Osborn, J. A.—No. J3
Page, Lorne A. and W. M. Woodward—No. Q8
Palevsky, H. and A. O. Hanson—No. X11
Parzen, P. and L. Goldstein—No. S3
Pearlstein, E. and R. B. Sutton—No. K11
Pell, E. M. and D. H. Tomboulian—No. H5
Pellam, John R.—No. H13
Penfield, Robert and Henry Zatzkis—No. C10
Peshkin, Murray—No. M8
Peterson, R. E., R. K. Adair, H. H. Barschall, and C. K. Bockelman—No. L2
Petritz, R. L. and A. J. F. Siegert—No. K1
Phillips, G. C.—No. W12
Pierce, J. R.—No. A4
Pines, David and David Bohn—No. S5
Plotkin, H. H. and J. E. Goldman—No. J9
Pratt, W. W., F. I. Boley, and R. T. Nichols—No. G1
Pugh, E. M., R. Heine-Geldern, and E. C. Mutschler—No. R10
Rau, R. Ronald and G. G. Harris—No. F4
Reber, Grote—No. T2
Rediker, R. H. and H. S. Bridge—No. F5
Reed, Ronald L. and M. Dresden—No. C8
Reynolds, John H.—No. Y8
Richards, H. T., S. Bashkin, D. S. Craig, D. Donahue, V. R. Johnson, and D. Martin—No. W5
Richardson, John M.—No. C6
Riddell, R. J., Jr.—No. C5
Ridgeway, S. L.—No. Y7
Roberts, T. R. and Alfred O. Nier—No. B6
Robertson, Harry S. and G. H. Dieke—No. S8
Rutledge, W. C., A. E. Stoddard, C. E. Branyan, J. LeBlanc, and J. M. Cork—No. V9
Ryan, Alden H.—No. P7
Sachs, R. G. and L. L. Foldy—No. M9
Sanders, J. H., K. W. Allen, E. Almqvist, J. T. Dewan, and T. P. Pepper—No. W2
Saur, A. J., P. Axel, L. G. Mann, and J. Ovadia—No. V8
Scheidegger, A. E. and L. Infeld—No. C12
Schwertz, F. A. and Jeanne E. Brow—No. N10
Seriff, A. J., R. B. Leighton, C. Hsiao, E. W. Cowan, and C. D. Anderson—No. E3
Serin, B., C. A. Reynolds, and M. P. Garfunkel—No. H8
Shea, Ruth C. and Gladys A. Anslow—No. U2
Sher, R., J. Halpern, and W. E. Stephens—No. X2
Sheridan, John and Walter Gordy—No. O4
Shockley, W.—No. J14
Shoemaker, F. C., J. E. Faulkner, S. G. Kaufman, and G. M. B. Bouricius—No. Q7
Siegel, Keeve M.—No. R1
Simpson, J. Arol—No. J11
Sitte, K.—No. E2
Smith, E. C. and J. W. Beams—No. N1
Staker, W. P. and W. O. Davis—No. F8
Stone, Orville—No. G7
Strait, E. N., D. M. Van Patter, and W. W. Buechner—No. W14
Strauch, Karl—No. X8
Stump, Robert and Sherman Frankel—No. Y6
Sturrock, P. A.—No. J13
Sun, K. H., R. A. Charpie, F. A. Pecjak, B. Jennings, J. F. Nechaj, and A. J. Allen—No. B4
Swann, C. P. and C. E. Mandeville—No. X1
Swann, W. F. G.—No. J1
Swift, C. J.—No. N5
Tamor, Stephen—No. M7
Taylor, H. S.—No. A2
Taylor, W. J., C. W. Beckett, J. Y. Tung, R. B. Holden, and H. L. Johnston—No. U4
Temmer, G. M.—No. Q5
Ter-Pogossian, Michel, Fred T. Porter, and C. Sharp Cook—No. Y9
Terrell, James—W10
Thomsen, John S. and T. H. Berlin—No. D10
Ting, Yu, Roy C. Weidler, and Dudley Williams—No. P6
Tinlot, J. H. and B. P. Gregory—No. E7
Townes, C. H. and W. Low—No. B8
Trambarulo, Ralph and Walter Gordy—No. O6
Trounson, E. P., D. F. Bleil, and L. R. Maxwell—No. P8
Truesdell, C.—No. R2
Van Allen, J. A. and S. F. Singer—No. F1
Van Patter, D. M. and W. W. Buechner—No. W13
Van Patter, D. M., E. N. Strait, and W. W. Buechner—No. W14
Van Tuyl, A. H.—No. R8
Waggoner, M. A., M. L. Moon, and A. Roberts—No. V3
Walker, R. L., B. D. McDaniel, and M. B. Stearns—No. X10
Watanabe, K., F. S. Johnson, and R. Tousey—No. K10
Waymouth, J. F., Jr.—No. S11
Welton, T. A.—No. X7
White, David—No. U13
White, David, Abraham S. Friedman, and Herrick L. Johnston—No. U10, U11
White, David and Herrick L. Johnston—No. U12
Whitehead, W. D.—No. W6
Wilcox, H. A., W. F. Cartwright, C. Richman, and M. N. Whitehead—No. B10
Wilkinson, Michael K.—No. S10
Williams, R. W., L. M. Spetner, W. L. Kraushaar, H. W. J. Courant—No. F10
Williams, Quitman and Walter Gordy—No. O7
Wilson, Robert R.—No. E1
Witmer, Enos E.—No. B7
Wrinch, Dorothy—No. D12
Yadoff, Oleg—No. N11
Yager, W. A., J. K. Galt, F. R. Merritt, E. A. Wood, and B. T. Matth No. J5
Yagoda, Herman—No. F11
York, Herbert—No. F12
Zar, Jacob L. and M. H. Shamos—No. F7
Zucker, A. and W. W. Watson—No. X3